VOL. 652 NO. 1 OCTOBER 15, 1993

5th Int. Symp. on High Performance Capillary Electrophoresis
Orlando, FL, January 25–28, 1993
Part I

JOURNAL OF CHROMATOGRAPHY A

INCLUDING ELECTROPHORESIS AND OTHER SEPARATION METHODS

SYMPOSIUM VOLUMES

ELSEVIER

JOURNAL OF CHROMATOGRAPHY A

INCLUDING ELECTROPHORESIS AND OTHER SEPARATION METHODS

Scope. The *Journal of Chromatography A* publishes papers on all aspects of **chromatography, electrophoresis** and related methods. Contributions consist mainly of research papers dealing with chromatographic theory, instrumental developments and their applications. In the *Symposium volumes*, which are under separate editorship, proceedings of symposia on chromatography, electrophoresis and related methods are published. *Journal of Chromatography B: Biomedical Applications* —This journal, which is under separate editorship, deals with the following aspects: developments in and applications of chromatographic and electrophoretic techniques related to clinical diagnosis or alterations during medical treatment; screening and profiling of body fluids or tissues related to the analysis of active substances and to metabolic disorders; drug level monitoring and pharmacokinetic studies; clinical toxicology; forensic medicine; veterinary medicine; occupational medicine; results from basic medical research with direct consequences in clinical practice.

Submission of Papers. The preferred medium of submission is on disk with accompanying manuscript (see *Electronic manuscripts* in the Instructions to Authors, which can be obtained from the publisher, Elsevier Science Publishers B.V., P.O. Box 330, 1000 AH Amsterdam, Netherlands). Manuscripts (in English; *four* copies are required) should be submitted to: Editorial Office of *Journal of Chromatography A*, P.O. Box 681, 1000 AR Amsterdam, Netherlands, Telefax (+31-20) 5862 304, or to: The Editor of *Journal of Chromatography B: Biomedical Applications*, P.O. Box 681, 1000 AR Amsterdam, Netherlands. Review articles are invited or proposed in writing to the Editors who welcome suggestions for subjects. An outline of the proposed review should first be forwarded to the Editors for preliminary discussion prior to preparation. Submission of an article is understood to imply that the article is original and unpublished and is not being considered for publication elsewhere. For copyright regulations, see below.

Publication information. *Journal of Chromatography A* (ISSN 0021-9673): for 1994 Vols. 652–682 are scheduled for publication, *Journal of Chromatography B: Biomedical Applications* (ISSN 0378-4347): for 1994 Vols. 652–662 are scheduled for publication. Subscription prices for *Journal of Chromatography A*, *Journal of Chromatography B: Biomedical Applications* or a combined subscription are available upon request from the publisher. Subscriptions are accepted on a prepaid basis only and are entered on a calendar year basis. Issues are sent by surface mail except to the following countries where air delivery via SAL is ensured: Argentina, Australia, Brazil, Canada, China, Hong Kong, India, Israel, Japan, Malaysia, Mexico, New Zealand, Pakistan, Singapore, South Africa, South Korea, Taiwan, Thailand, USA. For all other countries airmail rates are available upon request. Claims for missing issues must be made within six months of our publication (mailing) date. Please address all your requests regarding orders and subscription queries to: Elsevier Science Publishers, Journal Department, P.O. Box 211, 1000 AE Amsterdam, The Netherlands. Tel.: (+31-20) 5803 642; Fax: (+31-20) 5803 598. Customers in the USA and Canada wishing information on this and other Elsevier journals, please contact Journal Information Center, Elsevier Science Publishing Co. Inc., 655 Avenue of the Americas, New York, NY 10010, USA, Tel. (+1-212) 633 3750, Telefax (+1-212) 633 3764.

Abstracts/Contents Lists published in Analytical Abstracts, Biochemical Abstracts, Biological Abstracts, Chemical Abstracts, Chemical Titles, Chromatography Abstracts, Current Awareness in Biological Sciences (CABS), Current Contents/Life Sciences, Current Contents/Physical, Chemical & Earth Sciences, Deep-Sea Research/Part B: Oceanographic Literature Review, Excerpta Medica, Index Medicus, Mass Spectrometry Bulletin, PASCAL-CNRS, Referativnyi Zhurnal, Research Alert and Science Citation Index.

US Mailing Notice. *Journal of Chromatography A* (ISSN 0021-9673) is published weekly (total 52 issues) by Elsevier Science Publishers (Sara Burgerhartstraat 25, P.O. Box 211, 1000 AE Amsterdam, Netherlands). Annual subscription price in the USA US$ 5132.25 (US$ price valid in North, Central and South America only) including air speed delivery. Second class postage paid at Jamaica, NY 11431. **USA POSTMASTERS**: Send address changes to *Journal of Chromatography A*, Publications Expediting, Inc., 200 Meacham Avenue, Elmont, NY 11003. Airfreight and mailing in the USA by Publications Expediting.

See inside back cover for Publication Schedule, Information for Authors and information on Advertisements.

0021-9673/93/$06.00

Printed in the Netherlands

For Contents see p. VII.

JOURNAL OF CHROMATOGRAPHY A

VOL. 652 (1993)

JOURNAL OF CHROMATOGRAPHY A

INCLUDING ELECTROPHORESIS AND OTHER SEPARATION METHODS

SYMPOSIUM VOLUMES

ELSEVIER
AMSTERDAM — LONDON — NEW YORK — TOKYO

0021-9673/93/$06.00

SYMPOSIUM ISSUE

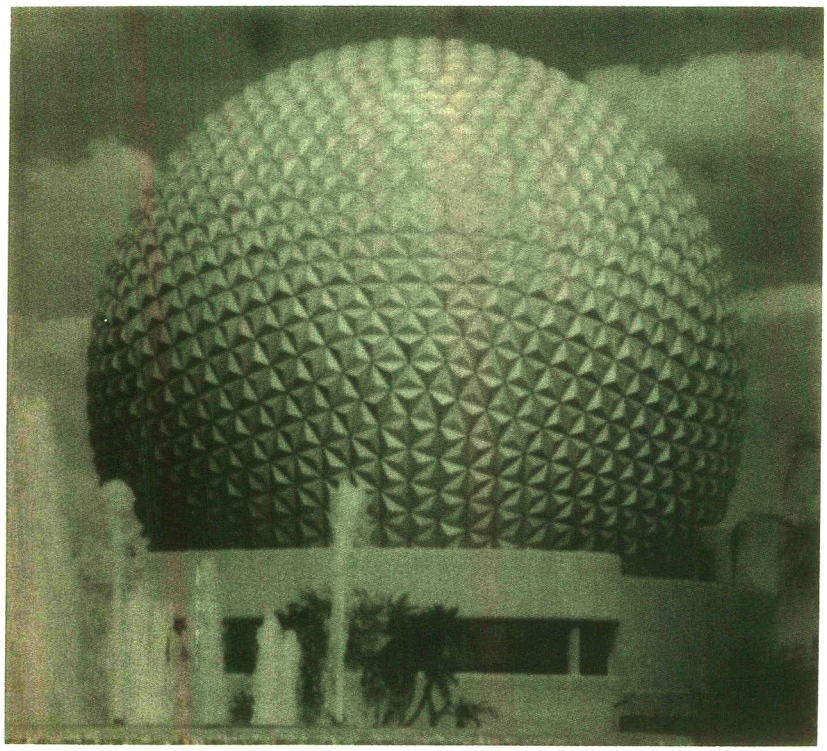

FIFTH INTERNATIONAL SYMPOSIUM ON HIGH PERFORMANCE CAPILLARY ELECTROPHORESIS

Orlando, FL (USA), January 25–28, 1993

Guest Editor

B.L. KARGER

(Boston, MA, USA)

VOL. 652, NO. 1 JOURNAL OF CHROMATOGRAPHY A OCTOBER 15, 1993

CONTENTS

5TH INTERNATIONAL SYMPOSIUM ON HIGH PERFORMANCE CAPILLARY ELECTROPHORESIS, ORLANDO, FL, JANUARY 25–28, 1993

PART I: VOLUME 652, NO. 1

CHIRAL SEPARATIONS

FUNDAMENTALS

Journal of Chromatography A, 652 (1993) 1
Elsevier Science Publishers B.V., Amsterdam

CHROM 25 486

Foreword

The *5th International Symposium on High Performance Capillary Electrophoresis, HPCE '93*, was held in Orlando, FL, January 25–28, 1993. By any measure, this was the most successful meeting of the series to-date, with over 600 participants, 26 exhibition booths and 270 papers. The popularity of the meeting is such that instrument manufacturers continually introduce new CE products at this symposium. Beyond the expanded interest in new developments in CE, two broad trends were clearly seen. First, researchers at an even greater rate are using CE to solve real separation and analytical problems. The increase in applications can also be realized from this symposium issue where a significant fraction of the 67 papers is in applications of CE. Secondly, the special feature of CE as a practical tool for miniaturized analysis was emphasized, whether assays on chips or the manipulation of flows or ions in nanosystems.

The success of the meeting is in large measure a result of many individuals. Special thanks are due Tom Gilbert for the key role he has played in all five HPCE symposia. Shirley Schlessinger again did a fine job in running the administrative tasks of the symposium. Rich and Julie Pumphrey of the Barnett Institute also were most helpful in a myriad of details. The program was carefully put together with the advice and assistance of my co-members of the Scientific Committee —Frans Everaerts, Stellan Hjertén, Jim Jorgenson and Shigeru Terabe. I also want to thank Dr. Zdenek Deyl for his fine editorship of this special issue.

Finally, it is my great pleasure to invite you to HPCE '94 to be held in San Diego on January 31–February 3, 1994. The chairman of the meeting will be Professor Shigeru Terabe, Himeji Institute of Technology, Japan.

Boston, MA (USA) Barry L. Karger

Journal of Chromatography A, 652 (1993) 3–16
Elsevier Science Publishers B.V., Amsterdam

CHROM. 25 137

Capillary electrophoresis of DNA in uncross-linked polymer solutions

Annelise E. Barron*, David S. Soane and Harvey W. Blanch

Department of Chemical Engineering, University of California, Berkeley, 201 Gilman Hall, Berkeley, CA 94720 (USA)

ABSTRACT

We have used dilute and semi-dilute uncross-linked hydroxyethyl cellulose (HEC) solutions as separation matrices for capillary electrophoresis of DNA restriction fragments. In these experiments, we investigated the effects of HEC molecular weight* and concentration on resolution, attempting to relate these parameters to the polymer entanglement threshold concentration.

The entanglement thresholds of seven molecular weight fractions of hydroxyethyl cellulose were determined from viscosity-concentration data; the entanglement threshold was found to scale as $N^{-1.2}$, where N = number of HEC monomers. This finding is not in agreement with classical scaling arguments. We present a relationship to predict the observed entanglement threshold of HEC in solution as a function of number average molecular weight.

It was found that excellent separation of ΦX174/*Hae*III DNA restriction fragments (72–1353 base pairs) by capillary electrophoresis in HEC solutions can be achieved significantly below the entanglement threshold, depending on DNA size and HEC molecular weight. The mechanism of separation in these uncross-linked polymer solutions must therefore be reexamined. Our experiments show that the entanglement threshold is a useful parameter in predicting a range of HEC concentrations which will separate certain DNA fragments for a given HEC molecular weight. However, the presence of a fully entangled network is not a prerequisite for separation.

INTRODUCTION

Capillary electrophoresis in uncross-linked polymer solutions has been shown to be a promising technique for the rapid and efficient separation of DNA restriction fragments up to 23 000 base pairs (bp) in size [1–6]. While cross-linking a homogeneous and stress-free gel within a capillary can be problematic, the use of uncross-linked polymer solutions enables high-resolution DNA separations to be carried out in an uncoated capillary [4]. Solutions of several different polymers have been employed as separation media for capillary electrophoresis, with varying degrees of success: hydroxyethyl cellulose [4], hydroxypropylmethyl cellulose [2,7], methyl cellulose [1], and polyvinyl alcohol [7], as well as liquified agarose [6,7] and uncross-linked polyacrylamide [3,7]. Solutions of uncross-linked polymers have been found to have separation potential over a wide range of concentrations, from semi-dilute, low-viscosity solutions [4] to extremely concentrated, "syrupy" solutions which are so viscous that they cannot be injected into a capillary and must be polymerized *in situ* [8]. Potentially, the more concentrated solutions have the resolving power to be used for DNA sequencing. It appears that the more dilute solutions will be more suited to mapping and sizing applications, as single base pair resolution for DNA greater than 100 bp in length has not yet been achieved. It has not been established whether the mechanism of DNA separation in an extremely dilute solution is the same as that which occurs in a gel-like, "syrupy" solution. Furthermore, for uncross-linked polymer solu-

* Corresponding author.

* Upon request of the authors, the term "molecular weight" is used in this paper, rather than the standard "molecular mass" which is preferred in this journal.

0021-9673/93/$06.00

tions in general, the relationship between the resolution and the molecular weight and concentration of the polymer is not yet fully understood. No theory exists to accurately predict the appropriate polymer size and concentration for a desired separation.

The mechanism of DNA separation in uncross-linked polymer solutions continues to be a matter of controversy. Some groups have asserted that the mechanism is essentially the same as that in traditional slab gel electrophoresis [2,4], while others attribute separation to the attraction and interaction of DNA fragments with the cellulose derivatives in the buffer [1,5]. Still others have theorized that the separation involves a mechanism of exclusion from the polymer fiber network similar to that occurring in gel permeation chromatography [9].

We address these questions both experimentally and theoretically, employing hydroxyethyl cellulose (HEC) solutions as a separation matrix for capillary electrophoresis. We discuss the structural characteristics which allow solutions of HEC (and other cellulosic polymers) to act as an effective separation matrix for electrophoresis of DNA. In fact, the mechanism of DNA separations in dilute and semi-dilute uncross-linked HEC solutions may involve entanglement coupling between the DNA and the uncross-linked HEC. We present the results of rheological and capillary electrophoresis experiments with several different molecular weights of HEC, and present evidence that for fine resolution, the average distance between entanglement points in the HEC solution must be approximately equal to the contour length of the DNA molecules of interest.

BACKGROUND AND THEORY

Structure of hydroxyethyl cellulose

Cellulose is a naturally occurring high polymer in which β-D-glucopyranoside units are condensed through a 1,4′-linkage to form a linear molecule. HEC is a hydrophillic cellulose derivative, synthesized commercially by reacting alkali cellulose with ethylene oxide at high temperatures [10]. Substitution may be expressed in terms of the moles of ethylene oxide per anhydroglucose unit, designated as the molar substitution (M.S.). On average, HEC has an M.S. of 2.5, giving an average monomer molecular weight of 272 g/mol. A typical structural element of the HEC molecule is shown in Fig. 1.

Properties of HEC in solution

The dissolution of HEC in water is accomplished by the expansion of the structure by the bulky substituent groups, especially the polyethylene oxide side chains which terminate in the hydrophillic hydroxyethyl group [10]. Cellulose derivatives such as HEC are known to be highly extended and inflexible in solution. While a typical non-cellulosic polymer has a Porod–Kratky persistance length of only 0.8–1.0 nm, that of HEC in water has been estimated at 8.3 nm [10]. Stiff and extended molecules are known to exhibit more pronounced effects of entanglement than highly flexible polymers [11]. The experiments of Saunders *et al.* [12] show that for cellulosic polymers the presence of bulky side chains, such as the bulky ethylene oxide group in HEC, does not significantly affect the onset of entanglement coupling. Thus, it is thought that these stiff, extended molecules form an entangled network through a long-range looping of chains, rather than through short-range interactions such as local kinks [13]. Fig. 2 is a schematic representation of this type of long-range looping. Although a mesh formed by long-range interactions of inflexible, extended HEC

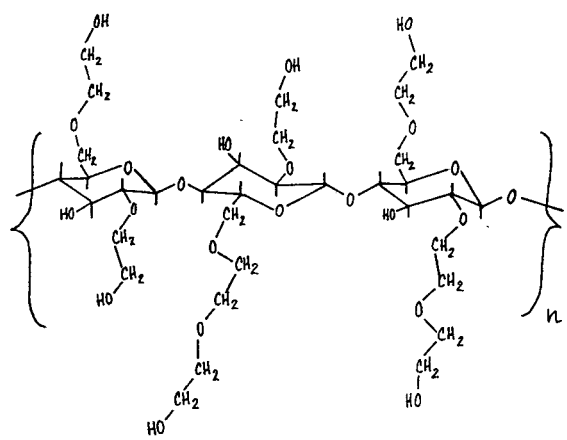

Fig. 1. A typical structural element of a hydroxyethyl cellulose chain (three monomers shown).

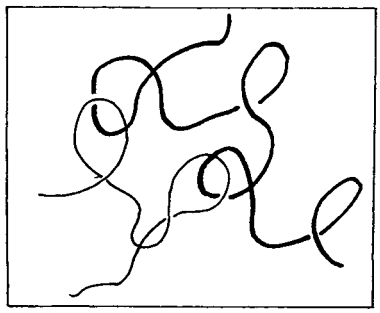

Fig. 2. Long-range entanglement coupling between two polymers. Since the presence of bulky side-groups, like the ethylene oxide group of HEC, does not inhibit the onset of entanglement coupling in solutions of cellulosic polymers, it seems likely that these interactions involve long-range looping rather than short-range kinking or knotting [12].

molecules will be fairly stiff, it will not be tightly "knotted" and therefore will have a dynamic structure.

Entanglement coupling between HEC and DNA

It is important to note that DNA molecules can also be described as stiff and extended in solution, even more so than HEC. In fact, the Porod–Kratky persistance length of double-stranded DNA is about 45 nm at an ionic strength of 0.2 *M* [14]. Therefore, it is likely that DNA experiences some degree of entanglement coupling with HEC molecules in solution, the effects of which are augmented by the stiffness of the two participants in the interaction. This entanglement coupling, theoretically, could sufficiently alter the frictional characteristics of the DNA molecules moving under the influence of the electric field so as to render size-dependent separations possible. This mechanism of separation is quite different from that postulated to occur in cross-linked polyacrylamide or agarose gels.

Consider the frictional characteristics of a molecule when no entanglement coupling is present. Einstein showed that in general, for large particles,

$$D = \frac{kT}{\text{(molecular friction factor)}} \qquad (1)$$

where D is the diffusion coefficient, k is Boltzmann's constant, T is the temperature, and the "molecular friction factor" is defined as the force required to pull the undeformed molecule through its surroundings at unit velocity [15]. It has been demonstrated by Bueche [16] that this molecular friction factor is strongly affected by entanglement coupling, and the following discussion closely follows his work.

Consider a freely orienting polymer, consisting of N subunits, that is not entangled with other polymers. If a force f_0 is needed to pull a single freely orienting segment through its surroundings at unit velocity, then the total frictional coefficient for the non-entangled polymer is Nf_0, where f_0 is a "segmental friction factor." Substitution of this relationship into eqn. 1 gives

$$D = \frac{kT}{Nf_0} \quad \text{(no entanglements)} \qquad (2)$$

Now, consider a polymer molecule which is entangled with other polymer molecules in solution. In this case, a force larger than Nf_0 is required to pull the polymer through the solution at unit velocity. Assume that all of the polymer molecules are identical and that entanglement points exist at uniform distances along a molecule, where L_e is the average molecular contour length between entanglement points.

If a particular molecule, the primary molecule, is pulled along at unit velocity, a force Nf_0 is required to pull its constituent segments through solution. A number of other molecules will be entangled with the primary molecule in such a way as to slow its progress (see Fig. 3). Since these molecules are not firmly attached to the primary molecule, they will slip as the primary

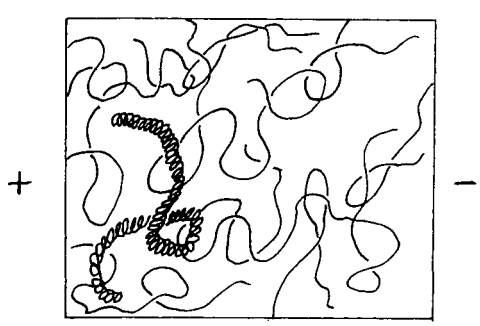

Fig. 3. A schematic representation of the entanglement coupling interaction of DNA, moving under the influence of an electric field, with the HEC molecules in the buffer.

molecule moves through solution. They will be transported at some velocity which is less than the velocity of the primary molecule.

In turn, those molecules which are entangled with the primary molecule will pull with them still other molecules; these molecules will pull with them still other molecules, and so on. The net effect of these entanglement couplings is to require the application of a force much larger than Nf_0 if the primary molecule is to be pulled through solution at unit velocity. Furthermore, this increase in the molecular friction factor will be dependent on N, the number of polymer segments; for the longer the polymer is, the more entanglement points which will exist, and the slower the polymer will progress through solution. Indeed, this behavior is observed in the capillary electrophoresis of DNA in entangled polymer solutions, where electrophoretic mobility decreases with increasing size [4]. This general trend, however, is the same when DNA is electrophoresed in a cross-linked gel, which has an interconnected system of semi-rigid pores. In order to show that the mechanism is different, we must show that good separations can occur before the separation matrix in the buffer is fully entangled; *i.e.*, before any porous network-like structure could exist.

Determination of entanglement threshold

The *entanglement threshold* (Φ^*) is defined as the concentration at which polymer molecules begin to overlap and interact strongly in solution. This critical concentration has been identified as the point at which *network formation* through chain entanglement becomes possible; *i.e.*, below Φ^* there may be some entanglement coupling between isolated molecules, but it does not extend throughout the system [17].

Experimentally, the concentration at which polymer chains in a given narrow molecular weight range form an entangled network can be determined from a log–log plot of specific viscosity (η_{sp}) *vs.* polymer weight fraction (Φ). At low concentrations ($\Phi < \Phi^*$), where the polymer molecules do not interact extensively in solution, specific viscosity is linear with concentration. At the entanglement threshold ($\Phi \approx \Phi^*$), the η_{sp} *vs.* Φ data exhibit a break and an increase in slope, since the presence of an entangled polymer network makes a large contribution to solution viscosity [18].

For any given polymer, Φ^* will have a unique dependence on molecular weight. DeGennes [19] recognized that Φ^* was an essential scaling parameter, and used polymer physics to derive a scaling relationship between Φ^* and molecular weight. This expression is based on the assumption that when $\Phi \approx \Phi^*$, the bulk concentration of the solution is the same as the concentration inside a single coil. For randomly coiling polymers in an athermal solvent, it follows that

$$\Phi^* \sim N^{-0.8} \tag{3}$$

where N is the number of monomer units. This expression states that Φ^* *scales as* $N^{-0.8}$, but in order to use this relationship in a predictive fashion, one must know the coefficient and additive constant. To this end, in our study of HEC we compared the molecular weight dependence of the entanglement threshold with that predicted by deGennes. We did not expect perfect agreement with this scaling relationship, since (1) HEC is stiff and extended in solution and therefore deviates appreciably from the model of a random coil, and (2) water is a good solvent for HEC, not an athermal solvent.

Average mesh size of an entangled network

In addition, deGennes [19] assumed that at polymer concentrations above the entanglement threshold, an entangled network of polymers could be characterized with an "average mesh size," designated ξ. He assumed first that for $\Phi > \Phi^*$, ξ depends only on Φ and not on the number of monomer units in the chain; *i.e.*, the average mesh size is less than the contour length of the polymer. Secondly, he assumed that when $\Phi \approx \Phi^*$, the mesh size is about the same as an individual polymer coil (R_g). With these assumptions the following scaling relationship was obtained:

$$\xi(\Phi) \sim a\Phi^{-0.75} \quad (\Phi^* < \Phi < 1) \tag{4}$$

where the units of ξ are nanometers, and a is the statistical segment length of HEC, a constant tabulated as 0.425 nm [20]. Once again, how-

ever, this is simply a *scaling* relationship, and no direct or approximate equality is implied. It was suggested by Grossman and Soane [4] that since combining eqns. 3 and 4 leads to the relationship $\xi(\Phi^*) \sim aN^{0.60}$, it should be possible to tailor the mesh size at Φ^* simply by using the correct HEC length.

The average molecular contour length between entanglement points

It is interesting to compare the scaling of the average mesh size discussed above, a concept which is only meaningful for a fully entangled mesh, to the average molecular contour length between entanglement points (L_e), a meaningful quantity both above and below the entanglement threshold. L_e provides a means of describing entanglement interactions which may occur at concentrations *below* Φ^*. Once again drawing from the work of Bueche [16], we can derive the scaling relationship between L_e and the concentration of polymer in solution (Φ). In fact, L_e will be inversely proportional to Φ. This becomes obvious if one considers that one can dilute a highly entangled network of polymers with a good solvent until the polymer concentration in solution is so low that molecules no longer overlap, and no entanglements between molecules will exist. It follows that L_e will increase as Φ decreases. There will be concentrations below the entanglement threshold where transient entanglement coupling between individual molecules occurs, so that on average L_e will be only slightly less than the contour length of the polymer molecule. Thus, L_e can take on a continuum of values, both below and above the entanglement threshold.

This concentration dependence of L_e can be justified more rigorously. Consider a polymer molecule in solution which is looped around itself in several places, so that if another polymer molecule passed through one of these loops it could form a point of entanglement. The number of other polymer molecules passing through one of these loops will be proportional to the total concentration of polymers in solution, Φ [16]. Thus, the probability that a given loop in a polymer is entangled with another polymer is proportional to Φ. Since L_e equals the total contour length of the polymer divided by the number of entanglement points, it follows that $L_e \sim 1/\Phi$. This leads to the relationship

$$L_e \Phi = \text{constant} \tag{5}$$

This equation assumes that a given polymer in an entangled network always has more possible points along its length where other entanglements *could* occur, if the concentration of polymer in solution were greater. Due to steric hindrances and other factors, the number of possible entanglement points per molecule probably reaches some asymptotic value at high concentrations which is related to its structure.

At the entanglement threshold, the average mesh size given in eqn. 4 should be comparable to the average contour length between entanglements. However, an additional relationship is required to make this comparison. This is provided by Ferry [21], who states that at the entanglement threshold there must be on average two entanglement points per molecule. By analogy with the theory of cross-linked gels, the entanglement coupling may extend throughout the system if, statistically, each molecule has two entanglement points. In other words, at the entanglement threshold,

$$L_c = 2L_e \quad (\Phi = \Phi^*) \tag{6}$$

where L_c is the average total contour length of the polymer molecule, a quantity which may be calculated easily, given knowledge of the number-average molecular weight (M_n), monomer molecular weight (M_0), and the monomer dimensions (L_m):

$$L_c = \left(\frac{M_n}{M_0}\right) L_m \tag{7}$$

Combining eqns. 5, 6 and 7, one arrives at the relationship

$$\Phi^* \sim M_n^{-1} \tag{8}$$

Since the number of monomers (N) can be calculated by dividing M_n by the monomer molecular weight (M_0), Eqn. 8 is equivalent to stating that $\Phi^* \sim N^{-1}$, which is different from deGennes' [19] result in eqn. 3. We have determined Φ^* for several different molecular

weights of HEC in order to compare experimental results with the predictions of eqns. 3 and 8.

EXPERIMENTAL

Instrumentation

The capillary electrophoresis apparatus used in these studies employs a straight length of fused-silica capillary with an external coating of polyimide (Polymicro Technologies, Phoenix, AZ, USA) and no internal coating, 50 cm in length (35 cm to the detector), with 51 μm I.D. and 360 μm O.D. The capillary connects the anodic reservoir with the electrically grounded cathodic reservoir. A high-voltage power supply with a 30 000-V capacity (Gamma High Voltage Research, Ormand Beach, CA, USA) was used to drive electrophoresis. Current was measured over a 1-kΩ resistor in the return circuit of the power supply, using a digital multimeter (Model 3465B, Hewlett-Packard, Palo Alto, CA, USA). On-column detection was by UV absorbance at 260 nm, using a modified variable-wavelength detector (Model 783, Applied Biosystems, Foster City, CA, USA). Data were collected using an integrator (Model 3390, Hewlett-Packard).

Materials

A ΦX174/*Hae*III restriction digest was obtained from Bethesda Research Labs (Bethesda, MD, USA). Mesityl oxide was used as a neutral marker (Aldrich, Milwaukee, WI, USA). The buffer used in all experiments was 89 m*M* tris(hydroxymethyl)aminomethane (Tris) and 89 m*M* boric acid, with 5 m*M* ethylenediaminetetraacetic acid (EDTA) added as a chelating agent, pH 8.15 (all buffer reagents purchased from Sigma Molecular Biology, St. Louis, MO, USA). Varying amounts of hydroxyethyl cellulose (HEC) were added to buffer solutions; mixtures were vigorously shaken and then mixed for 24 h by tumbling (mixing by mechanical stirring sometimes led to incomplete dissolution). Seven different (number-average) molecular weight fractions of HEC were used: samples with molecular weight ranges of $M_n \approx 24\,000$–$27\,000$, $M_n \approx 90\,000$–$105\,000$, and $M_n \approx 140\,000$–$160\,000$ g/mol were obtained from Polysciences (Warrington, PA, USA). (Hereafter these samples will be referred to as M_n 27 000, M_n 105 000, M_n 160 000, for brevity.) Samples with average molecular weights $M_n \approx 35\,900$, $M_n \approx 63\,800$, $M_n \approx 306\,000$ and $M_n \approx 438\,800$ were donated by the Aqualon (Wilmington, DE, USA) and were designated as Natrosol 250L, 250EXR, 250MR, and 250H, respectively. The average molecular weights of these Natrosol products were previously determined by Sperry [22] using intrinsic viscosity measurements. The molecular weight ranges of the HEC samples from Polysciences were determined by the company. The ratio of weight-average molecular weight to number-average molecular weight (a measure of sample polydispersity) has not yet been measured for these HEC samples.

Methods

Capillary zone electrophoresis. Before each experiment, the uncoated inner capillary wall was conditioned first with 1 *M* NaOH for 10 min, then with 0.1 *M* NaOH for 10 min, and finally with the electrophoresis buffer (containing dissolved HEC) for 20 min. The electric field was turned on and left on until current through the capillary had stabilized, usually 10–15 min. Buffer solutions were degassed immediately prior to use. Samples were introduced to the anodic end of the capillary by applying a vacuum of 4 inch Hg (13546 Pa) for a specific time which depended on the buffer viscosity, so as to introduce approximately 3 nl ($3 \cdot 10^{-6}$ cm^3) of sample for each run. After the sample slug was drawn into the capillary, the anodic end of the capillary was placed back into the electrophoresis buffer, together with the anodic electrode, and the electrophoretic voltage was applied. All experiments were run at 11 kV (220 V/cm). The capillary was surrounded by agitated air at a temperature of 30.0 ± 0.1°C in all experiments.

Note that DNA, which is negatively charged, would remain at the anodic end of the capillary were it not drawn toward the UV absorbance detector and the cathode by strong electroosmotic flow. Thus, the largest DNA fragment, which has the smallest electrophoretic mobility in the direction of the anode, will pass the detector first, followed by the smaller ones in

order of size. A description of the method used to calculate electrophoretic mobilities can be found elsewhere [23]. The capillary electrophoresis apparatus used in these studies is configured in such a way that electrokinetic injection at the cathode is difficult; because of this limitation, hydrodynamic injection at the anode required that uncoated capillaries, which engender strong electroosmotic flow, be used to drive the DNA past the detector.

Each new, uncoated capillary was treated with 1 *M* NaOH for three hours before performing the first run, to etch the fused-silica surface completely clean. After the initial 3-h treatment with 1 *M* NaOH, 10-min treatments with base between runs sufficed to clean out the previous buffer–HEC mixture and refresh the necessary wall condition for excellent separations.

Viscosity measurements. Viscosity measurements were performed with an Ostwald viscometer which had been previously characterized with two viscometer constants, α and β [18]. Previous experiments with HEC in water have shown that the effect of shear rate on viscosity may be neglected [10]. Densities of the HEC–buffer solutions were determined by weighing sample volumes of 25 cm^3 at room temperature. During all experiments the viscometer was thermostatted in a water bath at 25.0 ± 0.1°C.

RESULTS AND DISCUSSION

Determination of entanglement threshold

The entanglement threshold, Φ^*, was determined for seven molecular weight fractions of HEC, shown in Table I. Since in our comparison with theoretical entanglement threshold scaling the important parameter is the *number of monomers*, it is appropriate to use the *number-average* molecular weight, a measure of the average number of repeat units per polymer molecule, rather than the viscosity-average molecular weight or the weight-average molecular weight [24]. Fig. 4 shows a representative plot of log η_{sp} *vs.* log Φ used to determine Φ^* for each HEC molecular weight. In each case, Φ^* was taken to be the point at which the data begin to deviate significantly from a straight line. Table I summarizes the values of Φ^* [as % (w/w) HEC in buffer solution for each HEC molecular weight. It is important to note that this measured entanglement threshold reflects the concentration at which an infinite entangled *network* begins to form; below this concentration, an individual HEC molecule has, on average, less than two points of entanglement [21].

TABLE I

EXPERIMENTALLY DETERMINED ENTANGLEMENT THRESHOLDS

M_n = Number-average molecular weight of HEC. Φ^* = Entanglement threshold, weight percent HEC in buffer.

M_n (g/mol)	Φ^* (%, w/w)
27 000	1.80
35 900	1.25
63 800	0.68
105 000	0.37
160 000	0.21
306 000	0.11
438 800	0.09

The number of monomers, N, was calculated by dividing the number-average molecular weight by the monomer molecular weight of HEC (M.S. = 2.5) of 272 kg/kmol. If we plot log Φ^* *vs.* log N (Fig. 5), we see that Φ^* scales as $N^{-1.2}$ rather than $N^{-0.8}$ as deGennes [19] predicts in eqn. 3 or as $N^{-1.0}$ as Bueche predicts in eqn. 8 [16]. Thus, the onset of entanglement is a stronger function of molecular weight for HEC than that predicted for a randomly coiling poly-

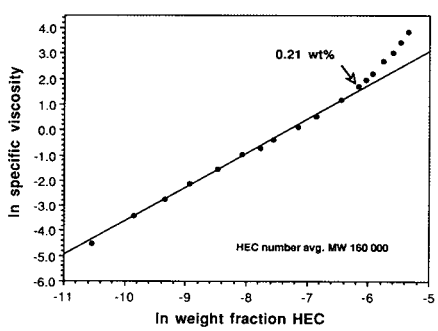

Fig. 4. A representative plot of the logarithm of the specific viscosity *vs.* the logarithm of HEC weight fraction, used to find the entanglement threshold (Φ^*) for each HEC molecular weight. In this case, the HEC has a number average molecular weight of 160 000 g/mol.

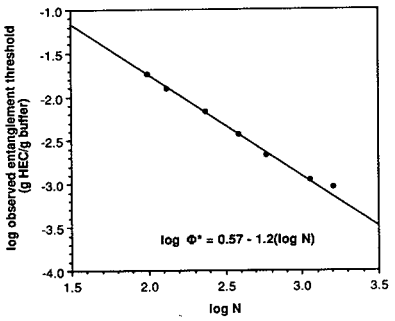

Fig. 5. A plot of the logarithm of the entanglement threshold (g HEC/g buffer) *vs.* the logarithm of the number of HEC monomers in the chain, showing that Φ^* scales as $N^{-1.2}$.

mer, consistent with the known stiffness of HEC in solution. Fig. 6 shows a plot of Φ^* *vs.* $N^{-1.2}$; the data are a good fit to a line with a positive intercept at $1.18 \cdot 10^{-4}$ g HEC/g buffer. Thus, a solution of "infinitely" long HEC molecules would be entangled even at this low concentration. Furthermore, the following relationship may be used to predict entanglement threshold for any HEC molecular weight fraction for which the number-average molecular weight is known:

$$\Phi^* = 3.63\left[\frac{M_n}{M_0}\right]^{-1.2} + 1.18 \cdot 10^{-4} \quad (9)$$

where Φ^* is measured as g HEC/g solvent and M_0 is the average monomer molecular weight, which will vary with the molar substitution (M.S.). Most HEC has an M.S. of 2.5, which gives an M_0 of 272 g/mol.

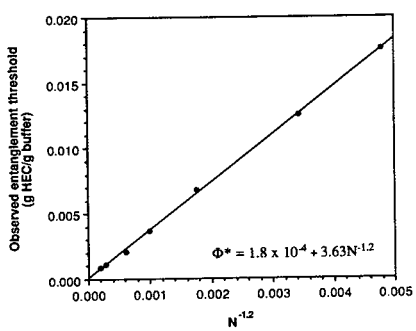

Fig. 6. A plot of the entanglement threshold (Φ^*) *vs.* $N^{-1.2}$. Note that the line which fits this data has a positive intercept of $1.18 \cdot 10^{-4}$.

Capillary electrophoresis experiments

We wished to test the importance of the entangled network of HEC chains in DNA separations; specifically, whether a definite mesh-like structure in HEC solutions is necessary for DNA separation. It has been proposed by Grossman and Soane [4] that this entangled network plays the same role as a cross-linked gel network in the electrophoretic separation of DNA restriction fragments, *i.e.*, that the mechanism of separation was essentially the same in cross-linked and uncross-linked sieving matrices. In our experiments, however, we found that the existence of a fully entangled network is not a necessary condition for separation. That is, an HEC solution used to fill an uncoated capillary

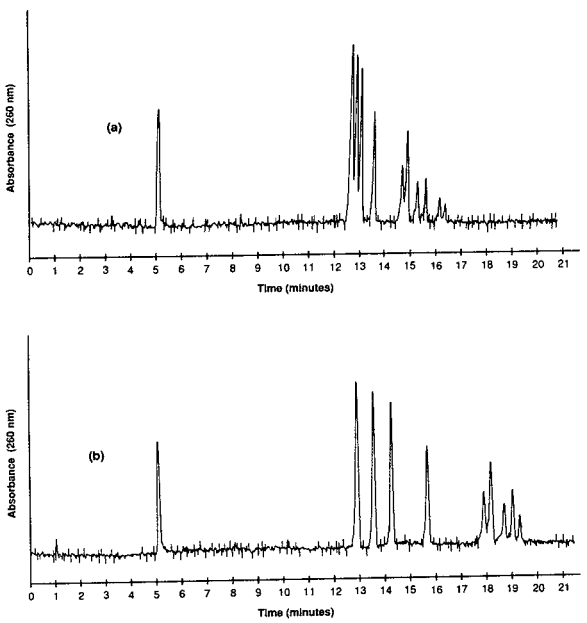

Fig. 7. Capillary electrophoresis of eleven ΦX174/*Hae*III restriction fragments ranging in size from 72 to 1353 bp in (a) 0.35% (w/w) M_n 27 000 HEC, and (b) 0.09% (w/w) M_n 105 000 HEC, both in 89 m*M* Tris–89 m*M* boric acid–5 m*M* EDTA. Reading from left to right (not including the first peak, which is a neutral marker), the species are (a) 1353, 1078, 872, 603, 310, 281 + 271, 234, 194, 118, and 72 bp in length, and (b) 1353, 1078, 872, 603, 310, 281 + 271, 234, 194 + 118, 72 bp in length, respectively. Conditions: field strength 221.4 V/cm; current (a) 7.2 μA, (b) 7.1 μA; UV detection at 260 nm; capillary dimensions, 50 cm total length (35 cm to detector) × 51 μm I.D.; temperature, 30 ± 0.1°C. R.S.D. of absolute electrophoretic mobilities: (a) 0.21%, $n = 5$; and (b) 0.37%, $n = 6$.

may be at a concentration significantly below its entanglement threshold and still well separate DNA restriction fragments. Fig. 7a shows the electrophoretic separation of ΦX174/*Hae*III restriction fragments in a buffer containing 0.35% (w/w) M_n 27 000 HEC. HEC of this molecular weight does not form an entangled network at concentrations below 1.8% (w/w). (In all electropherograms, peak heights are attenuated by a factor of 4.0.) In Fig. 7b the same restriction digest is separated in buffer containing 0.09% (w/w) M_n 105 000 HEC, although the entanglement threshold of this HEC fraction is 0.37% (w/w). Similar examples could be cited for electrophoresis in buffer solutions containing HEC of molecular weights up to M_n 438 800. UV absorbance peaks for the ΦX174/*Hae*III restriction fragments were identified from integrated peak areas, as shown in Fig. 8 by a representative plot of peak area *vs.* number of base pairs.

The question could be raised as to whether the solution within the capillary is homogeneous in concentration, *i.e.*, whether HEC adsorption on the capillary walls perhaps creates local regions with HEC concentration higher than the bulk concentration. If this were the case, concentrations near the wall could be *above* the entanglement threshold of the solution, although the bulk solution is well below this concentration. Our experiments show that this is probably not the case. Since we were constrained to use uncoated capillaries with our apparatus (see *Methods*), and we etched the capillary walls with strong base prior to each replacement of the HEC–buffer solution, the ζ potential of the capillary wall was quite high, even in the presence of HEC–buffer solution. This is evidenced by the strong electroosmotic flow in our experiments (a neutral marker typically eluted after about five minutes at a field strength of 220 V/cm). Were the HEC strongly adsorbed to the wall, or adsorbed in thick layers, negative charges on the wall would be effectively shielded and electroosmotic flow would be much reduced. Also, if the concentration profile within the capillary were inhomogeneous, with a higher concentration of HEC near the wall, DNA molecules near the wall would experience different amounts of sieving than those in the center of the capillary, and peaks would be broadened. But it can be seen that even in Fig. 7a, where the HEC concentration is well below the entanglement threshold and DNA separation definitely occurs, that peaks are quite sharp. Since peaks are sharp and electroosmotic flow is strong, since buffer pH is high (pH 8.2), and since temperature is also relatively high (30°C), there is more likely a rapid adsorption/desorption process which leads to ineffective shielding of the negative charges on the wall and a homogeneous concentration within the capillary.

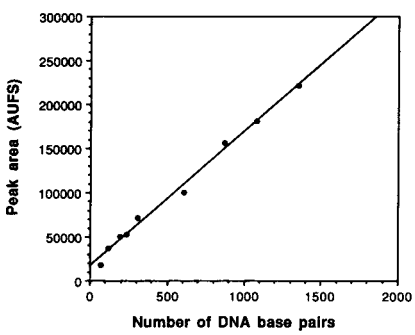

Fig. 8. A representative plot of UV absorbance peak area *vs.* number of DNA base pairs. This particular plot was obtained for electrophoresis at 220 V/cm of ΦX174/*Hae*III restriction fragments in a buffer containing 0.22% (w/w) M_n 105 000 HEC.

However, an investigation needs to be conducted into the importance of electroosmotic flow and the condition of the capillary walls on the success of DNA separations in uncoated capillaries in dilute HEC solutions. Note that at typical fields, with DNA injection at the anodic end of the capillary, electroosmotic mobility is *twice* the electrophoretic mobility of the DNA, and opposite in direction. This situation may be quite different from that of a DNA molecule moving through a stagnant solution. Work is proceeding in our laboratory now to reproduce these separations in a *coated* capillary with no electroosmotic flow.

It was clear from our experiments that the HEC length strongly affected the "window of DNA separation," that is, the size range of the restriction fragments which could be separated with good resolution. In general, the larger HEC molecular weights (M_n 105 000, 160 000, 306 000,

and 438 800 HEC) could well separate the larger ΦX174/*Hae*III fragments (1353, 1078, 872, and 603 bp) within a certain concentration range which was specific to each HEC molecular weight. Generally, above a certain minimum HEC concentration (unrelated to the entanglement threshold), the larger DNA fragments were better resolved at *low* HEC concentrations. The smaller HEC, on the other hand, did not resolve these larger DNA fragments well even at low concentrations, and could not resolve them at all above a certain HEC concentration. This is illustrated by the electropherogram in Fig. 9a, in which ΦX174/*Hae*III restriction fragments are separated in a buffer containing 0.95% (w/w) M_n 35 900 HEC. From these results we conclude that the mechanism of separation is related to the relative sizes of the DNA and HEC. We postulate that if the HEC molecules are too small, in their interactions with these larger DNA restriction fragments they are unable to form the firm entanglements that will significantly hinder DNA electrophoretic motion, and thus they are unable to introduce a size-dependence to the DNA molecular friction factor.

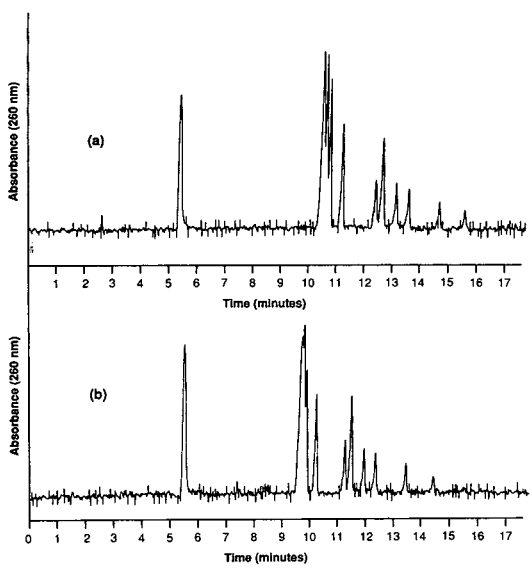

Fig. 9. Capillary electrophoresis of ΦX174/*Hae*III restriction fragments ranging in size from 72 to 1353 bp in (a) 0.95% (w/w) M_n 35 900 HEC, and (b) 1.35% (w/w) M_n 35 900 HEC, both in 89 m*M* Tris–89 m*M* boric acid–5 m*M* EDTA. Reading from left to right (not including the first peak, which is a neutral marker), the species are 1353, 1078, 872, 603, 310, 281 + 271, 234, 194, 118, and 72 bp in length, respectively. Conditions: field strength 221.4 V/cm; current (a) 8.8 μA, (b) 9.3 μA; UV detection at 260 nm; capillary dimensions, 50 cm total length (35 cm to detector) × 51 μm I.D.; temperature, 30 ± 0.1°C. R.S.D. of absolute electrophoretic mobilities: (a) 1.16%, $n = 5$; and (b) 0.93%, $n = 7$.

Considering the separation shown in Fig. 9a once again, we remark that this is still below the entanglement threshold for this polymer [1.25% (w/w)], and that the only fragments which are not resolved in this 11-fragment mixture are the 271/281 bp fragments. [We note that it is likely that with smaller sample volumes (*i.e.*, less than 3 nl) and a more sensitive method of detection, such as fluorescence, better resolution of these fragments could be achieved; however, we are interested only in the *relative* performance of our apparatus at different HEC concentrations, as it reflects on the mechanism of DNA separation.] If the concentration of this M_n 35 900 HEC is increased beyond the entanglement threshold the 271/281 bp fragments remain unresolved, and in fact resolution of the larger fragments declines, as shown in Fig. 9b with M_n 35 900 HEC at 1.35% (w/w). It is interesting that resolution of the larger DNA fragments is almost completely lost when the concentration of HEC is increased. If one was attempting to explain the results in terms of conventional gel electrophoresis models, one might expect, as the HEC network tightened, that the larger DNA fragments would enter the reptation regime, in which the electrophoretic mobility scales as $1/N$. If the larger DNA fragments began to reptate, resolution would *improve* as the HEC network tightened. Since this does not occur, we postulate that perhaps reptation cannot occur these dilute uncross-linked solutions, since there are no semi-rigid pores to force the DNA to take a tortuous path. Instead, once the solution reaches a high enough concentration to confine the motion of the larger DNA to an "effective tube," it moves immediately in the biased reptation regime, moving through the solution at a steady-state velocity independent of DNA length. This may be because confining the range of motion of the DNA makes it less probable that entanglement coupling with HEC can occur; yet since the tube "walls" are not semi-rigid like those of a gel, but are probably dilating on a time scale much shorter than the DNA residence time in this tube, neither is the DNA forced to follow a

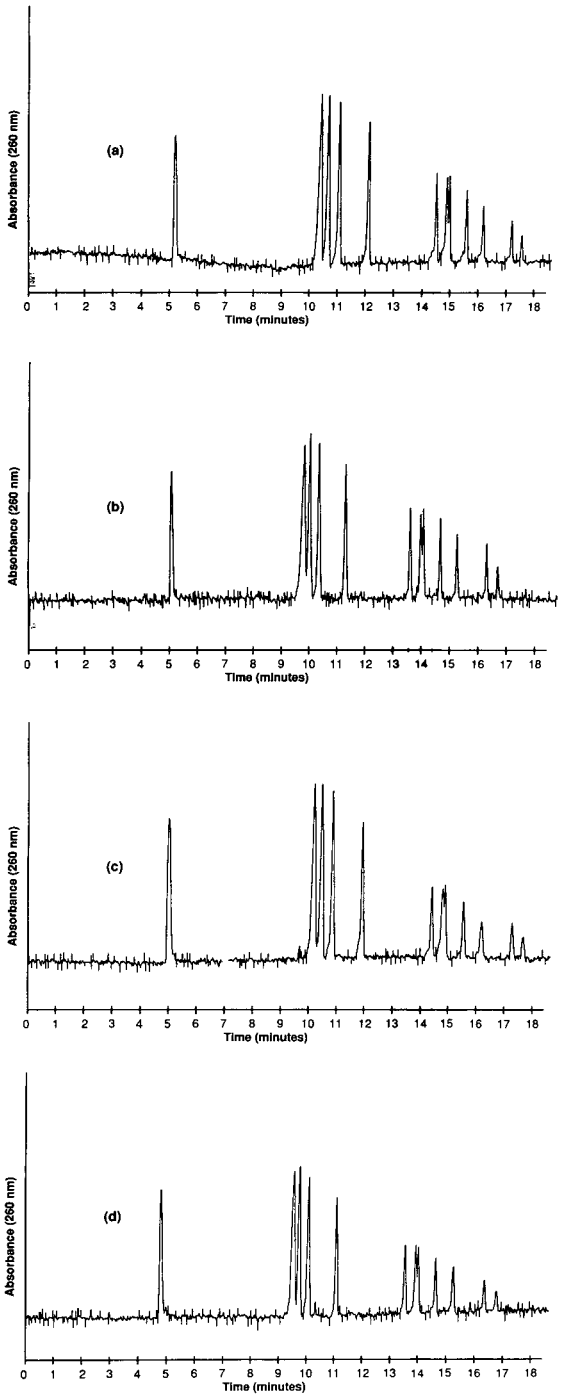

Fig. 10. Capillary electrophoresis of ΦX174/*Hae*III restriction fragments ranging in size from 72 to 1353 bp in (a) 0.225% (w/w) M_n 105 000 HEC, (b) 0.225% (w/w) M_n 160 000 HEC, (c) 0.22% (w/w) M_n 306 000 HEC, (d) 0.225% (w/w) M_n 438 800 HEC, all in 89 m*M* Tris–89 m*M* boric acid–5 m*M* EDTA. Reading from left to right (not including the first peak, which is a marker), the species are 1353, 1078, 872, 603, 310, 281, 271, 234, 194, 118, and 72 bp in length, respectively. Conditions: field strength 221.4 V/cm; current (a) 7.1 μA, (b) 7.1 μA, (c) 7.4 μA, (d) 7.3 μA; UV detection at 260 nm; capillary dimensions, 50 cm total length (35 cm to detector) × 51 μm I.D.; temperature, 30 ± 0.1°C. R.S.D. of absolute electrophoretic mobilities: (a) 0.30%, $n = 7$; (b) 0.24%, $n = 6$; (c) 0.23%, $n = 5$; and (d) 0.81%, $n = 7$.

tortuous path. We have not considered here concentrated HEC solutions [i.e., above 2% (w/w)]; it is possible that when HEC concentration is high enough, the network may become stiff and confining, allowing DNA reptation to occur as it is postulated to occur in rigid, cross-linked gels. While it is certain that a striking difference in structure and motion exists between a dilute, uncross-linked polymer solution and a semi-rigid cross-linked gel, there may be very little difference between an extremely concentrated, "syrupy" polymer solution and the aforementioned gel.

We note as well that Beebe-Poli and Schure [25] performed capillary electrophoresis in uncross-linked HEC, separating different lengths of poly(styrenesulfonate), a stiff, rod-like polymer which is negatively charged in proportion to its length, like DNA. These workers concluded after extensive analysis of their data that the mechanism of separation was neither Ogston-type sieving nor reptation, and that in fact conventional electrophoresis theories could not model their data.

We found that neither the M_n 27 000, M_n 35 900, nor the M_n 63 800 HEC was capable of separating the 271/281 bp fragments at *any* concentration above or below the entanglement threshold, even when the capillary was loaded with sample volumes less than 2 nl. However, an interesting finding is that the 271/281 bp fragments *can* be separated in uncross-linked HEC solutions, using the same larger HEC molecular weights that separate large restriction fragments well (M_n 105 000, M_n 160 000, M_n 306 000, and M_n 438 800 HEC). This is illustrated in Fig. 10a [0.225% (w/w) M_n 105 000 HEC], Fig. 10b [0.225% (w/w) M_n 160 000 HEC], Fig. 10c [0.22% (w/w) M_n 306 000 HEC], and Fig. 10d [0.225% (w/w) M_n 438 800 HEC]. Since we found that for these dilute solutions these two fragments could only be separated in a narrow

concentration range of HEC in the buffer [±0.05% (w/w)], it is striking that optimum resolution is at about 0.22% (w/w) for all four HEC molecular weights which can separate them.

The concept of the contour length between entanglements (L_e) can be used to attempt an explanation of this. Recall Ferry's assertion [11] that on average, $L_c = 2L_e$ at the entanglement threshold (eqn. 6). It is known that the dimensions of HEC in water are 0.519 nm per anhydroglucose unit [10]. Thus, $L_e(\Phi^*)$ can be determined for all seven HEC molecular weight fractions used in this study, and compared to the contour lengths of the restriction fragments of interest (Table II). Assuming 0.34 nm per base pair [14], DNA restriction fragments of 271 and 281 bp are 92.1 and 95.5 nm in length, respectively. Consider in particular the value of $L_e(\Phi^*)$ for M_n 160 000 HEC. For M_n 160 000 HEC, the entanglement threshold [0.21% (w/w)] is quite near the concentration of interest [0.22% (w/w)]. It can be seen in Table II that $L_e(\Phi^*)$ is equal to about 150 nm, somewhat longer than the 271/281 bp fragments. Slightly above the entanglement threshold, at $\Phi = 0.22\%$ (w/w), L_e(optimum) must be somewhat *less* than 150 nm, since $M_e \sim 1/\Phi$.

Based on this, we postulate that for electrophoretic separations in dilute HEC solutions L_e must be comparable and perhaps a bit larger than restriction fragment contour length in order to give fine resolution. Referring to Table II again, consider $L_e(\Phi^*)$ for M_n 105 000 HEC. Since for this polymer, $L_e(\Phi^*) \approx 100$ nm, shorter than the postulated L_e(optimum) of about 150 nm, M_n 105 000 HEC concentration must be *less* than Φ^* [0.37% (w/w)] for separation of the 271/281 bp fragments, as is the case for HEC smaller than M_n 105 000. Since for M_n 160 000, M_n 306 000, and M_n 438 800 HEC, L_e is too large to provide separation of 271/281 bp fragments at the entanglement threshold, these polymers must all be at a concentration *greater* than their entanglement thresholds in order to reach the optimum L_e; and the larger $L_e(\Phi^*)$ is, the further the solution must be past Φ^*.

We propose a tentative explanation for the finding. If L_e is a great deal shorter than the contour length of the DNA, then the probability that the DNA will form a strong entanglement with that loop in the HEC network is small, since this will not present a significant hindrance to the DNA motion. At the other extreme, if the HEC loop between two entanglement points is much larger than the contour length of the DNA, the smaller DNA molecule will have a high probability of passing through the loop easily without becoming entangled. Therefore, in order for strong entanglement interactions to occur between a DNA fragment and a given

TABLE II

THE MOLECULAR CONTOUR LENGTH BETWEEN ENTANGLEMENT POINTS AT $\Phi = \Phi^*$

M_n = Number-average molecular weight of HEC.
L_e = The contour length between entanglement points.

M_n	Φ^* (%, w/w)	$L_e(\Phi^*)$ (nm)
27 000	1.80	25.7
35 900	1.25	34.2
63 800	0.68	60.7
105 000	0.37	100.1
160 000	0.21	152.5
306 000	0.11	292.1
438 800	0.09	417.6

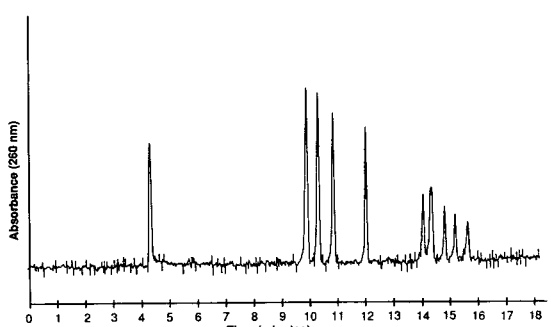

Fig. 11. Capillary electrophoresis of ΦX174/*Hae*III restriction fragments ranging in size from 72 to 1353 bp in 0.12% (w/w) M_n 438 800 HEC, 89 m*M* Tris–89 m*M* boric acid–5 m*M* EDTA. Reading from left to right (not including the first peak, which is a marker), the species are 1353, 1078, 872, 603, 310, 281 + 271, 234, 194, 118 + 72 bp in length, respectively. Conditions: field strength 221.4 V/cm; current 7.1 μA; UV detection at 260 nm; capillary dimensions, 50 cm total length (35 cm to detector) × 51 μm I.D.; temperature, 30 ± 0.1°C. R.S.D. of absolute electrophoretic mobilities: 0.54%, $n = 3$.

HEC loop formed between entanglement points, they must be of comparable length. And since HEC is more flexible than DNA in solution, perhaps the HEC must be a bit longer in order to present enough resistance to hang up the DNA.

Another finding of interest is that the largest HEC molecular weight, M_n 438 800, resolved the largest ΦX174/*Hae*III restriction fragments quite easily (Fig. 11), and *could* resolve still larger fragments. In fact, if larger HEC were used, perhaps DNA restriction fragments which are quite large (>20 000 bp) could be separated with uncross-linked cellulosic polymers. Work is proceeding in our laboratory to confirm this prediction.

CONCLUSIONS

We have shown that, theoretically, an entanglement coupling interaction between HEC molecules and DNA molecules during electrophoresis is capable of imparting a strong size-dependence to the electrophoretic mobility of the DNA by altering its frictional characteristics. We suggest, therefore, that this is the mechanisms by which DNA is separated in uncross-linked HEC solutions.

We have correlated the entanglement threshold of HEC molecules with number-average molecular weight, and shown that $\Phi^* \approx N^{-1.2}$, a scaling dependence which is not compatible with the predictions of either deGennes [19] or Bueche [16]. The reason for this incompatibility is probably related to the fact that HEC is stiff and extended in solution. As such, it exhibits the effects of entanglement coupling to a larger degree than the highly flexible, random coil-like polymers for which these theories were derived. We have presented a relationship which allows calculation of the observed entanglement threshold for any HEC sample in water, given that the number-average molecular weight is known or can be estimated.

We have demonstrated that a fully entangled network of uncross-linked HEC is not necessary for separation of DNA restriction fragments by electrophoresis (*i.e.*, the HEC solution can be significantly below its entanglement threshold). It is highly unlikely that the mechanism of separation in this case is the same as that applicable to the semi-rigid, porous network of a cross-linked gel.

Furthermore, we have shown that using uncross-linked HEC with a number-average molecular weight greater than 105 000, it is possible to separate restriction fragments that differ by only 10 base pairs. Our experiments show that for four different HEC molecular weights, the optimum concentration for separating these two restriction fragments is the same [0.22% (w/w) HEC], regardless of the length of the HEC. These findings support the assertion that beyond the entanglement threshold, the distance between entanglement points is independent of molecular weight and dependent only on concentration. We have used the concept of the average contour length between entanglements to infer that the optimum distance between HEC entanglements to separate a given mixture of restriction fragments is comparable to the average contour length of the DNA fragments in solution.

Based on this mechanism, there is no obvious limit to the size of the DNA which can be separated by this entanglement coupling between the DNA and uncross-linked polymers in solution.

ACKNOWLEDGEMENTS

We thank Maria Helen Kleemiss at the Max-Planck-Institut für Kohlenforschung for helpful discussions.

REFERENCES

1 M. Strege and A. Lagu, *Anal. Chem.*, 63 (1991) 1233.
2 H.E. Schwartz, K. Ulfelder, F.J. Sunzeri, M.P. Busch and R.G. Brownlee, *J. Chromatogr.*, 559 (1991) 267.
3 D.N. Heiger, A.S. Cohen and B.L. Karger, *J. Chromatogr.*, 516 (1990) 33.
4 P.D. Grossman and D.S. Soane, *Biopolymers*, 31 (1991) 1221.
5 A.M. Chin and J.C. Colburn, *Am. Biotech. Lab.*, 7 (1989) 16.
6 P. Bocek and A. Chrambach, *Electrophoresis*, 13 (1992) 31.

7 A. Chrambach and A. Aldroubi, *Electrophoresis*, 14 (1993) 18.
8 M. Chiari, M. Nesi, M. Fazio and P.G. Righetti, *Electrophoresis*, 13 (1992) 690.
9 H. Pulyaeva, D. Wheeler, M.M. Garner and A. Chrambach, *Electrophoresis*, 13 (1992) 608.
10 W. Brown, *Ark. Kemi*, 18 (1961) 227.
11 J.D. Ferry, *Viscoelastic Properties of Polymers*, Wiley, New York, 3rd ed., 1980.
12 P.R. Saunders, D.M. Stern, S.F. Kurath, C. Sakoonkim and J.D. Ferry, *J. Colloid Sci.*, 14 (1959) 222.
13 F. Bueche, *J. Polym. Sci.* 25 (1957) 243.
14 C.R. Cantor and P.R. Schimmel, *Biophysical Chemistry, Part III: The Behavior of Biological Macromolecules*, Freeman, New York, 1980.
15 A. Einstein, *Ann. Physik*, 17 (1905) 549.
16 F. Bueche, *Physical Properties of Polymers*, Wiley, New York, 1962.
17 T.G. Fox and S. Loshaek, *J. Appl. Phys.*, 26 (1955) 1080.
18 H.R. Allcock and F.W. Lampe, *Contemporary Polymer Chemistry*, Prentice-Hall, Englewood Cliffs, NJ, 1981.
19 P.G. deGennes, *Scaling Concepts in Polymer Physics*, Cornell University Press, Ithaca, NY, 1979.
20 J. Brandrup and E.H. Immergut, *Polymer Handbook*, Wiley, Ithaca, 1989.
21 J.D. Ferry, *Viscoelastic Properties of Polymers*, Wiley, New York, 1st ed., 1961.
22 P.R. Sperry, *J. Colloid Interface Sci.*, 87 (1982) 375.
23 P.D. Grossman, J.C. Colburn and H.H. Lauer, *Anal. Biochem.*, 179 (1989) 28.
24 F. Rodriguez, *Principles of Polymer Systems*, Hemisphere Publishing, New York, 1989.
25 J. Beebe-Poli and M.R. Schure, *Anal. Chem.*, 64 (1992) 896.

Journal of Chromatography A, 652 (1993) 17–22
Elsevier Science Publishers B.V., Amsterdam

CHROM. 25 201

Review

Polymeric separation media for electrophoresis: cross-linked systems or entangled solutions

Young C. Bae* and David Soane

Soane Technologies, Inc., Hayward, CA 94545 (USA)

ABSTRACT

The current status of separation media development for capillary electrophoresis is reviewed in light of well-known electrophoretic migration and entangled polymer solution theories. The relative strengths and weaknesses of crosslinked systems and entangled solutions are also examined. The residence time limit of DNA in a mesh is estimated and compared with the relaxation time of both a typical entangled polymer solution and a cross-linked gel. By advancing the concept of analyte residence time and life time of a characteristic network mesh, we can highlight the differences between the operative mechanism governing separation in these two types of electrophoresis media.

CONTENTS

1. INTRODUCTION

Capillary electrophoresis (CE) has found widespread applications in analytical and biomedical research. The scope and sophistication of CE are rapidly increasing. CE can perform analytical separations that are often substantially better than those using established chromatographic methods such as high-performance liquid chromatography (HPLC). Conventional electrophoretic methods are slow, labor-intensive, prone to relatively poor reproducibility and have limited quantitative capability. Furthermore, it has been difficult to fully automate the process. This situation has been greatly improved by the advent of CE. The major advantages of CE are that it can be fully automated, it offers high resolution, and it can quantitate minute amounts of samples [1]. These capabilities lie far beyond those of traditional electrophoretic methods.

CE has recently been used in the analysis of an extremely wide variety of molecules, including organic and inorganic anions and cations, drugs,

* Corresponding author.

0021-9673/93/$24.00

dyes and their precursors, vitamins, carbohydrates, catecholamines, amino acids, proteins and peptides, nucleic acids, nucleotides, and oligonucleotides. Among standard separation methodologies, CE is the best known for its ability to separate a wide range of molecular weights. It is possible to separate in the same column species ranging in size from free amino acids to large proteins associated with complex molecular matrices. From the detection point of view, HPLC provides better concentration sensitivity while CE provides better mass sensitivity. However, initial attempts to resolve complex mixtures of biological macromolecules in open CE columns were disappointing. Proteins present a serious problem when using untreated fused-silica capillaries due to their adsorption onto the walls of the capillary. With oligonucleotides, the unfavorable charge-to-mass ratio tends to cause comigration of larger mixture components.

A highly innovation solution to overcome these difficulties was the development of gel-filled capillaries [2–8]. Remarkably high separation efficiencies have been obtained by gel-filled CE. To accomplish size selection in electrophoretic separation of mixtures of nucleic acids and sodium dodecyl sulfate denatured proteins, a cross-linked gel matrix is employed. However, the routine preparation of homogeneous stress-free gels in capillaries is difficult due to polymerization-induced shrinkage and appearance of bubbles inside the capillaries.

As an alternative to cross-linked gels, solutions of entangled polymer, such as polyethylene glycol, linear non-cross-linked polyacrylamides or (hydroxyethyl)cellulose (HEC) have been tested as macromolecular sieving media [9–14]. This approach provides ease of filling and flushing of the separation capillary after each analysis, thus avoiding the possible contamination of analyte from the previous run. However, entangled polymer solutions in the capillaries exhibit lower resolution than cross-linked gels.

The resolving power of CE using entangled polymer solution as the separation media is not good for large analyte molecules, presumably as a result of the relevant time scales of the sieving polymers and analyte molecules. The residence time (or passage time) of an analyte molecule in a mesh is controlled by the size and electrophoretic mobility of the analyte, mesh size of the network, and the imposed electric field strength. The life time of an entanglement is dictated by the mobility of strands forming the mesh, the network integrity, and the length and concentration of macromolecules constituting the network. In order to achieve good resolution, the relaxation time of the entangled polymer solution should be orders of magnitude greater than the residence time of the analyte molecules. Otherwise, an entirely different mechanism must be occurring to make separation of mixtures possible. These time-scale considerations are the focus of this paper.

2. BACKGROUND AND THEORY

2.1. Electrophoretic migration theory

There are two well-known theories for the migration of a flexible macromolecule through a polymer network: The Ogston model and the reptation model. Here, we briefly summarize these two models.

The Ogston model is schematically illustrated in Fig. 1. It assumes that the matrix consists of a random network of interconnected pores having an average pore size ξ. The migrating solute behaves as an undeformable particle of radius R_g. In this model, smaller molecules migrate faster because they have access to a larger fraction of the available pores, giving the following expressions [9,10,15]

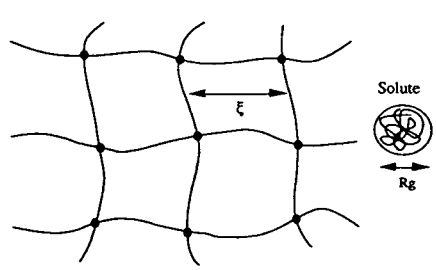

Fig. 1. Schematic of a solute migrating through a polymer network by the Ogston mechanism.

$$\mu = \mu_0 \exp[-Cb(R_g + r)^2] \quad (1)$$

or

$$\mu = \mu_0 \exp\left[-\frac{1}{4}\pi\left(\frac{R_g + r}{\xi}\right)^2\right] \quad (2)$$

where μ is the electrophoretic mobility of the analyte in the matrix, μ_0 is its free solution electrophoretic mobility, C is the concentration of polymer network, b is a constant and r is the thickness of the strand. This model, however, does not take into account for the electric field (E) effects on R_g. Therefore, eqns. 1 and 2 hold only in the limit of $E \rightarrow 0$. The Ogston model reduces to the celebrated Ferguson plot for $R_g \gg r$, where a plot of log (μ/μ_0) *vs.* C gives a straight line with a slope proportional to R_g^2.

The Ogston model assumes the migrating solute to be an undeformable spherical particle moving through a mesh network. Therefore, when $R_g > \xi$, this model ceases to be applicable. It is well known that a long and flexible chain molecules such as DNA can migrate even when $R_g \gg \xi$. This can be explained by the reptation model which assumes that the migrating solute moves as an unraveled coil from head to tail.

Assuming that one linear chain is moving in a given network, as shown in Fig. 2 [16]. The network is described by fixed obstacles O_1, O_2, etc. The chain is not allowed to penetrate any of these obstacles, but it can travel between them in a snakelike fashion. This motion is called "reptation". To understand the effect of the obstacles on the electrophoretic mobility, it is convenient to consider the chain to be contained within a certain imaginary tube [17]. In a unit time, parts of the tube are lost on the tail end while new parts of the tube are created on the headside. Lerman and Frisch [18] first introduced the reptation concept to the electrophoresis of biopolymers. In the limit of zero electric field strength,

$$\mu \approx \frac{1}{N} \quad (3)$$

where N is the number of repeat units of the analyte. Eqn. 3 suggests that the electrophoretic mobility μ is inversely proportional to the analyte molecular mass at low electric fields.

A modified reptation model that extends to strong electric fields is the biased reptation model. Under the influence of strong electric fields, the solute becomes more elongated. In the limit, the solute acquires a rod shape. This is schematically illustrated in Fig. 3. In the limiting of the biased reptation model, the electrophoretic mobility is no longer dependent on molecular size. Lumpkin expressed this effect by [23]

$$\mu \approx K\left(\frac{1}{N} + bE^2\right) \quad (4)$$

where K is constant and b is function of ξ, charge and persistence length of the migrating solute. As we can see from eqn. 4, the dependence of mobility on molecular size decreases when the electrical field or the molecular size increases. This is why DNA can be separated by using conventional electrophoretic technique at low fields up to approximately 20 000 base pairs [9].

2.2. Entangled polymer solution theory

To understand entangled polymer solutions, we need to introduce a simple scaling law by De Gennes [16]. Three regimes of polymer solutions can be imagined: (1) dilute solutions, (2) semi-

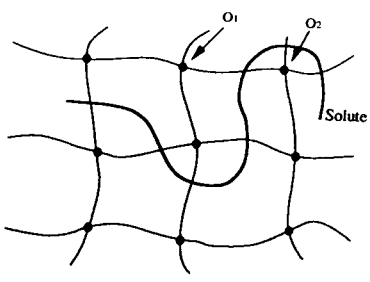

Fig. 2. Schematic of a solute migrating through a polymer network by the reptation mechanism.

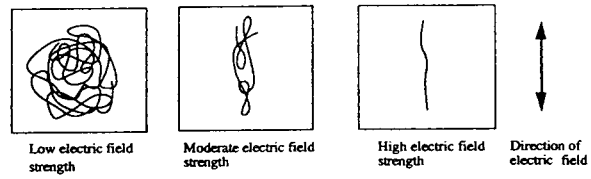

Fig. 3. Schematic of the elongation effect of the electric field on a migrating molecule.

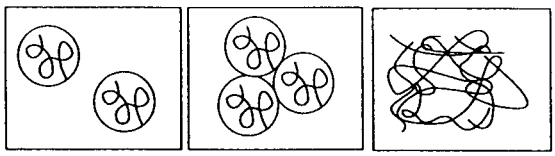

Fig. 4. Crossover between dilute and semi-dilute solutions: (a) dilute, (b) overlap, (c) semi-dilute.

dilute solutions and (3) concentrated solutions. Only dilute and semi-dilute solutions are important for separation. Transition from the dilute to the semi-dilute regime occurs at the overlap threshold. The overlap threshold where the polymer chains begin to be densely packed. This threshold is not sharp; it is more properly defined as a region of crossover between regimes (a) and (c) in Fig. 4. At the overlap threshold concentration, Φ^*, the bulk solution concentration is equal to the local concentration inside a single polymer chain. In an athermal solvent, this implies

$$\Phi^* \approx N_p^{-0.8} \tag{5}$$

where N_p is the number of segments in the polymer chain. Note that for large N_p, Φ^* is very small.

Now we discuss the concept of correlation length or mesh size (ξ), which characterizes an entangled polymer solution. This is illustrated in Fig. 5. The scaling law of ξ in the semi-dilute regime for an athermal solvent has been derived with the following assumptions: (i) For $\Phi > \Phi^*\xi$ depends only on concentration and not on the degree of polymerization N_p; (ii) for $\Phi \approx \Phi^*$ where the polymer chains are in contact but not yet interpenetrating ξ must be comparable with the size of a polymer chain R_g.

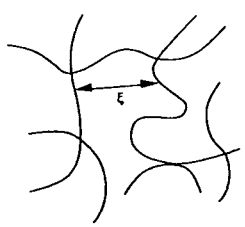

Fig. 5. Schematic of a characteristic mesh with size ξ.

The rescaling relation between ξ and Φ in an athermal solvent obeys the following form

$$\xi(\Phi) \approx a\Phi^{-0.75} \tag{6}$$

where a is a scaling constant. Eqn. 6 shows that ξ decreases rapidly with concentration.

Grossman and Soane [9,10] proposed the optimum conditions for CE using entangled polymer solutions to correspond to the lowest possible viscosity which maintains an entangled network, *i.e.* $\Phi \approx \Phi^*$. For such condition, combining eqns. 5 and 6 give

$$\xi(\Phi^*) \approx a\Phi^{0.6} \tag{7}$$

Eqn. 7 shows that in order to create a large ξ while minimizing the viscosity of the solution, one should choose a high-molecular-mass polymer. No consideration, however, was given to the integrity or longevity of the entangled network at the threshold condition. This aspect of the problem is now a subject of study.

3. DISCUSSION

We now closely scrutinize an entangled polymer solution mesh in contrast with a cross-linked gel mesh. This is illustrated schematically in Fig. 6. As we previously discussed, the entangled mesh is a spatial property, being temporally transient and not a permanent state. A given entangled mesh persists at best up to the relaxation time of the polymer chains constituting the mesh. The residence time of analyte molecule in this mesh is controlled by the size and electrophoretic mobility of the analyte, the mesh size of the network, and the imposed electric field strength. According to either the Ogston model

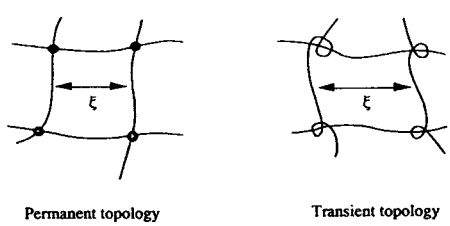

Fig. 6. Comparison of permanent network and transient network, corresponding to a cross-linked gel and a polymer solution.

or the reptation mechanism, in order to achieve good resolution, the relaxation time of the entangled polymer solution should be orders of magnitude greater than the residence time of the analyte molecules. In this manner, the mesh is maintained during transit of the analyte, so the matrix serves as an effective sieving medium.

It is well known that the relaxation times of polymer solutions and cross-linked gels can be measured by dynamic light scattering. A photon correlation function obtained by dynamic light scattering generates the underlying relaxation time spectrum. Such a spectrum often consists of slow and fast, and sometimes intermediate modes, indicative of different types of motion. We assume the mesh integrity is governed by the longest relaxation time, *i.e.*, the slow mode. In the ensuing comparison, the longest relaxation time is taken as the life time of the mesh. A typical DNA molecule is chosen as the model analyte. Specifically, the suitability of the gel and the solution networks as potential separation media for sequencing applications is investigated. The residence time of DNA can be estimated from the literature [9,10,19] by assuming two extremes (Ogston and biased reptation). In these two extremes, the residence time, τ_{res},

$$\left(\frac{\text{mesh size}}{\text{electrophoretic velocity}}\right)_{\text{Ogston}} < \tau_{res} < \left(\frac{\text{DNA contour length}}{\text{electrophoretic velocity}}\right)_{\text{biased reptation}} \quad (8)$$

where subscript Ogston means that the migrating solute is approximated as an undeformable particle (Ogston model). For biased reptation under the influence of large electric fields, the solute becomes more elongated, and the motion mimics that of a snake threading its way through the network. In the biased reptation mode, DNA moves by repeated stretching, slippage, relaxation and re-extension. The transient polymer network is momentarily under stress when interacting with the passing analyte. This is schematically illustrated in Fig. 7. Therefore, the correct time scale is estimated by employing the DNA contour length in the numerator of eqn. 8.

One can obviously question the driving force behind mesh destruction during electrophoresis.

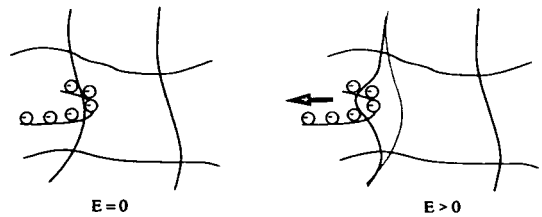

Fig. 7. Schematic of the transient interaction of a DNA molecule with one of the strands constituting and entangled mesh. Note the forces acting on the strand, causing dissociation of the mesh.

We propose at least two mechanisms. The first is the locally elevated osmotic pressure resulting from the increased local concentration of macromolecules during analyte passage. The second is the transient tethering the stretching action of the network strand as depicted in Fig. 7. Regardless of the origin of network disengagement around the mesh, it is the aforementioned two relevant time scales that govern the performance of the separation media.

The relaxation times of entangled polyacrylamide solution and cross-linked polyacrylamide gel are reported as following [20]:

$$\tau = 5.9 \cdot 10^{-4}\ \text{s}\ (T = 3\%,\ 25°C),\ \text{for entangled solutions}$$
$$\tau = 4.0 \cdot 10^{-3}\ \text{s}\ (T = 3\%,\ 25°C),\ \text{for cross-linked gel} \quad (9)$$

[T = (g acrylamide + g N,N′-methylenebisacrylamide)/(g acrylamide + g N,N′-methylenebisacrylamide + g H_2O)]. The calculated residence time limits of DNA are as follows [7,19]: For the two migrating extremes

Experimental results for 30 base pairs:

$$1.5 \cdot 10^{-5}\text{–}1.8 \cdot 10^{-4}\ \text{s}$$

Experimental results for 100 base pairs:

$$1.5 \cdot 10^{-5}\text{–}8.2 \cdot 10^{-4}\ \text{s} \quad (10)$$

The calculated residence times of 100 base pairs are extrapolated from 30-base pair data based on a hydrodynamic diameter per base pair of 3.3 Å

[21,22]. The results show clearly that the relaxation time of the entangled polymer and residence time of DNA are very close. Therefore, sharp resolution cannot be expected for the high molecular mass of DNA (*e.g.* beyond 100 base pairs) using entangled polymers. The network imposing the sieving medium fails before the analyte moves through a mesh completely. This problem does not exist for chemically cross-linked systems.

As a final note, we point out other possibilities for different electrophoretic mobilities for analytes of varying sizes, even below the critical overlap threshold. An example is the momentary interaction of the analyte with the surrounding matrix molecules as it streams by the former. The longer the analyte, the higher probability for this type of interaction, with consequential retardation of mobility. It is yet unclear whether this type of interaction is sufficient for DNA sequencing applications.

4. CONCLUSIONS

We have reviewed the current status of CE and the basic theories related to the two key types of sieving media. We also have contrasted the relative strengths and weaknesses of cross-linked and entangled systems as sieving media by advancing the concepts of analyte residence time and life time of a characteristic network mesh. Our calculations show that it would be difficult to achieve high resolution for high molecular masses of DNA using entangled polymer solutions that are neither concentrated nor extremely viscous as the sieving media. We are in the process of developing novel polymer systems that possess low viscosity during fill but retain a high resolving power during analysis. Experimental results of such work will be reported in further publications.

REFERENCES

1 N.A. Guzman, L. Hernandez and S. Terabe, in Cs. Horváth and J.G. Nikelly (Editors), *Analytical Biotechnology (ACS Symposium Series*, No. 434), American Chemical Society, Washington, DC, 1990, Ch. 1.
2 S. Hjertén, *J. Chromatogr.*, 270 (1983) 1.
3 A.S. Cohen, D. Najarian, J.A. Smith and B.L. Karger, *J. Chromatogr.*, 458 (1988) 323.
4 A. Guttman, A.S. Cohen, D.N. Heiger and B.L. Karger, *Anal. Chem.*, 62 (1990) 137.
5 A. Paulus, E. Gassmann and M.J. Field, *Electrophoresis*, 11 (1990) 702.
6 A. Paulus and J.I. Ohms, *J. Chromatogr.*, 507 (1990) 113.
7 H.F. Yin, J. Lux and G.J. Schomburg, *J. High Resolut. Chromatogr.*, 13 (1990) 624.
8 H. Swerdlow, J.Z. Zhang, D.Y. Chen, H.R. Harke, R. Grey, S. Wu and N. Dovichi, *Anal. Chem.*, 63 (1991) 2835.
9 P.D. Grossman and D.S. Soane, *Biopolymers*, 31 (1991) 1221.
10 P.D. Grossman and D.S. Soane, *J. Chromatogr.*, 559 (1991) 257.
11 M.J. Bode, *FEBS Lett.*, 65 (1991) 56.
12 M. Zhu, D.L. Hansen, S. Burd and F. Gannon, *J. Chromatogr.*, 480 (1989) 311.
13 A.M. Chin and J.C. Colburn, *Am. Biotech. Lab.*, 7 (1989) 16.
14 D. Tietz, M.M. Gottlieb, J.S. Fawcett and A. Chrambach, *Electrophoresis*, 7 (1986) 217.
15 A.G. Ogston, *Trans. Faraday Soc.*, 54 (1958) 1754.
16 P.G. de Gennes, *Scaling Concepts in Polymer Physics*, Cornell Univ. Press, Ithaca, NY, 1979.
17 M. Doi and S.F. Edwards, *J. Chem. Soc., Faraday Trans. II*, 79 (1978) 1789.
18 L.S. Lerman and H.L. Frisch, *Biopolymers*, 21 (1982) 995.
19 J. Sudor, F. Foret and P. Boček, *Electrophoresis*, 12 (1991) 1056.
20 T. Hino, *MS Thesis*, University of California, Berkeley, CA, 1991.
21 K.S. Schmitz, *An Introduction to Dynamic Light Scattering by Macromolecules*, Academic Press, New York, 1990.
22 V.A. Broomfield, in R. Pecora (Editor), *Dynamic Light Scattering*. Plenum Press, New York, 1985, Ch. 10.
23 O.J. Lumpkin, P. Dejardin and B.H. Zimm, *Biopolymers*, 24 (1985) 1573.

Journal of Chromatography A, 652 (1993) 23–30
Elsevier Science Publishers B.V., Amsterdam

CHROM. 25 138

Simultaneous determination of the migration coefficient of each base in heterogeneous oligo-DNA by gel filled capillary electrophoresis

Takashi Satow* and Tadao Akiyama

Beckman Instruments (Japan) Ltd., 6, Sanbancho, Chiyoda-ku, Tokyo 102 (Japan)

Akiko Machida

11-11, 5-Chome, Nijoh, Kitagou, Shiraishi-ku, Sapporo 003 (Japan)

Yushi Utagawa and Hidesaburo Kobayashi

Faculty of Science, Josai University, Keyakidai, Sakado-shi, Saitama-ken 350-02 (Japan)

ABSTRACT

The direct determination of migration coefficients was achieved by analysing the migration time of heterogeneous oligo-DNA with a gel filled capillary using the Gauss least-squares method for the observation functions, assuming that the migration time of oligo-DNA is dependent on its base composition and chain length. By using the coefficients obtained, the migration time of oligo-DNA of any known sequence that does not have a secondary structure can be estimated with an accuracy of less than 0.5-mer of cytidine. In addition, from the deviation of the actual migration time from the calculated migration time in certain specially designed base sequences, the existence of a secondary structure such as a hairpin structure was strongly suggested even in the presence of 7 *M* urea. From the investigation of the effects of secondary structure on migration time, it was concluded that this approach will give qualitative information on secondary structure, which may be applicable in work such as single strand conformational polymorphism (SSCP) analysis or antisense DNA analysis, in which secondary structure plays an important role in accelerating or decelerating migration times. The results of the analysis also predict the apparent chain length reversal from short to long together with a reduction in the actual chain length in DNA sequencing using capillary electrophoresis.

INTRODUCTION

Since capillary electorphoresis (CE) was first successfully achieved by Jorgenson and Lukacs [1], many different separation modes, such as micellar electrokinetic capillary chromatography (MECC) [2] have been developed not only for small compounds but also for biological macromolecules, as reviewed by Kuhr [3] and by Kuhr and Monnig [4]. One of the most useful separation modes is capillary gel electrophoresis (CGE) originally developed by Karger's group for protein [5] and DNA [6] separations. Especially for DNA separations, the performance of CGE has been continuously improved through improvements of the gel matrices and experimental conditions. Recently a few groups have achieved as high as $1 \cdot 10^7$–$3 \cdot 10^7$ theoretical plates [7–9] by using homogeneous oligo-DNA as the sample.

On the other hand, only a limited number of studies have been carried out using heterogeneous oligo-DNA samples to describe the migra-

* Corresponding author.

0021-9673/93/$06.00

tion behaviour of the sample components in the gel [10,11]. As the conclusion was that the oligo-DNA was not separated by chain length alone [10], and as the migration time slightly changed in each run, we have developed a novel means of determining the migration coefficient for each base in a single run by using several heterogeneous oligo-DNAs as standards followed by statistical analysis with the Gauss least-squares method for observation functions [12].

EXPERIMENTAL

CE instrument

For CE analysis, a Beckman (Fullerton, CA, USA) P/ACE System 2100 was used with Beckman Gold Workstation software on an IBM personal computer to operate the P/ACE instrument and to analyse the data. Some of the data were saved in the ASCII format on an IBM computer and transferred to an Apple Macintosh computer for further analysis with Microsoft Excel. For electrophoresis the polarity was reversed (cathode on the injection side and anode on the detector side).

The gel-filled capillary employed was eCAP gel U100P (Beckman) of 37 cm total length and 100 μm I.D. containing polyacrylamide gel in 7 *M* urea. Monitoring was effected with an on-column UV detector at 254 nm.

Oligo-DNA

Standard heterogeneous oligo-DNAs were a gift from Takara (Kyoto, Japan). Other oligo-DNAs including specially designed sequences for the analysis of the secondary structure effects were synthesized with a Milligen DNA synthesizer (Cyclone Plus DNA Synthesizer; Millipore, Bedford, MA, USA). The base sequences of the heterogenous oligo-DNAs are summarized in Table I and Fig. 3.

Procedure

In most instances, the sample concentration was adjusted to 0.01–0.005 absorbance units at 260 nm with water. For each injection we used 40–60 μl of sample solution in a modified polyethylene micro vial. Samples were injected electrokinetically at 5 kV for 2 S. Electrophoresis was performed at 300 V/cm, the capillary being kept at 30°C during the experiments by using the liquid cooling system of the P/ACE instrument.

Statistical analysis (Gauss least-squares method for observation functions)

Pilot experiments with heterogeneous oligo-DNA showed that the separation was not based on the chain length alone. We therefore assumed that the migration time is described as follows, assuming that the migration time of heterogeneous oligo-DNA is probably a function of the chain length and the base composition:

$$[A]a + [G]g + [T]t + [C]c + k = M \quad (1)$$

where [A], [G], [T] and [C] are the numbers of each base in the chain, a, g, t and c are the migration coefficients (in minutes per number of bases), k is a constant or the time required for oligo-DNA of zero length to move to the detector (in minutes) and M is the migration time in minutes obtained from an electropherogram.

It is possible to determine the parameters of the above function by using five heterogeneous oligo-DNAs of different base compositions by constructing simultaneous functions if there is no experimental error. However, in reality, all the experimentally obtained values include some degree of error. To minimize the effects of experimental errors, the statistical analysis of migration times was done basically following the Gauss least-squares method for observation functions [12], which is popular in experimental physics for calculating the coefficients of function(s).

We modified eqn. 1 into the following forms to remove the effects of observation errors and to obtain five different functions for the calculation of the parameters (coefficients):

$$[AA]a + [AG]g + [AT]t + [AC]c + [A]k = [AM]$$

$$[AG]a + [GG]g + [GT]t + [CG]c + [G]k = [GM]$$

$$[AT]a + [GT]g + [TT]t + [CT]c + [T]k = [MT]$$

$$[AC]a + [CG]g + [CT]t + [CC]c + [C]k = [CM]$$

$$[A]a + [G]g + [T]t + [C]c + [K]k = [M] \quad (2)$$

where K is the number of the constant (=1), $[AA] = \Sigma_i A_i A_i$, $[AT] = \Sigma_i A_i T_i$ and $[A] = \Sigma_i A_i$.

By solving the simultaneous eqns. 2, we can determine the migration coefficients (a, g, t and c) for A, G, T and C. The actual calculation was time consuming as we had to repeat a large number of simple calculations. We therefore developed a template on Microsoft Excel with a Macintosh computer to obtain the normal equations and to solve the simultaneous equations simply by inputting the base compositions and migration times of standard heterogeneous oligo-DNAs actually measured in a single experiment. This template also gives the estimated migration time of any known sequence. A limited number of templates for Microsoft Excel on Macintosh are available on request from the authors for research purposes only.

RESULTS AND DISCUSSION

Analysis of standard sample

CGE is a high-resolution technique and shows its resolving power particularly when using oligo-DNAs as the sample. For example, a few groups have achieved more than 10^7 theoretical plates/m [7–9]. In most work to improve the resolution of the gel-filled capillary, homogeneous oligo-DNAs were used as the sample, and showed a very linear relationship between chain length and migration time, which gives equal time differences between the peak of an n-mer and the $(n + 1)$-mer. Unlike homogeneous oligo-DNA, however, no linear calibration graph is obtained when using heterogeneous oligo-DNAs. A typical electorpherogram obtained with a heterogeneous oligo-DNA standard is shown in Fig. 1 and the base sequences are summarized in Table I. The peak assignment was done by varying the concentration of each oligo-DNA.

As can be seen in Fig. 1, the fact that the migration time differences between the 20–21-mers, 29–30-mers, 30–31-mers, 40–41-mers and 50–51-mers were different strongly suggested an effect of base composition on the migration time, as was reported by Guttman *et al.* [10]. Rapid heat treatment to eliminate the possibility of complex formation through hydrogen bonding had no significant effect on the separation.

Repetitive injection caused a slight change in

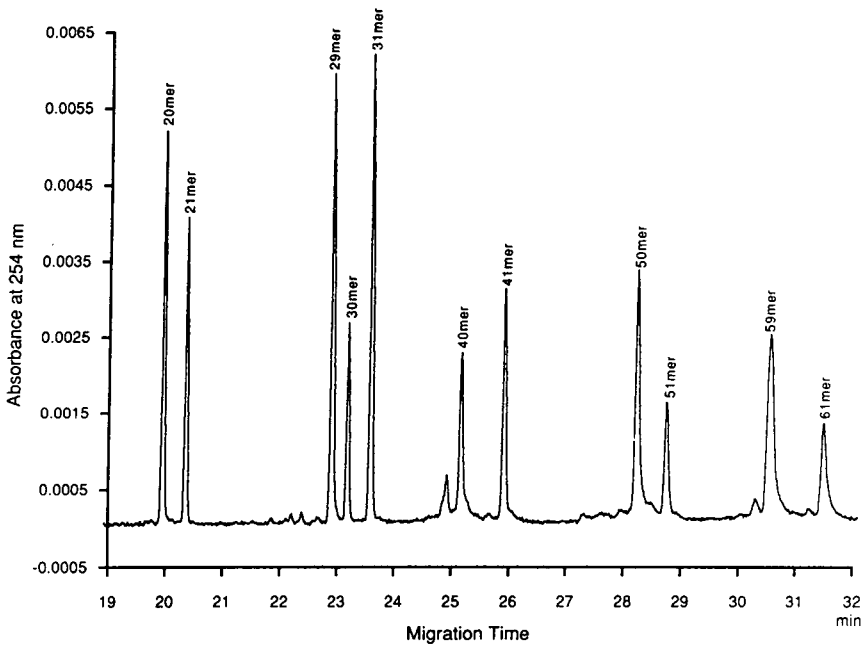

Fig. 1. Separation of heterogeneous oligo-DNA standards. The actual sequences of oligo-DNAs and CE separation conditions are summarized in Table I and under Experimental, respectively.

TABLE I

HETEROGENEOUS OLIGO-DNA STANDARD USED IN THE EXPERIMENTS

For experimental conditions, see Experimental.

Oligomer	Sequence
20-mer	5'-AAGAAAGCAGCAACTGCATT-3'
21-mer	5'-AGTACGTGCCAGTGCCAGCGT-3'
29-mer	5'-ATTACAGTTCATCGTGCACAGCTTTCTGA-3'
30-mer	5'-AGTTCATCGTGCTCAAATTTCTGATCATCG-3'
31-mer	5'-GATCCGTTTCAGGTCTGATTGAAAGCGGTAC-3'
40-mer	5'-AGAGCATCAGATCACCTGGGACCCCATCGATGGACGCGTT-3'
41-mer	5'-ATCCTGGGATTAAATAAAATAGTAAGAATGTATAGCCCTAC-3'
50-mer	5'-CCTCCGGAAGTGGACGTTGACGACGAGCCAGAAGAAGAATAAGGATCCGG-3'
51-mer	5'-TATTTATGGAGTTCAGACACTCAGCACAGCAGGGTCCTGAGCTTATATAAT-3'
59-mer	5'-CGGATGAGCTAAGGGATGAGGATGAGAGCAAGAGCAAAAGAAGGAGCAACAACTTCATC-3'
61-mer	5'-TCGAGATGAAGTTGTTGCTCCTTCTTTTGCTCTTGCTCTCATCCTCATCCCTTAGCTCATC-3'

migration time, as shown in Fig. 2, which makes it critical to use an internal migration standard such as Orange G, as Guttman *et al.* used [10] to compensate for the results obtained in different runs or to determine the migration coefficients in each run based on multiple oligo-DNA markers in a sample mixture. We used the latter method to describe the migration properties of the heterogeneous oligo-DNA by expanding the Gauss least-squares method for observation functions, which can give information on the exact separation in a run.

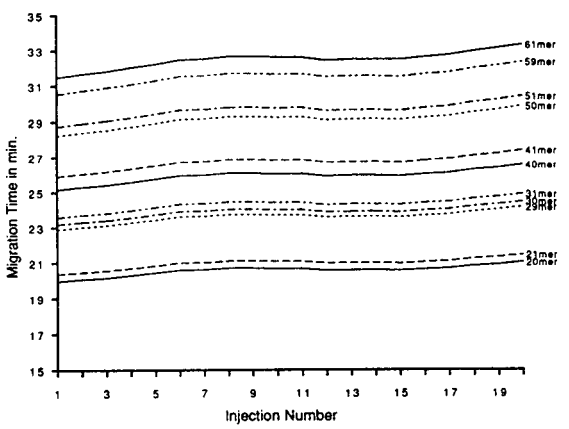

Fig. 2. Migration time shift during the first twenty successive injections. A newly prepared eCAP gel U100P capillary was subjected to the continuous separation of the heterogeneous oligo-DNA standard. The sample was freshly prepared every three injections as the peak height decreased to less than one third of that for the first injection owing to the inherent nature of electrokinetic injection. The electrolytes in 4-ml anodic and cathodic vials were changed every five injections. Other experimental conditions are summarized under Experimental. After 100 injections, no serious decrease in resolution was observed.

The results for the migration coefficient of each base analysed by this method are given in Table II. The calculated migration coefficients (a, g, t and c) varied with the bases, but in more than 20 successive runs they consistently showed that $t > g > a > c$ immigration coefficients and C > A > G > T in migration speed within the range of relative standard deviations 1.8% (G)–2.5% (T). Guttman *et al.* [10] observed a relative migration order of A > C > G > T, which is slightly different from our results. The reason for this is not clear, but the difference in oligo-DNA type and length may be critical as Guttman *et al.* mainly used homogeneous oligo-DNAs of 12–18-mers whereas we used heterogeneous 20–61-mers.

Attempts at averaging or normalization were made to improve the accuracy of the analysis, but no significant improvement in the probable error was achieved, as is shown in the last two rows of Table II.

The calculated migration time based on the migration coefficients agreed well with the actual migration times, as is shown in Table III, although some of the sequences gave a 0.16 min maximum difference after nearly 30 min of migration (even in this instance the deviation was as small as 0.5%). The reason for the variation

TABLE II

MIGRATION COEFFICIENTS FOR TWENTY SUCCESSIVE RUNS

a, *g*, *t* and *c* are migration coefficients for A, G, T and C, respectively, and *k* is a constant determined in each run or after averaging or normalization. The average migration coefficients ("Average") were calculated by averaging the migration times of each peak obtained by twenty successive runs, before Gauss least-squares analysis of observation functions. For the "Normalized" values, the migration times of each peak in twenty successive runs were corrected by assuming the migration time of the 61-mer to be 32 min before the analysis. The experimental conditions are summarized under Experimental.

Expt. No.	*a*	*g*	*t*	*c*	*k*	ΔM [a]	Δ/C [b]
1st	0.229	0.331	0.348	0.162	14.889	0.077	0.475
6th	0.238	0.343	0.360	0.166	15.345	0.079	0.476
11th	0.240	0.345	0.362	0.168	15.803	0.079	0.470
16th	0.240	0.345	0.363	0.169	15.353	0.076	0.450
20th	0.246	0.345	0.372	0.173	15.618	0.079	0.457
Average	0.238	0.343	0.361	0.168	15.309	0.078	0.464
Normalized	0.234	0.338	0.355	0.165	15.078	0.076	0.461

[a] ΔM = probable error of the migration time in minutes.
[b] Δ/C = probable error as the number of C.

remains unclear. Although in the set of experiments shown in Table III we used eleven heterogeneous oligo-DNAs as markers, as few as six markers gave equally good results.

We applied this technique to synthesized heterogeneous oligo-DNAs to examine the migration times, and found out that the calculated results agreed well with actual migration time in most instances. By using the migration coefficients obtained, we can easily predict that oligo-dC_{40}, for example, may migrate faster than oligo-dT_{20} as the expected migration times are 21.68 and 22.18 min, respectively.

Effects of secondary structure on migration time

One of the interesting applications of this approach is the determination of the migration

TABLE III

COMPARISON OF ACTUAL AND CALCULATED MIGRATION TIMES

A, G, T and C represent the numbers of dA, dG, dT and dC in each DNA fragment; t_M is the actual migration time and t_M (calc.) is the calculated migration time based on the Gauss least-squares method. Δ is the difference between the actual and calculated migration times.

Oligomer	A	G	T	C	t_M (min)	t_M (calc.) (min)	Δ (min)
20-mer	9	4	3	4	20.57	20.58	−0.01
21-mer	4	7	4	6	20.98	21.11	−0.13[a]
29-mer	7	5	10	7	23.61	23.47	0.14[a]
30-mer	7	5	11	7	23.90	23.83	0.07
31-mer	7	9	9	6	24.32	24.32	0.00
40-mer	10	11	7	12	25.95	26.00	−0.05
41-mer	17	7	11	6	26.72	26.73	−0.01
50-mer	16	17	6	11	29.12	28.96	0.16[a]
51-mer	15	11	15	10	29.65	29.74	−0.09[a]
59-mer	24	19	7	9	31.53	31.58	−0.05
61-mer	8	9	25	19	32.49	32.50	−0.01

[a] Differences of more than 0.5-mer C.

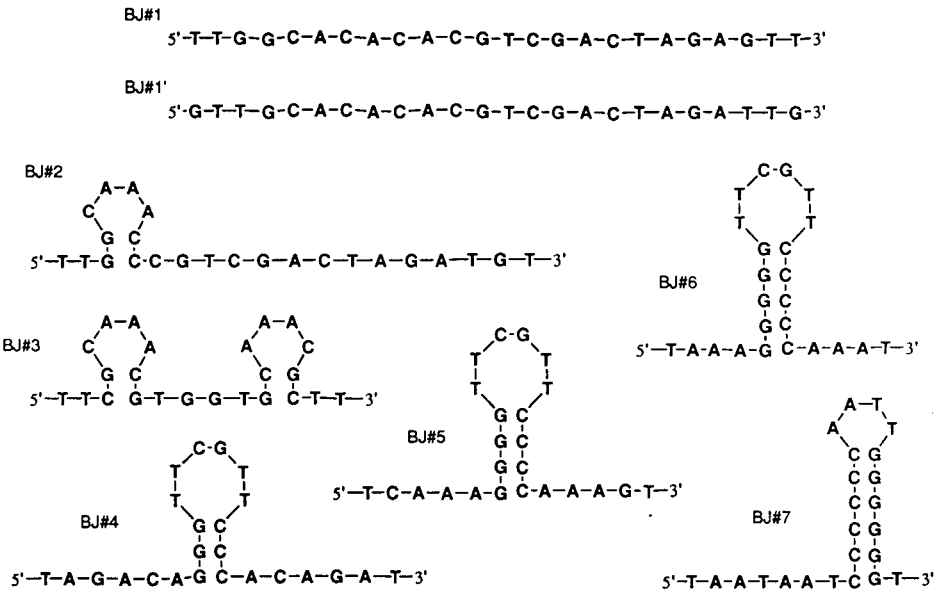

Fig. 3. Heterogeneous oligo-DNA used in the analysis for the effect of secondary structure on migration time. Most probable secondary structures are illustrated.

time of structural isomers of oligo-DNAs which may or may not have a secondary structure, because in this mathematical treatment the effect of such a structure was not taken into account. To minimize the effects of the difference in base compositions and the effect of the bases of the 5′- and 3′-termini, we designed and synthesized the 24-mer DNAs, which may or may not have secondary structure. All of them contained six of all four bases, having T at both ends except for BJ#1′, as shown in Fig. 3.

Contrary to the expectation that all these sequences would show the same migration time in the presence of 7 *M* urea, most of the sequences (except BJ#1 and #4) were separated from each other, as summarized in Table IV and

TABLE IV

MIGRATION TIMES OF DNA FRAGMENTS THAT MAY HAVE SECONDARY STRUCTURES

Each DNA fragment was run with the heterogeneous standard marker as described under Experimental. As there were small migration time drifts of the DNA standards, correction was done by assuming the migration time of the 31-mer in the standard to be 24.32 min [t_M (corr.)]. Migration coefficients were then calculated for every DNA fragment and were used for the calculation of estimated migration time [t_M (calc.)]. Δ is the difference between the corrected and calculated migration times.

Sequence	t_M (corr.) (min)	t_M (calc.) (min)	Δ (min)
BJ#1	23.13	22.83	0.30
BJ#1′	23.22	22.85	0.37
BJ#2	23.19	22.85	0.34
BJ#3	22.92	22.87	0.05
BJ#4	23.10	22.88	0.22
BJ#5	22.95	22.82	0.13
BJ#6	22.37	22.86	−0.49
BJ#7	20.76	22.88	−2.12

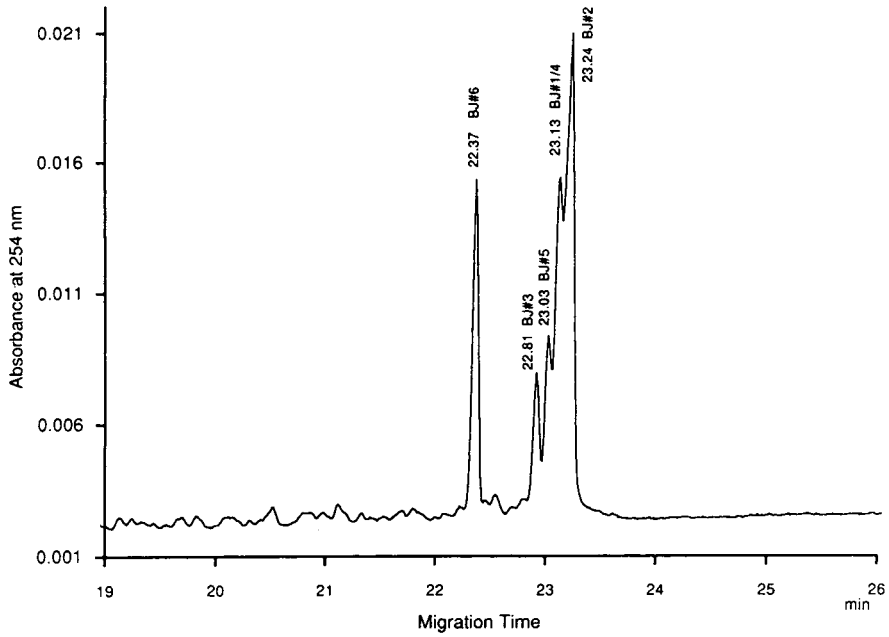

Fig. 4. Separation of heterogeneous oligo-DNAs that may have secondary structures in the presence of 7 *M* urea. The actual sequences #1–#6 are summarized in Fig. 3 with possible secondary structures. Separation conditions as in Fig. 1.

Fig. 4. This strongly suggested the existence of secondary structures. The deviation of the migration time of BJ#1 (linear oligo-DNA) from the calculated value was fairly large (0.30 min). One of the reasons for this is that different bases at the 3′- and 5′-termini must have different effects on the migration time. In fact, G at both termini (BJ#1′) had a 0.09 min longer migration time than that with T at both ends (BJ#1). The sequence that had a short G and C base pair stem (BJ#2) showed a slightly longer migration time than the linear sequence (BJ#1). As the difference was as small as 0.06 mins, it was not significant.

The parallel relationship between the decrease in migration time and the increase in the G and C base pair number in the sequences (Fig. 5) strongly suggested that the secondary structure due to hydrogen bonds or base stacking between the G and C bases plays an important role in maintaining the secondary structure even under such circumstances as in the presence of 7 *M* urea. The effect of having five or six G and C base pairs (BJ#6, 7) was so strong that the migration time was reduced by *ca.* 2% and 10% compared with linear oligo-DNA or calculated migration time, respectively.

Two loops in an oligo-DNA (BJ#3) seemed to have a greater effect on the migration time shift than one loop (BJ#2), which were clearly separated from each other as shown in Fig. 4.

Konrad and Pentoney [11] reported similar findings of an increment in mobility in cases where there was intermolecular base pairing at the 3′-end of single-stranded DNA molecules. However, this phenomenon may be generalized to most DNA fragments which have secondary structure, as we observed a decrease in migration time of oligo-DNA fragments that have a loop structure in the middle of the chain. They also reported the compression phenomena in DNA sequencing (Fig. 2 in ref. 11), which may be easily understood by assuming the existence of a loop and subsequent un-looping along with the decrease in the chain length from the 3′-terminus. As the effect of the decrease in migration time was as large as 10% of the calculated migration time in some instances (BJ#7), it may

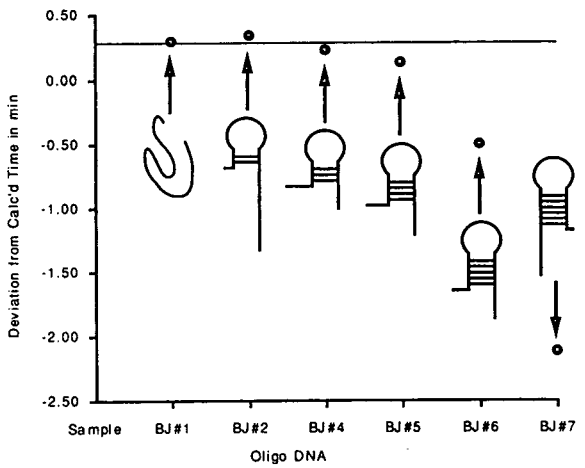

Fig. 5. Migration times and secondary structure. The results in Table IV are visualized by plotting the deviation of the actual migration time from calculated migration time *vs.* the number of possible hydrogen bonds. Although we are not sure whether there were hydrogen bonds or base stacking between the G and C bases to maintain the secondary structure in the presence of 7 *M* urea in the case of the small number of the G and C base pairs, the decrease in migration time and the increment of the number of G and C base pairs are directly correlated. This strongly suggests that hydrogen bonds or base stacking plays an important role in affecting the migration time, probably via secondary structure.

explain the peak compression phenomena. In addition, this predicts the apparent chain length reversal along with the decrease in the actual chain length in DNA sequencing experiments (data not shown).

CONCLUSIONS

By using the Gauss least-squares method for observation functions, we can describe the apparent migration phenomena with probable errors of less than 0.5-mer C with a limited number of oligo-DNA standards (at least six). This method gives separation information for each run as the migration coefficients are calculated every time based on a run. This statistical treatment showed that the migration time of heterogeneous oligo-DNA is the function of the chain length and the base composition. Typical migration coefficients are 0.165 (c), 0.234 (a), 0.338 (g), 0.355 (t) and 15.078 (k) under the present experimental conditions. The existence of secondary structures even in the presence of 7 *M* urea was strongly suggested from the experiments with specially designed oligo-DNAs which may have secondary structures. By changing the urea concentration or other constituents of the gel, such as the Mg^{2+} concentration, it may be possible to detect secondary structures of different magnitudes. As this migration time analysis based on the Gauss least-squares method for observation functions can given an indication of whether there is secondary structure or not, one of the most important applications of this technique may be point mutation detection following the polymerase chain reaction–single strand conformational polymorphism (PCR-SSCP) method on conventional slab gels [13]. As gene regulation via the triple helix is becoming an increasingly important subject of investigation [14,15], CGE may be a useful technique for evaluating such structures if appropriate gels and experimental conditions are developed.

REFERENCES

1 J.W. Jorgenson and K.D. Lukacs, *Anal. Chem.*, 53 (1981) 1298–1302.
2 S. Terabe, K. Otsuka, K. Ichikawa, A. Tsuchiya and T. Ando, *Anal. Chem.*, 56 (1984) 111–113.
3 W.G. Kuhr, *Anal. Chem.*, 62 (1990) 403R–414R.
4 W.G. Kuhr and C.A. Monnig, *Anal. Chem.*, 64 (1992) 389R–407R.
5 A.S. Cohen and B.L. Karger, *J. Chromatogr.*, 397 (1987) 409–417.
6 A.S. Cohen, D.R. Nagarian, A. Polus, A. Guttman, J.A. Smith and B.L. Karger, *Proc. Natl. Acad. Sci. U.S.A.*, 85 (1988) 9660–9663.
7 A. Guttman, A.S. Cohen, D.N. Heiger and B.L. Karger, *Anal. Chem.*, 62 (1990) 137–141.
8 J.A. Luckey, H. Drossman, A.J. Kostichka, D.A. Mead, J.D'Cunha, T.B. Norris and L.M. Smith, *Nucleic Acids Res.*, 18 (1990) 4417–4421.
9 Y. Baba, T. Matsuura, K. Wakamoto, Y. Morita, Y. Nishitsu and M. Tsuhako, *Anal. Chem.*, 64 (1992) 1221–1225.
10 A. Guttman, R.J. Nelson and N. Cooke, *J. Chromatogr.*, 593 (1992) 297–303.
11 K.D. Konrad and S.L. Pentoney, Jr., *Electrophoresis*, in press.
12 M. Ichinose, *Gosaron*, Baifukan, Tokyo, 1953 (in Japanese).
13 M. Orita, H. Iwahana, H. Kanazawa, K. Hayashi and T. Sekiya, *Proc. Natl. Acad. Sci. U.S.A.*, 86 (1989) 2766–2770.
14 K. Yoon, C.A. Hobbs, J. Koch, M. Sardaro, R. Kutny and A.L. Weis, *Proc. Natl. Acad. Sci. U.S.A.*, 89 (1992) 3840–3844.
15 R.W. Roberts and D.M. Crothers, *Science*, 258 (1992).

Journal of Chromatography A, 652 (1993) 31–39
Elsevier Science Publishers B.V., Amsterdam

CHROM. 24 997

Movement of DNA fragments during capillary zone electrophoresis in liquid polyacrylamide

Marcella Chiari and Marina Nesi

Istituto di Chimica degli Ormoni, CNR, Via Mario Bianco 9, Milan 20131 (Italy) and Department of Biomedical Sciences and Technologies, University of Milan, Via Celoria 2, Milan 20133 (Italy)

Pier Giorgio Righetti*

Faculty of Pharmacy and Department of Biomedical Sciences and Technologies, University of Milan, Via Celoria 2, Milan 20133 (Italy)

ABSTRACT

Migration of DNA fragments in the 51–23 130 base pair (bp) size range was investigated by capillary zone electrophoresis in solutions of linear polyacrylamide of concentration from 4 to 10%. Plots of log (mobility) *vs.* log [size (in bp)] clearly indicate three different migration regimes: according to Ogston (*i.e.*, as spherical globules) up to 200 bp, reptation-without-stretching up to 3000–4000 bp and reptation with partial stretching for larger fragments. Guidelines on what percentage of the polymer should be used for optimum resolution can be obtained from plots of peak spacing (in seconds per base pair) *versus* percentage of polymer in solution and from standard plots of peak resolution *versus* percentage of polymer. An optimum linear polyacrylamide concentration, allowing for good resolution of most fragments, from small to large, is found at a level of 6% polymer. It is hypothesized that *in situ* polymerization allows for the formation of a large distribution of polymer sizes (centred at $M_r \approx 100\,000$), thus facilitating simultaneous separation of short and long DNA fragments based on the principle that shorter polyacrylamide chains will sieve shorter DNA fragments and *vice versa*.

INTRODUCTION

It is well known that the electrophoretic mobility of double-stranded (ds) DNA in free solution is independent of molecular size, as the charge to mass ratio is essentially constant. Therefore, in order to effect an electrophoretic separation of dsDNA mixtures, one has to resort to separations in cross-linked, rigid gel matrices which alter the frictional characteristics of DNA in such a way as to introduce a molecular mass dependence on its electrophoretic mobility [1]. While agarose slab electrophoresis has been the preferred technique, in the last few years capillary zone electrophoresis (CZE) has become increasingly popular owing to the speed of separation, the minute amounts of analyte required and the automation of the technique, allowing on-line data acquisition. The earliest reports appeared in 1988 [2,3], and demonstrated the feasibility of both single-stranded DNA analysis (in, *e.g.*, 7.5%T, 3.3%C polyacrylamide gel-filled capillaries in 7 *M* urea)* [2] or dsDNA separations in, *e.g.*, 3%T, 5%C polyacrylamide gels [3]. Such separations were truly unique, in that they proved the possibility of filling troughs of capillary dimensions (typically 75–100 μm I.D.) with a functioning polyacrylamide matrix, while avoiding such frustrating events as air-bubble formation, which would automatically impede electric current flow through the circuit.

* Corresponding author.

* C = g N,N′-methylenebisacrylamide (Bis)/%T; T = (g acrylamide + g Bis)/100 ml solution.

0021-9673/93/$06.00

Prior to this application, ultrathin polyacrylamide matrices (as thin as 50 μm) had only been described for isoelectric focusing in flat slabs, where the gelling technique is simple [4]. A host of applications soon followed, a substantial portion of them being centred on the separation of single-stranded oligonucleotides, aimed at single-base resolution in an attempt to confirm CZE as a valid alternative, for human genome sequencing, to the standard flat-slab techniques. All sorts of gel formulations were tried, *e.g.*, 2.5%T, 3.3%C [5], 3%T, 5%C [6,7], 4%T, 3.3%C [8] or 4%T, 5%C [9], 5%T, 5%C [10], 6%T, 5%C [11,12] and even 7.5%T, 3.3%C [13]. Only recently has there been an attempt to evaluate the effect of total percentage of acrylamide (%T) on the resolution, peak spacing and plate count in the sequencing of short DNA fragments [14].

More recently, however, the trend has shifted towards the use of non-cross-linked polyacrylamide or, tout-court, of polymer networks. The reasons are that bubble-free cross-linked gels are extremely difficult to prepare, the life span of gel matrices is short (sometimes limited to only a few runs, notwithstanding the claims of >100 runs from some laboratories!) and gel matrices tend to accumulate sample precipitates at the injection port, with rapid clogging of the pores. The use of polymer networks stems from an original observation by Bode [15,16], who, in 1977, concluded that the mechanism of sieving in liquid linear polyacrylamide is similar to that occurring in cross-linked polyacrylamide gels. Bode's model views macromolecules migrating through "dynamic pores" which are formed by the fluctuating polymer chain network. This thesis found a theoretical support in the classical work of De Gennes [17], who expounded the concept that, once a polymer solution reaches a critical concentration in solution (called overlap or entanglement threshold), it will exert sieving on a particle migrating through it much like a gel does.

Among the earliest reports, Heiger *et al.* [18] described the use of low- and non-cross-linked polyacrylamides for the separation of DNA restriction fragments. Sudor *et al.* [19] reported the advantage of using linear polyacrylamide columns, as the capillary content can be refilled once the polymer network is exhausted (although Chiari *et al.* [20] clearly demonstrated that, owing to the very high viscosity, this is only possible up to 6% polyacrylamide concentrations). Guttman *et al.* [21] demonstrated the possibility of improving separations of dsDNA restriction fragments in 4% linear polyacrylamide by using field strength gradients. Pentoney *et al.* [22] adopted 10% linear polyacrylamide, in manganese buffers, for DNA sequence determination and reported a single-fluor approach offering a sensitivity of 2 zmol ($2 \cdot 10^{-21}$ mol). The use of polymer networks was soon extended to other types of linear macromolecules. Grossman and Soane [23], in reviving De Gennes' theory of entanglement threshold and reptation, demonstrated that hydroxyethylcellulose (HEC), around the entanglement threshold (set at *ca.* 0.4% polymer), could be an excellent medium for DNA fractionation. In a more recent report, the same group were able to derive the relationship between polymer concentration and the mesh size of the entangled network, and found that the average pore radius (R_p) would diminish from 21 nm in 0.5% HEC to 8.5 nm in 2% HEC [24], according to the law $\langle R_p \rangle = 6.0\ C^{-0.68}$ (where C is the polymer concentration), in general agreement with De Gennes' theory. They proposed that the average mesh size of entangled polymer solutions of HEC is about one order of magnitude less than that of agarose gels of comparable concentration [25], the migration mechanism of DNA fragments, however, being much the same as that found in traditional rigid-gel matrices. HEC as a sieving medium was also used by Oefner *et al.* [26], who used 0.5% HEC for DNA separations in both coated and uncoated capillaries (in the last instance, Rb or Cs salts were used for quenching the zeta potential). The same group recently extended their work to a systematic study covering a concentration range of HEC from 0.3 to 0.7% [27]. In a similar approach, other polymers have been proposed, such as 0.5% methylcellulose (MC) [28] and low-melting agarose above its gelling temperature [29,30].

Hydroxypropylmethylcellulose (HMC) was used as a sieving polymer for both proteins and DNAs by Hjertén *et al.* [31] and Zhu *et al.* [32].

As we feel that the future in electrophoretic sieving in CZE will go more and more towards fillings made of viscous solutions, we decided to investigate systematically the properties of one such polymer solution, namely linear polyacrylamide, because, owing to the ease of preparation of such polymers and the possibility of *in situ* polymerization, polyacrylamides appear to be a unique and versatile sieving medium. We give here general guidelines and some basic rules on the optimum %T to be adopted according to the size of the particle to be separated. Such guidelines are based on the evaluation of some basic separation parameters, such as peak spacing and resolution, for given adjacent pairs of DNA fragments, as a function of polymer concentration (%T at 0% C).

EXPERIMENT

Materials

Acrylamide, tris(hydroxymethyl)aminomethane (Tris), ammonium peroxodisulphate and *N*,*N*,*N*′,*N*′-tetramethylethylenediamine (TEMED) were obtained from Bio-Rad Labs. (Richmond, CA, USA). 3-(Trimethoxysilyl)propyl methacrylate (Bind Silane) and ethylenediaminetetraacetic acid (EDTA) were purchased from Aldrich Chemie (Steinheim, Germany). The DNA molecular mass markers marker V (a mixture of fragments from cleavage of plasmid pBR322 DNA with restriction endonuclease *Hae*III), marker II (a mixture of fragments from cleavage of lambda DNA with restriction endonuclease *Hind*III) and marker III (a mixture of fragments from cleavage of lambda DNA with restriction endonucleases *Hind*III and *Eco*RI) were obtained from Boehringer (Mannheim, Germany) and were available as 250 μg ml^{-1} solutions in 10 m*M* Tris–HCl (pH 8.2). The 1000 base pair (bp) ladder (up to 12 kbp) was supplied by Bethesda Research Labs. (Gaithersburg, MD, USA) at a concentration of 920 μg ml^{-1} in 10 m*M* Tris–HCl (pH 8.2). Fused-silica capillaries (100 μm I.D., 370 μm O.D.) were obtained from Polymicro Technologies (Phoenix, AZ, USA).

Capillary zone electrophoresis

CZE was performed in a Waters Quanta 4000 capillary electrophoresis system (Millipore, Milford, MA, USA). For the DNA marker separations, the analysis was run in 100 m*M* Tris–borate–2 *M* EDTA buffer (pH 8.2) at 100 V cm^{-1} in a 40 cm × 100 μm I.D. capillary. The samples were loaded by electromigation for 3 s at 4 kV. The detector was set at 254 nm and the runs were carried out at 24°C under reverse polarity (anode at the detection side).

Coating of the capillary inner wall

The capillary was first cut to the desired length and a 2–3-mm window burned. The capillary was washed and filled with 100 μL of 1 *M* NaOH and allowed to stand for 6 h. The capillary was rinsed and filled with 100 μl of 0.1 *M* HCl, incubated for 30 min and then rinsed with 100 μl of 0.1 *M* NaOH. After incubating the capillary for 1 h, it was rinsed with water and then with acetone. The capillary was filled with Bind Silane–acetone (1:1, v/v) mixture and incubated overnight. The capillary was washed with 100 μl of methanol and then with water, both liquids being pumped through at a slow rate (1 μl^{-1}). The capillary was filled with a 6%T (0% C) acrylamide solution in 100 m*M* Tris–borate–2 m*M* EDTA (pH 8.2) buffer, degassed and containing the appropriate amount of catalysts (4 μl of 10% peroxodisulphate and 2 μl of pure TEMED per millilitre of gelling solution). Polymerization was allowed to proceed for 12 h at room temperature.

Filling of the capillary with polymer networks

The coated capillaries were emptied and then filled with the appropriate solutions of acrylamide (in the absence of cross-linker) in 100 m*M* Tris–borate buffer (pH 8.2) in presence of 2 m*M* EDTA and of the standard amount of catalysts (4 μl of 10% peroxodisulphate and 2 μl of pure TEMED per millilitre of gelling solution). Linear polyacrylamide solutions of 4%, 6%, 8% and 10% concentration were tested.

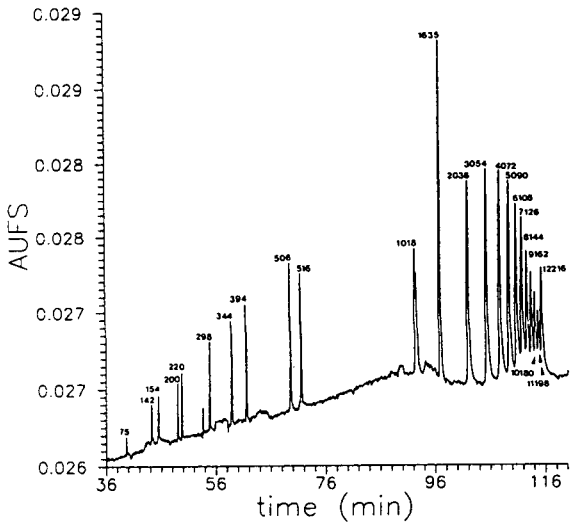

Fig. 1. CZE separation of the 1-kb ladder. Conditions: 47 cm × 100 μm I.D. capillary, in 100 m*M* Tris–borate buffer (pH 8.2)–2 m*M* EDTA, containing 4.5%T polyacrylamide (at O% C). Sample injection, 3 s at 4000 V; run, 4000 V at 10.5 μA; detection at 254 nm. Waters Quanta 4000 capillary unit with forced air cooling. The numbers on each peak represent the fragment length.

Polymerization was allowed to proceed for 12 h. Prior to sample application, the capillaries were conditioned by electrophoresis for 1 h at 4 kV in order to remove the charged catalysts.

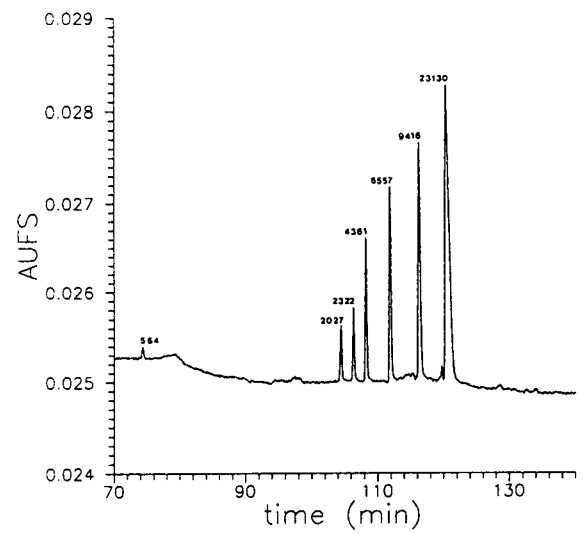

Fig. 2. CZE separation of the marker II DNA fragments. Details as in Fig. 1.

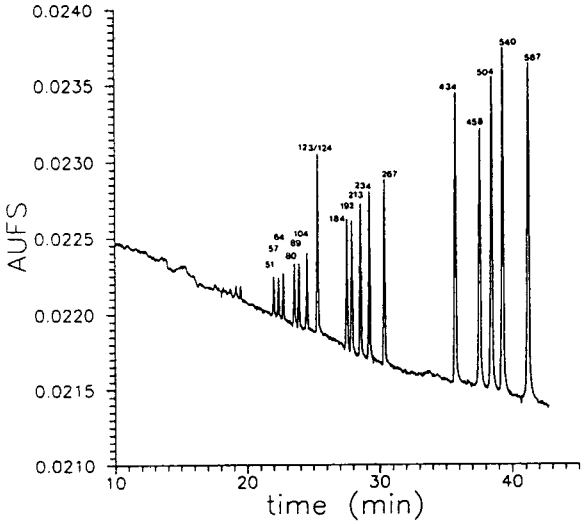

Fig. 3. CZE separation of the marker V DNA fragments. Conditions: 40 cm × 100 μm I.D. capillary, in 100 m*M* Tris–borate buffer (pH 8.2)–2 m*M* EDTA, containing 4.0% T polyacrylamide (at 0% C). Other details as in Fig. 1.

RESULTS

Figs. 1–3 show the electropherograms obtained with the 1-kb ladder (Fig. 1, in a 4.5%T linear polyacrylamide at 4 kV), with marker II (Fig. 2, in 4.5%T linear polyacrylamide at 4 kV) and with marker V (Fig. 3, in 4%T linear polyacrylamide at 4 kV). It is seen that this polymer concentration allows very good separations of relatively small fragments (Fig. 3, from 51 to 587 bp), rather large fragments (Fig. 1, from 75 to 12 216 bp) up to 23 130 bp (Fig. 2). The size selectivity of linear polyacrylamide fillings can be characterized by the well known Ferguson plots, relating the mobility to the %T (at 0% C in our case) as follows:

$$\log \mu = \log \mu_0 - K_R(\%T)$$

where μ is the measured mobility (in $cm^2\ V^{-1}\ s^{-1}$), μ_0 the extrapolated mobility in free solution and K_R the retardation coefficient. We ran a series of fragments in different capillaries containing from 4% to 10% T polymer and assessed the relative mobilities at progressively higher %T. The data are summarized in the Ferguson plot in Fig. 4: it is seen that the relatively smaller

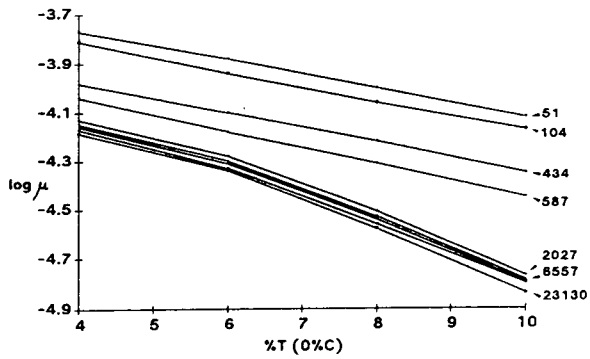

Fig. 4. Ferguson plot of log (mobility) *vs.* percentage of polymer in solution for different DNA fragment sizes. Note the slight downward curvature from fragments longer than 2000 bp.

fragments (*e.g.*, from 51 to 587 bp) exhibit a linear relationship as expected, whereas the larger fragments, *e.g.*, from 2027 up to 23 130 bp) exhibit a downward curvature at the higher %T. In addition, whereas the smaller fragments display progressively steeper slopes, as expected from progressively larger fragment sizes, the set of longer fragments (from 2027 up to 23 130 bp) reveals almost identical slopes, as though size discrimination were progressively lost.

An interesting insight into the migration of DNA fragments can be obtained when the data are expressed in a double-logarithmic plot of μ *vs.* L (the contour length of a DNA molecule, 340 nm per kbp) as suggested by Noolandi [33]. We constructed this plot for 30 DNA fragments, ranging in size from 51 up to 23 130 bp, in four different polymer solutions, of 4%, 6%, 8% and 10%T. The results are summarized in Fig. 5 and it is evident (see also Discussion) that at least three different migration regimes can be evinced: an Ogston dependence, for smaller fragments, reptation without stretching for intermediate sizes and reptation with partial stretching for the upper ladder. These three regimes are particularly evident in the curve pertaining to the 10% T linear polymer, where the transitions to the different migration modes are defined by sharp inflection points. In our case, it appears that the transition from the Ogston regime (when DNAs are considered to migrate as "blobs" or globules) to the reptation mode (where DNAs start slithering head-on through the gel, becoming oriented in the field) occurs already at around 200 bp. Surprisingly, reptation with partial stretching is already apparent at around 3000–4000 bp.

We then tried to obtain some parameters of separation efficiency, in order to allow users to evaluate the proper amount of polymer to be adopted according to the size of the fragments under analysis. One way of expressing the data is to calculate the peak spacing (in seconds per bp increment) as a function of sieving polymer concentration. Fig. 6A and B summarize the data for smaller and intermediate fragments, respectively, using as separation parameter the distance between adjacent peaks in the electropherogram (*e.g.*, 80/89 bp, and so on). It is seen that, for all smaller fragments analysed, the peak spacing strongly increases at progressively higher polymer concentrations (from 4 to 10% T), as it should if they migrate in an Ogston regime (note, however, that for relatively larger fragments, which already start following a reptation regime, such as the pair 458/504 bp, the increment is much less pronounced) (Fig. 6A). For the larger fragments (from 3054 up to 5090 bp, Fig. 6B) two phenomena are evident: (a) the absolute values of peak spacing strongly decrease and (b) little is gained in going from a 4 to a 10%

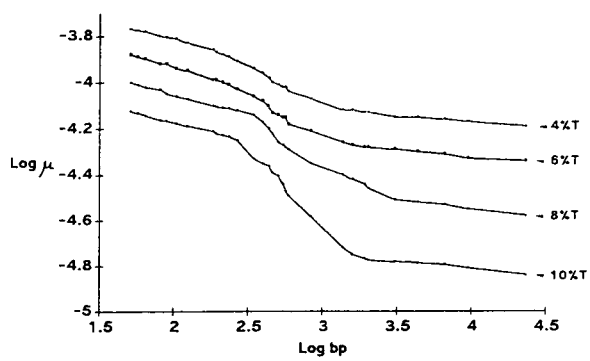

Fig. 5. Double logarithmic plot of mobility *vs.* fragment length (in bp) for 30 DNA fragments (ranging in size from 51 up to 23 310 bp). The plot was calculated for four different polymer concentrations, from 4 up to 10% T. Note the sharp transitions from the Ogston regime to reptation without stretching at *ca.* 200 bp and to reptation with (partial) stretching at 3000–4000 bp.

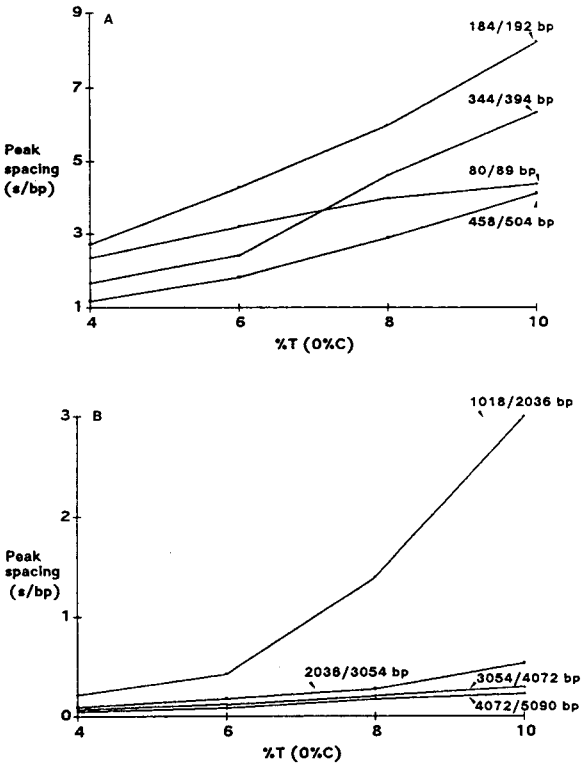

Fig. 6. Plot of peak spacing (in seconds per base pair) *vs.* percentage of polymer in solution. (A) For small fragment pairs (80/89, 184/192, 344/394 and 458/504 bp); (B) for larger fragment pairs (1018/2036, 2036/3054, 3054/4072 and 4072/5090 bp).

T. This is probably due to the fact that, as %T increases, reptation becomes more pronounced, thus diminishing the effective peak distance.

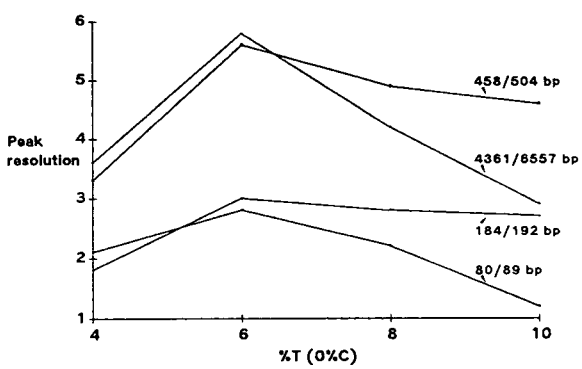

Fig. 7. Plot of peak resolution *vs.* percentage of polymer in solution. Resolution was calculated for the following adjacent pairs: 80/89, 184/192, 458/504 and 4361/6557 bp.

As a final criterion for choosing the optimum polymer concentration, we have plotted in Fig. 7 peak resolution *vs.* %T in the 4–10% T range. It is clearly seen that a sharp resolution optimum is found for most fragments at 6% T, which thus appears to be a good compromise between efficient sieving and reasonable analysis times.

DISCUSSION

Our results begin to shed some light on choosing optimum polymer concentrations when performing DNA fragment analysis in entangled polymer solutions, a field which is rapidly gaining momentum. We shall examine here the different aspects of such sieving polymer solutions.

Sieving of polyacrylamide solutions

We feel that, among all possible polymers listed in the Introduction, polyacrylamide still appears to be the most versatile for the following reasons. First, as several detection methods rely on DNA absorbance at 254 nm, polyacrylamide is completely transparent in this region, thus offering a medium with no background absorbance, which enhances the sensitivity even for minute amounts of DNA by increasing the signal-to-noise ratio at high signal amplification. In principle, this would not apply to polyacrylamide, as it is almost impossible to drive the reaction to 100% consumption of double bonds; however, we have described a scavenging method, based on addition of unreacted double bonds to free SH groups, able to abolish completely the background absorbance of unreacted acrylamide [20]. In addition, polyacrylamide allows complete freedom of selection of sieving ranges, as it can be polymerized *in situ* from non-viscous monomer solutions. With other polymers (*e.g.*, HEC, MC and agarose solutions), concentrated solutions are so viscous as to be unwieldy for any pumping process. In addition, polyacrylamide solutions appear to be surprisingly efficient in sieving mixtures of DNA fragments ranging from small to fairly large (*e.g.*, in the example in Fig. 1, from as little as 75 up to 12 216 bp). It might be asked why this is so. According to Grossman and Soane [23], "in order to create larger pores,

one wants to use a longer polymer and in order to create small pores one wants to use a shorter polymer". We would extend this idea as follows: longer chains will sieve larger objects, whereas shorter chains will act as efficient obstacle toward smaller objects. *i.e.*, we apply to molecular sieving the old adage of organic chemistry: "similar dissolves similar". If this is so, it might be advantageous to use *in situ* polymerization of acrylamide, as it produces a large distribution of chain lengths. We believe that, under our polymerization conditions (as measured by the average viscosity of these solutions), the average chain length is of the order of M_r 100 000, extending from perhaps 50 000 up to as much as 150 000. This provides a vast range of chain lengths for simultaneously sieving both short and long DNA fragments. This is in principle similar to pore-gradient gel electrophoresis, where sharp resolution is obtained for both small and large proteins, owing to the approach to the pore limit [34]. If this is the case, it might be preferable to use *in situ* polymerization rather than dissolve a single-size string (*e.g.*, like the commercially available M_r $5 \cdot 10^6$ polyacrylamide chain, as suggested by some workers), which presumably cannot perform as efficiently for the vast range of DNA sizes commonly found in restriction nuclease fragments (if it does, this would mean that such a chain is highly heterodisperse in size!).

Migration modes of DNA in entangled polymer solutions

In free solution, DNA behaves like a uniformly charged chain and so adopts a fairly open, randomly coiled configuration through which solvent can readily flow. Consequently, the frictional drag it experiences is simply proportional to its length. As the electrical force is also proportional to the length, it follows that the electrophoretic mobility of large DNAs in solution is independent of size [35]. In sieving media, the Ogston model [36] would predict that the mobility of a DNA "globule" would rapidly fall to zero as the diameter of the particle would be slightly larger than the average pore diameter in the gel. However, contrary to this model, it was found that DNA of sizes much larger than the gel pores could also enter the gel and migrate, to a point at which, above 50 kbp, all fragments would migrate at the same speed (*i.e.*, above this size limit, the mobility becomes independent of molecular mass, a most unfortunate behaviour). It was finally understood by Lerman and Frisch [37] that large DNA molecules would start slithering head-on through the gel, a type of motion called reptation, thus becoming oriented by the field [38].

This insight rapidly led to the discovery, by Schwartz and Cantor [39], that periodically changing the direction of the electric field restored the lost sieving mechanism. In addition to a regime of "reptation without stretching", a third regime is prevalent when very high field strengths, or very large fragments, or very small pore size gels are used: "reptation with stretching". When a regime of full stretching is reached, the mobility in a gel becomes again independent of length. Physically this means that for stretched molecules both the electric force and opposing friction scale with length, and the mobility is determined by the force per unit length, which is independent of the actual length, a situation analogous to that experienced by DNA globules in solution.

Noolandi [33] was able to reconstruct these three regimes in a schematic log–log plot of reduced mobility *vs.* molecular size L (see Fig. 2 in ref. [33]). To our knowledge, an actual experimental validation of these three regimes was still not available and we feel that our Fig. 5 (especially in the bottom curve pertaining to 10% polymer) illustrates well these three migration mechanisms. Interestingly, the transition from the Ogston to the reptation without stretching regimes occurs in our polymer solutions at 200 bp, whereas this limit had been set at *ca.* 2000 bp in slab-gel electrophoresis. Moreover, the transition from this last regime to reptation with (partial) stretching occurs in our case at *ca.* 3000–4000 bp, whereas in agarose gel electrophoresis it had been set at around 50 000 bp. The reasons for these discrepancies could be twofold: (a) the higher field strengths (typically extending up to 500 V cm^{-1}) used in CZE as opposed to slab-gel electrophoresis (in fact, in CZE, resolution in DNA analysis decreases above 100 V

cm^{-1}); (b) the smaller pore size of entangled polymer solutions as compared with true gels of similar matrix content. For example, Grossman and Soane [23] estimated an average pore size for entangled polymer solutions *ca.* one order of magnitude smaller than equivalent rigid gels. As the reptation regime begins at a critical value at which $R_g \approx 1.4\ R_p$ (where R_g is the radius of gyration of the particle and R_p is the average pore radius of the gel matrix), this explains why reptation begins in polymer solutions with fragments much smaller than expected. Even this last hypothesis, though, might only be valid when comparing agarose gels with polymer solutions. In polyacrylamide matrices, as commonly used for DNA sequencing, according to Noolandi's group, reptation might already begin at above 500 bases in length, as above this critical length all longer sequences are highly compressed. When pulsed fields were applied to such gels, sequence reading was dramatically improved up to 2300 bases in length [40].

CONCLUSIONS

Polymer networks consisting of linear polyacrylamides appear to be versatile in DNA analysis. Good indicators of the percentage of polymer needed for a given analysis appear to be plots of peak resolution (in seconds per base pair) *vs.* percentage of polymer and also standard plots of resolution [according to the well known equation $(t_2 - t_1)/2(w_1 + w_2)$, where t_2 and t_1 and w_2 and w_1 are the transit times and peak widths (standard deviation), respectively, of bands 2 and 1]. A good compromise appears to be 6% polymer solutions, as they allow for optimum resolution of all fragments in the mixture within reasonable analysis times. However, for very small fragments (up to 100 bp) we have successfully used up to 10% T polymer networks.

ACKNOWLEDGEMENTS

This work was supported in part by grants from the Agenzia Spaziale Italiana (ASI, Rome), by a grant from the European Community and by Consiglio Nazionale delle Ricerche (CNR, Rome), Progetti Finalizzati Chimica Fine II and Biotecnologie e Biostrumentazione.

REFERENCES

1 B.M. Olivera, P. Baine and N. Davidson, *Biopolymers*, 2 (1964) 245–251.
2 A. Guttman, A. Paulus, A.S. Cohen, B.L. Karger, H. Rodriguez and W.S. Hancock, in C. Schafter-Nielsen (Editor), *Electrophoresis '88*, VCH, Weinheim, 1988, pp. 151–159.
3 T.J. Kasper, M. Melera, P. Gozel and R.G. Brownlee, *J. Chromatogr.*, 458 (1988) 303–312.
4 B.J. Radola, *Electrophoresis*, 1 (1980) 43–56.
5 A. Paulus, E. Gassmann and M.J. Field, *Electrophoresis*, 11 (1990) 702–708.
6 A.S. Cohen, D.R. Najarian and B.L. Karger, *J. Chromatogr.*, 516 (1990) 49–60.
7 A. Guttman, A.S. Cohen, D.N. Heiger and B.L. Karger, *Anal. Chem.*, 62 (1990) 137–141.
8 X.C. Huang, S.G. Stuart, P.F. Bente, III and T.M. Brennan, *J. Chromatogr.*, 600 (1992) 289–295.
9 H. Drossman, J.A. Luckey, A.J. Kostichka, J. D'Cunha and L.M. Smith, *Anal. Chem.*, 62 (1990) 900–903.
10 Y. Baba, T. Matsuura, K. Wakamoto and M. Tsuhako, *J. Chromatogr.*, 558 (1991) 273–284.
11 M.J. Rocheleau, R.J. Grey, D.Y. Chen, H.R. Harke and N.J. Dovichi, *Electrophoresis*, 13 (1992) 484–486.
12 D.Y. Chen, H.P. Swerdlow, H.R. Harke, J.Z. Zhang and N.J. Dovichi, *J. Chromatogr.*, 559 (1991) 237–246.
13 A. Paulus and J.I. Ohms, *J. Chromatogr.*, 507 (1990) 113–123.
14 H.R. Harke, S. Bay, J.Z. Zhang, M.J. Rocheleau and N.J. Dovichi, *J. Chromatogr.*, 608 (1992) 143–150.
15 H.J. Bode, *Anal. Biochem.*, 83 (1977) 204–210.
16 H.J. Bode, *Anal. Biochem.*, 83 (1977) 364–371.
17 P.G. De Gennes, *Scaling Concepts in Polymer Physics*, Cornell University Press, Ithaca, NY, 1979, Ch. 3.
18 D.N. Heiger, A.S. Cohen and B.L. Karger, *J. Chromatogr.*, 516 (1990) 33–48.
19 J. Sudor, F. Foret and P. Bocek, *Electrophoresis*, 12 (1991) 1056–1058.
20 M. Chiari, M. Nesi, M. Fazio and P.G. Righetti, *Electrophoresis*, 13 (1992) 690–697.
21 A. Guttman, B. Wanders and N. Cooke, *Anal. Chem.*, 64 (1992) 2348–2351.
22 S.L. Pentoney Jr., K.D. Konrad and W. Kaye, *Electrophoresis*, 13 (1992) 467–474.
23 P.D. Grossman and D.S. Soane, *J. Chromatogr.*, 559 (1991) 257–266.
24 P.D. Grossman, T. Hino and D.S. Soane, *J. Chromatogr.*, 608 (1992) 79–83.
25 P.G. Righetti, B.C.W. Brost and R.S. Snyder, *J. Biochem. Biophys. Methods*, 4 (1981) 347–357.
26 P.J. Oefner, G.K. Bonn, C.G. Huber and S. Nathakarkitkool, *J. Chromatogr.*, 625 (1992) 331–340.

27 S. Nathakarkitkool, P.J. Oefner, G. Bartsch, M.A. Chin and G.K. Bonn, *Electrophoresis*, 13 (1992) 18–31.
28 M. Strege and A. Lagu, *Anal. Chem.*, 63 (1991) 1233–1236.
29 P. Bocek and A. Chrambach, *Electrophoresis*, 12 (1991) 1059–1061.
30 P. Bocek and A. Chrambach, *Electrophoresis*, 13 (1992) 31–34.
31 S. Hjertén, L. Valtcheva, K. Elenbring and D. Eaker, *J. Liq. Chromatogr.*, 12 (1989) 2471–2476.
32 M. Zhu, D.L. Hansen, S. Burd and F. Gannon, *J. Chromatogr.*, 480 (1989) 311–319.
33 J. Noolandi, *Adv. Electrophoresis*, 5 (1992) 1–57.
34 E. Gianazza and P.G. Righetti, in P.G. Righetti, C.J. van Oss and J.W. Vanderhoff (Editors), *Electrokinetic Separation Methods*, Elsevier, Amsterdam, 1979, pp. 293–311.
35 J.L. Viovy, T. Duke and F. Caron, *Contemp. Phys.*, 33 (1992) 25–40.
36 A.G. Ogston, *Trans. Faraday Soc.*, 54 (1958) 1754–1758.
37 L.S. Lerman and H.L. Frisch, *Biopolymers*, 21 (1982) 995–1001.
38 O.J. Lumpkin and B.H. Zimm, *Biopolymers*, 21 (1982) 2315–2320.
39 D.C. Schwartz and C.R. Cantor, *Cell*, 37 (1984) 67–75.
40 C. Turmel, E. Brassard and J. Noolandi, *Electrophoresis*, 13 (1992) 620–622.

Journal of Chromatography A, 652 (1993) 41–46
Elsevier Science Publishers B.V., Amsterdam

CHROM. 25 065

Use of glucomannan for the separation of DNA fragments by capillary electrophoresis

Tomonori Izumi*

Department of Chemistry, Faculty of Science, Tokyo Metropolitan University, Minami-Ohsawa, Hachiouji, Tokyo 192-03 (Japan)

Masato Yamaguchi

R & D Planning Department, Research and Development Division, Kurita Water Industries Ltd., Nishi-Shinjuku, Shinjuku, Tokyo 160 (Japan)

Kenichi Yoneda, Toshiaki Isobe, Tsuneo Okuyama and Tomotaka Shinoda

Department of Chemistry, Faculty of Science, Tokyo Metropolitan University, Minami-Ohsawa, Hachiouji, Tokyo 192-03 (Japan)

ABSTRACT

Glucomannan, a natural polysaccharide extracted from *Amorphophallus konjac*, was employed as a sieving additive for the separation of restriction DNA fragments in capillary electrophoresis. A stable solution of entangled glucomannan was successfully prepared under mild conditions. The separation capillary filled with 0.25% glucomannan exhibited excellent resolution and reproducibility on separation of DNA fragments over the range of *ca.* 1400 base pairs. The separation was dependent on the size of the fragments, which allowed the determination of the size of separated DNAs directly from the migration time. In addition to these separation characteristics, glucomannan has practical advantages in its chemical stability, non-toxicity and ease of handling. Because the method is applicable to the separation and characterization of the DNA fragments generated by digestion with restriction enzymes or produced by polymerase chain reactions, it is concluded that glucomannan is a good alternative to the conventional sieving additives for capillary electrophoresis, such as polyacrylamide and hydroxymethylcellulose.

INTRODUCTION

The separation of biological macromolecules such as DNA is an important technique in modern biological science. For instance, molecular cloning of a gene requires many experimental steps for the analysis and separation of DNA fragments generated by restriction enzyme digestion or produced by polymerase chain reaction (PCR). Because most of these procedures are currently performed manually by polyacrylamide or agarose slab gel electrophoresis, the separation and analysis of DNA fragments are laborious and often time-consuming steps in gene cloning studies.

Capillary electrophoresis has been developed for the determination of various substances, including biological macromolecules [1–7]. The advantages of this method are high resolution, rapid and sensitive analysis and easy operation and automation. The efficient separation of polynucleotides has been achieved using a capillary filled with polymer gel or entangled polymer

* Corresponding author.

0021-9673/93/$06.00

solution such as cross-linked or non-cross-linked polyacrylamide gels [8], polyethylene glycol [9] and fibrous polysaccharide derivatives such as hydroxypropylmethylcellulose [9,10]. The advantages and disadvantages of these materials have been discussed previously [8–11]. In this mode of separation, polynucleotides are basically resolved according to their size. Thus the matrices of these materials are thought to serve as pores to sieve the polynucleotide molecules. As the separation depends on the pore size, a matrix with large pores is generally suitable for the separation of large DNA fragments such as phage DNA, and *vice versa*.

Glucomannan, a natural polysaccharide extracted from *Amorphophallus konjac*, is a linear polymer mainly consisting of D-glucose and D-mannose [12], and the gel form of this material is known as a Japanese traditional food, "konjac". We intended to use this material as an entangled polymer solution for the capillary electrophoresis of DNA fragments because it is chemically stable and non-toxic, and has a pore size larger than that of agarose [13]. In this work, we prepared entangled glucomannan solution and examined its separation characteristics in the separation of DNA fragments.

EXPERIMENTAL

Apparatus

A CE-800 capillary electrophoresis system (JASCO, Tokyo, Japan), equipped with a high-voltage d.c. power supply (Model 890-CE) providing up to 30 kV and a UV–Vis spectrophotometer (Model 875-CE) for on-column detection, was employed. For data acquisition and processing, a Model 807-IT intelligent integrator (JASCO) was used. Electrophoresis was performed in a fused-silica capillary with the inner surface coated with DB-Wax (J&W Scientific, Folsom, CA, USA) (50 cm × 100 μm I.D. × 375 μm O.D.).

Chemicals

Glucomannan, purified from konjac flour by ethanol precipitation [14], was obtained from Kurita Water Industries (Tokyo, Japan). The preparation used in this study has an average molecular mass of $1.3 \cdot 10^6$ as estimated from the viscosity of the aqueous solution. All other chemicals used were of analytical-reagent grade. ΦX174 DNA digested with restriction enzyme *Hae*III was obtained from Nippon Gene (Tokyo, Japan) and used at a sample concentration of 0.47 mg/ml in 10 m*M* Tris–HCl containing 20 m*M* NaCl and 1 m*M* EDTA (pH 7.9). Restriction fragments of plasmid DNA were prepared by digestion of Bluescript II SK(+) (Stratagene, La Jolla, CA, USA) with restriction enzyme *Dde*I (Toyobo, Tokyo, Japan). The digestion was performed under the conditions recommended by the supplier. The digest was precipitated with ethanol, redissolved in distilled water and then subjected to electrophoresis. Polymerase chain reaction (PCR) product of the mRNA encoding the η-chain of 14–3–3 protein [15] was prepared using two synthetic primers (primer 1,5′ - TCGAATTCATGGGTGACCGCGAGC-A-3′; primer 2,5′-GATAGGATCCGCACTGG-ATACTTAGT-3′).

Preparation of entangled glucomannan solution

Because the glucomannan forms an insoluble gel on boiling in an alkaline solution [16], the entangled glucomannan solution was carefully prepared under mild conditions. The particles of glucomannan were added to an electrolyte solution at a concentration of 0.25% (w/w) and swollen by heating at 60°C in a water-bath. The swelling was completed within 4 h. The partially solubilized glucomannan, in the form of a clear paste, was then mixed on a vortex mixer with occasionally heating in boiling water until the preparation became almost homogeneous. The preparation was allowed to come to room temperature, centrifuged to remove small insoluble material and degassed by aspiration. Alternatively, the entangled glucomannan solution could be prepared by continuous stirring of the mixture at 60°C for 6 h. The glucomannan solution thus obtained was stable at room temperature at least for several months. Excessive heating of glucomannan (100°C, more than 1 h) should be avoided because a white gel is irreversibly formed.

Capillary electrophoresis

As an electrolyte solution, 70 m*M* Tris–HCl (pH 8.2) containing 14 m*M* EDTA was used. Prior to each analysis, 20 μl of glucomannan stock solution were injected into the coated fused-silica capillary using a glass syringe with a joint of PTFE tubing. Samples were injected electrophoretically from the cathode end of the capillary at 5 kV for 1 s. Electrophoresis was run at a constant voltage of 5 kV (100 V/cm for a 50-cm capillary) and the UV absorbance at 260 nm was measured at 20 cm from the cathode end.

RESULTS AND DISCUSSION

Separation of HaeIII digest of ΦX174 DNA

To examine the separation performance of the glucomannan-filled capillary, we chose an *Hae*III restriction digest of ΦX174 plasmid DNA as a standard DNA sample. Based on the nucleotide sequence of the plasmid DNA and the known specificity of *Hae*III, the digest should contain eleven fragments ranging from 72 to 1353 base pairs [17]. Fig. 1 shows a separation pattern of the *Hae*III digest of ΦX174 DNA using a 0.25% glucomannan-filled capillary. The method resolved all eleven fragments in less than 30 min. The peaks were identified by co-electrophoresis of the digest with each fragment isolated by conventional 6% polyacrylamide slab gel electrophoresis (shown in Fig. 1a). The fragments in peaks 5 and 6, which differ in length by only ten base pairs, could be separated by the present method employing an electrolyte solution containing 14 m*M* EDTA. However, a similar electrolyte solution containing lower or higher concentrations of EDTA gave poor resolution and broadening of some peaks (Fig. 1b and c).

A calibration graph of migration time *versus* the size of the fragments separated on the glucomannan-filled capillary is shown in Fig. 2. The migration time of the fragments is correlated with the size of the fragments over the range of *ca.* 1400 base pairs, indicating the size-dependent migration of the DNA fragments in the glucomannan-filled capillary.

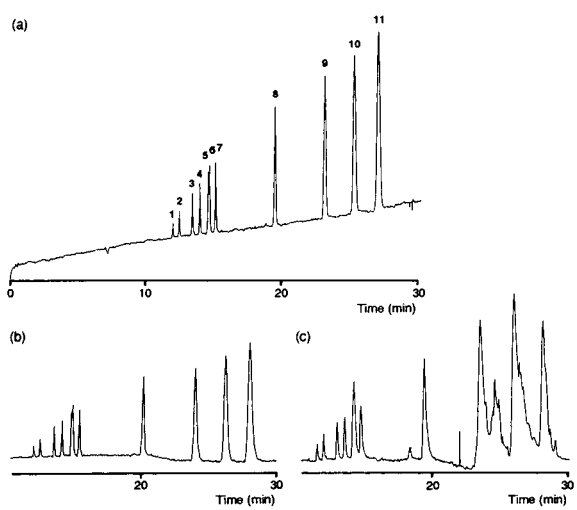

Fig. 1. Separation of *Hae*III digest of ΦX174 DNA using a 0.25% glucomannan-filled capillary. Peaks: 1 = 72; 2 = 118; 3 = 194; 4 = 234; 5 = 271; 6 = 281; 7 = 310; 8 = 603; 9 = 872; 10 = 1078; 11 = 1353 base pairs. Conditions: capillary, DB-WAX, was filled with 0.25% glucomannan dissolved in 70 m*M* Tris–HCl (pH 8.2) containing (a) 14, (b) 2 and (c) 26 m*M* EDTA. Effective length, 20 cm; total length, 50 cm; applied field, 100 V/cm; sample, injected electrophoretically at 5 kV for 1 s. Current generated: (a) 40; (b) 25; (c) 56 μA.

Ferguson plot analysis

The separation characteristics of the glucomannan-filled capillary were further examined by Ferguson plot analysis [18,19], where the logarithm of the mobility of the restriction fragments was plotted against the concentration of the glucomannan solution in the range 0.05–0.7% (Fig. 3). At glucomannan concentrations up to 0.25%, the DNA fragments ranging from 72 to 1353 base pairs exhibit a good linear relationship described by the equation

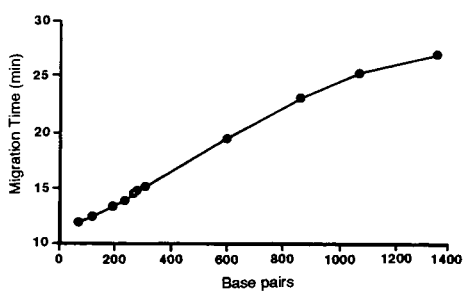

Fig. 2. Size calibration graph for *Hae*III digest of ΦX174 DNA in 0.25% glucomannan. Conditions as in Fig. 1a.

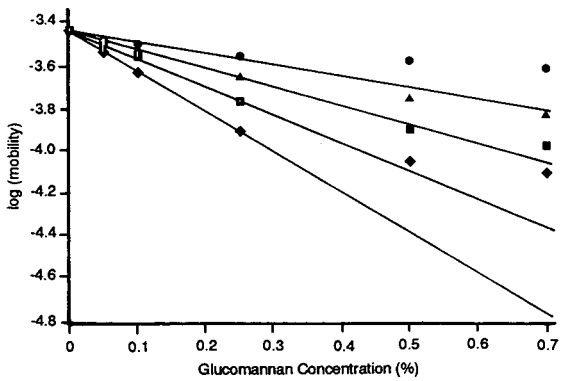

Fig. 3. Ferguson plots for entangled glucomannan solution. The lines represent the mobility of *Hae*III fragments of ΦX174 DNA as a function of glucomannan concentration (%, w/w). ○ = 72; ▲ = 310; □ = 603; ◆ = 1353 base pairs. Conditions as in Fig. 1a.

$$\log \mu = \log \mu_0 - k_R c \quad (1)$$

where μ is the measured mobility ($cm^2/V \cdot s$), μ_0 is the mobility in free solution, k_R is the slope (called the retardation coefficient) and c is the glucomannan concentration (%). The value of the retardation coefficient, k_R, is varied from −0.47 for the 72 base pair fragment to −1.9 for the 1353 base pair fragment. These values decrease with increasing size of the fragments, suggesting sieving of the DNA fragments in the entangled glucomannan solution. However, at glucomannan concentrations higher than 0.25%, these DNA fragments exhibit larger values of the mobility than those estimated from the above equation. Whether this is caused by changes in the conformation of DNA or in the structure of the glucomannan matrix awaits further investigation.

Reproducibility

The stability and reproducibility of the glucomannan-filled capillary were examined using the *Hae*III digest of ΦX174 DNA. In this experiment, electrophoresis was performed repeatedly with a single capillary without refilling the glucomannan solution. The capillary could be used for at least four analytical cycles without a detectable alteration in separation performance (Fig. 4a,b). The profile was similar even after ten consecutive analytical cycles, except that the separation between the two small fragments, of 271 and 281 base pairs, became insufficient (data not shown). A significant deterioration in peak resolution was observed after the fourteenth cycle, in which the fragments smaller than 281 base pairs were not separated (Fig. 4c). Fig. 4c also shows that the migration time of each fragment gradually decreased during the series of analytical cycles. However, the performance of the capillary was restored completely by refilling it with fresh glucomannan solution (Fig. 4d). The capillary exhibited a run-to-run reproducibility in migration time of 0.7% ($n = 5$) and a day-to-day reproducibility of 2.4% ($n = 5$) for the 1353 base pair peak. These results suggest that the glucomannan-filled capillary can be used for pattern analysis about ten times with satisfying performance of the separation without refilling and is also usable for further analysis such as the determination of the size of DNA frag-

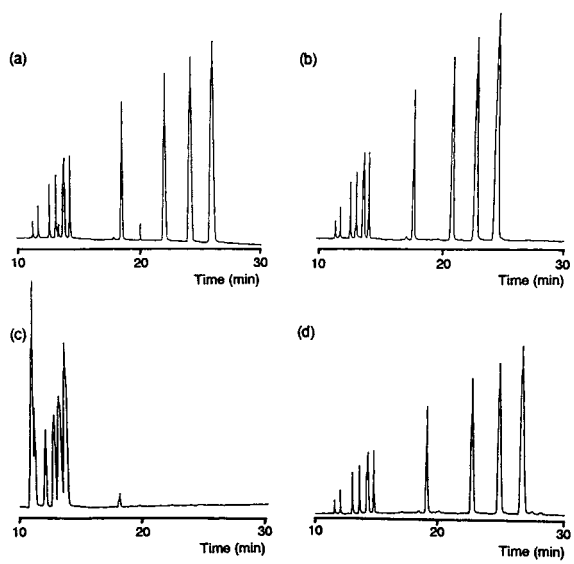

Fig. 4. Stability of the glucomannan-filled capillary. Sample: *Hae*III digest of ΦX174 DNA. The glucomannan-filled capillary was used repeatedly without refilling: (a) cycle 1; (b) cycle 4; (c) cycle 14. After the fourteenth analytical cycle, the capillary was refilled with the glucomannan solution, and the pattern of cycle 1 is shown in (d). All other conditions as in Fig. 1a.

ments directly from the migration time by replacing it.

Application to the analysis of plasmid DNA and PCR product

The glucomannan-filled capillary was applied to the analysis of plasmid DNA and its restriction fragments. Bluescript II SK(+) is a closed 2961 base pair DNA and produces four fragments of 166, 409, 540 and 1846 base pairs on digestion with *Dde*I. As shown in Fig. 5a, this 2961 base pair plasmid DNA appeared as a broad peak at 34.1 min, following some impurities at 14–15 min present in the commercial preparation. After digestion for 1 h with *Dde*I, the intact DNA disappeared and four fragments were generated (Fig. 5b). Based on the calibration graph in Fig. 2, the size of each fragment was estimated as 186 base pairs for peak 1, 440 base pairs for peak 2, 578 base pairs for peak 3 and 2000 base pairs for peak 4. These values are in good agreement with the size of the restriction fragments expected from the sequence of this plasmid DNA as described above, although the use of internal standards, such as the *Hae*III digest of ΦX174 DNA, allowed a more precise estimation of the size of the fragments. The rough estimation of the size of separated DNAs is even satisfactory for practical gene cloning studies.

The product of the polymerase chain reaction (PCR) of the η-chain of the brain 14–3–3 protein

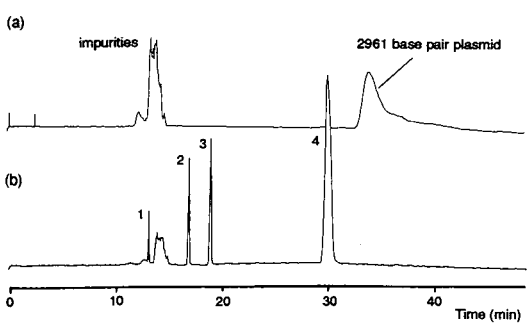

Fig. 5. Analysis of plasmid DNA and its restriction digest. Sample: Bluescript II SK(+), (a) before digestion and (b) after digestion with *Dde*I for 1 h. The digest was desalted and concentrated as described under Experimental and subjected to electrophoresis. Conditions as in Fig. 1a.

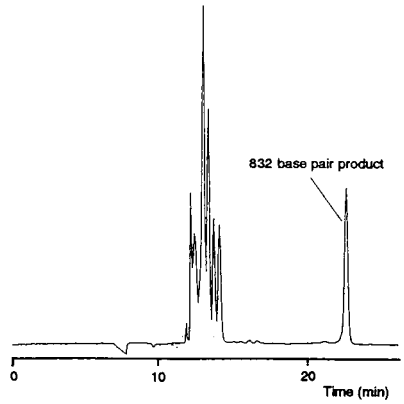

Fig. 6. Analysis of polymerase chain reaction (PCR) product. PCR product of η-chain of brain 14–3–3 protein prepared as described under Experimental was directly injected. Conditions as in Fig. 1a.

[15] was also analysed by the present method (Fig. 6). Following six peaks at 12–14 min due to NTPs and PCR primers, a single peak was detected at 22.5 min. From the migration time, the size of the product was estimated to be 822 base pairs. This value is close to the theoretical size of the fragment (832 base pairs), suggesting that the PCR procedure generated a single DNA as we expected.

CONCLUSIONS

This is the first report to describe the use of glucomannan in capillary electrophoresis. The entangled glucomannan solution, prepared easily under the mild conditions, was stable for at least several months and could be used as a sieving additive for capillary electrophoresis. The glucomannan-filled capillaries exhibited a size-dependent separation of DNA fragments. Because of its excellent resolution and reasonable reproducibility, the method should be applicable to the separation and analysis of a wide range of DNA samples such as plasmid DNA, restriction DNA fragments and PCR products. In addition, because glucomannan has two physical states, solution and gel, future studies may provide valuable information on the sieving mechanism of DNA fragments in electrophoresis.

ACKNOWLEDGEMENTS

The authors thank Dr. M. Senda, JASCO (Hachiouji, Tokyo, Japan), for providing the CE-800 capillary electrophoresis system. This work was supported in part by a grant-in-aid from the Human Science Foundation (Tokyo, Japan).

REFERENCES

1 P. Delmotte, *Sci. Tools*, 24 (1977) 33.
2 C.J. Holloway and W. Heil, in R.C. Allen and P. Arnaud (Editors), *Electrophoresis '81*, Walter de Gruyter, Berlin, 1981, p. 753.
3 K. Kojima, T. Manabe and T. Okuyama, in H. Hirai (Editor), *Electrophoresis '83*, Walter de Gruyter, Berlin, 1983, p. 511.
4 G. Schmitz, U. Borgman and G. Assmann, *J. Chromatogr.*, 320 (1985) 253.
5 T. Manabe, H. Yamamoto and T. Okuyama, *Electrophoresis*, 10 (1989) 172.
6 H. Yamamoto, T. Manabe and T. Okuyama, *J. Chromatogr.*, 480 (1898) 331.
7 T. Izumi, T. Nagahori and T. Okuyama, *J. High Resolut. Chromatogr.*, 14 (1991) 351.
8 D.N. Heiger, A.S. Cohen and B.L. Karger, *J. Chromatogr.*, 516 (1990) 33.
9 M. Zhu, D.L. Hansen S. Burd and F. Gannon, *J. Chromatogr.*, 480 (1989) 311.
10 H.E. Schwartz, K.J. Ulfelder, F.J. Sunzeri, M.P. Busch and R.G. Brownlee, *J. Chromatogr.*, 559 (1991) 267.
11 B.L. Karger, A.S. Cohen and A. Guttman, *J. Chromatogr.*, 492 (1989) 585.
12 K. Nishida and H. Hashima, *J. Dep. Agric. Kyushu Imp. Univ., Fukuoka, Jpn.*, 2 (1930) 277.
13 S. Ogasawara, H. Yamazaki and W. Nunomura, *Seibutsu Butsuri Kagaku*, 31 (1987) 155.
14 B. Sugiyama, H. Shimahara and T. Andoh, *Bull. Chem. Soc. Jpn.*, 45 (1972) 561.
15 T. Isobe, T. Ichimura, T. Sunaya, T. Okuyama, N. Takahashi, R. Kuwano and Y. Takahashi, *J. Mol. Biol.*, 217 (1991) 125.
16 T. Hata, Y. Ohno and S. Toda, *Kougyou Kagaku*, 54 (1951) 105.
17 F. Sanger, A.R. Coulson, T. Friedmann, G.M. Air, B.G. Barrell, N.L. Brown, J.C. Fiddes, C.A. Hutchison, III, P.M. Slocombe and M. Smith, *J. Mol. Biol.*, 125 (1978) 225.
18 K.A. Ferguson, *Metabolism*, 13 (1964) 1985.
19 A.T. Andrews, *Electrophoresis*, Clarendon Press, Oxford, 2nd ed., 1986.

Journal of Chromatography A, 652 (1993) 47–56
Elsevier Science Publishers B.V., Amsterdam

CHROM. 25 202

Separation of DNA restriction fragments by polymer-solution capillary zone electrophoresis

Influence of polymer concentration and ion-pairing reagents

Ram P. Singhal* and Jun Xian

Chemistry Department, Wichita State University, 1845 N. Fairmount Street, Wichita, KS 67260-0051 (USA)

ABSTRACT

To achieve sensitive and fast separations of the DNA fragments, polymer-solution capillary zone electrophoresis (PS-CZE) is examined. A systematic study of the influence of the linear polymer concentration on the separation of restriction fragments indicates that the larger DNA fragments are resolved with greater efficiency by using a lower concentration of the polymer, while the smaller ones are better resolved with a higher polymer concentration, when added to the buffer. A specific concentration of the polymer provides a certain limit of dynamic "porosity" (sieving), which is appropriate for a given range of the DNA fragments.

Several ion-pairing reagents are examined here to improve resolutions of both small and large DNA fragments in PS-CZE. These reagents cause no interactions between the ammonium cations (reagent) and the silanol groups (capillary surface). However, they interact with the linear polymer, perhaps by hydrophobic functions, and change its physical properties, such as dynamic viscosity and sieving ability. Enhanced retention (interactions) of the DNA fragments is observed by increasing the ion-pairing contents in the polymer solution. The increased peak retention strongly suggests presence of interactions between the reagent and the DNA fragments. Different ion-pairing reagents produce different degrees of peak retentions. The interactions results from relatively *greater* hydrophobic interactions and *smaller* ionic interactions between the reagent and the polynucleotides.

The study of ethidium bromide (EdBr) additon in PS-CZE indicates that a small concentration of EdBr reduces peak widths and decreases retention of all the fragments, but has little influence on the electroosmotic flow. However, a larger EdBr concentration results in broader peak widths and causes little change in their retention. Ion-pairing and intercalating reagents interact with the DNA fragments by different mechanisms. An anion-pairing agent appears to interact predominantly by hydrophobic interactions with the purine and pyrimidine bases, while EdBr intercalates with G:C base pairs and alter the chain length.

Satisfactory separations of *both* larger and smaller fragments can be achieved by adding an appropriate ion-pairing reagent along with the linear polymer to the buffer. Critical concentrations of the linear polymer and the ion-pairing reagent must be determined in order to achieve satisfactory separations for a given range (size) of the DNA fragments.

INTRODUCTION

Non-cross-linked polymers have been used as sieving media, such as in centrifugation and electrophoresis to yield a sieving medium in capillary zone electrophoresis (CZE) [1,2]. This "polymer-solution capillary zone electrophoresis" (PS-CZE) involving the use of a free polymer in the solution has not been fully exploited for the separation of proteins and nucleic acids. The cross-linked gel matrix in classical polyacrylamide gel electrophoresis

* Corresponding author.

0021-9673/93/$06.00

(PAGE) offers an anticonvective medium to prevent convection of analytes which may result from Joule heating and a sieve for size exclusion (size-dependent separation). The heat dissipation in CZE is achieved because of tiny capillary with large surface-to-volume ratio, *i.e.* Joule heat is well dissipated and natural convection is not a problem. The linear polymers offer sieving similar to that of a gel-based system. The separation of DNA fragments have recently been achieved in dilute polymer solutions with the use of a linear chain polymer, but without the aid of a cross-linked gel matrix [3–6]. Polyacrylamide [4], methylcellulose and hydroxypropylmethylcellulose [3] have been employed as sieving agents in PS-CZE for the separation of oligonucleotides and DNA fragments. The separation of nucleic acids by PS-CZE offers size-based separations, and has several advantages over capillary-gel CE (CGE). The technique is simple, fast, and offers a variety of sieving systems without requiring a change of the capillary. In order to enhance DNA separations in PS-CZE, as well as in CGE, efforts have been made to complex DNA fragments by intercalation with ethidium bromide (EdBr) [7,8]. (For full details on PS-CZE and CGE of nucleic acids, see a recent review article, ref. 9.)

The effect of linear polymer concentrations on the separation of restriction endonuclease DNA fragments is studied here. Interactions of ion-pairing reagents with DNA fragments, a linear polymer, and the capillary surface are examined. A series of ion-pairing reagents are employed for this purpose. Effects of ion-pairing reagents are compared with those of the EdBr and mechanisms of interactions of both additives are discussed here.

EXPERIMENTAL

Materials

The DNA restriction fragments mixtures, ΦX174 DNA/*Hae*III digest and pGEM-3 DNA/*Hinf*I, *Rsa*I and *Sin*I digest were obtained from Promega (Madison, WI, USA). Samples were diluted with water to 0.2 mg/ml before injection and stored at −20°C. Hydroxyethyl cellulose, tetrabutylammonium dihydrogenphosphate (TBAP) and tetrahexylammonium bromide (THAB) were from Aldrich (Milwaukee, WI, USA). Tetramethylammonium hydroxide (TMAH), triethylamine (TEA), and EdBr were from Sigma (St. Louis, MO, USA) and Fisher Scientific (Fair Lawn, NJ, USA). Buffer solutions were pre-filtered through a 0.2-μm pore filter (Gelman, Ann Arbor, MI, USA).

Capillary zone electrophoresis system

The CE equipment, designed in this laboratory [10], consisted of the following four basic components: (a) A polyimide-coated fused-silica capillary tubing [80 cm × 75 μm I.D. × 280 μm O.D., 30 (or 50) cm effective length]; anodic reservoir electrically grounded. (b) A specifically designed on-line Z-shaped flow cell with a light path of 3 mm (LC Packing, San Francisco, CA, USA). (c) A variable-wavelength UV monitor (Spectroflow 757; Kratos Analytical Instruments, Ramsey, NJ, USA), which was modified to accommodate the above mentioned flow cell. (d) A high-voltage power supply (0 to 30 kV) with features of programmable, reversible-polarity output (Bertan, Hicksville, NY, USA). The direction of the solution flow during the CE was changed by simply changing the electrode polarities. The electric current was monitored by a digital multimeter (John Fluke, Everett, WA, USA). An elution pump (Waters, Milford, MA, USA) was used for washing the column and initiating the sample injection. The signals from the detector were fed to a strip-chart recorder for instant monitoring of the results. In addition, data were acquired with an IBM-compatible personal computer by using an analog-to-digital interface, and retrieved with the help of Nelson Analytical (Cupertino, CA, USA) software. Sample was injected from the anode side and the detector installed on the cathode side. The operation temperature was controlled at 20 ± 0.5°C.

Diverse methods

The electroosmotic flow measurement was carried out according to the method of Lukacs and Jorgenson [11]; phenol was used as a neutral marker. The injected volume was established by introducing a standard solution of adenosine and determining its concentration from the peak area as a function of time. The specific viscosity of the solutions containing polymer of different concentrations was measured by using an Ostwald

viscometer in relation to pure water at 20 ± 0.5°C [5,12].

Equipment operation

The capillary column was first washed by pumping a buffer through it and allowing the pressure to reach a constant value. The liquid flow was then disconnected and the capillary dipped into the sample contained in a miniature conical polyethylene tube. The positive liquid flow current generated by the pump and the gravitational force were enough to allow introduction of the sample into the fine capillary column. The sample flow was allowed for a specific time (between 5 and 20 s). This method of sample application was found to be very reproducible. For example, a 20-s injection introduced 7.9 nl of the sample into the capillary column. This value having a standard deviation of 0.05, was based on six different injections.

RESULTS

The effect of a linear polymer concentration on the separation of DNA fragments

The separation of DNA fragments derived from ΦX174 digested with restriction endonuclease *Hae*III is shown in Fig. 1. Panels a, b and c show these separations while using an increasing amount of hydroxyethylcellulose (HEC). The results indicate that larger DNA fragments [1353 base pairs (bp) to 872 bp, peaks 1 to 3] are resolved with greater efficiency by employing a lower HEC concentration (0.25%), while the smaller ones (234 bp to 72 bp, peaks 7 to 11) are resolved with significantly enhanced resolutions by adding a higher polymer concentration to the buffer (0.50% to 0.75% HEC). The polymer provides a certain range of dynamic "porosity" (sieving effect) for the DNA fragments. Though larger fragments fail to resolve with a higher concentration of the polymer, the smaller ones undergo fractionation. Similarly, larger fragments tend to fractionate with a lower polymer concentration, but the smaller ones fail to resolve.

The effect of ion-pairing reagents in CZE

The effect of ion-pairing reagents on electroosmotic flow, and also on the emergence of unresolved DNA fragments from the capillary, is shown in Table I. None of the four ion-pairing reagents alters the electroosmotic flow in CZE,

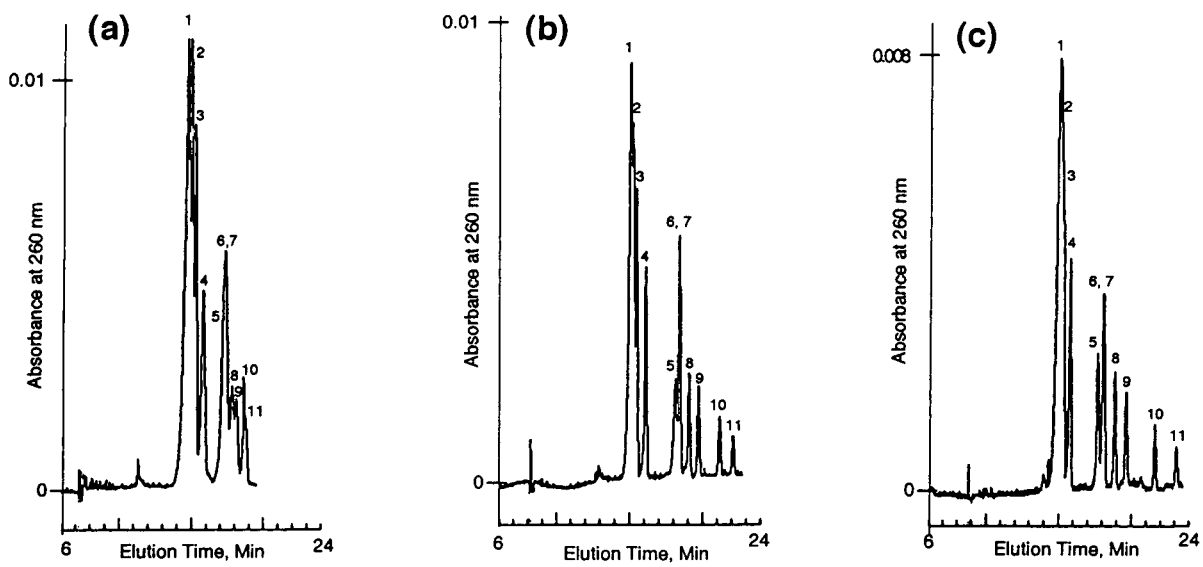

Fig. 1. The separation of ΦX174 DNA/*Hae*III fragments with different concentrations (w/v) of hydroxyethylcellulose (HEC): (a) 0.25%, (b) 0.5% and (c) 0.75%. Buffer, in addition to HEC, contained 50 m*M* Tris–borate, 2 m*M* EDTA and 7 *M* urea, pH 8.85. The column was an untreated capillary, 80 cm × 75 μm I.D. (effective length, 50 cm); applied voltage, 250 V/cm; detection at 260 nm, 20°C. Approximately 1.6 ng of the sample was injected. The peak numbers correspond to various DNA fragments of the listed base pairs (peak No.): 1353 (1), 1078 (2), 872 (3), 603 (4), 310 (5), 281, 271 (6,7), 234 (8), 194 (9), 118 (10) and 72(11).

TABLE I

EFFECT OF ION-PAIRING REAGENTS IN CZE

Ion-pairing reagent[a]	Electroosmotic flow[b] (±0.05)	Retention time (min)[c] (±0.1)
None[a]	4.3	20.4
Triethylamine, 5 m*M*	4.2	23.8
Tetramethylammonium hydroxide, 5 m*M*	4.3	23.2
Tetrabutylammonium dihydrogenphosphate, 5 m*M*	4.3	26.4
Tetrahexylammonium bromide, 5 m*M*	4.3	21.4

[a] Buffer contained 50 m*M* Tris–borate, 2 m*M* EDTA and 7 *M* urea, pH 8.85.
[b] Electroosmotic flow is expressed in $cm^2\ V^{-1}\ s^{-1} \times 10^{-4}$.
[c] Emergence of unresolved pGEM DNA fragments.

suggesting that no interaction occurs between the ammonium cations (weak acid) and silanol groups (weak base). The bulky alkyl chains can prevent this interaction with the capillary surface.

Polymer addition progressively decreases the electroosmotic flow, but dramatically increases the solution viscosity. For example, three HEC concentrations (0.25, 0.50 and 0.75%) produced electroosmotic flow values of 4.13, 3.89 and $3.71 \cdot 10^{-4}$ $cm^2\ V^{-1}\ s^{-1}$, respectively; and relative viscosity of 1.66, 3.82 and 7.26, respectively. The loss in electroosmotic flow is apparently caused by an increase in the viscosity, thus lowering the "bulk movement" of the solution in CZE.

Different reagents retain the DNA fragments for different times in CZE, although the ion-pairing reagents have no resolving power (all fragments emerge unresolved). In each case, the fragments are retained for a longer period of time than the buffer itself. The increased reten-

TABLE II

EFFECT OF ION-PAIRING REAGENTS ON ELECTROOSMOTIC FLOW IN PS-CZE

Ion-pairing reagent[a]	Concentration (m*M*)	Electroosmotic flow[b]
None[a]	0	3.9
Triethylamine	3	3.6
Triethylamine	5	3.6
Triethylamine	7	3.6
Tetramethylammonium hydroxide	1	3.8
Tetramethylammonium hydroxide	3	3.6
Tetramethylammonium hydroxide	5	3.6
Tetrabutylammonium dihydrogenphosphate	1	3.8
Tetrabutylammonium dihydrogenphosphate	3	3.6
Tetrabutylammonium dihydrogenphosphate	5	3.4
Tetrabutylammonium dihydrogenphosphate	7	3.2
Tetrahexylammonium bromide	1	3.7
Tetrahexylammonium bromide	3	3.5
Tetrahexylammonium bromide	5	3.5

[a] Buffer contained 50 m*M* Tris–borate, 2 m*M* EDTA, 7 *M* urea and 0.5% hydroxyethylcellulose, pH 8.85.
[b] Electroosmotic flow is expressed in $cm^2\ V^{-1}\ s^{-1} \times 10^{-4}$.

tion strongly suggests interactions between the reagent and the DNA fragments (for nature of this interaction, see Discussion).

The effect of ion-pairing reagents in PS-CZE

The ion-pairing reagents exhibit no influence on the electroosmotic flow as observed in Table I. However, some reduction in the electroosmotic flow is observed when the reagent is added with a linear polymer (0.5% HEC) to the buffer. This loss in electroosmotic flow (2 to 22%), as shown in Table II, is directly related to the amount of the ion-pairing reagent present in the polymer solution.

The effect of ion-pairing reagents on the retention of DNA fragments in PS-CZE

The separation of eleven DNA fragments, derived from ΦX174/*Hae*III, are examined in the presence of four different ion-pairing reagents, and with several concentrations of each reagent. The results, shown in Fig. 2, confirm enhanced retention (interactions) of DNA fragments with increasing amounts of the ion-pairing reagent in the polymer solution. Different ion-pairing reagents produce different degrees of retention enhancement. Once a critical concentration of the reagent is achieved (such as 5 m*M* TBAP), no significant enhancement in their resolutions can be attained by further addition of the reagent (Fig. 2a).

TEA, in excess of 1 m*M* concentration, fails to show any improvement in resolution (Fig. 2b). Though the addition of TMAH and THAB enhances resolution, TBAP provides the most dramatic improvement in resolutions for these DNA fragments (compare Fig. 2c and d with a).

The effect of intercalation of G:C base pairs with EdBr on electroosmotic flow and retention of DNA fragments in PS-CZE

The results in Table III indicate that a small concentration of EdBr reduces peak widths and decreases retention of all the fragments, but has little influence on the electroosmotic flow. However, a larger EdBr concentration, such as 0.15 m*M*, results in broader peak widths and causes little change in their retention. With EdBr as an additive, the larger DNA fragments fail to resolve and all the fragments emerge earlier than in the absence of EdBr. Though the separation of the large DNA fragments is not favorably influenced, the fragments of 271 bp and 281 bp are partially resolved in the presence of >60 μM EdBr. In general, small concentrations of EdBr tend to make the peaks sharper, but a larger concentration produces broader peaks. The ion-pairing reagent, such as TBAP, alone appears to resolve both larger and smaller DNA fragments and produces moderate peak widths, but retains the peak longer. A combination of EdBr and TBAP slightly decreases the electroosmotic flow, broadens all the peaks, and prolongs peak emergence from the column.

Examples of the separation of DNA fragments with a combination of an ion-pairing agent and a linear polymer by PS-CZE

Results in Fig. 3 indicate improvement in the resolution of the DNA fragments with the addition of an ion-pairing reagent, such as TBAP. Satisfactory separations of *both* larger and smaller DNA fragments are observed with the addition of an appropriate ion-pairing reagent along with the linear polymer to the buffer. A lower concentration of the reagent (3 m*M* TBAP) can be employed if the capillary length is increased (Fig. 3a). Conversely, the use of a shorter capillary (30 cm) requires a higher concentration of the reagent (Fig. 3b).

Another example of the separation of DNA fragments (pGEM-3 digested with restriction endonucleases *Hind*I, *Rsa*I and *Sin*I) by PS-CZE involving a combination of an ion-pairing agent and a linear polymer is shown in Fig. 4. The addition of the ion-pairing reagent, such as TBAP, improves resolution of *both* larger and smaller DNA fragments, ranging from 36 to 2645 bp.

Comparison of separations achieved by two different detection methods

A flow cell of Z-type (light path, 3 mm) used in this study, offers significant detection sensitivity by UV absorption, for example the detection of 8 ng (0.8 fmol or 71 n*M*) DNA fragments. However, the fragments differing by a small chain length (such as 179 bp from 222 bp fragments) could not be resolved while employing a

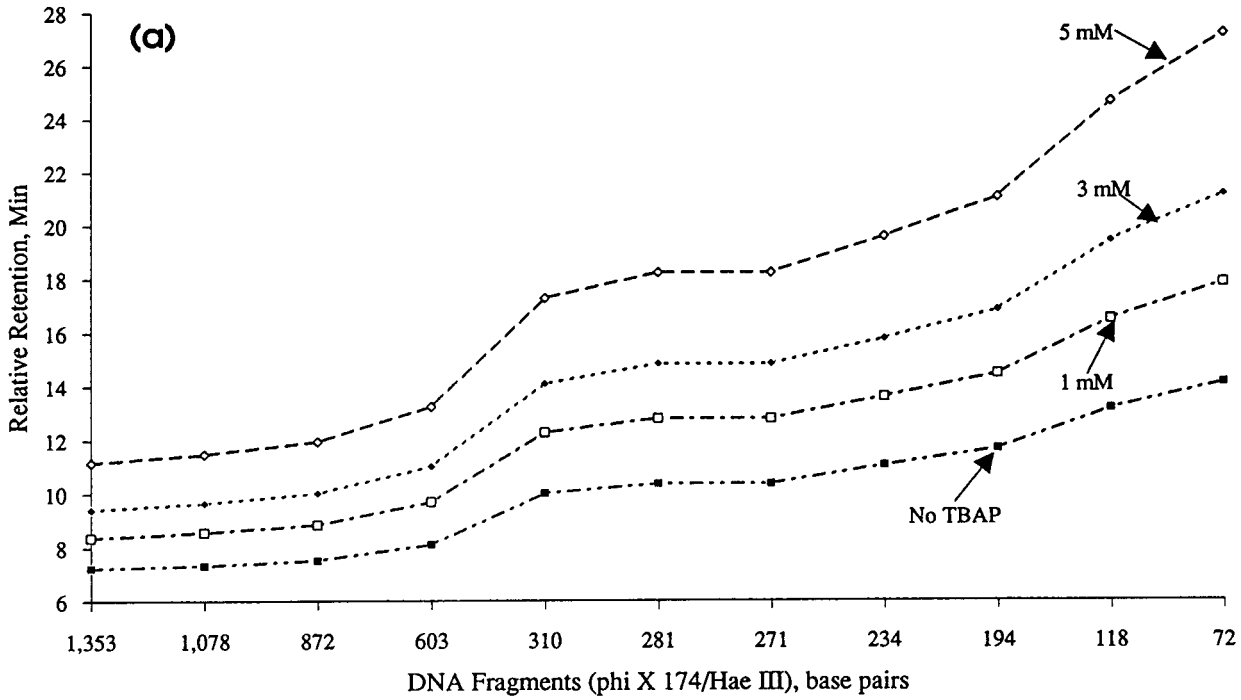
(a)
Relative Retention, Min
28
26
24
22
20
18
16
14
12
10
8
6
5 mM
3 mM
1 mM
No TBAP
1,353
1,078
872
603
310
281
271
234
194
118
72
DNA Fragments (phi X 174/Hae III), base pairs

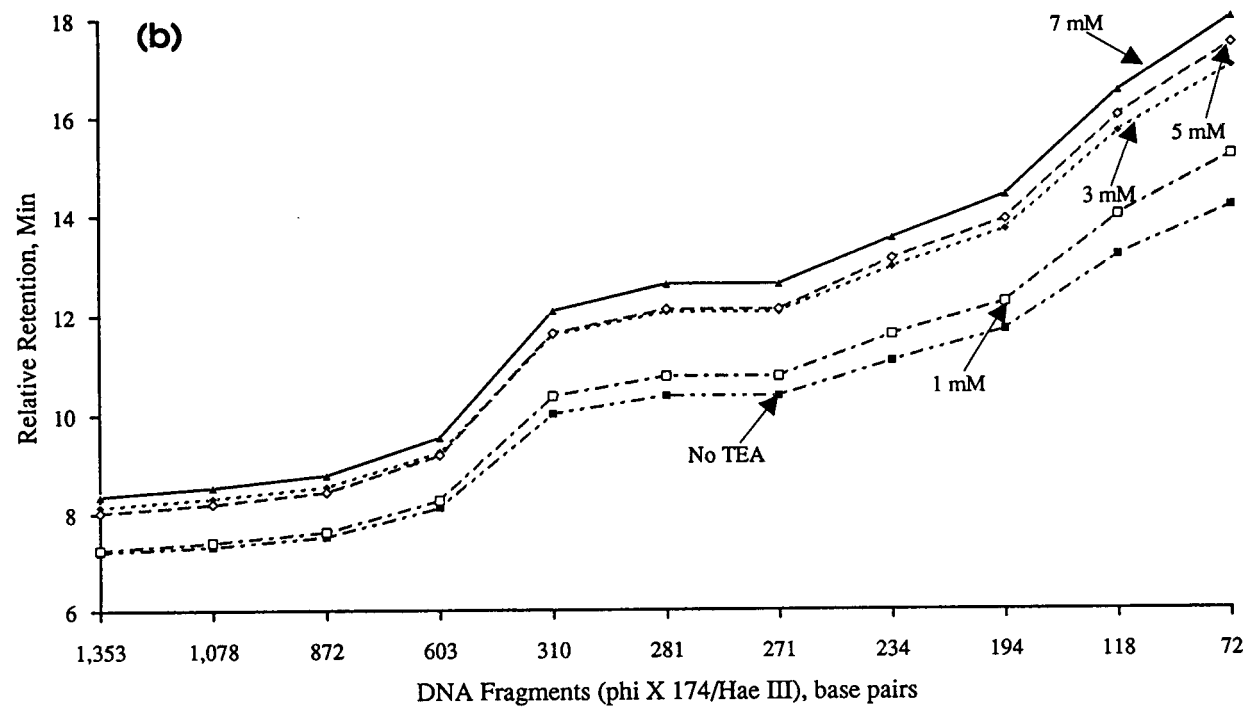
(b)
Relative Retention, Min
18
16
14
12
10
8
6
7 mM
5 mM
3 mM
1 mM
No TEA
1,353
1,078
872
603
310
281
271
234
194
118
72
DNA Fragments (phi X 174/Hae III), base pairs

Fig. 2.

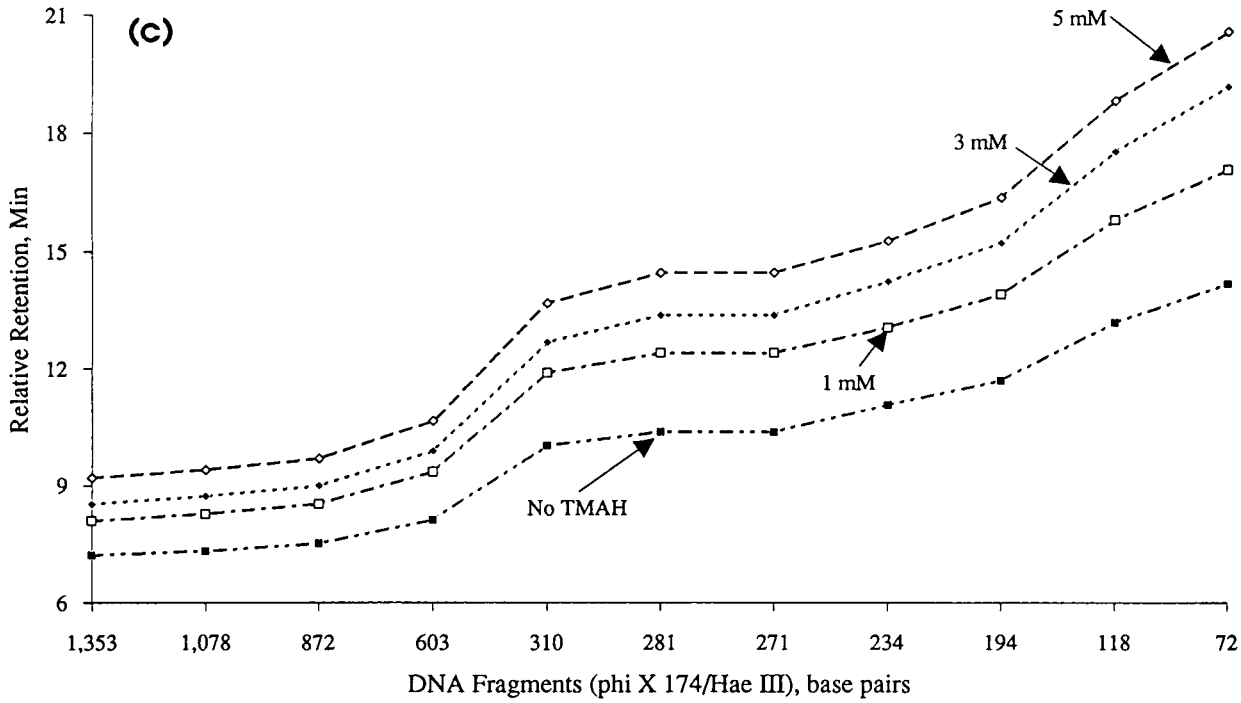

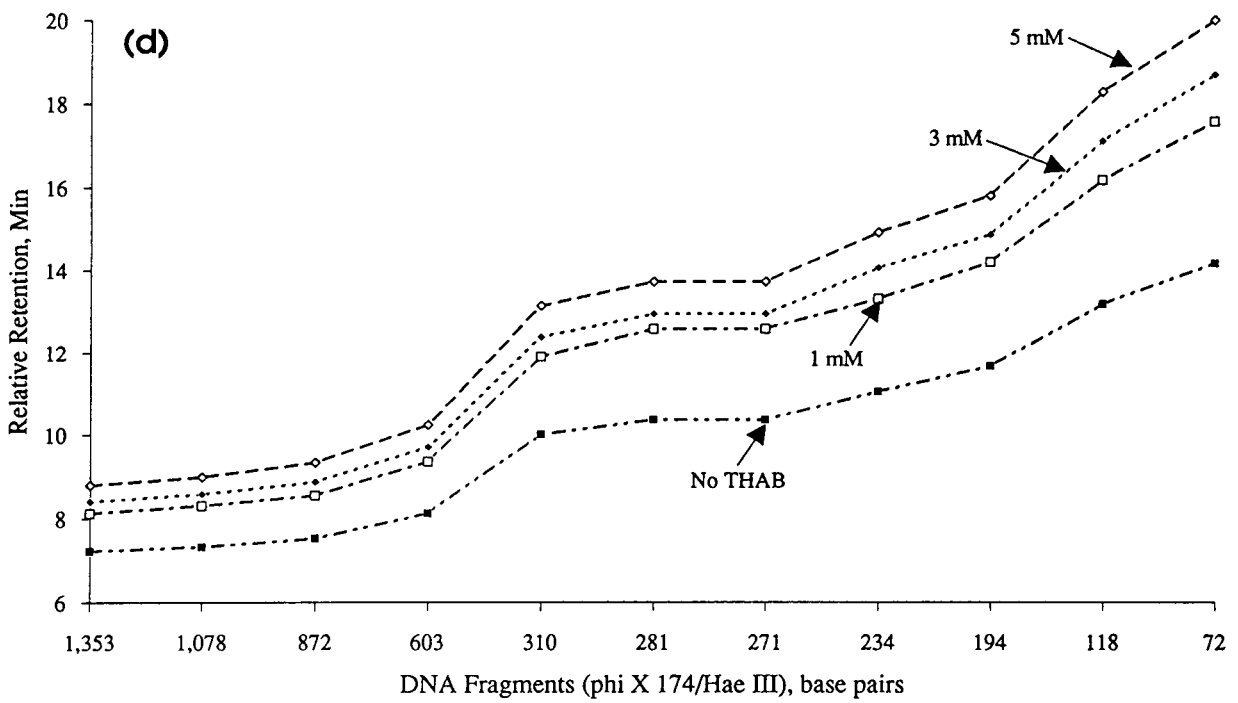

Fig. 2. The emergence of ΦX174 DNA/*Hae*III fragments in the presence of different ion-pairing reagents: (a) TBAP, (b) TEA, (c) TMAH and (d) THAB. The buffer contained 0.5% HEC; for other experimental details, see caption to Fig. 1. The relative retention time is expressed as $t_R - t_0$, where t_0 is the front peak of benzene and t_R is the retention of the DNA fragment.

TABLE III

EFFECT OF ETHIDIUM BROMIDE ADDITION ON THE SEPARATION OF DNA FRAGMENTS

Additive[a]	Concentration	Electroosmotic flow[b]	Peak width (min)[c], DNA fragments			Relative retention time (min)[d], DNA fragments		
			603 bp	194 bp	72 bp	603 bp	194 bp	72 bp
None	0	3.5	0.36	0.32	0.36	10.2	17.0	21.6
Ethidium bromide	1 μM	3.4	0.28	0.30	0.26	10.5	16.9	22.6
Ethidium bromide	60 μM	3.4	0.26	0.17	0.22	8.2	13.4	19.2
Ethidium bromide	150 μM	3.3	0.37	0.42	0.23	7.9	13.0	19.2
Ethidium bromide and TBAP	60 μM 5 mM	3.1	0.38	0.33	0.37	10.7	18.2	27.5
TBAP	5 mM	3.4	0.31	0.28	0.31	13.3	21.1	27.2

[a] Buffer contained 50 mM Tris–borate buffer, 2 mM EDTA, 7 M urea, 0.5% hydroxyethyl cellulose, and any additive, pH 8.85.
[b] Electroosmotic flow is expressed in $cm^2\ V^{-1}\ s^{-1} \times 10^{-4}$.
[c] Peak widths at half-maximum height of the fragments derived from ΦX174 DNA.
[d] Relative retention time is expressed as $t_R - t_0$, where t_0 is the front peak of benzene and t_R is the retention of the DNA fragment.

flow cell of such a large volume (13.3 nl). A commercially available detector (Isco Model CV[4]) having a light path of the capillary diameter (75 μm) also produced identical separations, but exhibited approximately five times less sensitivity. However, the plate numbers were substantially increased (such as, from 33 000 to 70 000) with the use of the narrow-bore light path detector.

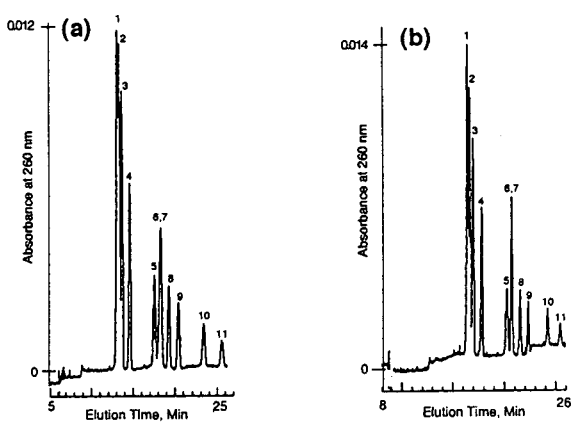

Fig. 3. The separation of ΦX174 DNA/*Hae*III fragments with different TBAP concentrations and column lengths: (a) 3 mM TBAP, 50 cm effective column length and (b) 5 mM TBAP, 30 cm effective column length. The buffer contained 0.5% HEC; for other experimental details and peak identities, see caption to Fig. 1.

DISCUSSION

DNA fragments in PS-CZE (uncoated capillaries) migrate upstream (towards the injector),

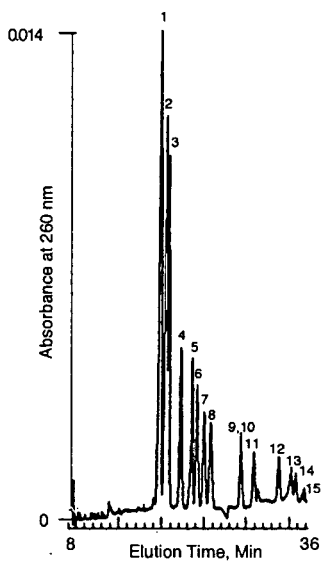

Fig. 4. The separation of pGEM-3 DNA (digested with restriction endonucleases *Hind*I, *Rsa*I and *Sin*I) fragments. The buffer contained 0.5% HEC and 5 mM TBAP; for other experimental details, see caption to Fig. 1. Approximately 8 ng of the sample were injected. The peak numbers correspond to various DNA fragments of the listed base pairs (peak No.): 2645 (1), 1605 (2), 1198 (3), 676 (4), 517 (5), 460 (6), 396 (7), 350 (8), 222, 179 (9,10), 126 (11), 75 (12), 65 (13), 51 (14), 36 (15).

against electroosmotic flow due to the anionic charges of the phosphate groups which are present in the DNA molecule. The electrophoretic mobility and electroosmotic flow are of unequal strength; the electroosmotic flow exerts a greater velocity and tends to *sweep* or *comb* the molecules towards the detector (cathode). Consequently, the larger fragments exit prior to the smaller ones even though the former fragments exhibit a greater degree of negative (phosphate) charge than the smaller fragments.

The interaction between the ion-pairing reagent and the DNA fragments can occur in two ways. One involving an ionic interaction between the phosphate anions (polynucleotides) and the ammonium cations of the reagent. The other attraction can involve hydrophobic interactions between the purine and pyrimidine bases and the alkyl chains of the reagent. These interactions, singly or in combination, produce a DNA–reagent complex, having a greater molecular mass and diminished anionic character, *i.e.* electrophoretic migration. Though a loss in the electrophoretic migration should decrease the peak retention, the electroosmotic flow remains unaltered. Therefore, the enhanced retention is the result of relatively *greater* hydrophobic interactions and *smaller* ionic interactions. For example, TEA and TMAH influence DNA separations similarly; both reagents have similar alkyl chains (hydrophobicity), while they exhibit significantly different cationic charges at pH 8.8.

The ion-pairing reagents apparently interact with the linear polymers, perhaps by hydrophobic interactions, and change their physical properties, such as dynamic viscosity and dynamic "porosity". Besides the concentration effect, different ion-pairing reagents appear to influence the electroosmotic flow differently; for example, compare the effect of TEA with that of TBAP in Table II.

A critical concentration of the linear polymer must be determined for satisfactory separation of a given range (size) of the DNA fragments. Though an increase in the polymer concentration enhances resolution of the smaller fragments, increased viscosity can make the operation impractical. A moderate concentration of 0.5% HEC (relative viscosity of 3.82) appears to be appropriate for the separation of both ranges of the DNA fragments from the two organisms used in this study. Nevertheless, no polymer concentration can resolve DNA fragments exhibiting only very small mass differences (such as 281 bp and 271 bp, peaks 6 and 7), at least under our detection system (3-mm flow cell, 13-nl volume).

Schwartz *et al.* [13] have studied the separation of DNA fragments with a polysiloxane-coated capillary and polymeric buffer additives. An addition of EdBr to the buffer solution results in longer migration times of the DNA fragments and better peak resolutions. The authors propose that in addition to the sieving effect, the linear polymer may cause an additional dynamic coating on the capillary surface, and consequently can suppress the electroosmotic flow. The results in Figs. 1 and 2 indeed confirm a loss in the electroosmotic flow when a linear polymer is added to the buffer.

An enhancement in the separation of the pBR322 plasmid fragments was observed with the addition of EdBr to a separation medium containing 0.5% HEC. DNA fragments differing only by a few base pairs can be resolved by the inclusion of EdBr [8]. Guttman and Cooke [7] have also observed enhancement in the separation of DNA fragments, ranging from 20 to 2000 bp by CGE with the addition of EdBr.

Our results in Table III confirm these observations in quantitative terms. The consequences of the two additives, an ion-pairing agent and an intercalating agent are also compared in Table III. These two reagents interact with the DNA fragments by different mechanisms. An anion-pairing agent appears to interact predominantly by hydrophobic interactions with the purine and pyrimidine bases, while EdBr intercalates with G:C base pairs and alters the chain length. EdBr can fill one site for every other base pair, thus increasing the DNA length (fully saturated DNA chain is increased by 50%) [14,15]. This increase in the chain length caused by EdBr appears to be the reason of early emergence of DNA fragments from the capillary column.

Application of different types of detection methods, *i.e.* light paths of 3 mm or 75 μm, surprisingly produced almost identical resolutions of the DNA fragments (Fig. 3b and Fig. 4), but the narrow-bore detector produced higher

efficiency (small peak widths). These results are thus repeatable irrespective of the instrument, origin of capillaries or type of detector.

In conclusion, a critical concentration of the linear polymer must be determined appropriate for the given range of DNA fragments. An ion-pairing reagent improves the resolution of the DNA fragments, but different reagents yield different degrees of enhancement. EdBr as an additive in PS-CZE, also improves resolution of the fragments, but by a different mechanism.

REFERENCES

1 D. Langevin and F. Rondelez, *Polymer*, 19 (1978) 875–882.
2 D. Tietz, M.H. Gotlieb, J.S. Fawcett and A. Crambach, *Electrophoresis*, 7 (1986) 217–220.
3 M. Zhu, D.L. Hansen, S. Burd and F. Gannon, *J. Chromatogr.*, 480 (1989) 311–319.
4 D.N. Heiger, A.S. Cohen and B.L. Karger, *J. Chromatogr.*, 516 (1990) 33–48.
5 P.D. Grossman and D.S. Soane, *J. Chromatogr.*, 559 (1991) 257–266.
6 R. Rodriguez, M. Zhu and T. Wehr, *Am. Biotech. Lab.*, Feb. (1992) 21–22.
7 A. Guttman and N. Cooke, *Anal. Chem.*, 63 (1991) 2038–2042.
8 S. Nathakarnkitkool, P.J. Oefner, G. Bartsch, M.A. Chin and G.K. Bonn, *Electrophoresis*, 13 (1992) 18–31.
9 R.P. Singhal and J. Xian, in D.M. Radzik and S.M. Lunte (Editors), *Application of Capillary Electrophoresis to Pharmaceutical and Biochemical Analysis*, Pergamon, Oxford, in press.
10 R.P. Singhal, D. Hughbanks and J. Xian, *J. Chromatogr.*, 609 (1992) 147–161.
11 K.D. Lukacs and J.W. Jorgenson, *J. High Resolut. Chromatogr. Chromatogr. Commun.*, 8 (1985) 407–411.
12 R.J. Sime, *Physical Chemistry: Methods, Techniques and Experiments*, Part 3, Saunders College Publishing, Philadelphia, PA, 1990, p. 522.
13 H.E. Schwartz, K. Ulfelder, F.J. Sunzeri, M.P. Busch and R.G. Brownlee, *J. Chromatogr.*, 559 (1991) 267–283.
14 C. Tsai, S.C. Jain and H.M. Sobell, *Proc. Natl. Acad. Sci., U.S.A.*, 72 (1975) 628–632.
15 H.M. Sobell, C. Tsai, S.C. Jain and S.G. Gilbert, *J. Mol. Biol.*, 114 (1977) 333.

Journal of Chromatography A, 652 (1993) 57–66
Elsevier Science Publishers B.V., Amsterdam

CHROM. 25 302

Separation of DNA fragments by capillary electrophoresis using replaceable linear polyacrylamide matrices

Y.F. Pariat, J. Berka[☆], D.N. Heiger[☆], T. Schmitt[☆☆], M. Vilenchik[☆☆☆], A.S. Cohen[☆☆☆], F. Foret[☆☆] and B.L. Karger*

Barnett Institute and Department of Chemistry, Northeastern University, 102 Hurtig Hall, 360 Huntington Avenue, Boston, MA 02115 (USA)

ABSTRACT

The use of low percent (1.5–6%T) replaceable linear polyacrylamide (LPA) network matrices for rapid separation of double-stranded DNA fragments was explored. Separations of fragments ranging from 20 to 23 000 base pairs were readily achieved. Typically, $4 \cdot 10^6$ theoretical plates/m were obtained in less than 30 min. Short separation times under 2 min were also possible, using the DNA intercalating dye, ethidium bromide, along with high electric fields. The high resolving power of linear polyacrylamide was demonstrated in the separation of two fragments which differ by a single base pair (123/124 base pairs) using 6%T LPA and ethidium bromide intercalation. This LPA composition allowed for the possible single base-pair resolution of dsDNA fragments up to 300 base pairs in length. Several concentrations of the linear polyacrylamide for different ranges of fragment lengths have been employed. In addition, replaceable LPA offers the advantage of a fresh separation matrix for each run, thus overcoming column stability problems and minimizing needs for sample cleanup. Electroosmotic flow was substantially reduced using stable capillary coatings, which were required for obtaining high efficiencies and good reproducibility.

INTRODUCTION

The separation of double-stranded DNA fragments is a basic requirement in recombinant DNA technology [1,2]. Improvements in resolution, speed, quantitation, and automation are among the characteristics that capillary electrophoresis offers relative to electrophoresis in the conventional slab gel format [3]. Due to the anti-convective nature of the walls of the capillary, low-viscosity sieving media which cannot normally be successfully applied to a slab may be employed for DNA separations, *e.g.* linear (*i.e.* noncrosslinked) polyacrylamide [4–6], cellulose and its derivatives [7–11], liquified low melting point agarose [12] or polyethylene glycol [13]. For a review on this topic see ref. 14.

For the most part, slab gel electrophoresis has been limited to the use of either agarose or crosslinked polyacrylamide or related polymeric matrices [15]. The mesh size of crosslinked polyacrylamide is generally too small to separate efficiently DNA fragments larger than 2000 base pairs (bp). While agarose slab gels are employed for both small (200–1000 bp) and large (up to 10 000 kbp) DNA molecule separations, resolution and speed are often insufficient. Capillary electrophoresis using crosslinked polyacrylamide gel filled capillaries provides high separation

* Corresponding author.
☆ Present address: Hewlett Packard, Waldbronn, Germany.
☆☆ Present address: University of Saarlandes, Saarbrücken, Germany.
☆☆☆ Present address: Hybridon, Inc., Worcester, MA, USA.

0021-9673/93/$06.00

efficiencies for synthetic single-stranded oligonucleotides and short restriction dsDNA fragments [16–18], but any stress conditions leading to a gel failure result in a need of the whole column replacement. For these reasons we continue our efforts in DNA separations using linear (*i.e.* noncrosslinked) polyacrylamide in capillary electrophoresis with the aim of a single base-pair resolution and extension of the size range of separated DNA fragments [4,5,19].

Linear polyacrylamide (LPA) has been shown to offer many desirable analytical characteristics and to provide for high resolving power. In this work we explore the use of linear polyacrylamide concentrations between 1.5 and 6%T.[a] These compositions have a low to moderate viscosity and can easily be refilled in the column. This replaceable matrix, as well as other commonly used polymer networks, increase the flexibility of capillary electrophoresis since problems such as polyacrylamide degradation or column fouling are eliminated. Moreover, these replaceable matrixes are simple to work with and yield reproducible results of high resolution.

EXPERIMENTAL

Equipment

The basic laboratory-made CE instrumentation has been previously described [4]. A 60 kV direct current power supply (Model PS/MK 60; Glassman, Whitehouse Station, NJ, USA) was used for continuous field electrophoresis. A UV–Vis spectrophotometer (Model 100; Spectra-Physics, San Jose, CA, USA) was employed at 260 nm to detect the DNA fragments. Column temperature was controlled by means of a water jacket connected to a heating/cooling thermostatic circulation water bath. Each end of the capillary was placed in buffer reservoirs (3 ml) with platinum wire electrodes. For all experiments, placing 3%T LPA in the reservoirs was found to be beneficial in avoiding ion depletion in the matrix with subsequent changes of current and migration times [20]. Buffer reservoirs were positioned at the same level and any coiling of the capillary after filling it with LPA was avoided to prevent the distortion of the structure of the low viscosity polymer networks [21].

Electrophoresis was performed in fused-silica capillaries (Polymicro Technologies, Phoenix, AZ, USA) of 50 and 75 μm I.D. and 360 μm O.D., which had a 2–4 mm portion of the polyimide coating removed for UV detection. The electropherograms were acquired at 5 Hz sampling rate using Turbochrom software (version 3.2) and stored on a IBM-compatible 486 DX-2 computer by means of an A/D converter interface (Model 762 SB, PE/Nelson, Cupertino, CA, USA).

Reproducibility experiments under controlled temperature conditions were performed using a Beckman P/ACE 2000 system (Palo Alto, CA, USA). It was operated in both the normal- and reverse-polarity configurations, depending upon the desired column length (*i.e.* the distance from the detector window to one of the reservoirs was fixed at 6.7 cm). Data were collected and integrated using Beckman System Gold software (version 403) and transferred to Lotus 1-2-3 (Cambridge, MA, USA) for further manipulation.

Capillary coating

The capillary coating was prepared according to Hjertén [22], cross-linked maltoside surfactant coating developed in this laboratory [40], or a recently developed procedure [23], using 6%T linear polyacrylamide. In the latter case, linear polyacrylamide is grafted to a highly cross-linked polymeric sublayer. Because all coatings suppress highly electroosmotic flow, differences in resolution and efficiency were not observed. However, the latter two procedures led to the longer column lifetimes [23].

Preparation of linear polyacrylamide

In this work, both laboratory polymerized and commercially available linear polyacrylamide were used. 6%T LPA matrices were prepared as follows: 6% (w/v) acrylamide solution was dissolved in 1 × TBE buffer (100 m*M* Tris, 100 m*M* boric acid, 2 m*M* Na_2EDTA, pH 8.4) and vacuum degassed for 2 h. Polymerization was initiated by adding 0.2% (v/v) N,N,N′,N′-tetramethylethylenediamine (TEMED) (Bio-Rad, Richmond, CA, USA) and 0.04% (w/v) am-

[a] T = [g acrylamide + g N,N′-methylenebisacrylamide (Bis)]/100 ml solution.

monium persulfate (ICN, Costamesa, CA, USA), and continued at 4°C for 48 h. 3%T and 1.5%T LPA matrices were prepared by dilution of a prepolymerized stock of 6%T. 5%T LPA M_r 700 000–1 000 000 (Polysciences, Warrington, PA, USA) was diluted from 10% aqueous stock solution and running buffer was adjusted to final concentration 1 × TBE. All LPA matrices were stored in a refrigerator at 4°C and replaced in the capillary using 100-μl syringes connected to capillary by piece of PTFE tubing. Prior to storage, polymerization byproducts were removed by electrolysis.

Chemicals

Ultrapure Tris base, boric acid and Na_2EDTA were obtained from Schwartz/Mann Biotech (Cleveland, OH, USA). Acrylamide was purchased from ICN and the silane reagents from Petrarch Systems (Bristol, PA, USA). Ethidium bromide (Sigma, St. Louis, MO, USA), 10 mg/ml aqueous solution was diluted in water and added to both the separation matrix and LPA used in the electrode reservoirs. All other reagents were of the highest quality available from Sigma. Buffer and acrylamide solutions were prepared in a Millipore Alpha-Q system purified water (Millipore, Bedford, MA, USA) and filtered through a 0.2-μm pore size filter (Schleicher & Schuell, Keene, NH, USA) prior to use.

DNA Samples

Restriction digests ΦX174/*Hae* III, pBR322/Msp I and λ/*Hind* III were obtained from New England Biolabs (Beverly, MA, USA), pBR322/Hae III digest from Sigma, 123 bp ladder and 1 kbp ladder from Gibco BRL (Gaithersburg, MD, USA). All DNA samples were used at a final concentration of 100 μg/ml in water for electrokinetic or pressure injection into the capillary.

RESULTS AND DISCUSSION

DNA Restriction fragment separations

The use of low %T (≤6) linear polyacrylamide for the resolution of DNA restriction fragments was examined. A number of size-dependent separations were developed, with emphasis on analytical characteristics (*e.g.* time, efficiency and separation). While higher %T composition (6 to 14%T in ref. 4) have been useful principally for oligonucleotides, DNA sequencing reaction products, and small restriction fragment separations, the lower-viscosity systems are able to separate a wide size range of restriction fragments from tens of base pairs to twenty or greater kilobase pairs. Linear polyacrylamide compositions ≤6%T have significantly lower viscosities than those previously presented [4]. These compositions can be replaced or regenerated in the capillary column, allow pressurized sample injection, and offer versatility in sample clean-up (*e.g.* the column can be refilled, providing a fresh matrix for each separation). Four LPA concentrations are used in this work, 1.5% T, 3% T, 5% T and 6% T. The 1.5% T and 3% T matrices can be replaced with current commercial CE instrumentation. On the other hand, 5% T and 6% T matrices are more viscous and, depending on conditions, generally require *ca.* 500 p.s.i. (1 p.s.i. = 6895 Pa) for replacement. At present, this is easily done with a high-pressure syringe.

A representative restriction fragment separation is shown in Fig. 1. Here the 11 fragments of ΦX174 DNA cut with *Hae* III are resolved on 3% T (diluted from 6% T laboratory-polymerized stock) linear polyacrylamide in less than 10 min. Similar to the higher % T compositions previously presented [4], peak efficiency for the 3% T was high. At an applied electric field of 300 V/cm, the 603 bp fragment in Fig. 1 exhibited >400 000 plates in 20 cm ($2 \cdot 10^6$ N/m), as calculated using the method of Foley and Dorsey [24] to account for non-Gaussian peaks. (At such high plate counts, the assumption of symmetrical peaks may significantly overestimate column efficiency [25]).

It can be seen in Fig. 1 that peak heights and areas increase progressively for the longer fragments. This result is expected for a restriction fragment digest since equal numbers of each fragment are present but larger fragments have a proportionally greater number of chromophores. This relationship between fragment size and peak area may be useful in the initial assignment

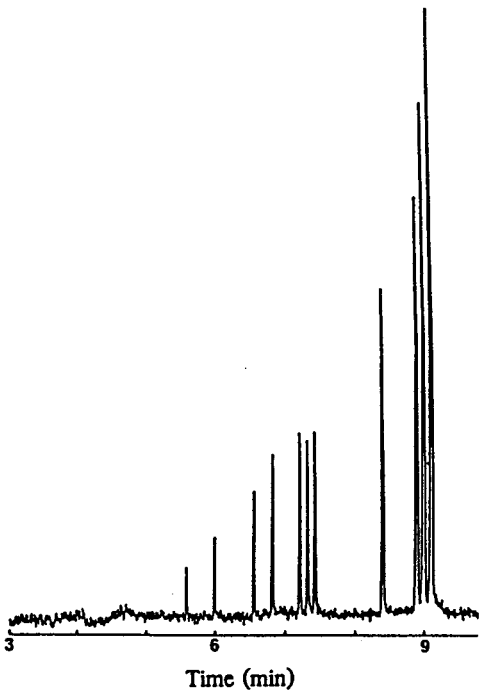

Fig. 1. Separation of ΦX174/*Hae* III using 3% T linear polyacrylamide. The eleven fragments range from 72 to 1353 bp. Conditions: l (length to detector) = 20 cm, L (column length) = 40 cm, E (voltage) = 300 V/cm, I (current) = 16 μA, capillary I.D. = 75 μm, O.D. = 360 μm, 1 × TBE buffer, electrokinetic injection at 75 V/cm for 4 s.

of migration order for this type of sample. Note also the baseline resolution of three peaks 271, 281 and 310 bp in length.

Using the ΦX174/*Hae* III restriction fragment digest as a test mixture, repetitive separations were performed using 3% T LPA at the column temperature 30°C to determine run-to-run reproducibility. Reproducibility experiments were performed using capillaries with inner walls coated with 6% T LPA [40] as described in the experimental section and the Beckman P/ACE system. Between each run, the polyacrylamide was blown out of the column and refilled. Comprehensive reproducibility data is summarized in Table I for the number of 418 separations performed. Table I demonstrates high stability of column coating and very reproducible migration times under the controlled conditions. Other coatings such as in ref. 23 work equally as well.

Another example of the separation of DNA

TABLE I

MIGRATION TIME REPRODUCIBILITY OF ΦX174/*Hae* III DIGEST ON A 3% T LINEAR POLYACRYLAMIDE COLUMN

Conditions: l = 25 cm, E = 300 V/cm, I = 23 μA, capillary I.D. = 75 μm, O.D. = 375 μm, column temperature = 30°C, running buffer 1 × TBE, pH 8.3, electrokinetic injection at 150 V/cm, 5 s. Beckman P/ACE system.

	603 bp	1353 bp
Absolute migration		
t_r average [min]	6.34	6.79
σ	$9.80 \cdot 10^{-2}$	$1.11 \cdot 10^{-1}$
n	418	418
R.S.D. (%)	1.55	1.63
Relative migration	1353/603 bp	
Δt_r [min]	1.07	
σ	$1.79 \cdot 10^{-3}$	
n	418	
R.S.D. (%)	0.17	

fragments on a laboratory-made 3% T linear polyacrylamide matrix is demonstrated in Fig. 2. This electropherogram shows separation of a 123 bp ladder (*e.g.* 123 bp fragments ligated to form 123 bp multimers). Twenty-six ladder species, of

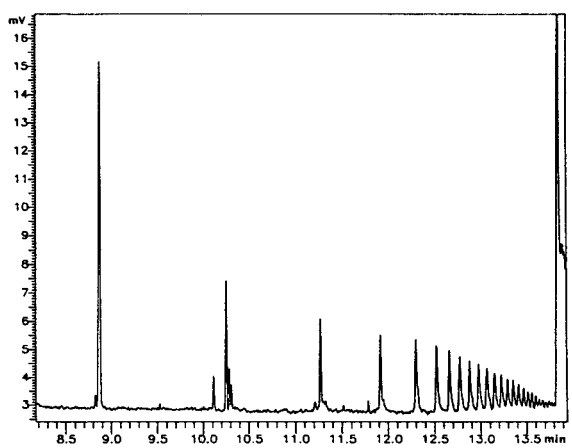

Fig. 2. Electropherogram of 123 bp DNA ladder using 3% T linear polyacrylamide. 26 fragments are separated ranging from 123 to 3198 bp. Conditions as in Fig. 1, except: l = 30 cm, electrokinetic injection at 200 V/cm for 2 s.

lengths between 123 bp and 3198 bp, are resolved in less than 15 min. High efficiencies are obtained with a maximum of $8.5 \cdot 10^6$ plates/m reached for the peak 3 (369 bp). The broad peak eluting after 13.8 min is assumed to be higher order multimers which were not resolved. The peak area (and peak height) decrease with increase in base number opposite to that of the *ΦX174/Hae* III digest in Fig. 1. Since the ladder is prepared by enzymatic ligation of the smallest unit (*e.g.* 123 bp), the smaller fragments are in the highest concentration for the specific reaction time.

We next examined the performance of the laboratory-made 3% T polymer network matrix with the separation of DNA restriction fragments up to 12 kbp. The electropherogram shown in Fig. 3 demonstrates the separation of a 1 kbp DNA ladder up to 12 kbp in less than 30 min. Peak 4 of the ladder exhibits a high efficiency of $4.4 \cdot 10^6$ plates/m. This sample consisted of 11 species in addition to the 12 species from the 1018 bp ligated monomer ladder. The additional fragments ranging from 72 to 1636 bp arise from enzymatic digestion of the pBR 322 plasmid DNA which was used in the preparation of the sample. A total of 23 fragments ranging from 72 to 12 216 bp were expected and were observed. This separation is comparable to one, shown previously using a crosslinked (3% T, 0.5% C)[a] gel filled capillary [4].

Next, separation of the sample pBR322/MspI was performed using a commercially available industrial linear polyacrylamide matrix, previously also used by other authors [26]. The sieving matrix was a 5% T LPA in 1 × TBE (Polysciences, molecular mass distribution of the polyacrylamide chains ranges from 700 000 to 1 000 000). The sample contains 26 fragments ranging in size from 9 bp to 622 bp. The first detectable peak consisted of the two fragments of 26 bp in length, the second peak consisted of the two 34 bp long fragments. Roman numeral I in Fig. 4 shows the base line separation of two 147 bp fragments. Roman numeral II shows the partial separation of the two fragments 160 bp. Similar resolutions of equivalent fragments have been shown previously using high % T nonreplaceable LPA matrix [5].

The separation of two fragments of the same length is a result of conformational differences between the two species. Similar migration phenomena have been observed by Stellwagen and

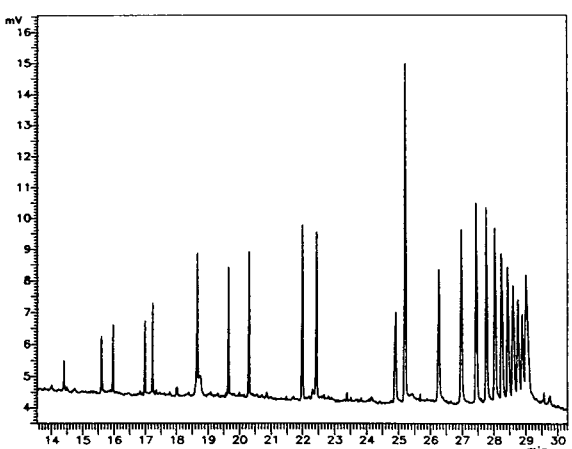

Fig. 3. Separation of the 1 kbp DNA ladder using 3% T linear polyacrylamide. Fragments range from 72 bp up to 12 216 bp. Conditions as in Fig. 1, except: $l = 40$ cm, $L = 70$ cm, electrokinetic injection at 10 kV for 0.5 s.

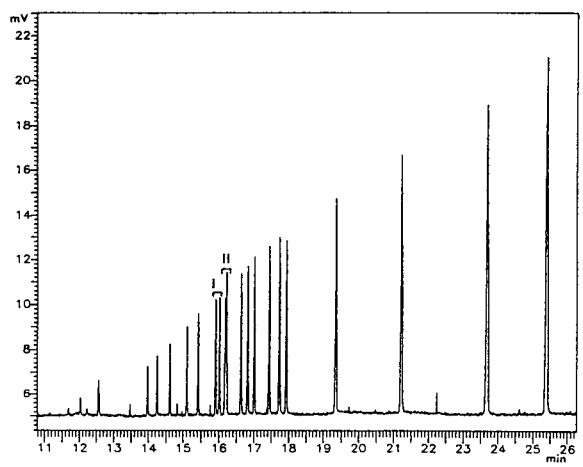

Fig. 4. Separation of the pBR322/Msp I digest using 5% T LPA Polysciences (M_r 700 000–1 000 000). Fragments range from 9 to 622 bp. The first fragment observed here is the fragment of 26 bp. Conditions as in Fig. 1, except: electrokinetic injection at 4 kV for 1 s.

[a] C = g Bis/% T.

Stellwagen [27] in crosslinked polyacrylamide slab gels. It was concluded that numerous AT-rich regions in one of the 147 bp fragments imparted a bend to the molecule, causing it to migrate more slowly than the other 147 bp fragment. Differences in tertiary structures are analogously assumed to be the reason for partial separation of the two 160 bp fragments. Thus, the high resolving power of linear polyacrylamide can potentially be used to probe structural differences between DNA fragments of the same or similar size, but of a different origin. DNA conformation dependent separations using capillary electrophoresis with linear polyacrylamide matrices is a subject of a separate paper [28].

The separation in Fig. 4 shows the possible usefulness of commercially available linear polyacrylamide solutions; however, in the present work we have found poor batch-to-batch reproducibility of the commercial product, compared to laboratory made matrixes. There are several linear polyacrylamide molecular mass standards on the market, which may yield improved reprodubility. It can be noted, nevertheless, that the current polymerization procedure is quite straightforward, and the resultant material highly reproducible [19].

We next extended the DNA size range by decreasing our laboratory-polymerized LPA concentration to 1.5% T. A separation of λ/*Hind* III digest on such a matrix is shown in Fig. 5. The λ/*Hind* III digest contains 8 fragments ranging from 125 bp to 23.1 kbp. The 125 bp fragment, the smallest of the digest, is not observed in the figure due to its relatively low absorbance (since absorbance ∝bp). The peak for this fragment could be observed by loading more sample onto the column; however, overloading of the larger fragments occurred. Peak assignment was made by peak height analysis.

An interesting feature in Fig. 5 is the broad 23.1 kbp peak. Similar separation of λ/*Hind* III on 0.5% methylcellulose matrix was previously shown and broadening of the 23.1 kbp fragment was explained by reptation with stretching model [29]. This phenomenon is, however, believed to be caused by *cos*-end annealing of the 4361 bp and 23.1 kbp fragments, resulting in a 27 kbp

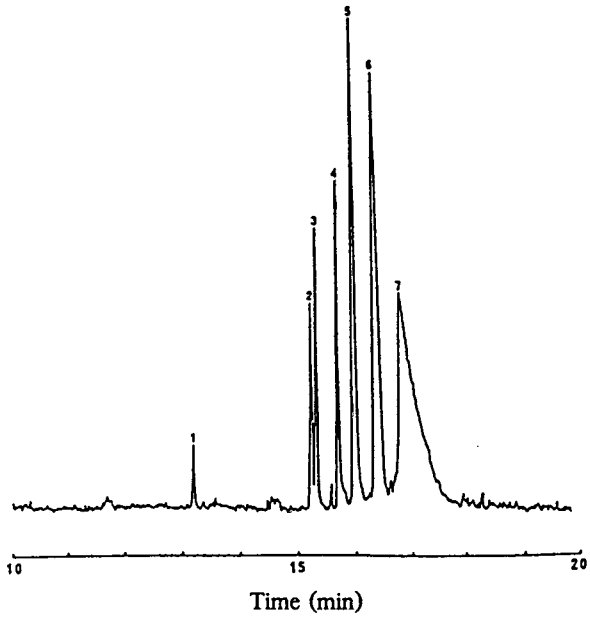

Fig. 5. Electropherogram of λ/*Hind* III DNA using 1.5% linear polyacrylamide. Presumed peak identification: 1 = 564 bp; 2 = 2.0 kbp; 3 = 2.3 kbp; 4 = 4.4 kbp; 5 = 6.6 kbp; 6 = 9.4 kbp; 7 = 23.1 kbp. Conditions as in Fig. 1, except: 1.5% T, $l = 30$ cm, sample heated to 65°C then chilled on ice, injection by siphoning ($\Delta h = 10$ cm, 2 s.)

species [30]. Evidence of this was obtained by loading the sample after immediate removal from −20°C storage. In this case, the 4361 bp peak was not observed and the 23.1 kbp peak was further broadened, due to strong annealing (Fig. 6A). Heating of the sample or addition of urea to the running buffer disrupted this interfragment annealing and single, sharper peaks were obtained (Fig. 6B).

Addition of ethidium bromide

The conformation of DNA, and thus its mobility, can be affected chemically. A common fluorescent dye, ethidium bromide (EtBr), alters the conformation by intercalating into the DNA helix [31,32]. EtBr is known to bind to DNA in a ratio of 1:5 and the binding constant ($1.5 \cdot 10^5$ M^{-1}) is sequence independent [32]. Intercalation of EtBr increases the contour length, but decreases the persistence length of DNA molecules, as the result of reduced DNA rigidity upon neutralization of phosphate groups after

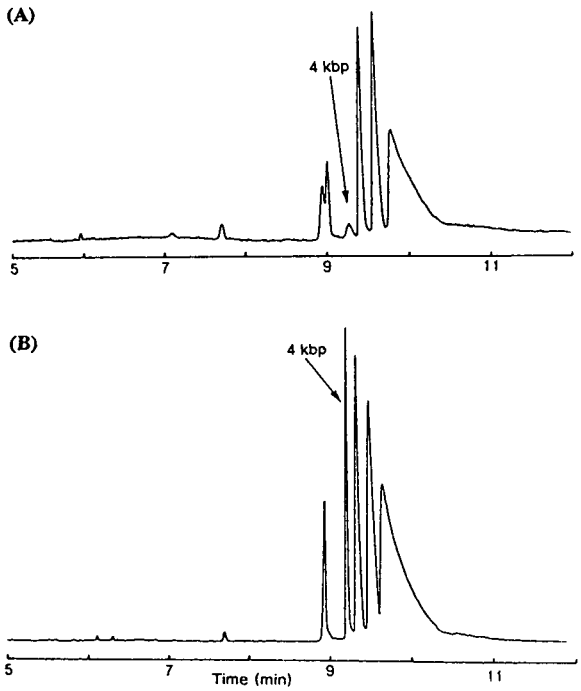

Fig. 6. Use of 1.5% T linear polyacrylamide with 0.05% agarose for λ/*Hind* III separation. See text for details. l = 20 cm, $E = 200$ V/cm, $I = 12$ μA. Injection by siphoning (Δh = 10 cm, 2 s.) (A) Sample at 4°C from −20°C; (B) sample at 25°C after heating to 65°C.

intercalation of the positively charged EtBr [33]. These properties of ethidium bromide and other DNA ligands are believed to remove sequence induced DNA curvature [34].

The separation of the sample ΦX174/*Hae* III, using 6% T LPA and electric field of 300 V/cm, exhibits changes in peak order in which DNA fragments no longer migrate according their molecular mass, *i.e.* length. The triplet of 271, 281 and 310 bp fragment in Fig. 7A is most likely not migrating according to increasing fragment length based on peak areas and relative positions. Furthermore, the peak for fragment 872 bp comigrates with peak 1078 bp (confirmed by fragment spiking experiments). For the same electrophoretic conditions, the addition of EtBr to the running buffer clearly eliminates these problems (see Fig. 7B). As another consequence of DNA charge neutralization, the migration time of DNA fragments increases, as can be seen in Fig. 7B. The relationship between changes in

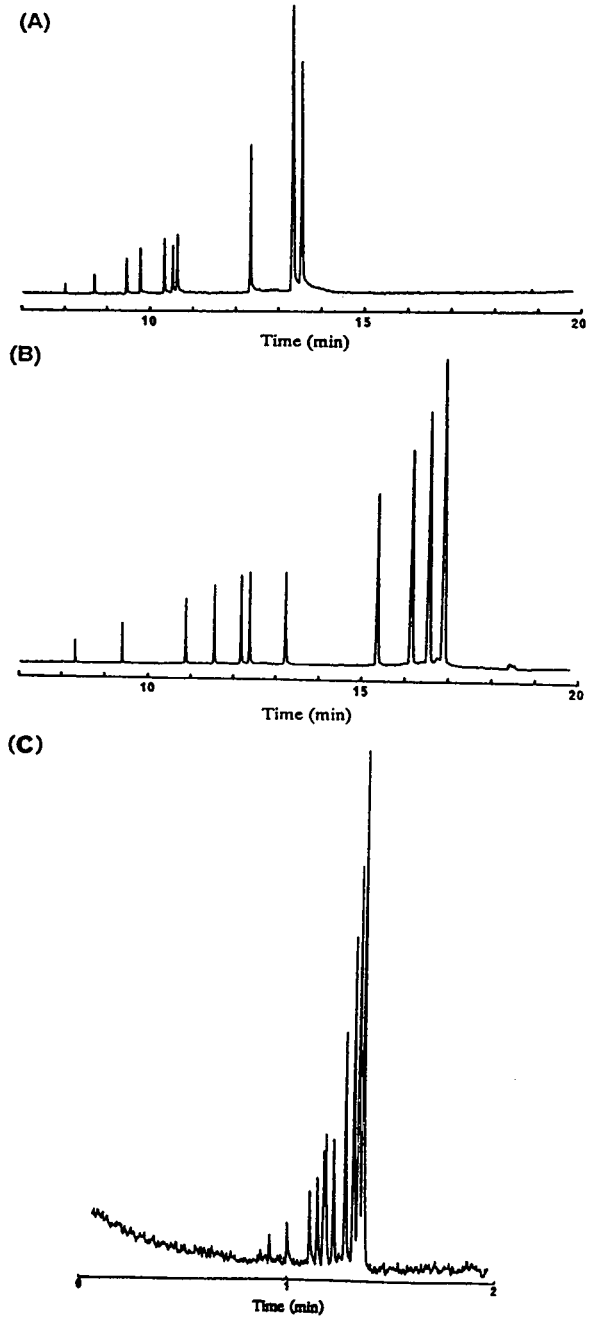

Fig. 7. Effect of ethidium bromide in migration behavior of ΦX174/*Hae* III DNA. (A) 6% T linear polyacrylamide without ethidium bromide; (B) 6% T linear polyacrylamide with 0.5 μg/ml ethidium bromide added to the running buffer. Conditions: $l = 20$ cm, $E = 300$ V/cm, other conditions as in Fig. 1. (C) Rapid separation of ΦX174/*Hae* III using 3% T linear polyacrylamide. Conditions: $E = 700$ V/cm, $I = 19$ μA, capillary I.D. = 25 μm, 0.5 μg/ml EtBr.

DNA fragment conformation and the correct migration pattern (increasing UV absorbance) is not fully understood. Nevertheless, the use of intercalating agents as well as other DNA-binding chemicals to modify DNA tertiary structures seems to be promising [28,34,35]. Other parameters such as temperature, field strength, buffer ionic strength, and matrix composition have also been studied in order to recover normal migration patterns for anomalous DNA fragments [27]. The role of these parameters, and others, on DNA separations using CE will be discussed separately [28].

The combined advantage of both ethidium bromide addition into the running buffer and the high plate counts on linear polyacrylamide allow separation under high electric fields. Migration times can be on the order of 1 min, as shown in Fig. 7C. Here, the analysis time for the ΦX174/*Hae* III digest was decreased to 1.5 min by increasing the field to 700 V/cm. Since the low viscosity of the 3% T polyacrylamide solution yields current generation similar to that observed in the open-tube mode (in contrast to the low currents found for the high %T gels), the column I.D. was reduced from 75 to 25 μm, limiting the power generation to <0.6 W/m. At this level, significant Joule heating is not expected [36,37].

Comparing the differences in the electropherograms of Fig. 7B and C, it can be seen that separation of the 271/281 bp doublet was worse in the high field experiment. This trade-off between speed and separation power, however, may be acceptable for many applications, such as in on-line polymerase chain reaction (PCR) product analysis [38], monitoring an enzymatic digest, or any type of time-dependent reaction. In fact, depending on the separation required, sub-minute analysis times can be readily realized.

In order to examine further the separation abilities of linear polyacrylamide, we have next chosen the plasmid pBR 322/*Hae* III restriction digest. This sample contained 22 fragments ranging from 8 to 587 bp, including the doublet 123/124 bp. The first detectable peak was for fragment 18 bp long and 19 peaks were detected using 6% T LPA, as shown in Fig. 8A. The seventh major peak represents comigrating fragments 123 and 124 base pairs, which were not separated on 6% T LPA, under the described conditions. Fig. 8A further shows positions of the last five peaks (434 to 587 bp) which do not correspond to the fragment lengths, based on the expected peak area increase with migration position for the restriction digest. Fragments 458 bp and 587 bp of this digest contain regions with tertiary structures which can cause retardation in polyacrylamide gels [27]. Fig. 8B shows the effect of ethidium bromide addition upon the

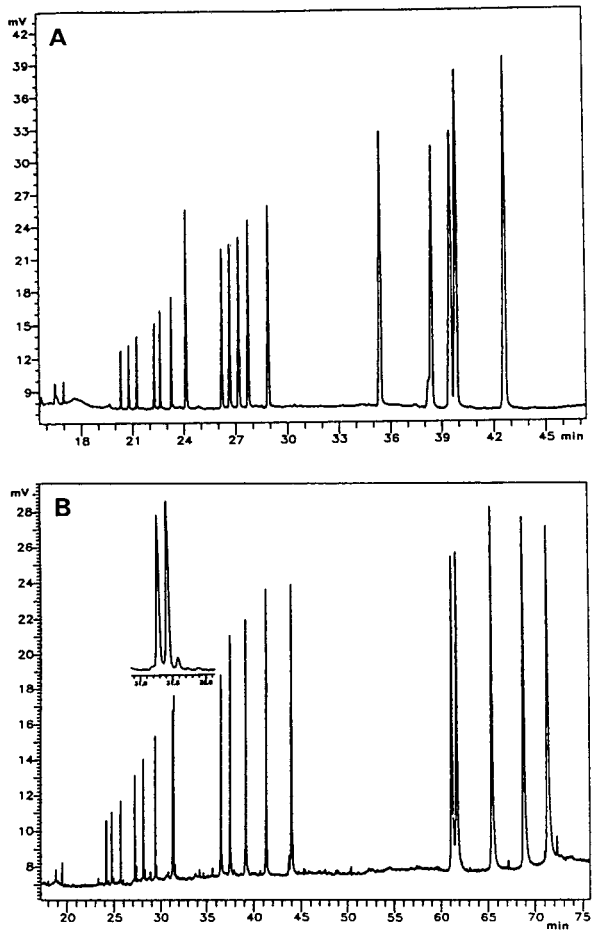

Fig. 8. Electropherogram of the pBR 322/*Hae* III sample separation from peak 18 bp to 587 bp using 6% T LPA without (A) or with (B) 1 μg/ml ethidium bromide. Conditions: 1 × TBE running buffer, $E = 150$ V/cm, $L = 45$ cm, $l = 30$ cm, column temperature 30°C, electrokinetic sample injection at 10 kV/2.5 s.

separation of pBR 322/*Hae* III. Note baseline resolution of peaks for fragments 123 and 124 bp (insert at Fig. 8B) and correct migration order of peaks for fragments 434–587 bp (based on peak areas). On the other hand, overall migration time increased to 72 min.

Fig. 9 shows a plot of migration time (mobility^{-1}) *vs.* bp number, N for the electropherogram in Fig. 8B. It can be seen that a close to linear relationship exists at least to 267 bp. The number of peaks that can be resolved in this region (51–267 bp) can be determined from

$$N = \frac{(t_{r267} - t_{r51})}{W} \quad (1)$$

where W = average peak width. For the given time window (*ca.* 20 min) and peaks widths ($4 \cdot 10^6$ plates/m), it is determined that single base pair resolution is possible in this region, assuming the DNA molecules do not anomalously migrate.

In Fig. 9, it can be seen that the slope of the last five peaks is lower than for the shorter fragments, probably as a consequence of the early stages of DNA stretching [39]. In addition, relative peak widths tend to be wider. As a consequence, the bp resolution changes to 2–3 bp in this region. Further optimization may decrease this number. However, what is important is that whereas in Fig. 8A the peaks do not appear to migrate in terms of increasing bp size (as determined from peak areas), the order is correct when ethidium bromide is the agent.

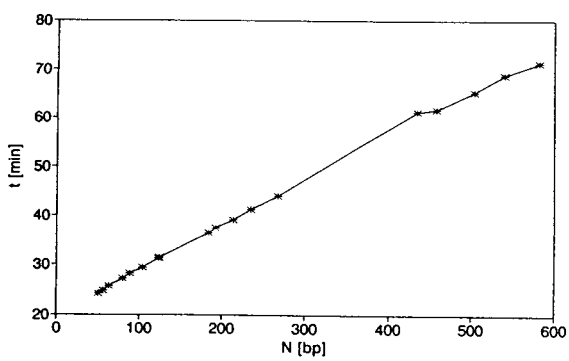

Fig. 9. Plot of migration time *vs.* base number for pBR 322/*Hae* III for electropherogram in Fig. 8B.

However, as seen in Fig. 9, there appears still to be a small amount of anomalous migration. These points will be discussed separately [28].

CONCLUSIONS

This paper presents results on the separation of double-stranded DNA molecular mass standards using replaceable linear polyacrylamide. Close to 1-min size-dependent separations were achieved using high electric field and ethidium bromide as an additive in the running buffer. Single base pair resolution of dsDNA fragments of 123 and 124 bp in length was attained with ethidium bromide in the running buffer. Possible single base pair resolving power of the 6% T linear polyacrylamide matrix was calculated in the range up to 267 bp. We have also demonstrated the sensitivity of linear polyacrylamide matrices to sequence induced DNA curvature of double-stranded DNA fragments.

With the perspective of an automated multicapillary instrument, equipped with the fluorescence detection, replaceable sieving matrices will allow the use of various compositions of separation media during consecutive runs without replacing and aligning new capillaries. This includes various pore-size matrixes optimized for specific size ranges of dsDNA fragments, native or denaturing compositions for mapping and detection of mutations, or finally, high resolution denaturing linear polyacrylamide for DNA sequencing [19]. Such a design would be cost effective and accessible to many research, clinical and forensic laboratories.

ACKNOWLEDGEMENTS

Authors gratefully acknowledge support by Department of Energy (DOE)–Human Genome Initiative grant No. DE-FG02-90ER60985. Support by DOE does not constitute an endorsement of the views expressed in this particle. The authors also acknowledge Dr. Dieter Schmalzing for his assistance with the preparation of capillary coatings and useful discussions. Contribution No. 577 from the Barnett Institute.

REFERENCES

1 J. Sambrook, E.F. Fritsch and T. Maniatis, *Molecular Cloning: A Laboratory Manual*, Cold Spring Harbor Laboratory, Cold Spring Harbor, NY, 1989.
2 D. Rickwood and B.D. Hames, *Gel Electrophoresis of Nucleic Acids: A Pracical Approach*, IRL Press at Oxford University press, Oxford, 1990.
3 B.L. Karger and F. Foret, in N. Guzman (Editor), *Capillary Electrophoresis: Theory, Methodology, and Applications*, Marcel Dekker, New York, 1993, pp. 3–63.
4 D.N. Heiger, A.S. Cohen and B.L. Karger, *J. Chromatogr.*, 516 (1990) 33.
5 A. Guttman and N.J. Cooke, *J. Chromatogr.*, 63 (1991) 2038.
6 A. Paulus and D. Hüsken, *Electrophoresis*, 14 (1993) 27.
7 H.E. Schwartz, K. Ulfelder, F.J. Sunzeri, M.P. Busch and R.G. Brownlee, *J. Chromatogr.*, 559 (1991) 267.
8 P.D. Grossman and D.S. Soane, *Biopolymers*, 31 (1991) 1221.
9 W.A. MacCrehan, H.T. Rasmussen and D.M. Northrop, *J. Liq. Chromatogr.*, 15 (1992) 1063.
10 B.R. McCord, J.M. Jung and E.A. Holleran, *J. Liq. Chromatogr.*, 16 (1993) 1963.
11 S. Nathakarnkitkook, P.J. Oefner, G. Bartsch, M.A. Chin and G.K. Bonn, *Electrophoresis*, 13 (1992) 18.
12 P. Boček and A. Chrambach, *Electrophoresis*, 13 (1992) 31.
13 M. Zhu, D.L. Hansen, S. Burd and F.J. Gannon, *J. Chromatogr.*, 480 (1989) 63.
14 J.P. Landers, R.P. Oda, T.C. Spelsberg, J.A. Nolan and K.J. Ulfelder, *Bio/Techniques*, 14 (1993) 98.
15 P.G. Righetti, *J. Biochem. Biophys. Methods*, 19 (1989) 51.
16 A.S. Cohen, D.R. Najarian, A. Paulus, A. Guttman, J.A. Smith and B.L. Karger, *Proc. Natl. Acad. Sci. U.S.A.*, 85 (1988) 9660.
17 A. Guttman, A.S. Cohen, D.N. Heiger and B.L. Karger, *Anal. Chem.*, 62 (1990) 137.
18 T.J. Kasper, M. Melera, P. Gozel and R.G. Brownlee, *J. Chromatogr.*, 458 (1988) 303.
19 M.C. Ruiz-Martinez, J. Berka, A. Belenkii, F. Foret and B.L. Karger, *Anal. Chem.*, in press.
20 H. Swerdlow, J.Z. Zhang, D.Y. Chen, H.R. Harke, R. Grey, S. Wu and N.J. Dovichi, *Anal. Chem.*, 63 (1991) 2835.
21 S. Wicar, M. Vilenchik, A. Belenkii, A.S. Cohen and B.L. Karger, *J. Microcol. Sep.*, 4 (1992) 339.
22 S.J. Hjertén, *J. Chromatogr.*, 347 (1985) 191.
23 D. Schmalzing, C.A. Piggee, F. Foret, E. Carrilho and B.L. Karger, *J. Chromatogr. A*, 652 (1993) 149.
24 J.P. Foley and J.G. Dorsey, *Anal. Chem.*, 55 (1983) 730.
25 J.J. Kirkland, W.W. Yau, H.J. Stoklosa and C.H. Dilks, Jr., *J. Chromatogr. Sci.*, 15 (1977) 303.
26 H. Pulyaeva, D. Wheeler, M.M. Garner and A. Chrambach, *Electrophoresis*, 13 (1992) 608.
27 A. Stellwagen and N.C. Stellwagen, *Biopolymers*, 30 (1990) 309.
28 Y.F. Pariat, J. Berka, O. Müller, F. Foret, D. Smisek and B.L. Karger, in preparation.
29 M. Strege and A. Lagu, *Anal. Chem.*, 63 (1991) 1233.
30 J. Ballantyne, G. Sensabaugh and J.A. Witkowski, *DNA Technology and Forensic Science, Banbury Center Report No. 33*, Cold Spring Harbor Press, Cold Spring Harbor, NY, 1989.
31 J.-B. LePecq and C.J. Paoletti, *J. Mol. Biol.*, 27 (1967) 87.
32 C. Cuniberti and M. Guenza, *Biophys. Chem.*, 38 (1990) 11.
33 E. Nordmeier, *J. Phys. Chem.*, 96 (1992) 6045.
34 F. Barcelo, G. Muzard, R. Mendoza, B. Revet, B.P. Roques and J.-B. Le Pecq, *Biochemistry*, 30 (1991) 4863.
35 H.E. Schwartz and K.J. Ulfelder, *Anal. Chem.*, 64 (1992) 1737.
36 R.J. Nelson, A. Paulus, A.S. Cohen, A. Guttman and B.L. Karger, *J. Chromatogr.*, 480 (1989) 111.
37 S. Hjertén, *Electrophoresis*, 11 (1990) 665.
38 H.H. Kazarian, in H.A. Erlich (Editor), *PCR Technology*, Stockton Press, New York, 1989.
39 M. Lalande, J. Noolandi, C. Turmel, R. Brousseau, J. Rousseau and G.W. Slater, *Nucleic Acids Res.*, 16 (1988) 5427.
40. B.L. Karger, R.W. Giese and E. Szoko, *US Pat.*, 5 089 106 (1992).

Journal of Chromatography A, 652 (1993) 67–73
Elsevier Science Publishers B.V., Amsterdam

CHROM. 25 254

Optimization of capillary electrophoretic separation of DNA fragments based on polymer filled capillaries

David A. McGregor and Edward S. Yeung*

Ames Laboratory–US Department of Energy and Department of Chemistry, Iowa State University, Ames, IA 50011 (USA)

ABSTRACT

The separation of ΦX174RF DNA-*Hae* III fragments is studied in a 0.5% methycellulose polymer solution as a function of temperature and applied voltage. The migration times decreased with both increasing temperature and increasing field strength, as expected. However, the relative migration rates of the fragments (selectivity) did not change with temperature but are affected by the applied field. A clear transition from the Ogston mechanism to the reptation mechanism is observed. The use of 0.5% methyl cellulose and 202 m*M* borate buffer at pH 8.2 allows the separation of the 271/281 base pair fragments, even without the addition in intercalating agents. At 700 V/cm and 20°C, complete separation of all fragments is achieved in less than 4 min with an average plate number of $2.5 \cdot 10^6$/m.

INTRODUCTION

The identification and codification of the human genome is a continuing worldwide scientific goal. A committee for The Human Genome Initiative has proposed a 15-year time table for the completion of the human genome project [1]. To ultimately achieve this goal, critical reevaluation of current separation techniques must be done, to substantially increase the speed, reliability, and sensitivity in gene mapping and in DNA sequencing applications. For example, to identify the $3 \cdot 10^9$ base pairs (bp) of the human genome would require sequencing individual bases, even at a rate of 23 000 bp/h, for the next 15 years. However, completion of this task will aid us in better understanding and possibly treating the more than 4000 genetic disorders that afflict humankind [2]. Although this daunting task appears impossible, great strides have been made recently.

Slab gel separations of deoxyribonucleic acid (DNA) has been the standard technology for many years, but tends to be very time consuming [3,4]. More recently, the union of DNA separations and high-performance capillary electrophoresis (HPCE) have been achieved for separations of DNA fragments under *ca.* 12 kilobase pairs (kb) [5]. The principal advantages of HPCE in DNA separation have been increased efficiencies, shortened separation times, and reduced amounts of sample needed. Separation of DNA in HPCE has been ongoing for several years. In many cases, adaptation of existing slab-gel methodology was applied to the relatively new technique of HPCE. Examples include filling capillaries with a proven separation medium such as agarose [6,7] or cross-linked polyacrylamide [5,8,9]. A leading advantage of HPCE is the decrease in Joule heating of the separation medium, which allows for increased voltages and consequently decreasing separation times. This combination also offers improved results over slab gels such as separation efficiency.

Problems exist in filling the capillary with the traditional separation media. When an immobilized separation medium such as agarose or

* Corresponding author.

0021-9673/93/$06.00

crosslinked polyacrylamide is introduced into the capillary, care must be exercised to maintain the integrity of the gel. Formation of polyacrylamide inside a capillary is very difficult and careful polymerization must be achieved. Otherwise voids in the gel will occur and the capillary will be useless. Instead of using an immobilized matrix in capillaries, polymer networks can be used. These include liquified agarose [6,7,10], non-cross-linked (linear) polyacrylamide [5,11–13], and viscous polymers [14–18]. These polymers can emulate the sieving effect of the fixed matrix and similar separations can be achieved. The ability to replenish the medium with fresh polymer or to vary the concentration of the polymer is a definite advantage over immobilized gels.

We will describe here optimization of electrophoretic separations in methyl cellulose solutions as an alternative to immobilized gels. With this simple polymer matrix in solution, less current is drawn and higher velocities can be achieved along with the capability of achieving extremely high resolution in a relatively short column. This results in drastically reduced separation times. Viscous polymers such as hydroxypropylmethylcellulose [14,17,18], hydroxyethylcellulose [16], polyethylene glycol [14] and methylcellulose [15] have been applied to DNA separations before. In this work, the influence of temperature and field strength on the separation of DNA fragments from 72 to 1353 bp derived from *Φ*X174RF DNA-*Hae* III based on methylcellulose solutions is examined. Comparisons with the behavior in linear polyacrylamide solutions [12,13] will be made.

EXPERIMENTAL

Materials

*Φ*X174RF DNA-*Hae* III digest from United States Biochemical (Cleveland, OH, USA) was diluted to 250 ng/μl. The TBE buffer consisted of tris[hydroxymethyl]-aminomethane (THAM), boric acid and ethylenediaminetetraacetic acid (EDTA), all from Sigma (St. Louis, MO, USA). The polymer was methyl cellulose 4000 (Sigma) which has a viscosity rating of 4000 cP for a 2% solution at 25°C.

Apparatus

DB-1 coated GC capillaries, 50 μm I.D. × 360 μm O.D. (J & W Scientific, Folsom, CA, USA) with 0.2 μm coating thickness was used without any further modification. The capillary length was 43 cm total, 35 cm effective length. A SpectraPHORESIS 1000 system (Spectra-Physics, Fremont, CA, USA) was used for all separations in the constant voltage mode. Temperature control to ±0.1°C was achieved by the peltier cooling system of the SpectraPHORESIS-1000. Electrokinetic injection was used throughout at 1 s at 200 V/cm. Detection of nucleic acids were monitored at 260 nm. Because of the small width of the peaks, the time constant was set to zero on the CE instrument to prevent any biasing of peak shapes.

Methods

The buffer solution contained 100 m*M* each of THAM and boric acid, both being the free base and acid respectively, with EDTA added as a chelating agent for divalent cations that could activate DNAases. The pH of the solution at the 202 mM TBE was 8.2 and was not further adjusted. A 19.90-ml volume of buffer was mixed with 0.5% (w/w) of methyl cellulose (0.10 g) and sonicated for 15 min. When the methyl cellulose appeared thoroughly wetted the solution was stirred until it appeared homogeneous. To further clarify the solution the stirring was continued on ice for at least 15 min. This caused the solution to appear transparent, leaving only small methyl cellulose needles in solution. Filtration was performed on the cooled solution through a 0.8 μm cellulose acetate filter (Alltech, Deerfield, IL, USA) and the solution was stored at 4°C until used.

Once the capillary was pressure filled it was allowed to equilibrate at running voltages for 5 min. The polymer did not degrade significantly over 30 to 40 runs and could be easily refilled once separation times started to change significantly. Column lifetimes were in excess of 100 injections.

RESULTS AND DISCUSSION

In Figs. 1–3, we show the separation of DNA fragments at various temperatures and at various

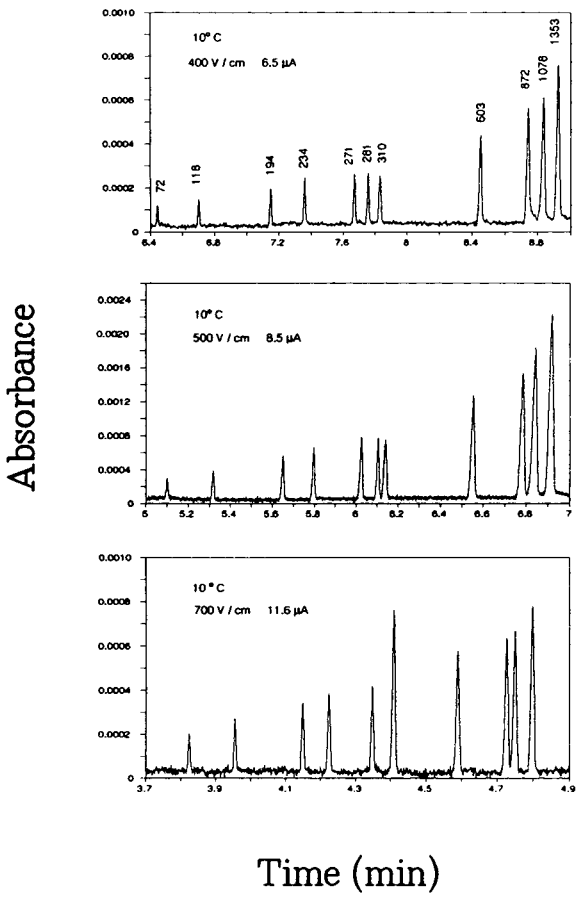

Fig. 1. Separation of ΦX174RF DNA-*Hae* III fragments at various field strengths. Conditions: 202 m*M* TBE buffer, 0.5% methyl cellulose 4000, 45 cm (35 cm to detector) × 50 μm I.D. DB-1 coated capillary, all electropherograms are at 10°C.

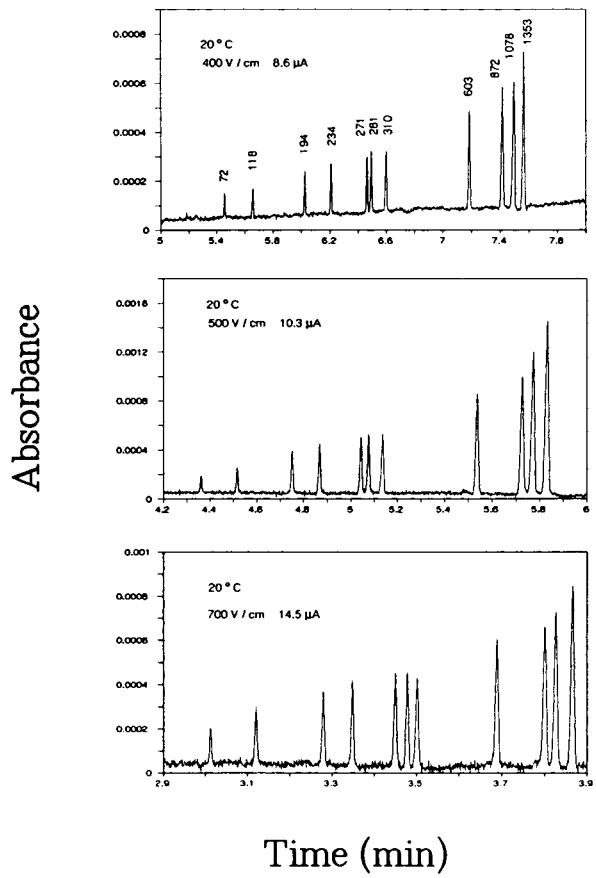

Fig. 2. Separation of ΦX174RF DNA-*Hae* III fragments at various field strengths. Conditions as in Fig. 1 except all electropherograms are at 20°C.

electric field strengths. It is clear that there are differences in migration times, efficiencies, and resolution between pairs of fragments. Several important observations can be made.

First, the migration times decrease with increasing temperature in each case. This is consistent with published results in linear polyacrylamide gel systems [12], where the viscosity of the gel–buffer system decreases with temperature. In that study, the migration times decreased roughly by a factor of 2 over a 20°C temperature range. Here, we observe a factor of 1.3 decrease over the same temperature range. In effect, the activation energy for viscous flow is smaller in methylcellulose by a factor of 0.65 [12]. Fig. 4 shows the temperature dependence of mobilities of the DNA fragments at fixed field strengths. For comparisons, the mobilities are normalized to that of the smallest (72 bp) fragment. Overall, the relative mobilities show little temperature dependence, indicating that there is negligible change in the effective pore size of the polymer matrix [19] and that the DNA conformation stayed constant over this temperature range.

Second, the separation efficiencies generally decrease with increasing fragment size, increasing temperature and increasing electric field strength, as shown in Table I. The peak widths should have negligible contributions from the injection process, since both the injection times and the injection voltages are lower. At higher temperatures and at higher applied fields, the

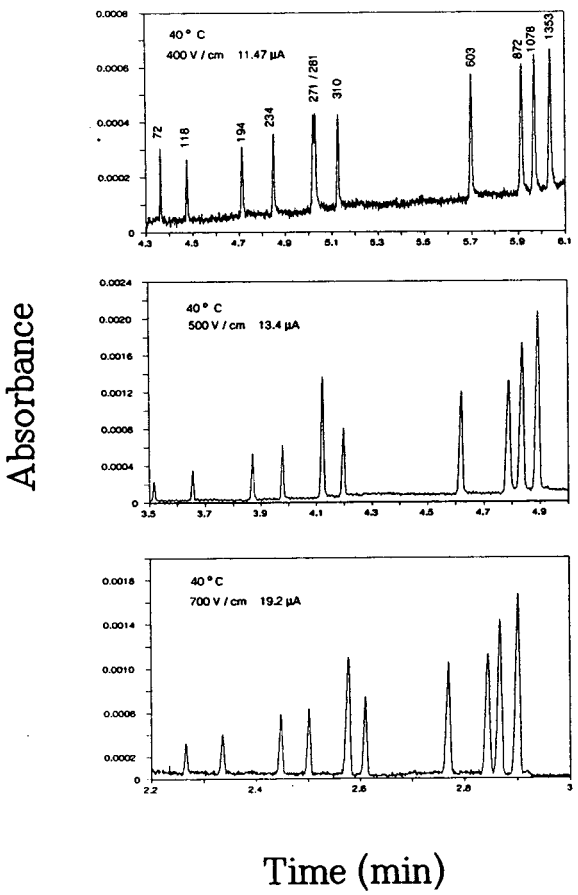

Fig. 3. Separation of ΦX174RF DNA-*Hae* III fragments at various field strengths. Conditions as in Fig. 1 except all electropherograms are at 40°C.

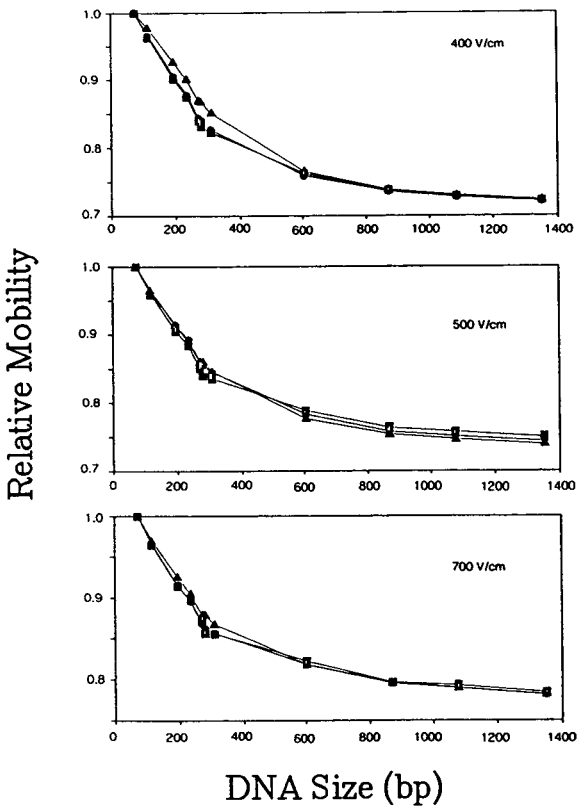

Fig. 4. Normalized mobilities *versus* DNA size for (a) 400 V/cm, (b) 500 V/cm, (c) 700 V/cm at various temperatures. □ = 10°C; ○ = 20°C; △ = 40°C.

half-width of the bands actually decreased for a given DNA fragment, but the shorter migration times in each case led to lower numbers of theoretical plates. The concept of theoretical plates strictly should be modified since the migration times past the detector are not constant. A closer examination reveals that the physical lengths of the zones on column are insensitive to the temperature or the electric field strength. This means that one can in general shorten the running time by increasing the temperature or the field strength without introducing band broadening. Diffusional broadening of the DNA fragment bands should be minor based on the short residence times and the large molecular masses (sizes) involved. We can conclude that the primary contributor to the observed peak widths is a mismatch in the mobilities of the fragments compared to that of the buffer ions [20], leading to skewed, triangular peaks. This is consistent with the fact that the widths of the peaks for the larger fragments, even after correction for migration times, are larger than those for the smaller fragments. In these studies, we cannot decrease the injected amounts further because of the lack of detector sensitivity. Also, the buffer ionic strength cannot be increased if joule heating is to be avoided at these high field strengths.

Third, the migration times decrease as the applied field strength is increased. This goes beyond the normal linear dependence of migration velocity on field strength, as is depicted in Fig. 5. There, the mobilities of each series of fragments had been normalized to that of the 72

TABLE I

NUMBER OF THEORETICAL PLATES (MILLIONS) FOR THE SEPARATION OF DNA FRAGMENTS UNDER VARIOUS CONDITIONS

Size (bp)	Theoretical plates ($\times 10^6$)								
	10°C			20°C			40°C		
	400 V/cm	500 V/cm	700 V/cm	400 V/cm	500 V/cm	700 V/cm	400 V/cm	500 V/cm	700 V/cm
72	2.9	1.3	1.8	3.0	1.3	1.2	5.1	1.1	1.0
118	2.6	2.3	1.5	2.0	1.2	1.4	2.1	1.1	1.0
194	2.2	1.8	1.3	1.9	1.1	1.4	1.7	1.2	0.9
234	2.3	1.9	1.5	2.3	1.1	1.4	1.8	1.2	1.3
271	2.0	1.8	1.4	2.1	1.0	1.1	1.5	1.2	0.8
281	2.2	1.7	1.2	2.7	1.1	1.2	2.3	1.2	0.8
310	1.3	1.2	1.2	1.9	0.9	1.0	1.9	1.2	1.0
603	1.6	1.4	1.4	1.8	0.7	1.0	1.9	1.0	1.0
872	1.3	1.1	1.1	1.6	0.5	1.0	1.7	0.8	0.9
1078	1.2	1.0	1.2	1.3	0.6	0.9	1.8	0.8	1.1
1353	1.2	1.0	1.3	1.3	0.5	0.9	1.8	0.8	1.1

bp fragment. The smaller fragments (<250 bp) show little dependence on field strength, a result that is similar to typical small-molecule separations in CE. The larger fragments clearly show a higher relative mobility with increased field strength. The explanation of this effect could be attributed to the mechanism which drives this separation. The Ogston or sieving mechanism which describes analyte through a porous medium states that the analyte can be viewed as a hard sphere and is immutable [21,22]. Since the porous medium is made up of a range of pore sizes, the smaller the analyte sphere the more pores become available for the analyte to travel through, hence the "sieving" effect. This explains the behavior of the smaller fragments. Obviously, DNA is not a hard sphere but more closely represented by a long chain. This is more pronounced for the larger (>250 bp) DNA fragments. When this happens the Ogston mechanism fails and another theory must be applied. The new mechanism will more closely resemble reptation that describes the DNA as snaking through a porous medium [22]. This explains the plateau-like behavior for the larger fragments in Figs. 4 and 5. When higher voltages are applied the DNA is certainly more stretched out parallel to the field that is applied. The plateaus therefore shift to larger values as the electric force per unit length of the molecule increases [22].

Fourth, we are able to resolve the 271/281 pair of fragments under certain experimental conditions (see Figs. 1–3), *i.e.* certain combinations of temperature and field strength. Such a separation is almost never achieved for a cellulose [14,17] or agarose [6,7] medium except if an intercalator such as ethidium bromide is used. This is in contrast to a linear polyacrylamide medium, where the native 271/281 fragments are well separated [5,11–13]. A possible explanation is that polyacrylamide is formed with a wide distribution in pore sizes. This allows the small difference between the two fragments to affect separation. Cellulose solutions are generally of one viscosity rating and are not diverse enough to optimize separation in the 280 bp range simultaneously with the larger and the smaller fragments. Fortunately, 280 bp lies just about at the transition point between the sieving and the reptation mechanisms (Figs. 1–3) for this polymer type, size and concentration. Since the applied field only affects the larger fragments, the migration of the 281 and larger fragments can be "tuned" to optimize their resolution from

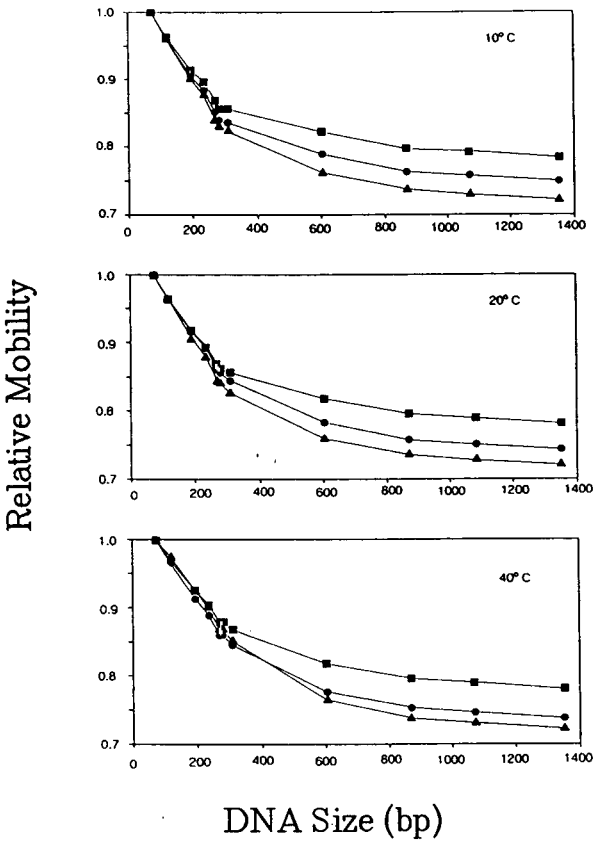

Fig. 5. Normalized mobilities *versus* DNA size for 10, 20 and 40°C at various field strengths. ▲ = 400 V/cm; ○ = 500 V/cm; □ = 700 V/cm.

the 271 and smaller fragments. This then constitutes a systematic approach for enhancing the resolution of a narrow range of DNA fragments in polymer solutions.

Fifth, there are some differences in resolution between our results and those reported in the literature. High electric field strengths have been found to degrade the resolution between the larger DNA fragments in polyacrylamide gels [5,13]. Such is not the case in Figs. 1–3, even though some of the runs are at very high fields (700 V/cm). The degradation of resolution of the larger fragments at high fields is also not always observed in polyacrylamide gels (Fig. 3 *vs.* Fig. 8 in ref. 5). One can thus rule out field-induced DNA alignment as the cause, since alignment should be matrix independent. These results may indicate some inherent differences between cellulose *versus* polyacrylamide matrixes, such as the latter being less rugged at high fields.

Sixth, because of the very high fields used, the complete separation of all ΦX174RF DNA-*Hae* III fragments was accomplished in record time. The best result along these lines is for separation at 700 V/cm and 20°C, requiring less than 4 min. The number of theoretical plates averaged better than $1 \cdot 10^6$ (*ca.* $2.5 \cdot 10^6$ plates per meter). A direct comparison is given in Table II. Even higher plate numbers have been obtained for DNA sequencing runs [23,24], but those involve run times of up to an hour.

TABLE II

SEPARATION OF ΦX174RF DNA-*Hae* III FRAGMENTS UNDER DIFFERENT CONDITIONS

MC = Methylcellulose; PA = polyacrylamide; HPMC = hydroxypropylmethylcellulose; EB = ethidium bromide; ND = not determined.

Ref.	Medium	Conditions	Total time (min)	Average plate number ($\times 10^6$)
This work	0.5% MC	20°C, 700 V/cm	3.8	1.1
13	linear PA	20°C, 400–100 V/cm	9.3	0.2
5	linear PA	20°C, 300 V/cm	12	ND
12	linear PA	40°C, 400 V/cm	14	ND
11	linear PA	25°C, 250 V/cm	16	1.2
5	crosslinked PA	20°C, 250 V/cm	16	2
13	linear PA	20°C, 200 V/cm	27	0.2
17	0.5% HPMC, EB	25°C, 175 V/cm	32	ND
14	0.5% HPMC, EB	25°C, 175 V/cm	33	1

In summary, we have demonstrated effective control of the separation of DNA fragments in a 0.5% methylcellulose polymer solution. We expect this system to be a reasonable alternative to the use of linear polyacrylamide, particularly if one can further optimize the performance towards the higher mass range by suitable combinations of polymers of different specific viscosities and molecular mass [19].

ACKNOWLEDGEMENT

The Ames Laboratory is operated for the US Department of Energy by Iowa State University under Contract No. W-7405-Eng-82. This work was supported by the Director of Energy Research, Office of Health and Environmental Research.

REFERENCES

1 *National Research Council Report of the Committee on Mapping and Sequencing the Human Genome*, Board of Basic Biology, Commission on Life Sciences, National Academy Press, Washington, DC, 1988.
2 *Joint Report DOE/ER-0452P: Understanding Our Genetic Inheritance —The US Human Genome Project: The First Five Years*, US Department of Energy and US Department of Health and Human Services, Washington, DC, April 1990.
3 F.M. Ansubel, R. Brent, R.E. Kingston, D.D. Moore, J.G. Seidman, J.A. Smith and K. Struhl (Editors), *Short Protocols in Molecular Biology*, Wiley, New York, 1992.
4 J. Sambrook, E.F. Fritsch and T. Maniatis (Editors), *Molecular Cloning: A Laboratory Manual*, Cold Spring Harbor Press, Cold Spring Harbor, NY, 1989.
5 D.N. Heiger, A.S. Cohen and B.L. Karger, *J. Chromatogr.*, 515 (1990) 33.
6 P. Bocek and A. Chrambach, *Electrophoresis*, 13 (1992) 31.
7 P. Bocek and A. Chrambach, *Electrophoresis*, 12 (1991) 1059.
8 A.S. Cohen, D.R. Najarian, A. Paulus, A. Guttman, J.A. Smith and B.L. Karker, *Proc. Natl. Acad. Sci. U.S.A.*, 85 (1988) 9660.
9 A. Guttman, A.S. Cohen, D.N. Heiger and B.L. Karger, *Anal. Chem.*, 62 (1990) 137.
10 P. Bocek and A. Chrambach, *Electrophoresis*, 12 (1991) 620.
11 A. Guttman and N. Cooke, *Anal. Chem.*, 63 (1991) 2038.
12 A. Guttman and N. Cooke, *J. Chromatogr.*, 559 (1991) 285.
13 A. Guttman, B. Wanders and N. Cooke, *Anal. Chem.*, 64 (1992) 2348.
14 H.E. Schwartz, K. Ulfelder, F.J. Sunzeri, M.P. Busch and R.G. Brownlee, *J. Chromatogr.*, 559 (1991) 267.
15 M. Strege and A. Lagu, *Anal. Chem.*, 63 (1991) 1233.
16 S. Nathakarnkitkool, P.J. Oefner, G. Bartsch, M.A. Chin and G.K. Bonn, *Elecrophoresis*, 13 (1992) 18.
17 K.J. Ulfelder, H.E. Schwartz, J.M. Hall and F.J. Sunzeri, *Anal. Biochem.*, 200 (1992) 260.
18 M. Zhu, D.L. Hansen, S. Burd and F. Gannon, *J. Chromatogr.*, 480 (1989) 311.
19 P.D. Grossman and D.S. Soane, *J. Chromatogr.*, 559 (1991) 257.
20 F.E.P. Mikkers, F.M. Everaerts and Th.P.E.M. Verheggen, *J. Chromator.*, 169 (1979) 11.
21 A.G. Ogston, *Trans. Faraday Soc.*, 54 (1958) 1754.
22 G.W. Slater and J. Noolandi, *Biopolymers*, 28 (1989) 1781.
23 H. Swerdlow, J.Z. Zhang, D.Y. Chen, H.R. Harke, R. Grey, S. Wu, N.J. Dovichi and C. Fuller, *Anal. Chem.*, 63 (1991) 2835.
24 A.S. Cohen, D.R. Najarian and B.L. Karger, *J. Chromatogr.*, 516 (1990) 49.

Journal of Chromatography A, 652 (1993) 75–82
Elsevier Science Publishers B.V., Amsterdam

CHROM. 25 411

Capillary electrophoresis of polymerase chain reaction-amplified DNA using fluorescence detection with an intercalating dye

Bruce R. McCord*, David L. McClure☆ and Janet M. Jung

FBI Laboratory, FBI Academy, Forensic Science Research and Training Center, Quantico, VA 22135 (USA)

ABSTRACT

The application of the fluorescent intercalating dye, YO-PRO-1 to the analysis of polymerase chain reaction-generated DNA fragments from 120 to 400 base pairs in size was investigated. Analysis of samples was performed using a non-gel sieving buffer containing Tris–borate, hydroxyethyl cellulose, and the intercalating dye. Minimum detectable concentrations were less than 500 pg/ml DNA. For samples requiring resolution of four base pairs or less, it was necessary to add a second intercalating agent, ethidium bromide to the buffer. Using this procedure, a number of loci of interest in genetic typing were examined.

INTRODUCTION

The polymerase chain reaction (PCR) enables the amplification of specific fragments of DNA that are present in trace amounts of biological material [1–3]. Capillary electrophoresis (CE), with its high throughput and resolving power, has great potential for application to the analysis of such samples. Generally these types of analyses have been performed using gel-filled capillaries due to the high resolution required [4–8].

Recently, CE separation of DNA fragments has been developed using non-gel sieving buffers [8–12]. These buffers can be flushed out of the capillary following each run. Analyses carried out using buffers containing hydroxyethyl cellulose (HEC) have provided impressive separation efficiencies [12]. We have used similar buffer systems to obtain 4 base pairs (bp) resolution of a mixture of alleles in the 200–300 bp size range with UV detection [13].

The goal of this work has been to develop the application of laser induced fluorescence to the analysis of PCR-amplified DNA. The DNA fragments used in this study are a series of PCR-amplified alleles resulting from variable number tandem repeats (VNTRs) with repeat units 4 bp in length. The resolution of DNA fragments with differences in size this small presents a particularly challenging separation.

The use of laser fluorescence has the potential to improve the sensitivity and selectivity of the analysis. The PCR process can generally produce sufficient material for analysis by UV detection, (μg/ml quantities). However, due to the sample extraction and amplification process, occasionally an insufficient sample may be presented for analysis. Also, residual salts in the PCR mixture can inhibit the electrokinetic injection process, reducing sensitivity. These factors make the improved sensitivity obtainable though fluorescence attractive.

Since DNA has little native fluorescence, PCR products must either be tagged using fluorescent primers, or stained using a fluorescent dye [14,15]. The use of fluorescent dyes to stain or intercalate the DNA is inherently more sensitive

* Corresponding author.
☆ Visiting scientist from South Carolina Law Enforcement Division, P.O. Box 21398, Columbia, SC 29221-1398, USA.

0021-9673/93/$06.00

than tagging via the PCR as the maximum number of fluorescent tags per PCR product is only two, one for each primer. Fluorescent intercalating dyes, however, can bind at multiple sites on the DNA molecule. For example, thiazole orange was found in one experiment to bind to the DNA fragment at a ratio of one dye molecule per every two bp of DNA [6].

We began this study with an investigation of the concentration dependence of YO-PRO-1, {1-(4-[3-methyl-2,3-dihydro-(benzo-1,3-oxazole) - 2-methyidene]-quinolinium)-3-trimethylammonium propane diiodide}, when used as a visualizing and intercalating agent for the laser-induced fluorescence detection of double-stranded DNA fragments. In our earlier work with UV detection, we had used ethidium bromide in the buffer to improve the resolution by intercalating the DNA [13]. Our goal was to replace the ethidium bromide in the buffer with YO-PRO-1, the YO-PRO-1 providing florescence detection as well as resolution enhancement through intercalation. The YO-PRO-1 dye has a strong binding constant to DNA and little intrinsic fluoresence unless bound to DNA [17].

Experiments were performed to determine if the resolution obtained would permit the analysis of the small differences in size of DNA fragments used in genetic typing. The studies revealed that while high sensitivity can be obtained with this procedure, for resolution better than 6 bp, the addition of ethidium bromide was still necessary.

MATERIALS AND METHODS

Sample preparation

The pBR322 *Hae*III digested DNA (Sigma, St. Louis, MO, USA) was diluted to 0.005 μg/ml with deionized water. Biological samples were prepared by extracting the DNA [18] and amplifying via the PCR [1]. Samples containing mixtures of alleles were prepared by amplification and recovery of specific alleles present in blood samples obtained from specific donors. The amplified DNA was diluted to 2 ml with deionized water and desalted using dialysis via centrifugation at 1000 *g* through a Centricon 100 ultrafiltration device (Amicon, Boston, MA, USA). Following ultrafiltration, the sample was dialyzed further by pipeting it onto a 0.1-μm VSWP membrane filter (Millipore, Bedford, MA, USA) which was floating in a petri dish filled with deionized water. Dialysis was carried out on the floating filter for 30 min [19]. The dual filtration process was developed to remove salts and excess primers which can interfere with sample injection by preferentially migrating into the capillary during electrokinetic injection [13]. Following the filtration steps, the samples were pretreated with YO-PRO-1 (Molecular Probes, Eugene, OR, USA) by diluting 1:10 with distilled water containing 50 ng/ml of the dye.

Capillary electrophoresis

A P/ACE 2050 capillary electrophoresis instrument (Beckman, Palo Alto, CA, USA) was used with a Laser Module 488 argon ion laser (Beckman). The instrument was operated in the constant current mode at 38 μA (approximately −13 kV) and 25°C. The separation buffer was prepared using a modification of a procedure published by Nathakarnkitkool *et al.* [12]. The column was 60 cm effective length × 0.1 μm I.D. DB-17 (J&W, Folsom, CA, USA) with 0.1 μm phase thickness. The buffer was prepared in the following manner: 0.1 m*M* EDTA (Sigma) was added to 100 m*M* Trizma (Tris) base (Sigma) and 100 m*M* boric acid (Sigma) pH adjusted to 8.7 with cesium hydroxide (Sigma). HEC with a viscosity range of 86–113 cP for a 2% solution (Aldrich, Milwaukee, WI, USA) was dissolved in this buffer at a concentration of 1.0% (w/v), and the solution was filtered through a 0.45-μm cellulose acetate disposable filter (Corning 25943; Corning Glass Works, Corning, NY, USA). Prior to analysis ethidium bromide (Sigma) was added to the run buffer to a concentration of 1.27 μM and YO-PRO-1 dye was added to a concentration of 50 ng/ml. In the analysis of pBR322 *Hae*III digested DNA, ethidium bromide was not added and the YO-PRO-1 concentration was 5 ng/ml.

When fresh capillaries were prepared, the new columns were hand-flushed by attaching a syringe to the end of the capillary column and forcing buffer through the length of the capillary. Each day, the capillary column was rinsed for 20

min with HPLC-grade methanol (Fisher Scientific, Fair Lawn, NJ, USA) and then for 20 min with buffer. Prior to each individual run, the columns were rinsed for 2 min with methanol and 6 min with buffer [13]. Following the methanol and buffer wash, the samples were injected electrodynamically at 5 kV for 10 s. Typical run times were 35 min.

RESULTS AND DISCUSSION

The YO-PRO-1 dye was selected for these studies due to its compatibility with the argon-ion laser excitation 488 line, good photostability, and a partition coefficient between DNA and a 10% ethanol solution of $8 \cdot 10^6$ [17]. While there is also a dimer available with an even higher partition coefficient of $6 \cdot 10^8$, (YOYO-1), we did not pick this dye for our initial experiments due to concern about irreversible binding to the column walls [20]. Another advantage to YO-PRO-1 is that it has virtually no fluorescence unless bound to DNA [17]. This property was especially significant given that our intention was to add the dye directly to the sieving buffer. Unbound fluorescent dye without this property could significantly reduce sensitivity and enhance the background signal.

Initial experiments were carried out in order to determine the proper ratio of dye to DNA. Work carried out by Schwartz and Ulfelder [14] on thiazole orange (a dye similar in structure to YO-PRO-1) suggested that the ratio of dye to DNA would be critical in maintaining separation efficiency. Ethidium bromide did not produce such dramatic effects, although there is a rela-

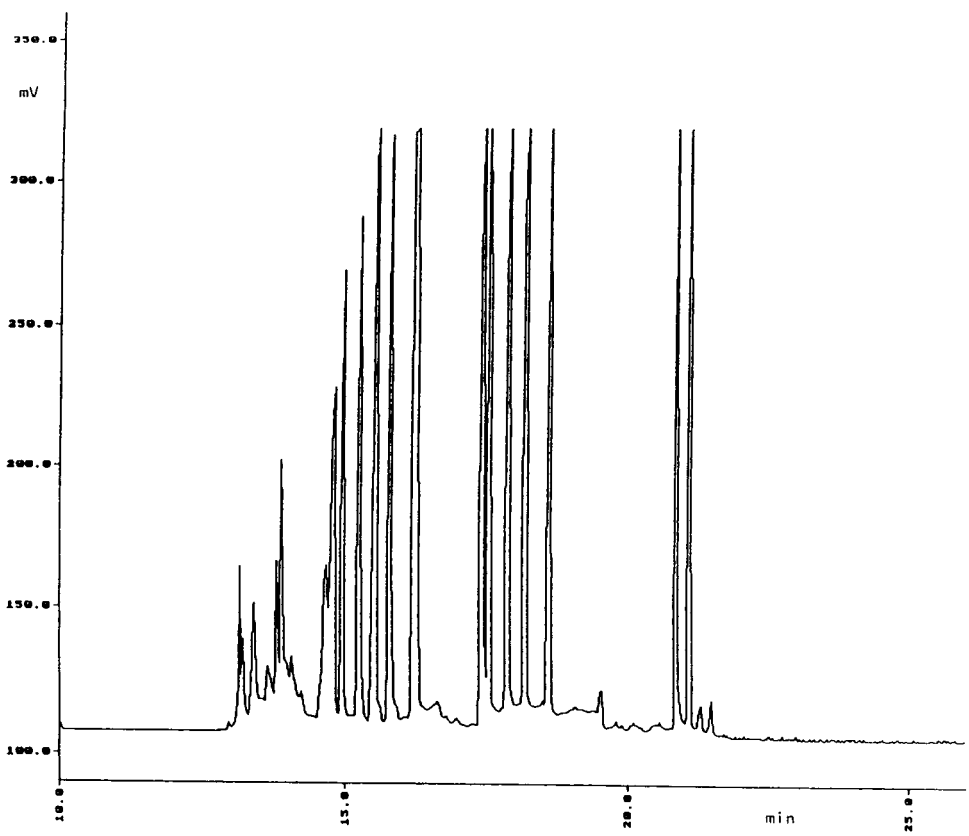

Fig. 1. pBR322 *Hae*III digested DNA (50 μg/ml) showing effect of depletion of intercalating dye in the buffer. Note the reduced fluorescence of the late eluting peaks. Buffer: 100 m*M* Tris–borate, pH adjusted to 8.7 with CsOH, 0.75% HEC, 1.27 μM ethidium bromide, 50 ng/ml YO-PRO-1.

tionship between efficiency and the concentration of this dye in the buffer [13,21].

It is our opinion that studies of this nature must be carried out with extreme care, as the dynamic interactions between column surface and buffer can have an overwhelming effect on the quality of the separation, obscuring secondary effects such as small differences in dye concentration. Different capillary columns can produce dramatically different separations and dye molecules and buffer components can irreversibly bind to the walls of these columns.

Initially we examined 50 μg/ml of the pBR322 sample using 50 ng/ml YO-PRO-1 dye in the presence of 1.27 μg/ml ethidium bromide (Fig. 1). This figure shows an effect which we ascribe to the depletion of the YO-PRO-1 dye as the DNA moves through the buffer. Note how the three late-eluting peaks show minimal fluorescence. Presumably, dye throughout the column has been depleted before these peaks have had a chance to come in contact with it. This effect illustrates the high binding constant of YO-PRO-1 with DNA. We also saw effects resulting from adsorption of the dye to the walls. Even after removing both ethidium bromide and YO-PRO-1, and washing out the column for 30 min with methanol and dye-free running buffer, significant fluorescence was seen for early eluting peaks in a subsequent analysis.

Further work revealed that when ethidium bromide was not present, the optimum concentration of the YO-PRO-1 dye was 5 ng/ml with a DNA concentration of 500 ng/ml. At dye concentrations higher than this, the DNA peaks of 434 bp and above broadened and became poorly resolved. However, even at a concentration of 100 ng/ml the resolution of peaks from 80 to 267 bp was not greatly diminished. Fig. 2 shows the effect of YO-PRO-1 concentration on the selectivity of the method. Note that only at a YO-PRO-1 concentration of 5 ng/ml were the peaks of 434 bp and 458 bp separated.

The effect of changing the concentration of the pBR322 DNA standard from 500 to 5 ng/ml, with a YO-PRO-1 concentration of 5 ng/ml, was minimal. In fact, with DNA:dye ratios from 100:1 to 1:10, the number of theoretical plates determined for the 267 bp peak varied only from

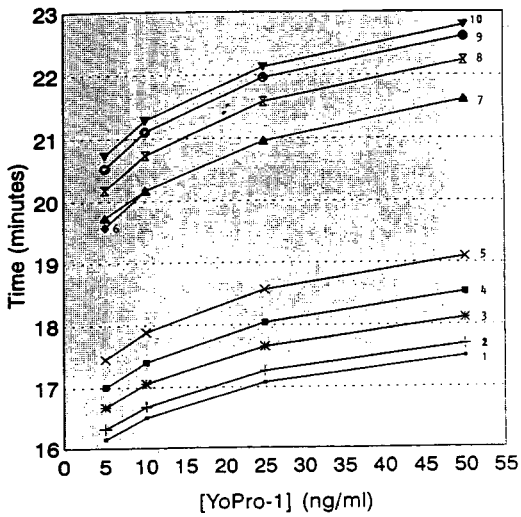

Fig. 2. Selectivity effects of increasing YO-PRO-1 dye concentration for 5 ng/ml pBR322 *Hae*III digested DNA. 1 = Peak 184; 2 = peak 192; 3 = peak 213; 4 = peak 234; 5 = peak 267; 6 = peak 434; 7 = peak 458; 8 = peak 504; 9 = peak 540; 10 = peak 587.

$4 \cdot 10^5$ to $7 \cdot 10^5$, and resolution ranged from 6 to 9 bp. These experimental data do not suggest a major effect on efficiency due to DNA:dye ratio.

In general for the pBR322 *Hae*III digested DNA we obtained excellent results with DNA concentration ranges from 5 to 500 ng/ml using 5 ng/ml of YO-PRO-1 dye in the buffer. Fig. 3 gives an example of the pBR322 standard at the 5 ng/ml concentration. The minimum detectable concentration at which the last 11 major peaks could be determined was 500 pg/ml of pBR322 *Hae*III digested DNA using a 30-s injection at 5 kV. This high sensitivity is due to the dye's near-zero fluorescence unless bound to DNA [17].

Analysis of samples

In this laboratory, we are currently exploring a number of genetic markers for application to forensic analysis. By combining all the major alleles present in a sample population into a single reference standard, the ability of the CE method to resolve any given pair of alleles can be experimentally verified. Three loci containing VNTRs with repeat units of 4 bp were selected for this study to determine if a viable technique

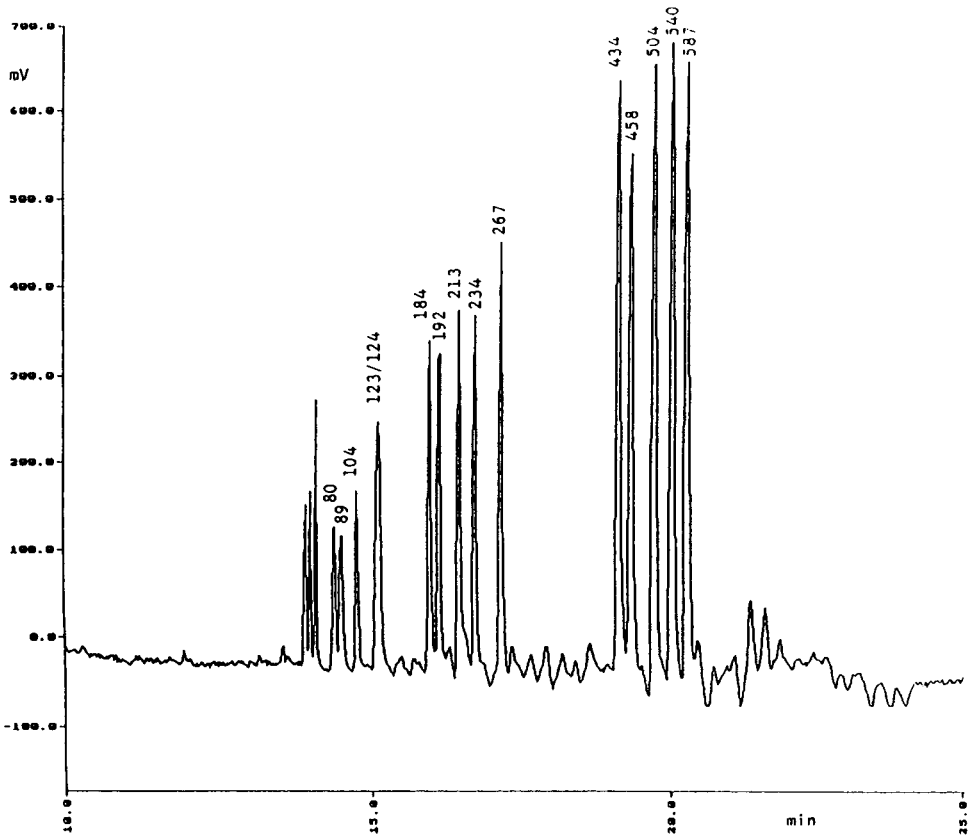

Fig. 3. pBR322 *Hae*III digested DNA (5 ng/ml). Buffer as in Fig. 1 except no ethidium bromide in buffer and YO-PRO-1 concentration of 5 ng/ml.

for the analysis of such samples could be developed using CE with laser fluorescence and non-gel sieving buffers.

Each of these samples contained a series of alleles which consist of 4 bp repeats. The first locus examined was HUMTHO1 (TC-11) located on chromosome 11. The alleles used in this sample contained 7 DNA fragments ranging from 183 to 207 bp [15,22]. One problem was immediately apparent. The resolution obtained in preliminary experiments with pBR322 DNA and a YO-PRO-1 concentration of 5 ng/ml was not adequate to resolve these samples. Resolution of 4 bp or better was needed. Fig. 4 shows that even with the concentration of HEC increased to 1%, it is not possible to resolve a mixture of alleles from the TC-11 genetic locus.

In a further attempt to improve resolution, ethidium bromide was added to a concentration of 1.27 μM. The results yielded resolution of nearly 4 bp, but sensitivity was reduced more than 10-fold. This concomitant loss of sensitivity may be the result of two factors: the higher background fluorescence of ethidium bromide, and a competition between ethidium bromide and YO-PRO-1 for active sites on the DNA molecules.

To help improve the sensitivity, the concentration of YO-PRO-1 in the buffer was increased to 50 ng/ml and the PCR samples were diluted 10:1 with distilled water containing 50 ng/ml YO-PRO-1 dye prior to analysis. Fig. 5 shows the result using a buffer containing 1.27 μM ethidium bromide and 50 ng/ml YO-PRO-1. Peak intensity is equivalent to that shown in Fig. 4, with all 7 alleles clearly distinguished. Thus, the addition of ethidium bromide is necessary for improved efficiency even when YO-PRO-1 dye is

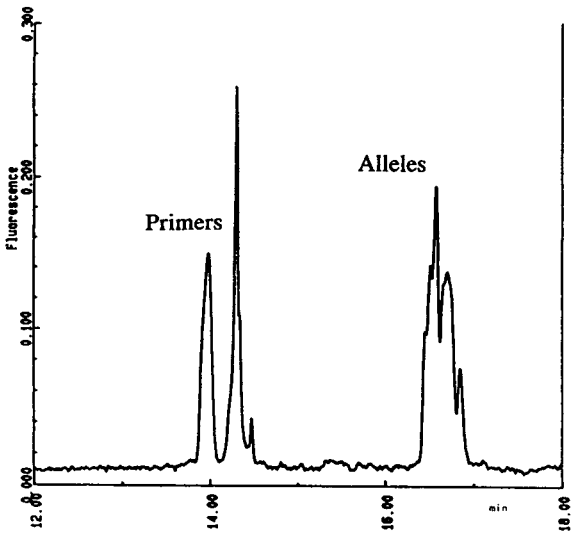

Fig. 4. Mixture of 7 HUMTHO1 alleles amplified via the PCR with each allele 4 bp apart. Buffer: 100 m*M* Tris–borate, pH adjusted to 8.7 with CsOH, 1.0% HEC, 5 ng/ml YO-PRO-1.

present. Increasing the HEC polymer concentration to 1% further enhanced the column efficiency.

The improved resolution of the sample peaks

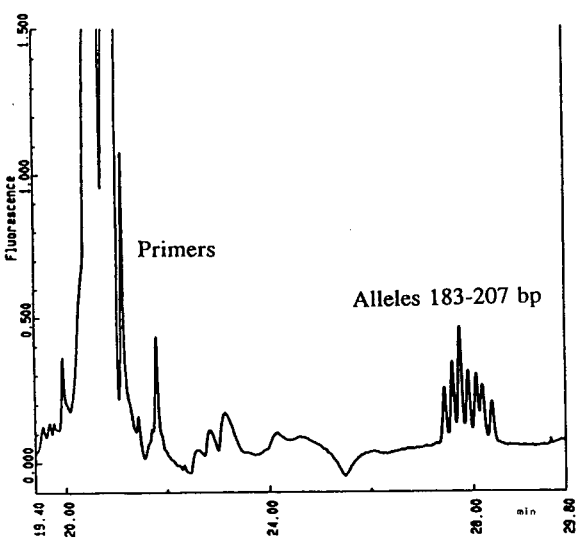

Fig. 5. Mixture of 7 HUMTHO1 alleles amplified via the PCR with each allele 4 bp apart. Buffer: 100 m*M* Tris–borate, pH adjusted to 8.7 with CsOH, 1.0% HEC, 5 ng/ml YO-PRO-1, 1.27 μM ethidium bromide. Sample diluted 1:10 with 50 ng/ml YO-PRO-1.

may result from a specific effect of ethidium bromide. In addition to being usable at a higher concentration than YO-PRO-1, ethidium bromide has a single positive charge and a nonpolar end. The ethidium bromide may reduce wall effects of the capillary by ion pairing with residual silanol groups with have been missed in the column coating process. Subsequently, the exposed non-polar end may lower electroosmotic flow and increase overall resolution. The higher ethidium bromide concentration in the buffer may also play a role in the resolution enhancement, as the YO-PRO-1 dye concentration may not be sufficient to completely intercalate the DNA.

While the major improvement in sensitivity came as a result of the increase in YO-PRO-1 concentration, pretreatment of the sample with the YO-PRO-1 dye did appear to improve sensitivity as well. Further experimentation is required to determine the actual rates of exchange between bound and unbound dye in the presence of ethidium bromide and other buffer components. It has been shown that similar dye–DNA complexes dissociate under gel electrophoresis conditions in the absence of free dye [23]. As shown above (Fig. 1), in the presence of excess DNA the amount of YO-PRO-1 in the run buffer can be locally depleted, resulting in variable fluorescence intensity. For this reason pretreatment of unknown quantities of DNA with YO-PRO-1 is desirable.

The second genetic marker analyzed was a 4 bp repeat located on chromosome 12 within intron 40 of the Von Willenbrand Factor gene [24]. This locus has been given the name vWA. The sample contained a mixture of 7 alleles ranging in size from 138 to 162 bp. The concentration of this PCR product was not as high as that for the TC-11 system. For this reason, the sample was diluted 1:1 with 50 ng/ml YO-PRO-1 and the injection time was increased to 20 s. Fig. 6 shows this sample. The results reveal excellent resolution of all 7 alleles.

The last genetic marker examined was a pair of VNTRs located 5′ to the human myelin basic protein gene on chromosome 18g22-qter [25]. This locus, identified as MBP, contains two VNTRs, each with a 4 bp repeat. The first

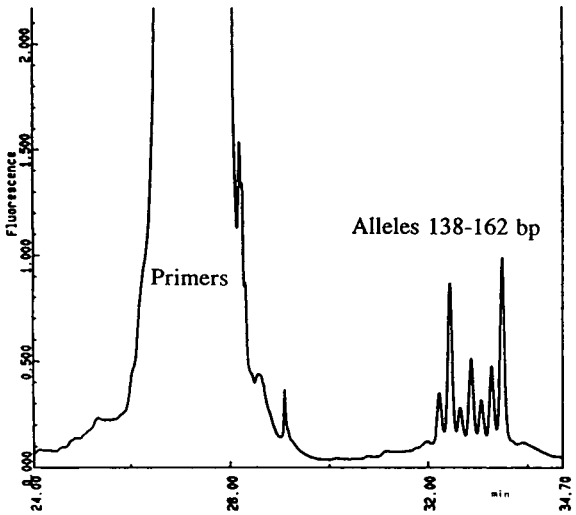

Fig. 6. Mixture of 7 vWA alleles amplified via the PCR with each allele 4 bp apart. Buffer as in Fig. 5. Sample diluted 1:1 with 50 ng/ml YO-PRO-1.

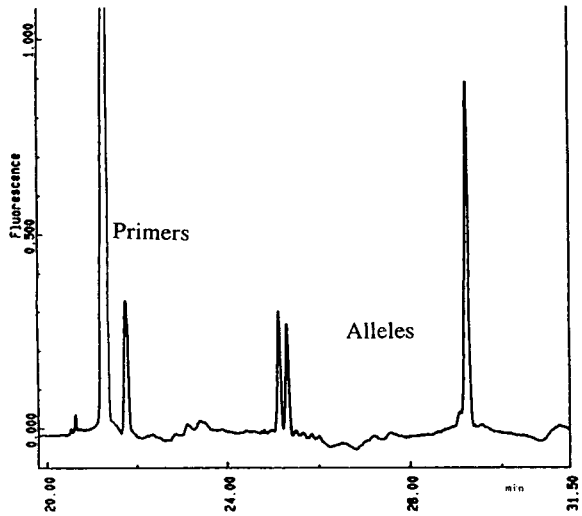

Fig. 8. Single set of MBP alleles extracted from liquid blood sample and amplified via the PCR. Buffer as in Fig. 5.

VNTR contains alleles from 122 to 142 bp in length while the second VNTR contains alleles from 208 to 232 bp in length.

Fig. 7 shows a mixture of alleles from this locus. The 3′ PCR primer for the MBP system can attach at two different locations, both before and after the second VNTR in the region, allowing the two VNTRs to be amplified at the same time. The size of the second set of alleles is a function of the length of both VNTRs. The CE buffer system easily separates both sets of alleles simultaneously.

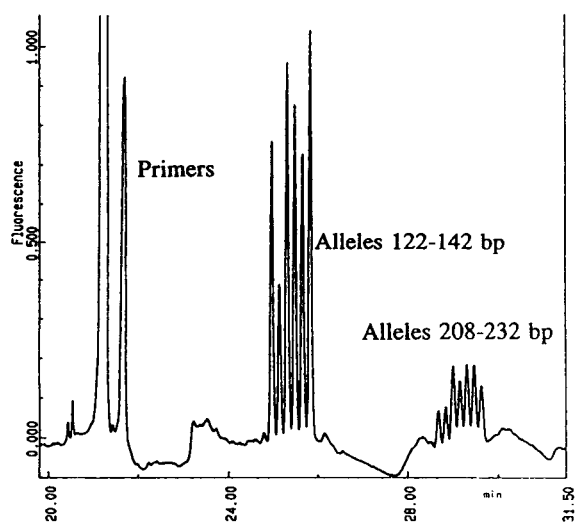

Fig. 7. Mixture of 13 MBP alleles amplified via the PCR. Note that this is a binary system. Buffer as in Fig. 5.

Fig. 8 shows the analysis of a sample of DNA extracted and amplified at the MBP locus. The lower-molecular-mass VNTR shows two alleles while a single peak is seen from the higher-molecular-mass VNTR, thus both of the DNA fragments obtained from the second VNTR have the same apparent molecular mass.

CONCLUSIONS

The results presented here show that CE has great potential in the analysis of PCR-amplified DNA of forensic interest. By using non-gel sieving buffers coupled with fluorescence detection, sensitive and specific detection of PCR-amplified DNA can be achieved. The intercalating dye YO-PRO-1 has been shown to facilitate sensitive detection of DNA fragments and to allow a wide range of concentration ratios of DNA/dye with little degradation in performance. For the analysis of samples requiring high separation efficiency, it is necessary to add

ethidium bromide to the buffer as well as YO-PRO-1. Using this procedure, alleles from a number of VNTRs of interest in genetic typing were investigated. Further work will be performed to examine the role ethidium bromide plays in improving column performance and to develop internal standards for the precise determination of sample retention times.

ACKNOWLEDGEMENTS

The authors would like to thank the South Carolina Law Enforcement Division for support of D.McC. as a Visiting Scientist to the FBI Laboratory. We would also like to thank Dr. Catherine Comey, Dr. Greg Parsons and Ms. Jeri Replogle for help in the preparation of samples and for many useful discussions.

This is publication No. 93-09 of the Laboratory Division of the Federal Bureau of Investigation. Names of commercial manufacturers are provided for identification only and inclusion does not imply endorsement by the Federal Bureau of Investigation.

REFERENCES

1 P.K. Saki, S. Scharf, F. Faloona, K.B. Mullis, G.T. Horn and H.A. Erlich, *Science*, 230 (1985) 1350–1354.
2 S.J. Odelberg and R. White, in J. Ballantyne, G. Sensabaugh and J. Witkowski (Editors), *DNA Technology and Forensic Science*, Cold Spring Harbor Press, Cold Spring Harbor, NY, 1989, p. 257.
3 G.F. Sensabaugh and C. von Beroldingen, in M.A. Farley and J.J. Harrington (Editors), *Forensic DNA Technology*, Lewis Publishers, Chelsea, MI, 1991, pp. 63–82.
4 A.S. Cohen and B.L. Karger, *J. Chromatogr.*, 387 (1987) 409.
5 A. Guttman and N. Cooke, *J. Chromatogr.*, 559 (1991) 285.
6 A. Guttman and N. Cooke, *Anal. Chem.*, 63 (1991) 2038.
7 X.C. Huang, S.G. Stuart, P.F. Bente III and T.H. Brennan, *J. Chromatogr.*, 600 (1992) 289.
8 W.A. MacCrehan, H.T. Rasmussen and D.M. Northrup, *J. Liq. Chromatogr.*, 15 (1992) 1063.
9 M. Zhu, D.L. Hansen, S. Burd and F. Gannon, *J. Chromatogr.*, 480 (1989) 311.
10 P.D. Grossman and D.S. Sloane, *Biopolymers*, 31 (1991) 1221.
11 H.E. Schwartz, K. Ulfelder, F.J. Sunzeri, M.P. Busch and R.G. Brownlee, *J. Chromatogr.*, 559 (1991) 267.
12 S. Nathakarnkitkool, P.J. Oefner, G. Bartsch, M.J. Chin and G.K. Bonn, *Electrophoresis*, 13 (1992) 18–31.
13 B. McCord, J. Jung and B.A. Holleran, *J. Liq. Chromatogr.*, 16 (1993) 1963.
14 H.E. Schwartz and K.J. Ulfelder, *Anal. Chem.*, 64 (1992) 1737.
15 A. Edwards, A. Civitello, H.A. Hammond and C.T. Caskey, *Am. J. Hum. Genet.*, 49 (1991) 746.
16 L.G. Lee, C.H. Chen and L.A. Chiu, *Cytometry*, 7 (1986) 508.
17 *Product Literature WN 9.3/9.4*, Molecular Probes, Eugene, OR, May 13, 1992.
18 B. Budowle, J.S. Waye, G.G. Schutler and F.S. Baechtel, *J. Forensic Sci.*, 35 (1989) 530.
19 R. Marusyk and A. Sergent, *Anal. Biochem.*, 104 (1980) 403.
20 K. Ulfelder, personal communication.
21 P. Oefner, G.K. Bonn, C.G. Huber and S. Nathakarnkitkool, *J. Chromatogr.*, 625 (1992) 331.
22 A. Edwards, H.A. Hammond, L. Jin, C.T. Caskey and R. Chakraborty, *Genomics*, 12 (1992) 241.
23 H.S. Rye, S. Yue, D.E. Wemmer, M.A. Quesada, R.P. Haugland, R.A. Mathies and A.N. Glazer, *Nucleic Acids Res.*, 20 (1992) 2803.
24 C. Kimton, A. Walton and P. Gill, *Human Molecular Genetics*, 1 (1992) 287.
25 K.B. Boylan, T.M. Ayres, B. Popko, N. Takahashi, L.E. Hood and S.B. Prusiner, *Genomics*, 6 (1990) 16.

Journal of Chromatography A, 652 (1993) 83–91
Elsevier Science Publishers B.V., Amsterdam

CHROM. 25 305

Electrophoretic separations of polymerase chain reaction-amplified DNA fragments in DNA typing using a capillary electrophoresis–laser induced fluorescence system

Kannan Srinivasan

Biotechnology Division, Chemical Sciences and Technology Laboratory, National Institute of Standards and Technology, Room A 353, Building 222, Gaithersburg, MD 20899 (USA)

James E. Girard

Department of Chemistry, The American University, Washington, DC 20016 (USA)

Patrick Williams, Rhonda K. Roby and Victor W. Weedn

Armed Forces DNA Identification Laboratory, Washington, DC 20306 (USA)

Sam C. Morris

Beckman Instruments, Columbia, MD 21045 (USA)

Margaret C. Kline and Dennis J. Reeder*

Biotechnology Division, Chemical Sciences and Technology Laboratory, National Institute of Standards and Technology, Room A 353, Building 222, Gaithersburg, MD 20899 (USA)

ABSTRACT

Analysis of polymerase chain reaction (PCR)-amplified DNA fragments for human identification requires high-resolution separation and efficient detection of amplified alleles. Capillary electrophoresis (CE) with its speed, automation, high resolution and efficiency shows promise for analyzing the amplified DNA fragments. CE with UV detection, however, suffers from lack of detector sensitivity owing to the limited detection path length of the capillary. By the use of intercalating dyes (TOTO and YOYO) a laser-induced fluorescence (LIF) detection system can provide much greater sensitivity for detecting DNA fragments. Femtogram quantities of dsDNA (ΦX174 *Hae*III restriction digest mixture) per nanoliter of injected volume have been detected. Application of CE–LIF to analysis of PCR-amplified DNA fragments from three different genetic loci (apolipoprotein B, VNTR locus D1S80, mitochondrial DNA) is shown here. Further, the resolving power of a polymer-network capillary separation system is compared to that of a capillary-gel separation system.

* Corresponding author.

0021-9673/93/$06.00

INTRODUCTION

The ability of the polymerase chain reaction (PCR) to make multiple copies from minute quantities of DNA extracted from blood, hair or semen has enabled new forensic approaches in human identification [1,2]. Generally DNA identification is based on differences in inherited genetic markers. Analytical techniques are employed following the PCR reaction to distinguish individuals based on these genetic differences. Techniques such as slab gel electrophoresis, various hybridization strategies, dot blot assays and direct sequencing are used to analyze the amplified PCR products [3]. Capillary electrophoresis (CE), due to its automation, speed and ability to analyze small sample volumes shows high potential for PCR product analysis.

At present, DNA fragments are analyzed by two major CE approaches: a polymer-network capillary separation system [4–7] and a capillary-gel separation system [8–10]. The polymer-network system is based on buffers containing additives such as methylcellulose, hydroxypropylmethylcellulose, dextran or polyethylene glycol, which create a gel-like matrix inside the capillary. The migrating DNA fragments interact with the dynamic pores of this matrix resulting in separations based on size. The capillary-gel system on the other hand, uses an *in situ* polymerized acrylamide gel cross-linked to the walls of the capillary. Fixed pores in the gel retard migration of the DNA fragments in a manner similar to that in slab gels and, consequently, results in separations based on size. These approaches have their own limitations. The gel-filled capillaries are difficult to manufacture with sufficiently large pores, suffer from matrix contraction problems and often have problems associated with air bubbles, thus restricting their useful life. Nevertheless, gel-filled capillaries have proven useful in high-resolution separation of oligonucleotides or of smaller double-stranded DNA (dsDNA) fragments. Polymer-network capillaries owing to their wider range of pore sizes offer comparable or better separations to the gel-filled capillaries [11]. They are, however, restricted by the viscosity of the buffer–polymer mixtures, making it difficult to completely fill the capillaries. In addition to the buffer, capillary dimensions, applied field, injection, the amount of polymer as well as the chain length of the polymer affect the separations in both systems.

Since the validity of DNA typing increases with the number of marker systems used, we tested both CE approaches for their ability to effectively separate polymorphic PCR-amplified DNA fragments. We used three different genetic systems: (1) apolipoprotein system (apo B) [700–1000 base pairs (bp)] [12], (2) Variable number tandem repeat (VNTR) locus D1S80 (300–700 bp) [13] and (3) mitochondrial DNA system (mtDNA) (130–140 bp) [14]. The goal of this study was to find a separation system that would be useful in analyzing PCR-amplified DNA fragments from loci that differ in number of base repeats and in size.

Initial efforts to analyze PCR-amplified products failed when we used UV detection at 260 nm both in capillary gels and in polymer-network capillaries [15]. Nonetheless, we were able to analyze the same products using slab-gel electrophoresis with silver staining (data not shown). We have observed that some PCR-amplified samples are not amenable for analysis by UV, even when samples are desalted or dialyzed [16]. Failure to observe PCR products could be a result of amplification problems associated with the PCR or lack of sensitivity of UV detection. To compete with the sensitivity of silver staining, we employed a laser-induced fluorescence (LIF) detection system.

The utility of a CE–LIF system for analyzing PCR products was first shown by Schwartz and Ulfelder [17] who used thiazole orange dye in the CE run buffer. They showed roughly 400 times better sensitivity than that achieved with UV. We investigated asymmetric cyanine dyes TOTO (TOTO-1) and YOYO (YOYO-1) (Molecular Probes, Eugene, OR, USA)[a] based on a report of enhanced detection of DNA fragments

[a] Certain commercial equipment, instruments and materials are identified in this paper in order to specify experimental procedures as completely as possible. In no case does such identification imply a recommendation or endorsement by the National Institute of Standards and Technology nor does it imply that the material, instrument or equipment identified is necessarily the best available for the purpose.

by Rye *et al.* [18]. TOTO and YOYO are non-fluorescent dyes when free but fluoresce upon binding to dsDNA; this property makes them useful in applications that require high sensitivity [19,20]. Our studies showed suitability of TOTO and YOYO in detecting PCR-amplified DNA fragments [21]. We have also shown the analysis of PCR-amplified DNA fragments without any sample pretreatment step (dialysis or filtration) in an earlier publication [22]. Our approach included prestaining the samples in addition to incorporating a small amount of the dye to the run buffer. In this study we compare the polymer-network capillaries to gel-filled capillaries for their usefulness in DNA typing by using a CE–LIF system with TOTO.

EXPERIMENTAL

Instrumentation

A P/ACE system 2100 CE apparatus coupled with an Ar ion laser source (Beckman Instruments, Fullerton, CA, USA) was used with negative source polarity. The laser source provides 4 mW excitation at 488 nm. A 530-nm band pass filter was used as an emission cut-off filter. Data were collected at 5 Hz and analyzed using System Gold software. The temperature was set at 25°C and electrophoretic runs were performed at the conditions specified in the figure captions. The coated capillary was flushed with buffer for 3 min between runs.

Capillaries

The polymer network separations were performed in a DB-17 (50% phenyl, 50% methyl silicone)-coated capillary (J&W Scientific, Sunnyvale, CA, USA). The gel separations were performed in 3%T, 3%C[a] urea and non-urea based gel-filled capillaries (J&W Scientific). The dimensions of the capillaries are indicated in the figure captions.

Dyes

TOTO was supplied as a 1 m*M* solution. [TOTO-1 is 1,1′-(4,4,7,7-tetramethyl-4,7-diazundecamethylene)-bis-4-[3-methyl-2,3-dihydro-(benzo-1,3-thiazole)-2-methylidene]-quinolinium tetraiodide].

Buffers

CE run buffer (1 ×) for all the polymer-network separations consisted of 89 m*M* Tris, 89 m*M* boric acid, 2 m*M* EDTA at pH 8.5. To this buffer was added 0.5% (w/w) methylcellulose (Sigma, St. Louis, MO, USA). Just prior to the CE analysis, 1 μl of a 1 m*M* dye solution of TOTO was added to 15 ml of the run buffer. Gel separations were performed on (urea and non-urea based) μPage buffers (J & W Scientific) and supplemented by the addition of 1 μl of 1 m*M* TOTO to 15 ml of the buffer.

Polymerase chain reaction protocol

DNA was extracted using a modified Chelex-100 procedure [23] by incubating three human hair roots in a 5% Chelex-100 suspension overnight at 56°C. After a 5-min heating in a boiling-water bath, the samples were ready for PCR amplification on a Perkin-Elmer Cetus 9600 thermal cycler. The region coding for the genetic system D1S80 [13] and apo B [12] were amplified using prescribed primers at a concentration of $2.5 \cdot 10^{-5}$ μM $MgCl_2$ was added to achieve a 2.0 m*M* concentration in the PCR reaction tube. Each cycle was programmed to denature at 94°C for 10 s, anneal for 20 s at 68°C and extend at 72°C for 30 s. The samples were analyzed after 30 amplification cycles. The mtDNA PCR samples were amplified using DNA extracted from whole blood with 100 ng of prescribed primers [14] in a total volume of 50 μl. The conditions of PCR include 1 cycle at 94°C for 30 s followed by 30 cycles programmed to denature at 94°C for 10 s, anneal at 50°C for 10 s and extend at 72°C for 1 s.

Samples and standards

Samples of ΦX174 *Hae*III DNA (BRL Labs., Gaithersburg, MD, USA) restriction fragments were diluted to the required concentration using deionized water. The PCR samples were pretreated on a 0.025 μm pore size, 25 mm diameter MF-Millipore membrane filter (Millipore, Milford, MA, USA) for 20 min [16]. For prestaining, the DNA samples were always added to

[a] T = [2.91 g acrylamide monomer + 0.09 g N,N′-methylenebisacrylamide (Bis)]/100 ml solution; C = g Bis/%T.

the dye as recommended by Molecular Probes, at the desired DNA base pair-to-dye molar ratio of 5:1. The samples were incubated at room temperature for at least 20 min before analysis. The PCR samples were prestained by diluting 1 μl of the 1 m*M* dye to 1 ml and adding 1–20 μl of the sample.

RESULTS AND DISCUSSION

The purpose of this work was to identify a single separation method for analysis of PCR-amplified DNA fragments of forensic origin (irrespective of the marker system under consideration). High-resolution separation and sensitive detection of the amplified products are primary requirements for typing. Our earlier work has shown the suitability of methylcellulose polymer-based separation systems in analyzing VNTR locus D1S80 alleles with TOTO as an additive. Using the same system we show here the analysis of both apo B DNA (14 bp repeat) and mtDNA (2 bp repeat).

Fig. 1 (inset) demonstrates the sensitivity of the CE–LIF system with an analysis of a standard DNA ladder (0.5 pg/μl) consisting of 11 fragments. Femtogram amounts are detected per nanoliter of injected volume. The peak marked 118 contains roughly 2% of the total amount of DNA injected (assuming that equal amounts of the different fragments are injected). The migration times at two different concentrations 150 pg/μl and 0.5 pg/μl showed very little difference, indicating that the effect of DNA concentration on migration was minimal in the presence of TOTO under the conditions shown here. At low DNA concentrations, however, we have observed that some smaller-sized fragments showed higher relative fluorescence than the larger ones. This is possibly associated with differences in dye binding kinetics. Reproducibility studies with a ΦX174 *Hae*III digest using an internal standard (PCR-LIF kit, Beckman In-

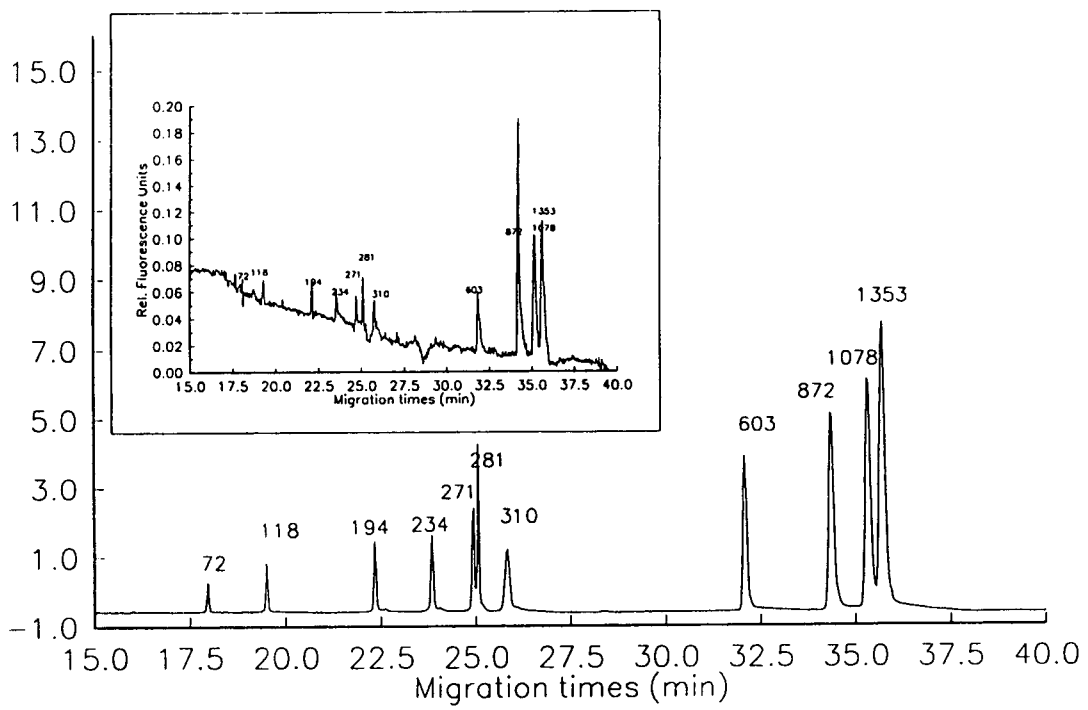

Fig. 1. Analysis of a ΦX174 DNA restriction fragment mixture with sizes as indicated. Conditions: A DB-17 capillary from J & W Scientific (40 cm × 100 μm); electrophoretic run at constant voltage of 10 kV; injection at 10 kV for 5 s; Sample 0.15 ng/μl ΦX174 DNA *Hae*III digest. Inset shows the analysis of the same digest at a concentration of 0.5 pg/μl under the same conditions.

struments) showed a relative standard deviation (R.S.D.) of less than 1.5% in migration times ($n = 10$).

Resolution and DNA typing

In DNA typing applications it is important to differentiate heterozygous from homozygous individuals. Lack of resolution of the PCR-amplified fragments would result in inaccurate typing results. To optimize resolution of apo-B PCR-amplified products, we varied the applied voltage. Reducing the field strength improved separations of the larger fragments at the expense of time as shown in Fig. 2. In addition to voltage effects, increased resolution may also be attributed to increased interactions with the sieving matrix. Fig. 3 shows the effect of sample load on separation; increased sample loads decreased both resolution and efficiency of separations. A 10 kV s injection was found to be optimal for analyzing PCR-amplified DNA fragments.

Analysis of the apo B PCR-amplified DNA fragments from four different individuals is shown in Figs. 4 and 5. Using the polymer-network capillary separation system we could distinguish all four. Average efficiencies of greater than $1.5 \cdot 10^6$ plates/m were achieved. A 3%T, 3%C urea-based gel-filled capillary, when used for analyzing one of the apo B samples, resulted in multiple peaks with excessive band broadening (Fig. 6). Additionally, the same PCR-amplified products when analyzed on a 3%T, 3%C non-urea gel were not optimally resolved and showed broad peaks as shown in Figs. 7 and 8.

We hypothesize that the 3%T, 3%C urea-based gel-filled capillaries are not as effective in

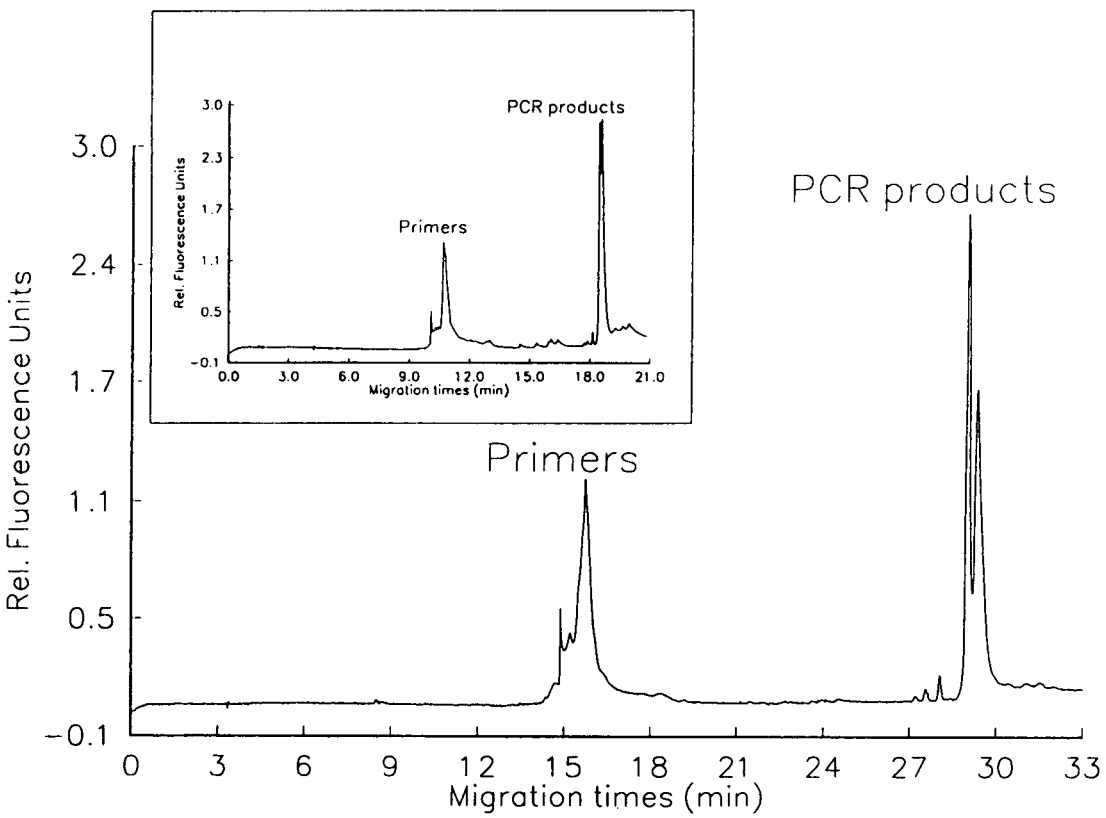

Fig. 2. Analysis of PCR-amplified DNA fragments coding for the apo B gene at two different voltages. Conditions: A DB-17 capillary from J & W Scientific (50 cm × 50 μm); electrophoretic run at constant voltage of 10 kV; injection at 10 kV for 5 s. Inset shows separation of the same product at constant voltage of 15 kV; injection at 10 kV for 5 s.

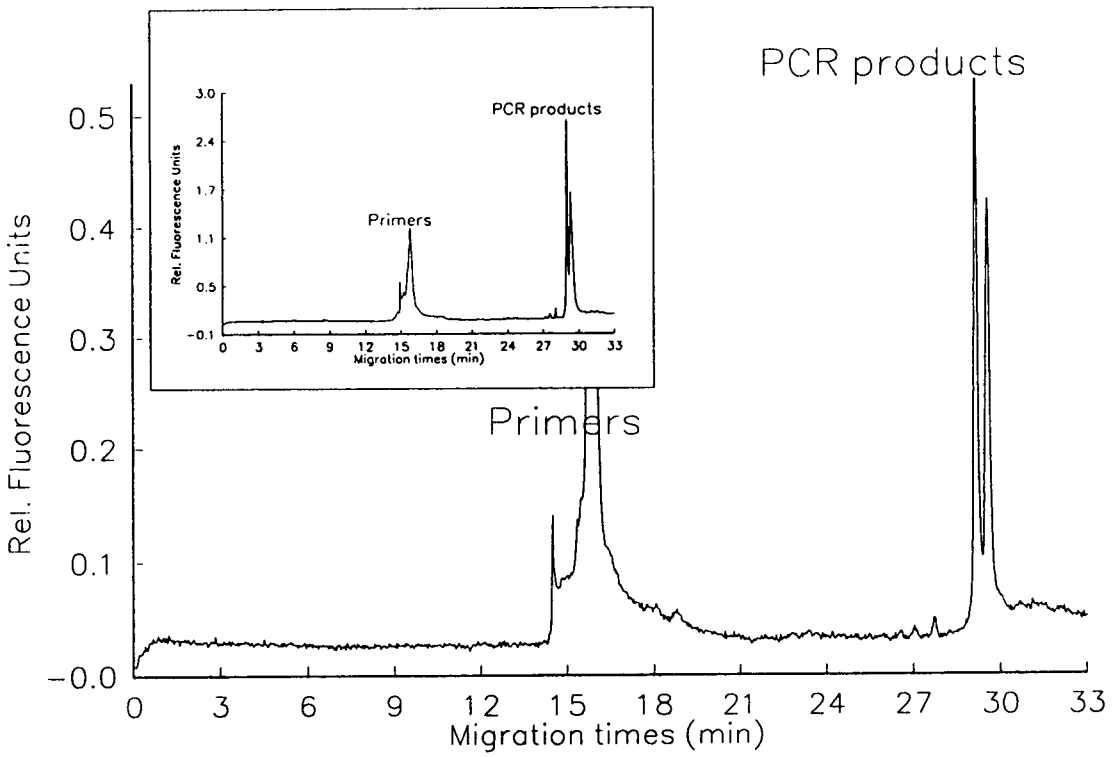

Fig. 3. Analysis of PCR-amplified DNA fragments coding for the apo B gene at two different injections. Conditions: A DB-17 capillary from J & W Scientific (50 cm × 50 μm); electrophoretic run at constant voltage of 10 kV; injection at 10 kV for 1 s. Inset shows separation of the same product at 10 kV; injection at 10 kV for 5 s.

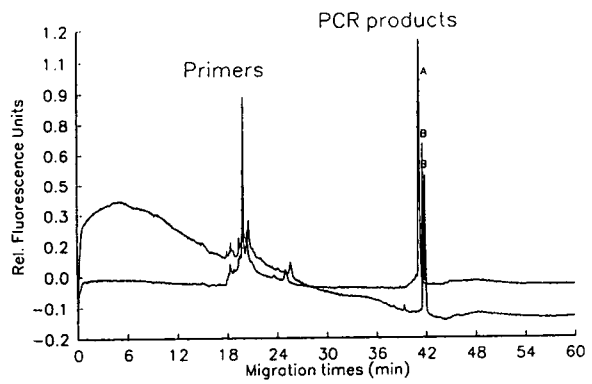

Fig. 4. Analysis of PCR-amplified DNA fragments coding for the apo B gene of a homozygous and a heterozygous individual A and B. Conditions: A DB-17 capillary from J & W Scientific (50 cm × 50 μm); electrophoretic run at constant voltage of 8 kV; injection at 10 kV for 1 s.

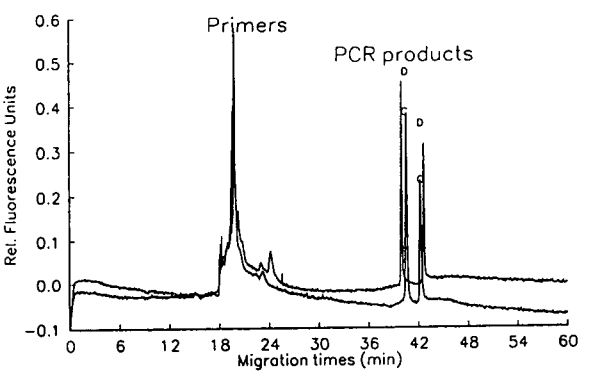

Fig. 5. Analysis of PCR-amplified DNA fragments coding for the apo B gene of two different heterozygous individuals C and D. Conditions as in Fig. 4.

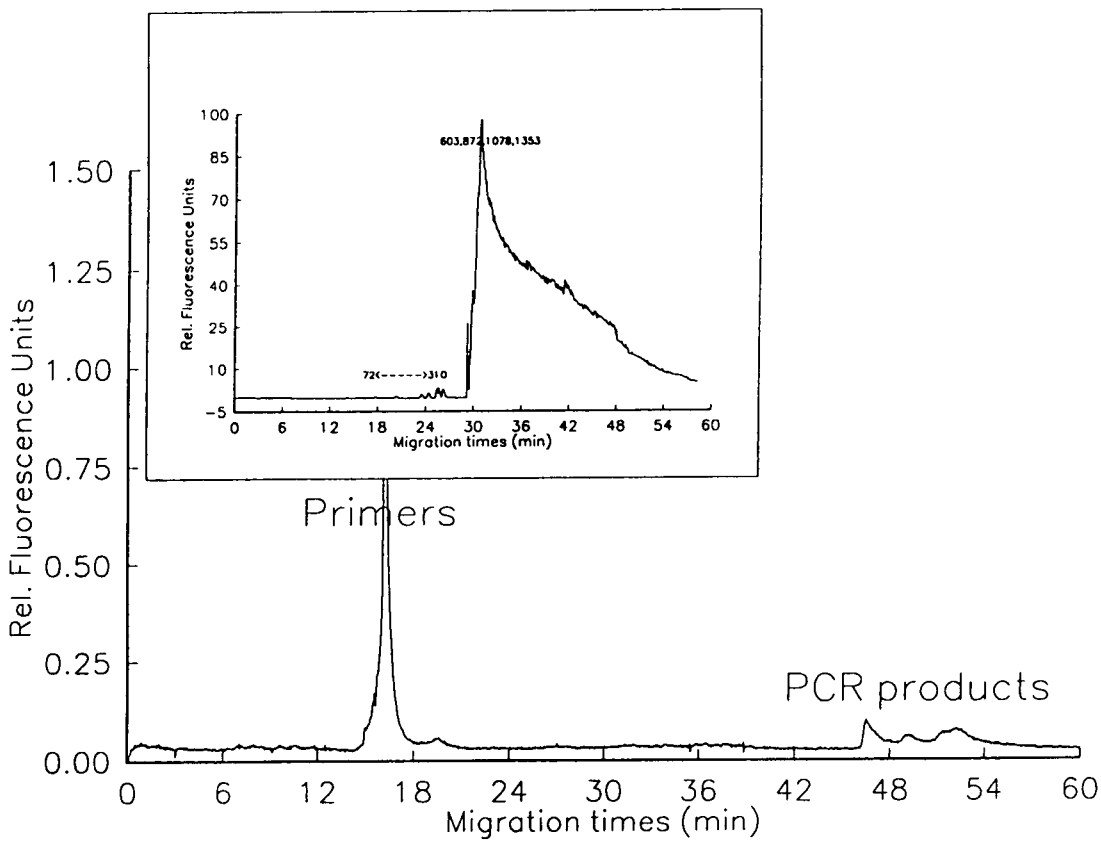

Fig. 6. Analysis of PCR-amplified DNA fragments coding for the mt locus of an individual. Conditions: A 3%C, 3%T urea-gel capillary from J & W Scientific (40 cm × 50 μm); electrophoretic run at constant voltage of 10 kV; injection at 5 kV for 5 s. Multiple peaks with band broadening are observed for this heterozygous individual. Inset shows the analysis of a ΦX174 DNA restriction fragment mixture showing the same behavior for the bigger fragments.

resolving larger DNA fragments due to increased non-specific interactions with the intercalating dye. Urea is known to denature DNA fragments, even at low urea concentrations. TOTO has a high binding affinity for DNA and, in a denaturing environment, binds to single strands of DNA to induce further conformational changes. In addition, we speculate that the TOTO in the run buffer binds to the limited number of free capillary surface silanols that were not masked by the gel-coating process resulting in cationic sites being available along the capillary walls for interaction (TOTO has 4 cationic charges available). These charges may interact with DNA fragments resulting in band broadening. These effects are more obvious for the larger fragments possibly due to their size and longer residency in the capillary column. Use of a non-urea-based gel provided us with separations of some of the higher-molecular-mass species showing that urea has some deleterious effect. In this case, resolution was not optimal possibly due to the rigid pore structure of these gels.

Comparisons of the separation times of the amplified mtDNA fragments on both systems showed very little difference (Figs. 9 and 10). However, the gel-filled capillary separations showed broad peaks with much lower efficiencies and resolution. The polymer-network capillaries show better separations and a broader range of applicability than the gel-filled capillaries used in this study. Fig. 11 shows the separation of the larger D1S80 alleles of a single individual using the polymer-network capillary system. The poly-

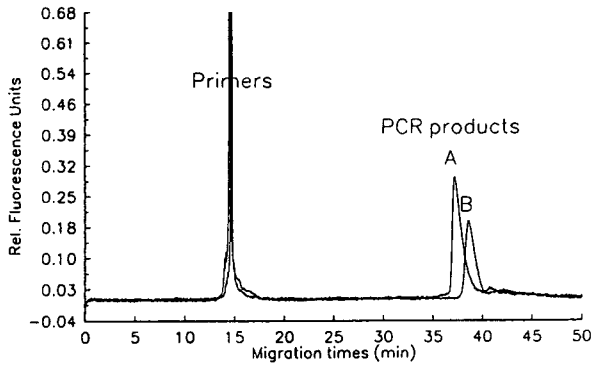

Fig. 7. Analysis of PCR-amplified DNA fragments coding for the apo B gene of a homozygous and a heterozygous individual A and B. Conditions: A 3%C, 3%T non-urea gel capillary from J & W Scientific (40 cm × 50 μm); electrophoretic run at constant voltage of 10 kV; injection at 5 kV for 5 s. The heterozygous individual B appears homozygous in this separation.

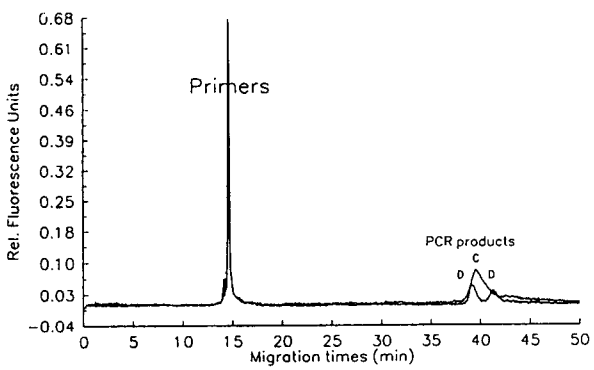

Fig. 8. Analysis of PCR-amplified DNA fragments coding for the apo B gene of two different heterozygous individuals C and D. Conditions as in Fig. 7. The heterozygous individual C appears as homozygous in this case.

mer-network capillaries may have a broader effective size range due to their flexible and larger effective pore structure.

CONCLUSIONS

CE–LIF detection results in a powerful approach to analyze PCR-amplified DNA fragments. The polymer-network capillaries offer higher separation efficiencies and resolution when compared to gel-filled capillaries used in this study. The polymer-network capillaries also have a broader DNA size range of effectiveness

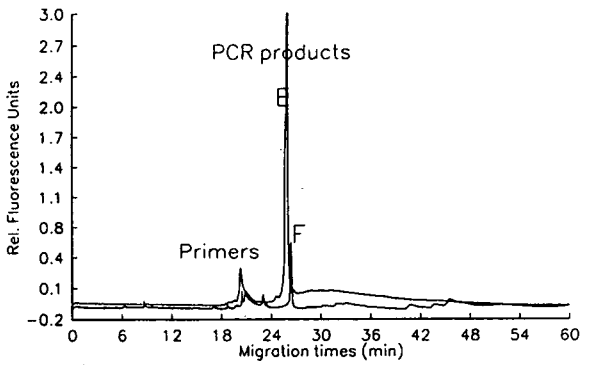

Fig. 9. Analysis of PCR-amplified mtDNA fragments of two different individuals E and F using a polymer-network capillary. Conditions as in Fig. 4.

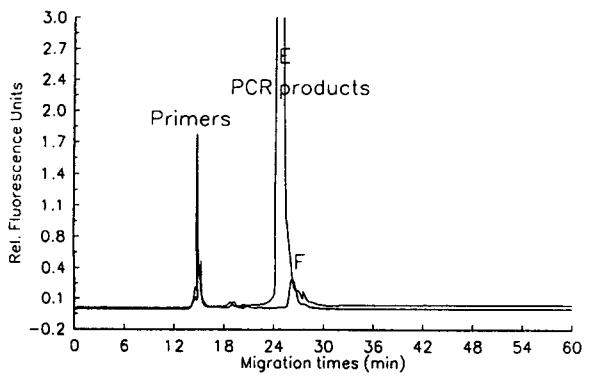

Fig. 10. Analysis of PCR-amplified mtDNA fragments of two different individuals E and F using a non-urea gel-filled capillary. Conditions as in Fig. 7.

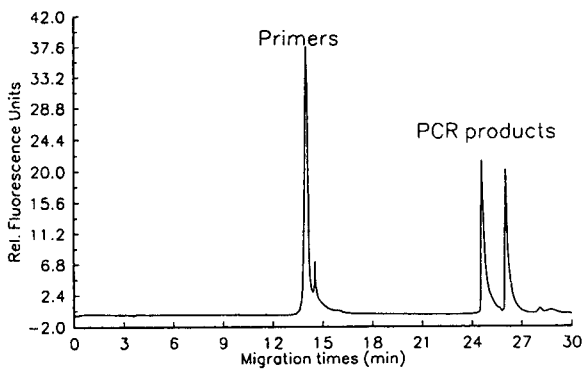

Fig. 11. Analysis of PCR-amplified DNA fragments coding for the VNTR locus D1S80 of an individual using a polymer-network capillary. Conditions of this run as in Fig. 1.

as demonstrated by the separations of various PCR-amplified fragments from different VNTR loci. The gel-filled capillaries did not provide us with efficient separations possibly due to interactions of the dye with the capillary and with the separation matrix. Further studies in terms of interactions of the dyes TOTO and YOYO with dsDNA [24] and the separation matrix are being pursued.

ACKNOWLEDGEMENTS

The National Institute of Justice provided support for this work through an interagency agreement with the National Institute of Standards and Technology (NIST). We thank Dr. David T. Mao of J & W Scientific for providing us capillaries for this study. We also thank Dr. Jess Edwards of NIST for helpful discussions.

REFERENCES

1 K.B. Mullis and F. Faloona, *Methods Enzymol.*, 155 (1987) 335.
2 R.K. Saiki, D.H. Gelfand, S. Stoffel, S.J. Scharf, R. Higuchi, G.T. Horn and H.A. Erlich, *Science*, 239 (1988) 487.
3 R. Reynolds, G. Sensabaugh and E. Blake, *Anal. Chem.*, 63 (1991) 2.
4 M. Zhu, D.L. Hansen, S. Burd and F. Gannon, *J. Chromatogr.*, 480 (1989) 311.
5 M. Strege and A. Lagu, *Anal. Chem.*, 63 (1991) 1233.
6 W.A. MacCrehan, H.T. Rasmussen and D.M. Northrop, *J. Liq. Chromatogr.*, 15 (1992) 1063.
7 P.D. Grossman and D.S. Soane, *J. Chromatogr.*, 559 (1991) 257.
8 D.K. Heiger, A.S. Cohen, B.L. Karger, *J. Chromatogr.*, 516 (1990) 33.
9 A. Guttman and N. Cooke, *Anal. Chem.*, 63 (1991) 2038.
10 B. L Karger, A.S. Cohen and A. Guttman, *J. Chromatogr.*, 492 (1989) 585.
11 H.E. Schwartz, K. Ulfelder, F.J. Sunzeri, M.P. Busch and R.G. Brownlee, *J. Chromatogr.*, 559 (1991) 267.
12 E. Boerwinkle, S.S. Lee, R. Butler, V.N. Schumaker and L. Chan, *Atherosclerosis*, 81 (1990) 225.
13 K. Kasai, Y. Nakumara, and R. White, *J. Forensic Sci.*, 35 (1990) 1196.
14 A. Bodenteich, L.G. Mitchell, M.H. Polymeropoulos and C.R. Merril, *Human Molecular Genetics*, 1 (1992) 40.
15 K. Srinivasan, J.E. Girard, D.J. Reeder, R.K. Roby, P. Williams and V.W. Weedn, presented at the *5th International symposium on High Performance Capillary Electrophoresis, Orlando, FL, Jan. 1992*, Poster T205.
16 P. Williams, in *CE Application Note No. 2*, J & W Scientific, Sunnyvale, CA, August 1992.
17 H.E. Schwartz and K.J. Ulfelder, *Anal. Chem.*, 64 (1992) 1737.
18 H.S. Rye, S. Yue, D.E. Wemmer, M.A. Quesada, R.P. Haugland, R.A. Mathies and A.N. Glazer, *Nucleic Acids Res.*, 20 (1992) 2803.
19 I.D. Johnson, E.M. Marcus, S. Yue and R.P. Haugland, *Biophys. J.*, 61 (1992) A314.
20 A.N. Glazer and H.S. Rye, *Nature*, 359 (1992) 859.
21 K. Srinivasan, J.E. Girard, S.C. Morris and D.J. Reeder, presented at the *3rd Annual Frederick Conference on Capillary Electrophoresis, Frederick, MD, Oct. 1992*, Poster p28.
22 K. Srinivasan, S.C. Morris, J.E. Girard, M.C. Kline and D.J. Reeder, *Appl. Theor. Electrophoresis*, in press.
23 P.S. Walsh, D.A. Metzger and R. Higuchi, *BioTechniques*, 10 (1991) 506.
24 K. Srinivasan, S.C. Morris, J.E. Girard and D.J. Reeder, in preparation.

Journal of Chromatography A, 652 (1993) 93–99
Elsevier Science Publishers B.V., Amsterdam

CHROM. 25 107

Effect of urea concentration on the base-specific separation of oligodeoxynucleotides in capillary affinity gel electrophoresis

Yoshinobu Baba* and Mitsutomo Tsuhako

Kobe Women's College of Pharmacy, Kitamachi, Motoyama, Higashinada-ku, Kobe 658 (Japan)

Tomohiro Sawa and Mitsuru Akashi*

Department of Applied Chemistry and Chemical Engineering, Faculty of Engineering, Kagoshima University, Korimoto, Kagoshima 890 (Japan)

ABSTRACT

Base-specific separations of oligodeoxynucleotides were achieved with high resolution by electrophoresis, using a urea-gel capillary, in which poly(9-vinyladenine) (PVAd) was utilized as an affinity ligand. The migration behaviour and the plate number of oligodeoxynucleotides were investigated as a function of urea concentration between 2 and 10 *M* in capillary gel electrophoresis (CGE) as well as capillary affinity gel electrophoresis (CAGE). The migration time in CGE separation increases as urea concentration increases. An increase in the viscosity of the gel buffer medium as well as a change in the conformation of oligodeoxynucleotides is found to be a predominant factor for an increase in the migration time. The migration time and the plate number of oligothymidylic acids, which interact with PVAd in CAGE, is manipulated by differing urea concentration, which leads to the change in the dissociation process of a specific hydrogen bonding between oligothymidylic acids and PVAd. The migration time of oligodeoxyadenylic acids, which do not interact with PVAd in CAGE, increases with an increase in urea concentration as in CGE separation. The plate number of oligodeoxyadenylic acid was not affected by the urea concentration.

INTRODUCTION

Over the past decade, capillary electrophoresis (CE) has become an important technique for the separation of complex mixtures in the area of analytical biotechnology [1–9]. CE comprises several modes, including capillary zone electrophoresis (CZE) [2,3], micellar electrokinetic chromatography (MEKC) [4,5], capillary gel electrophoresis (CGE) [6–8] and capillary isoelectric focusing [9]. More recently capillary affinity gel electrophoresis (CAGE), which is another important mode of CE, has been introduced for the biospecific separation of oligodeoxynucleotides [10–14], DNA restriction fragments [15] and optical isomers [16]. CAGE, in which an affinity ligand is incorporated within a gel, provides a general means of manipulating the selectivity of CGE separations for biologically important molecules.

We demonstrated the selective and sensitive base-specific recognition of oligodeoxynucleotides with high efficiencies by using the CAGE system, in which poly(9-vinyladenine) (PVAd) was used as an affinity ligand [10–14]. PVAd is a non-degradable biomaterial that can interact to form complexes with naturally occurring nucleic acids by complementary hydrogen bonding in an aqueous solution [17,18] and is also an efficient

* Corresponding author.

0021-9673/93/$06.00

affinity ligand in high-performance affinity chromatography [19,20] and affinity gel electrophoresis [21,22] as well as CAGE for the recognition of nucleobases of naturally occurring or synthetic nucleosides, oligonucleotides and polynucleotides.

Oligothymidylic acids were selectively separated from a mixture of oligodeoxynucleotides by CAGE using PVAd as an affinity ligand [10–12]. Additionally, the sequence isomers of hexadeoxynucleotides (TTATTT, TTTATT, TTTTAT and TTTTTA) that could not be separated by CGE [13] were completely separated by CAGE [13,14]. The electrophoretic behaviour of oligodeoxynucleotides in CAGE was strongly affected by several parameters, such as size of PVAd, capillary temperature and concentration of PVAd and urea [10–12]. Preliminary experiments [10] showed some relationship between the migration time in CAGE and the concentration of urea. In this study, the details of the effect of urea concentration on the migration behaviour of oligodeoxynucleotides were investigated in CAGE and CGE separations. We demonstrate that CAGE in the presence of excess urea is effective for the high-performance base-specific separation of oligodeoxynucleotides.

THEORY

PVAd, as an affinity ligand (L), interacts with oligodeoxynucleotide (N) as expressed by eqn. 1.

$$N + L \rightleftharpoons N \cdot L \quad K_a = \frac{[N \cdot L]}{[N][L]} \tag{1}$$

where K_a is the apparent association constant between oligodeoxynucleotide and an affinity ligand. The migration time, t, of an oligodeoxynucleotides in CAGE is expressed as follows [10]:

$$t = t_0(1 + K_a[L]_t) \tag{2}$$

where t_0 is the migration time of oligodeoxynucleotide in the absence of affinity ligand, *i.e.* CGE migration time, and $[L]_t$ is the total L concentration.

A change in urea concentration leads to changes in the conformation of oligonucleotides [23], the viscosity of the surrounding gel–buffer medium and the association process, as expressed in eqn. 1. The first two effects are related to t_0 as formulated in eqn. 3 [24], and the last effect is related to K_a.

$$t_0 = l \cdot 6\pi r\eta / EQ \tag{3}$$

where l is the effective length of the capillary up to the detection point, η is the viscosity of the surrounding gel–buffer medium, E is the applied field, Q is the net charge of oligonucleotides and r, which is the root mean square radius of the oligonucleotide, is related to the conformational change. The relationship between urea concentration and K_a has not been formulated.

EXPERIMENTAL

Chemicals

Tris(hydroxymethyl)aminomethane (Tris) from Sigma (St. Louis, MO, USA), boric acid, ammonium peroxodisulphate and urea from Nakarai Tesque (Kyoto, Japan) were of reagent grade. Electrophoretic grade acrylamide, N,N′-ethylenebis(acrylamide) (Bis) and N,N,N′,N′-tetramethylethylenediamide (TEMED) were purchased from Nakarai Tesque. Oligodeoxyadenylic acids, pdA_{12-18}, and oligothymidylic acids, pdT_{12-18}, were obtained from Pharmacia (Uppsala, Sweden). Other oligodeoxynucleotides were chemically synthesized using an Applied Biosystems (ABI, Foster City, CA, USA) Model 391 DNA synthesizer. Samples were diluted to 2.5 units per 500 μl with distilled water and stored at −15°C until use. PVAd was prepared by the method reported previously [10,17,18]. The PVAd samples thus obtained had molecular masses ranging from 10 000 to 30 000.

Apparatus

CAGE and CGE separations were carried out by using a CE-800 capillary electrophoretic system (Jasco, Tokyo, Japan). A Shimadzu (Kyoto, Japan) CR-3A was used as a data processor for CAGE and CGE separations. Polyimide-coated fused-silica capillaries (375 μm O.D. and 100 μm I.D., GL Sciences, Tokyo, Japan) were used, with an effective length of 30 cm and a total length of 50 cm. The buffer was a

mixture of 0.1 *M* Tris and 0.1 *M* boric acid with 2–10 *M* urea (pH 8.6) for the preparation of the gel-filled capillaries, as well as the running buffer. Capillaries filled with polyacrylamide–PVAd-conjugated gel (8% T, 5% C and 0.02–0.03% PVAd)[a] and polyacrylamide gel (8% T and 5% CA)-filled capillaries were prepared by the method previously reported [10–12, 25–27]. The percentage of PVAd was calculated by the equation, 100 × PVAd (g)/[acrylamide (g) + Bis (g) + PVAd (g)]. Gel-filled capillaries were mounted in the CE-800 system and run with buffer solution at 10 kV (200 V/cm) for 30 min prior to actual measurements in order to remove non-reacted monomer, peoxosulphate and TEMED. Samples were electrophoretically injected into the capillary by applying a voltage of 10 kV for 0.1–1 s. The applied voltage was 10 kV during the measurement. Oligonucleotides were detected at 260 nm. The viscosity of the buffer solution was measured by using an Ostwald viscometer.

RESULTS AND DISCUSSION

The base specificity of CAGE, using capillary filled with polyacrylamide gel entrapping PVAd as an affinity ligand, was based on the formation of complementary hydrogen bonding between PVAd and oligodeoxynucleotides [10–14]. Although urea is extensively used in gel electrophoresis as a denaturant to abolish the secondary structure of DNA and RNA [23], significant interaction between oligothymidylic acids and PVAd is observed in the presence of an excess of urea such as 7 *M* [10]. This indicates that the PVAd–DNA hybrid is more stable than normal double-stranded DNA, because the repulsion between anionic charges on the sugar–phosphate backbones in double-stranded DNA is significantly diminished in the hybrid of DNA and PVAd, having a non-charged polyvinyl backbone.

[a] C = g Bis/% T; T = (g acrylamide + g Bis)/100 ml solution.

Effect of urea concentration in the capillary gel electrophoretic separations

We first measured the migration time, t_0 in eqn. 3, of oligodeoxyadenylic acids and oligothymidylic acids using polyacrylamide gel (8% T and 5% C)-filled capillaries without an affinity ligand to examine the effect of urea concentration on the electrophoretic mobility (Fig. 1). Fig. 1 illustrates that an increase in the

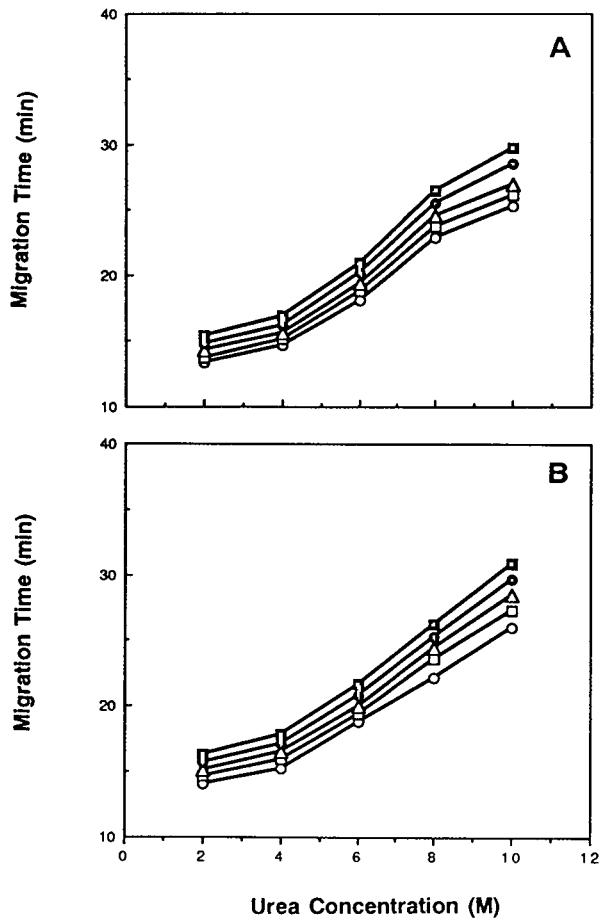

Fig. 1. Effect of the concentration of urea on the migration time of oligodeoxyadenylic acids (A) and oligothymidylic acids (B) in capillary gel electrophoresis. Conditions: capillary 100 μm I.D., 375 μm O.D., 50 cm length, 30 cm effective length; running buffer, 0.1 *M* Tris–borate and urea, pH 8.6; gel, 8% T and 5% C; capillary temperature, room temperature; field, 200 V/cm; current, 10 μA; injection, 10 kV for 1 s; detection, 260 nm. ○ = 8mer; □ = 10mer; △ = 12mer; ● = 14mer; ■ = 16mer.

concentration of urea results in an increase in the migration time of both oligodeoxyadenylic and oligothymidylic acids. This effect is caused by the change in the viscosity of the gel buffer medium and the root mean square radius of oligodeoxynucleotides, *i.e.* the conformational change, as expressed in eqn. 3. The root mean square radius increases with an increase in urea concentration, because self-associated oligonucleotides under non-denaturing conditions are transformed to the expanded conformation in the presence of an excess of urea. The viscosity of the buffer solution was measured by Ostwald viscometer at different urea concentrations and shown to increase with an increase in the urea concentration, as depicted in Fig. 2. It can be seen in Figs. 1 and 2 that the relationship between the migration time and the urea concentration is similar to that between the viscosity and the urea concentration. The viscosity, to which little attention has been paid, is proved to be a significant factor in this instance. Consequently, the migration time in CGE separation increases as the urea concentration increases in accordance with the relationship between the migration time and both the viscosity and the root mean square radius of oligodeoxynucleotides (eqn. 3).

Effect of urea concentration in the capillary affinity gel electrophoretic separations

The migration time, t in eqn. 2, of oligodeoxyadenylic and oligothymidylic acids was measured by using polyacrylamide–PVAd-conjugated gel-filled capillary (8% T, 5% C and 0.02% PVAd). Preliminary experiments [10] gave some relationship and qualitative considerations, because we measured t at only three urea concentrations. Therefore, the measurements were expanded to the wider range of the urea concentration to examine the details of the effect of the urea concentration and obtain some quantitative interpretations. Fig. 3 shows the relationship between the migration time and the urea concentration in CAGE separations. The migration time of oligodeoxyadenylic acid increases as urea

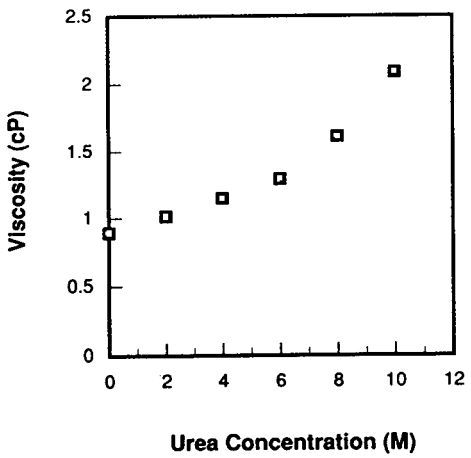

Fig. 2. The plot of the viscosity of buffer (0.1 *M* Tris–borate and urea) at 25°C *vs.* the concentration of urea.

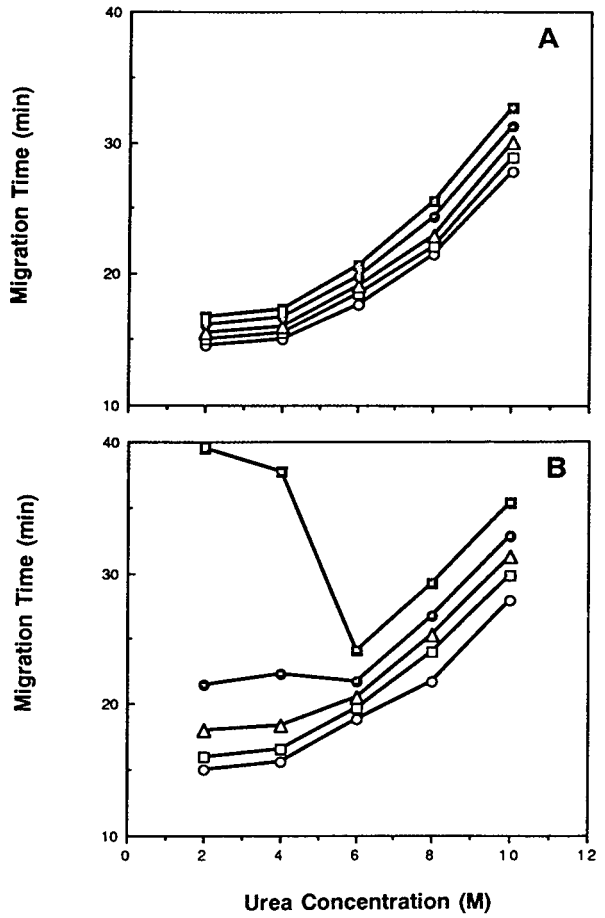

Fig. 3. Effect of the concentration of urea on the migration time of oligodeoxyadenylic acids (A) and oligothymidylic acids (B) in capillary affinity gel electrophoresis. The gel contained 8% T, 5% C and 0.02% poly(9-vinyladenine) with a molecular mass range of 10 000–30 000. Other conditions are as in Fig. 1. ○ = 8mer; □ = 10mer; △ = 12mer; ● = 14mer; ■ = 16mer.

concentration increases, as shown in Fig. 3A. The result in Fig. 3A was similar to that in Fig. 1A. This indicates that the effect of urea concentration on K_a in eqn. 2 is not taken into account in this instance, because the interaction of oligodeoxyadenylic acids with PVAd is negligible.

The effect of the urea concentration on the migration time of oligothymidylic acid as shown in Fig. 3B was different from that in CGE (Fig. 1B). Fig. 3B illustrates that an increase in the concentration of urea up to 6 *M* results in a decrease in migration time of larger oligothymidylic acids such as 14mer and 16mer, in contrast to the results in Fig. 1B. Urea will be effective in weakening the interaction between N and L, since it can break the hydrogen bonding of the base-paired complex. A decrease in the association constant (K_a in eqn. 2) caused by the dissociation of hydrogen bonding leads to a decrease in the migration time of larger oligothymidylic acid. The relationship between the migration times of shorter oligothymidylic acids such as 8–12mer and urea concentration is almost the same as that in CGE separations, as shown in Fig. 1B. The effect of the urea concentration over 6 *M* on the migration time of each oligothymidylic acid is also similar to that in Fig. 1B. Accordingly, larger oligothymidylic acids can interact with PVAd even in the presence of 2–6 *M* urea, but very weak interaction of smaller oligothymidylic acids with PVAd is exhibited. Urea at higher concentration over 6 *M* almost completely breaks the complementary hydrogen bonding of the oligothymidylic acids and PVAd hybrid.

Effect of urea concentration on the plate number

Fig. 4A and B compare the separations of a mixture of pdA_{12-18} and pdT_{15} by CAGE at different urea concentration. The relative migration time of pdT_{15} *vs.* oligodeoxyadenylic acids is reduced significantly at elevated concentration of urea. In addition, the band width of pdT_{15} decreases with an increase in urea concentration, as shown in Fig. 4, whereas that of oligodeoxyadenylic acid was insensitive to the urea concentration. Plate numbers in both the CAGE and the CGE separation were estimated and are

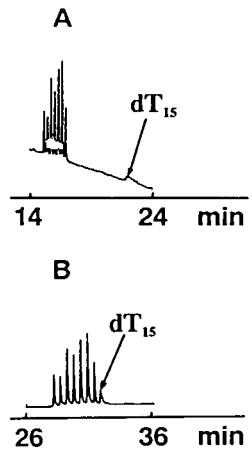

Fig. 4. Capillary affinity gel electrophoresis of a mixture of pdA_{12-18} and pdT_{15}. The gel contained 8% T, 5% C and 0.02% poly(9-vinyladenine) with a molecular mass range of 10 000–30 000. Running buffer, 0.1 *M* Tris–borate and urea, pH 8.6. Concentration of urea: 4 *M* (A) and 8 *M* (B). Other conditions are as in Fig. 1.

compiled in Table I. The plate number of oligodeoxyadenylic acid was kept almost constant during all measurements.

The plate number of oligothymidylic acid in CAGE separation was very sensitive to the urea concentration as listed in Table I. For example, the plate number of pdT_{15} at 6 *M* urea was 28 times larger than that at 4 *M* urea in CAGE separation. Since the affinity ligand would bind tightly to pdT_{15} by hydrogen bonding, the pdT_{15} band was severely broadened at lower concentrations of urea. Dissociation of hydrogen bonding, which occurred at higher concentrations of urea. Dissociation of hydrogen bonding, which occurred at higher concentrations of urea, resulted in sharper bands of oligothymidylic acid. The results show that the base-specific separation was achieved with high resolution only in the presence of an excess of urea.

High performance base-specific separation of oligodeoxynucleotides

We tried the base-specific separation of a complex mixture of pdT_{12-18} and pdA_{12-18} by using 10 *M* urea–gel capillary, as shown in Fig. 5. The pdT_{14-18} bands were selectively separated from pdA_{12-18}, whereas the pdT_{12} band co-migrated with the pdA_{16} band and the pdT_{13} band partially overlapped the pdA_{18} band. The pdT_{17}

TABLE I

PLATE NUMBER OF OLIGODEOXYNUCLEOTIDES IN CAPILLARY AFFINITY GEL ELECTROPHORESIS AND CAPILLARY GEL ELECTROPHORESIS

Sample	Concentration of PVAd (%)	Concentration of urea (*M*)	Plate number per metre
pdT_{12}	0	4.0	$5.7 \cdot 10^5$
	0.02	4.0	$2.8 \cdot 10^4$
	0.02	6.0	$4.6 \cdot 10^5$
pdT_{15}	0	4.0	$6.4 \cdot 10^5$
	0.02	4.0	$1.2 \cdot 10^3$
	0.02	6.0	$3.4 \cdot 10^4$
pdA_{12}	0	4.0	$5.1 \cdot 10^5$
	0.02	4.0	$3.2 \cdot 10^5$
	0.02	6.0	$1.2 \cdot 10^5$
pdA_{15}	0	4.0	$5.7 \cdot 10^5$
	0.02	4.0	$5.5 \cdot 10^5$
	0.0	6.0	$2.4 \cdot 10^5$

and pdT_{18} bands were severely broadened owing to the powerful interaction with PVAd. Although the temperature programming technique [12] was demonstrated to be essential to the base-specific separation of the mixture of oligodeoxynucleotides, complete resolution of such complex mixture was not realized even by using the temperature-programmed CAGE [12]. The result in Fig. 5, therefore, demonstrates that the CAGE using urea–gel capillaries as well as temperature-programmed CAGE [12] is very effective for improving the resolution in base-specific separation. In conclusion, a urea–gel capillary is indispensable to the analytical purpose of CAGE, because severe band broadening was significantly reduced and high-performance base-specific separation was accomplished.

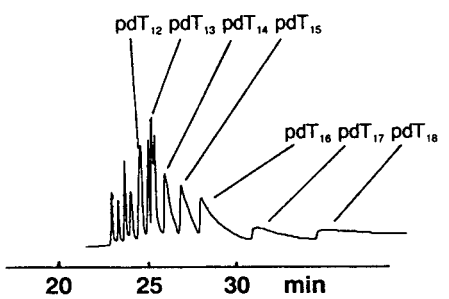

Fig. 5. Capillary affinity gel electrophoresis of a mixture of pdA_{12-18} and pdT_{12-18}. The gel contained 8% T, 5% C and 0.03% poly(9-vinyladenine) with a molecular mass range of 10 000–30 000. Running buffer, 0.1 *M* Tris–borate and 10 *M* urea, pH 8.6. Other conditions are as in Fig. 1.

ACKNOWLEDGEMENTS

The authors gratefully acknowledge support for this research by a travel grant from the Kato Memorial Foundation for Bioscience Research. This work was partly supported by a Grant-in-Aid for a Creative Basic Research (Human Genome Program) and a Grant-in-Aid for Scientific Research from the Ministry of Education, Science, and Culture, Japan.

REFERENCES

1 S.F.Y. Li, *Capillary Electrophoresis—Principles, Practice and Applications*, Elsevier, Amsterdam, 1992.
2 F.E.P. Mikkers, F.M. Everaerts and Th.P.E.M. Verheggen, *J. Chromatogr.*, 169 (1979) 11.
3 J.W. Jorgenson and K.D. Lukacs, *Anal. Chem.*, 53 (1981) 1298.
4 S. Terabe, K. Otsuka, K. Ichikawa, A. Tsuchiya and T. Ando, *Anal. Chem.*, 56 (1984) 111.
5 S. Terabe, K. Otsuka and T. Ando, *Anal. Chem.*, 57 (1985) 834.
6 S. Hjertén, *J. Chromatogr.*, 270 (1983) 1.

7 A.S. Cohen, D.R. Najarian, A. Paulus, A. Guttman, J.A. Smith and B.L. Karger, *Proc. Natl. Acad. Sci. USA*, 85 (1988) 9660.
8 Y. Baba and M. Tsuhako, *Trends Anal. Chem.*, 11 (1992) 280.
9 S. Hjertén, J.L. Lia and K. Yao, *J. Chromatogr.*, 387 (1987) 127.
10 Y. Baba, M. Tsuhako, T. Sawa, E. Yashima and M. Akashi, *Anal. Chem.*, 64 (1992) 1920.
11 T. Sawa, E. Yashima, M. Akashi, Y. Baba and M. Tsuhako, *J. High Resolut. Chromatogr.*, 16 (1993) in press.
12 Y. Baba, M. Tsuhako, T. Sawa and M. Akashi, *J. Chromatogr.*, 632 (1993) 137.
13 M. Akashi, T. Sawa, Y. Baba and M. Tsuhako, *J. High Resolut. Chromatogr.*, 15 (1992) 625.
14 T. Sawa, M. Akashi, Y. Baba and M. Tsuhako, *Nucleic Acids Res., Symp. Ser.*, 27 (1992) 51.
15 A. Guttman and N. Cooke, *Anal. Chem.*, 63 (1991) 2038.
16 S. Brinbaum and S. Nilsson, *Anal. Chem.*, 64 (1992) 2872.
17 M. Akashi, H. Iwasaki, N. Miyauchi, T. Sato, J. Sunamoto and K. Takemoto, *J. Bioactive Compatible Polym.*, 4 (1989) 124.
18 E. Yashima, T. Tajima, N. Miyauchi and M. Akashi, *Biopolymers*, 32 (1992) 811.
19 M. Akashi, M. Yamaguchi, H. Miyata, M. Hayashi, E. Yashima and N. Miyauchi, *Chem. Lett.*, (1988) 1093.
20 E. Yashima, T. Shiiba, T. Sawa, N. Miyauchi and M. Akashi, *J. Chromatogr.*, 603 (1992) 111.
21 E. Yashima, N. Suehiro, M. Akashi and N. Miyauchi, *Chem. Lett.*, (1990) 1113.
22 E. Yashima, N. Suehiro, N. Miyauchi and M. Akashi, *J. Chromatogr.*, in press.
23 J. Sambrook, E.F. Fritsch and T. Maniatis, *Molecular Cloning*, Cold Spring Harbor Laboratory Press, Plainview, 2nd ed., 1989.
24 K. Kleparnik and P. Bocek, *J. Chromatogr.*, 569 (1991) 3.
25 Y. Baba, T. Matsuura, K. Wakamoto, Y. Morita, Y. Nishitsu and M. Tsuhako, *Anal. Chem.*, 64 (1992) 1221.
26 Y. Baba, T. Matsuura, K. Wakamoto and M. Tsuhako, *Chem. Lett.*, (1991) 371.
27 Y. Baba, T. Matsuura, K. Wakamoto and M. Tsuhako, *J. Chromatogr.*, 558 (1991) 273.

Journal of Chromatography A, 652 (1993) 101–108
Elsevier Science Publishers B.V., Amsterdam

CHROM. 25 152

Capillary gel electrophoresis and the analysis of DNA phosphorothioates

Lawrence DeDionisio

Lynx Therapeutics Inc., 465 Lincoln Centre Drive, Foster City, CA 94404 (USA)

ABSTRACT

Capillary gel electrophoresis (CGE) is recognized as an effective method for the analysis of normal phosphodiester deoxyoligonucleotides (DNA). However, it was found that when the same electrophoretic principles were applied to the analysis of phosphorothioate DNA, peak broadening due to the phosphorothioate moiety made CGE's utility questionable. Therefore, optimization of several parameters is necessary for CGE to be effective in leading to the precise and accurate analysis of phosphorothioate DNA. Phosphorothioates are oligonucleotide analogs acknowledged as potential antisense therapeutics in the treatment of viral diseases and certain cancers. In order to improve a CGE approach to the analysis of this class of therapeutics, several parameters were investigated and improved upon. Three factors which proved critical in providing high resolution and good gel to gel reproducibility were: gel concentration, buffer additives, and pH.

INTRODUCTION

The advantages of capillary gel electrophoresis (CGE) in the analysis of synthetic oligonucleotides lie not only in its potential to resolve single base deletion products or failure sequences from the full-length oligonucleotide, but also in its capability to automate the electrophoretic analysis of these compounds in general [1,2]. However, in order for automated electrophoresis to occur via CGE, a gel-filled capillary must first prove itself resilient and at the same time, give reproducible results from run to run.

It is generally recognized that 7 to 8 *M* urea used as a denaturant in gel electrophoresis will denature all intermolecular secondary structures [3]. In lieu of high urea concentration, conducting CGE at elevated temperatures in conjunction with a rigid gel matrix provides adequate denaturing for the analysis of normal phosphodiester oligonucleotides. However, it was found that in the analysis of phosphorothioates these measures were not enough to overcome peak broadening that results in the loss of resolution between thioates differing in length by one base.

It has since been found that the pH of the buffer system has significant effects on the migration properties of oligonucleotides within a capillary gel [4,5]. Therefore, in the absence of a denaturing agent like urea, it is believed that by simply raising the pH of the buffer system, an effective denaturing gel could be achieved. We shall demonstrate that optimization of gel buffer pH, buffer concentration, and gel composition can lead to improved CGE performance in the separation of phosphorothioate DNA differing only by a single base in length, and to longer gel working lifetimes.

MATERIALS AND METHODS

Synthesis and purification of oligos

Phosphorothioate oligonucleotides were chemically synthesized using proprietary methods developed by Lynx Therapeutics on an Applied Biosystems (ABI, Foster City, CA, USA) 380B DNA synthesizer [6]. Truncating particular mixed base sequences by one base increments at the 3′ end created representative "failure" sequences. After these sequences were

0021-9673/93/$06.00

synthesized, cleaved off the solid support, and deprotected, the resulting crude solutions were purified on a Perkin-Elmer (Norwalk, CT, USA) HPLC system (Series 4) using an ABI 1783A detector and a Polymer Labs. (Amherst, MA, USA) PLRPS reversed-phase column (150 × 4.6 mm I.D., 8 μm). Chromatographic conditions were as follows: buffer A was 2% acetonitrile, 0.1 *M* triethylammonium acetate (TEAA) pH 7.5; buffer B was 100% acetonitrile; flow-rate of 1 ml/min. A linear gradient of 5–35% buffer B over 35 min was applied, and Trityl-on DNA (phosphorothioate), monitored at 300 nm, was collected at approximately 25 min. The purified DNA was detritylated with 80% acetic acid (*ca.* 5 ml total volume) for 15 min, dried to a residue under vacuum, and reconstituted in 1–2 ml NH_4OH (10%). An extraction was then carried out with ethyl acetate (2–4 ml) to remove free trityl group. The aqueous layer was retained, evaporated under a vacuum to a residue, and reconstituted in 1 *M* NaCl (1–2 ml). Three ethanol precipitations were done [7 parts ethanol to 3 parts NaCl (1 *M*)] to rid DNA of all organic solvents used in its synthesis and HPLC purification. The resulting purified "failure" sequences were mixed together in equimolar amounts along with their parent full-length oligo, and these "mixes" were used as standards to measure the resolution capabilities and gel-to-gel reproducibility of the different gel-filled capillaries.

Capillary electrophoresis

All capillary electrophoresis was conducted with an ABI 270A instrument. Capillaries (50 cm (30 cm to detector window) × 100 μm I.D. purchased from Polymicro Technologies (Phoenix, AZ, USA), were filled with ABI's Micro-Gel™ [7], and various buffer systems were used. All buffer reagents were purchased from Aldrich (Milwaukee, WI, USA). Runs were conducted with (−) polarity and a constant voltage of 22 kV was applied unless otherwise indicated. Injections were electrokinetic for 5.0 s (−8 kV). Detection was set at 260 nm, and temperature was kept at 55°C. Sample concentrations (total absorbance units/ml at 260 nm) were pre-determined and set at 0.5 absorbance units/ml unless otherwise indicated. The equation $R_s = 2(t_y - t_x)/w_y + w_x$ was used to determine resolution (R_s) between peaks, where y and x refer to any two peaks of interest, t is retention time in decimal min, and w is peak width in decimal min at the base.

RESULTS AND DISCUSSION

We evaluated several CGE parameters, including (1) buffer concentration, (2) buffer pH, (3) gel concentration, and (4) organic additive, and these systems are summarized in Table I. Figs. 1 and 2 illustrate the results of two different gel concentrations and two different buffer systems. In system I (Fig. 1), methanol is used as a preservative; however, these gels gave results that varied from gel to gel, and they often did not last beyond a few runs. It was soon discovered that the relatively high buffer concentration (75 m*M*) was contributing to excessive Joule heating within the gel, which resulted in premature gel failure. Thus, the buffer concentration was diluted to 35 m*M* and methanol was replaced with ethylene glycol (EG) (system II, Fig. 2). EG served not only as a preservative but, due to its viscosity, also produced a more rigid gel that was less likely to form voids or air bubbles. Neither of these systems gave sufficient resolution ($\bar{R}_s = 0.84$), and they were deemed inefficient gel capillaries for the analysis of phosphorothioates.

After it was discovered that lowering the buffer concentration increased the lifetime of the gel, improving the resolution of the gel was the next area of focus. It was felt that increasing the gel concentration would enhance peak resolution, and Fig. 3 is an example of a 10% gel (system III). Gels of 11 and 12% were also prepared, but they were prone to instability and air bubbles often developed. Although resolution ($\bar{R}_s = 1.07$) did improve with gels of higher concentration, the goal was to obtain gel-filled capillaries that would at least give near baseline resolution ($R_s \geq 1.2$).

As mentioned earlier, the pH of the buffer system has a direct effect on capillary-gel performance [4,5]. It has also been found that intramolecular secondary structure within single stranded DNA is not easily denatured even with

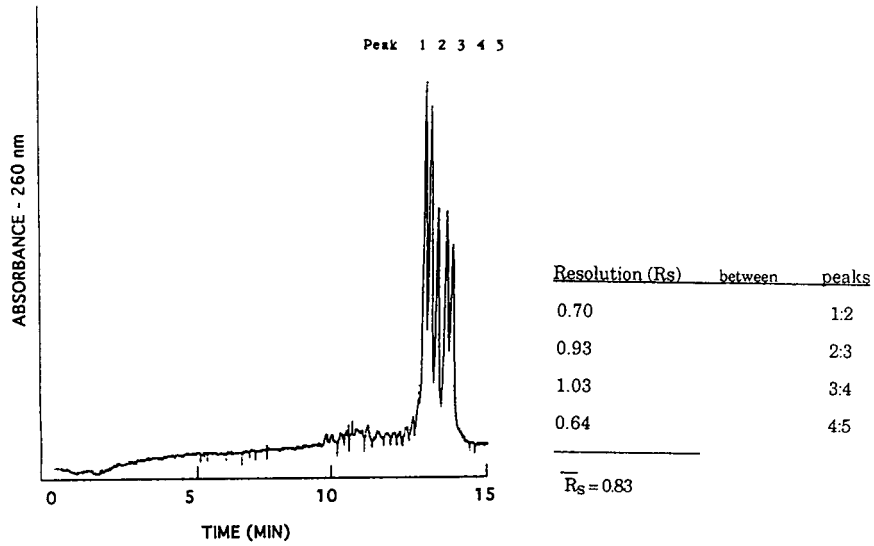

Fig. 1. Electropherogram of a mixture of different length phosphorothioates (22–26-mer). Sample concentration was 0.1 absorbance units/ml. Electrophoresis was conducted with an electrokinetic injection at −5 kV for 5 s, a running voltage of −10 kV, and buffer system I.

7 to 8 *M* urea [8,9]. Conceivably, intramolecular secondary structure, caused primarily by H-bonding, contributes to peak broadening and the loss of resolution which was illustrated in Figs. 1, 2 and 3. It was concluded that buffers of higher pH (>8.0) should help to denature intramolecular secondary structure caused by H-bonding.

The first attempt at a higher pH gel involved

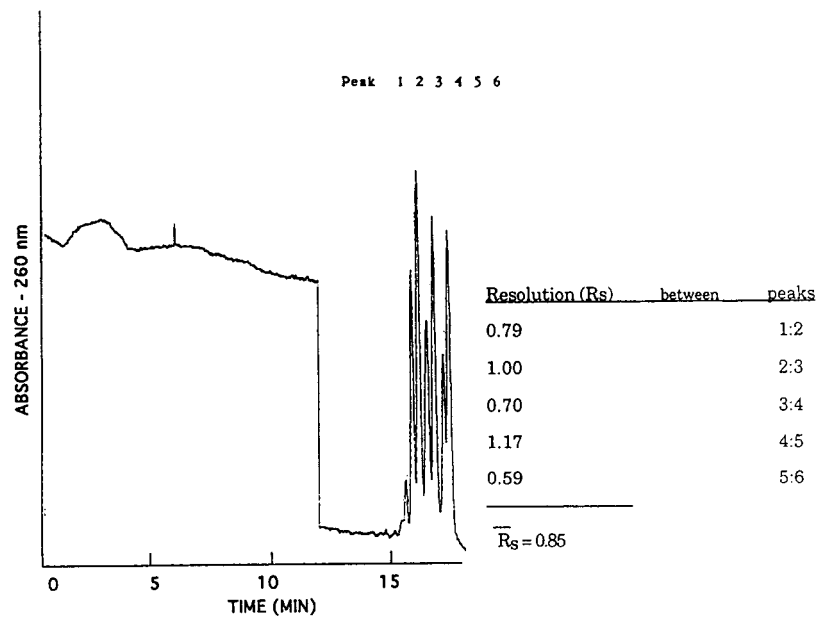

Fig. 2. Electropherogram of a mixture of different length phosphorothioates (16–21-mer). Sample concentration was 0.5 absorbance units/ml. Electrophoresis was conducted with an electrokinetic injection at −8 kV for 5 s, a running voltage of −22 kV, and buffer system II.

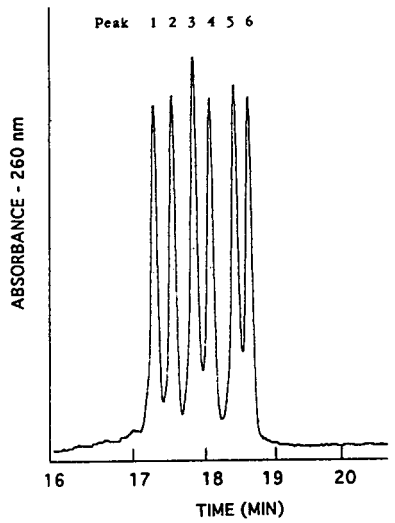

Resolution (Rs) between peaks
1.04 1:2
1.20 2:3
0.92 3:4
1.37 4:5
0.82 5:6

$\overline{R_S} = 1.07$

Fig. 3. Electropherogram of the phosphorothioate mixture from Fig. 2. Buffer system III was used, and other running conditions were the same as in Fig. 2.

Tris alone (system IV) as the buffer (Fig. 4). In this electropherogram, peaks are more uniform in shape and size, and resolution was slightly improved. However, at pH 10, Tris loses its buffering capacity, since it has a pK_a of 8.3. Consequently, these gels did not give consistent results, which can be attributed to a marked decrease in the pH of the Tris solution over time. Several other high pH buffer systems were tried, but the best results utilized a Tris–borate system (system V, Fig. 5A, B). It was found that a pH of 9.5 was still not low enough to maintain a true buffer involving Tris, and consequently, the gels utilizing 1.5 m*M* borate (Fig. 5A) did not give reproducible data. Gel system VI (10% Micro-Gel, 35 m*M* Tris, 5.6 m*M* borate, pH 9.0) exhibited good resolution ($\overline{R_s} = 1.95$) and, more importantly, reproducible data, and is the system shown in Fig. 5B. These gels continue to give consistent data and exhibit good gel to gel reproducibility; each gel lasts for approximately 30–40 injections.

Table I summarizes the results from the electropherograms of Figs. 1–5. Although system VI

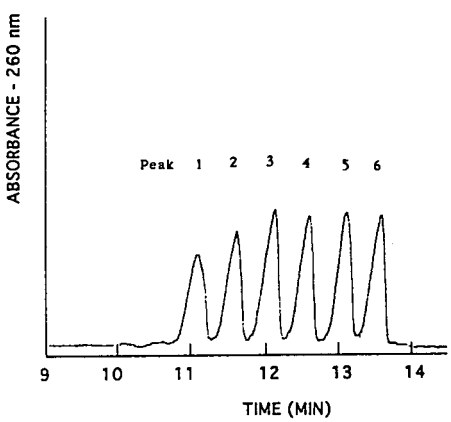

Resolution (Rs) between peaks
1.07 1:2
1.18 2:3
1.07 3:4
1.17 4:5
1.05 5:6

$\overline{R_S} = 1.11$

Fig. 4. Electropherogram of the same phosphorothioate mixture from Fig. 2. Buffer system IV was used, and other running conditions were the same as in Fig. 2.

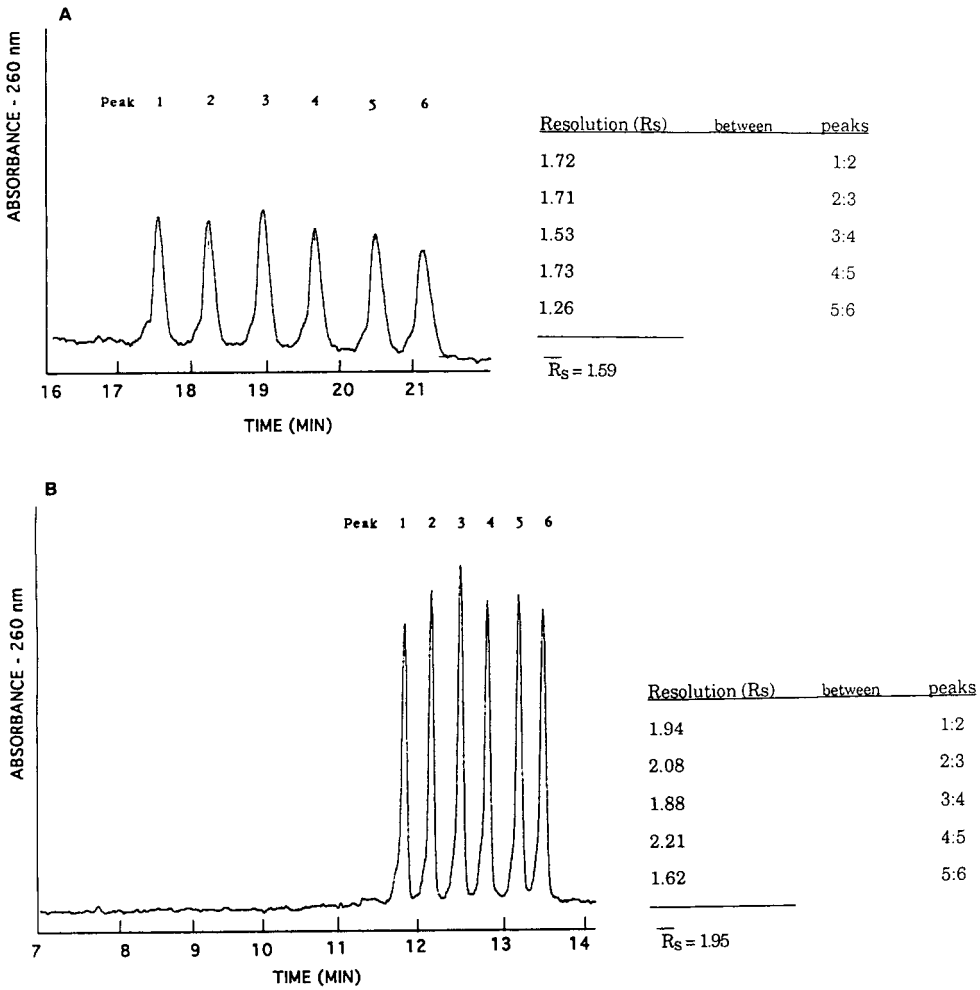

Fig. 5. Electropherogram of the phosphorothioate mixture from Fig. 2. The buffer system parameters were: (A) system V and (B) system VI. Other running conditions were the same as in Fig. 2.

(Fig. 5B) gave the best resolution, the gels used for Fig. 5A gave baseline resolution ($\overline{R}_s = 1.59$), but as stated earlier, these gels proved unstable. In all these gel systems, resolution varied slightly from gel to gel.

Table II shows the resolution data from three representative capillaries using system VI. Average resolution varied from 1.47 to 1.70; however, all resolutions were 1.20 or greater. These gel-filled capillaries proved to not only give superior resolution but also exhibited the resilience to last several runs.

Fig. 6A is an example of a 24-mer of unknown purity co-injected with the thioate-mix (21–16-mer) seen in previous figures. The mix is acting like an internal marker. Since the oligonucleotide lengths of the mix are known, the unknown product is checked for full-length integrity. Counting up from the 16-mer in the mix verifies that a 24-mer is indeed the main constituent of the analysis.

Fig. 6B depicts the analysis of the 24-mer (phosphorothioate) seen in Fig. 6A. Presently, it is difficult to always obtain baseline resolution for the $n - 1$-mer and $n + 1$-mer when present in an analysis. This loss in resolution is due to peak broadening caused not only by the phosphorothioate moiety, but also from base composition.

TABLE I

RESOLUTION DATA FROM 6 DIFFERENT BUFFER SYSTEMS

Capillary 50 cm × 100 μm I.D., constant running voltage (−22 kV), sample injection at −8 kV for 5 s, UV detection at 260 nm.

System	Gel parameters	Average resolution ($\overline{R_s}$)
I	10% Micro-Gel, 75 m*M* Tris–phosphate (TP), 10% methanol, pH 7.5	0.83
II	8.5% Micro-Gel, 35 m*M* TP, 15% ethylene glycol, pH 8.0	0.85
III	10% Micro-Gel, 35 m*M* TP, 15% ethylene glycol, pH 8.0	1.07
IV	10% Micro-Gel, 35 m*M* Tris, 15% ethylene glycol, pH 10.0	1.11
V	10% Micro-Gel, 35 m*M* Tris, 1.5 m*M* borate, 15% ethylene glycol, pH 9.5	1.59
VI	10% Micro-Gel, 35 m*M* Tris, 5.6 m*M* borate, 15% ethylene glycol, pH 9.0	1.95

TABLE II

RESOLUTION DATA FROM 3 GEL-FILLED CAPILLARIES MANUFACTURED ON DIFFERENT DATES

Capillary 50 cm × 100 μm I.D., 10% Micro-Gel, 35 m*M* Tris, 5.6 m*M* borate, 15% ethylene glycol, pH 9.0, constant running V (−2.2 kV), sample (thioate-mix 16–21-mer) injection −8 kV for 5 s, UV detection at 260 nm.

Gel	Resolution ($\overline{R_s}$)	between peaks
1	1.67	1:2
	1.78	2:3
	1.60	3:4
	1.97	4:5
	1.49	5:6
Average	1.70	
2	1.54	1:2
	1.59	2:3
	1.40	3:4
	1.61	4:5
	1.20	5:6
Average	1.47	
3	1.52	1:2
	1.68	2:3
	1.52	3:4
	1.86	4:5
	1.36	5:6
Average	1.59	

Overall $\overline{R_s}$ for above data = 1.59

It is known that base composition plays a role in the electrophoretic mobility of DNA [3]. For the gel-filled capillaries utilized here, oligos with high guanine content, like the oligonucleotide analyzed in Fig. 6, often give broader peaks that move at slightly slower rates when compared to oligonucleotides of the same length with relatively less guanine in their base composition.

Fig. 7 shows the analysis of a 21-mer identical to the 21-mer used in the thioate-mix. A 21-base phosphorothioate DNA is representative of those commonly synthesized for biological studies. This particular compound exhibits a typical $n-1$ mer and is used as a gel performance control. If the 20-mer does not resolve from the 21-mer in this sample, it is often a sign that the gel is breaking down and needs replacing. Most gel-filled capillaries of this type last approximately 30–40 runs.

CONCLUSIONS

The analytical results of phosphorothioates by CGE have always been unsatisfactory when compared to results obtained from phosphodiester DNA analysis. Phosphorothioates typically give broader peaks which cause poor resolution between oligos that differ only by one base. Gel concentration was shown to be a critical factor in reducing peak broadening. While a rigid gel is

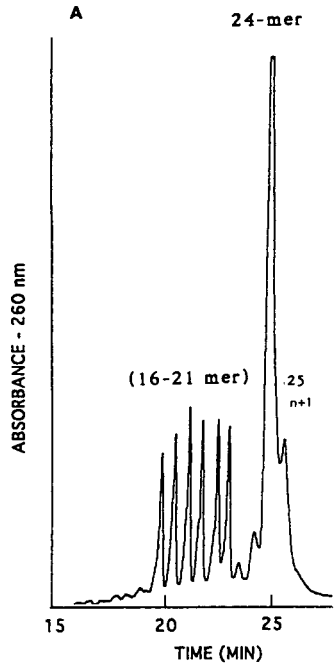

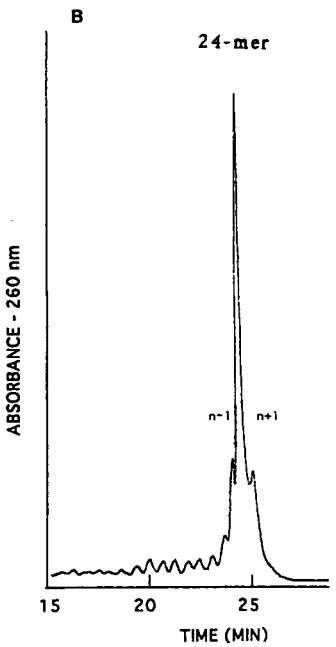

Fig. 6. (A) Analysis of the phosphorothioate mixture from Fig. 5A and B combined with a mixed base phosphorothioate (24-mer), and (B) the analysis of the 24-mer by itself. Gel parameters and running conditions were the same as in Fig. 5B.

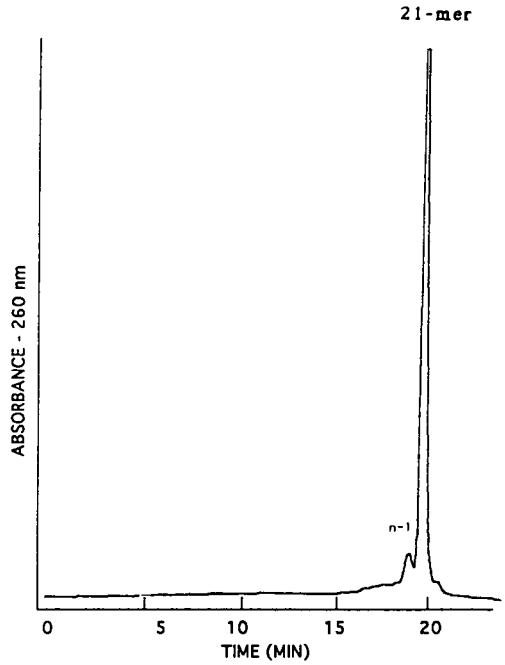

Fig. 7. Analysis of a phosphorothioate 21-mer. This oligo is used as a control sample because of the prominent 20-mer ($n-1$ mer) it contains. Gel parameters and running conditions were the same as in Fig. 5B.

crucial in obtaining resolutions higher than 1.0, gel concentrations higher than 10% give capillaries that often form air bubbles and fail prematurely. The use of ethylene glycol as a buffer additive was also found to increase the rigidity of the gel which served to prolong its lifetime on the instrument.

Since peak broadening could be a consequence of typical intramolecular secondary structures that neither high temperature (55°C) nor denaturing agents, *i.e.* 7–8 *M* urea, can completely disrupt, it was also demonstrated that by raising the pH of the buffer, markedly better electrophoretic conditions are achieved for the phosphorothioates. A pH of 9.0 gave the best resolution when compared to lower pH; however, a stable buffering system with a pH $\geq$ 10.0 would be more suitable since this would insure complete denaturation.

Finally, in data not shown here, it was found that buffer systems that contained Na^+ greatly reduced the chances of a gel surviving for more than a few runs. This is directly related to high

currents and joule heating, a consequence of high ionic strength within sodium buffers. For this reason, buffer systems that utilized dibasic or tribasic sodium phosphate failed. Therefore, organic buffers are most desirable, since their ionic strength is often relatively lower than buffers that contain high amounts of inorganic salt.

REFERENCES

1 A. Paulus and J.I. Ohms, *J. Chromatogr.*, 507 (1990) 113–123.
2 A.S. Cohen, D.R. Najarian, A. Paulus, A. Guttman, J.A. Smith and B.L. Karger, *Proc. Natl. Acad. Sci. U.S.A.*, 85 (1988) 9660–9663.
3 R. Frank and H. Koster, *Nucl. Acids Res.*, 6 (1979) 2069–2087.
4 A. Guttman, A. Arai and K. Magyar, *J. Chromatogr.*, 608 (1992) 175–179.
5 A. Guttman, R.J. Nelson and N. Cooke, *J. Chromatogr.*, 593 (1992) 297–303.
6 G. Zon and T.G. Geiser, *Anti-Cancer Drug Des.*, 6 (1991) 539–568.
7 R. Dubrow, *Am. Lab.*, March (1991) 64–67.
8 J.M. Bowling, K.L. Bruner, J.L. Cmarik and C. Tibbets, *Nucl. Acids Res.*, 19 (1991) 3089–3097.
9 M.S. Broido and D.R. Kearns, *J. Am. Chem. Soc.*, 104 (1982) 5207–5216.

Journal of Chromatography A, 652 (1993) 109–117
Elsevier Science Publishers B.V., Amsterdam

CHROM. 25 048

Utility of high resolution capillary electrophoresis for monitoring peptide homo- and hetero-dimer formation

James P. Landers*, Robert P. Oda, Jane A. Liebenow and Thomas C. Spelsberg☆

Department of Biochemistry and Molecular Biology, Mayo Clinic, Rochester, MN 55905 (USA)

ABSTRACT

The monomer and disufide-linked homo-dimer of two different peptides, one with an amino-terminal cysteine, the other with a cysteine at the carboxy-terminal, are shown to be baseline resolved by capillary electrophoresis in less than 15 min. Time-course for homo-dimer formation with both peptides, either under mild (air) or stronger (hydrogen peroxide oxidizing conditions, was easily monitored. Confirmation that the second peak appearing under oxidizing conditions was indeed the homo-dimer was obtained with mass spectrometry. The possibility that stronger oxidizing conditions led to the production of the sulfonic acid derivative of the monomeric peptide, was ruled out through generation of the derivative by performic acid oxidation. As expected, the negative charge of the sulfonic acid moiety gives the peptide a slower electrophoretic mobility than both the monomer and the dimer. Moreover, as would be expected with a sulfonic acid derivative, oxidation to the dimeric form was not possible. This was consistent with the observation that the homo-dimer peak could be reduced to monomeric form in the presence of dithiotreitol. Co-oxidization of the amino- and carboxy-terminal peptides led to the expected production of both homo-dimers and the hetero-dimer, all of which were resolved.

INTRODUCTION

High-performance capillary electrophoresis (HPCE) is an analytical technique applicable to both small and macromolecular components of biological interest. The capability of attaining separation efficiencies superior to those with high-performance liquid chromatography (several hundred thousand to one million theoretical plates) in a rapid, automated and reproducible manner has set the stage for HPCE to become a premier method for the separation of complex mixtures of molecules having a diverse size and nature [1–4]. Electrophoretic separation is carried out in a capillary having an internal diameter of less than 100 μm and a total volume of no greater than several microliters. The simplicity of using a polyimide-coated fused-silica capillary allows for the efficient dissipation of Joule heat and, hence, for electrophoretic separations to be carried out in free-solution under high potentials (up to 30 000 V).

The development of conditions for reproducible peptide analysis by CE was one of the first successes for the technique. Low pH buffer systems reduce the negative character of the inner capillary wall, thus minimizing interaction with peptides. Under these conditions, CE has been shown to be an excellent technique for separating acidic peptides which are typically difficult to resolve by reversed-phase HPLC methods. The selectivity of CE has ben highlighted by the ability to resolve peptides with small structural differences such as deamidation [5], single amino acid substitutions which do not change the calculated peptide net charge [6], and geometrical isomers which vary only in the surface of the peptide exposed to the run buffer matrix [7]. Collectively, these studies suggest that the isoelectric point (p*I*) should be used

* Corresponding author.
☆ George M. Eisenberg Professor of Biochemistry.

0021-9673/93/$06.00

with caution as a predictive method for peptide migration in CE, since it does not account for variable surface presentation and amino acid sequence which induce "nearest neighbor" effects. This has been demonstrated in an elegant study by Field *et al.* [8] who used strategically located histidine and arginine residues in "shuffled" peptide sequences (same total composition, shuffled amino acid order). These peptides, all theoretically possessing the same charge-to-mass (q/m) ratio were found to have dramatically different mobilities. While there have been attempts to model peptide mobility on altered p*I* predictions which take the nearest neighbor phenomenon into consideration [9], larger peptides, which are non-linear molecules, still do not behave in a theoretically predictable manner.

With the high selectivity inherent in CE, it seems probable that this technique could be exploited for the analysis of disulfide-mediated peptide dimerization. A single illustration in the review by Grossman *et al.* [1] showing the reduction of STP-3 peptide by dithiothreitol provided the first intimation that such analyses could be done with CE. In the present work, we demonstrate this to be the case. The rapid analysis times associated with CE make it ideal for monitoring disulfide-mediated dimerization/reduction processes quantitatively and qualitatively, as well as providing information with respect to homo- and hetero-dimer formation.

EXPERIMENTAL

Materials

Citric acid was a Gold Label reagent purchased from Aldrich. Sodium hydroxide, phosphoric acid (85%) and hydrogen peroxide (30%) were purchased from Fisher Scientific. All chemicals for peptide synthesis were purchased from Applied Biosystems (ABI, Foster City, CA, USA). Dithiothreitol (DTT) was purchased from Sigma (St. Louis, MO, USA).

Peptide synthesis

The synthetic peptide, N-terminal cysteine (Ntc), CFLGIPFAEPPVGSRRFMPPEPKRPWSGVL contained residues 32–60 from mouse RNA acetylcholinesterase with the addition of an amino-terminal cysteine. A second synthetic peptide contained a 13 amino acid sequence from a proprietary protein, with the addition of a carboxy-terminal cysteine. This peptide, TFQTNPDGTIQFRC, is denoted as the carboxy-terminus cysteine peptide or Ctc. Both were synthesized by 9-fluorenylmethoxycarbonyl (FMOC) amino acid strategy on an ABI 431A peptide synthesizer using the protocols and reagents provided by the manufacturer. Each peptide was purified by reversed phase HPLC using a Vydac C_{18} column (25 × 2.2 cm) using a trifluoroacetic acid–acetonitrile buffer system. Peptide integrity was monitored by either amino acid analysis or positive ion mass spectrometry.

Peptide dimerization

Dimerization was carried out under mild conditions through air oxidation. The peptide was dissolved in water to a final concentration of 0.1 mg/ml. The pH was adjusted to 8.0 with NH_4OH and the solution was stirred at room temperature for up to 18 h. Under these conditions, oxidation was monitored through the concentration of free cysteine using Ellman's reagent [5,5′-dithio-bis-(2-nitrobenzoic acid)] to a zero absorbance at 412 nm [10]. For HPCE time course analysis of the dimerization process, the sample was allowed to stand in a microvial (suspended in the sample vial containing 1 ml of water and sealed with a rubber cap) in the HPCE vial tray which maintained a temperature of *ca.* 27°C or in a refrigerator at 4°C. Dimerization was reversed by the addition of DTT at a final concentration of 1 m*M* (addition from a 1 *M* stock solution). Homo-dimer formation was enhanced by the addition of H_2O_2 at a final concentration of 0.015% added to the sample from a 0.3% stock solution.

Formation of the peptide sulfonic acid derivative

Performic acid oxidation was carried out by the method described by Hirs [11]. Briefly, 50 μl of 30% H_2O_2 was added to 950 μl of 88% formic acid and reacted for 2 h at room temperature. A 50-μg amount of peptide was dissolved in 2.5 μl

formic acid and 0.5 μl methanol and cooled at −20°C. A 5-μl volume of performic acid was added, and the reaction allowed to proceed for 2 h at −20°C. The reaction was stopped by dilution with 250 μl of water and the solution speed vacuumed to dryness. The residue was dissolved in 100 μl of water and stored at −20°C until analysis.

Buffer and sample preparation

Citrate buffer (20 m*M*) was made by solubilizing citric acid and adjusting the pH using either NaOH or HCl. Phosphate buffer was made by diluting a 0.1 *M* phosphoric acid stock solution and adjusting the pH with NaOH. All buffers were made with Milli-Q (Millipore) water, and filtered through an 0.2-μm filter (Gelman) before use. The monomeric and dimeric forms of the peptides were solubilized in Milli-Q purified water at a final concentration of 1 mg/ml.

Instrumentation

HPCE separation was carried out on a Beckman P/ACE System 2050 interfaced with an IBM 55SX computer utilizing System Gold software (version 7.1) for control and data collection. All peak information (migration time) was obtained through the System Gold software.

Capillary electrophoresis separation conditions

For peptide analyses, running buffer was either 20 m*M* citrate or 50 m*M* phosphate buffer, pH 2.5, and the following method was typically used: a three-column-volumes rinse with running buffer, 3 s pressure injection of peptide, separation at 25 kV (constant voltage with the inlet as the anode and the outlet as the cathode), a five-column-volumes wash with 0.1 *M* NaOH followed by a five-column-volumes rinse with running buffer. Capillaries were polyimide-coated fused silica with a 57 cm in length (50 cm to the detector) × 50 μm I.D. All electrophoretic separations were carried out at 25 kV constant voltage and capillary temperature was maintained at 28°C. Detection was by absorbance was at 200 nm.

RESULTS AND DISCUSSION

Oxidation of the peptide monomer results in homo-dimer formation

Two unrelated peptides were used to evaluate the utility of HPCE for separation of peptide monomers from their disulfide-linked dimers. The N-terminal cysteine peptide was a 30-mer containing residues 32–60 of the mouse mRNA acetylcholinesterase, has a molecular mass of 3369 and is termed the N-terminal cysteine or Ntc peptide. The second peptide used in this study was a 14-mer containing 13 residues from a proprietary protein and a C-terminal cysteine. It has a molecular mass of 1629 and is referred to as the Ctc peptide.

For CE analysis of the monomers and homo-dimer of each of the respective peptide systems, the purified homo-dimer was generated via air oxidation. Oxidation was found to be complete with stirring at room temperature overnight (≈18 h) at which point no free cysteine could be detected using Ellman's reagent [10]. Positive ion mass spectrometric analysis of the peptide before and after oxidation yielded molecular masses consistent with the monomer and the dimer. CE analysis of the freshly dissolved, HPLC-purified Ntc peptide monomer in low-pH buffer (pH 2.5) showed that the peptide ran as a single discrete peak at *ca.* 8.2 min, indicating that there was minimal contamination from either incomplete synthesis/deprotection or side reactions (Fig. 1A). CE analysis of the oxidized product shows that the disulfide-linked homo-dimer had a markedly faster electrophoretic mobility (migration time of 7.2 min) and appeared to be baseline resolved from the monomer (Fig. 1B). Similar profiles were seen in both 50 m*M* phosphate and 20 m*M* citrate. While the peaks were somewhat sharper in the phosphate buffer, the migration times were longer.

Two lines of evidence supported the postulate that the identity of the oxidized product was indeed the disulfide-linked dimer. First, the purified homo-dimer co-migrates with the faster migrating peak which appears in time-dependent manner under oxidizing conditions. Second, a mixture containing the purified homo-dimer and monomer could be reversibly converted to either

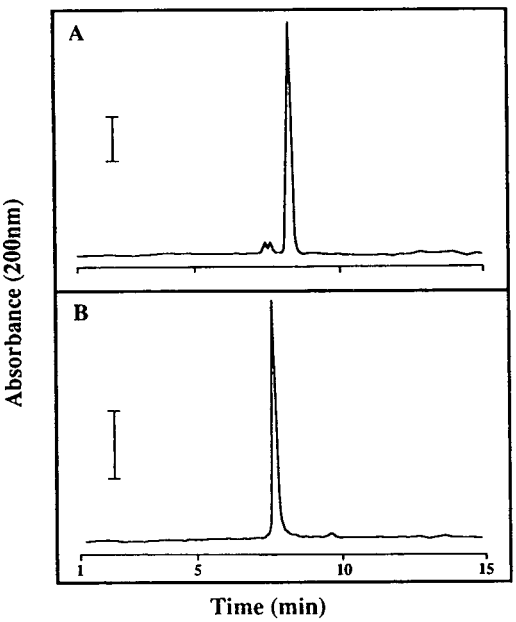

Fig. 1. CE separation of Ntc monomer and the disulfide-linked dimer. Purified Ntc monomer (A) and dimer (B) were dissolved in water at 0.5 mg/ml. Separation was carried out in 20 m*M* citrate buffer, pH 2.5. Bar represents 0.005 AU.

the monomer under reducing conditions (DTT) or the homo-dimer under oxidizing conditions (H_2O_2). This is shown in Fig. 2 (left panels) where, upon addition of DTT at a final concentration of 1 mM, an initial 1:2 mixture of Ntc monomer–dimer is immediately and almost completely converted to the monomeric form (96% as determined by peak areas). In contrast, a 2:1 monomer–dimer mixture is rapidly converted to the dimeric form (90% as determined by peak areas) with the addition H_2O_2 at a final concentration of 0.015% (v/v) (Fig. 2, right panels). In both of these cases, injection and subsequent electrophoretic separation of the oxidized/reduced mixture was carried out within 2–3 min of addition of the reagent. This highlights the rapid rate of conversion between the Ntc monomeric and dimeric forms. In both cases conversion was 100% complete after 30 min.

The possibility that the H_2O_2 had oxidized the sulfhydryl group of the monomer to sulfonic acid (as opposed to generating the disulfide-linked dimer) was thought to be unlikely for two reasons. First, analysis of both preparations on positive ion mass spectrometry gave molecular masses expected for the monomer and dimer. Second, it is unlikely that a sulfonic acid moiety on the peptide would lead to a more rapid electrophoretic mobility than the monomer. In fact, the additional negative charge on the peptide, due to the ionized sulfonic acid at pH 2.5, would presumably lead to a slower electrophoretic mobility (*i.e.* a longer migration time). This was confirmed by generating the sulfonic acid derivative of the Ntc peptide by performic acid oxidation [11]. As predicted, the presence of a sulfonic acid moiety markedly slows the electrophoretic mobility of the Ntc peptide (Fig. 3). Injection of a mixture containing the Ntc monomer, homo-dimer and monomeric sulfonic acid derivative shows that the order in which they migrate is as would be predicted. However, the migration times for all components have been increased as result of residual formic acid in the sample matrix. Addition of DTT to untreated monomer and the sulfonic acid derivative showed that only the former could be oxidized to the dimer. These results indicate that the peak signified with an arrow in Fig. 2 (lower right panel) is most likely the sulfonic acid derivative. Under the strong oxidizing conditions afforded by H_2O_2, some sulfonic acid derivative is formed as a minor side reaction during the dimerization process. The oxidation of the Ntc monomer to the disulfide-linked homo-dimer was substantially rapid at room temperature. Fig. 4 shows approximately 32% conversion of the Ntc monomer (as determined by peak areas) within 2 h at 27°C. The temperature-dependent nature of this process is indicated by the slower loss of monomer at 4°C. It is clear that the loss of the monomer (peak at 8.2 min) and corresponding appearance of the peak at 7.2 min does not represent some type of degradation process, since the purified homo-dimer is apparently unaffected within the same time-frame under identical conditions.

Similar studies were carried out with a second peptide having a carboxy-terminal cysteine and these studies clearly show the utility of CE for time course analysis if peptide dimerization (Fig. 5). Analysis of the purified Ctc monomer and homo-dimer showed the Ctc monomer to have a

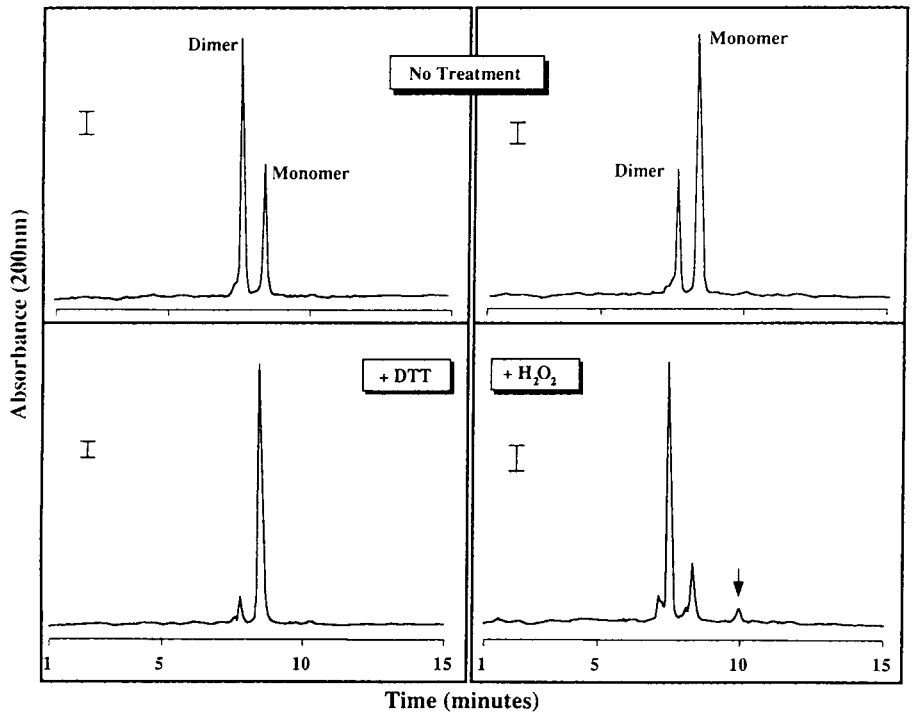

Fig. 2. Oxidization and reduction of an Ntc monomer–dimer mixture. A 1:2 mixture of monomer–dimer is reduced in the presence of 1 m*M* DTT (left panels) while a 2:1 mixture monomer–dimer is oxidized in the presence of 0.015% H_2O_2 (right panels). Separation was carried out in 20 m*M* citrate buffer, pH 2.5. Bar represents 0.002 AU.

migration time of 11.3 min while the dimer, formed more rapidly under the strongly oxidizing conditions, has a migration time of 9.6 min. Consistent with the Ntc system, the Ctc homo-dimer had a more rapid electrophoretic mobility than the Ctc monomer and, thus, they are baseline resolved. Oxidation of the Ctc monomeric peptide was markedly slower at 27°C than that observed with the Ntc peptide (compare with Fig. 4C), with only negligible conversion to homo-dimer observed after 8 h. In order to induce substantial conversion of the monomer to the dimer, H_2O_2 was added at a final concentration of 0.015% (v/v) at which point a more accelerated conversion to the homo-dimer occurred. Where similar conditions (H_2O_2) led to complete monomer-to-dimer conversion of the Ntc system within minutes, Ctc dimerization was only 59% complete after 8 h. This suggests that either the nature of the peptide itself (size, amino acid composition, primary structure), the different location of the cysteine (N- *vs.* C-terminal) or both are playing a role in the rate of dimerization.

CE analysis of homo- and hetero-dimer formation

It is clear from a comparison of Figs. 4C and 5 that the Ntc dimerization is markedly faster than that observed with the Ctc system (under mild or strong oxidizing conditions). To determine whether CE could resolve both homo-dimers, as well as the heterodimer, a solution containing both the purified Ntc and Ctc monomer was incubated at 27°C in the absence of H_2O_2 due to the comparatively rapid oxidation of the Ntc monomer (Fig. 2). Beginning initially with pure Ntc and Ctc monomer (Fig. 6A), incubation for 2 h and 46 min resulted in the formation of substantial Ntc homo-dimer (migration time 8.0 min) representing *ca.* 16% conversion (Fig. 6B). In contrast, a negligible amount of Ctc monomer had been oxidized to the homo-dimeric state (signified by the arrow at 9.4 min). In addition,

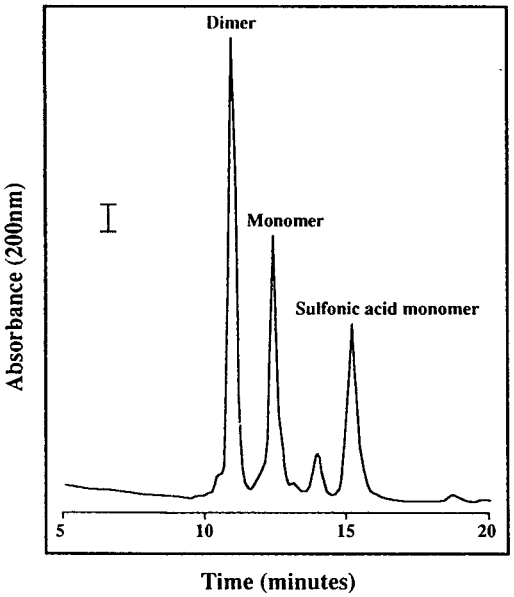

Fig. 3. CE analysis of the Ntc monomer, homo-dimer and sulfonic acid derivative. A mixture of purified monomer (1.0 mg/ml), dimer (0.5 mg/ml) and sulfonic acid derivative (0.5 mg/ml) obtained as described in the Experimental section was injected into the capillary which contained 50 m*M* phosphate buffer, pH 2.5. Bar represents 0.005 AU.

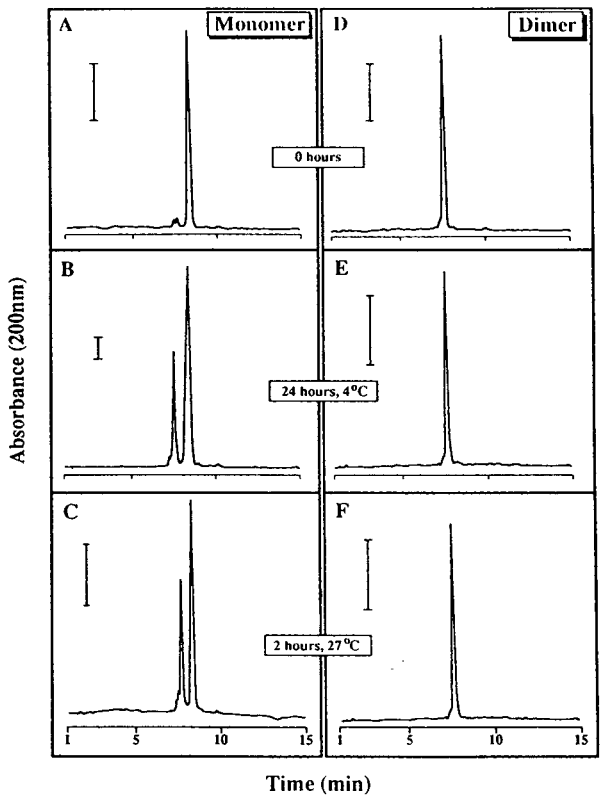

Fig. 4. Oxidization of Ntc peptide. Purified Ntc monomer and dimer were dissolved in water (1 mg/ml), analysed immediately (0 h) and after incubation at 27°C for 2 h and 4°C for 24 h. Bar represents 0.005 AU.

there is the appearance of a peak between the Ntc monomer and homo-dimer that was not previously observed. This represents the first intimation of heterodimer formation between the Ntc and Ctc peptide monomers (8.6 min). This peak appears to increase in concert with the Ntc homo-dimer peak (Fig. 6B and C). Only after *ca.* 11 h is there a clearly definable amount of Ctc homo-dimer (Fig. 6D). As would be predicted from the comparatively slow rate of dimerization (relative to the Ntc peptide), the magnitude of the Ctc homo-dimer peak is small in comparison with those of the Ntc homo-dimer and Ntc-Ctc heterodimer.

After incubation of this same sample for 24 h at 27°C, the profile given in Fig. 7A was observed. From the rapid rate of dimerization of the Ntc peptide and the comparatively slow rate of Ctc dimerization, it is predicted that after this period of time, there should be little or no monomeric Ntc but detectable levels of Ctc monomer. This appears to be the case. Co-injection of pure Ctc (Fig. 7B) and Ntc (Fig. 7C) monomer with the mixture clearly shows that, as would be predicted from migration times, peaks 6 and 3 represents residual monomeric Ctc and Ntc respectively, while peaks 4 and 1 respectively represent the Ctc and Ntc dimers. It follows that peak 2 represents the Ctc:Ntc hetero-dimer and that peak 5 represents the sulfonic acid derivative of the Ntc peptide. As would be expected from the mobility of the Ntc and Ctc monomers, the hetero-dimer has a mobility that is median to both. It is interesting that the heterodimer appears to be in a slightly higher concentration (assuming equal molar absorptivity) than both of the homo-dimers. This may indicate that both monomers have a slightly higher affinity for hetero- rather than homo-dimerization. This is particularly the case for the Ctc monomer and raises some interesting questions regarding the physical characteristics of

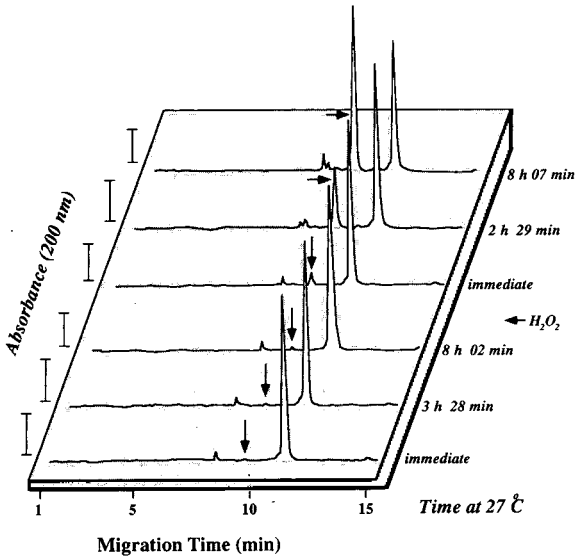

Fig. 5. CE time-course analysis of the Ctc dimerization process. Ctc peptide (1 mg/ml in water) was incubated at 27°C and analysed at 0 min (immediately), 3 h 28 min, 8 h 2 min. Hydrogen peroxide was added and analysis carried out at 0 min (immediately), 2 h 29 min, 8 h 7 min. Separation was carried out in 20 m*M* citrate buffer, pH 2.5. Bar represents 0.005 AU.

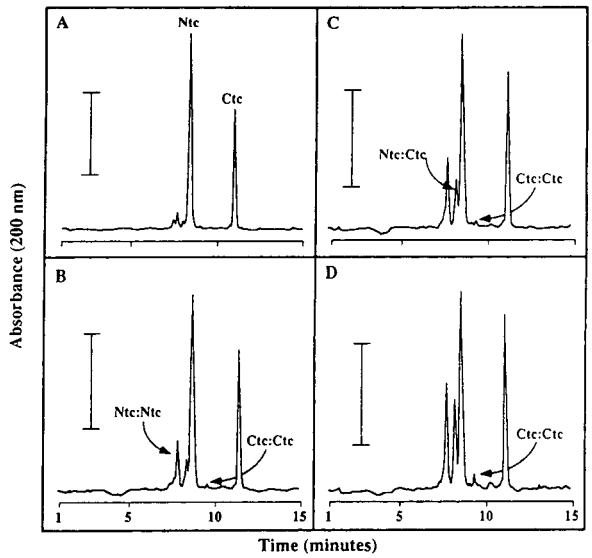

Fig. 6. Co-oxidization of the Ctc and Ntc peptides. A mixture of the purified Ntc and Ctc monomers was incubated at 27°C and analysed at 0 min (A), 2 h 46 min (B), 5 h 31 min (C) and 11 h 1 min (D). Separation was carried out in 20 m*M* citrate buffer, pH 2.5. Bar represents 0.005 AU.

each of the peptides that result in the observed dimerization properties.

Resolution of the monomer and dimer

An interesting question arises from the observation that the monomer and dimer in both systems are baseline resolved by CE. Can the baseline resolution of the monomer and dimer be explained by differences in mass/charge properties? Covalent dimerization through oxidation of the terminal cysteines involves only the loss of two hydrogen atoms with no obvious change in net charge. Hence, from the perspective of simple mass-to-charge ratio (m/q), which is the basis for separation in free solution CE, the difference between the monomer and the homodimer appears negligible (0.034%). However, the 1966 study by Offord [12] demonstrated that the relationship between the mass/charge properties of a peptide and its electrophoretic mobility was linear when expressed as a quotient of mass$^{2/3}$/charge ($m^{2/3}/q$). This was shown to be a reasonable postulate with a mixture of peptides which included bradykinin, angiotensin, leucine enkephalin, methionine enkephalin, and oxytocin (Fig. 8). The charge on each peptide at pH 2.5 was calculated with a program that compensated for the presence of amidated or acetylated residues[a] and the $m^{2/3}/q$ ratios calculated accordingly. A plot of the $m^{2/3}/q$ *vs.* migration time shows a reasonably linear relationship between these two parameters with a correlation coefficient (r) of 0.971. Co-injection of Ntc and Ctc monomer/dimer with the standard peptides allowed for the determination of their respective mobilities relative to the standards. Determining the net charge at pH 2.5 for the Ntc monomer (+4.88), Ntc dimer (+8.85), Ctc monomer (+1.969) and Ctc dimer (+3.390), $m^{2/3}/q$ values of 46.32, 37.51, 70.32 and 55.90 result respectively. The differences in the calculated $m^{2/3}/q$ for the monomer and dimer in both peptide systems suggest that, indeed, they should resolve

[a] The net charge on a peptide was calculated using the NCHARGE software written by Dr. L. Holladay of Alza Corporation. Parameters for the calculation including temperature of 28°C (capillary temperature), ionic strength of the buffer and a C-terminal pK_a of 2.90.

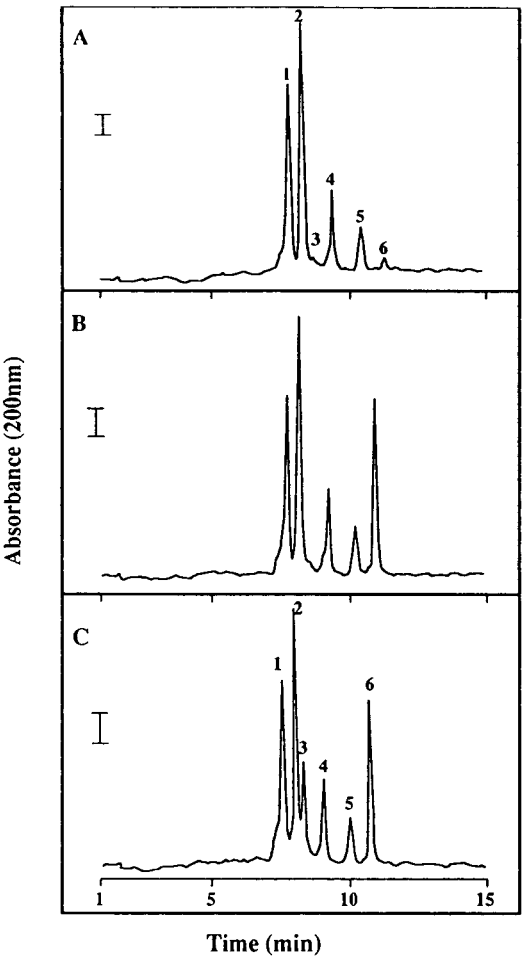

Fig. 7. Confirmation of peak identity through co-injection of peptide monomers. (A) The oxidized mixture described in Fig. 6 except after incubation at 27°C for 28.5 h. By co-injection of purified components with the mixture, peaks 6 and 3 are shown to represent the Ctc (B) and Ntc (C) monomers respectively. As indicated by migration times, peaks 1 and 4 represent the Ntc and Ctc dimer while peak 2 represents the Ntc:Ctc hetero-dimer and peak 5 the sulfonic acid derivative of the Ntc monomer. Separation was carried out in 20 mM citrate buffer, pH 2.5. Bar represents 0.001 AU.

by CE and that the homo-dimer should have a faster electrophoretic migration than the monomer. When these values are plotted on the curve obtained with standard peptides, it becomes clear that the Ctc monomer and homo-dimer both behave ideally, *i.e.* do not deviate from the linear relationship between charge/mass and

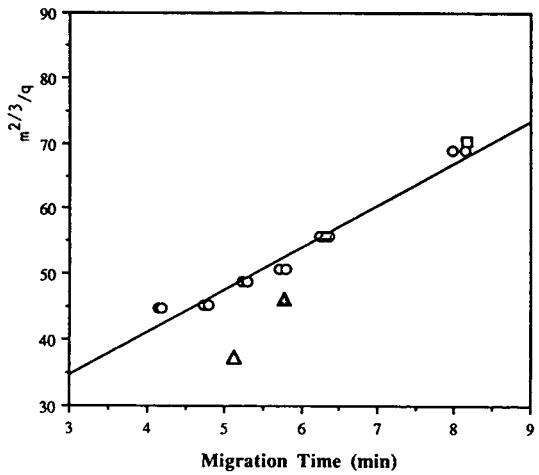

Fig. 8. Plot of mass-to-charge ratio ($m^{2/3}/q$) *vs.* migration time. Calculated values for $m^{2/3}/q$ were plotted against the migration times for two analyses (hollow circles) and linear regression analysis done on the combined data set (standard peptides include bradykinin, angiotensin, leucine enkephalin, methionine enkephalin, and oxytocin). Calculated values plotted for comparison: ○ = standard peptides ($r = 0.971$); □ = Ctc monomer; ■ = Ctc dimer; ▲ = Ntc monomer; △ = Ntc dimer.

electrophoretic mobility. In contrast, neither the Ntc monomer nor homo-dimer appear to behave ideally. Previous studies have shown that larger peptides are typically not linear and, hence, are less likely to behave ideally. Therefore, whether this observed deviation from linearity is a function a peptide size, character or both, is not clear.

It is reasonable to suggest that the differences in the $m^{2/3}/q$ values for the monomers and dimers reflect some type of secondary structure in the dimeric form, which ultimately results in the dimer having more charge per unit mass than the monomer. This could simply be due to "nearest neighbor" effects induced by the secondary structure of the dimer. The study by Field *et al.* [8] showed the dramatic outcome of the "nearest neighbor effect" on the mobility of peptides. They found that a series of peptides containing the identical amino acid composition (and little or no secondary structure) but differing in their primary structure (*i.e.* amino acid sequence) were separable by HPCE under the appropriate conditions. They argued that the

residues flanking charged amino acids (*i.e.* their environment) can alter the pK_a of the charged amino acid. Their data were also consistent with the concept that varying the primary sequence may lead to subtle changes in secondary structure, which ultimately may affect electrophoretic mobility. While there is no evidence that any type of secondary structure exist in the Ntc and Ctc systems (as predicted using the Chow–Fasman or Garnier–Osguthorpe–Robson methods[a]), we can not rule out the possibility that random secondary structure of the dimer is affecting the pK_a values of charged residues when in proximity to certain residues of the covalently-bound complimentary peptide. This most certainly is a possibility with the larger Ntc system which, as per Fig. 8, coincidently does not behave ideally from an electrophoretic mobility point of view.

CONCLUSIONS

This study demonstrates the utility of CE for the analysis of peptide dimerization through disulfide linkages. Selectivity is highlighted by the ability to resolve, not only monomers and dimers, but disulfide-linked homo- and hetero-dimers. The advantages of CE for this type of analysis include all the characteristics that make it useful as a microanalytical technique for biomolecules [13], the most important of which are selectivity, rapid analysis time and automation. The time-course analysis of the oxidization of peptide monomer to the dimeric form is easily automated, the results revealing qualitative and quantitative information about monomeric, homo-dimeric and hetero-dimeric components. This presents the possibility that CE could be used for measuring the kinetics of dimerization.

ACKNOWLEDGEMENTS

The authors would like to thank Ms. Colleen Allen for her excellent clerical assistance and both the Medical Research Council (Canada) and Mayo Foundation for support of this work. We also thank Dr. Richard Palmieri of Beckman Instruments and Ben Madden of the protein sequencing facility (Mayo Clinic) for stimulating discussions on this subject and Dr. L. Holladay for the NCharge software.

REFERENCERS

1 P.D. Grossman, J.C. Colburn, H.H. Lauer, R.G. Nielsen, R.M. Riggin, G.S. Sittampalam and E.C. Rickard, *Anal. Biochem.*, 179 (1989) 28.
2 M.J. Gordon, X. Huang, S.L. Pentoney, Jr. and R.N. Zare, *Science*, 242 (1988) 224.
3 B.L. Karger, A.S. Cohen and A. Guttman, *J. Chromatogr.*, 585 (1989) 492.
4 J.P. Landers, R.P. Oda, T.C. Spelsberg, J.A. Nolan and K.J. Ulfelder, *BioTechniques*, 14 (1993) 98.
5 R. Palmieri, *Applications Data Sheet DS-749*, Beckman, Fullerton, CA, 1989.
6 M. Field, R. Keck and J. O'Connor, presented at the *200th American Chemical Society National Meeting, Washington, DC, August 26, 1990.*
7 H. Ludi and E. Gassman, *Anal. Chim. Acta*, 213 (1988) 215.
8 M. Field, J. O'Connor and R. Palmieri, *Application Data*, Beckman, Fullerton, CA, 1990.
9 E.C. Rickard, M.M. Strohl and R.G. Nielsen, *Anal. Biochem.*, 197 (1991) 197.
10 A.F.S.A. Habeeb, *Methods Enzymol.*, 16 (1972) 457.
11 C.W.H. Hirs, *Methods Enzymol.*, 11 (1967) 197.
12 R.E. Offord, *Nature*, 211 (1966) 591.
13 J.P. Landers, *BioEssays*, 13 (1991) 253.

[a] Obtained through the "Peptide Structure Program" contained within the GCG (Genetics Computer Group) sequence analysis software (version 7.0). Idem., Ibid.

Journal of Chromatography A, 652 (1993) 119–129
Elsevier Science Publishers B.V., Amsterdam

CHROM. 25 066

Capillary electrophoresis of abnormal hemoglobins associated with α-thalassemias

Mingde Zhu, Tim Wehr,* Viktorya Levi, Roberto Rodriguez, Kathleen Shiffer and Zhu A. Cao

Bio-Rad Laboratories, 2000 Alfred Nobel Drive, Hercules, CA 94547 (USA)

ABSTRACT

Capillary electrophoresis was evaluated for separation of hemoglobin species associated with α-thalassemias, and for identification of hemoglobin variants commonly found in the same human populations. Separation of hemoglobins was achieved using capillary isoelectric focusing with chemical mobilization; visible-wavelength absorbance detection was used to identify hemoglobins against a background of nonheme-containing proteins. This technique could easily differentiate hemoglobins Bart's and H (associated with α-thalassemias) from hemoglobin variants. Analysis of globin chains derived from intact hemoglobins was performed by free zone capillary electrophoresis under denaturing conditions. This technique was useful for distinguishing Hb Bart's and Hb H, and for confirming the identity of hemoglobin variants.

INTRODUCTION

Thalassemias are blood disorders associated with reduced production of the globin chains of hemoglobin. In α-thalassemias, reduction of α-globin production most commonly arises from deletion of one or more of the four α-globin genes, resulting in anemias of varying degrees of severity from asymptomatic to lethal [1,2]. As a consequence of reduced α-globin chain production, α-thalassemias are characterized by appearance of abnormal hemoglobin species in varying amounts depending upon the nature and severity of the genetic defect. In the most severe form of α-thalassemia, hemoglobin Bart's *hydrops fetalis*, there is no α-globin chain production and the fetus dies before or soon after birth. Hemoglobin Bart's is characterized by the appearance of a tetramer composed of four chains of γ-hemoglobin. Hemoglobin H disease, usually manifested by milder forms of anemia, is characterized by the presence of Hb H, a tetramer composed of four β-globin molecules.

Particular hemoglobin disorders are known to occur at higher frequencies in certain geographical areas and within certain ethnic groups. Thalassemias are prevalent in Southeast Asia, and α-thalassemia gene frequencies approach 40% in northern Thailand and Laos [2]. A number of hemoglobin variants are also common in Southeast Asian populations, and these may give rise to anemias which mimic the symptoms of thalassemias or may be coinherited with α-globin gene deletions and potentiate their effects [2]. Hemoglobin E, a variant found in high frequency in the region joining Thailand, Laos and Cambodia, results from a replacement of glutamic acid by lysine in position 26 of the β-globin gene. The hemoglobin E mutation results in reduced β-globin production and a β-thalassemia phenotype. The hemoglobin Constant Spring variant (Hb CS) arises from a mutation in the α-globin chain termination codon which results in a 24–26 amino acid addition to the α-globin polypeptide. The Hb CS globin mRNA is unstable, and the resulting reduction in α-globin production leads to an α-thalassemia condition. Coinheritance of hemoglobin E or

* Corresponding author.

0021-9673/93/$06.00

Constant Spring mutations with α-globin chain deletions results in complex phenotypes with varying levels of Hb Bart's and H, Hb CS and Hb E.

In a previous report [3] we described the separation of normal hemoglobins and hemoglobin variants using capillary isoelectric focusing (cIEF), and separation of globin chains by free zone capillary electrophoresis under denaturing conditions. In this report we have extended the study using cIEF to characterize the hemoglobin species associated with α-thalassemias and hemoglobin variants common in Southeast Asian populations; globin chain analysis was also performed using free zone capillary electrophoresis. In addition, hemoglobins and globin chains from a patient carrying the G Philadelphia and C variants were analyzed; these mutations (an asparagine-to-lysine replacement in position 48 of the α-globin chain, and a glutamic acid-to-lysine replacement in position 6 of the β-globin chain, respectively) are common among some populations in the USA.

EXPERIMENTAL

Materials

Hemoglobin AF electrophoresis control was obtained from Isolab (Akron, OH, USA). Hemoglobin AFSE reference standard, Bio-Lyte pH 3–10 ampholytes, and AG 501-X8 resin were obtained from Bio-Rad Labs. (Hercules, CA, USA). Reduced Triton X-100 was obtained from Aldrich (Milwaukee, WI, USA). Patient samples of hemoglobin E were generously provided by Childrens Hospital, Oakland, CA, USA. Patient samples of hemoglobin Bart's, hemoglobin H, hemoglobin G Philadelphia/C, and hemoglobin Constant Spring were generously provided by Kaiser Permanente Hospital, Oakland, CA, USA.

Gel isoelectric focusing of hemoglobins

Whole blood samples (50 μl) were lysed by 1:10 dilution with deionized water. Hemoglobin content was measured by conversion of cyanomethemoglobin using Drabkin's reagent [4] and spectrophotometric determination at 540 nm. Samples were diluted to 17 mg/ml hemoglobin, and 170 μg hemoglobin were applied to each lane of the gel. Isoelectric focusing was carried out using Pharmacia Ampholine PAG plate isoelectric focusing gels, pH 5.5–8.5 (Pharmacia LKB Biotechnology, Piscataway, NJ, USA). The anolyte solution was 0.5 *M* acetic acid + 0.1% KCN and the catholyte solution was 0.5 *M* ethanolamine + 0.1% KCN. Following isoelectric focusing, heme protein-containing bands were selectively stained with *o*-dianisidine in the presence of hydrogen peroxide [1]. In this procedure, *o*-dianisidine is oxidized by the heme portion of the hemoglobin molecule, producing an insoluble brown precipitate which is proportional to the amount of hemoglobin present.

Preparation of hemoglobin samples for capillary electrophoresis

Whole blood samples (50 μl) containing hemoglobin Bart's, hemoglobin E, hemoglobin G Philadelphia C, or hemoglobin Constant Spring were added to 250 μl isotonic saline (0.9% sodium chloride) and centrifuged at 2000 *g* for 10 min. After removal of the supernatant, erythrocytes were lysed by the addition of 1 ml of deionized water. Whole blood samples (50 μl) containing hemoglobin H were lysed directly by addition of 1 ml deionized water. Hemoglobin content was measured by conversion to cyanomethemoglobin using Drabkin's reagent [4] and spectrophotometric determination at 540 nm. All samples were diluted with deionized water to a final hemoglobin concentration of 2.4 mg/ml.

Preparation of globin chains

One volume of hemoglobin sample was mixed with 20–40 volumes of acidic acetone [2% concentrated hydrochloric acid (36%) in acetone] and stirred briefly. The mixture was held at 4°C for 30 min, then centrifuged for 2 min in a microcentrifuge. After drawing off the supernatant, the precipitate was washed twice with acetone and dissolved in 10 m*M* sodium phosphate buffer (pH 2.5) + 7 *M* urea + 0.1% reduced Triton X-100. Prior to use, the buffer + urea solution was stirred with AG-501-X8 resin to remove urea impurities.

Capillary electrophoresis

All separations were performed with the BioFocus 3000 automated capillary electrophoresis system (Bio-Rad Labs.). All capillaries used in this study were coated internally with a covalently attached hydrophilic linear polymer [5]. Capillaries were enclosed in a cartridge format and thermostated at 20°C by liquid cooling. The distance from the monitor point to the capillary outlet was 4.6 cm.

Isoelectric focusing of hemoglobins was carried out using 17 cm × 25 μm I.D. coated capillaries. Capillaries were purged with water and 10 m*M* phosphoric acid between separations. Hemoglobin samples were mixed with pH 3–10 ampholytes to a final ampholyte concentration of 2% and total hemoglobin concentration of 240–480 μg/ml. The sample + ampholyte mixtures were pressure-injected into the capillary at 100 p.s.i. (689 476 Pa) for 60 s. Focusing was carried out at 10 kV constant voltage for 5 min using 40 m*M* sodium hydroxide as catholyte and 20 m*M* phosphoric acid as anolyte. Cathodic mobilization was performed by replacing the catholyte was a proprietary zwitterionic solution (Bio-Rad Labs.). Mobilization voltage was 10 kV. Detection was at 415 nm. Free zone electrophoresis of globin chains was carried out using 36 cm × 50 μm I.D. coated capillaries. The electrophoresis buffer was 100 m*M* sodium phosphate (pH 2.5) + 7 *M* urea + 1% reduced Triton X-100. Samples were pressure-injected for 5 p.s.i. · s and separated at 8 kV constant voltage. Detection was at 210 nm.

RESULTS AND DISCUSSION

Capillary isoelectric focusing of hemoglobins

cIEF provides extremely high resolution of proteins based on small differences in their isoelectric points. This is due to the use of high field strengths (typically 400–600 V/cm) combined with good heat dissipation using narrow-bore (25 μm I.D.) capillaries with liquid cooling. Once focused, protein zones may be mobilized past the detector monitor point by changing the composition of the anolyte or catholyte solutions [6]. In this investigation, proteins were mobilized towards the cathode by exchanging the 40 m*M* NaOH for a zwitterion solution; in this process proteins across the full pH range from 4 to 10 are efficiently mobilized [7], and sharp zones are maintained by application of high voltage during the mobilization process. The use of coated capillaries eliminated electroosmosis which would otherwise disrupt the focusing process. The resolving power of cIEF is seen in the separation of a hemoglobin reference standard containing hemoglobins A, F, S and E (Fig. 1). These species have isoelectric points of 7.10, 7.15, 7.25 and 7.42, respectively. In this and other cIEF separations of hemoglobins, detection was performed at 415 nm, which allowed high-sensitivity detection of hemoglobins against a background of non-heme-containing proteins (Fig. 2).

CE of hemoglobin Bart's

The cIEF profile of a sample from a patient with hemoglobin Bart's disease revealed a major peak for normal adult hemoglobin A_0 and an elevated level of fetal hemoglobin F (Fig. 3). In addition, there were a series of minor peaks migrating late in the separation (18.5–19.5 min), corresponding to heme-containing proteins with isoelectric points much lower than normal hemoglobins and known hemoglobin variants. These were observed in all Hb Bart's samples separated by cIEF, and are thought to include the γ-chain tetramer characteristic of this α-

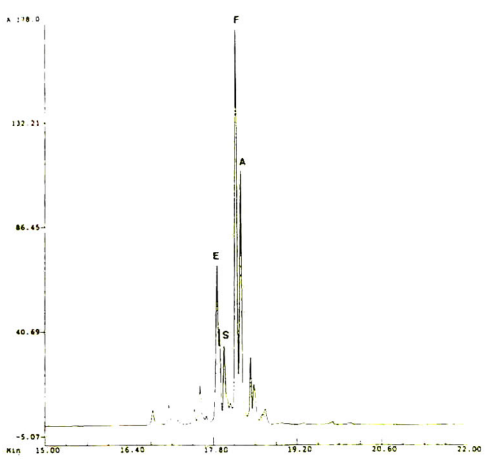

Fig. 1. Capillary isoelectric focusing of hemoglobin A, F, S and E reference standard.

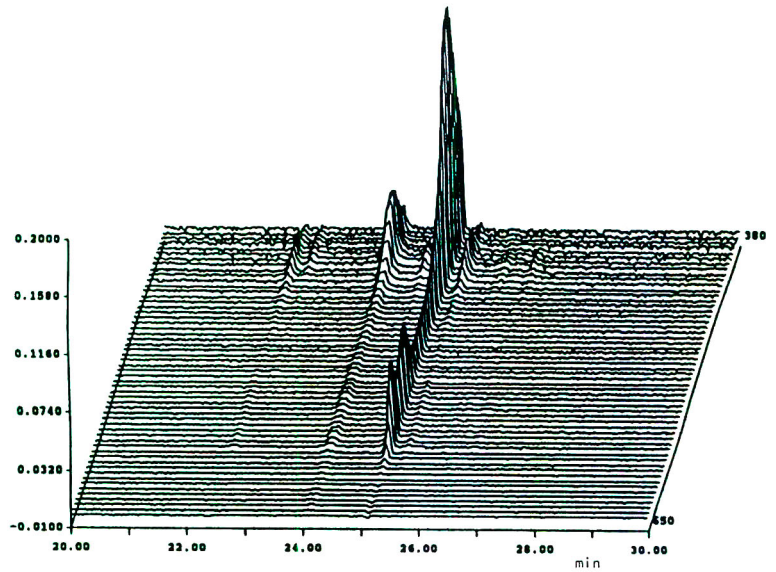

Fig. 2. Capillary isoelectric focusing of hemoglobin A using scanning detection in the 380–650 nm spectral region. The major peak migrating at 25 min is hemoglobin A_0 and the minor peak migrating at 24 min is hemoglobin A_2. The hemoglobin A_0 spectrum exhibits a maximum at 415 nm. *x*-Axis, time (min); *y*-axis, absorbance; *z*-axis, wavelength (nm).

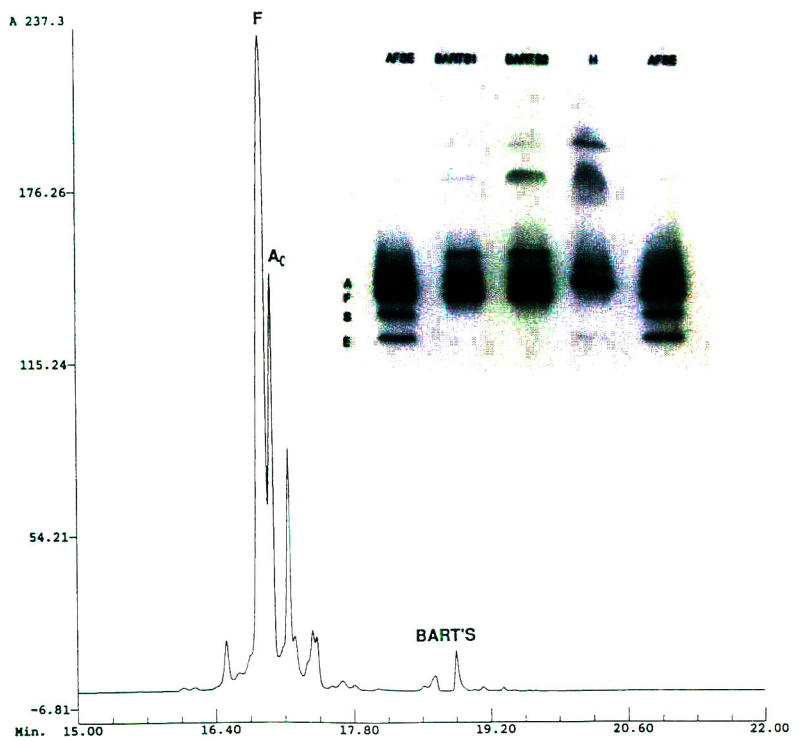

Fig. 3. Capillary isoelectric focusing of hemoglobins from a patient with hemoglobin Bart's disease. Inset: isoelectric focusing gel of hemoglobin samples stained with *o*-dianisidine (1st and 5th lanes: hemoglobin AFSE reference standard; 2nd and 3rd lanes: hemoglobin Bart's samples; 4th lane: hemoglobin H). The sample separated by cIEF is the one shown in lane 3 of the IEF gel.

thalassemia. The series of peaks migrating after Hb A_0 (17–18 min) have not been identified, but probably represent glycated forms of Hb A_0, acetylated Hb F, and degradation products.

Comparison of the cIEF profile with the band pattern on a conventional isoelectric focusing gel (Fig. 3 inset, 2nd and 3rd lanes) revealed similar patterns. The gel showed major bands for Hb A_0 and F, a series of minor bands focusing above the Hb A_0 band, and an Hb Bart's band focusing in the acidic portion of the gel, corresponding to an approximate pI of 6. A comparison of the two Hb Bart's samples indicated a higher level of Hb Bart's in the 3rd lane, which was in agreement with cIEF peak area percent values obtained for the two samples (data not shown).

The globin chain content of the Hb Bart's sample was analyzed by free zone capillary electrophoresis under denaturing conditions. This separation was carried out in the presence of 7 *M* urea with detection at 210 nm; at this wavelength the globin chains could be detected with satisfactory sensitivity and minimal interference from the urea in the electrophoresis buffer (Fig. 4). The electropherogram showed the presence of the normal α-, β- and γ-globin chains but in altered ratios (Fig. 5), with γ-globin elevated relative to β-globin.

CE of hemoglobin H

The cIEF profile of a sample from a patient with hemoglobin H disease exhibited a major peak for normal adult hemoglobins A_0 and A_2 and a small amount of Hb F (Fig. 6). In addition, a late-migrating doublet peak was observed which was assumed to represent the β-chain tetramer associated with Hb H disease. The isoelectric focusing gel pattern of this sample (Fig. 6 inset, 4th lane) showed the same major band for Hb A_0 and a band focusing in the acidic part of the gel. There were two differences observed between the IEF pattern and the band pattern of the conventional IEF gel. First, the gel exhibited a diffuse band focusing in the same position as Hb Bart's, which may represent degradation products. This material was either not detected in cIEF, or co-migrated with Hb H. Second, an Hb A_2 band was not observed in the

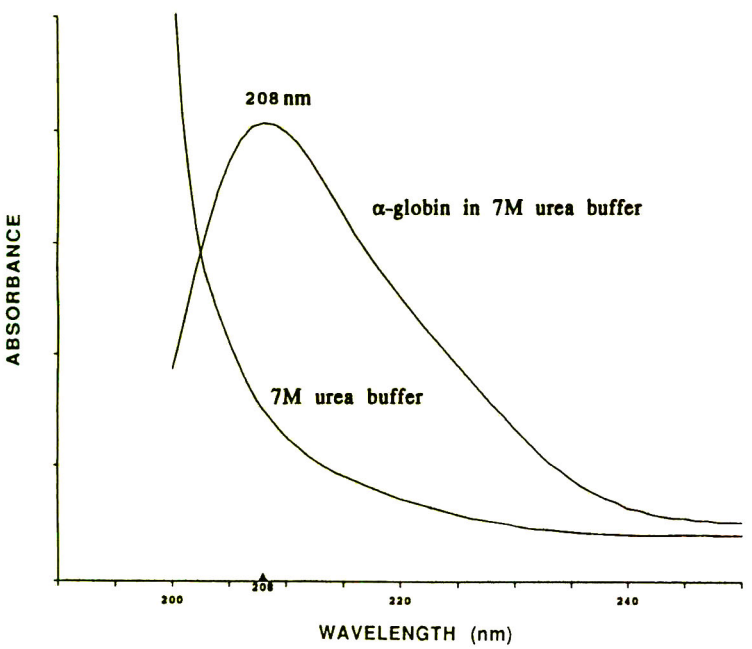

Fig. 4. UV spectra obtained during free zone capillary electrophoresis with scanning detection. (Lower trace) background absorbance of electrophoresis buffer (100 m*M* sodium phosphate, pH 2.5, +0.1% reduced Triton X-100 + 7 *M* urea). (Upper trace) spectrum of α-globin in electrophoresis buffer.

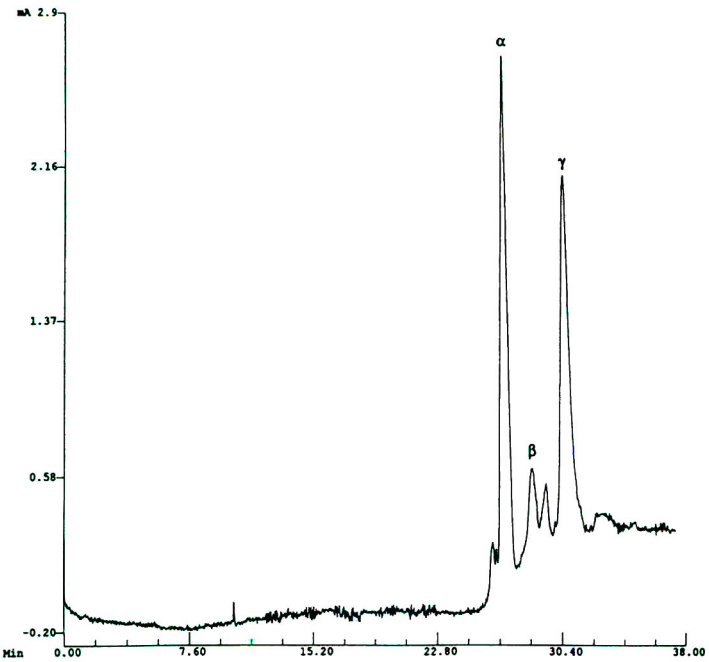

Fig. 5. Free zone capillary electrophoresis separation of globin chains from the hemoglobin Bart's sample shown in Fig. 3.

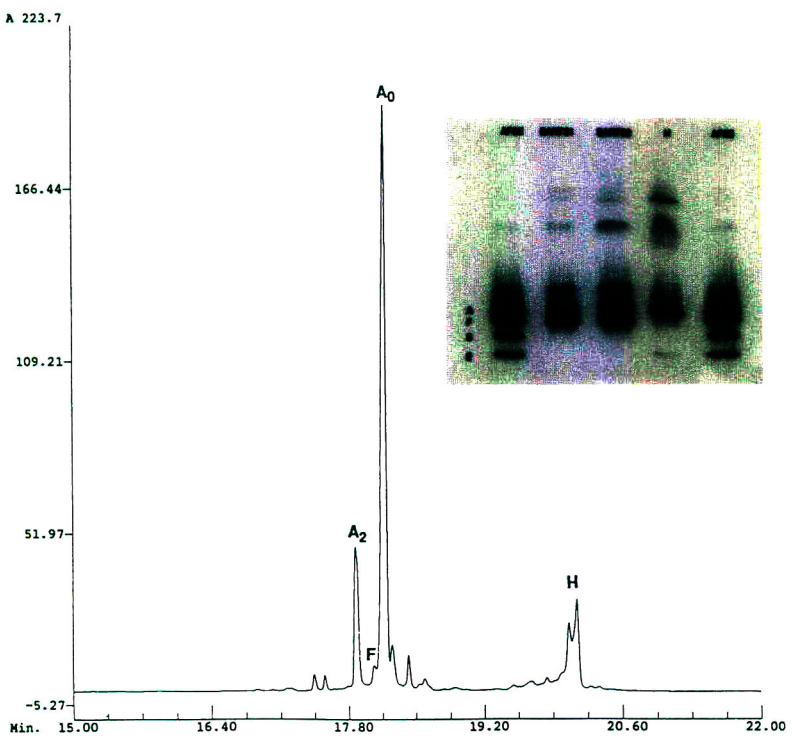

Fig. 6. Capillary isoelectric focusing of hemoglobins from a patient with hemoglobin H disease. Inset: isoelectric focusing gel of hemoglobin samples stained with *o*-dianisidine (1st and 5th lanes: hemoglobin AFSE reference standard; 4th lane: hemoglobin H sample; 2nd and 3rd lane: hemoglobins Bart's).

gel pattern, while a distinct peak migrating in the position of Hb A_2 was observed in the cIEF electropherogram. We have no explanation for this difference. Globin chain analysis of the Hb H sample (in contrast to the results obtained with Hb Bart's) showed major peaks for α- and β-globin, with only a minor amount of γ-globin (Fig. 7).

CE of hemoglobin E

The cIEF profile for a sample obtained from a patient homozygous for the Hb E mutation exhibited a single major peak for hemoglobin E and two minor peaks (Fig. 8). Since both β-globin genes carry the Hb E mutation, only β-globin polypeptides with the glutamic acid-to-lysine replacement at position 26 are synthesized, and no Hb A_0 should be formed. The two minor peaks probably represent glycated Hb E and fetal Hb F. The identity of the second minor peak was confirmed in another homozygous Hb E sample by capillary isoelectric focusing of the sample following addition of an Hb AF electrophoresis control (Fig. 9).

The gel IEF profile (Fig. 8, inset) exhibited a band pattern similar to the cIEF peak profile, *e.g.* a single major band for Hb E and indistinct minor bands. Free zone CE globin chain analysis of the Hb E sample exhibited only a single major peak (Fig. 10); we believe this to represent comigration of the mutated β-globin chains with α-globins due to increased β-globin mobility imparted by the substitution of the basic lysine residue for glutamic acid.

CE of G Philadelphia C

This patient carried two hemoglobin mutations, Hb G Philadelphia (asparagine to lysine replacement at position 68 in the α-globin gene) and Hb C (glutamic to lysine replacement at position 6 in the β-globin gene). Therefore at least four hemoglobin species would be expected: $\alpha\beta$, $\alpha_G\beta$, $\alpha\beta_C$ and $\alpha_G\beta_C$. The cIEF profile showed four major peaks (Fig. 11) which agreed with the gel IEF band pattern observed for the same sample (Fig. 11 inset). Globin chain analysis also displayed the expected profile of four peaks (Fig. 12). Since reference standards are not readily available, the peak assignments for

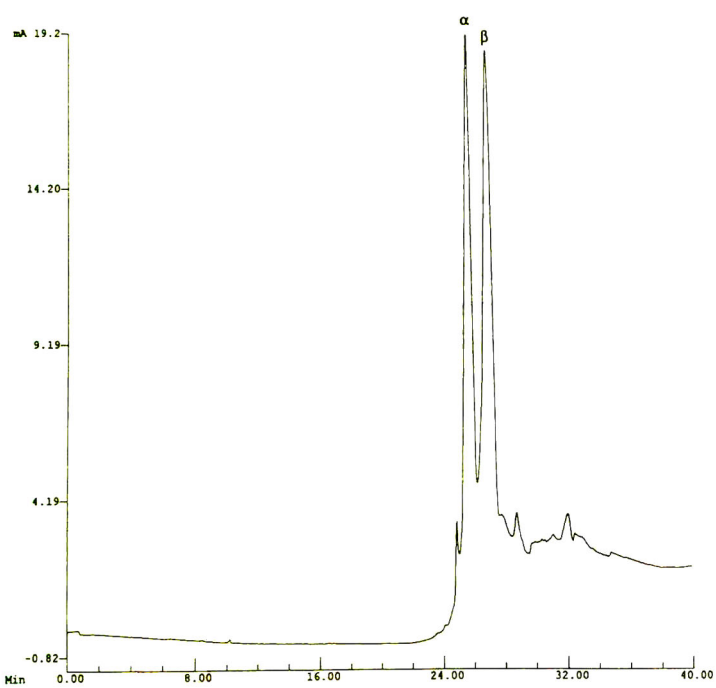

Fig. 7. Free zone capillary electrophoresis separation of globin chains from the hemoglobin H sample shown in Fig. 6.

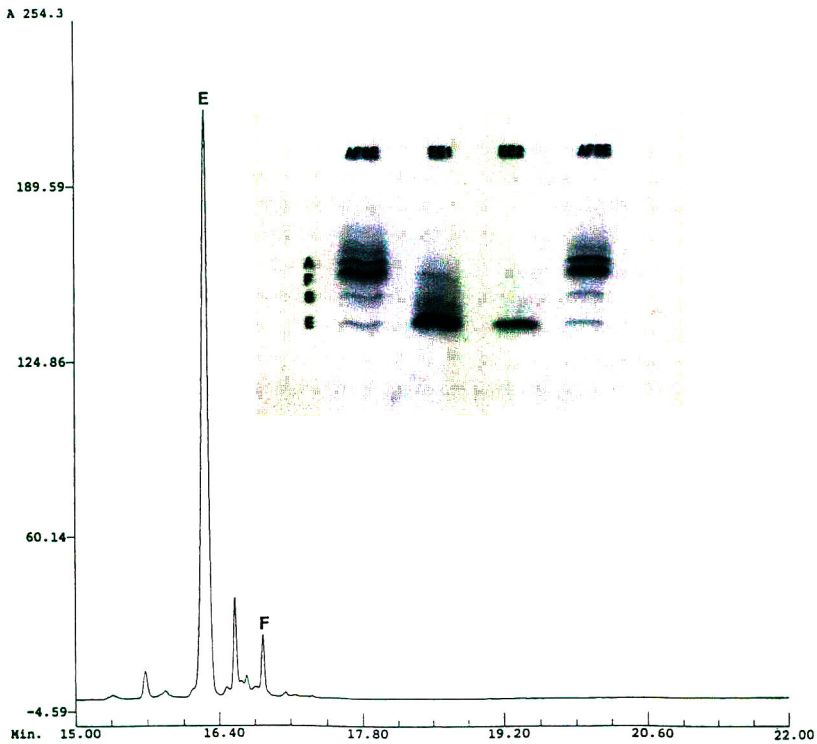

Fig. 8. Capillary isoelectric focusing of hemoglobins from a patient homozygous for the hemoglobin E mutation. Inset: isoelectric focusing gel of hemoglobin samples stained with *o*-dianisidine (1st and 4th lanes: hemoglobin AFSE reference standard; 2nd and 3rd lanes: hemoglobin E samples). The sample separated by cIEF is the one shown in the 2nd lane of the IEF gel.

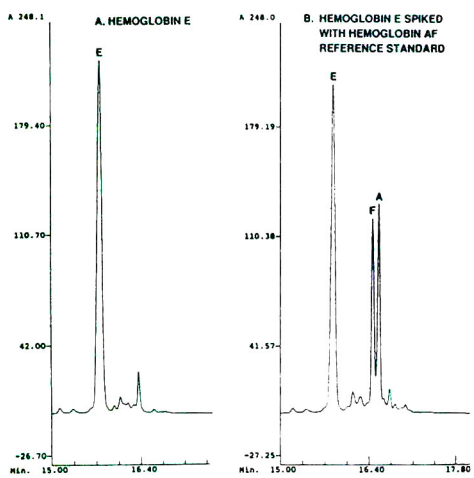

Fig. 9. Capillary isoelectric focusing of the Hb E sample shown in Fig. 8 after addition of a hemoglobin AF electrophoresis control.

β_C and α_G in Fig. 12 are tentative and based on assumptions drawn from the amino acid substitutions.

cIEF of hemoglobin Constant Spring

In conventional isoelectric focusing gels, hemoglobin Constant Spring focuses towards the very basic end of the pH gradient with an apparent pI of about 7.47 [8]. We have obtained preliminary cIEF results with a sample containing about 1% Hb Constant Spring which indicated a minor component migrating in the basic region of the electropherogram (Fig. 13). However, because of the low concentration of this species and its instability, confirmation of this component will require additional work with samples containing larger concentrations of Hb Constant Spring.

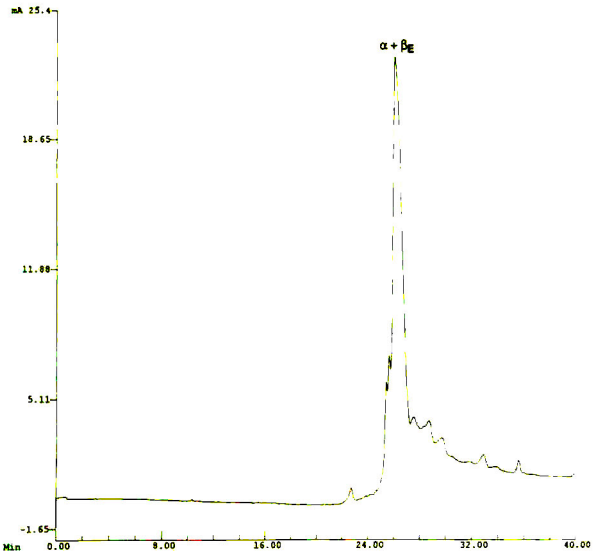

Fig. 10. Free zone capillary electrophoresis separation of globin chains from the hemoglobin E sample shown in Fig. 8.

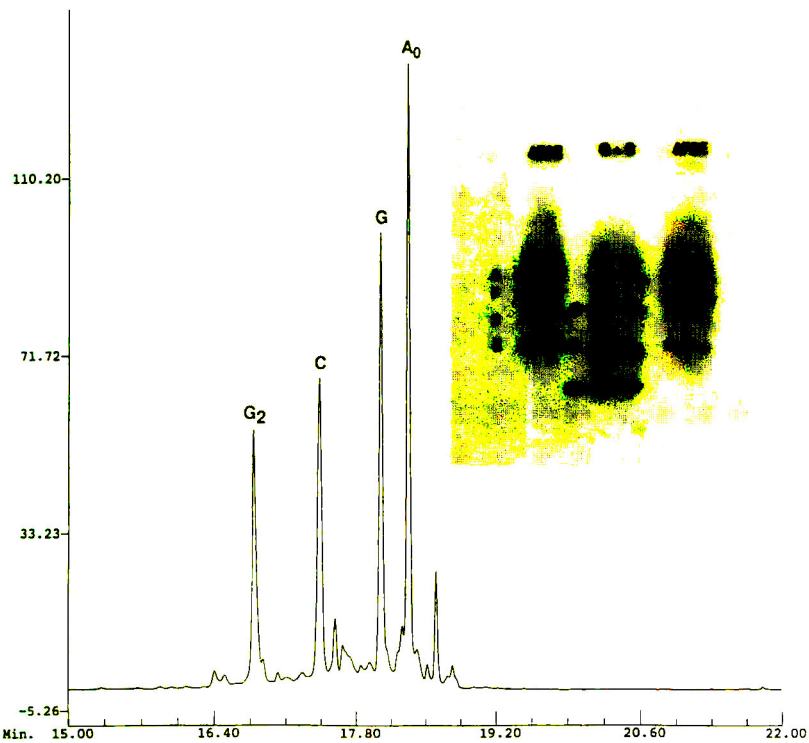

Fig. 11. Capillary isoelectric focusing of hemoglobins from a patient carrying the Hb G Philadelphia and Hb C mutations. Inset: isoelectric focusing gel of hemoglobin samples stained with *o*-dianisidine (1st and 3rd lanes: hemoglobin AFSE reference standard; 2nd lane: hemoglobin G Philadelphia C sample).

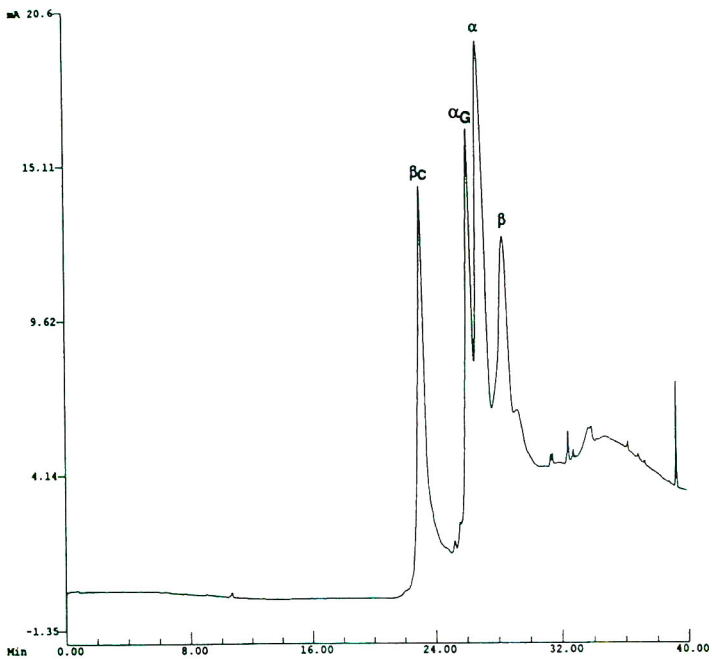

Fig. 12. Free zone capillary electrophoresis separation of globin chains from the Hb G Philadelphia C sample shown in Fig. 11.

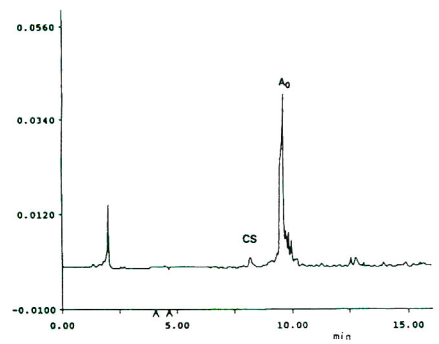

Fig. 13. Capillary isoelectric focusing of hemoglobins from a patient carrying the Hb Constant Spring mutation. *x*-Axis, time (min); *y*-axis, absorbance.

CONCLUSIONS

cIEF provides rapid, high-resolution separation of hemoglobin species, and specific detection of heme proteins in the visible region is highly sensitive and free of interferences. Hemoglobins Bart's and H, characteristic of α-thalassemia conditions common in Southeast Asia, can be easily distinguished by late-migrating components in the acidic portion of the pH gradient. Normal hemoglobins and known hemoglobin variants do not migrate in this region in cIEF. Hemoglobin H and hemoglobin Bart's samples were differentiated from each other by the distribution of globin chains analyzed by free zone electrophoresis under denaturing conditions. Hb Bart's samples exhibited major peaks for α- and γ-globin, while predominantly α- and β-globin chains were observed in Hb H samples.

The common hemoglobin variants could be distinguished from α-thalassemia samples (and from each other) by the presence of early-migrating species in the cIEF profile. Hemoglobin variants E, S, C, G Philadelphia, and Constant Spring all have isoelectric points higher than normal hemoglobins A_0 and F. Our results indicate that hemoglobins E, S, C, and G. Philadelphia are resolved from Hb A_0 and F. In addition, hemoglobins E, C, G Philadelphia can be distinguished by altered mobility of the mutant

globin chains using free zone capillary electrophoresis under denaturing conditions. This confirmatory analysis could be particular useful for identification of Hb E, which co-focuses with normal hemoglobin A_2 in conventional gel IEF.

REFERENCES

1 V.F. Fairbanks (Editor), *Hemoglobinopathies and Thalassemias, Laboratory Methods and Case Studies*, Brian C. Dekker, New York, 1980.
2 S. Fucharoen and P. Winichagoon, *Southeast Asean J. Trop. Med. Public Health*, 23 (1992) 647.
3 M. Zhu, R. Rodriguez, T. Wehr and C. Siebert, *J. Chromatogr.*, 608 (1992) 225.
4 E.J. van Kampen and W.G. Zijlstra, *Adv. Clin. Chem.*, 8 (1965) 141.
5 S. Hjertén, *J. Chromatogr.*, 247 (1985) 191.
6 S. Hjertén, J.-L. Liao and K. Yao, *J. Chromatogr.*, 387 (1987) 127.
7 M. Zhu, R. Rodriguez and T. Wehr, *J. Chromatogr.*, 559 (1991) 479.
8 P. Basset, F. Braconnier and J. Rosa, *J. Chromatogr.*, 227 (1982) 267.

Journal of Chromatography A, 652 (1993) 131–138
Elsevier Science Publishers B.V., Amsterdam

CHROM. 25 082

Effect of detergents on the electrophoretic behaviour of plasma apolipoproteins in capillary electrophoresis

Tanya Tadey and William C. Purdy*

Department of Chemistry, McGill University, 801 Sherbrooke Street West, Montréal, Québec H3A 2K6 (Canada)

ABSTRACT

The influence of various detergents on the capillary electrophoretic behaviour of plasma apolipoproteins was studied. Electrophoretic mobility increased in the presence of anionic detergents sodium deoxycholate (DOC) and sodium dodecyl sulfate (SDS), and decreased in the presence of non-ionic Triton X-100. Apolipoproteins from plasma low-density lipoproteins (LDLs) and high-density lipoproteins (HDLs) exhibited different affinities for DOC and SDS. Optimal separation and reproducibility of HDL and LDL apolipoproteins was obtained using high-pH buffers containing SDS. Good resolution of very-low-density lipoprotein (VLDL) apolipoproteins was obtained on addition of either SDS or cetyl trimethylammonium bromide to the running buffer. For VLDL apolipoproteins the use of polyacrylamide coated capillaries yielded better results.

INTRODUCTION

The use of capillary electrophoresis (CE) for clinical diagnostistic applications is growing in prominence. Large biomolecules can be separated rapidly in an instrumental format that delivers the resolving power of traditional electrophoresis. Furthermore, CE does not suffer from slow mass transfer rates which lead to band broadening in HPLC separations of proteins and peptides.

To date, there has been a number of papers describing the use of CE for analyzing biological samples [1–6]. Chen *et al.* [1] used CE to screen for abnormalities in serum, urine and cerebrospinal fluid. By employing high voltage gradients and high ionic strength buffers, serum proteins were separated in less than 100 s. The addition of ethylene glycol to the separation buffer was also shown to improve resolution of serum proteins [3]. Josic *et al.* [4] demonstrated the separation of intrinsic and extrinsic membrane proteins from the liver using urea-containing buffers.

We are interested in the use of CE for screening of plasma apolipoproteins. There is growing evidence that the apolipoprotein distribution in the plasma is a better marker of coronary heart disease (CHD) than the cholesterol level [7,8]. Some apolipoproteins, such as apoA-I, participate in the removal of cholesterol from the bloodstream and are therefore classified as antiatherogenic. Conversely, elevated levels of other apolipoproteins, such as apoB, indicate an increased risk of CHD, even in the individuals with normal cholesterol levels. As research into these effects of apolipoproteins grows there is increased demand for a fast and simple method for their analysis.

Recently, we reported preliminary results on the separation of plasma apolipoproteins by CE [9]. By adding the detergent sodium dodecyl sulfate (SDS) to the separation buffer, the main apolipoproteins of plasma high-density lipoproteins (HDLs) and low-density lipoproteins (LDLs) were resolved in less than 12 min. A distinct advantage to this method was that both LDL and HDL apolipoproteins could be sepa-

* Corresponding author.

0021-9673/93/$06.00

rated under the same conditions in a single run. This is generally not the case for either slab gel [10] or chromatographic [11] separations of apolipoproteins.

There have been no previous reports describing free-zone CE separations of protein-detergent complexes. Capillary SDS–polyacrylamide gel electrophoresis (PAGE) separations of protein–SDS complexes have been achieved [12]. However, in these cases separation was due to differences in size and detergent binding occurred only with the addition of heat and reducing agents. In cases where low concentrations of detergents were used as buffer modifiers, the role of detergent was only to modify the surface of the capillary [13,14]. This is because in the absence of heat or prolonged equilibration times, most proteins do not complex with detergents. However, since apolipoproteins have much higher affinity for detergents, their electrophoretic behavior can be significantly influenced by using detergents as buffer modifiers.

In this paper, the influence of various detergents on apolipoprotein CE is presented. The purpose of this work is to find the optimal detergent additive for apolipoprotein resolution. The detergents chosen as buffer modifiers have been shown to undergo complexation with apolipoproteins. The effects of detergent type, detergent concentration, and pH on electrophoretic behaviour of apolipoproteins are presented. CE separations of apolipoproteins from very-low-density lipoproteins (VLDLs) as well as HDL and LDL plasma fractions are shown.

EXPERIMENTAL

Apparatus

The CE system used a Bertan Model 230R (Bertan Associates, Hicksville, NY, USA) power supply and an Isco CV^4 (Isco, Lincoln, NE, USA) detector. The output of the power supply was connected to the buffer reservoir via platinum electrodes (Bioanalytical Systems, West Lafayette, IN, USA). Fused-silica capillaries (Polymicro Technologies, Phoenix, AZ, USA) of 50 μm I.D. and 375 μm O.D. were used. Electropherograms were collected on a 486DX-compatible computer using the Waters Maxima 820 (Millipore, Milford, Mass, USA) chromatography software.

Chemicals

Doubly distilled, deionized water was used for all experiments. Ultra-pure SDS, tris(hydroxymethyl)methylamine (Tris), and acrylamide were obtained from ICN Biochemicals (Montreal, Canada). Sodium tetraborate (borax) and 3-(trimethoxysilyl)propyl methacryalte were from Aldrich (Milwaukee, WI, USA). Electrophoresis grade N,N,N′,N′-tetramethylethylenediamine (TEMED) and ammonium persulfate (Biorad, Mississauga, Canada) were used. Glacial acetic acid and hydrochloric acid were purchased from J.T. Baker (Phillipsburg, NJ, USA). Sodium deoxycholate (DOC), tetredecyltrimethylammonium bromide (TDAB) and cetyltrimethylammonium bromide (CTAB) were from Sigma (St. Louis, MO, USA). Apolipoprotein A-I, A-II and B standards were purchased from Sigma and apolipoprotein C-III was purchased from Biodesign International (Kennebunkport, ME, USA).

Preparation of apolipoprotein samples

Blood from a fasting male donor was collected into tubes containing 0.01% EDTA. A hypertriglyceridemic donor was used for isolation of VLDL lipoproteins in order to increase yields. Plasma was isolated by centrifugation at 1000 *g* and 4°C for 20 min. Plasma lipoprotein fractions were obtained using standard procedures [15]. Ultracentrifugation was performed at 142 200 *g* and 5°C using a Beckman L8-80 centrifuge equipped with a Ti-50.3 rotor. The lipoproteins were isolated at the following density ranges: VLDL ($d < 1.006$ g/ml), LDL ($d = 1.019$–1.063 g/ml) and HDL ($d = 1.063$–1.21 g/ml). To remove contamination due to serum albumin, the HDL fraction was diluted 1:3 with a NaCl/NaBr solution of $d = 1.21$ g/ml and recentrifuged for 20 h. All lipoprotein fractions were dialysed against 0.9% NaCl.

The HDL fraction was delipidated using diethyl ether and ethanol [16] and dissolved in a pH 6, 0.1 *M* Tris buffer containing 6 *M* urea. The LDL and VLDL fractions were not delipi-

dated since solubility in aqueous solution decreased dramatically upon delipidation.

Preparation of polyacrylamide-coated capillaries

The method of Hjertén [17] was used with some modifications. The capillary was first conditioned using a 15-min rinse with 1 *M* NaOH followed by a 5-min rinse with water. A solution containing 30 μl of 3-(trimethoxysilyl)propyl methacrylate in 1 ml of acetic acid–water (1:1, v/v) was drawn through the capillary using house vacuum. After 1 h, this solution was removed. The polymerizing solution was prepared by adding 10 μl of TEMED and 100 μl of 10% (w/v) ammonium persulfate to 10 ml of degassed 4% (w/v) acrylamide. The capillary was filled with this solution and left in a horizontal position for about 45 min. After polymerization was completed the excess polyacrylamide was removed and the capillary was rinsed with water.

CE procedures

Uncoated fused-silica capillaries had a total length of 75 cm and a separation length of 50 cm. Polyacrylamide coated capillaries were 80 cm long and had a separation length of 55 cm. A wavelength of 220 nm was used for detection. The applied voltage was 25 kV for all separations. The pH of borax buffers was adjusted by titrating with appropriate amounts of HCl and NaOH. Bare silica capillaries were conditioned between runs by two-minute rinses with 0.1 *M* NaOH and water. Samples were injected hydrodynamically at a height of 15 cm and an injection time of 8–10 s.

RESULTS AND DISCUSSION

CE behaviour of apolipoprotein–detergent complexes

To understand the nature of interaction between apolipoproteins and detergents a closer look at apolipoprotein assembly within lipoprotein particles is necessary. A diagram of a typical lipoprotein particle is shown in Fig. 1 [18]. The apolipoproteins normally exist on the periphery of the lipoprotein particle. One side of the apolipoprotein is in contact with the aqueous plasma environment and is therefore hydrophilic. The other side is hydrophobic since it is associated with the lipid core of the lipoprotein particle. This dual nature allows apolipoproteins to readily associate with other amphiphiles such as detergents.

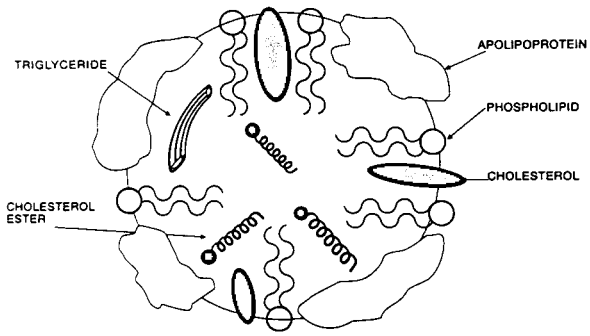

Fig. 1. Schematic of lipoprotein particle.

Discrete, non-interacting detergent binding sites on apolipoproteins have been observed at low detergent concentrations ($<10^{-4}$ *M*) [19]. These sites are hydrophobic in nature and involve only the monomeric detergent. Formation of the apolipoprotein–detergent complex can therefore be represented by:

$$A + nD \rightarrow AD_n \quad (1)$$

where A is the apolipoprotein, D is the detergent and n is the number of bound detergent monomers.

The number of discrete binding sites and maximum amount of bound detergent for HDL and LDL apolipoprotein detergent complexes are shown in Table I [19,20]. The values for Triton X-100 and DOC are expecially interesting since hydrophilic proteins do not bind these detergents even after prolonged equilibration. The binding of detergent to apolipoprotein molecules alters the Stokes radius and in the case of ionic detergents, the charge of the protein. This causes a change in the electrophoretic mobility of the protein since [21]:

$$\mu_e = \frac{Q}{R_S}\left(\frac{1}{6\pi\eta}\right) \quad (2)$$

where μ_e is the electrophoretic mobility, Q is the total charge, R_S is the Stokes radius and η is the viscosity. Changes in electrophoretic mobility

TABLE I

NUMBER OF PROTEIN BINDING SITES AND AMOUNT OF DETERGENT BOUND IN APOLIPOPROTEIN–DETERGENT COMPLEXES

Apolipoprotein	Detergent	n	Detergent/protein (w/w)
Apo-AI[a]	SDS	4	1.4
	DOC	1	0.4
	TDAB	4	1.1
Apo-AII[a]	SDS	4	1.4
	DOC	1	0.4
	TDAB	10	1.1
Apo-B[b]	DOC		0.64
	Triton X		0.52

[a] From ref. 19, detergent binding data obtained by equilibrium dialysis.
[b] From ref. 20, detergent binding data obtained by gel filtration of the proteins in the presence of detergent.

upon detergent binding to apolipoproteins can be used therefore to estimate the effect of detergent on protein size and charge. The value of μ_e can be experimentally determined using:

$$\mu_e = \frac{l_d L}{V}\left(\frac{1}{t_{eo}} - \frac{1}{t}\right) \quad (3)$$

where l_d is the detection length of the capillary, L is the total length, V is the applied voltage, t_{eo} is the retention time of the neutral marker and t is the analyte retention time.

The effect of three surfactants on resolution of HDL and LDL apolipoproteins is illustrated in Fig. 2. The concentrations of added detergent ensured maximum binding to apolipoproteins. The presence of anionic detergents SDS and DOC resulted in complete resolution of all components. Addition of the neutral detergent Triton X-100 resulted in separation of A and B apolipoproteins. Resolution of apoA-I, apoA-II and apoB-100, apoB-48 pairs however, was not possible. The extra peaks in Fig. 2C were found to be due to sample buffer components.

The cationic detergent TDAB was also studied as a buffer modifier since the values in Table I indicate that it undergoes significant binding with apolipoproteins. The resulting electropherogram (not shown) exhibited a noisy baseline and protein peaks were not observed after 30 min. It is possible that under these conditions the electrophoretic and electroosmotic velocities are similar in magnitude but in opposite directions. Addition of another cationic detergent, CTAB, also gave poor results.

Changes in apolipoprotein electrophoretic mobility on addition of surfactants are shown in Table II. Triton X-100 caused a decrease in the

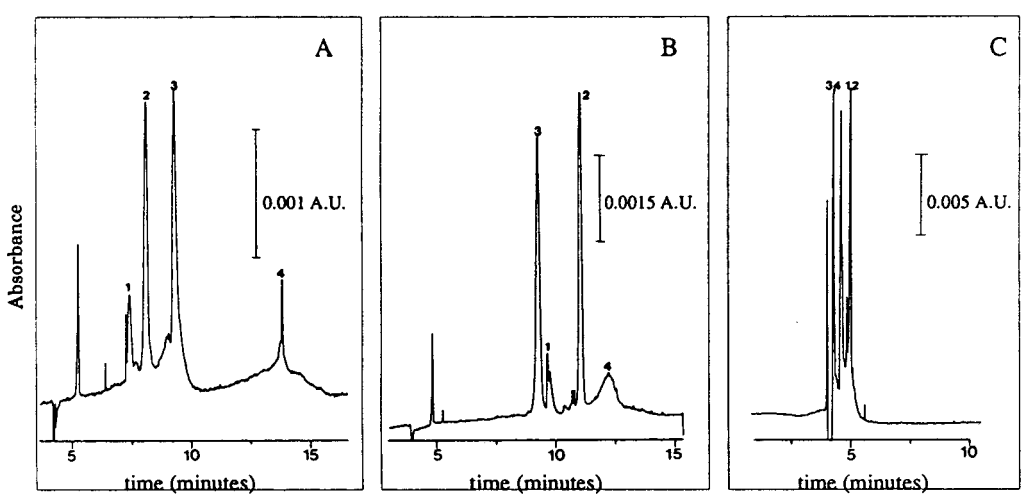

Fig. 2. Effect of various detergents of resolution of apolipoproteins. Conditions: 30 mM borate buffer pH 9. (A) 10 mM DOC; (B) 3.5 mM SDS; (C) 3.5 mM Triton X-100. Peaks: 1 = apoA-II; 2 = apoA-I; 3 = apoB-100; 4 = apoB-48.

TABLE II

EFFECT OF DETERGENTS ON ELECTROPHORETIC MOBILITIES OF APOLIPOPROTEINS

CE conditions as in Fig. 2.

Protein	Mobility, μ_e (10^{-4} cm^2/V s)				$(\mu_{e2} - \mu_{e1})$ (10^{-4} cm^2/V s)		
	Borate buffer (μ_{e1})	SDS (μ_{e2})	DOC (μ_{e2})	Triton X (μ_{e2})	SDS	DOC	Triton X
ApoA-I	1.40	4.06	2.82	0.92	2.66	1.42	−0.48
ApoA-II	1.40	3.74	2.57	0.92	2.34	1.17	−0.48
ApoB-100	1.40	3.64	3.21	0.84	2.24	1.81	−0.06

electrophoretic mobility for all three proteins. This is because binding of this detergent causes an increase in the protein's Stokes radius and a concomitant decrease in total charge. The net result, as shown by eqn. 2, is decreased mobility.

Both anionic detergents caused a significant increase in apolipoprotein electrophoretic mobility. The effect of SDS was more pronounced, however, for all proteins. Mikano *et al.* [19] showed that Stokes radii of apoA–DOC and apoA–SDS complexes were similar. However, since four times as much SDS as DOC is bound to the protein, the SDS complexes exhibit a higher negative charge and consequently increased electrophoretic mobility.

It is interesting to note that elution order of apoA-I and apoB-100 is different in DOC and SDS. This can be explained by the relative hydrophobicities of the proteins. LDL lipoproteins contain a higher fraction of lipid compared to HDL particles and the main protein of LDL, apoB, is much more hydrophobic than apoA-I which is found in HDL. Since DOC is derived from cholesterol it more closely resembles the natural lipoprotein environment. Consequently, apoB binds more strongly to DOC and experiences a greater change in its electrophoretic mobility.

On examination of the electropherograms in Fig. 2, addition of either DOC or SDS to the running buffer appears to give good resolution of apolipoproteins. However, reproducibility of the separation must also be considered. This is especially true for routine clinical diagnostic applications. We found that the behaviour of apoB was not reproducible in the DOC system. The apoB peak tended to degrade over time. This may have been due to adsorption of the protein complex to the capillary wall. As illustrated in Fig. 3, electropherograms obtained in SDS-containing buffers were found to be highly reproducible in retention time and peak area. Further studies were therefore concentrated on SDS buffers.

Fig. 4 shows the retention profile of apolipoproteins at different SDS concentrations. When the buffer contained less than 2.7 m*M* SDS, the individual apolipoproteins could not be distinguished. Instead the mixture appeared as a broad series of peaks between 6 and 12 min. Injection of individual apolipoprotein standards produced similar electrophoretic patterns. This behavior is most likely due to the binding characteristics of SDS–apolipoprotein complexes. Reynolds and Simon [22] showed binding to

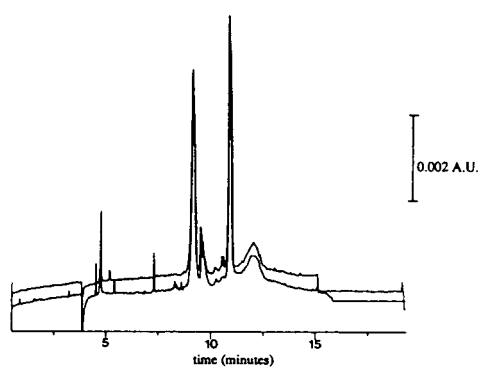

Fig. 3. Overlay showing reproducibility of first and eleventh run in SDS containing buffers. Conditions and peaks as in Fig. 2B.

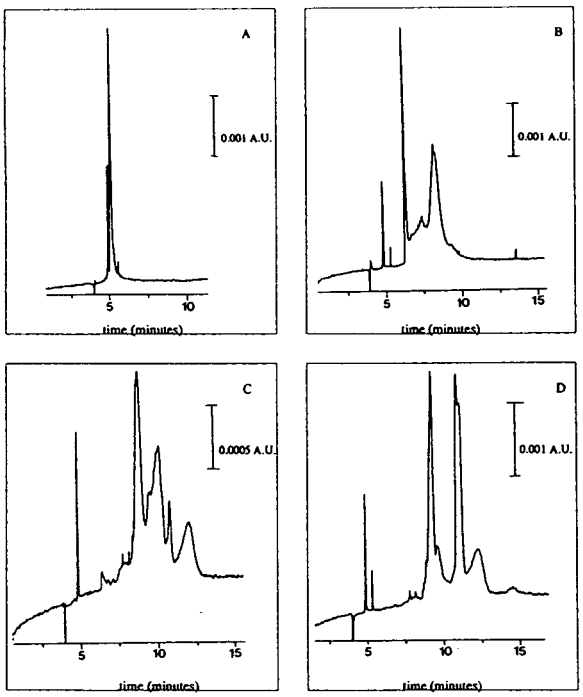

Fig. 4. Effect of SDS concentration on apolipoprotein CE. (A) No SDS; (B) $9 \cdot 10^{-4}$ *M* SDS; (C) $1.7 \cdot 10^{-3}$ *M* SDS; (D) $2.6 \cdot 10^{-3}$ *M* SDS. Other conditions as in Fig. 2.

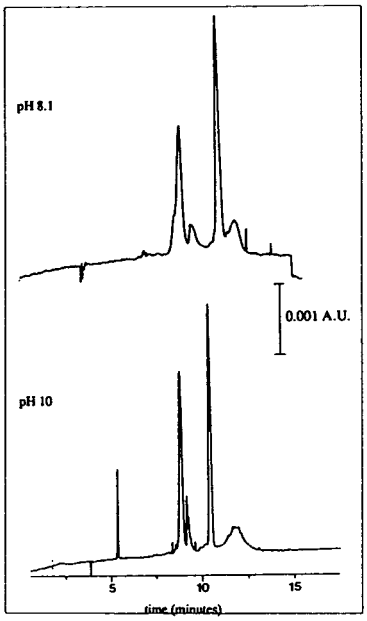

Fig. 5. Effect of buffer pH on resolution. Conditions: borate buffer, 25 kV, 40 μA for both runs.

apoA-I begins at about 0.1 m*M* SDS and plateaus at about 3 m*M* SDS. Therefore, the elution patterns obtained in Fig. 4 are likely due to the existence of apolipoproteins with varying degrees of binding to SDS.

The effect of adding detergent to apolipoprotein samples was also studied. In this case the running buffer contained no detergent and the sample contained 3.5 m*M* SDS. There was no significant improvement in resolution compared to the electropherogram in Fig. 3. The retention time of the peak did increase, however, by over two minutes. This indicates that SDS remains in a complex with the proteins throughout the run. However, the absence of SDS in the running buffer means that protein-protein interactions can still occur. This causes the proteins to elute as a single peak. When both the sample and running buffer contained SDS, electropherograms similar to those in Fig. 3 were obtained.

Effect of pH

The effect of pH on apolipoprotein resolution is illustrated in Fig. 5. The ionic strength of the borate buffer was adjusted to maintain the same current in both runs. Both resolution and efficiency were improved at the higher pH. This can be partially attributed to decreased adsorption. It is now well known that proteins undergo pH-dependent association with silanol groups of fused silica. It is also possible that SDS–apolipoprotein association is weakened at lower pH values.

CE of VLDL apolipoproteins

The main apolipoproteins found in plasma VLDL particles are apoB-100 (M_r 500 000), apoB-48 (M_r 250 000), apoE (M_r = 35 000), apoC-III (M_r 8750), apoC-II (M_r = 8800) and apoC-I (M_r 6500) [18]. The apolipoproteins in this fraction are the most heterogeneous with respect to their size and hydrophobicity. This makes their separation by chromatographic techniques difficult. The effect of detergent addition on the separation of VLDL apolipoproteins is

shown in Fig. 6. As in the case of HDL and LDL fractions, the VLDL apolipoproteins migrate as a single species in the absence of detergent in the buffer.

All three detergents had a dramatic effect on the elution profile of VLDL apolipoproteins. Addition of DOC (Fig. 6B) appears to result only in the bulk separation of hydrophobic apoB from the more hydrophilic apoC proteins. Results obtained with SDS and CTAB are more promising. At least four major components can be distinguished when either of these detergents is added to the buffer. The effect of CTAB is especially interesting since we had found it to be a poor choice for resolution of HDL and LDL apolipoproteins.

Separations of apolipoproteins in polyacrylamide capillaries are shown in Fig. 7. A significant increase in resolution was observed in these capillaries. This is another difference from

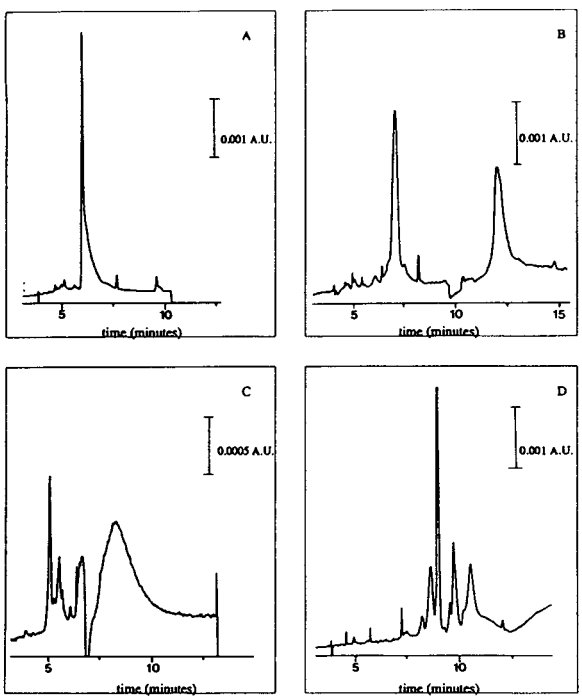

Fig. 6. Effect of detergent addition on VLDL apolipoprotein resolution in fused-silica capillaries. Conditions: 30 m*M* borate buffer pH 9; (A) no detergent added; (B) 10 m*M* DOC; (C) 3.5 m*M* CTAB; (D) 3.5 m*M* SDS.

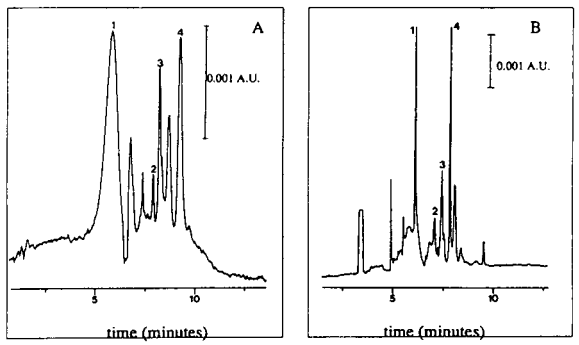

Fig. 7. Separation of VLDL apolipoproteins in acrylamide-coated capillaries. Conditions: 30 m*M* borate pH 9, (A) 3.0 m*M* CTAB; (B) 3.5 m*M* SDS. Peaks: 1 = apoB; 2, 3 = apoCIII variants; 4 = albumin.

CE separations of HDL and LDL apolipoproteins where resolution was not affected by coating the capillary [9]. In both the SDS- and CTAB-containing buffers over 7 different components of VLDL could be distinguished.

Since standards of all VLDL apolipoproteins were not available, it was difficult to assign all of the peaks in Fig. 7. This also made it difficult to draw conclusions regarding which detergent is better for these separations. The efficiency in SDS-buffers was somewhat higher. However, as illustrated in Fig. 8, CTAB showed better results for resolving charged variants of apoC-III. The isoforms of apoC-III occur as a result of varying degrees of sialization. For now, it appears that

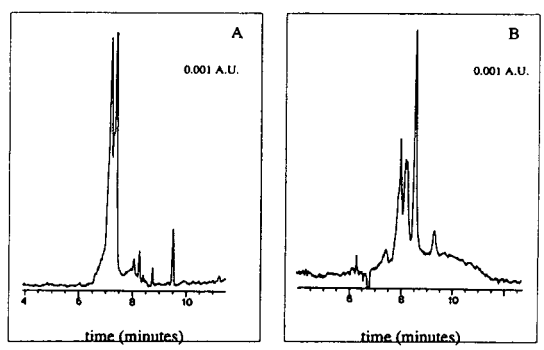

Fig. 8. Separation of apoC-III charged variants. (A) 3.5 m*M* SDS; (B) 3.0 m*M* CTAB buffer. Other conditions as in Fig. 7.

either detergent is very effective for obtaining VLDL profiles.

CONCLUSIONS

The electrophoretic behaviour of apolipoproteins can be modified by addition of surfactant to the running buffer. Addition of anionic detergents results in optimal resolution of HDL and LDL proteins. Both cationic and anionic detergents improve the resolution of VLDL apolipoproteins. The CE procedures in this paper are advantageous since one buffer system can be used for resolving all apolipoproteins. Furthermore, detergent modified CE of apolipoproteins does not require extensive sample treatment as in the case of chromatography or slab electrophoresis. CE therefore appears to be well-suited for rapid screening of all major plasma apolipoproteins. Future work is being directed at using CE to identify apolipoprotein abnormalities in plasma.

ACKNOWLEDGEMENTS

The authors are indebted to the National Research Council of Canada for financial support of this work.

The authors also wish to thank the Lipid Research Center of the Royal Victoria Hospital in Montreal for use of their facilities in preparing the lipoprotein fractions and Merck Frosst Canada for their assistance in purchasing the CE equipment.

REFERENCES

1 F.A. Chen, C.M. Liu, Y.Z. Hsieh and J.C. Sternberg, *Clin. Chem.*, 37 (1991) 14.
2 F.A. Chen, *J. Chromatogr.*, 559 (1991) 445.
3 M.J. Gordon, K.J. Lee, A.A. Arias and R.N. Zare, *Anal. Chem.*, 63 (1991) 69.
4 D. Josic, K. Zeilinger, W. Reutter, A. Bottcher and G. Schmitz, *J. Chromatogr.*, 516 (1990) 89.
5 K.J. Lee and G.S. Heo, *J. Chromatogr.*, 559 (1991) 317.
6 H. Yamamoto, T. Manabe and T. Okuyama, *J. Chromatogr.*, 515 (1990) 659.
7 H.K. Naito, *Clin. Chem.*, 34 (1988) B84.
8 N. Rifai, J.F. Chapman, L.M. Silverman and J.T. Gwynnes, *Ann. Clin. Lab. Sci.*, 18 (1988) 429.
9 T. Tadey and W.C. Purdy, *J. Chromatogr.*, 583 (1992) 111.
10 C. Edelstein and A.M. Scanu, *Methods Enzymol.*, 128 (1986) 339.
11 A. Aviram, S. Mokady and U. Cogan, *Chem. Biochem. Physiol.*, 93B (1989) 279.
12 A.S. Cohen and B.L. Karger, *J. Chromatogr.*, 397 (1987) 409.
13 W.G.H.M. Muijselar, C.H.M.M. de Bruijn and F.M. Everaerts, *J. Chromatogr.*, 605 (1992) 115.
14 J.K. Towns and F.E. Regnier, *Anal. Chem.*, 63 (1991) 1126.
15 R.J. Havel, H.A. Eder and J.M. Bragdon, *J. Clin. Invest.*, 34 (1955) 1345.
16 A.M. Scanu and C. Edelstein, *Anal. Biochem.*, 44 (1971) 576.
17 S. Hjertén, *J. Chromatogr.*, 347 (1985) 191.
18 A.M. Gotto, Jr. (Editor), *Plasma Lipoproteins*, Elsevier, New York, 1987, Ch. 3.
19 S. Mikano, C. Tanford and J.A. Reynolds, *J. Biol. Chem.*, 249 (1974) 7379.
20 A. Helenius and K. Simons, *J. Biol. Chem.*, 247 (1972) 3656.
21 Y. Walbroehl and J.W. Jorgenson, *J. Microcol. Sep.*, 1 (1989) 43.
22 J.A. Reynolds and R.H. Simon, *J. Biol. Chem.*, 249 (1974) 3937.

Journal of Chromatography A, 652 (1993) 139–147
Elsevier Science Publishers B.V., Amsterdam

CHROM. 25 105

Evaluation of sodium dodecyl sulfate non-acrylamide, polymer gel-filled capillary electrophoresis for molecular size separation of recombinant bovine somatotropin

Kiyoshi Tsuji

Control Biotechnology, Pharmaceutical Product Control Division, The Upjohn Company, Kalamazoo, MI 49001 (USA)

ABSTRACT

Sodium dodecyl sulfate (SDS) non-acrylamide, polymer gel-filled capillary electrophoresis was examined as an alternative to the high-performance size-exclusion chromatographic (HPSEC) method for the analysis of recombinant bovine somatotropin (bovine growth hormone, rbSt). A calibration curve for the molecular mass of protein standards (M_r 14 000 to 97 000) was linear ($r^2 = 0.998$) when the molecular mass of the proteins and their peak migration time were plotted on a logarithmic (log–log) scale. Relative standard deviation (R.S.D.) of the molecular mass determination was approximately 2–3%. A pre-production as well as a production lot of the SDS gel-filled capillary columns were examined. Performance of both of these columns were equivalent. Peak migration time remained relatively constant beyond 140 sample injections. Gradual loss of theoretical plates was noted over the course of the assay; however, the peak resolution remained adequate for the analysis of rbSt.

Peaks corresponding to monomer, dimer, trimer, and tetramer of rbSt were base-line resolved by the SDS gel-filled capillary electrophoresis. Theoretical plate of the monomer peak was approximately 28 000–30 000 per 40 cm column. Both the monomer and the dimer recovery studies indicated that the calibration curves are linear ($r^2 > 0.993$) and the slopes are no different from one. Amounts of the components in rbSt determined by the SDS gel-filled capillary electrophoresis compared well with those of the HPSEC method. The results of this study indicated that the SDS non-acrylamide gel-filled capillary electrophoresis may be a viable alternative to the HPSEC method for the molecular size separation and analysis of recombinant proteins.

INTRODUCTION

Recombinant proteins are posing a considerable challenge to analytical chemistry. High-performance size-exclusion chromatography (HPSEC) is routinely employed to determine the composition of recombinant proteins. However, peak resolution capability of the HPSEC method is not always ideal and difficulty has been experienced in obtaining reliable/usable columns for the assay of recombinant bovine somatotropin (rbSt). The difficulty was traced to changes made in the column manufacturing processes.

Sodium dodecyl sulfate–polyacrylamide slab gel electrophoresis (SDS-PAGE) is an indispensable technique for the separation of proteins based on their apparent molecular mass. In spite of impressive advances made in recent years [1], electrophoresis still represents a collection of labor-intensive and time consuming techniques and quantification by means of an optical scanning apparatus is often sub-optimum.

Recent developments in the commercialization of high-performance capillary electrophoresis (HPCE) instrument [2–5] have made it possible to exploit potential of SDS gel-filled capillary column for separation of proteins with promises of rapid and automated analysis with improved reproducibility and quantification. Hjertén [6] was the first to demonstrate utility of a polyacrylamide gel filled column for separation of a membrane protein. He utilized an uncoated, home made, ordinary glass capillary column filled with polyacrylamide gel. Cohen and Karger [7] also applied SDS polyacrylamide gel-filled

capillaries for electrophoresis of peptides and proteins, but no quantitative data was presented. Tsuji [8] prepared an SDS polyacrylamide gel-filled capillary column filled with cross-linked acrylamide gel and provided quantitative data for molecular mass separation and analysis of SDS–protein complexes.

Zhu *et al.* [9] expanded molecular sieving action of linear polymers, *e.g.* dextran, methylcellulose, and polyethylene glycol, and used them as additives in the HPCE buffer to facilitate separation of DNA and proteins. Ganzler *et al.* [10] substituted polyacrylamide with a dextran polymer and/or a linear polyethylene glycol polymer network and successfully achieved molecular mass separation of proteins. Just recently, the SDS non-acrylamide, polymer gel-filled capillary column became commercially available [11]. Such columns were examined as an alternative to the HPSEC method for the analysis of rbSt.

EXPERIMENTAL

Instrumentation

A Beckman P/ACE system 2100 HPCE instrument (Beckman Instruments, Fullerton, CA, USA) was used. Each analytical run consists of rinsing a coated capillary column (parts No. 241521, Beckman; 100 μm I.D. × 375 μm O.D.; effective length, 40 cm) with 1.0 *M* HCl for 2 min and the column was filled with an SDS non-acrylamide, polymer gel solution (parts No. 241522, Beckman) for 4 min. Use of a coated capillary column is required to eliminate electroendosmosis.

About 1 mg protein per ml solution was injected for 60 s under nitrogen pressure (total injection volume, *ca.* 60 nl) onto the SDS gel-filled capillary column and the peaks migrating in the capillary were monitored on-column by UV at 214 nm. The column temperature was maintained at 20°C by a circulating coolant to minimize band diffusion for effective size separation. An electrophoretic run was conducted at −14.1 kV (−300 V/cm, 24 μA) using the SDS gel solution as reservoirs at both anode and cathode terminals. The area under the peak was integrated by means of an in-house GC/LC program residing on a VAX mainframe computer and with an electronic integrator (Model 3392A, Hewlett-Packard, Palo Alto, CA, USA).

A series II 1090 Liquid Chromatograph with a low-volume autosampler/injector (Hewlett-Packard) was used for the HPSEC assay. Peaks eluting from the Zorbax GF-250 column (25 cm × 9.4 mm I.D.; MAC-MOD Analytical, Chadds Ford, PA, USA) were monitored at 280 nm.

Reagents

The molecular mass protein standard solution containing hen egg white lysozyme (molecular mass: 14 400), soybean trypsin inhibitor (21 500), bovine carbonic anhydrase (31 000), hen egg white ovalbumin (45 000), bovine serum albumin (BSA, 66 200), rabbit muscle phosphorylase *b* (97 400) was obtained from Bio-Rad Labs. (No. 161-0304, SDS-PAGE Low Range Molecular Weight Standard, Richmond, CA, USA).

The sample buffer solution, containing 1% SDS (Sigma, St. Louis, MO, USA) in 0.12 *M* Tris–HCl, pH 6.6 (part No. 241525, Beckman), was used to dilute the protein sample. The 2-mercaptoethanol (Sigma) was used to reduce the protein sample.

For the HPSEC assay, a thoroughly de-gassed mobile phase composed of 150 m*M* NaCl (Mallinckrodt, Paris, KY, USA), 25 m*M* NaH_2PO_4 (J.T. Baker, Phillipsburg, NJ, USA) at pH 8.0 and 0.1% SDS was pumped at a flow-rate of approximately 1.0 ml/min.

Preparation of protein samples

Molecular mass protein standard. A 5-μl volume of the molecular mass protein standard solution was diluted in 40 μl of the sample buffer solution. After through mixing, 2 μl of 2-mercaptoethanol was added and the mixture was heated at 80°C for 5 min.

rbSt. Samples of rbSt used in this study were manufactured by The Upjohn Company (Kalamazoo, MI, USA). Approximately 1 mg of rbSt samples was dissolved in 100 μl of a weak ammonium solution [10 μl of NH_4OH (Mallinckrodt) per 10 ml of water (Burdick & Jackson, Muskegon, MI, USA)] and diluted in 900 μl of the sample buffer solution just prior to the

analysis. An aliquot of 20 μl of the dimer-enriched sample (*ca.* 4.5 mg protein per ml) was dissolved in 10 μl of the weak ammonium solution. After through mixing, the solution was diluted in 70 μl of the sample buffer just prior to the analysis.

To reduce and denature the protein, 2 μl of 2-mercaptoethanol was pipetted into a solution with *ca.* 1 mg protein concentration per ml. After through mixing, the sample was heated at 80°C for 5 min.

For a standard addition/recovery study, several different quantities of the dimer-enriched sample was pipetted into the monomer-enriched sample to prepare seven solutions containing the dimer ranging from 5 to 30%.

For the HPSEC analysis, approximately 10 mg of rbSt per ml of the weak ammonium hydroxide solution containing 0.1% SDS was prepared. About 100 μl of the sample solution was injected onto the size-exclusion column.

RESULTS AND DISCUSSION

SDS gel-filled capillary electrophoresis

The SDS non-acrylamide gel-filled capillary electrophoresis separates SDS–protein complexes based on their apparent molecular mass [9–11] similar in the principal as that of the conventional SDS-PAGE technology [12]. A typical HPCE electropherogram indicating separation of the molecular mass protein standards is shown in Fig. 1-I. A linear relationship ($r^2 = 0.998$) existed when the molecular mass of protein stan-

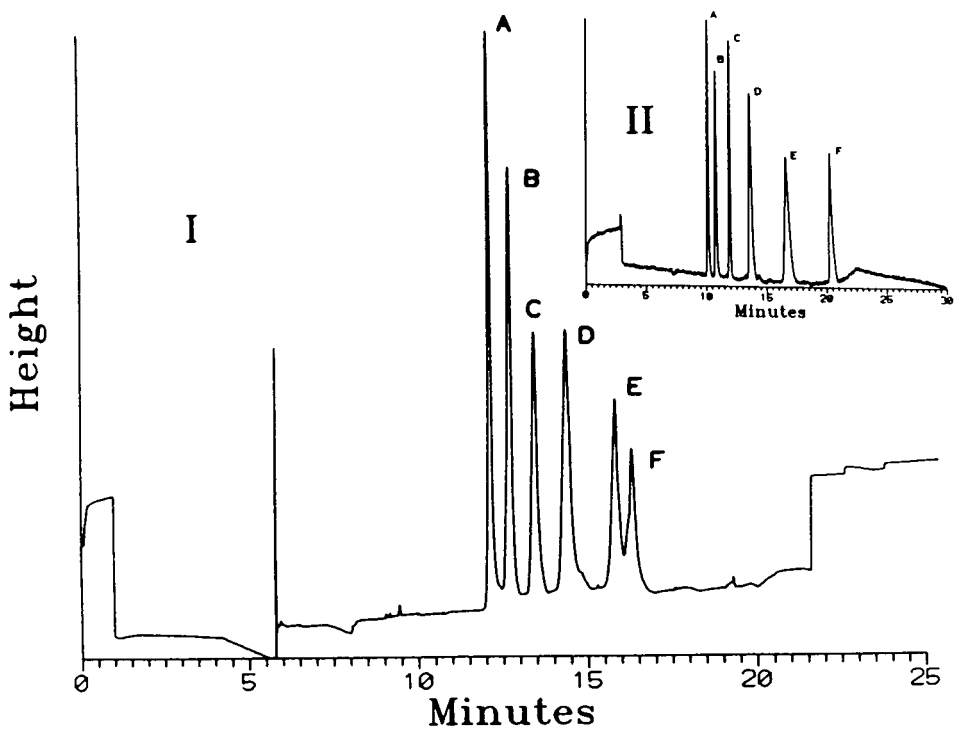

Fig. 1. SDS gel-filled capillary electrophoretic separation of the molecular mass protein reference standards as monitored at 214 nm. Peak migration order, A = lysozyme (M_r 14 400); B = trypsin inhibitor (21 500); C = carbonic anhydrase (31 000); D = ovalbumin (45 000); E = BSA (66 400); and F = phosphorylase *b* (97 400). (I) SDS non-acrylamide, polymer gel-filled capillary column [8,9]. Conditions, −300 V/cm (24 μA); column temperature: 20°C; effective peak migration distance: 40 cm; coated capillary: 100 μm I.D.; running buffer: SDS non-acrylamide, polymer gel solution. (II) SDS polyacrylamide gel-filled capillary column [7]. Conditions, −83 V/cm (12 μA); column temperature: 25°C; peak migration distance: 7 cm; coated capillary filled with 5% T [T = (5 g acrylamide + 0.13 g N,N'-methylenebisacrylamide)/100 ml solution] polyacrylamide gel: 75 μm I.D.; running buffer: 375 m*M* Tris, pH 8.8, 0.1% SDS, 2.5 *M* ethylene glycol.

dards, ranging from approximately 14 000 to 97 000, was plotted against their electrophoretic mobilities or peak migration time on a logarithm (log–log) scale. Unlike the excellent peak resolution efficiency of the SDS polyacrylamide gel-filled capillary column (Fig. 1-II) [8], complete separation of BSA (M_r 66 200) from phosphorylase *b* (M_r 97 400) was not attained nor minor components in carbonic anhydrase and ovalbumin resolved by this commercially available SDS non-polyacrylamide gel-filled capillary column (Fig. 1-I).

Beckman uses a proprietary, non-polyacrylamide, hydrophilic, low-viscosity, linear polymer as the gel matrices to obtain size separations [11]. Use of a low-viscosity linear polymer as a sieving matrices has an advantage over a cross-linked polymer in that the low-viscosity polymer can be removed and the column rinsed and re-filled with the fresh polymer for each sample analysis. Thus, the problem of column instability due to accumulation of slow eluting impurities experienced by Tsuji [8] on a cross-linked polyacrylamide gel-filled capillary column has been effectively eliminated.

Precision of the protein peak migration time was determined by repeatedly injecting a rbSt solution at approximately 1 mg protein per ml. Relative standard deviation R.S.D. for the monomer peak migration time is approximately 0.3% (Table I).

Analysis of rbSt

Baseline resolution of peaks corresponding to the monomer, dimer, trimer, and tetramer of rbSt is typified by the SDS gel-filled capillary electrophoresis of a dimer-enriched sample (Fig. 2). When sensitivity of the detector near the minor, monomer peak region of a typical electropherogram of a rbSt sample (Fig. 3-I) was increased, the sample was shown to contain fragment, dimer, and trimer (Fig. 3-II). The dimer peak was further resolved into four peaks; the molecular masses of which differ by approximately 1000. Approximately M_r 1000 was determined to be the limit of the peak resolution capability of the SDS gel-filled capillary electrophoresis (Fig. 3-II) [8].

Performance of the SDS gel-filled capillary column was examined by use of a pre-production and a production lots of the capillary columns. As shown in Table II, performance of these two

TABLE I

PRECISION OF THE SDS GEL-FILLED CAPILLARY ELECTROPHORESIS FOR THE DETERMINATION OF MOLECULAR MASS OF MONOMER IN AN rbSt SAMPLE

Non-reduced rbSt sample was used.

Sample injected	Monomer	
	Peak migration (min)	M_r
1	12.88	21 870
2	12.82	21 300
3	12.82	21 300
4	12.79	21 000
5	12.77	20 800
6	12.75	20 700
7	12.77	20 800
8	12.76	20 700
Average	12.80	21 070
R.S.D. (%)	0.3	1.9

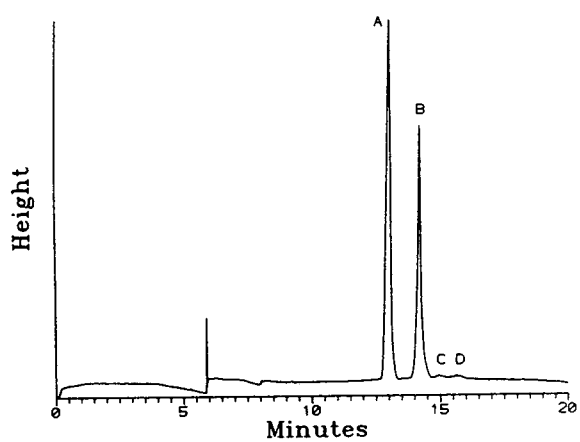

Fig. 2. SDS gel-filled capillary electropherogram of a dimer-enriched rbSt sample indicating a base-line resolution of monomer, dimer, trimer, and tetramer peaks. Conditions, −300 V/cm (24 μA); detector: 214 nm; column temperature: 20°C; migration distance: 40 cm; coated capillary: 100 μm I.D.; running buffer: SDS non-acrylamide, polymer gel solution. Peaks: A = monomer; B = dimer; C = trimer; D = tetramer.

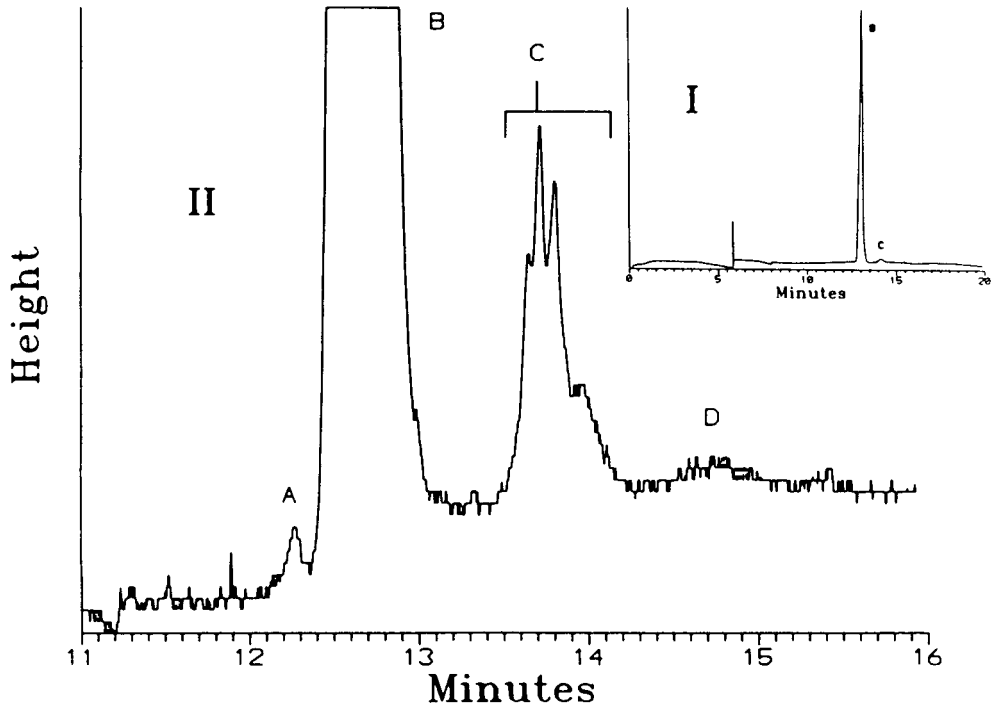

Fig. 3. (I) A typical SDS gel-filled capillary electropherogram of an rbSt sample as monitored at 214 nm. Peak identification, B = monomer; C = dimer. (II) Expanded electropherogram of the rbSt sample indicating resolution of the dimer peak into 4 sub-peaks differing by $M_r \approx 1000$. Peaks: A = fragment; B = monomer; C = dimer; D = trimer. Conditions, −300 V/cm (24 μA); column temperature: 20°C; peak migration distance: 40 cm; coated capillary: 100 μm I.D.; running buffer: SDS non-acrylamide, polymer gel solution.

columns were equivalent as indicated by similarities of the theoretical plate number (28 000 to 30 000 per 40 cm), the R.S.D. of the assay (R.S.D.: 14 to 19%), peak capacity factor (data not shown), and resolution ($R_s > 1$) between the monomer and the dimer peaks.

Molecular mass determination. Using a dimer-enriched sample against the molecular mass protein reference standard, the molecular mass of the components in rbSt (Fig. 3-II) were calculated. The molecular mass of the fragment, monomer, dimer, trimer, and oligomer were calculated to be approximately 15 000–16 000, 20 000–21 000, 46 000–47 000 and >62 000, respectively, with R.S.D.s of 2 to 3% for the monomer and the dimer determination. The observed masses determined by the HPSEC for the monomer, dimer and oligomer were 19 200, 43 500 and >68 000, and 20 400, 41 800 and >126 000 by the conventional SDS-PAGE technique, respectively. The theoretical, average mass of the rbSt is 21 812. The protein reference standard solution used to construct the calibration curve for the determination of the molecular mass was reduced and denatured but not the rbSt samples (refer to the following paragraph for the reason of not reducing the rbSt sample). Discrepancy of the observed molecular mass of the monomer from its theoretical value may be due to the non-reduced state of the rbSt molecule. Unless the protein is completely reduced to disrupt its secondary structure, the protein cannot unfold to full length and tend to run faster than expected resulting in lower observed molecular mass in an SDS-gel system [1]. For a precise measurement of the molecular mass of the protein, a separate technique, such as a capillary electrophoresis interfaced with an electrospray mass spectrometer [13], must be utilized.

When reduced and denatured, the majority of

TABLE II

THEORETICAL PLATE NUMBER OF THE SDS GEL-FILLED CAPILLARY ELECTROPHORESIS FOR THE DETERMINATION OF rbSt

Theoretical plate (N) of the monomer peak was calculated and expressed as N per the effective column length of 40 cm. About 60 nl of a rbSt sample solution at 1 mg protein per ml was injected onto the SDS gel-filled capillary column, 47 cm × 100 μm I.D. Migrating peaks were monitored at 214 nm; column temperature, 20°C; −300 V/cm.

Sample injection	Theoretical plates per 40 cm column	
	Pre-production column	Production column
1	23 100	29 700
2	22 900	37 100
3	22 900	26 600
4	25 000	33 000
5	31 100	26 500
6	34 900	33 000
7	31 100	24 000
8	34 800	29 500
Average	28 200	29 900
R.S.D. (%)	18	14

TABLE III

PRECISION OF THE SDS GEL-FILLED CAPILLARY ELECTROPHORESIS FOR THE DETERMINATION OF MONOMER AND DIMER CONTENTS IN AN rbSt SAMPLE

About 60 nl of a rbSt sample at 1 mg protein per ml was repeatedly injected onto the SDS gel-filled capillary column, 100 μm I.D. with an effective length of 40 cm. Migrating proteins were monitored at 214 nm; column temperature, 20°C; −300 V/cm.

Sample injected	Monomer		Dimer	
	Area	%	Area	%
1	3 276 000	96.1	134 100	3.9
2	3 375 000	96.3	129 900	3.7
3	3 315 000	96.4	123 700	3.6
4	3 286 000	96.0	135 800	4.0
5	3 197 000	96.2	125 100	3.8
6	3 202 000	96.4	119 900	3.6
7	3 237 000	96.3	124 900	3.7
Average	3 270 000	96.3	127 600	3.7
R.S.D. (%)	1.9	0.2	4.6	4.1

the dimer in the dimer enriched sample reverted to monomer indicating that the dimer is formed by an intra-molecular disulfide bonding during the protein re-folding processes. However, approximately 15–16% dimer remained after the treatment suggesting an existence of a dimer species with another bonding mechanism [14].

Peak area measurement. Precision for the determination of rbSt was examined by repeated injection, eight times, of a rbSt sample solution at the protein concentration of approximately 1 mg/ml. The R.S.D.s for measurement of the area under the monomer and the dimer peaks were approximately 2 and 5%, respectively (Table III). Since the sample was injected under a nitrogen pressure into the column filled with a highly viscous polymer solution, variability in quantitative injection may be an inherent nature of the SDS gel-filled capillary electrophoretic assay operation. Variability in the sample injection did not affect precision for the determination of components when expressed in the relative percentage, however.

When a sample with the protein concentration of over 2 mg/ml was analyzed, the gel-filled capillary column severely over-loaded resulting in a skewed peak shape with a significant loss of theoretical plate, 6300 from 29 000 per 40 cm. Theoretical plate number of the monomer peak nearly doubled, from 29 000 to *ca.* 60 000 per 40 cm, when a sample with the protein concentration of less than 0.5 mg/ml was analyzed. However, variability (R.S.D.) of the dimer peak area increased significantly.

Relative response factor. The calibration curve for the monomer peak area is linear ($r^2 = 0.998$) with the linear equation of $y = 6.26x + 1.01$. The calibration curve for the dimer was also linear ($r^2 = 0.999$) with the linear equation of $y = 7.07x - 1.03$. From the ratio of the slopes of the monomer and the dimer curves the relative response factor for the dimer peak was determined to be 1.1. The rbSt sample used contained too small quantities of fragment, trimer, and

tetramer to effectively obtain their relative response factor.

In order to calculate the relative response factors for the dimer, trimer, and tetramer, the dimer-enriched sample solution, ranging from 2 to 0.14 mg protein per ml was injected onto the column. From the regression analysis the relative response factors for the dimer, trimer, and tetramer were calculated as 1.0, 1.0, and 1.2, respectively. Differences in the relative response factor for the dimer between the two studies, 1.1 and 1.0, are within the assay error.

Sensitivity of the SDS gel-filled capillary electrophoresis for detection of the monomer and the dimer is approximately 5 fmol, respectively.

Recovery study. Various amounts of the dimer-enriched sample were added to the monomer-enriched sample creating the solution with the dimer contents ranging from 5 to 30%. These solutions were analyzed by the SDS gel-filled capillary electrophoresis. Calibration curves for recovery of the two components from the preparation were linear ($r^2 = 0.993$ and $r^2 = 0.994$) with the linear regression equations of $y = 1.01x + 0.334$ and $y = 0.998x + 0.209$ for the monomer and the dimer of rbSt, respectively. The slopes of these regression equations were not significantly different from one and the y-intercepts were not significantly different from zero.

Assay precision. Precision of the SDS gel-filled capillary electrophoresis for the determination of isoforms and fragments was examined using both a pre-production and a production lots of the coated capillary column and the non-acrylamide, polymer gel solution. Composition of monomer, dimer, trimer, and fragment contents in a rbSt sample determined by use of the production lot of the coated capillary column were 96, 4, <1, and <1%. R.S.D.s or the determination of monomer and the dimer were 0.1–0.2 and 4%, respectively (Table III). Performance of the pre-production lot of a coated capillary column was similar (data not shown).

SDS gel-filled capillary electrophoresis vs. HPSEC. Table IV presents data obtained by use of the SDS gel-filled capillary electrophoresis and the HPSEC methods for the analysis of rbSt. Percentage of isoforms and fragments in rbSt samples examined by the SDS gel-filled capillary electrophoresis correlated well with those of the HPSEC method. The values determined by the HPSEC were well within the inter-day variability of the SDS gel-filled capillary electrophoresis method.

TABLE IV

COMPARATIVE ANALYSIS OF rbSt SAMPLES BY THE SDS GEL-FILLED CAPILLARY ELECTROPHORESIS (HPCE) AND THE HIGH-PERFORMANCE SIZE-EXCLUSION CHROMATOGRAPHY (HPSEC)

rbSt			Composition (%)			
			Fragments	Monomer	Dimer	Trimer
Sample 1	HPCE	day 1	<1	94.6	4.1	1.1
		day 2	<1	95.8	3.7	<1
	HPSEC	day 1	<1	96	4.2	<1
		day 2	<1	95.6	4.0	<1
Sample 2	HPCE		<1	95.9	2.8	1
	HPSEC		<1	98	2.3	<1
Sample 3	HPCE	day 1	<1	96.7	2.1	1.2
		day 2	<1	97.5	2.1	<1
	HPSEC		<1	98	1.7	<1
Sample 4	HPCE		<1	97.0	2.1	<1
	HPSEC		<1	98	1.9	<1

Ruggedness

Ruggedness of the SDS gel-filled capillary electrophoresis system was evaluated during the course of the assay operation. In order to examine reliability of the coated capillary column, both a pre-production and a production lots of the columns were examined. Performance of both of these columns was equivalent in terms of the theoretical plate number and precision of the assay (refer to Table II). As shown in Fig. 4, peak migration time of the molecular mass protein standards remained relatively constant for approximately 140 sample injections. Stability of the peak migration time may be due to the use of new gel matrices for each assay operation. The peak area also remained relatively constant throughout the experiment.

Theoretical plate of the protein standards gradually decreased during the course of the sample analysis (data not shown). Decrease of the theoretical plate number may be caused by the protein slowly coating/accumulating on the surface of the column, even though the column was rinsed with 1 *M* HCl after each assay operation. The peak resolution remained adequate for the analysis of rbSt, however.

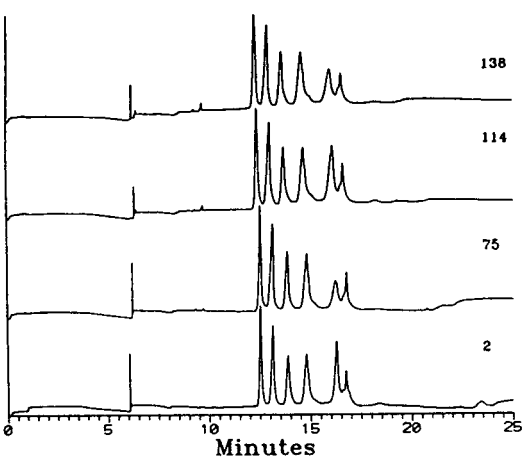

Fig. 4. Composite electropherograms of the molecular mass protein reference standard solution analyzed by the SDS gel-filled capillary electrophoresis indicating ruggedness of the coated capillary column. Number on each electropherogram indicates the number of samples injected on the column. Peak migration order: lysozyme, trypsin inhibitor, carbonic anhydrase, ovalbumin, BSA and phosphorylase *b*.

Because of accumulation of slow eluting compounds, the custom made SDS polyacrylamide gel-filled capillary column of Tsuji [8] requires periodic back-washing. During the column back-washing operation by reversal of the polarity, bubbles frequently formed in the capillary making the column useless. This limits the life of the custom made column life to 20–40 sample injections.

CONCLUSIONS

Peak resolution capability of the commercially available SDS non-polyacrylamide gel-filled capillary column is less than the custom-made SDS polyacrylamide gel-filled capillary column. Conventionally, linear range for the determination of the molecular mass may be extended by modifying the composition and the degree of cross-linking of the polyacrylamide gel matrix [1,8,11]. However, no such provision has yet to be made for the non-polyacrylamide gel-filled capillary column. Nevertheless, the SDS non-polyacrylamide gel-filled capillary column represents significant advantages over the custom-made SDS polyacrylamide gel-filled capillary column for convenience, adequate peak resolution of proteins with M_r values ranging from 10 000 to 50 000, and above all longevity of the column life.

Results obtained in this study indicated that the SDS gel-filled capillary electrophoresis may be a viable alternative to the HPSEC method for the analysis of recombinant proteins.

ACKNOWLEDGEMENTS

Technical assistance of G.A. Walker and Devon K. Andres, the latter a student intern, are greatly acknowledged. L.C. Eaton, and T.R. Urban are thanked for rbSt samples. R.L. Garlick is acknowledged for the dimer-enriched rbSt sample. J.A. Nolan of Beckman Instruments is thanked for providing a pre-production lot of the eCAP SDS 200 capillary electrophoresis kits.

REFERENCES

1 F.M. Ausubel, R. Brent, R.E. Kingston, D.D. Moore, J.G. Seidman, J.A. Smith and K. Struhl (Editors), *Current Protocols in Molecular Biology*, Wiley, New York, 1990, p. 10.0.5.
2 R.A. Wallingford and A.G. Ewing, *Adv. Chromatogr.*, 29 (1989) 1.
3 F.E.P. Mikkers, F.M. Everaerts and Th.P.E.M. Verheggen, *J. Chromatogr.*, 169 (1979) 11.
4 J.W. Jorgenson and K.D. Lukacs, *Science*, 222 (1983) 266.
5 B.L. Karger, A.S. Cohen and A. Guttman, *J. Chromatogr.*, 492 (1989) 585.
6 S. Hjertén, in H. Hirai (Editor), *Electrophoresis '83*, Walter de Gruyter, New York, 1984, p. 71.
7 A.S. Cohen and B.L. Karger, *J. Chromatogr.*, 397 (1987) 409.
8 K. Tsuji, *J. Chromatogr.*, 550 (1991) 823.
9 M. Zhu, D.L. Hansen, S. Burd and F. Gannon, *J. Chromatogr.*, 480 (1989) 311.
10 K. Ganzler, K.S. Greve, A.S. Cohen and B.L. Karger, *Anal. Chem.*, 64 (1992) 2665.
11 A. Guttman, J.A. Nolan and N. Cooke, *J. Chromatogr.*, 632 (1993) 171.
12 U.K. Laemmli, *Nature*, 227 (1970) 680.
13 K. Tsuji, L. Baczynskyj and G.E. Bronson, *Anal. Chem.*, 64 (1992) 1864.
14 B.N. Violand, M. Takano, D.F. Curran and L.A. Bentle, *J. Protein Chem.*, 8 (1989) 619.

Journal of Chromatography A, 652 (1993) 149–159
Elsevier Science Publishers B.V., Amsterdam

CHROM. 25 303

Characterization and performance of a neutral hydrophilic coating for the capillary electrophoretic separation of biopolymers

Dieter Schmalzing, Christine A. Piggee, Frantisek Foret[☆], Emanuel Carrilho[☆☆] and Barry L. Karger*

Northeastern University, Barnett Institute, Boston, MA 02115 (USA)

ABSTRACT

Polyvinylmethylsiloxanediol (50% vinyl) was synthesized and combined with a cross-linker for static coating onto fused-silica columns. After cross-linking and binding to the surface, linear polyacrylamide was grafted to the double bonds of the siloxanediol; subsequently, this linear polymer matrix was cross-linked with formaldehyde. The grafted neutral polymeric layer provided suppression of electroosmotic flow and minimized adsorption. This combination yielded successful open tube and polymer network separations of proteins, peptides and DNA molecules. Very high efficiencies (*ca.* $1 \cdot 10^6$ plates/m) were achieved for open tube protein separations, and hundreds of consecutive runs were performed with minimal change in migration times.

INTRODUCTION

Capillary zone electrophoresis (CZE) is rapidly developing as a powerful separation tool [1]. One of the major applications of CZE is the analysis of biopolymers such as peptides, proteins, DNA fragments and carbohydrates where CZE can provide ease of operation, speed and high separation efficiency [2]. Unfortunately, many macromolecules, and proteins in particular, tend to adsorb to the surface of the capillary tube due to coulombic and hydrophobic interactions [3]. Adsorption leads to significant zone broadening, non-reproducible migration times, and errors in quantitation.

Two different approaches to preventing the interaction between proteins and the fused-silica surface are currently being explored. In one approach, high [4,5] or low pH [3,6], high salt concentrations [7,8] and/or specific additives [9–13] have been applied to adjust the buffer composition. In a number of cases, the additives become an adsorbed coating to modify the fused-silica surface [14,15]. High or low pH of the background electrolyte can potentially cause sample degradation and limit the operational pH range for optimization of the separation. Furthermore, high salt concentrations might result in extra band broadening due to Joule heating. Using smaller inner diameters will minimize heating effects but may also introduce additional difficulties in injection and detection. Additives may interact with the sample, potentially distorting results when intermolecular interactions are important, *e.g.* affinity capillary electrophoresis [16], or may obliterate the sample signal in capillary electrophoresis–mass spectrometry (CE–MS). Furthermore, in this regard,

* Corresponding author.
☆ On leave from the Institute of Analytical Chemistry, Ververi 97, Brno, Czech Republic.
☆☆ On leave from the University of São Paulo, IFQSC/DQFM, 13560 São Carlos, São Paulo, Brazil.

0021-9673/93/$06.00

high salt concentrations can destabilize the electrospray.

A second strategy involves the chemical alteration of the fused-silica surface by a fixed coating [17–26]. In principle, this approach may be less limiting than the previous one in allowing the separation conditions to be adapted more freely to the needs of the analytical problem. We have taken this approach in this work and have set the following goals for a permanent coating: (1) ease of preparation; (2) high batch-to-batch reproducibility; (3) high efficiencies over a wide pH range of the buffer; (4) good pH stability and (5) negligible electroosmotic flow (EOF).

There are three reasons we have sought to minimize EOF. First, migration time reproducibility should in principle be high, since the lower the EOF, the less susceptible migration times will be to changes in bulk flow. Second, in all columns with EOF (coated and uncoated), there could be local differences in flow, creating electroosmotic mixing of the zones, and resulting in band broadening [27]. Finally, columns with negligible electroosmotic flow will have broad applicability in open tube and polymer network separations and potentially in IEF. One disadvantage of negligible flow will be the inability to separate positive and negative species in one run.

The basic strategy of the surface modification was to divide the coating into two polymeric layers (Fig. 1). The sublayer, a polymeric film, was present to provide a stable surface with high grafting capacity as a substitute for the fused-silica wall. The dense hydrophilic top layer was present to prevent adsorption and to minimize electroosmotic flow by means of its high viscosity. We have thus developed a coating composed of a vinyl siloxanediol as the sublayer where the OH groups were used for cross-linking and the vinyl groups for grafting the top layer of linear or cross-linked polyacrylamide. Moreover, the usual pretreatment of the fused-silica surface could be neglected, and coating and cross-linking of the sublayer could be performed in one single step at room temperature without further manipulation, *e.g.* thermal treatment. The second part of this work consisted of the extensive evaluation of the coating in terms of EOF,

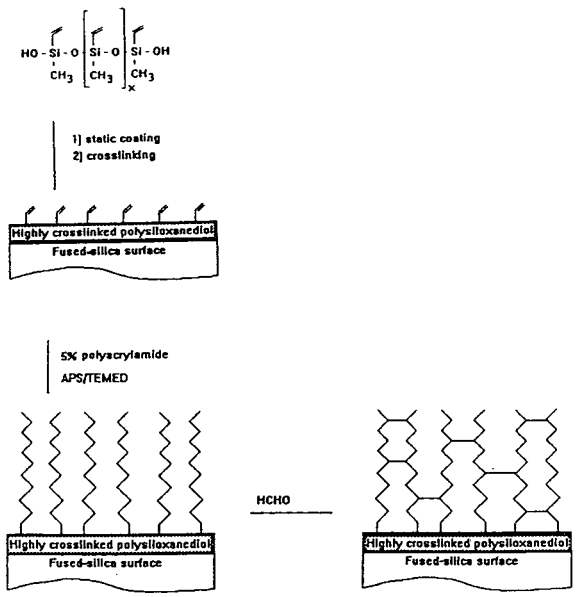

Fig. 1. Synthetic scheme for the neutral hydrophilic coating.

efficiency, long-term stability, and batch-to-batch reproducibility.

EXPERIMENTAL

Instrumentation and electrophoresis

A P/ACE 2100 capillary electrophoresis instrument controlled by System Gold software (Beckman, Fullerton, CA, USA) was used for protein and peptide separations. For the DNA separations and the electroosmotic flow measurements, the system consisted of a Spectra 100 spectrophotometer (Spectra Physics, San Jose, CA, USA) and a Series EH high-voltage power supply (Glassman High Voltage, Whitehouse Station, NJ, USA). Proteins and peptides were detected at 214 nm, whereas DNA and acetone, as the neutral electroosmotic flow marker, were detected at 260 nm. The proteins were dissolved in the separation buffer at a concentration of 0.1 mg/ml. Peptides were dissolved in water to a concentration of 0.013 mg/ml. Between runs the columns were rinsed by high pressure with the separation buffer for 2.5 min. Electoosmotic flow was measured at 270 V/cm and pH 8.8 (20 m*M* TAPS/AMPD; see *Reagents and materials* for

abbreviations). Buffer in the vials was changed after every 27 runs.

Reagents and materials

Anhydrous ether, glacial acetic acid (HAc), formaldehyde (37%, w/v solution in water), and spermine were all obtained from Aldrich (Milwaukee, WI, USA). N,N,N′,N′-tetramethylethylenediamine (TEMED), ammonium persulfate (APS) and electrophoresis-grade acrylamide were from ICN (Cleveland, OH, USA). Proteins, peptides, cetyldimethylethylammonium bromide, cacodylic acid, N-tris(hydroxymethyl)methyl-3-aminopropanesulfonic acid (TAPS), and N-tris(hydroxymethyl)methyl-2-aminoethanesulfonic acid (TES) were supplied by Sigma (St. Louis, MO, USA). The 123 base pair ladder was received from GIBCO BRL (Bethesda, MD, USA). 6-Aminocaproic acid (EACA) and 2-amino-2-methyl-1,3-propanediol (AMPD) were from Fluka (Ronkonkoma, NY, USA). Ultra-pure electrophoresis grade Tris-base was obtained from Schwarz/Mann Biotech (Cambridge, MA, USA). Fused-silica capillaries of 50 and 75 μm I.D. were purchased from Polymicro Technologies (Phoenix, AZ, USA).

Coating procedure

An amount of 50 mg of the polymethylvinylsiloxanediol, prepared according to ref. 28, and a silane cross-linker was dissolved in 4.6 ml anhydrous ether and filled into the untreated fused-silica column (70 cm × 75 μm). The column was closed at one end with a septum, and a vacuum was applied at the other end (static method). After complete evaporation of the solvent, the septum was removed, and cross-linking took place overnight. The calculated film thickness was 0.2 μm [29].

To form the top layer, a solution of 50 mg acrylamide in 1 ml water was degassed for 30 min by bubbling through helium. Aliquots of TEMED (10 μl) (10%, w/v in water) and APS (10 μl) (10%, w/v in water) were then added, and the mixture was immediately pushed by means of a syringe into the siloxanediol-coated column. After 12 h the polymerized but not grafted part of the acrylamide was pushed out of the column. For cross-linking the polyacrylamide (PAA), a coated column was filled with a 37% solution of formaldehyde which was adjusted to pH 10 with NaOH. After three hours, the column was rinsed with water and was then ready for use.

RESULTS AND DISCUSSION

Surface modification

The chemistry used for the highly cross-linked hydrophobic polymeric siloxane sublayer (Fig. 1) is well-established for sealants and adhesives and is known as the room temperature vulcanizing (RTV) method [30]. The inner wall of the separation capillary was coated with a mixture of a polysiloxanediol (containing 50% vinyl and 50% methyl groups) and silane cross-linker dissolved in anhydrous diethyl ether. Cross-linking and binding to the silica surface took place in one step at room temperature: the cross-linker reacted with the Si–OH groups of the siloxanediol and the silica surface via the formation of Si–O–Si bonds. No prior treatment (*e.g.* etching) of the capillary wall was necessary since the amount of OH groups already present on the silica surface was sufficient for the effective binding of the polymer to the capillary wall. Moreover, column etching did not result in improved column performance.

Since cross-linking of the siloxane was performed at room temperature instead of at the commonly used elevated temperature [31], a high concentration of the temperature-sensitive vinyl groups were available for the dense grafting on the final hydrophilic top layer. A dense and highly viscous top layer should strongly suppress the EOF [17] and minimize protein adsorption. It must be further noted that the cross-linking of the siloxanediol was also important for the mechanical strength of the sublayer. Coatings with a non-cross-linked siloxanediol sublayer were destroyed by the shear force created when the highly viscous non-grafted excess of polyacrylamide was removed after polymerization.

The top layer, covalently attached to the polysiloxane sublayer, consisted of polymethylol acrylamide which could, in principle, be prepared in one step by direct polymerization inside

the capillary. However, the final polymer tended to cross-link spontaneously [32], preventing its subsequent removal from the capillary. Thus, it was decided to form the cross-linked top layer in two steps. In the first, linear polyacrylamide was grafted to the polysiloxane layer, and in the second, polyacrylamide chains were converted into polymethylol acrylamide by reacting with formaldehyde at pH 10 [32]. In this way a dense, cross-linked, hydrophilic layer was formed. Bisacrylamide, which is usually added for the cross-linking of acrylamide, was not used in this approach because polymerization of the acrylamide took place throughout the entire column volume. Even small amounts of bisacrylamide ($< 0.2\%$) resulted in the formation of a rigid gel which could not be pushed out from the column, unless careful control of the conditions and time of polymerization were established.

Electroosmotic flow

As mentioned in the introduction, one of the goals in developing this coating was to minimize electroosmotic flow. Unfortunately at present there is no agreed method for assessing the extent of electroosmotic flow, making it difficult to compare the results of different coatings. Our recommended procedure is to use sensitive conditions of buffers with high pH (*ca.* 9) and low ionic strength (*ca.* 20 m*M*), since the contribution of the buffer to the suppression of the EOF is then minimized. At pH 8.8, essentially all of the Si–OH groups on the fused-silica surface are deprotonated, and the EOF of bare fused silica is maximized [34]. Low ionic strength buffers further enhance the electroosmotic flow by increasing the zeta potential [18].

Columns coated with only the polysiloxanediol sublayer showed almost the same strong electroosmotic flow as plain fused-silica columns (under basic pH conditions). However, because the polysiloxane film was thicker than the electric double layer on the capillary wall, it is assumed that the flow was not caused by the negatively charged Si–OH groups on the fused silica surface. Given a uniform coating, one possible explanation is the fact that an electric double layer is always formed at the solid/liquid interface. For example, even PTFE capillaries exhibit electroosmotic flow in spite of the fact that no functional groups are present on the PTFE surface for deprotonation [34]. A second possible explanation is that the siloxanediol layer possessed some negative charge.

After attachment of the top polymeric layer the EOF was substantially decreased. At pH 8.8 and 20 m*M* buffer, the EOF for the linear polyacrylamide coating was found to be 300 times less than that of a plain fused-silica column and the polymethylol acrylamide coating showed an initial 150-fold reduction in EOF (see Fig. 5). It is reasonable to conclude that during the separation time of an analysis, the small EOF played no significant role. The major decrease in EOF indicated the dense grafting of the top layer to the polymeric siloxanediol sublayer. The difference in EOF of a factor of two between the linear and cross-linked polyacrylamide top layers was possibly caused by the hydrolysis of a small percentage of the amide bonds during the formaldehyde treatment at pH 10.

Other important quantitative parameters for the characterization of a coating are: run-to-run migration time reproducibility, efficiency, and batch-to-batch reproducibility. To examine the stability of the coating in terms of migration time and band width reproducibility, we have used the following sensitive testing conditions: high electric field (*ca.* 500 V/cm), acidic and basic buffers (pH 4.4, 8.0 and 8.8) with low ionic strengths (20 m*M*).

Protein separations at acidic pH

Basic proteins are known for being sensitive probes of the quality of the capillary wall treatment due to their positive net charge and the typical negative charge on the walls. On uncoated columns or poorly shielded surfaces such proteins tend to interact strongly with the negatively charged fused-silica surface, leading to irreversible adsorption and poor reproducibility in migration times. On the present coated columns no indications for interactions with the capillary wall could be observed for the separation of a basic protein test mixture at pH 4.4. The absolute change in migration times after 600 consecutive injections (150 hours of continuous run time) was negligible, and the relative stan-

TABLE I

REPRODUCIBILITY OF MIGRATION TIMES FOR CONSECUTIVE RUNS OF BASIC PROTEINS AT pH 4.4

Conditions as in Fig. 2. t_m = Migration time.

Peak number	Protein	t_m	R.S.D. (%)
1	Lysozyme	5.94[a]	0.31
		5.91[b]	0.34
2	Cytochrome *c*	6.04	0.29
		6.01	0.31
3	Myoglobin	8.64	0.36
		8.62	0.39
4	Trypsinogen	9.09	0.39
		9.08	0.39
5	α-Chymotrypsinogen A	9.26	0.41
		9.23	0.40

[a] $n = 100$ (run No. 1–100).
[b] $n = 100$ (run No. 500–600).

dard deviations (R.S.D.s) of the migration times were still less than 0.5% after the 600 runs (Table I, Fig. 2).

High efficiencies were obtained ranging between $4 \cdot 10^5$ and $6 \cdot 10^5$ plates per meter (N/m) (Table II, Fig. 2). Moreover, no loss in efficiency was found during the 600 consecutive injections [Table II]. It must be added that the initial peaks widths were caused to a certain extent by the widths of the injection plugs, since this sample of standard proteins was dissolved in the running buffer. By dissolving the sample in deionized water and making use of focusing techniques by sample stacking [1], the efficiencies could be increased up to $2 \cdot 10^6$ plates per meter.

The batch-to-batch reproducibility of the coating was evaluated with three batches, each batch consisting of three columns coated in the same manner. The columns were evaluated using the basic protein test mixture (conditions as in Fig. 2). The R.S.D.s for the migration times of the basis proteins were less than 1%, and the R.S.D. values for the efficiencies were less than 14%, confirming excellent reproducibility of the coating.

Protein separations at basic pH

To examine next the long-term performance of

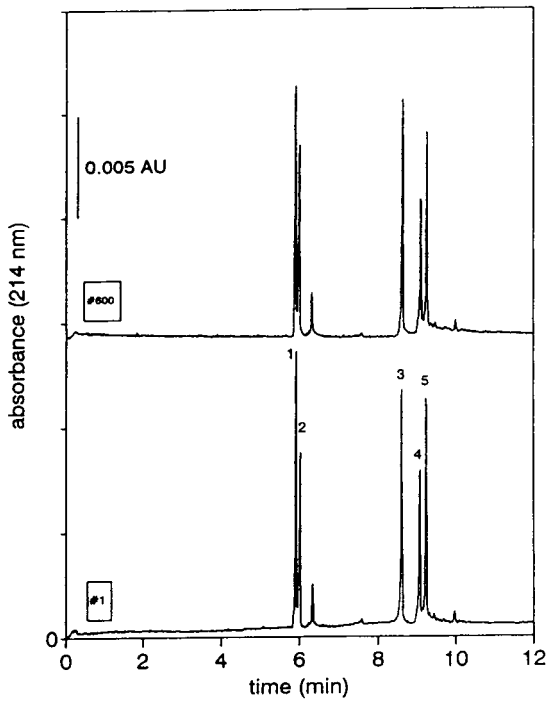

Fig. 2. Proteins as in Table I, 0.1 mg/ml in buffer; 8 s pressure injection; 20 m*M* EACA–HAc, pH 4.4; 214 nm; 526 V/cm, 17 μA, $l = 50$ cm (migration length), $L = 57$ cm (total length), 75 μm I.D.

the coating at basic pH, an acidic protein test mixture was run at pH 8.0. The R.S.D.s of migration times of the acidic proteins were again very low, less than 0.7% even after 600 consecutive runs (150 h of continuous run time) (Table III, Fig. 3). The efficiencies were as high as

TABLE II

COLUMN EFFICIENCIES FOR CONSECUTIVE RUNS OF BASIC PROTEINS AT pH 4.4

Conditions as in Fig. 2.

Peak number	Protein	N/m ($\cdot 10^3$)	
		Run No. 1	Run No. 600
1	Lysozyme	433	336
2	Cytochrome *c*	597	594
3	Myoglobin	515	575
4	Trypsinogen	472	605
5	α-Chymotrypsinogen A	592	735

TABLE III

REPRODUCIBILITY OF MIGRATION TIMES FOR CONSECUTIVE RUNS OF ACIDIC PROTEINS AT pH 8.0

Conditions as in Fig. 3.

Peak number	Protein	t_m	R.S.D. (%)
1	Glucose-6-phosphate dehydrogenase	5.53[a]	0.42
		5.45[b]	0.39
2	Trypsin inhibitor	6.47	0.48
		6.38	0.50
3	*l*-Asparaginase	10.05	0.42
		10.01	0.49
4	α-Lactalbumin	10.45	0.70
		10.41	0.69

[a] $n = 100$ (run No. 1–100).
[b] $n = 100$ (run No. 500–600).

$1 \cdot 10^6$ plates per meter at the beginning of the study, with only a 25% average decrease in efficiency found after the 600 runs (Table IV).

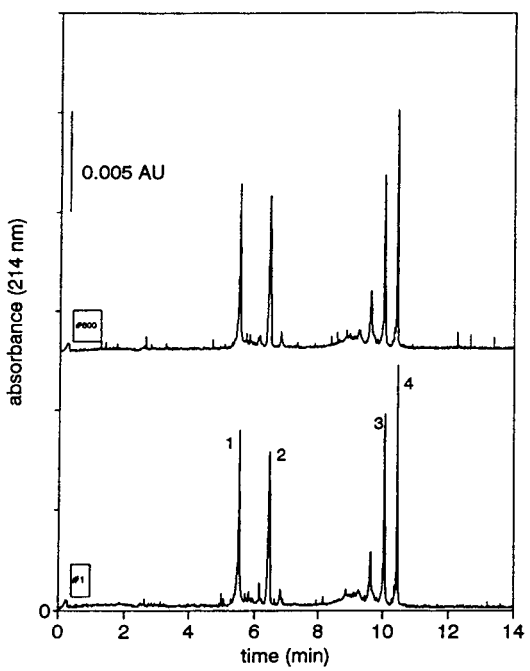

Fig. 3. Proteins as in Table III, 0.1 mg/ml in buffer; 8 s pressure injection; 20 m*M* TAPS–Tris, pH 8.0; 214 nm; 526 V/cm, 6 μA, $l = 50$ cm, $L = 57$ cm, 75 μm I.D.

TABLE IV

COLUMN EFFICIENCIES FOR CONSECUTIVE RUNS OF ACIDIC PROTEINS AT pH 8.0

Conditions as in Fig. 3.

Peak number	Protein	N/m ($\cdot 10^3$)	
		Run No. 1	Run No. 600
1	Glucose-6-phosphate dehydrogenase	295	240
2	Trypsin inhibitor	–[a]	–[a]
3	*l*-Asparaginase	820	610
4	α-Lactalbumin	975	694

[a] Not evaluated due to presence of double peak.

Nevertheless, the plate counts after the 600 runs was still greater than $6 \cdot 10^5$ plates per meter. The EOF was measured at pH 8.8 before and after the 150-h test period, and it was found that the EOF changed by 25% from an initial 160 times less than on a plain fused-silica column to 120 times less after the 600 runs.

From the results in Tables I–IV and measurements performed between pH 2 and 3 (results not shown) it can thus be concluded that the coating can be used for an extended period of time without significant loss in performance. The stability of the coating is probably the result of the cross-linked polymeric structure of the siloxanediol linker, which stabilizes the coating even if some damage to the sublayer occurs, and also to the formaldehyde cross-linking of the top layer, which decreases the rate of base hydrolysis of the amide bonds.

For the further investigation of the stability of the coating at basic pH, the coated column was studied with an acidic protein test mixture at pH 8.8. Even at this pH with 600 consecutive injections, the R.S.D.s of migration times for the first 100 runs were less than 0.7% and still less than 1.6% for the last 100 injections (runs No. 500–600) (Table V, Fig. 4). Furthermore, the absolute change in migration time over the 600 runs was less than 1%. Initially, efficiencies were as high as $1.1 \cdot 10^6$ plates per meter, but after 600

TABLE V

REPRODUCIBILITY OF MIGRATION TIMES FOR CONSECUTIVE RUNS OF ACIDIC PROTEINS AT pH 8.8

Conditions as in Fig. 4.

Peak number	Protein	t_m	R.S.D. (%)
1	Glucose-6-phosphate dehydrogenase	6.16[a]	0.39
		6.19[b]	0.48
2	Trypsin inhibitor	7.43	0.38
		7.47	0.57
3	β-Lactoglobulin B	8.30	0.43
		8.50	0.95
4	l-Asparaginase	10.87	0.44
		11.01	0.99
5	α-Lactalbumin	11.60	0.67
		11.73	1.55

[a] $n = 100$ (run No. 1–100).
[b] $n = 100$ (run No. 500–600).

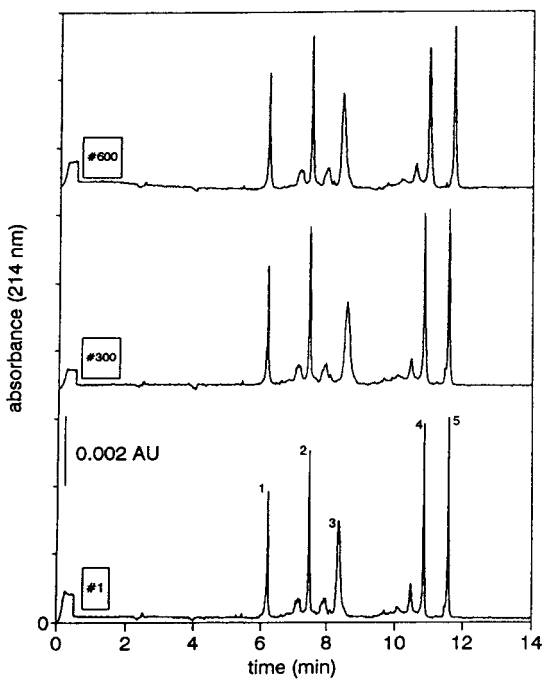

Fig. 4. Proteins as in Table V, 0.1 mg/ml in buffer; 8 s pressure injection; 20 m*M* TAPS–AMPD, pH 8.8; 214 nm; 526 V/cm, 14 μA, $l = 50$ cm, $L = 57$ cm, 75 μm I.D.

consecutive runs (150 h of continuous run time), and average loss in plate count of about 60% was observed (Table VI). However, as seen in Fig. 4, despite this decrease, the efficiencies were still sufficient for high resolution. (The low efficiency of β-lactoglobulin B (Fig. 4, Peak No. 3) was most likely due to the heterogeneity of this protein.) Furthermore, by changing the buffer after these 600 runs to pH 4.4, an average of $5 \cdot 10^5$ plates per meter could still be achieved for the basic protein test mixture.

Because of the decrease in efficiency found during the long term operation of pH 8.8, we decided to continuously monitor the EOF at this pH to see if changes in flow could be correlated with the observed loss in column performance. Both coatings, the linear and the crosslinked polyacrylamide, showed a slow increase in EOF over time, but the relative increase in the EOF for the polymethylol acrylamide coating was remarkably less than for the non-modified polyacrylamide coating (Fig. 5). After 156 h of continuous use at pH 8.8, the EOF of the polymethylol acrylamide coating was still about 100 times less than for a plain fused-silica column and remained constant at this value for another 160 h of continuous operation at pH 8.8. Moreover, as already discussed above, only a 25% change was observed for the polymethylol acrylamide coating at pH 8.0 during the 150-h testing period. The increase in EOF over time indicated

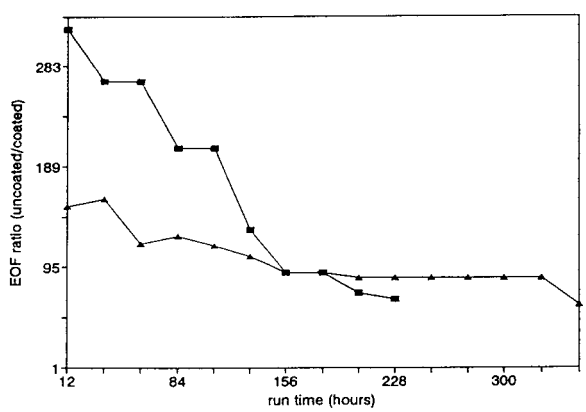

Fig. 5. EOF of (▲) cross-linked and (□) non-cross-linked polyacrylamide top layer with siloxanediol as sublayer. 20 m*M* TAPS–AMPD, pH 8.8; 7 μA, 268 V/cm; acetone used as EOF marker.

a gradual change on the capillary surface which might have been caused by the hydrolysis of amide bonds of the top layer and/or by the cleavage of Si–O–Si bonds of the siloxanediol sublayer [35]. The higher stability of the polymethylol acrylamide coating is probably the result of partial cross-linking along with the alkyl substitution of amide bonds slowing down the basic attack. The strong suppression of the EOF even after 150 h of continuous operation at pH 8.8 is in good agreement with the negligible changes in migration times observed. Furthermore, based on the results in Fig. 5, there would appear to be a relationship between the hydrolysis of the coating and the decrease in efficiency.

Coating stability and electric field

To test if the actual use of a column under high electric field operation had an influence on the stability of the coating, a coated column was stored without an applied electric field for 168 h filled with the pH 8.8 buffer. The comparison of the electropherograms run before and after this storage with the electropherograms of the column continuously run at pH 8.8 clearly demonstrated that the rate of deterioration depends on the operation of the electric field (Tables VI and VII). Indeed, little change in performance was observed for the column that was simply stored. A change in the pH of the buffer in the vials, caused by the redox processes occurring at the electrodes [33], can be excluded as an explanation for the effect of the electric field since all the electrolytes were well buffered and replaced after every 27 runs. One possibility is that the high electric field interacted with the permanent dipoles of the amide bonds, aligning the polyacrylamide fibers and thereby opening the three dimensional structure of the top layer for base attack. From the results of Table VI and VII it can be concluded that lifetime testing of a column should be on the basis of high electric field operation.

TABLE VI

COLUMN EFFICIENCIES FOR CONSECUTIVE RUNS OF ACIDIC PROTEINS AT pH 8.8

Conditions as in Fig. 4.

Peak number	Protein	N/m ($\cdot 10^3$)		
		Run No. 1	Run No. 2	Run No. 600
1	Glucose-6-phosphate dehydrogenase	544	469	266
2	Trypsin inhibitor	785	226	184
3	β-Lactoglobulin B	62	29	40
4	*l*-Asparaginase	1127	520	288
5	α-Lactalbumin	928	593	371

TABLE VII

INFLUENCE OF COLUMN STORAGE WITHOUT AN APPLIED ELECTRIC FIELD ON EFFICIENCY AT pH 8.8

Peak number	Protein	N/m ($\cdot 10^3$)	
		Before storage	After 168-h storage
1	Glucose-6-phosphate dehydrogenase	715	743
2	Trypsin inhibitor	642	613
3	β-Lactoglobulin B	98	92
4	*l*-Asparaginase	1112	980
5	α-Lactalbumin	1268	624

Protein separations at neutral pH

So far, only separations at acidic and basic pH have been discussed. However, since the selectivities of proteins in open tube CZE is governed mainly by charge differences, the coating should allow operation close to neutral pH. Moreover, this pH region is especially interesting since proteins often exist in native structures, and sample degradation is thus minimized in this region.

The test mixture of acidic proteins was separated over the pH range from 6 to 9 with high efficiencies in low ionic strength buffers (Fig. 6). For the basic protein test mixture, it was found

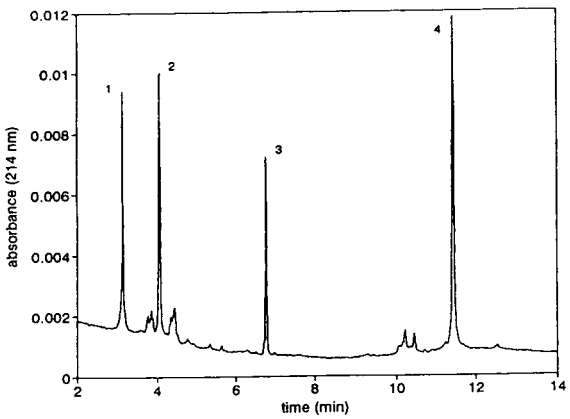

Fig. 6. (1) Glucose-6-phosphate dehydrogenase, (2) trypsin inhibitor (3), *l*-asparaginase, (4) α-lactalbumin, 0.1 mg/ml in water, 10 s pressure injection; 20 m*M* cacodylic acid + Bis-Tris, pH 6.2; 214 nm; 810 V/cm, 13 μA; $l = 37$ cm, $L = 30$ cm, 50 μm I.D.

that the addition of minute amounts of cationic additives to the low ionic strength background electrolyte were necessary for high separation efficiencies at pH 7. Fig. 7 depicts the separation of the basic proteins at this pH (10 m*M* phosphate–NaOH) in the presence of $2 \cdot 10^{-4}$ *M* spermine. It might be noted that not all of the peaks at pH 7 were totally symmetrical since the mobilities of several of the proteins were too low at this pH (*e.g. ca.* $4 \cdot 10^{-5}$ cm^2/Vs for the last peak) to match the mobilities of the buffer ions. Electropherograms similar to that in Fig. 7 were also obtained at pH 6.2 when $5 \cdot 10^{-5}$ *M* cetyldimethylethylammonium bromide was added to the running buffer (20 m*M* Tris–cacodylic acid) (results not shown). Since the conductivities of the background electrolytes were still low at neutral pH, very high electric fields could be applied (up to 1100 V/cm), keeping the separation times of the protein test mixtures to less than ten minutes. Moreover, the positively charged additives did not generate electroosmotic flow toward the anode as usually observed when such additives are used in uncoated columns [11,13].

Other applications

The coating has also been successfully used for open tube peptide and polymer network DNA separations. The peptides were separated in less than 80 s since very high fields (1100 V/cm) and a short column ($L = 27$ cm) could be utilized (Fig. 8). In the 123 bp DNA ladder polymer network separation very high resolution was achieved with efficiencies up to $1 \cdot 10^7$ plates per meter (peak No. 15) (Fig. 9). With replaceable linear polyacrylamide matrices, more than 500 DNA separations could be performed (pH 8.4)

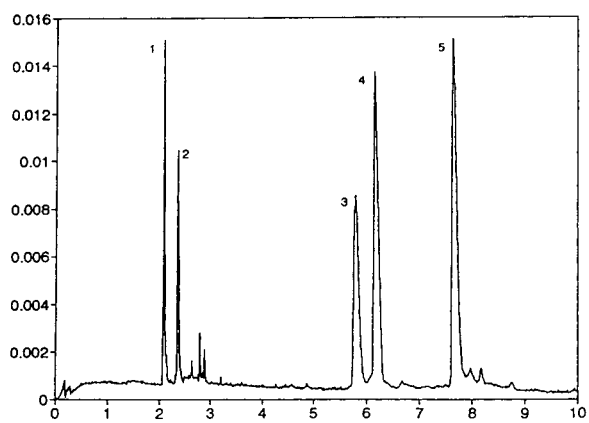

Fig. 7. (1) Lysozyme, (2) cytochrome *c*, (3) ribonuclease A, (4) α-chymotrypsinogen, (5) trypsinogen, 0.1 mg/ml in water; 8 s pressure injection; 10 m*M* H_3PO_4–NaOH, $2 \cdot 10^{-4}$ *M* spermine, pH 7.0; 214 nm; 1111 V/cm, 32 μA; $l = 20$ cm, $L = 27$ cm, 50 μm I.D.

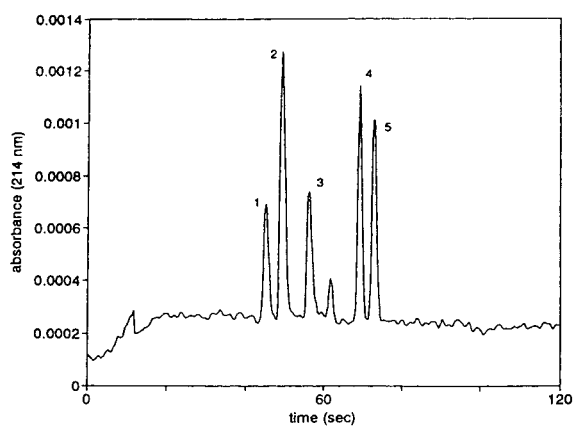

Fig. 8. (1) K-R-T-L-R-R, 0.05 mg/ml; (2) K-R-Q-H-P-G, 0.006 mg/ml; (3) R-P-K-P, 0.02 mg/ml; (4) R-P-K-P-Q-Q-F-F-G-L-M, 0.013 mg/ml; (5) R-P-K-P-Q-Q-F-F-G, 0.013 mg/ml all in water; 8 s pressure injection; 50 m*M* HAc, pH 3.0; 214 nm; 1111 V/cm, 8 μA; $l = 20$ cm, $L = 27$ cm, 50 μm I.D.

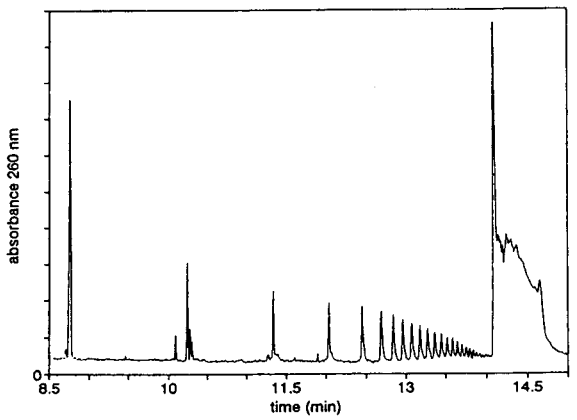

Fig. 9. 123 bp DNA ladder, 100 μg/ml in water; 2 s electrokinetic injection at 8 kV; 3%T PAA, 0.1 *M* Tris–boric acid, pH 8.4; 260 nm; 300 V/cm, 15 μA; $l = 30$ cm, $L = 40$ cm, 75 μm I.D.

with a single column before changes in migration times or efficiencies were noticeable.

CONCLUSIONS

A simple coating procedure has been developed with a high batch-to-batch reproducibility in which the EOF was greatly suppressed. Very high efficiencies were achieved for both acidic (pH 8–9) and basic proteins (pH 4.4) with low ionic strength buffers. Acidic proteins could be rapidly separated over the pH range from 6 to 9. For basic proteins, very small amounts of additives were necessary at or near neutral pH to achieve high performance. At both pH 8.0 and 4.4, hundreds of consecutive runs could be performed with excellent reproduciblities in migration times and efficiencies. The coating also showed high performance in peptide separations and for DNA mixtures using polymer network matrices. The recommended working range of the coating is between pH 2–9. Work is continuing on developing coatings that are stable for extended periods of time at extreme pH values.

ACKNOWLEDGEMENTS

The authors gratefully acknowledge NIH under GM 15847 for support of this work. The authors further thank Dr. Eva Szoko, Dr. Yvan Pariat and Roger Tim for their assistance on this project. E.C. thanks CNPq (Brazil) for a scholarship. C.A.P. acknowledges NSF for a Minority Graduate Fellowship. This is contribution No. 573 from the Barnett Institute.

REFERENCES

1 B.L. Karger and F. Foret, in N. Guzman (Editor), *Capillary Electrophoresis*, Marcel Dekker, New York, 1993, in press.
2 P.D. Grossman and J.C. Colburn (Editors), *Capillary Electrophoresis, Theory and Practice*, Part III, Academic Press, San Diego, 1992.
3 R.M. McCormick, *Anal. Chem.*, 60 (1988) 2322–2328.
4 H.H. Lauer and D. McManigill, *Anal. Chem.*, 58 (1986) 166–170.
5 Y. Walbroehl and J.W. Jorgenson, *J. Microcol. Sep.*, 1 (1989) 41–45.
6 H. Lindner, W. Helliger, A. Dirschlmayer, M. Jaquemar and B. Puschendorf, *Biochem. J.*, 283 (1992) 467–471.
7 M.M. Bushey and J.W. Jorgenson, *J. Chromatogr.*, 480 (1989) 301–310.
8 F.A. Chen, L. Kelly, R. Palmieri, R. Biehler and H. Schwartz, *J. Liq. Chromatogr.*, 15 (1992) 1143–1611.
9 M.J. Gordon, K.J. Lee, A.A. Arias and R.N. Zare, *Anal. Chem.*, 63 (1991) 69–72.
10 M. Zhu, R. Rodriguez, D. Hansen and T. Wehr, *J. Chromatogr.*, 516 (1990) 123–131.
11 A. Emmer, M. Jansson and J. Roeraade, *J. High Resolut. Chromatogr.*, 14 (1991) 738–740.
12 M.A. Strege and A.L. Lagu, *J. Chromatogr.*, 630 (1993) 337–344.
13 W.G.H.M. Muijselaar, C.H.M.M. de Bruijn and F.M. Everaerts, *J. Chromatogr.*, 605 (1992) 115–123.
14 J.E. Wiktorowicz and J.C. Colburn, *Electrophoresis*, 11 (1990) 769–773.
15 K. Tsuji and R.J. Little, *J. Chromatogr.*, 594 (1992) 317–324.
16 Y.-H. Chu, L.Z. Avila, H.A. Biebuyck and G.M. Whitesides, *J. Med. Chem.*, 35 (1992) 2915–2917.
17 S.J. Hjertén, *J. Chromatogr.*, 347 (1985) 191–198.
18 G.J.M. Bruin, J.P. Chang, R.H. Kuhlman, K. Zegers, J.C. Kraak and H. Poppe, *J. Chromatogr.*, 471 (1989) 429–436.
19 K.A. Cobb, V. Dolník and M. Novotny, *Anal. Chem.*, 62 (1990) 2478–2483.
20 W. Nashabeh and Z. El Rassi, *J. Chromatogr.*, 559 (1991) 367–383.
21 J.E. Sandoval and J.J. Pesek, *Anal. Chem.*, 63 (1991) 2634–2641.
22 J. Kohr and H. Engelhardt, *J. Microcol. Sep.*, 3 (1991) 491–495.
23 J.K. Towns and F.E. Regnier, *Anal. Chem.*, 63 (1991) 1126–1132.
24 M. Huang, W.P. Vorkink and M.L. Lee, *J. Microcol. Sep.*, 4 (1992) 233–238.

25 M. Gilges, H. Husmann, M.-H. Kleemiss, S.R. Motsch and G. Schomburg, *J. High Resolut. Chromatogr.*, 15 (1992) 452–457.
26 S.A. Swedberg, *Anal. Biochem.*, 185 (1990) 51–70.
27 L.-G. Oefverstedt, G. Johansson, G. Froeman and S. Hjertén, *Electrophoresis*, 2 (1981) 168–172.
28 J.F. Hyde, *US Pat.*, 2 490 357 (1949).
29 K. Grob, *Making and Manipulating Capillary Columns for Gas Chromatograph*, Hüthig, New York, 1986, pp. 159–160.
30 W. Noll, *Chemistry and Technology of Silicones*, Academic Pres, New York, 1968, Ch. 8.
31 K. Grob, *Making and Manipulating Capillary Columns for Gas Chromatography*, Hüthig, New York, 1986, Ch. 3.4.
32 R.H. Hunt and D.E. Nagy, *US Pat.*, 3 214 420 (1965).
33 M.A. Strege and A.L. Lagu, *J. Liq. Chromatogr.*, 16 (1) (1993) 51–60.
34 K.D. Lukacs and J.W. Jorgenson, *J. High Resolut. Chromatogr. Chromatogr. Commun.*, 8 (1985) 407–411.
35 M.G. Voronkov, *The Siloxane Bond*, Consultants Bureau, New York, 1978, pp. 146–163.

Journal of Chromatography A, 652 (1993) 161–170
Elsevier Science Publishers B.V., Amsterdam

CHROM. 25 251

High-efficiency capillary electrophoretic separation of basic proteins using coated capillaries and cationic buffer additives

Evaluation of protein–capillary wall interactions

A. Cifuentes, J.M. Santos, M. de Frutos and J.C. Diez-Masa*

Institute of Organic Chemistry (CSIC), Juan de la Cierva 3, 28006 Madrid (Spain)

ABSTRACT

The joint use of basic cationic additives (morpholine and several tetraazamacrocycles) in the buffer and chemically bonded cross-linked polyacrylamide-coated capillaries was evaluated as a method for decreasing the adsorption of basic proteins on the fused-silica capillary wall. The superiority of the tetraazamacrocycle Cyclen (1,4,7,10-tetraazacyclododecane) over morpholine and other tetraazamacrocycles is demonstrated. Using 20 m*M* phosphate–60 m*M* Cyclen buffer (pH 5.5) and cross-linked polyacrylamide-coated capillaries, separation efficiencies in the range of 10^6 plates/m were obtained for basic proteins. A simplified model that allows the quantification of the interactions between proteins and the capillary wall was developed. The model was assessed using the different buffers and capillaries evaluated in the first part. As the model predicts, a straight line for the plot of the inverse of the migration time *versus* the electric field strength with an intercept different from zero was observed. The value of the intercept correlates with the separation efficiency observed for the basic proteins studied and, therefore, with the interaction strength between proteins and the capillary wall.

INTRODUCTION

Theoretically, more than 10^6 plates/m could be obtained in the separation of proteins using Capillary Electrophoresis (CE). However, mainly owing to adsorption of proteins on the fused-silica surface of the capillaries used in CE, the efficiency values obtained in the separation of these biopolymers is lower than that predicted by theory [1,2]. The main cause of protein adsorption on the capillary wall is the electrostatic interaction between the protein's positively charged residues and the negatively charged silanol groups intrinsic to the silica surface. In the case of proteins, the cooperative effect [3,4] could play a major role in the adsorption and the mass transfer term of the proteins during separation processes. This effect is related to the flexibility of the polypeptidic chain of the proteins, and has the result that with adsorption of the protein molecule at one site of the surface, the adsorption of this molecule at a second point of the surface is made easier or more probable.

Different methods have been developed in CE to avoid interactions between proteins and the capillary surface. These procedures include manipulation of the buffer (use of extreme pH [5,6] or the use of cationic or zwitterionic additives in the buffer [2,7,8]) or manipulation of the silica surface (see ref. 9 for an up-to-date review) to shield the active sites on the capillary wall. Each method has its advantages and drawbacks, which are summarized in ref. 9. Some of the procedures involving cationic additives in the buffer [10] and some of those using hydrophilic polymeric coatings chemically bonded to the capillary wall [11,12] have allowed the achievement of

* Corresponding author.

0021-9673/93/$06.00

very high efficiencies (more than 10^6 plates/m) in protein separations.

We have demonstrated previously [13] that the joint use of cross-linked polyacrylamide-coated capillaries and buffers containing basic organic compounds (quaternary ammonium salts, linear amines, morpholine, etc.) is very efficient in decreasing the adsorption of proteins on the capillary surface. Separation of proteins using capillaries with a bonded polyacrylamide coating but without a cationic additive in the buffer gave rise to lower efficiencies than those achieved using coated capillaries with such compounds in the separation buffer. This result could be due to the fact that the polymeric layer does not cover the fused-silica surface completely or that it is not thick enough to mask the residual effect of the negatives charges on the surface [14]. We showed that the stronger the interaction between a cationic additive and surface charges, the higher are the efficiencies obtained for the separation of basic proteins. This result led us to speculate that other basic compounds able to interact more strongly with the negatively charged silanol groups of the surface could be better masking agents for the separation of basic proteins.

Tetraazamacrocycles are cyclic polyamines bearing four atoms of nitrogen in a rigid structure, several of which are completely ionized at the pH used in CE for the separation of basic proteins (pH 3–9). Their cyclic structure, where the nitrogen atoms are symmetrically distributed around the cavity whose size depends on the number of carbon atoms in the ring, may contribute more effectively to the masking effect of the silica negative charges by taking advantage of the preorganization principle observed in macrocyclic compounds [15]. The superior efficiency of these compounds as maskers of the silanophilic effect compared with other monoamine and linear polyamine compounds has been already demonstrated in HPLC [16].

The primary objective of this work was to study the effect of several tetraazamacrocyclic compounds as masking agents of the negative charges on the surface of silica capillaries used in CE.

On the other hand, it has been theoretically [1,17] and experimentally [2,5–8,12,13] demonstrated that the efficiency loss observed in the separation of proteins by CE is related to the interactions between proteins and the capillary wall. However, to the best of our knowledge, facile methods allowing the quantification of such interactions do not exist. The efficiency of the different procedures developed to reduce or preclude protein–capillary wall interactions has been evaluated so far in terms of the plate number per metre of column obtained for basic proteins separated in acidic buffers [2,5–9,13,14] or in terms of the recovery of such proteins [4].

Second, a simplified model was developed that allows the quantification of the interaction between proteins and the capillary wall. The model uses only the data obtained from the variation of the migration time of each protein with the electric field. It is easily implemented under any separation conditions (buffer and modified capillary), allowing the comparison of several methods developed to decrease the adsorption of the proteins on the capillary wall. The validity of the method was thereby established by comparing the data obtained from the model with the efficiency obtained for some basic proteins on cross-linked polyacrylamide-coated capillaries and separation buffers containing basic organic additives (morpholine or 1,4,7,10-tetraazacyclododecane) or those containing no additives.

EXPERIMENTAL

Instrumentation

Separations were carried out using a laboratory-made electrophoresis system. The apparatus included a Glassman (Whitehouse Station, NJ, USA) PS/EH50R2 power supply and a Linear Instruments (Reno, NV, USA) M-200 variable-wavelength UV–Vis detector operated at 230 nm with a laboratory-modified flow cell. The cooling of the capillaries at room temperature was achieved with a fan. Electropherograms were recorded and analysed using an A/D converter (Flytech, Taiwan), a laboratory-built amplifier, a Model 500 PC Acer computer (Multitech, Taiwan) and a PASCAL program developed in this laboratory. During electrophoresis, the current through the capillary was

measured using a Fluke (Everett, WA, USA) Model 83 multimeter. Fused-silica capillaries of 25 μm I.D. and 360 μm O.D., were obtained from Polymicro Technologies (Phoenix, AZ, USA). The total and the effective (from the injection point to the detector) lengths of each capillary used are given under Results and Discussion. The method utilized to prepare the cross-linked polyacrylamide-coated capillaries has been described previously [13]. Injection was carried out in the anode by electromigration.

All the experiments involving efficiency determination and reproducibility were accomplished in a P/ACE 2000 HPCE electrophoresis apparatus (Beckman, Fullerton, CA, USA) controlled by an IBM PS/2 286 computer. The fused-silica capillaries used in this apparatus were similar to those used in the laboratory-made apparatus, but with a 27 cm total length and 20 cm effective length. In this case, the external temperature of the capillaries was maintained at 22°C. Injection was carried out in the anode using nitrogen pressure (0.5 p.s.i.; 1 p.s.i. = 6894.76 Pa). Detection took place at 214 nm. Data were collected and analysed using System Gold software from Beckman running on the IBM PS/2 286 computer. In order to increase migration time reproducibility, the capillaries were successively rinsed for 30 s each with water, air and buffer between injections.

Samples and chemical

Lysozyme (chicken egg white) (Lys), cytochrome *c* (horse heart) (Cyt *c*), ribonuclease A (bovine pancreas) (Rib A) and α-chymotrypsinogen (bovine pancreas) (α-Chy) were purchased from Sigma (St. Louis, MO, USA) and used as received. The proteins were dissolved at the concentrations indicated (ranging from 0.2 to 1 mg ml^{-1}) in water purified using a Milli-Q system (Millipore, Bedford, MA, USA), stored at −5°C and warmed to room temperature before use. Phosphoric acid, sodium dihydrogenphosphate (both from Merck, Darmstadt, Germany), morpholine, 1,4,7,10-tetraazacyclododecane (Cyclen), 1,4,8,12-tetraazacyclopentadecane ([15]aneN_4) and 1,4,8,11-tetraazacyclotetradecane (Cyclam) (all from Aldrich, Steinheim, Germany) were used as received in the preparation of the different running buffers. Hydrochloric acid, sodium hydroxide (both from Merck), 3-methacryloxypropyl-3-trimethoxysilane (ABCR, Karlsruhe, Germany), acrylamide, N,N′-methylenebisacrylamide, ammonium peroxidisulphate, and N,N,N′N′-tetramethylenediamine (TEMED) (all from Schwarz, Cleveland, OH, USA) were used for the preparation of the cross-linked polyacrylamide-coated capillaries.

Buffers

A stock solution of 20 m*M* phosphate buffer (pH 5.5) was prepared by dissolving the weighed amount of sodium dihydrogenphosphate in Milli-Q-purified water and adding 1 *M* sodium hydroxide to adjust the pH to 5.5. Aliquots of this solution were used to prepare the buffers which contained the cationic additives. The additives (morpholine or one of the three tetraazamacrocycles tested) were dissolved in the phosphate buffer at the concentrations indicated. The pH of these solutions was returned to 5.5 using concentrated phosphoric acid. The buffers were stored at 4°C and heated to room temperature before use.

Electroosmotic flow measurements

The electroosmotic flow of uncoated and coated capillaries was measured using acetone dissolved in 20 m*M* phosphate buffer (pH 5.5). The same buffer was used as the separation buffer for these tests. The acetone sample was injected by electromigration (10 kV, 20 s). The test was run until acetone left the column or until 3 h had elapsed.

THEORY

In electrophoresis, the main driving force for a charged particle is the electric field. If a particle *p* having a net positive electric charge Q_p is introduced into an electric field whose voltage gradient or electric field strength is *E*, a constant electric force F_e is exerted on the particle. Simultaneously, as the wall of the fused-silica capillary is negatively charged, it behaves as an electric charge Q_c, generating an electric field inside the capillary. Let us assume that this

internal field is uniform along the capillary and, although much smaller than the external field, is not negligible and exerts a force F_i on the particle. The force F_i will have two components: the component F_{ix} directed along the capillary tube, and the component F_{iy} perpendicular to the capillary wall. The component F_{iy} could be considered as the component of F_i responsible for the adsorption of the particle on the capillary and F_{ix} as the component of F_i decreasing the migration velocity of the particle. If, as in the Hückel model [18], we suppose that the particle is very small but the double layer is thick enough to assume that the effect of viscous forces F_v is important, then

$$F_v = F_e - F_{ix} \quad (1)$$

The value of F_e is given by

$$F_e = Q_p E \quad (2)$$

and, according to the Stokes equation,

$$F_v = 6\pi\eta v_p a_p \quad (3)$$

where η is the buffer viscosity, v_p is the particle velocity and a_p its radius.

Combining eqns. 1, 2 and 3, we obtain

$$6\pi\eta v_p a_p = Q_p E - F_{ix} \quad (4)$$

The component x of the force between the capillary wall and the particle is given by

$$F_{ix} = \frac{Q_p Q_c}{\varepsilon x^2} \quad (5)$$

where ε is the dielectric constant of the buffer and x is the average distance between the surface and the particle.

By substituting eqn. 5 in eqn. 4, we obtain

$$v_p = \frac{1}{6\pi\eta a_p}\left(Q_p E - \frac{Q_p Q_c}{\varepsilon x^2}\right) \quad (6)$$

As the movement of the particle in the capillary is uniform, time t needed to move it a distance l from the injection to the detection point is given by

$$\frac{1}{t} = \frac{\mu_p}{l} \cdot E - \frac{\mu_p Q_c}{l\varepsilon x^2} \quad (7)$$

where μ_p is the electrophoretic mobility of the particle.

It can be deduced from eqn. 7 that a plot of $1/t$ against E should give a straight line whose slope depends on the electrophoretic mobility of the particle. Its intercept is also a function of both the electrophoretic mobility of the particle and the electric charge of the capillary surface. The intercept of the plot gives, therefore, a value related to the electric charge of the wall for a given particle and separation conditions. Only in those cases where the surface capillary behaves as if it were not charged ($Q_c = 0$) could the migration time be given by the classical equation

$$1/t = \mu_p E/l \quad (8)$$

For proteins, which are large non-spherical particles, moving in an electrophoretic buffer these equations must be corrected considering the effective charge and radius of the protein as a function of the buffer composition, which does not substantially modify eqn. 7. In this model, the electroosmotic flow was considered to be zero. In fact, using the cross-linked polyacrylamide coating described in this paper, the electroosmotic flow in the capillaries, if any, is at least two orders of magnitude smaller than that obtained with uncoated capillaries, as will be shown under Results and Discussion.

RESULTS AND DISCUSSION

Masking effect of tetraazamacrocycles on the silica surface negative charges

Tetraazamacrocycles are extremely basic compounds, able to interact with both inorganic and organic anions [19]. The tetraazamacrocycles evaluated in this work (Table I) can bear positive charges at the pH 5.5 used. As demonstrated [19,20] for azamacrocycles larger than those used in this work, the stability of the complex formed between these compounds and several types of anions (inorganic and organic) is related to the macrocycle charge, the size of its cavity compared with the anion size, the conformational characteristics of the anion and the hydrophobicity of the anion. It is possible that the capacity of the small-sized tetraazamacrocy-

TABLE I

PROTONATION CONSTANTS OF THE TETRAAZAMACROCYCLES USED

Compound	Formula	pK	Temperature (°C)	Conditions	Ref.
1,4,7,10-Tetraazacyclododecane (Cyclen)	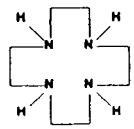	(1) 10.5 (2) 9.4 (3) ~1.6 (4) ~0.8	35	H_2O, 0.2 M $NaClO_4$	26
1,4,8,11-Tetraazacyclotetradecane (Cyclam)	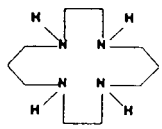	(1) 11.2 (2) 10.3 (3) ~1.5 (4) ~0.8	35	H_2O, 0.2 M $NaClO_4$	26
1,4,8,12-Tetraazacyclopentadecane ([15]aneN$_4$)	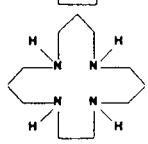	(1) 11.1 (2) 10.4 (3) 5.3 (4) 3.6	25	H_2O, 0.5 M KNO_3	27

cles used in our work to mask the negative charges on the silica surface is also related to the structural characteristics of the macrocyclic compound, such as size cavity.

To explore the role of the macrocycle size in the masking capacity for silica-surface negative charges, three tetraazamacrocycles (Cyclam, Cyclen and [15]aneN$_4$) were compared in terms of the plate number obtained for several basic proteins (Lys, Cyt c, Rib A, α-Chym) separated on uncoated silica capillaries using phosphate buffer (pH 5.5). Under these very demanding separation conditions, the proteins had a net positive charge, being able to adsorb on the ionized silanol groups on the silica. The relative influence of the three tetraazamacrocycles was clearly shown. When an unused capillary was employed for the separation of the basic proteins with 20 mM phosphate buffer (not containing any tetraazamacrocycle), the proteins were not recovered from the column. This fact helped to deduce the strong interactions between proteins and silica surface. In contrast, when 50 mM [15]aneN$_4$ was added to the 20 mM phosphate buffer (pH 5.5), the four proteins migrated out of an unused capillary, but the efficiency obtained for their peaks was very poor. Better efficiency was obtained for the proteins on unused capillaries with 20 mM phosphate buffer containing 50 mM Cyclam (pH 5.5) (Lys $1 \cdot 10^5$, Cyt c $1 \cdot 10^5$, Rib A $2.5 \cdot 10^5$ and α-Chym $2.5 \cdot 10^5$ plates/m). Finally, the best efficiency on unused, uncoated capillaries was achieved when a 20 mM phosphate buffer containing 60 mM Cyclen (pH 5.5) was used (Lys $2.5 \cdot 10^5$, Cyt c $1.3 \cdot 10^5$, Rib A $4.5 \cdot 10^5$ and α-Chym $3.6 \cdot 10^5$ plates/m). This result clearly demonstrates that Cyclen has a higher masking effect than the two other tetraazamacrocycles tested. As deduced from Table I, under our separation conditions [15]aneN$_4$ could have at least two protonated amino groups whereas Cyclam and Cyclen could have only two. The fact that the shielding effect increases in the order [15]aneN$_4$ < Cyclam < Cyclen, which is the same order as the decreasing cavity radius, shows the important role of the macrocycles size on their masking effect.

Morpholine has been used in protein separations by HPLC as a masking agent to avoid the detrimental effect of silanol groups [21]. Using this idea, we demonstrated in a previous study [13] that the use of cross-linked polyacrylamide-coated capillaries and buffers containing morpholine systematically led to better separation efficiencies for basic proteins than in those cases where the same buffer was used with uncoated fused-silica capillaries. It was therefore considered of interest to study the effect of buffers

containing tetraazamacrocycles on the separation of basic proteins with cross-linked polyacrylamide-coated capillaries. The separation of several basic proteins using coated capillaries and a 20 m*M* phosphate–60 m*M* Cyclen buffer (pH 5.5) is shown in Fig. 1. The efficiencies obtained for the protein peaks were in the range of a 10^6 plates/meter (Lys $1 \cdot 10^6$, Cyt *c* $1.1 \cdot 10^6$, Rib A $0.8 \cdot 10^6$ and α-Chym $0.8 \cdot 10^6$ plates/m). Under the same separation conditions, but using a 20 m*M* phosphate–0.25 *M* morpholine buffer (pH 5.5), efficiencies around 2–3 times smaller were observed. Good reproducibility in terms of efficiency [relative standard deviation (R.S.D.) = 3% ($n = 4$)] and migration time [R.S.D. = 0.5% ($n = 4$)] were obtained with Cyclen-containing buffers. These results demonstrate that the joint use of Cyclen and cross-linked polyacrylamide-coated capillaries is a very effective method of decreasing protein–capillary wall interactions.

As speculated previously [13], the residual adsorption effect observed for the polyacrylamide-coated capillaries could be due to the lack of a homogeneous capillary coating which could leave some areas of the fused silica uncoated, and/or to the fact that the polyacrylamide layer, which although covering homogeneously all the silica surface, could be thin enough to let the electric charges on the silica surface adsorb the proteins on top of the polymeric layer.

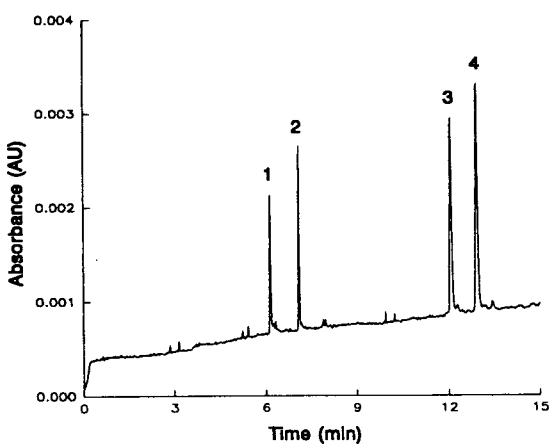

Fig. 1. Separation of basic proteins. Capillary, cross-linked polyacrylamide coated, 25 μm I.D., 360 μm O.D., 27 cm total length, 20 cm effective length; buffer, 20 m*M* phosphate–60 m*M* Cyclen (pH 5.5); temperature, 22°C; voltage, 12 kV (24 μA); injection, 2 s at 0.5 p.s.i. (nitrogen); detection, 214 nm. Peaks: 1 = 0.27 mg ml^{-1} lysozyme; 2 = 0.27 mg ml^{-1} cytochrome *c*; 3 = 0.35 mg ml^{-1} ribonuclease A; 4 = 0.81 mg ml^{-1} α-chymotrypsinogen.

In order to compare the efficiency achieved for basic proteins using polyacrylamide-coated capillaries and Cyclen-containing buffers with those predicted by theory, we used the Jorgenson's model [22], which considers that longitudinal diffusion dominates dispersion ($N = \mu VL/2Dl$). It is not easy to obtain reliable values for the diffusion coefficient (D) of the proteins in the buffers used in our experiments. However, accepting that for globular proteins the Stokes–Einstein equation [23] gives a reasonable estimation of D, one can calculate that D values could be around $1 \cdot 10^{-6}$ cm^2 s^{-1} for Lys, Cyt *c*, and Rib A (molecular mass *ca.* 15 000) and around $0.7 \cdot 10^{-6}$ cm^2 s^{-1} for α-Chym (molecular mass 25 000). Using these values and the electrophoretic mobilities deduced from Fig. 1, an estimation gives that a maximum efficiency of $2 \cdot 10^6$–$2.5 \cdot 10^6$ plates/m should be obtained for such proteins. Several causes of band broadening in CE have been described [1], including solute adsorption, Joule heat effect, electroendosmosis and extra-column (injection and detection) effects. The decrease in efficiency observed under our experimental conditions could be due to some residual adsorption of the basic proteins on the uncovered silica surface or on the polyacrylamide coating. Further, under our experimental conditions, for which no attempt had been carried out to optimize injection, this could also be a major cause of the difference in efficiency noted between theory and our results [24]. We have observed (results not shown) that the amount of protein injected (decreased by changing both the injection time and sample concentration) can dramatically increase (by more than 100%) the efficiency obtained for proteins. We are currently working on this issue.

In order to gain some practical knowledge about the effect of the concentration of basic additives on the separation efficiency and to compare Cyclen and morpholine as masking agents in CE, we compared the efficiencies obtained for several basic proteins with different

concentrations of these additives. The results are shown in Fig. 2. In general, an increase in the concentration of the additive (Cyclen or morpholine) in the buffer led to an increase in the efficiency achieved for the basic proteins. As a general rule, better efficiencies are obtained for the same proteins separated using Cyclen-containing buffers than for those containing morpholine. It should also be noted that the optimum masking effect of Cyclen is achieved at concentrations one order of magnitude lower than that of morpholine; this result again indicates the high efficiency of Cyclen as a negative charge masker. For a more extensive comparison

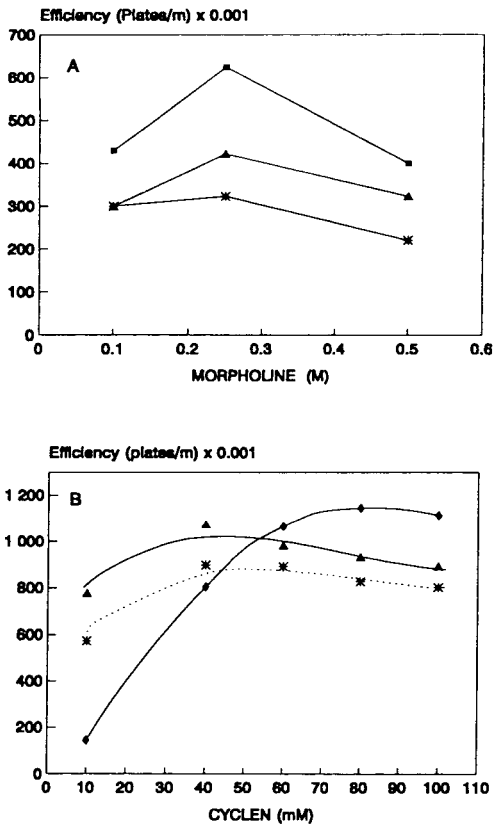

Fig. 2. Effect of (A) morpholine and (B) Cyclen concentration on the separation efficiency of several basic proteins. Buffers: (A) 20 m*M* phosphate–morpholine (pH 5.5); (B) 20 m*M* phosphate–Cyclen (pH 5.5). Voltage: (A) 14 kV; (B) 12 kV. Sample: □ = 0.27 mg ml^{-1} cytochrome *c*, ▲ = 0.35 mg ml^{-1} ribonuclease A; * = 0.81 mg ml^{-1} α-chymotrypsinogen; ◆ = 0.27 mg ml^{-1} lysozyme. Other separation conditions as in Fig 1.

between morpholine and Cyclen, it should be considered that the curve's general trend and efficiency values for lysozyme are similar to those obtained for cytochrome *c*. As indicated at Fig. 2, the efficiencies obtained for the proteins studied at a morpholine concentration higher than 0.25 *M* decrease slightly. This result could be due to the high electric conductivity of the buffer containing 0.5 *M* morpholine. Because of the large amount of morpholine in the buffer, a very large amount of phosphoric acid had to be added to the solution to return the pH to 5.5. As a result of the buffer's high conductivity, more than 3.5 W m^{-1} of power were generated in these conditions. A previous test (results not shown) with the thermostatic system used in this experiment demonstrated that it was posible to eliminate up to 2 W m^{-1} of dissipated power (for good power dissipation, the plot of voltage *versus* current values fit a straight line with a regression coefficient >0.999). This could explain why a better efficiency was obtained with buffer containing 0.25 *M* than with that containing 0.5 *M* morpholine. On the other hand, the maximum efficiency using Cyclen-containing buffers was obtained with a power dissipation of only 0.8 W m^{-1}. This is another advantage of this tetraazamacrocycle as an additive, which could be used in air-cooled electrophoretic systems where only powers as low as 1 W m^{-1} could be dissipated [25] without excessive rise of the buffer temperature and the subsequent risk of protein denaturation.

Experimental assessment of the model

The experimental results presented above form an array of separation conditions showing different efficiencies (plate number) for basic proteins depending on the additive used and its concentration in the separation buffer. Because all the data were obtained under the same experimental conditions, they show the correlation between efficiency and wall interaction for proteins. They were therefore used for a preliminary evaluation of the migration model presented in the Theory section. Two major conclusions can be drawn from this model. First, the representation of the inverse of the migration time (t) for a given protein against the field

strength (E) should give a straight line with an intercept different from zero (unless $Q_c = 0$). Second, the absolute value of the intercept for each protein is related to the electrostatic interaction between the protein and the capillary wall; this value is also related to the net charge of the protein and consequently to its electrophoretic mobility under the separation conditions.

Because the model was developed assuming that no electroosmotic flow existed in the cross-linked polyacrylamide coated capillaries, we verified that the electroosmotic flow in each column used, if any, was very small. The electroosmotic flow of each capillary used in the experiments described below was measured beforehand. For the polyacrylamide-coated columns used, we observed that the electroosmotic flow coefficient (μ_{eo}) was smaller than $4 \cdot 10^{-6}$ cm^2 V^{-1} s^{-1}, that is, roughly two orders of magnitude smaller than the μ_{eo} value observed for an uncoated column tested under the same experimental conditions.

All the experiments to evaluate the model were carried out using the laboratory-made electrophoresis apparatus where the capillary was cooled using a forced-flow air system. To prevent the effect of temperature increase inside the capillary on protein migration time, special care was taken to work only under conditions (field applied and electric current) for which the power dissipated during separation was easily eliminated by the cooling system (<1 W m^{-1}).

The plot of $1/t$ for different E values using buffers containing morpholine or Cyclen for several proteins is shown in Fig. 3. As the model predicts, (eqn. 7), straight lines were obtained. The intercepts, slopes and linear regression coefficients for these straight lines are given in Table II. For a given separation buffer, the absolute values of the intercepts (A values) decrease in the order Lys > Rib A > α-Chym, that is, in the order of decreasing electrophoretic mobility. For the 60 mM Cyclen buffer, the A values for the three proteins studied are very small, and, surprisingly, they increase slightly from Lys to α-Chym (decreasing order of net charge). This can be explained in terms of a loss of statistical significance of such results if A values are compared with their standard deviations (S.D.). This is related to the almost total elimination of the protein adsorption based on the high efficiency values (in the range of 10^6 plates/m) obtained for the basic proteins separated under these conditions (Figs. 1 and 2). Also, a decrease in the A values occurs for a given protein as the masking capacity of the additives increases. This effect is clearly seen when A values for no additive buffer are compared with those obtained with an additive. The same effect is observed for lysozyme on comparing the A value in 0.25 M morpholine buffer with that obtained in 60 mM Cyclen buffer. For other proteins (Rib A and α-Chym), this last

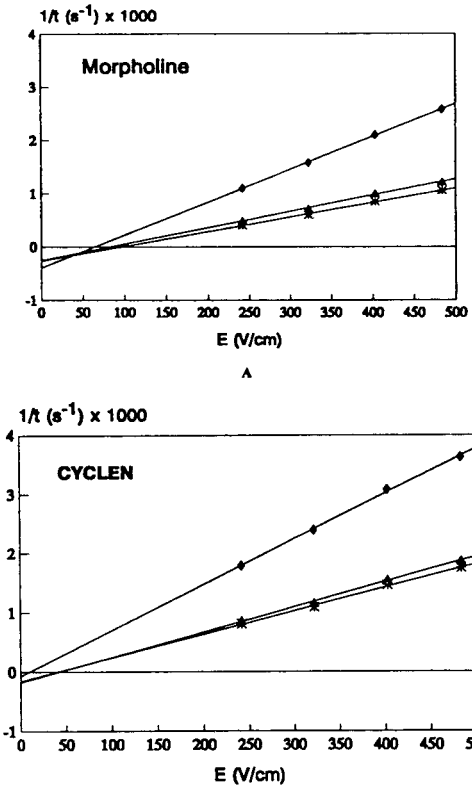

Fig. 3. Variation of $1/t$ with the field strength (E) under different conditions. Capillary, cross-linked polyacrylamide coated, 25 μm I.D., 360 μm O.D., 30 cm total length, 15 cm effective length; buffer, (A) 20 mM phosphate–0.25 M morpholine (pH 5.5) and (B) 20 mM phosphate–60 mM Cyclen (pH 5.5); room temperature; injection, electromigration, (A) 2 kV, 8 s and (B) 3 kV, 5 s; detection, 230 nm. Proteins: ◆ = lysozyme; ▲ = ribonuclease A; * = α-chymotrypsinogen.

TABLE II

EFFECT OF DIFFERENT BUFFER ADDITIVES ON PROTEIN–CAPILLARY WALL INTERACTIONS

Capillary, cross-linked polyacrylamide coated, 25 μm I.D., 360 μm O.D., 30 cm total length, 15 cm effective length; buffer, no additive = 20 m*M* phosphate (pH 5.5); 0.25 *M* morpholine = 20 m*M* phosphate–0.25 *M* morpholine (pH 5.5); 60 m*M* Cyclen = 20 m*M* phosphate–60 m*M* Cyclen (pH 5.5); detection, 230 nm. $A \times 10^3$ = intercept of $1/t$ *versus* E (s^{-1}). $B \times 10^3$ = slope of $1/t$ *versus* E ($cm\ V^{-1}\ s^{-1}$). r = Linear correlation coefficient of $1/t$ *versus* E. Values in parentheses are standard deviations of A and B values.

Additive	Lysozyme			Ribonuclease A			α-Chymotrypsinogen		
	A	*B*	*r*	*A*	*B*	*r*	*A*	*B*	*r*
No additive	−20.7 (6.6)	131 (1.3)	0.999	−9.7 (4.0)	79 (1.3)	0.999	−7.6 (3.5)	69 (1.4)	0.999
0.25 *M* Morpholine	−2.8 (0.6)	56 (0.7)	0.999	−0.7 (0.2)	27 (0.6)	0.999	−0.6 (0.1)	23 (0.2)	0.999
60 m*M* Cyclen	−0.4 (1.6)	76 (1.4)	0.999	−0.6 (0.4)	40 (0.7)	0.999	−0.7 (0.4)	37 (0.8)	0.999

comparison is blurred by the S.D. values obtained. Finally, the slope of the straight line of $1/t$ *vs.* E (B values) for a given buffer decreases with decreasing electrophoretic mobility of the proteins.

Other experimental data that could be explained using the model are those relating the morpholine to Cyclen concentrations in the buffer and their masking capacity. The values for the intercept and the slope for various proteins for different morpholine and Cyclen concentrations in the buffers are given in Tables III and IV, respectively. Using any of the buffer additives evaluated in this work, the intercept of the line decreases as the additive concentration in the buffer increases. As demonstrated above, an increase in morpholine or Cyclen concentration in the buffer, up to some value, led to a decrease in the interaction between basic proteins and the capillary wall. It should be noted that in the separation used in this experiment to obtain the plot of $1/t$ *vs.* E for buffer containing 0.5 *M* morpholine, the power dissipated was 2.9 W m^{-1}. The fact that this thermal effect considerably modifies the separation efficiency of the proteins (Fig. 2) but does not significantly modify the general trend of the A values could indicate that our model would be of some utility

TABLE III

EFFECT OF MORPHOLINE CONCENTRATION ON PROTEIN–CAPILLARY WALL INTERACTIONS

Capillary, cross-linked polyacrylamide coated, 25 μm I.D., 360 μm O.D., 50 cm total length, 25 cm effective length; buffer, 20 m*M* phosphate–0.1–0.5 *M* morpholine as indicated (pH 5.5); detection, 230 nm.

Parameter[a]	Cytochrome *c*			Ribonuclease A			α-Chymotrypsinogen		
	0.1 *M*	0.25 *M*	0.5 *M*	0.1 *M*	0.25 *M*	0.5 *M*	0.1 *M*	0.25 *M*	0.5 *M*
A	−6.6	−2.6	−1.9	−2.7	−2.1	−1.8	−1.8	−1.7	−0.3
B	8.4	5.4	3.3	5.1	3.4	2.2	4.4	3.0	1.4

[a] $A \times 10^4$ = intercept of $1/t$ *versus* E (s^{-1}). $B \times 10^6$ = slope of $1/t$ *versus* E ($cm\ V^{-1}\ s^{-1}$).

TABLE IV

EFFECT OF CYCLEN CONCENTRATION ON PROTEIN–CAPILLARY WALL INTERACTIONS

Capillary, cross-linked polyacrylamide coated, 25 μm I.D., 360 μm O.D., 31 cm total length, 15 cm effective length; buffer, 20 m*M* phosphate–10–60 m*M* Cyclen as indicated (pH 5.5); detection, 230 nm.

Parameter[a]	Lysozyme			Ribonuclease A			α-Chymotrypsinogen		
	10 m*M*	30 m*M*	60 m*M*	10 m*M*	30 m*M*	60 m*M*	10 m*M*	30 m*M*	60 m*M*
A	−32	−8.7	−0.4	−9.4	−2.7	−0.6	−6.6	−2.4	−0.7
B	120	96	75	64	50	39	56	46	37

[a] $A \times 10^3$ = intercept of $1/t$ *versus* E (s^{-1}). $B \times 10^3$ = slope of $1/t$ *versus* E (cm V^{-1} s^{-1}).

even in those instances where the small power dissipation of the cooling system could increase the temperature of the separation buffer.

ACKNOWLEDGEMENTS

This work was supported by DGCYT (Project PBB 88-00-34). A. C. and M. F. acknowledge MEC (Spain) for financial support. Special thanks are due to Beckman Instruments España for financial support of part of this work. The authors also thank Dr. M.V. Dabrio for writing one of the computer acquisition programs used and Dr. S. Penedés for fruitful discussions.

REFERENCES

1 S. Hjertén, *Electrophoresis*, 11 (1990) 659.
2 M.M. Bushey and J.W. Jorgenson, *J. Chromatogr.*, 480 (1989) 301.
3 F.E. Regnier and R.M. Chicz, in K.M. Gooding and F.E. Regnier (Editors), *HPLC of Biological Molecules*, Marcel Dekker, New York, 1990, Ch. 4, p. 86.
4 J.K. Towns and F.E. Regnier, *Anal. Chem.*, 63 (1991) 1126.
5 H.H. Lauer and D. McManigill, *Anal. Chem.*, 58 (1986) 166.
6 J.W. Jorgenson and K.D. Lukacs, *Science*, 222 (1983) 266.
7 J.S. Green and J.W. Jorgenson, *J. Chromatogr.*, 478 (1989) 63.
8 A. Emmer, M. Jasson and J. Roerrade, *J. High Resolut. Chromatogr.*, 14 (1991) 778.
9 S.F. Yi, *Capillary Electrophoresis —Principles, Practice and Applications*, Elsevier, Amsterdam, 1992.
10 Y. Walbroel and J.W. Jorgenson, *J. Microcol. Sep.*, 1 (1989) 41.
11 S. Wicar, M. Vilenchik, A. Balenskii, A.S. Cohen and B.L. Karger, *J. Microcol. Sep.*, 4 (1992) 339.
12 M. Giles and G. Schomburg, presented at the *19th International Symposium on Chromatography, Aix-en-Provence, September 1992.*
13 A. Cifuentes, M. de Frutos, J.M. Santos and J.C. Diez-Masa, *J. Chromatogr. A*, 655 (1993) in press.
14 J.K. Towns and F.E. Regnier, *J. Chromatogr.*, 516 (1990) 69.
15 D.J. Cram, *Angew. Chem., Int. Ed. Engl.*, 25 (1986) 1039.
16 P.C. Sadek and P.W. Carr, *J. Chromatogr. Sci.*, 21 (1983) 314.
17 J. Liu, V. Dolnik, Y.Z. Hsieh and M. Novotny, *Anal. Chem.*, 64 (1992) 1328.
18 R.S. Hunter, *Zeta Potential in Colloid Science*, Academic Press, London, 1981, Ch. 3.
19 H. Koda, Y. Kuramoto and E. Kimura, in E. Kimura (Editor), *Current Topics in Macrocyclic Chemistry in Japan*, Hiroshima University School of Medicine, Hiroshima, 1987, p. 136.
20 E. Kimura, A. Sakonaka, T. Yatsunami and H. Kodama, *J. Am. Chem. Soc.*, 103 (1981) 3041.
21 L.R. Snyder and H.A. Stadalius, in Cs. Horváth (Editor), *High-Performance Liquid Chromatography —Advances and Perspectives*, vol. 4, Academic Press, New York, 1986, p. 289.
22 J.W. Jorgenson and K.D. Luckacs, *Anal. Chem.*, 53 (1981) 1298.
23 G. Guiochon and M. Martin, *J. Chromatogr.*, 326 (1985) 3.
24 S.L. Delinger and J.M. Davis, *Anal. Chem.*, 64 (1992) 1947.
25 R.J. Nelson, A. Paulus, A.S. Cohen, A. Guttman and B.L. Karger, *J. Chromatogr.*, 480 (1989) 111.
26 Y. Machida, E. Kimura and M. Kodama, *Inorg. Chem.*, 22 (1983) 2055.
27 M. Micheloni, A. Sabatini and P. Paoletti, *J. Chem. Soc., Perkin Trans. 2*, (1978) 828.

Journal of Chromatography A, 652 (1993) 171–177
Elsevier Science Publishers B.V., Amsterdam

CHROM. 25 255

Buffer conditions affecting the separation of Maillard reaction products by capillary electrophoresis

Andy J. Tomlinson* and James P. Landers

Department of Biochemistry and Molecular Biology, Mayo Clinic, Rochester, MN 55905 (USA)

Ivor A.S. Lewis

Department of Chemistry, King's College, London, University of London, London WC2R 2CS (UK)

Stephen Naylor

Department of Pharmacology and Department of Biochemistry and Molecular Biology, Mayo Clinic, Rochester, MN 55905 (USA)

ABSTRACT

Capillary electrophoresis was applied to effect the separation of Maillard reaction products generated by the reaction of 5-hydroxymethylfurfural (5-HMF) with glycine. Since many components of this reaction mixture have not been previously identified an empirical approach was taken to develop separation conditions. Buffer composition, ionic strength and pH were all investigated. The effects of these parameters on the separation of a 5-HMF-glycine model Maillard reaction mixture are reported.

INTRODUCTION

Reactions involving amino acids, peptides, or proteins with reducing sugars (Maillard chemistry) are believed to be of great importance in food chemistry. It has been suggested that such reactions are central to the formation of flavours [1–4], colours [5–9], mutagens [10], and antioxidants [11] as foods are cooked or processed. Furthermore, it has been reported that these interactions can occur in dried foods (*e.g.*, milk powders) as they are stored, causing discolouration [12], production of off-flavours [13], and a possible loss of nutritional value [14,15]. In addition, Maillard chemistry has recently been shown to be involved in cross-linking of proteins [16] and nucleic acids [17], thereby influencing the metabolic fate of these biomolecules. Such reactions are also thought to occur *in vivo*, and their role in ageing has been postulated [18,19].

Investigation of the components formed during the reaction of amino compounds with sugars is often aided by analysis of model reaction systems. Typically a pure amino compound (usually an amino acid) is reacted, under a variety of conditions (*e.g.* changes in temperature, reactant concentrations, etc.), with a reducing sugar. These studies have shown that even model systems lead to extremely complex product reaction mixtures that are difficult to analyse [see, for example, refs. 5–9]. This is particularly evident in the investigations of coloured components (the melanoidins) that result from this

* Corresponding author.

0021-9673/93/$06.00

chemistry [20]. As a result, information regarding these reaction products is rather limited, and complete structural analyses have not been successful. Indeed, to date, despite many attempts, effective means of isolation of the melanoidins have not been established, and HPLC techniques have proved to be of limited use in their investigation [20].

Based on the observation that melanoidins possess amphoteric character [21], there have been attempts to separate them using classical electrophoretic techniques, such as gel and paper electrophoresis [21,22]. Both techniques enabled the separation of model reaction mixtures into a series of coloured bands, but in both instances, the resolution of individual components was reported to be poor. Other electrophoretic techniques applied to the attempted separation of melanoidins include those of electrofocusing and preparative electrofocusing [22]. These latter techniques are reported to enable the separation of amphoteric species that exhibit isoelectric points that differ by 0.005 pH units [23]. However, when applied to the separation of melanoidins, it was found that analysis times were lengthy, often taking up to 14 h to complete [22]. Also, as separations occurred at the gel surface, it was difficult to determine whether the observed coloured bands were real, or artifacts caused by oxidation of the labile melanoidins. Modification of these techniques is required to enable the separation of coloured components of Maillard reaction mixtures in a rapid manner under benign conditions.

A technique that is currently gaining widespread acclaim for the separation of a variety of compound mixtures is capillary electrophoresis (CE) [see refs. 24 and 25 for reviews]. In this form of free solution zone electrophoresis separations are performed in thin-walled, narrow bore (typically 50 μm internal diameter) fused-silica capillaries, that are filled with an aqueous buffer solution [25]. Application of a high voltage across the capillary affords very rapid, highly efficient separations, that are a function of the mass and charge of separated species. Capillary efficiencies in excess of $1 \cdot 10^6$ theoretical plates per meter are not uncommon. In addition, additives/buffer modifiers can be added to the buffers to change separation mechanisms, *e.g.*, the addition of surfactants to buffers (as in micellar electrokinetic capillary chromatography; MECC) can enhance separation by introducing a chromatography element to electrokinetic separation mechanisms [25].

The use of CE to separate Maillard reaction products has received scant attention [26,27]. In the first study, reaction products resulting from reactions of glucose or ribose with glycine, alanine and isoleucine were separated, before and after the formation of phenylthiocarbonyl or 2,4-dinitrophenylhydrazine derivatives [26]. We have recently reported the separation of reaction products (in particular the melanoidins) resulting from glucose–glycine and 5-hydroxymethylfurfural (5-HMF)–glycine model systems by reversed-phase HPLC (RP-HPLC) and CE [27].

The objective of the present study was to investigate CE conditions that effect the separation of reaction products formed by a 5-HMF–glycine model Maillard reaction mixture. The effects of buffer composition, ionic strength and pH on the separation of components of this reaction mixture are reported.

EXPERIMENTAL

Chemicals

5-HMF and glycine were analytical reagent grade obtained from Aldrich (Poole, UK). Buffer tablets were obtained from FSA (Loughborough, UK). Dichloromethane was HPLC grade from Rathburn (Walkerburn, UK). Gold-grade ammonium acetate was obtained from Aldrich (Milwaukee, WI, USA) and analytical reagent-grade potassium phosphate, sodium acetate and trifluoroacetic acid (TFA) were from Sigma (St. Louis, MO, USA). Ammonium hydroxide was from Baxter (Minneapolis, MN, USA). High-purity water was prepared in-house using a Sybron Banstead water purifier system (ex-Millipore) applied by VWR (Minneapolis, MN, USA).

Preparation of a 5-HMF–glycine model Maillard reaction mixture

5-HMF (1.5 g; 0.012 mol) was reacted for 8 h, under reflux conditions, with glycine (0.9 g; 0.012 mol) in aqueous solution (40 ml) buffered

to pH 7.0, with commercially available buffer tablets. After reaction, the mixture was cooled and extracted with dichloromethane (3 × 50 ml) to remove most of the reacted 5-HMF. The resultant aqueous fraction was then freeze-dried to yield a dark brown powder. This powder was reconstituted in deionised water, to produce a solution of 1 mg/ml, prior to separation by CE.

CE separation conditions

All CE separations were performed using a Beckman P/ACE model 2100 CE (Fullerton, CA, USA) coupled to an IBM PS2/76 PC with control and data capture by System Gold Software. An uncoated capillary 57 cm × 75 μm, 50 cm before detector) was used throughout this study. Prior to using the capillary and between each analysis, the capillary was rinsed with a 0.1 *M* solution of sodium hydroxide followed by water and conditioning with running buffer (5 column volumes of each). The following buffers were used during these investigations: 5 m*M* potassium phosphate (mono basic) + 5 m*M* sodium phosphate (dibasic) pH 7.0; 20 m*M* sodium acetate pH 7.0; 20 m*M* ammonium acetate pH 7.0; 10 m*M* potassium phosphate (monobasic) + 10 m*M* sodium phosphate (dibasic) pH 7.0; 40 m*M* sodium acetate pH 7.0; 40 m*M* ammonium acetate pH 7.0; 20 and 40 m*M* ammonium acetate adjusted to pH 4.6 with trifluoroacetic acid; 20 and 40 m*M* potassium phosphate (monobasic) adjusted to pH 4.6 with trifluoroacetic acid; and 20 and 40 m*M* ammonium acetate adjusted to pH 9.2 with ammonium hydroxide.

Samples were applied to the anodic end of the capillary using pressure injection (1 s) and separated by application of a voltage of 10 kV across the capillary. The capillary temperature was maintained at 25°C throughout separations. Components were detected spectrophotometrically at a wavelength of 214 nm.

RESULTS AND DISCUSSION

The complexity of model Maillard reaction mixtures has frequently been demonstrated [10]. In addition, the lack of suitable analytical techniques that affect the separation of components of such reaction mixtures has considerably detracted from the identification of, in particular, advanced Maillard reaction products (MRPs), such as the coloured melanoidins. While several semi-volatile reaction products have been recently identified [28], no advance MRPs have been structurally characterised. Development of separation techniques to effect the resolution of these compounds must therefore be conducted via an empirical approach. For CE, buffer composition, its ionic strength, and pH are parameters that are of primary importance in determining suitable separation conditions. However, it is recognised that capillary dimensions, applied voltage, and sample injection technique are also factors to be considered. In the present study, these latter parameters were fixed; hence, whilst it is understood that increasing capillary length can result in better resolution of components, the effects of buffers for separating MRPs produced by reaction of 5-HMF with glycine were of initial interest.

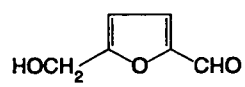

5-HMF

In all samples analysed, unreacted 5-HMF was detected, and under the pH conditions used, was present as the neutral species. Hence, it was utilised to determine electroosmotic flow (EOF). Therefore, since in forward polarity experiments (sample applied at anode and components detected at cathodic end of capillary), cations are detected before neutral compounds whereas anions are detected later, the ionic character of analytes in aqueous solutions of various pH can be determined. In the present study, we have used the migration times of reaction products, relative to 5-HMF, in electropherograms to gain an understanding of the ionic character of MRPs produced by the reaction of 5-HMF with glycine.

Electropherograms obtained from CE analysis of the 5-HMF–glycine model Maillard reaction mixture using three different buffer solutions of the same ionic strength and pH (7.0) are shown in Fig. 1. Comparison of the migration time of 5-HMF (peak 1) in each of these profiles indicates that EOF was fastest in the phosphate buffer (Fig. 1A) and slowest in the ammonium acetate experiment (Fig. 1C). The EOF of the sodium acetate system (Fig. 1B) was closest to

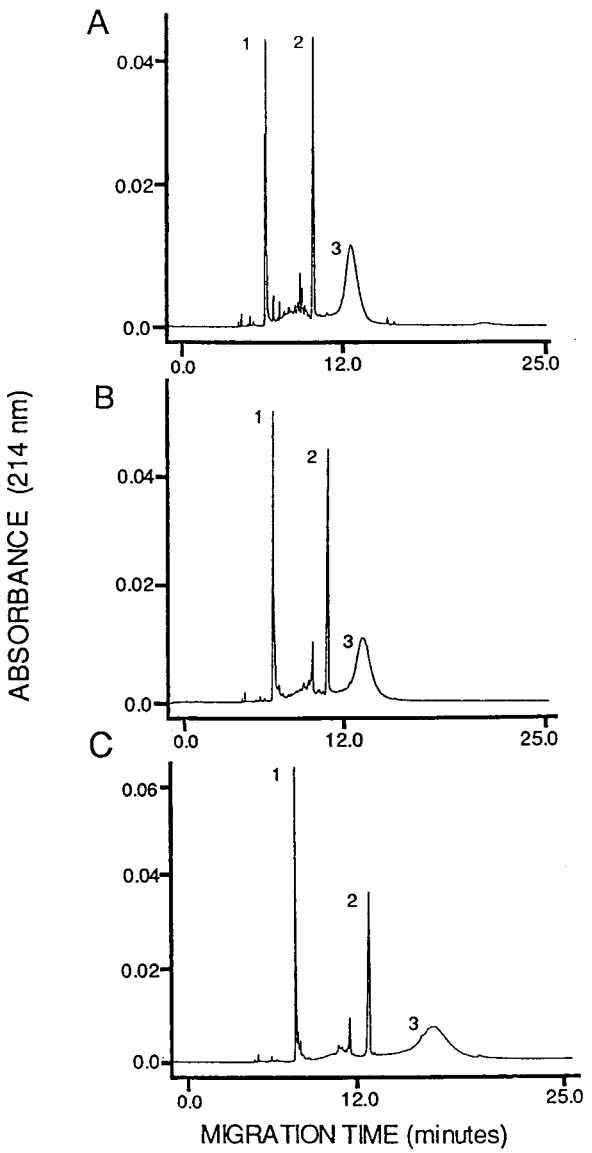

Fig. 1. Electropherograms recorded for a 5-HMF–glycine model Maillard reaction mixture at pH 7.0. (A) 5 m*M* KH_2PO_4 + 5 m*M* Na_2HPO_4 buffer; (B) 20 m*M* sodium acetate buffer; (C) 20 m*M* ammonium acetate buffer. Capillary 57 cm × 75 μm (50 cm prior to detector). Voltage 10 kV. Detection 214 nm. Peaks: 1 = 5-HMF, EOF; 2 = coloured melanoidin product; 3 = complex mixture of MRPs.

that of the phosphate buffer. The various differences of EOF are mirrored by the length of time MRPs are held on the capillary. Hence, in ammonium acetate, the total analysis time is 20 min, whilst in both phosphate and sodium acetate buffers, all components migrated within 15 min. In general, since it is expected that the longer components are on the capillary, the better their separation, it would be predicted that the best resolution of MRPs would be achieved using the ammonium acetate buffer. Indeed, considering the broad peak (peak 3) detected in each electropherogram, the separation of components, whilst poor in all examples, were partially resolved in the ammonium acetate buffer. These components were suspected to be polymeric, since their mass-to-charge ratios (the separation mechanism of free solution CE methods) were apparently very similar. However, for other MRPs of the reaction mixture (earlier migrating species), better resolution was achieved using the phosphate buffer, *e.g.*, a second compound that migrates with a time similar to that of a neutral species has been separated from 5-HMF in this buffer solution (peak 1 in Fig. 1A). This effect is likely to be due to a more effective prevention of analyte–analyte interactions in the phosphate buffer in comparison to the acetate buffers. In all three buffers at this pH (7.0), the major MRPs of this reaction mixture, including peak 2 (a response shown in previous study [27] to be the main melanoidin (coloured) component of the 5-HMF–glycine reaction mixture) migrate with longer times than 5-HMF. These compounds therefore possess anionic character at this pH.

Electropherograms obtained from CE separation of the 5-HMF–glycine model reaction mixture using buffers of twice the ionic strength but the same composition and pH (7.0) as those used to generate the profiles of Fig. 1 are shown in Fig. 2. Comparison of the migration time of 5-HMF (peak 1) in each of these buffers again indicates that EOF was fastest in the phosphate buffer (Fig. 2A) and slowest in the ammonium acetate system (Fig. 2C). However, the EOF of all buffer compositions was slower at increased ionic strength. This can be attributed to a change of zeta potential (the charge on the capillary wall) caused by occupation of the ionised silanol groups by cations, due to the increased concentration of these ions in solution. One effect of

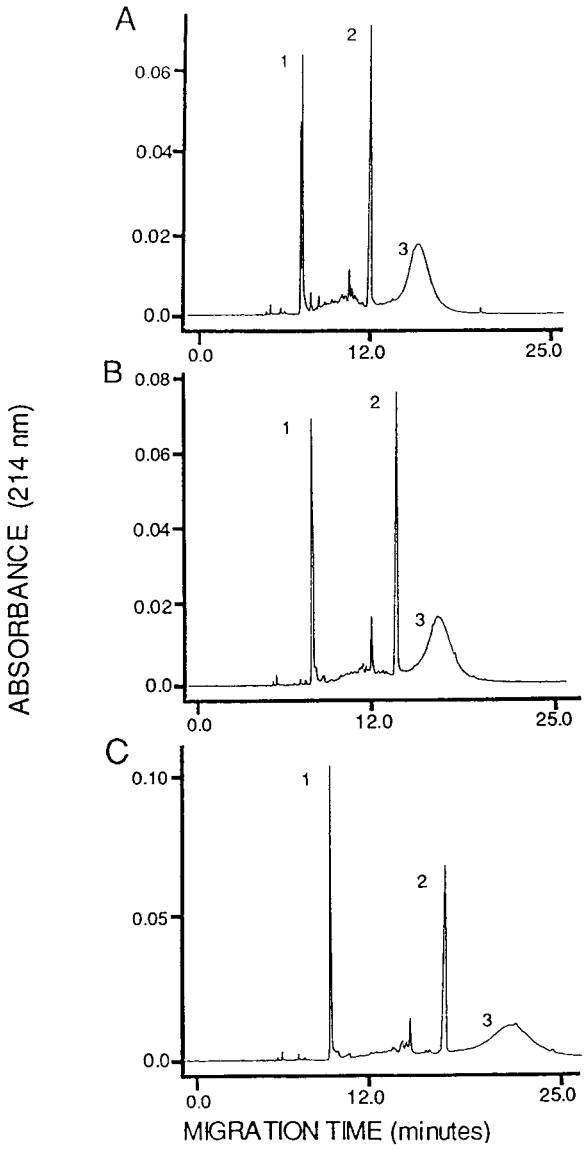

Fig. 2. Electropherograms recorded for a 5-HMF–glycine model Maillard reaction mixture at pH 7.0. (A) 10 m*M* KH_2PO_4 + 10 m*M* Na_2HPO_4; (B) 40 m*M* sodium acetate; (C) 40 m*M* ammonium acetate. Other parameters and assignments as noted in Fig. 1.

the slower EOF was to hold MRPs on the capillary for a longer time. This increases the resolution achieved in all buffers. Furthermore, since at a high ionic strength there are more buffer ions in solution, analyte-analyte interactions are reduced, the effect of which is also increased resolution of components. However, as observed with the lower ionic strength buffers, the best separation of the MRPs migrating prior to the major coloured response (peak 2) of the 5-HMF-glycine reaction mixture was achieved in phosphate buffer (Fig. 2A). In these higher ionic strength buffers, since the pH of solution was again 7.0, most MRPs possessed anionic character.

In addition to investigating the effects of increasing ionic strength of buffer solutions, the effect of changing buffer pH was studied. Changes in this parameter cause two major events in CE separations, both of which alter the separation of components. First, since the pK_a of the surface silanol group is *ca.* 2.7, these groups are ionised above a pH of 2.7. Since it is the interaction of the ionised silanol groups with buffer cations that leads to development of EOF, this parameter can be drastically affected by pH changes. Hence, it is observed that at low pH, EOF is slow, whilst at high pH, EOF is much faster. At pH values above 8.5, since all surface silanol groups are ionised, the effect on separation is caused by a change of charge on the analyte species. Hence, changing pH causes both a modification of EOF and a possible change of charge state of analytes.

Results of investigation of the affect of pH on the separation of MRPs of the 5-HMF–glycine reaction mixture are presented in Fig. 3 (ammonium acetate and phosphate buffers at pH 4.6) and Fig. 4 (ammonium acetate buffer at pH 9.2). At low pH, a dramatic change in the appearance of the electropherogram was observed for both buffers (Fig. 3). However, again increasing the ionic strength results, as expected, in increased resolution of components, and in both buffers, the broad response detected (peak 3) is flattened with increased ionic strength (Fig. 3B and D). An unexpected result was at this pH, the MRPs exhibited sizeable anionic character. In fact, this was also found in buffers of pH 1.7 (data not shown). This therefore tends to suggest that the majority of MRPs, and especially the melanoidins, contain a number of functional groups that possess low pK_a values, such that unless extremes of pH are encountered, these molecules exist in solutions as anions.

At high pH (Fig. 4A and B), the response due

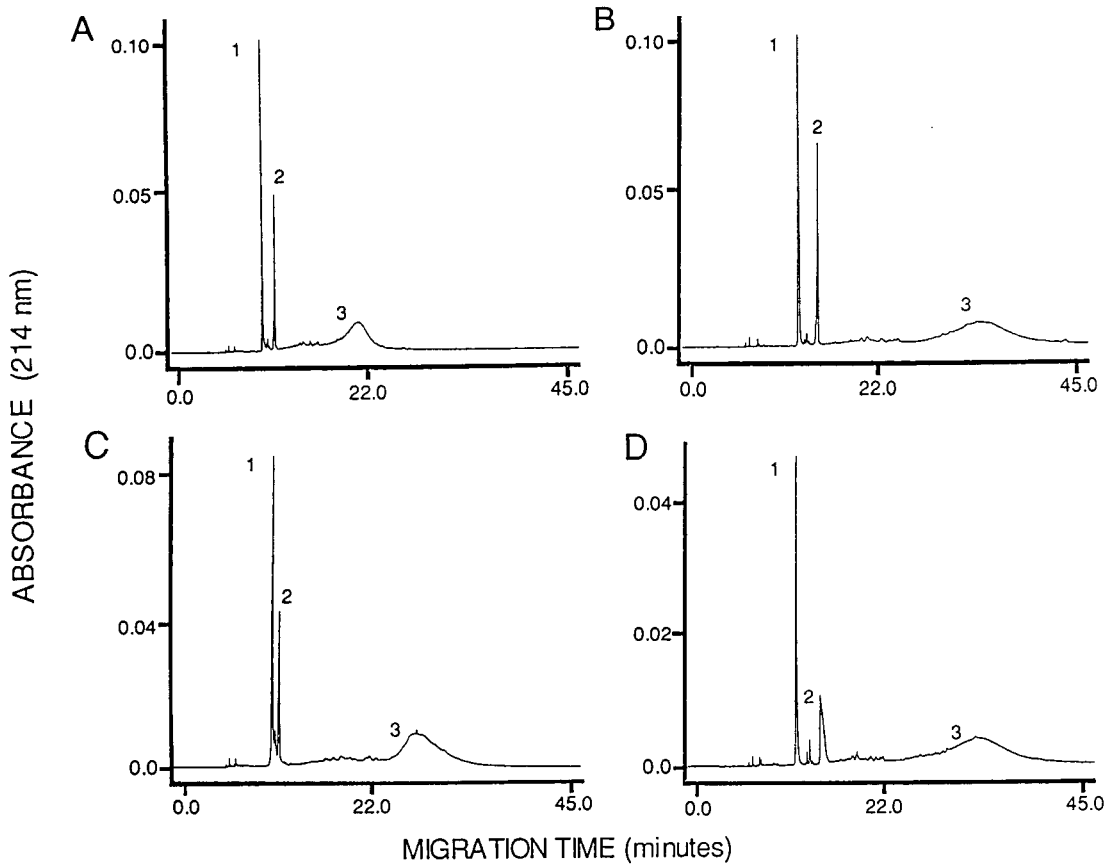

Fig. 3. Electropherograms recorded for a 5-HMF–glycine model Maillard reaction mixture at pH 4.6. (A) 20 m*M* ammonium acetate adjusted to appropriate pH with TFA; (B) 40 m*M* ammonium acetate adjusted to appropriate pH with TFA; (C) 20 m*M* KH_2PO_4; (D) 40 m*M* KH_2PO_4. Other parameters and assignments as noted in Fig. 1.

to 5-HMF (peak 1) was reduced, and new responses were detected in electropherograms. There responses also possessed anionic character. Thus, it was apparent that several components that were previously neutral in solution had been ionised. These latter components were therefore weakly acidic. Once again, as expected, resolution of components was increased at a higher ionic strength. The overall resolution of components was, however, not as good as was achieved in either pH 4.6 or 7.0 buffers.

CONCLUSIONS

The complexity of model Maillard reaction mixtures was demonstrated by separation of MRPs by CE produced on reaction of 5-HMF with glycine. Comparison of buffer composition, ionic strength, and pH for effecting the separation of these compounds indicated that at pH 7.0, a phosphate buffer would be of choice, whilst at pH 4.6, an ammonium acetate buffer gave improvements of component resolution.

Throughout these studies, the major MRPs of the 5-HMF–glycine reaction mixture were detected with longer migration times than 5-HMF (a neutral compound at all pH conditions used in this study). These compounds therefore possess at least partial anionic character in solution over a wide pH range. The amphoteric nature previously reported for such compounds was not detected [21,22]. This leads to suggestions that the MRPs formed in the reaction studied possess a number of acidic groups that exhibit low pK_a

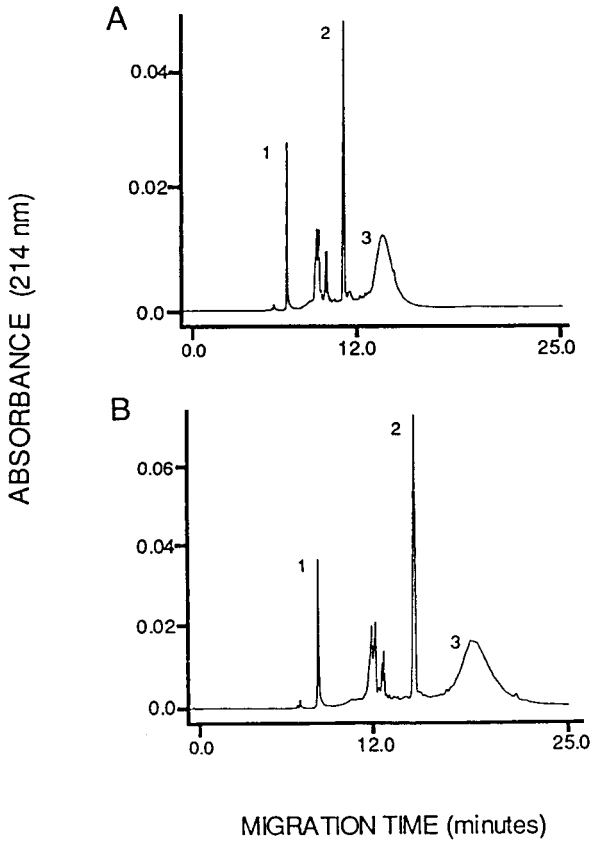

Fig. 4. Electropherograms recorded for a 5-HMF–glycine model Maillard reaction mixture at pH 9.2. (A) 20 m*M*; (B) 40 m*M* ammonium acetate (pH of both adjusted with ammonium hydroxide). Other parameters and assignments as noted in Fig. 1.

values. Hence, the formation of cationic species is unfavourable under common pH conditions.

ACKNOWLEDGEMENTS

The authors wish to acknowledge Mrs. Val Langworthy for her help in preparation of this manuscript for publication. One of us (J.P.L.) would like to thank the Medical Research Council of Canada for support.

REFERENCES

1 G. Verin and C. Paranyi, in G. Verin (Editor), *The Chemistry of Heterocyclic Flavouring and Aroma Compounds*, Ellis Horwood, Chichester, 1982, p. 151.
2 J.P. Danehy, *Adv. Food Res.*, 30 (1986) 77.
3 L.L. Buckholz, Jr., *Cereal Foods World*, 33 (1988) 547.
4 J.M. Ames, *Food Manuf.*, (1989) 61.
5 H.E. Nursten, *Food Chem.*, 6 (1981) 263.
6 H.E. Nursten, in D. MacCarthy (Editor), *Concentration and Drying of Foods*, Elsevier, Oxford, 1986, p. 53.
7 J.M. Ames, *Food*, (1987) 67.
8 J.M. Ames, *Chem. Ind., London*, (1987) 558.
9 F. Ledl, in P.A. Finot, H.U. Aeschbacher, R.F. Hurrell and R. Liardon (Editors), *The Maillard Reaction in Food Processing, Human Nutrition and Physiology*, Birkhauser, Basel, 1990, p. 19.
10 M. Namiki, *Adv. Food Res.*, 32 (1988) 115.
11 H. Lingnert and G. Hall, in M. Fujimaki, M. Namiki and H. Kato (Editors), *Amino-Carbonyl Reactions in Food and Biological Systems —Proc. 3rd Int. Symp. on the Maillard Reaction, Susono, Shizuoka, July 1–5, 1985 (Developments in Food Science*, Vol. 13), Elsevier, Amsterdam, 1986, p. 273.
12 K.M.S. Henry, S.K. Kon, C.H. Lea and J.C.D. White, *J. Dairy Sci.*, 15 (1948) 292.
13 A. Ferritti and V.P. Flanagan, *J. Dairy Sci.*, 54 (1971) 1764.
14 J. Mauron, *Prog. Food Nutr. Sci.*, 5 (1981) 5.
15 J. O'Brien and P.A. Morrissey, *Crit. Rev. Food Sci. Nutr.*, 28(3) (1989) 211.
16 M. Brownlee, A. Ceramic and H. Vlassara, *N. Engl. J. Med.*, 318 (1988) 1315.
17 R. Bucala, P. Model and A. Ceramic, *Proc. Natl. Acad. Sci. U.S.A.*, 81 (1984) 105.
18 V.M. Monnier, D.R. Sell, M. Satoshi and H.N. Ramanakoppa, in P.A. Finot, H.U. Aeschbacher, R.F. Hurrell and R. Liardon (Editors), *The Maillard Reaction in Food Processing, Human Nutrition and Physiology*, Birkhauser, Basel, 1990, p. 393.
19 J.J. Harding, H.T. Beswick, R. Ajiboye, R. Huby, R. Blakytny and K.C. Rixon, *Mech. Age Dev.*, 50 (1989) 7.
20 A.J. Tomlinson, *Ph.D. Thesis*, University of London, London, 1991.
21 H. Hashiba, *Agric. Biol. Chem.*, 42 (1978) 763.
22 R. O'Reilly, *Ph.D. Thesis*, University of Reading, Reading, 1982.
23 H. Hagland, in J.P. Arbuthnott and J.A. Becley (Editors), *Isoelectric Focusing*, Butterworths, London, 1975, p. 3.
24 J.P. Landers, R.P. Oda, T.C. Spelsberg, J.A. Nolan and K.J. Ulfelder, *Biotechniques*, 14(1) (1993) 98.
25 W.A. Kuhr, *Anal. Chem.*, 62 (1990) 403R.
26 Z. Deyl, I. Miksik and R. Struzinski, *J. Chromatogr.*, 516 (1990) 287.
27 A.J. Tomlinson, J.A. Mlotkiewicz and I.A.S. Lewis, *Food Chem.*, in press.
28 A.J. Tomlinson, J.A. Mlotkiewicz and I.A.S. Lewis, *Food Chem.*, in press.

Journal of Chromatography A, 652 (1993) 179–188
Elsevier Science Publishers B.V., Amsterdam

CHROM. 25 126

Capillary electrophoresis as a tool for the analysis of protein folding

Mark A. Strege and Avinash L. Lagu*

Lilly Research Laboratories, Eli Lilly and Company, Indianapolis, IN 46285 (USA)

ABSTRACT

The utility of capillary electrophoresis (CE) was demonstrated for the analysis of a model protein, bovine trypsinogen, as it underwent oxidation from a fully reduced molecule through a distribution of intermediate species until the disulfide bond conformation corresponding to that of the globular native structure was reached. Through the use of CE, completely refolded (native) trypsinogen was resolved from both the reduced protein and intermediate refolded conformations. In addition, the presence of polyethylene glycol in the separation buffer was determined to provide size-based protein separations of significantly higher resolution than those obtained in phosphate buffer alone. Quantitation of native trypsinogen in refolded material revealed an excellent correlation between CE determinations and analyses by established techniques such as biological activity assay and high-performance size-exclusion and cation-exchange chromatography. These results, together with a comparative consistency of CE separations with those obtained via non-denaturing slab gel electrophoresis and isoelectric focusing, suggest that CE can be an effective technique useful for the analysis of protein refolding.

INTRODUCTION

The formation of a protein inside a living cell is known to take place in two steps: the biosynthesis of the protein chain, followed by its folding into a native three-dimensional structure. While extensive work has been devoted toward the study of the first process, much less is understood concerning the latter. It is known that many proteins can fold *in vitro* from a completely unordered state [1], providing evidence that a polypeptide chain, in an aqueous environment, contains all of the information required for folding. Therefore, the study of protein folding *in vitro* is crucial to understanding the mechanism of protein self-organization.

Two fundamental experimental approaches, the determination of biological function (activity) and the determination of the state of association, have been traditionally employed to characterize the folding and association of proteins. Because of the structure–function relationship of proteins, activity represents the most sensitive criterion. However, studies monitored using UV [2–4], circular dichroism [5], fluorescence [6,7], NMR [8–10] and gel electrophoresis [11] have demonstrated that the protein denaturation–renaturation process is not always a two-state transition, *i.e.*, intermediate species can be detected. Various chromatographic techniques, such as high-performance size-exclusion [12–14], ion-exchange [13,15,16], and hydrophobic interaction chromatography [17–19], have demonstrated potential for non-denaturing protein separations, in addition to the analysis of folding intermediates. However, the number of analytical methods readily applicable to the separation, detection and quantitation of changes in covalent structure, such as those undergone by a protein during folding, remain quite limited.

Advances in the development of analytical methods for the analysis of changes undergone by a protein structure during refolding will

* Corresponding author.

0021-9673/93/$06.00

impact work upon the following two issues. A primary objective of the study of protein folding is the elucidation of the "second half of the genetic code" that is assumed to govern the spontaneous transition from the one dimensional structural information (encoded in a given primary structure) to the three-dimensional biologically active state [20]. If this folding code were known, not only structural predictions would be at hand, but hypothetical functions could also be deduced from given amino acid or DNA sequences. Secondly, the advent of the recombinant DNA revolution and the new biotechnology that derives from it has brought protein folding to the forefront of the awareness of the scientific community. Recent biotechnological advances have resulted in the development of genetically engineered cells which can be viewed as factories for the production of specific polypeptides. The polypeptide product is often in the form of an inclusion body, and the solubilization, purification, and refolding of the product are processes which can provide enormous challenges for separation scientists. Analytically, it is crucial to be able to detect the different conformational states of a protein in both process development and quality assurance.

In this paper, the use of a relatively new bioseparation technique, capillary electrophoresis (CE), is reported for the analysis of proteins differing in *covalent* structure as they undergo refolding. Separations of refolded proteins by CE, a quantitative electrophoretic technique, are demonstrated to compare favorably with analyses by other analytical methods (activity assay, high-performance liquid chromatography, native gel electrophoresis and isoelectric focusing) which have previously demonstrated application for determinations of this nature. Bovine trypsinogen was chosen as the protein of interest for this investigation. The refolding biochemistry of this serine protease zymogen has been investigated extensively [21–23].

EXPERIMENTAL

Materials

Bovine trypsinogen [phenylmethylsulfonyl fluoride (PMSF)-treated], bovine trypsin, dithiothreitol (DTT), cysteine, cystine, calcium chloride, phenylmethylsulphonyl fluoride (PMSF), Nα-*p*-tosyl-l-arginine methyl ester hydrochloride (TAME), trifluoroacetic acid (TFA) and urea were purchased from Sigma (St. Louis, MO, USA). Sodium acetate, glacial acetic acid and ethylenediaminetetraacetic acid (EDTA) were from EM Science (Gibbstown, NJ, USA), polyethylene glycol (PEG; M_r 40 000) was from Serva (New York, NY, USA), and glycerin was from Fisher (Fair Lawn, NJ, USA). Formic acid was obtained from Fluka (Ronkonkoma, NJ, USA). Analytical-grade acetonitrile was purchased from Burdick & Jackson (Muskegon, MI, USA).

Reduction of trypsinogen

A 50-mg sample of trypsinogen was dissolved in 10 ml 0.1 *M* Tris–HCl pH 8.5, 8 *M* urea, 1 m*M* EDTA, 0.1 *M* DTT and 0.2 m*M* PMSF. The reduction of disulfides was carried out at ambient temperature for 3 h under a nitrogen atmosphere. The presence of PMSF, a trypsin inhibitor, was found necessary for the minimization of enzymatic degradation via trypsin contaminant activity during the reduction. Following reduction, the pH was then lowered to pH 3.0 with concentrated formic acid, and the sample was then dialyzed overnight in a Spectra/Por 2000 M_r cut-off membrane (Spectrum, Houston, TX, USA) in 400 volumes of 100 m*M* acetic acid to remove salts.

Refolding of trypsinogen

Quantities (50 mg) of reduced trypsinogen were refolded through the use of techniques described by Jaenicke and Rudolph [20] and Light and Higaki [21]. Aliquots of the folding solution were removed at various time points, and the pH of these samples was immediately dropped to pH 3 by addition of concentrated formic acid. Samples analyzed by CE, native gel electrophoresis and isoelectric focusing were first dialyzed in 100 m*M* acetic acid to remove salts, and then concentrated in a SpeedVac concentrator (Key Scientific, Mt. Prospect, IL, USA) to a final volume corresponding to a concentration of 2.0 mg/ml total protein.

Activity assay of trypsinogen

Samples of refolded trypsinogen were solvent exchanged into 50 m*M* Tris–HCl pH 8.1, 10 m*M* calcium chloride and then activated to trypsin via incubation with a low concentration of trypsin (5 units of trypsin/mg trypsinogen) at ambient temperature for 6 h. Activity toward TAME was determined spectrophotometrically according to the procedure of Hummel [24], through the use of a Model DU-7400 UV–Vis diode array spectrophotometer (Beckman, Fullerton, CA, USA).

Capillary electrophoresis

CE was performed with an automated P/ACE 2100 instrument (Beckman Instruments, Palo Alto, CA, USA) controlled by an IBM PS/2 Model 80 386 computer fitted with PACE software (Beckman) running in a Windows (Microsoft, Redmond, WA, USA) environment. The capillary cassette was fitted with a 50 μm I.D. fused-silica capillary, 37 cm total length (30 cm inlet-to-detector window). All separations were obtained through the employment of a cathodic outlet reservoir, and injection of the sample was by low pressure (0.5 p.s.i.; 1 p.s.i. = 6894.76 Pa). On-column detection was performed by UV absorption at 200 nm, and the temperature was controlled at 25 ± 0.1°C. The capillaries employed in this study were fused-silica capillaries obtained from Polymicro Technologies (Phoenix, AZ, USA).

Cation-exchange HPLC

Chromatography was performed with a gradient HPLC system (Models 303 and 305 pumps, Model 811B dynamic mixer, Model 116 variable-wavelength UV detector, and a Model 231 sample injector equipped with a 100-μl sample loop (Gilson, Madison, WI, USA). Analog data were collected directly from the absorbance detector (280 nm) on an in-laboratory centralized chromatography computer system based on the Hewlett-Packard Model 1000 minicomputer. A ProGel-TSK SP-5PW column (Supelco, Bellefonte, PA, USA) (7.5×0.75 cm), a vinyl polymer-based strong cation exchanger, was used for this investigation, together with an in-line 0.25-μm filter frit preceding the analytical column. Mobile phase A was 25 m*M* sodium acetate pH 4.0, 2 *M* urea, 20% acetonitrile and mobile phase B was 25 m*M* sodium acetate pH 4.0, 2 *M* urea, 20% acetonitrile, 1 *M* NaCl. A linear 45-min gradient from 0 to 35% B was utilized with a 1.0 ml/min flow-rate, and the column was operated at ambient temperature.

Size-exclusion HPLC

Size-exclusion chromatography was performed on a Superose 12 column (30×1.0 cm) (Pharmacia) using the chromatography system described above and a flow-rate of 0.5 ml/min. An in-line 0.25-μm filter frit preceded the column. Isocratic elution, using a mobile phase containing 100 m*M* acetic acid, 100 m*M* NaCl and 2 *M* urea, was monitored at 280 nm. Fractions of refolded trypsinogen were collected through the use of a Model 203 fraction collector (Gilson).

Native gel electrophoresis

The protein samples (2 mg/ml total protein, 1 μl volume loaded) were electrophoresed using PhastGel Homogeneous 20 gels (Pharmacia/LKB Biotechnology, Piscataway, NJ, USA) and then stained with Coosmasie Brilliant Blue using a PhastSystem equipped with a reversed-polarity electrode assembly. The samples were separated, fixed, stained, and destained according to the procedures described in the product literature.

Isoelectric focusing

The protein samples (2 mg/ml total protein, 1 μl loaded) were focused using a PhastSystem and PhastGel IEF 3–9 gels (Pharmacia). The samples were fixed, silver stained, and destained as per the product literature. A p*I* marker mixture containing, among other proteins, native trypsinogen, was also purchased from Pharmacia.

RESULTS AND DISCUSSION

In this report, the native state of trypsinogen will be referred to as that conformation possessing the correct covalent structure, *i.e.* the disulfide bond arrangement present in protein which can be converted to active trypsin. Therefore, the term "refolding" will be employed to designate the reformation and interchange of disulfide

bonds occurring during the re-oxidation of the reduced protein, a process considered distinct in this study from the instantaneous reversible tertiary conformational changes experienced by the protein in response to changes in pH [25].

Refolded samples of bovine trypsinogen were generated following reduction of the commercially available native protein via the employment of a folding protocol derived from conditions suggested by Light and Higaki [21] and Jaenicke and Rudolph [20], as described in the Experimental section. Aliquots of material quenched with acid at various time points following the initiation of refolding were analyzed for activity via conversion of the protein to trypsin. By following the protocol described in this report, approximately 15% recovery of activity was observed after 22 h refolding. The low yield may in part be attributed to the formation of insoluble protein aggregates which were visible during refolding, and also to low levels of enzymatic degradation (occurring during reduction) caused by tryptic contamination.

Bovine trypsinogen is a basic protein, possessing a p*I* of *ca.* 9.3 in its native state [26]. Proteins of this nature have demonstrated a tendency to electrostatically adsorb to the negatively charged silanol groups present on the walls of silica capillaries, thereby seriously impairing the separation efficiency of these molecules during analysis by CE [27]. This phenomenon, together with poor recovery of the reduced and intermediate refolded species (which are known to exhibit pronounced hydrophobic character relative to native proteins), prevented the achievement of successful separations of the trypsinogen samples in both polyacrylamide- and octadecylsilane-derivatized capillaries in the presence of zwitterionic surfactant and non-ionic surfactant, respectively, at neutral pH. It has been demonstrated that basic proteins are separable by CE under acidic conditions (pH < 3), where the silica capillary walls are highly protonated and electrostatic adsorption is minimized [28]. Using this approach, 5 s injections of native and reduced trypsinogen were observed to separate successfully in a 25 m*M* sodium phosphate pH 2.0 buffer used in conjunction with a 37 cm bare silica capillary, 10 kV, and 200 nm UV

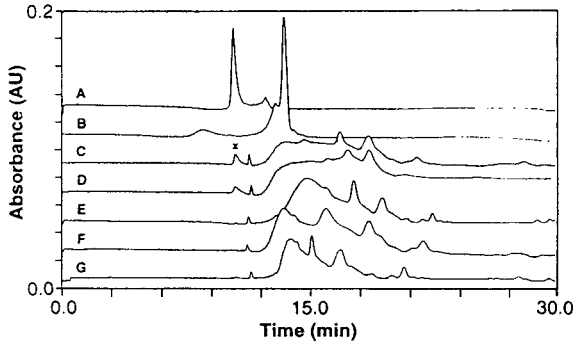

Fig. 1. Capillary electrophoretic separations of 5-s injections of 2 mg/ml samples of (A) native trypsinogen, (B) reduced trypsinogen, and (C) 22-h, (D) 7-h, (E) 1-h, (F) 30-min and (g) 10-min refolded trypsinogen obtained using 25 m*M* sodium phosphate pH 2.0 in a 37 cm, 50 μm bare silica capillary, 10 kV potential, and 200 nm detection. Refolded trypsinogen is marked by an "×".

detection (see Fig. 1). The minor peaks present in these separations were presumed to represent impurities in the commercially available material. Under these conditions, reduced trypsinogen was observed to migrate significantly slower than did the native protein. These results provide strong evidence for the dependence of the electrophoretic mobility of proteins, as observed via free-solution CE, upon the solvent-accessible charge. It appears that in the case of bovine trypsinogen, reduction of the molecule results in diminished basic character, perhaps through the exposure of acidic residues which are not accessible to the buffer when the protein is in its native, completely folded conformation.

Analyses of the refolded samples revealed a distribution of components, the majority displaying migration times equal to or greater than the reduced protein. These peaks are presumed to represent trypsinogen folding intermediates, the existence of which has been previously substantiated [21,22]. The distributions of electrophoretic mobilities displayed by the refolded species probably reflect differences in the solvent-accessible charges of these molecules. The viscous drag of the protein molecules as they migrate through the phosphate buffer appears to play at best a minor role in these separations, since trypsinogen folding intermediates have been demonstrated via size-exclusion chromatography (SEC)

to possess hydrodynamic radii significantly less than that of the completely unfolded protein [21,22]. It is important to note that a component which co-migrated with the native species (verified by spiking the refolded samples with native trypsinogen) was observed in the 1-, 7- and 22-h folded samples. This component probably represents completely refolded trypsinogen (corresponding to *ca.* 14% yield at 22 h), the presence of which was verified through the use of the activity assay.

Addition of 5% glycerine to 25 m*M* sodium phosphate pH 2.0 buffer facilitated an increase in the resolution of 10-s injections of the trypsinogen samples. These effects are visible in Fig. 2 where electropherograms (obtained using 10 kV) of the native, reduced, and 22-h refolded samples are displayed. The impact of the increased buffer viscosity seemed to be most evident in its effect upon the migration of the reduced protein, which possesses an extended unfolded conformation. In free solution the electrophoretic mobility of a macromolecule is expected to be inversely related to its frictional coefficient [29]. The frictional coefficient, in turn, depends upon not only the size and shape of a macromolecule, but also upon its interactions with the solvent (glycerine may associate hydrophilically with proteins). In the presence of 5% glycerine, reduced trypsinogen was observed to display a migration time approximately twice that of the native species.

Upon substitution of PEG, a hydrophilic nonionic polymer, for the glycerine in the separation buffer, resolution between the native and reduced trypsinogen increased to an even greater degree, and all of the partially refolded species displayed intermediate migration times (separations obtained using 30 kV), as presented in Fig. 3. The presence of PEG not only promoted a high viscosity, but may have also formed a network of intermeshed polymers which has been suggested to be capable of facilitating size-based macromolecule electrophoretic separations via sieving [30]. During the folding transition of a protein, the reduced form is converted to a distribution of rapidly interconverting conformations, some of which eventually may reach the compact and relatively fixed native state. At this time, the majority of these intermediate conformations are much more extended than the native conformation, but less extended than the reduced form. The order of migration of the native, reduced, and partially refolded trypsinogen appeared to correlate directly with the hydrodynamic radii of these species, as had been determined by studies employing SEC [21,22]. The viscosities of the phosphate buffer alone, the phosphate buffer with 5% glycerol, and the phosphate buffer with 5% PEG were determined

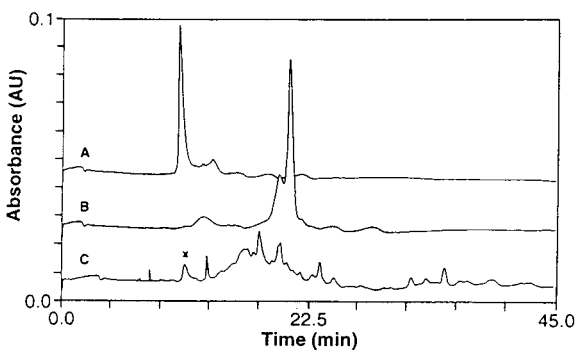

Fig. 2. Capillary electrophoretic separations of 10-s injections of 2 mg/ml samples of (A) native trypsinogen, (B) reduced trypsinogen and (C) 22-h refolded trypsinogen obtained using 25 m*M* sodium phosphate pH 2.0, 5% glycerine in a 37 cm, 50 μm bare silica capillary, 10 kV potential, and 200 nm detection. Refolded trypsinogen is marked by an "×".

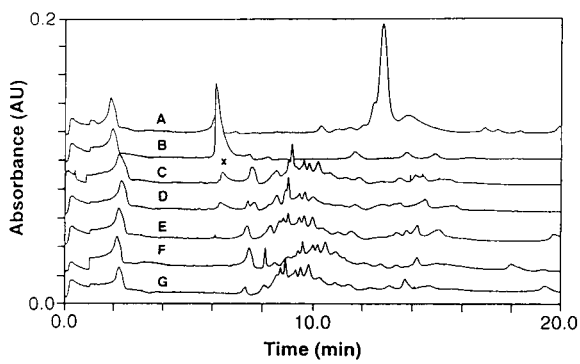

Fig. 3. Capillary electrophoretic separations of 15-s injections of 2 mg/ml samples of (A) reduced trypsinogen, (B) native trypsinogen, and (C) 22-h, (D) 7-h, (E) 1-h, (F) 30-min and (G) 10-min refolded trypsinogen obtained using 25 m*M* sodium phosphate pH 2.0, 5% PEG in a 37 cm, 50 μm bare silica capillary, 20 kV potential, and 200 nm detection. Refolded typsinogen is marked by an "×".

through the use of Poiseuille's law [31] and the CE instrument (the refractive index change occurring at the UV detector, zeroed *vs.* air, was used to measure the time required to pump buffer from the capillary inlet to the detector window) to equal 0.89, 1.01 and 4.60 cP, respectively (the viscosity of water at 25°C is 0.8904 cP [31]). From this data, it was not possible to determine whether viscosity effects or sieving, or a combination of the two, were responsible for the apparent size-based separation occurring in the buffer containing PEG.

Since Corbett and Roche [14] first demonstrated the displacement of sperm whale myoglobin toward shorter elution times following urea denaturation, SEC has been utilized to monitor the denaturation and refolding of a variety of proteins. Conformational changes in proteins are resolvable via SEC through changes in retention time, where distribution coefficients correlate with Stokes radii of protein conformers [14,32,33]. To compare high-performance SEC elution profiles of refolded trypsinogen with the CE electropherograms discussed earlier, acid-quenched refolded trypsinogen samples (50 μg/ml protein, 100-μl injections) were separated using a Superose 12 column and a mobile phase containing 100 m*M* acetic acid, 100 m*M* sodium chloride and 2 *M* urea at a flow-rate of 0.5 ml/min (absorbance monitored at 280 nm UV). The presence of urea was found to improve recovery of both the reduced protein and the partially refolded intermediates. Cysteine and cystine, two components present in the solutions of refolded material, appeared in the SEC chromatograms as large peaks appearing at *ca.* 35 min, following the elution of the trypsinogen conformers. The elution profiles displayed in Fig. 4 demonstrate the ability of the Superose packing to baseline resolve the native and reduced trypsinogen, and to provide partial resolution of the components present in the samples of refolded protein. Approximate quantitation of the material in the refolded samples demonstrated a 13% yield of completely refolded trypsinogen present after 22 h, in good agreement with both the activity assay and CE analysis.

A direct comparison of the SEC *vs.* CE analyses of refolded trypsinogen was achieved

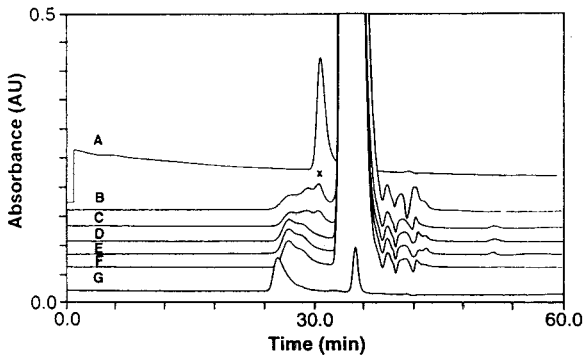

Fig. 4. SEC profiles of 50 μg/ml samples (100-μl injections) of (A) native trypsinogen, (B) 22-h, (C) 7-h, (D) 1-h, (E) 30-min, (F) 10-min refolded trypsinogen, and (G) reduced trypsinogen obtained via elution through a Superose 12 packing (30.0 × 1.0 cm) in the presence of 100 m*M* acetic acid pH 3.3, 100 m*M* sodium chloride, 2 *M* urea at a flow-rate of 0.5 ml/min monitored at 280 nm. Refolded trypsinogen is marked by an "×".

via isolation of the material corresponding to a 22-h refolded sample [concentrated 50-fold using a 150 ml OmegaCell 150 stir cell concentrator (Filtron, Northborough, MA, USA)] in four fractions (*ca.* 10 mg total protein collected), as indicated in Fig. 5a. The two later eluting peaks in the SEC profile were not fraction-collected, since they were determined to represent low-M_r components present in the fold solution (cysteine, cystine, urea, etc.). The fractions were dialyzed against 100 volumes of 1% acetic acid and then concentrated down to 1.0 ml final volume prior to analysis by CE. The CE buffer used for this study was 25 m*M* sodium phosphate pH 2.0, 5% PEG. The electropherograms of the SEC fractions displayed in Fig. 5b demonstrate, under these conditions, the dependence of protein electrophoretic migration time upon hydrodynamic volume. Refolded trypsinogen species appear to be present in fractions A–C (native trypsinogen is probably represented by the early-eluting peak in the electropherogram of fraction C), while the peaks generated by fraction D may represent peptides (from enzymatic degradation), or also cysteine or cystine.

High-performance ion-exchange chromatography has also demonstrated the ability to effect separations of various protein conformers under non-denaturing conditions [34–36]. The samples

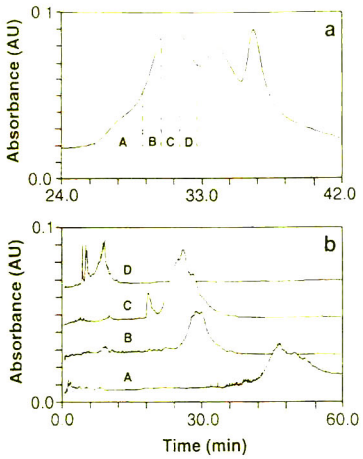

Fig. 5. (a) Fractionation of 0.5 mg of 22-h refolded trypsinogen, chromatographed using the conditions described in Fig. 4. (b) Capillary electrophoretic separations of 15-s injections of the dialyzed and concentrated SEC fractions (2.5 mg/ml final approximate total protein concentration) obtained using 25 m*M* sodium phosphate pH 2.0, 5% PEG in a 37 cm, 50 μm bare silica capillary, 10 kV potential, and 200 nm detection.

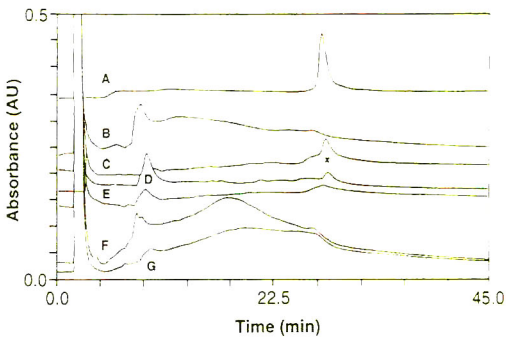

Fig. 6. Cation-exchange HPLC profiles of 50 μg/ml samples (100-μl injections) of (A) native trypsinogen, (B) reduced trypsinogen, (C) 22-h, (D) 7-h, (E) 1-h, (F) 30-min and (G) 10-min refolded trypsinogen obtained via elution through a Progel-TSK SP-5PW packing (7.5 × 0.75 cm) in the presence of 25 m*M* sodium acetate pH 4.0, 2 *M* urea, 20% acetonitrile and a 45 min 0.00–0.35 *M* sodium chloride gradient at a flow-rate of 1.0 ml/min monitored at 280 nm. Refolded trypsinogen is marked by an "×".

of refolded trypsinogen made for this study were separated using a Progel-TSK SP-5PW cation-exchange packing, a 25 m*M* sodium acetate pH 4.0, 2 *M* urea, 20% acetonitrile mobile phase with a 45-min linear gradient from 0 to 0.35 *M* NaCl, and a 1.0 ml/min flow-rate at ambient temperature. The presence of both the urea and acetonitrile was found to be necessary for the recovery of the reduced protein and the partially refolded intermediates. The separation profiles obtained under these conditions are presented in Fig. 6. The chromatograms reveal that the reduced protein elutes much earlier than the native conformer, suggesting that, in agreement with the CE results discussed earlier, reduced trypsinogen possesses significantly less basic character than does the native protein. The refolded samples appear in these separations as a distribution of components eluting between the reduced and native species. Quantitation of the peak co-eluting with the native protein (at *ca.* 29 min) indicated a 17% yield of completely refolded material in the 22-h sample.

Perhaps the technique most comparable to the use of viscous/sieving buffers employed in conjunction with CE for the separation of proteins is non-denaturing slab gel electrophoresis. Non-denaturing (native) gel electrophoresis has been successfully employed for the analysis of the conformations of proteins. Studies using non-denaturing gel electrophoresis have demonstrated that the reduction of the disulfide bonds in a protein lead to the formation of an extended unfolded conformation with reduced electrophoretic mobility [37,38]. Non-denaturing slab gel separations of the refolded trypsinogen samples generated for this study are displayed in Fig. 7. The outer lanes on both gels were loaded with a 2 mg/ml native trypsinogen standard, and the lanes adjacent with 2 mg/ml reduced protein. It was evident that the native conformer migrated much further through the gel matrix than did the reduced. A distribution of folding intermediates appeared as a stained haze migrating within the region between the native and reduced protein, and a band co-migrating with the native standard, probably representing completely refolded conformers, was visible in the lanes representing the 7- and 22-h folded samples. These observations correlated well with the CE and chromatography results discussed previously.

The majority of charged groups in native globular proteins, both acidic and basic, are

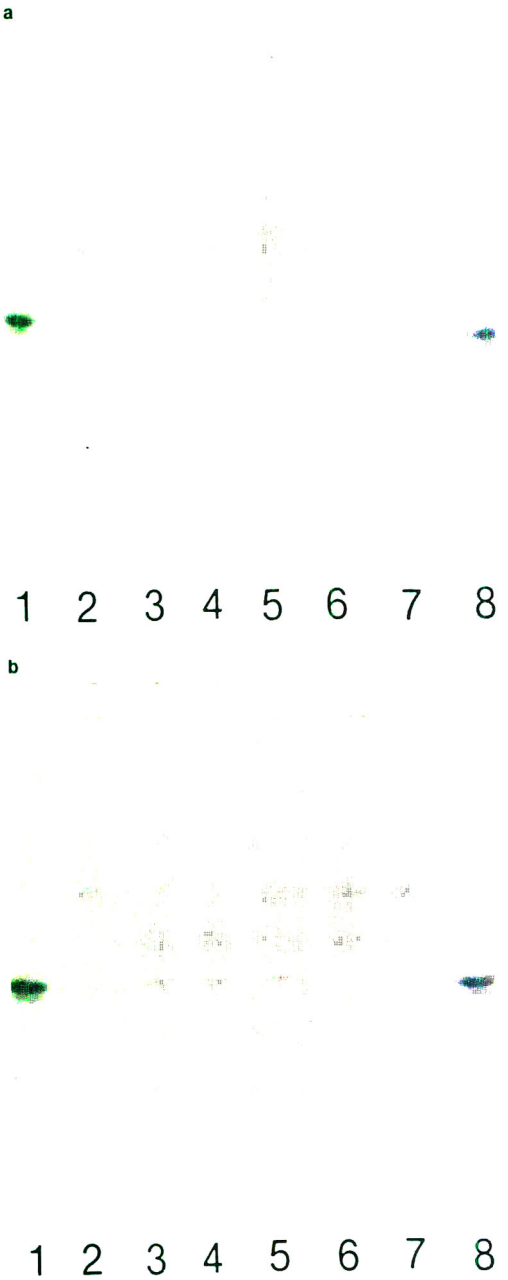

Fig. 7. Non-denaturing gel electrophoresis of samples (2 mg/ml, 1 μl loaded) of (lanes a1, a8, b1, b8) native trypsinogen; (a2, a7, b2, b7) reduced trypsinogen; (a6) 10-min refolded; (a5) 30-min refolded; (a4, b6) 1-h refolded; (a3, b5) 7-h refolded; (b3, b4) 22-h refolded trypsinogen obtained in Homogenous 20 PhastGels.

located on the surface of the molecules and are freely accessible to the solvent. However, some may be buried within the interior and only become accessible when the molecule is unfolded or denatured. In such cases the isoelectric point will then be altered as the protein is unfolded and these groups become exposed. Thus isoelec-

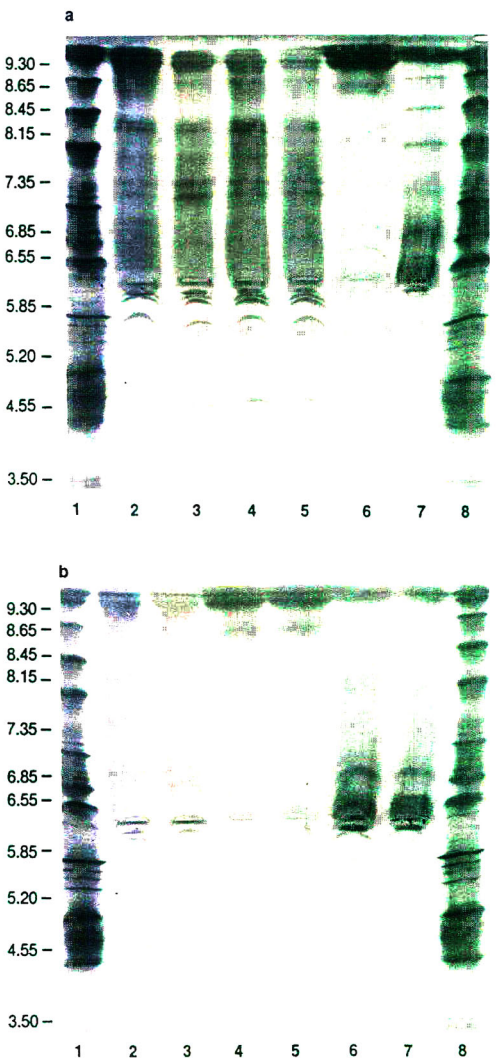

Fig. 8. Isoelectric focusing of samples (2 mg/ml, 1 μl loaded) of (lanes a1, a8, b1, b8) p*I* markers; (a7, b6, b7) reduced trypsinogen; (a6, b4, b5) native trypsinogen; (a5) 10-min refolded; (a4) 30-min refolded; (a3) 1-h refolded; (a2) 7-h refolded; (b2, b3) 22-h refolded trypsinogen obtained in PhastGel IEF 3–9 gels.

tric focusing (IEF), which is a highly sensitive technique in which changes in p*I* as small as 0.001 can be distinguished, can be used to study conformational changes [21,39–41]. The refolded trypsinogen samples of this study were analyzed by focusing on a p*I* 3–9 IEF PhastGel, and the results are presented in Fig. 8. Reduced trypsinogen (p*I* 6.5) was well resolved from native trypsinogen (p*I* 9.3). A dark well-focused band representative of the native species was evident at the top of the gels, its position aligning well with the trypsinogen present in the commercially available p*I* marker mixture. The minor bands observed in the native and reduced trypsinogen standards may represent impurities also observed in the CE electropherograms (see Figs. 1–3) (the reduced trypsinogen in Fig. 8a may also have been contaminated with the p*I* markers run in the adjacent lane). A number of components in the p*I* range of 6.5–9.3, and also several with p*I* values <6.0, were detected as the reduced trypsinogen underwent folding. A minor component focusing at p*I* ≈ 9 appeared in the reduced and early time point refolded samples, and perhaps corresponded to a contaminant possessing a p*I* ≥ 9; however, the bands focusing in this region darkened significantly as folding time increased, providing qualitative evidence for refolding of the protein to its native form.

CONCLUSIONS

By monitoring the re-oxidation of reduced bovine trypsinogen, CE proved to be an effective method capable of separating and quantitating native and reduced protein, and also intermediate conformations present during the refolding. The presence of components such as glycerine and PEG in the CE buffer was observed to facilitate size-based separations via viscosity and/or sieving effects. The progress curves for the regeneration of native trypsinogen calculated from four methods of analysis, enzyme activity, CE, SEC and cation-exchange HPLC, were in excellent agreement with one another, as displayed in Fig. 9. CE analyses also correlated well with qualitative separations obtained via non-denaturing gel electrophoresis and IEF. The results of this study suggest that

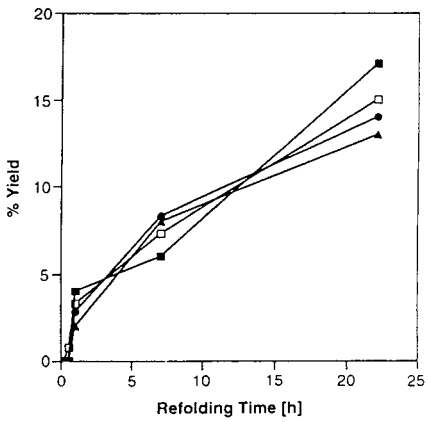

Fig. 9. Rate of appearance of refolded trypsinogen from analyses via (□) enzymatic activity following activation with trypsin, (▲) SEC, (■) cation-exchange HPLC, (●) CE in 25 m*M* sodium phosphate pH 2.0, 5% PEG.

CE can serve as a simple, rapid, and powerful analytical method capable of detecting and resolving changes in protein covalent structure. In this capacity, it may provide information crucial to the analysis of the protein folding process.

ACKNOWLEDGEMENTS

We wish to thank Mr. Doug Schmidt, Mr. Terry Stinger and Ms. Shelly Vanderstelt for their technical assistance.

REFERENCES

1 T.E. Creighton, *Proteins —Structure and Molecular Properties*, W.H. Freeman, New York, 1983.
2 A.M. Labhart, *Proc. Natl. Acad. Sci. U.S.A.*, 81 (1984) 7674.
3 T.Y. Tsong, R.I. Baldwin and P. McPhie, *J. Mol. Biol.*, 63 (1972) 453.
4 P.J. Hagerman and R.L. Baldwin, *Biochemistry*, 15 (1976) 1462.
5 A. Galat, C.C. Yang and E.R. Blout, *Biochemistry*, 24 (1985) 5678.
6 R.F. Kelley, J. Wilson, C. Bryant and E. Stellwagen, *Biochemistry*, 25 (1986) 728.
7 E.H. Zuniga and B.T. Nall, *Biochemistry*, 22 (1983) 1430.
8 D.N. Brems and R.L. Baldwin, *J. Mol. Biol.*, 180 (1984) 1141.
9 J.J. Osterhout, K. Muthukrishnan and B.T. Nall, *Biochemistry*, 24 (1985) 6680.

10 A.D. Blum, S.H. Smallcombe and R.L. Baldwin, *J. Mol. Biol.*, 118 (1978) 305.
11 D.P. Goldenburg and T.E. Creighton, *Anal. Biochem.*, 138 (1984) 1.
12 K.C. Ingham, T.T. Busby, D.H. Atha and H. Forastieri, *J. Liq. Chromatogr.*, 6 (1983) 229.
13 F.E. Regnier and K.M. Gooding, *Anal. Biochem.*, 103 (1980) 1.
14 R.J.T. Corbett and R.S. Roche, *Biochemistry*, 23 (1983) 79.
15 R.W. Stout, S.I. Sivakoff, R.D. Ricker and L.R. Snyder, *J. Chromatogr.*, 353 (1986) 439.
16 F.E. Regnier, *Anal. Biochem.*, 126 (1982) 1.
17 P. Strop and D. Cechova, *J. Chromatogr.*, 207 (1981) 55.
18 P. Strop, D. Cechova and V. Tomasek, *J. Chromatogr.*, 259 (1983) 255.
19 Y. Kato, T. Kitamura and T. Hashimoto, *J. Chromatogr.*, 266 (1983) 49.
20 R. Jaenicke and R. Rudolph, in T.E. Creighton (Editor), *Protein Structure: A Practical Approach*, IRL Press, Oxford, 1989, p. 191.
21 A. Light and J.N. Higaki, *Biochemistry*, 26 (1987) 5556.
22 A.M. Al-Obeidi and A. Light, *J. Biol. Chem.*, 263 (1988) 8642.
23 T.W. Odorzynski and A. Light, *J. Biol. Chem.*, 254 (1978) 4291.
24 B.C.W. Hummel, *Can. J. Biochem. Physiol.*, 37 (1959) 1393.
25 M. Lazdunski and M. Delaage, *Biochim. Biophys. Acta*, 140 (1967) 417.
26 N.M. Green and H. Neurath, in H. Neurath and K. Bailey (Editors), *The Proteins*, Vol. 2, Part B, Academic Press, New York, 1954, p. 1057.
27 J.S. Green and J.W. Jorgenson, *J. Chromatogr.*, 478 (1989) 63.
28 R.M. McCormick, *Anal. Chem.*, 60 (1988) 2322.
29 D.P. Goldenburg, in T.E. Creighton (Editor), *Protein Structure: A Practical Approach*, IRL Press, Oxford, 1989, p. 225.
30 M. Zhu, D.L. Hansen, S. Burd and F. Gannon, *J. Chromatogr.*, 480 (1989) 311.
31 R.C. Weast (Editor), *CRC Handbook of Chemistry and Physics*, CRC Press, Boca Raton, FL, 64th ed., 1984, p. F-36.
32 T. Imamura, K. Konishi and M. Yokoyama, *J. Liq. Chromatogr.*, 4 (1981) 613.
33 D.N. Brems, S.M. Plaisted, H.S. Havel, E.W. Kauffman, J.D. Stodola, L.C. Eaton and R.D. White, *Biochemistry*, 24 (1985) 7662.
34 E.S. Parente and D.B. Wetlaufer, *J. Chromatogr.*, 314 (1984) 337.
35 E.S. Parente and D.B. Wetlaufer, *J. Chromatogr.*, 288 (1984) 482.
36 J. Luiken, R. van der Zee and G.W. Welling, *J. Chromatogr.*, 284 (1984) 482.
37 T.E. Creighton, *J. Mol. Biol.*, 87 (1984) 579.
38 D.P. Goldenburg and T.E. Creighton, *J. Mol. Biol.*, 165 (1983) 407.
39 N. Ui, *Biochim. Biophys. Acta*, 229 (1971) 567.
40 N. Ui, *Ann. N.Y. Acad. Sci.*, 209 (1973) 198.
41 R.A. Stinson, *Biochem. J.*, 167 (1977) 65.

Journal of Chromatography A, 652 (1993) 189–198
Elsevier Science Publishers B.V., Amsterdam

CHROM. 25 154

High-performance capillary electrophoresis for the determination of trypsin and chymotrypsin inhibitors and their association with trypsin, chymotrypsin and monoclonal antibodies

Anne Marie Arentoft

Chemistry Department, Royal Veterinary and Agricultural University, 40 Thorvaldsensvej, DK-1871 Frederiksberg C (Denmark)

Hanne Frøkiær

Department of Biochemistry and Nutrition, Technical University of Denmark, Building 224, DK-2800 Lyngby (Denmark)

Søren Michaelsen

Department of Research in Fur Animals, National Institute of Animal Science, Research Centre Foulum, P.O. Box 39, DK-8830 Tjele (Denmark)

Hilmer Sørensen*

Chemistry Department, Royal Veterinary and Agricultural University, 40 Thorvaldsensvej, DK-1871 Frederiksberg C (Denmark)

Susanne Sørensen

Department of Biochemistry and Nutrition, Technical University of Denmark, Building 224, DK-2800 Lyngby (Denmark)

ABSTRACT

High-performance capillary electrophoresis (HPCE) was adapted for the determination of Kunitz soybean trypsin inhibitor, Bowman Birk inhibitor from soybean and protein-type proteinase inhibitors from pea (*Pisum sativum* L.). The method was developed for the determination and characterization of the inhibitors, the enzymes trypsin and chymotrypsin and the monoclonal antibodies (mAbs) raised against the inhibitors, and also the inhibitor–enzyme and inhibitor–mAb association complexes. The results from studies involving the use of various types of buffers revealed the advantages of having zwitterions such as trimethylammoniumpropyl sulphonate (AccuPure) or taurine included in the buffer. The use of capillaries dynamically coated with zwitterions efficiently reduced the interactions of the proteins with the silica capillary surface, which was important for the analyses for trypsin, chymotrypsin and mAbs and their association complexes with the inhibitors. The influence of temperature, voltage, pH and buffer type on migration times, resolution, peak areas and number of theoretical plates was investigated for the proteins studied. The proposed HPCE method is very suitable for studies of proteinase inhibitors compared with traditional inhibitor studies, and it gives efficient protein separations with the possibility of 245 000 plates/m.

* Corresponding author.

0021-9673/93/$06.00

INTRODUCTION

Trypsin (EC 3.4.21.4) and chymotrypsin (EC 3.4.21.1) are produced in the small intestine from the proenzymes synthesized in the pancreatic glands of animals. These digestive enzymes vary in structure and properties depending on the animal species producing them and on the age of the animals [1,2]. Protein-type inhibitors for both trypsin and chymotrypsin are widespread in plants, foods and feeds, and these inhibitors have attracted much interest as they are considered to be the cause of various nutritional problems, as reviewed in several papers [3–6]. Efficient analytical methods are needed for the determination of the inhibitors, and for this purpose monoclonal antibodies (mAbs) have been produced against the inhibitors Kunitz soybean trypsin inhibitor (KSTI), Bowman Birk inhibitor (BBI) and pea (*Pisum sativum* L.) protein-type proteinase inhibitor (PPI) [7]. Information on the structures and properties of the individual BBI, KSTI and PPI and their interactions with mAbs, trypsin and chymotrypsin requires special attention, which raises the need for analytical methods with the potential for high resolution of the individual proteins.

High-performance capillary electrophoresis (HPCE) has proved useful for the determination of various proteins [8,9], and this technique in various modifications has been used for studies of mAbs [10,11]. However, efficient separations of proteins in fused-silica capillaries can be hampered by adsorption of proteins on the capillary walls if the buffer pH is higher than about 3, resulting in band broadening, low resolution and low recovery of the proteins [12]. These complications are especially expected to create problems in unmodified capillaries with proteins having pI values higher than the buffer pH. Various methods have therefore been considered to counteract protein adsorption on the capillary wall, including capillary surface treatments, electrophoresis in buffers with pH > pI for the proteins and the use of buffers with pH < 3 [12,13]. The use of zwitterionic compounds in the HPCE buffers is another promising approach to solve the problems [13], as is the use of micellar electrokinetic capillary chromatography (MECC), introduced by Terabe *et al.* [14] in 1984. Studies of interactions between native proteins using MECC require, however, micelles formed from surfactants other than sodium dodecyl sulphate to avoid the possibilities of changed or limited binding between the proteins.

This study was aimed at developing HPCE methods for studies of the individual KSTI, BBI and PPI and their interaction or binding to trypsin or chymotrypsin and also the mAbs raised against these inhibitors. An efficient HPCE method based on MECC with cholate and buffers containing zwitterionic compounds was developed. The parameters studied include systematic evaluations of the effects of buffer pH, electrolyte and modifier concentrations, temperature and voltage on migration time, peak area, number of theoretical plates and resolution.

EXPERIMENTAL

Apparatus

The apparatus used was an ABI Model 270 A-HT capillary electrophoresis system (Applied Biosystems, Foster City, CA, USA) with a 760 mm × 0.05 mm I.D. fused-silica capillary. Detection was performed by on-column measurements of UV absorption at a position 530 mm from the injection end of the capillary. For data processing, a Shimadzu (Kyoto, Japan) Chromatopac C-R3A was used.

Samples and reagents

Bovine γ-globulin, Bowman Birk inhibitor (BBI) from soybean, Kunitz soybean trypsin inhibitor (Type I-S) (KSTI), porcine pancreas trypsin and bovine pancreas chymotrypsin were obtained from Sigma (St. Louis, MO, USA). Horseradish peroxidase (HRP) was purchased from Serva (Heidelberg, Germany) and β-lactoglobulin and α-lactalbumin (both from bovine milk) from BDH (Poole, UK). Proteinase inhibitors from pea and monoclonal antibodies raised against the inhibitors from pea and soybean were from the collection in this laboratory [7]. Trigonellinamide, disodium hydrogenphosphate, cholic acid and taurine (2-amino-

ethanesulphonic acid) were obtained from Sigma. Trimethylammoniumpropyl sulphonate (AccuPure Z1 Methyl reagent) was obtained from Waters (Milford, MA, USA). All chemicals were of analytical-reagent grade.

Procedure

All analyses with enzymes were made with solutions of enzymes in running buffer freshly prepared from standard solutions of enzymes in 1 m*M* HCl. The concentrations of the individual proteins ranged form 1 to 10 mg/ml.

Buffers with AccuPure as zwitterion contained 1 *M* AccuPure and 100 m*M* phosphate, with buffer of pH 7.0. Samples analysed with AccuPure as separation buffer were run at 10 kV and 28°C.

Other buffer solutions tested were based on phosphate, taurine and cholic acid with 1-propanol as modifier. The pH range tested was defined by considering the pK_a values of about 8.7 and 6.4 for taurine and cholic acid, respectively. The choice of buffers with cholate micelles was based on an interest in having solutions with positive effects on solubility and stability of the proteins, thus enhancing the possibility of binding reactions between proteins.

All buffers with taurine (50–300 m*M*) contained 35 m*M* cholate, which is well above the critical micelle concentration of cholate (*ca.* 10 m*M*). In addition, the buffers contained various amounts of sodium phosphate (25 and 100 m*M*) and 1-propanol (0–10%) as specified in the individual experiments. The samples were introduced from the positive end of the capillary by vacuum injection (1–3 s), resulting in injection volumes of a few nanolitres. Separations were performed at 30–40°C and 12–20 kV. On-column detection at 280 nm was applied. Standard conditions, while varying individual running parameters, were a temperature of 30°C, a voltage of 20 kV and electrolyte concentrations of 35 m*M* cholate and 100 m*M* sodium phosphate, a taurine concentration of 50 m*M* and a modifier concentration of 2% of 1-propanol. Buffer solutions were filtered through a 0.45-μm membrane filter before use.

The optimization of the MECC method for separation of proteins was performed using a mixture of proteins (HRP, γ-globulin, BBI, KSTI, β-lactoglobulin and α-lactalbumin). For the proteins run separately and for the binding studies, trigonellinamide was used as an internal standard. The protein mixture was dissolved in a buffer consisting of 50 m*M* phosphate, 35 m*M* cholate, 2% 1-propanol and 50 m*M* taurine (pH 8.7).

Calculations of relative migration time (*RMT*) and normalized peak area (*NA*) were performed according to the equations

$$RMT = MT_1/MT_2 \quad (1)$$

where MT_1 is the migration time of the actual protein and MT_2 that of α-lactalbumin, and

$$NA = A/MT \quad (2)$$

where A is the measured peak area. The number of theoretical plates (N) per metre of capillary and the resolution (R_s) was calculated as described elsewhere [15] with

$$N = 5.54(MT/\omega_{1/2})^2 \quad (3)$$

where $\omega_{1/2}$ is the peak width at half-height. To obtain the number of theoretical plates per metre of capillary, N is divided by the capillary length in metres from the injection end to the detector window. Washing with 0.1 *M* NaOH for 3 min and buffer for 5 min was performed between each analysis.

RESULTS AND DISCUSSION

Two separation systems with different zwitterions were investigated. The results obtained with AccuPure were comparable to those obtained with taurine as zwitterion. However, as taurine is much cheaper than AccuPure, the taurine system was used for optimization of the separation of proteins using zwitterions. Preliminary investigations with taurine buffers with and without cholate were performed, and it was decided to optimize on the system with cholate and taurine. As the critical micelle concentration of cholate (10 m*M*) was exceeded, the method presented is an MECC method.

The applied MECC method is based on the electrophoretic mobility of the analytes, elec-

troosmotic flow of the solvent and electrophoretic mobility of cholate micelles. The pH value of the applied buffer creates negatively charged silanol groups on the capillary wall. The positive ends of zwitterions compete with positively charged buffer ions and positively charged regions of macromolecules, thus preventing adsorption of proteins on the capillary wall. At the pH values applied, taurine is present as a zwitterion and therefore will not contribute to the conductivity of the operating buffer [13], whereas the cholate carboxylic acid group is present in its ionized form. Therefore, above the CMC there are possibilities of both ionic and hydrophobic interactions between cholate and proteins. Cholate in solution may be associated with hydrophobic protein domains adding negative charges to the molecules or by ion pairing with hydrophilic areas of the proteins adding hydrophobic groups to the proteins. The addition of negative charges on the proteins will both stabilize the molecules in the solution and reduce the possibilities of adsorption on the capillary wall.

Negatively charged cholate micelles move towards the anode in the opposite direction to the electroosmotic flow. With injection at the anode of negatively charged proteins the electroosmotic flow will be responsible for the migration of the proteins towards the cathode. Proteins with positive charges will be retarded by interaction with negatively charged cholate micelles or with the non-micellar associated free cholate in solution.

Modifications of the MECC method conditions implied changes of temperature, pH, voltage and composition of the buffer, including concentrations of phosphate and zwitterions.

The optimization studies consisted in the electrophoresis of several commercially available proteins with p*I* values from 4.5 to 9.5 and molecular masses from 8000 to 160 000.

Temperature

The influence of temperature was tested with a buffer of pH 8.0. Shorter migration times were seen with increasing temperature (Fig. 1), in agreement with the simultaneous decreases in the viscosity of the solvent in the capillary. The decrease in viscosity was also reflected by an

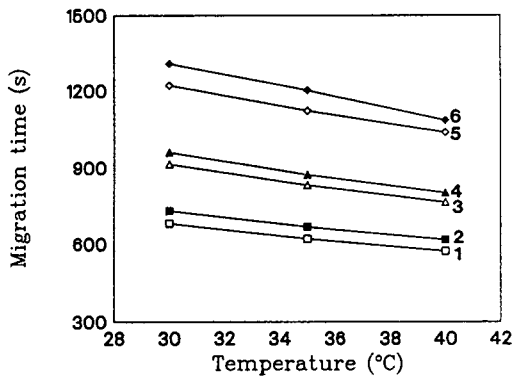

Fig. 1. Influence of temperature on migration times of proteins. Conditions: buffer, 35 m*M* cholate–100 m*M* phosphate–50 m*M* taurine (pH 8.0); voltage 20 kV; total length of capillary, 760 nm; length from injection end to detection, 530 mm; detection wavelength, 280 nm; vacuum injection for 1 s. 1 = HRP; 2 = γ-globulin; 3 = BBI; 4 = KSTI; 5 = β-lactoglobulin; 6 = α-lactalbumin.

increased current intensity. *RMT* values calculated relative to α-lactalbumin were almost unchanged from 30 to 40°C.

The *NA* values were not markedly affected by changes in temperature form 30 to 35°C, whereas a change from 35 to 40°C had different effects on the proteins present in the standard analyte solution. Corrections of peak areas (*NA*) were performed to eliminate the influence of alterations in migration time. However, under the present conditions, the corrections for changes in migration times were insufficient to keep the *NA* values constant for all of the proteins tested.

Increasing the temperature mainly affected the resolution of the proteins with the longest migration times, thus revealing several peaks originating from different proteins within the commercially available β-lactoglobulin and α-lactalbumin. The additional peaks are not believed to be a result of thermal denaturation at the applied electrolyte concentration, voltage and temperature. However, the improvement in peak separation at increased temperature was accompanied by reduced migration times, resulting in less space for baseline separations of proteins with closely related structures.

These conflicting effects are probably able to account for the different effects on the *N* values observed for the individual proteins when

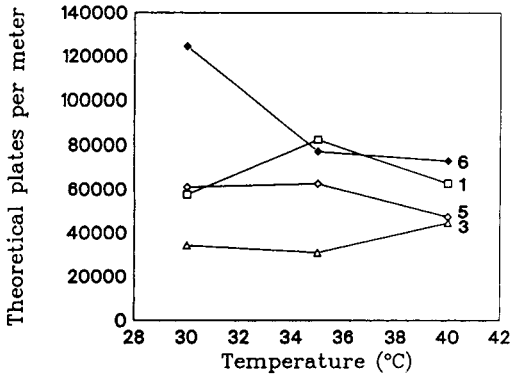

Fig. 2. Influence of temperature on theoretical plate number per metre of capillary. Numbers and other separation conditions as in Fig. 1.

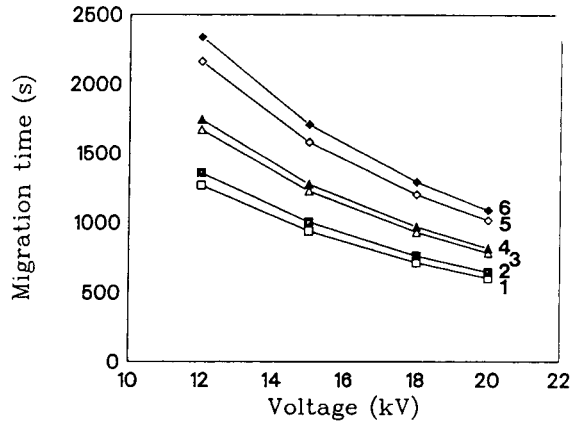

Fig. 3. Influence of voltage on migration times of proteins. Buffer pH, 8.7; temperature, 30°C. Numbers and other separation conditions as in Fig. 1.

changes in temperature were investigated, as illustrated in Fig. 2. The electropherograms forming the basis for the results presented in Fig. 2 were obtained using an injection time of 1 s in order to obtain a large number of theoretical plates. To evaluate the relative standard deviation, the analysis was also performed in triplicate with an injection time of 3 s. This resulted in relative standard deviations of 1–10% of the number of theoretical plates. With respect to migration time, the relative standard deviations were 0.2–0.8% with an injection time of 3 s.

Voltage

An increase in applied voltage resulted in a decrease in migration time, as illustrated in Fig. 3. The decreases were largest for compounds having long migration times, resulting in a considerable decrease in the total time of analysis at high voltage.

RMT values calculated relative to α-lactalbumin remained constant, whereas an increase in applied voltage had different effects on the *NA* values, with unchanged or decreasing *NA* values depending on the proteins in question. These differences could be due to the presence of several closely related proteins with overlapped peaks or to changing response factors of the proteins.

The *N* values were not greatly affected by an increase in applied voltage, although an increased field strength should lead to improved separation efficiency according to the theory of HPCE. This may be explained by limited removal of the developed heat, thus resulting in band broadening and less sharp peak profiles due to temperature increases in the capillary [8,16]. For α-lactalbumin an increase in *N* values was observed with increase in applied voltage, indicating less influence of increased temperature on band broadening for this protein.

pH

Changes in pH values were examined for a buffer containing 50 m*M* taurine. Changing the pH from 7.5 to 8.7 resulted in slightly lower migration times. This could be due to an increase in the electroosmotic flow because more of the surface silanols are ionized at pH 8.7 [13]. The *RMT* values (calculated relative to α-lactalbumin) remained constant. The *NA* values were not affected, except for α-lactalbumin, which showed a considerable decrease in *NA* values at pH 8.7, as demonstrated in Fig. 4.

Increased pH values also resulted in a large increase in *N* for α-lactalbumin. HRP and BBI showed minor decreases in *N* values, whereas the *N* values for the other proteins were less affected by changes in pH.

Electrolyte concentration

The effects of changes in the concentrations of cholate and phosphate ions in the running buffer

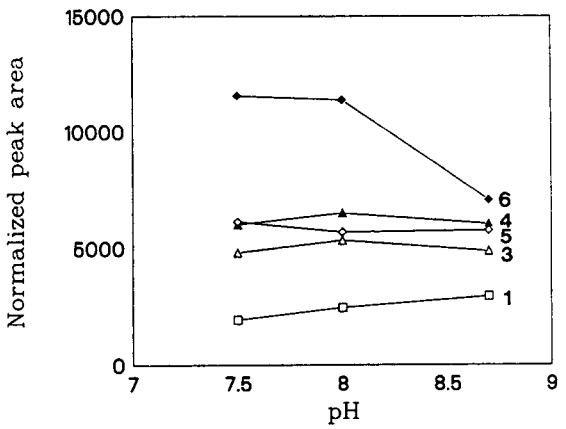

Fig. 4. Influence of buffer pH on normalized peak area. Temperature, 30°C. Numbers and other separation conditions as in Fig. 1.

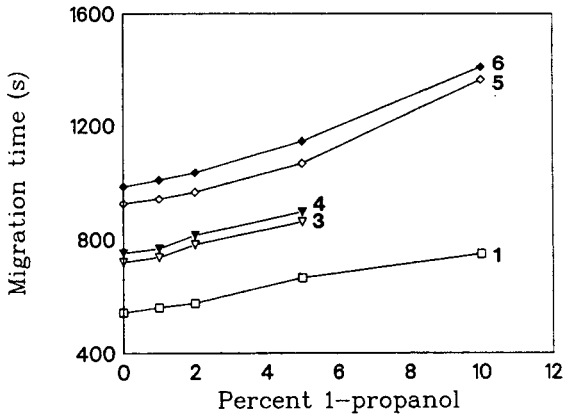

Fig. 5. Influence of 1-propanol concentration on migration time. Buffer pH, 8.7; temperature, 30°C. Numbers and other separation conditions as in Fig. 1.

were examined for a buffer containing 25 m*M* phosphate and 35 m*M* cholate and a buffer consisting of 100 m*M* phosphate and 35 m*M* cholate. With the electrolyte concentration in the latter buffer, the migration times and peak resolutions were appreciably improved and, therefore, this buffer was used in further analyses.

The zeta potential decreases with increasing electrolyte concentration, affecting the electroosmotic flow. The improved results with high electrolyte concentration could be explained by an increase in current followed by heat deposition, thus resulting in lower viscosity and shorter migration times for the proteins at high electrolyte concentrations. Moreover, a higher electrolyte concentration may result in a high degree of competition of electrolytes with proteins in the binding to the capillary wall dynamically coated with taurine.

Modifier concentration

The migration times increased with addition of 1-propanol to the running buffer (Fig. 5). The current decreased markedly at high concentrations of 1-propanol, which indicated a decreased electroosmotic flow. This explains the increased migration times seen on going from 0 to 10% of 1-propanol.

The *NA* values were essentially similar for 1 and 2% of 1-propanol added, whereas 5% of 1-propanol resulted in slight decreases in *NA* values.

No effects on *N* values were observed for KSTI and BBI, whereas the number of theoretical plates per metre of capillary for HRP, β-lactoglobulin and α-lactalbumin generally increased with the addition of up to 5% of 1-propanol and then decreased at 10% of 1-propanol (Fig. 6). As in Fig. 2, injection times of 1 s were used, resulting in high relative standard deviations.

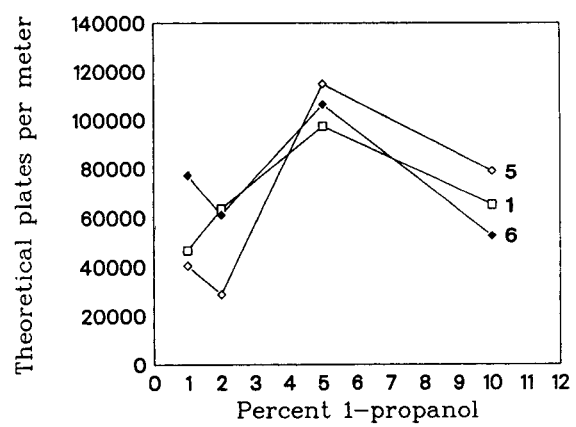

Fig. 6. Influence of 1-propanol concentration on theoretical plate number per metre of capillary. Buffer pH, 8.7; temperature, 30°C. Numbers and other separation conditions as in Fig. 1.

Taurine concentration

The influence of taurine concentration on the HPCE separation was examined for 50, 100 and 300 m*M* taurine. Slightly shorter migration times were seen with increasing taurine concentration. With respect to *NA* values the influence of taurine concentration showed individual effects on the examined proteins, as illustrated in Fig. 7.

The different behaviour of the proteins was also reflected by the influence on the theoretical plate number as some proteins were unaffected of changes in taurine concentration (γ-globulin, KSTI and BBI), whereas the others showed slightly increased *N* values with increasing taurine concentration.

Resolution (R_s) and N

The mixture of proteins used for optimization of the method did not consist solely of the proteins mentioned, as various other proteins were present in the commercially available proteins used in the standard mixtures. The results for *NA* and *N* values were therefore not as simple to interpret as when the individual proteins were analysed separately. As a consequence, the baseline separation was poorer and the normalized areas of the peaks were greater than those found for samples containing only a few proteins.

From the optimization investigations of the developed MECC method, some of the most relevant parameters were investigated for the individual proteins. Changes in voltage from 12 to 20 kV did not have a negative effect on *N* values, and 20 kV was chosen because of the reduced migration times obtained with this voltage. A buffer pH of 8.7 was chosen as increasing pH values resulted in a decrease in *MT* and a higher *N* value for α-lactalbumin. In Fig. 8 selected electropherograms of proteins from the standard analyte solution are shown. The presence of two peaks for β-lactoglobulin is probably due to the presence of both β-lactoglobulin A and B. Table I lists the *N* and R_s values obtained

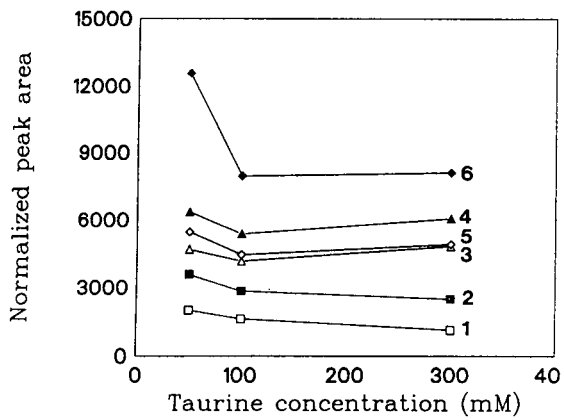

Fig. 7. Influence of taurine concentration on normalized peak area. Temperature, 30°C. Numbers and other separation conditions as in Fig. 1.

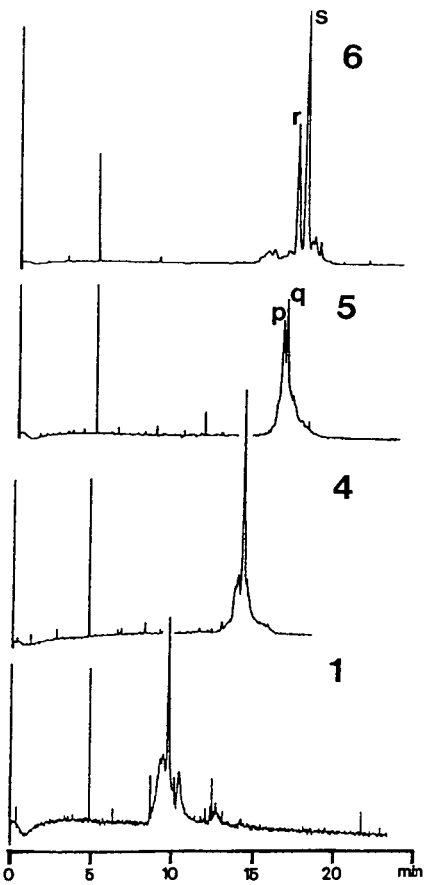

Fig. 8. Electropherograms of (1) horseradish peroxidase, (4) Kunitz soybean trypsin inhibitor, (5) β-lactoglobulin and (6) α-lactalbumin. Separation conditions as in Fig. 1 with buffer pH 8.7 and temperature 30°C; detection at 280 nm. For identification of peaks p, q, r and s, see Table I.

TABLE I

NUMBER OF THEORETICAL PLATES (N) PER METRE OF CAPILLARY AND RESOLUTION (R_s) FOR STANDARD ANALYTE PROTEINS UNDER DIFFERENT SEPARATION CONDITIONS

Conditions: all buffers contained 35 mM cholate and 100 mM phosphate in addition to the amounts of zwitterion and modifier indicated. Voltage, 20 kV; 1 s injection.

Protein		Zwitterion modifier and temperature					
		50 mM taurine, 2% 1-propanol, 30°C		300 mM taurine, 5% 1-propanol, 30°C		300 mM taurine, 5% 1-propanol, 35°C	
		N (m^{-1})	R_s	N (m^{-1})	R_s	N (m^{-1})	R_s
Horseradish peroxidase		46 830	–	116 521	–	136 478	–
Bowman birk inhibitor		75 974	–	114 107	–	129 254	–
Kunitz soybean trypin inhibitor[a]		96 396	–	136 544	–	36 285	–
β-Lactoglobulin[b]	p	59 219	0.64	113 275	1.15	36 285	0.76
	q	82 591		245 581		101 802	
α-Lactalbumin[b]	r	99 457	1.03	144 787	2.24	151 800	2.19
	s	104 936		151 713		149 751	
PPI[c]	t	208 781	0.66	392 779	1.03	376 519	0.68
	u	163 211		161 583		182 569	

[a] Electrophoresis of KSTI in the buffer with 300 mM taurine resulted in broad peaks around the main peak from KSTI which especially at 35°C strongly affected the N values.
[b] Peak letters as in Fig. 8.
[c] Two adjacent peaks (t and u) of several present in the electropherogram were chosen for the calculations.

with proteins run under different conditions in the developed MECC method.

It can be seen from Table I that the combination of 300 mM taurine with 5% of 1-propanol at 30°C resulted in the largest number of theoretical plates per metre of capillary and also the best resolutions between proteins. However, for KSTI the buffers with 300 mM taurine and 5% of 1-propanol resulted in considerable broadening at the peak base, although this phenomenon was not reflected in the N values, as there was no peak broadening at the peak half-height. Because of the undesirable peak broadening, the buffer containing 50 mM taurine was chosen for the binding studies.

Applications

The method described was applied to investigations of binding between inhibitors and enzymes and binding between inhibitors and antibodies, under conditions where all the investigated proteins were able to preserve their native structures and properties.

Fig. 9 shows electropherograms of trypsin, the proteinase inhibitors KSTI and BBI and monoclonal antibodies produced against these inhibitors, and also mixtures of inhibitors and antibodies or trypsin. Complexes between antibody and antigen in solution are believed to form rapidly (less than 30 s) and to be tightly bound [9]. From the sequence of electropherograms in Fig. 9A–C it appears that the migration time of the monoclonal antibody complex (C) was increased compared with the monoclonal antibody alone (A) as a result of binding between KSTI (B) and the monoclonal antibody produced against KSTI. In Fig. 9C the molar ratio of KSTI to antibody was 25:1 and therefore, as expected, all of the antibody seems to have formed a complex with KSTI, and a peak of unbound KSTI is present. Similarly, the binding of BBI (H) to a monoclonal antibody produced against BBI (G) resulted in a splitting

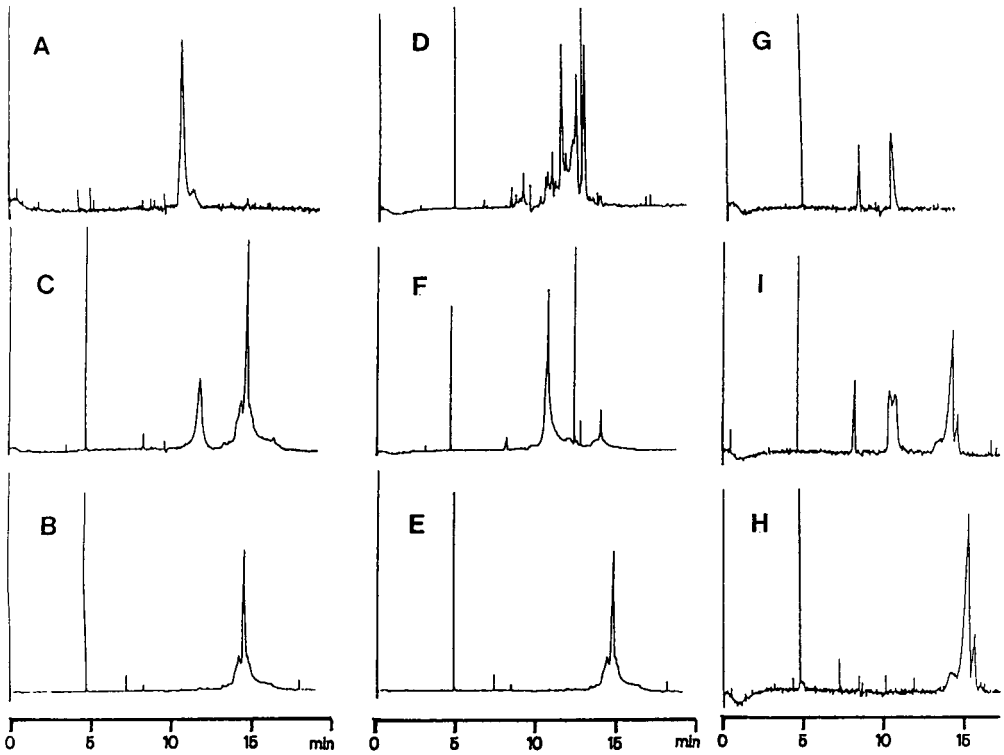

Fig. 9. Electropherograms obtained using buffer containing 50 m*M* taurine, 35 m*M* cholate, 100 m*M* phosphate and 2% 1-propanol at 20 kV, 30°C. Other conditions as in Fig. 8. (A) Monoclonal antibody against KSTI; (B) KSTI; (C) mixture of KSTI and monoclonal antibody against KSTI; (D) trypsin; (E) KSTI; (F) mixture of trypsin and KSTI; (G) monoclonal antibody against BBI; (H) BBI; (I) mixture of BBI and monoclonal antibody against BBI. The electropherograms were aligned according to the migration time of the internal standard, trigonellinamide (very sharp peak at *ca.* 5 min).

of the antibody peak (I), probably caused by the complex formation with BBI. Again, the molar ratio of antibody to inhibitor was 1:25 in the mixture, thus accounting for the presence of unbound BBI. The splitting of the antibody peak could be due to the presence of antibody with low or lost affinity for BBI, *e.g.*, caused by partial denaturation of the antibody during the purification steps. In the electropherograms in Fig. 9G and I the peaks at *ca.* 8 min. represent water from the samples. Other samples were dissolved in running buffer containing 50 m*M* phosphate.

An equimolar mixture of trypsin (D) with KSTI (E) also resulted in visible changes in the electropherogram of the mixture (F), indicating that binding between inhibitor and enzyme had occcurred. The presence of multiple peaks in the electropherogram of trypsin is probably due to several trypsin isoenzymes. In Fig. 9F only a complex peak and a small peak of residual KSTI appear, indicating that all isoenzymes present in D were able to form complexes with KSTI. Trypsin and KSTI have approximately equal molecular masses and the electrophoretic characteristics of KSTI therefore have a more pronounced influence on the electrophoretic mobility of the complex compared with the influence of KSTI on the complex of antibody and KSTI as the molecular mass of KSTI comprises only 13% of the antibody molecular mass. Similar results (not shown) were obtained with mixtures of BBI with trypsin and chymotrypsin and with mixtures of PPI and trypsin. With the chosen MECC system, the chymotrypsin and trypin electropherograms showed peaks with up to 250 000

and 91 000 theoretical plates per metre of capillary, respectively.

CONCLUSIONS

The optimum conditions for the separation of specific proteins vary with respect to especially taurine and 1-propanol concentrations.

With the applied MECC method it is possible to analyse mixtures of proteins with a wide range of p*I* values. The system allows the use of pH values below the p*I* values of proteins such as chymotrypsin and trypsin. Thereby, it is possible to study the complexes with enzyme inhibitors at the pH optimum of the enzymes. With respect to the antigen–antibody complexes the applied MECC method makes it possible physically to separate antibody–antigen complexes from unreacted reagents in non-denaturing environments. This gives the opportunity to prevent the problems associated with solid-phase immunoassays. The use of an internal standard (*e.g.*, trigonellinamide) gives the possibility of a relative determination of the amount of inhibitor before and after complex formation, thus giving information on, *e.g.*, which of several isoinhibitors have taken part in the complex formation.

ACKNOWLEDGEMENTS

The authors gratefully acknowledge support from the Danish Agricultural and Veterinary Research Council and the Danish Natural Research Council.

REFERENCES

1 A.M. Arentoft, K. Mortensen and H. Sørensen, *Aspects Appl. Biol.*, 27 (1991) 211.
2 P.T. Sangild, P.D. Grandwell, H. Sørensen, K. Mortensen, O. Noren, L. Wetterberg and H. Sjöström, in M.W.A. Verstegen, J. Huisman, L.A. van Hartog (Editors), *Proceedings of Vth Congress on Digestive Physiology in Pigs, Wageningen, April 1991*, Pudoc, Wageningen, 1991, p. 73.
3 M. Laskowski, Jr., and I. Kato, *Annu. Rev. Biochem.*, 49 (1980) 593.
4 I.E. Liener and M.L. Kakade, in I.E. Liener (Editor), *Toxic Constituents of Plant Foodstuffs*, Academic Press, New York, 2nd ed., 1980, p. 50.
5 Y. Birk, in A. Neuberger and K. Brocklehurst (Editors), *Hydrolytic Enzymes*, Elsevier, Amsterdam, 1987, p. 257.
6 H.-D. Belitz and J.K.P. Weder, *Food Rev. Int.*, 6 (1990) 151.
7 A.M. Arentoft, H. Frøkiær, H. Sørensen and S. Sørensen, in P. Plancquaert (Editor), *Proceedings of 1st European Conference on Grain Legumes, Angers, France, June 1992*, Edition Soft Publicité, Reims, 1992, p. 395.
8 B.L. Karger, A.S. Cohen and A. Guttman, *J. Chromatogr.*, 492 (1989) 585.
9 P.D. Grossman, J.C. Colburn and H.H. Lauer, *Anal. Chem.*, 61 (1989) 1186.
10 B.J. Compton, *J. Chromatogr.*, 559 (1991) 357.
11 S.J. Harrington, R. Varro and T.M. Li, *J. Chromatogr.*, 559 (1991) 385.
12 W. Nashabeh and Z.E. Rassi, *J. Chromatogr.*, 559 (1991) 367.
13 M.M. Bushey and J.W. Jorgenson, *J. Chromatogr.*, 480 (1989) 301.
14 S. Terabe, K. Otsuka, K. Ichikawa, A. Tsuchiya and T. Anto, *Anal. Chem.*, 56 (1984) 111.
15 S. Michaelsen, P. Møller and H. Sørensen, *J. Chromatogr.*, 608 (1992) 363.
16 J.W. Jorgenson and K.C. Lukacs, *Anal. Chem.*, 53 (1981) 1298.

Journal of Chromatography A, 652 (1993) 199–205
Elsevier Science Publishers B.V., Amsterdam

CHROM. 25 177

Characterization by capillary electrophoresis of the surface glycoproteins of ovine lentiviruses before and after treatment with glycosidic enzymes

Mary Jo Schmerr* and Kathryn R. Goodwin

National Animal Disease Center, USDA, Agricultural Research Service, 2300 Dayton Road, Ames, IA 50010 (USA)

ABSTRACT

Ovine lentiviruses are a group of viruses that infect sheep and goats. These viruses contain a surface glycoprotein (SU) that is very similar among the viral strains. Sera from infected animals react equally well with SU from each strain. Monoclonal antibodies produced to SU can distinguish among some of the viral strains. In order to delineate these differences we treated SU from several viral strains with the glycosidic enzymes. These enzymes included a mixture of exoglycosidases, β-N-acetyl glucosaminidase, neuraminidase and endoglycosidases D, F and H. After these treatments we observed changes in the reactivities of the monoclonal antibodies that were directed to SU. In order to characterize these changes on the surface epitopes, SU from the different viral strains were subjected to free zone capillary electrophoresis (CZE) using an 0.02 *M* phosphate buffer at pH 9.0 at a running voltage of 5 kV. Differences were readily seen between SU that had not been treated and SU that had been treated with the glycosidic enzymes. Each viral strain had a characteristic electropherogram. The electropherograms indicated that the heterogeneity of the charge on SU was increased after the enzyme treatments. From these results we have concluded that the carbohydrate moieties play an important role in contributing to the surface charge of SU. This charge affects the nature of its surface epitopes and has an impact on its biological function.

INTRODUCTION

Ovine lentiviruses belong to a family of retroviruses that infect sheep and goats and cause disease affecting multiple systems. The prototype virus, maedi-visna, was first isolated in Iceland in the 1950s [1,2]. Since this time, several additional strains of ovine progressive pneumonia virus (OPPV) have been isolated [3–5]. In cell culture these strains show characteristic differences [6–9]. Except for the nucleic acid sequence of a few of these viruses [10–12], structural properties that may cause these strain differences have not be explored. Advances in the adaptation of high-performance capillary electrophoresis for proteins point to this technique as an efficient analytical tool to observe differences in protein structures [13–16]. We chose this technique to observe changes that occur on the surface glycoprotein (SU) of ovine lentiviruses, after treatment with glycosidic enzymes. This glycoprotein plays an important role in the interaction of the host cell with the virus. Recently, the role that carbohydrate moieties play in immunogenicity and pathogenicity for lentiviruses in general (this family includes the human immunodeficiency virus, HIV) has taken on more significance. Hansen *et al.* [17] have shown that peripheral glycosylation of the surface glycoprotein of HIV may be a target for virus neutralization and, more recently, that monoclonal antibodies to carbohydrate epitopes of gp120 of HIV inhibit infection of lymphocytes [18]. Benjouad *et al.* [19] have suggested that carbohydrate moieties can modulate the specificity of the antibody response to the important V3 loop region of HIV. In other experiments, cell specific

* Corresponding author.

0021-9673/93/$06.00

glycosylation determined whether a strain of feline immunodeficiency virus was cytopathic or non-cytopathic [20]. In earlier work on caprine arthritis encephalitis virus (CAEV) Huso *et al.* [21] found that sialylation of CAEV made it resistant to degradation by proteolytic enzymes. The cross-reactivity that has been shown among lentiviruses, specifically equine infectious anemia virus reactivity with HIV antisera, is due to reaction with similar carbohydrate moieties [22]. We have found that treatment of SU from the ovine lentiviruses with glycosidic enzymes will reduce or cause a loss of the reactivity for some of the monoclonal antibodies produced to SU. In this study, we investigated differences in glycoproteins from different viral strains and changes both in antigenicity and in the electrophoretic mobility of SU after treatment with glycosidic enzymes.

MATERIALS AND METHODS[a]

Purification of the surface glycoprotein (SU)

Ovine fetal lung cells that had been persistently infected with a strain of an ovine lentivirus were grown for 2 weeks in Eagles's minimal media containing 10% ovine serum. The ovine lentiviral strains in this study were WLC-1, Visna, Howard and Runk. A caprine lentivirus, CAEV was also included. Each of the strains was cultured as above and then processed in the same manner. Culture fluids were harvested and precipitated with 50% saturated ammonium sulfate. The precipitates were harvested by centrifugation, resuspended, and dialyzed against 0.05 *M* sodium phosphate containing 0.15 *M* NaCl, pH 7.0 (phosphate-buffered saline, PBS). After dialysis, the concentrated culture fluids were placed over a lentil lectin Sepharose 4B column (Pharmacia LKB Biotechnology, Uppsala, Sweden). The column was washed with PBS and the glycoproteins eluted with 0.5 *M* α-D-methylmannoside in PBS. The eluted glycoproteins were precipitated with 50% saturated ammonium sulfate. The samples were dialyzed against PBS and placed on a protein G-Sepharose column to remove contaminating immunoglobulins. Chromatography was performed using the methods specified by the manufacturer (Pharmacia LKB Biotechnology). SU did not bind to this column. The unbound fractions were concentrated as above. When SU is prepared in this way, one diffuse band is observed on sodium dodecyl sulfate–polyacrylamide gel electrophoresis.

Enzyme treatments

The protein concentration of each of the glycoproteins from the different strains was determined [23] and made equivalent to 1.92 mg/ml. SU was dialyzed against 0.2 *M* phosphate–citrate buffer pH 5.5. After dialysis, SU was centrifuged to remove particulates. Exoglycosidases (*T. cornutus*, a mixture of several glycosidases, ICN, Costa Mesa, CA, USA) were used in a ratio of 1:1 (w/w) to SU at 37°C for 16 h. Neuraminidase was used in a ratio of 0.05 U/380 μg of glycoprotein and β-N-acetyl glucosaminidase, 0.06U/380 μg of glycoprotein. The above enzymes were obtained from Sigma (St. Louis, MO, USA). SU was incubated with each of these enzyme alones at 37°C for 16 h. In another experiment, SU was pretreated with neuraminidase for 4 h before the addition of the enzyme β-N-acetyl glucosaminidase. Those samples that were to be tested by radioimmunoassay were diluted 1/100 before enzymatic treatments. Those tested by capillary electrophoresis were not diluted further. When the detector was set at 214 nm *ca.* 60 ng were injected into the capillary. At 200 nm *ca.* 35 ng were injected into the capillary.

Capillary electrophoresis

Capillary electrophoresis was performed on a P/ACE system Model 2050 (Beckman, Fullerton, CA, USA) controlled by the System Gold software (Beckman). UV Absorbance was monitored by a fixed-wavelength detector at either 214 or 200 nm. The capillary was 57 cm long ×

[a] *Disclaimer:* No endorsements are herein implied. Brand names are necessary to report factually on available data; however, the USDA neither guarantees nor warrants the standards of the products, and the use of the names by the USDA implies no approval of the products to the exclusion of others that may also be suitable.

75 μm I.D. Two buffers and two different voltages were tried to establish conditions for separation of the glycoprotein. The buffer systems that were used were: 0.02 *M* phosphate buffer at two different pH values, 9.0 and 7.0, and 0.1 *M* sodium borate pH 8.5. The separating voltages of 5 kV and 10 kV were used. The separating buffer that was selected was 0.02 *M* phosphate buffer, pH 9.0 with a separating voltage of 5 kV at 25°C. When the detector was set at 214 nm the sample was injected by pressure for 5 s and at 200 nm, for 3 s. Electropherograms were produced for the glycoproteins from each of five different strains of the virus and for each of the enzyme treatments of each viral glycoprotein.

Solid-phase radioimmunoassay

Monoclonal antibodies had been previously produced to the purified SU. Each monoclonal antibody was purified by Protein G-Sepharose chromatography using the methods specified by the manufacturer. (Pharmacia LKB Biotechnology). The purified monoclonal antibody was iodinated using I-o-do-Gen (Pierce, Rockford, IL, USA) [24]. The solid-phase radioimmunoassay used was a modification of the procedure of Srikumaran *et al.* [25]. Briefly, 100 μl (*ca.* 2 μg) of the samples including the enzyme treated glycoprotein was adhered to the plates at 37°C for 2 h. After incubation, the plates were washed five times with a buffer containing 4 m*M* KCl, 140 m*M* NaCl, 1.5 m*M* KH_2PO_4 and 6 m*M* Na_2HPO_4, pH 7.3 and 1.0% bovine serum albumin. Approximately 100 000 cpm of the ^{125}I monoclonal antibody were added to the plate. The plate was incubated at 37°C for 2 h and then at 4°C overnight. The plates were washed as above, and the individual wells cut out and counted in a gamma counter. Two representative monoclonal antibodies, were chosen for this assay, one (9H4) that reacts specifically with the viral strains WLC-1, Visna and CAEV and another (10C10) that reacts with Howard and Runk. After subtracting the background cpm from both the sample cpm and total cpm the loss of activity and the % enhancement were calculated as follows:

$$\% \text{ loss of activity} = 100 \times \frac{\text{total cpm bound} - \text{sample cpm}}{\text{total cpm bound}}$$

$$\% \text{ enhancement} = 100 \times \frac{\text{sample cpm}}{\text{total cpm bound}}$$

The error in this assay was ±7.0%. The results obtained in these assays have been reproduced at least three times.

RESULTS

Profiles of SU run with phosphate buffer and borate buffer at 10 kV are shown in Fig. 1a. A lower voltage of 5 kV was used with these buffers (Fig. 1b). The wavelength at 200 nm was used with the phosphate buffer system at this voltage as well (Fig. 1b). At this wavelength (200 nm) an increase in sensitivity of *ca.* 2.5-fold was observed. These profiles were reproducible from capillary to capillary and from different preparations of SU.

Profiles of the enzymes, neuraminidase and β-N-acetyl glucosaminidase, that were used to treat the glycoproteins are shown in Fig. 2a and b. Little or no absorbance was observed for

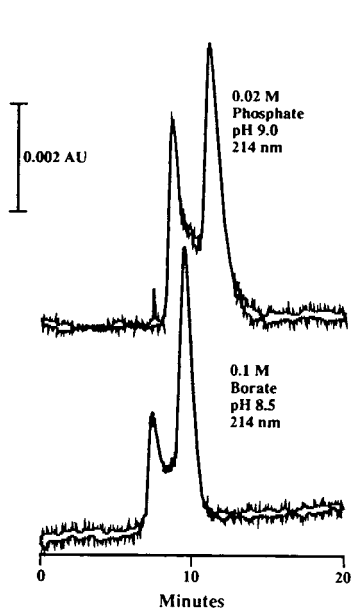

Fig. 1.

(Continued on p. 202)

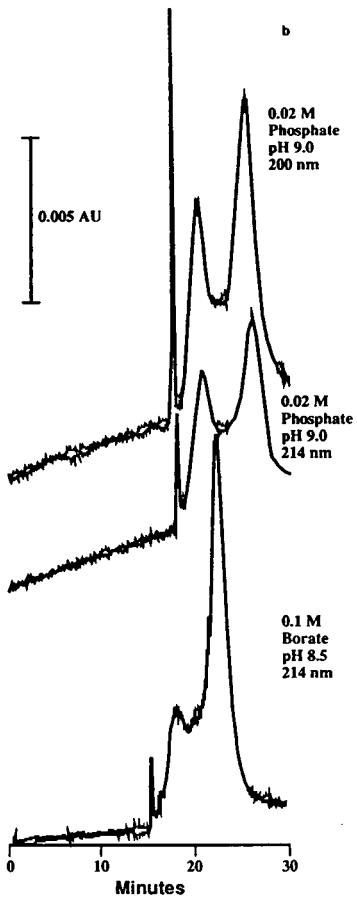

Fig. 1. Electropherograms of different conditions for SU from the strain of virus WLC-1. A Beckmann P/ACE was used. (a) 0.02 *M* sodium phosphate buffer, pH 9.0 and 0.1 *M* sodium borate buffer, pH 8.5 at 10 kV at 214 nm; (b) 0.02 *M* sodium phosphate buffer at 214 nm and 200 nm at 5 kV; 0.1 *M* sodium borate buffer, pH 8.5 at 214 nm at 5 kV.

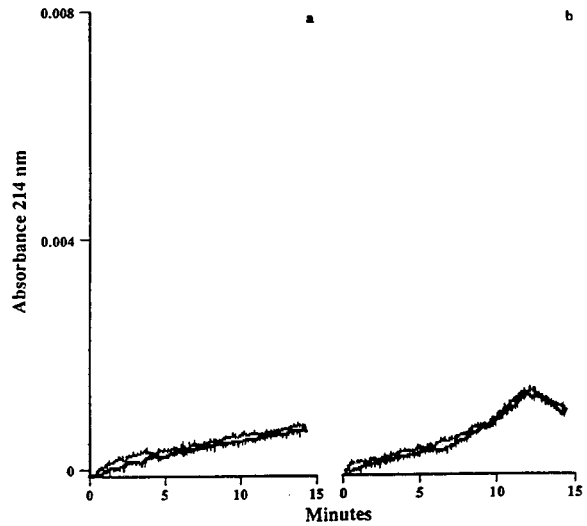

Fig. 2. Electropherograms of the enzymes neuraminidase and β-N-actyl glucosaminidase. The capillary was 57 cm × 75 μm I.D. and the separating voltage was 20.5 kV. UV absorbance was measured at 214 nm. The sample loaded into the capillary was 30 nl. A Beckman P/ACE was used. (a) β-N-Acetyl glucosaminidase; (b) neuraminidase.

these enzymes at the concentrations used to treat the glycoproteins. Profiles were obtained of SU from different viral strains after treatment with the mixed exoglycosidases. The exoglycosidases were used at a concentration equivalent to that of SU. The absorbance profile of the exoglycosidases alone was close to that of SU making the profiles of the enzyme treated samples difficult to interpret (data not shown). The exoglycosidases did cause a loss of antigenic activity of SU with the monoclonal antibodies (Table I). Removal of the sialic residues by neuraminidase appears to affect the profile of the strains by changing the mobility and the number of peaks in the electropherogram (Fig. 3b). Although the removal of these residues had little effect on the antigenicity of Howard or WLC-1,

TABLE I

LOSS OF ACTIVITY AFTER TREATMENT WITH EXOGLYCOSIDASES [%]

Monoclonal antibody	Virus strain				
	Runk	Howard	WLC-1	CAEV	Visna
10C10	77.5	89.9	–	–	–
9H4	–	–	75.7	47.7	59.5

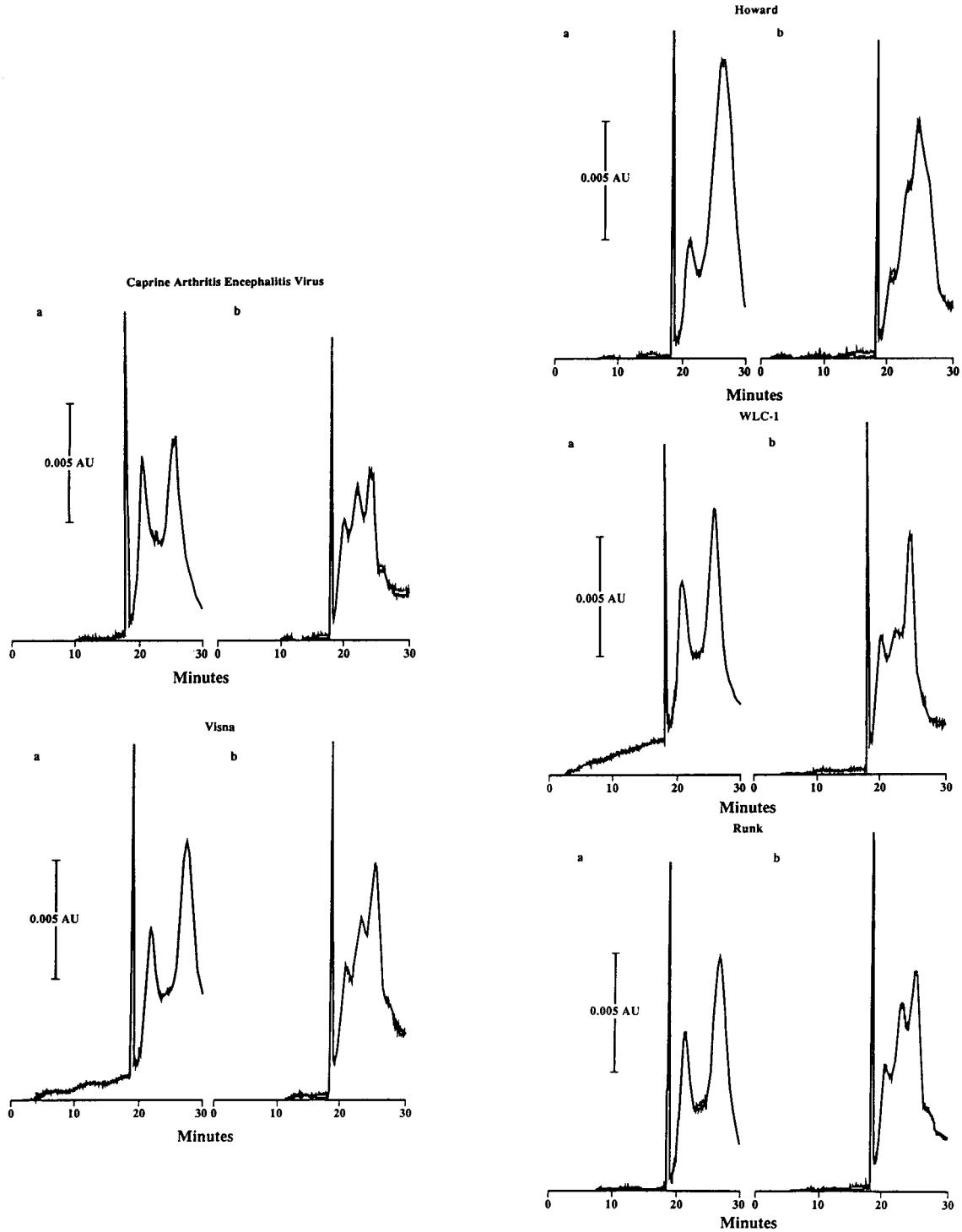

Fig. 3. Electropherograms of SU before and after treatment with neuraminidase. A Beckman P/ACE was used. The capillary was 57 cm × 75 μm I.D. and the separating voltage was 5 kV. UV absorbance was measured at 200 nm. The sample loaded into the capillary was 18 nl. The virus strain is indicated on the top of each panel. (a) The untreated glycoprotein; (b) the glycoprotein treated with neuramidase.

TABLE II

ENHANCEMENT OF ACTIVITY AFTER TREATMENT WITH NEURAMINIDASE [%]

Monoclonal antibody	Virus strain				
	Runk	Howard	WLC-1	CAEV	Visna
10C10	112.7	0	–	–	–
9H4	–	–	105.0	112.6	119.0

the antigenicity of Runk, Visna and CAEV was enhanced (Table II). The antigenicity of SU of the viral strain Howard does not appear to be affected by the enzymatic treatments. This is consistent with the different reactivities to this strain exhibited by a panel of monoclonal antibodies produced to the glycoprotein (unpublished data).

The enzymes, β-N-acetyl glucosaminidase and the endoglycosidases (data not shown), had little or no effect on any of the strains for capillary electrophoresis or for antigenicity. Prior treatment with neuraminidase followed by β-N-acetyl glucosaminidase did not alter the profile from that obtained with neuraminidase alone (Fig. 3b).

The monoclonal antibody 9H4 reacts poorly with the strains Runk and Howard while it reacts very well with WLC-1, Visna and CAEV. The monoclonal antibody 10C10 reacts in an opposite fashion. Treatment of the glycoproteins with neuraminidase enhanced the reactivity to the glycoproteins by the monoclonal antibody (9H4) for Visna and CAEV (Table I) and by the monoclonal antibody 10C10 for Runk (Table II). Exoglycosidases reduced the reactivity for all the glycoproteins between *ca.* 50% and 90%.

DISCUSSION

Capillary electrophoresis can be used to analyze significant changes that occur in biological systems. There has been considerable effort to define conditions for protein separation and for prevention of protein interaction with the capillary walls [26–29]. We used a simple phosphate buffer system without additives. We tried several ionic detergents and found that in some cases, the detergents caused negative peaks and interfered with the ultraviolet absorbance at the wavelengths that we wished to use. Landers *et al.* [28] have suggested that borate, itself, was a necessary component to obtain optimal resolution in the separation of glycoforms of ovalbumin. With SU borate buffer did not enhance the separation and the electropherograms were similar to those profiles obtained in the phosphate buffer system. Although we did not use buffer additives, perhaps a buffer additive such as putrescine as suggested by both Taverna *et al.* [30] and Landers *et al.* [28] would help to observe the microheterogeniety of glycoproteins based on their sialic acid content. When the method of Tran *et al.* [31] was followed in which the capillary was pre-equilibrated with the phosphate buffer at pH 4.0 several hours prior to obtaining the electropherogram, no peaks were obtained.

Capillary electrophoresis has contributed information that helps unravel the complex picture that affects the antigenicity of surface glycoproteins of strains of ovine lentiviruses after treatment with different glycosidic enzymes. Charge differences can explain the differences in reactivities to some of the monoclonal antibodies. Epitopes that are hidden by the sialic acids are exposed after treatment with neuraminidase and migration patterns are changed on the electropherograms. Sialic acids were noted to be important for the viral strain CAEV. Huso *et al.* [21] reported that the sialic acids conferred a degree of resistance to degradation of the virus by proteolytic enzymes and to neutralization of the agent by antibodies. He concluded that the sialylation pattern of the CAEV envelope is responsible for its poor antigenicity and inability

to induce neutralizing antibodies. He found that another strain, Visna, which has fewer sialic acids on its surface is an excellent inducer of neutralization antibodies. Our finding that the monoclonal antibodies' reactivity is enhanced by removal of the sialic acids agrees with these conclusions. Although the strain of CAEV used is not identical to the one used by Huso *et al.* [21], we also found an increase in the reactivity of monoclonal antibodies to CAEV after treatment with neuraminidase. This suggests that the carbohydrate configuration plays a role in biological function of these viruses as well as determining the antigenicity of SU. We can speculate that the host (sheep *vs.* goats) pattern of glycosylation of SU of this virus may help determine the course of pathogenicity and virulence of the virus. Although the correlation of virulence with glycoslyation was not studied, it is known that some strains of the virus cause clinical disease more readily than others do. The changes induced by the glycosidic enzyme treatments in the reactivity of the monoclonal antibodies to the glycoproteins of different strains and the profiles on capillary electrophoresis have demonstrated that the glycosylation patterns contribute directly to the antigenicity of SU and the surface charge of SU as determined by capillary electrophoresis.

ACKNOWLEDGEMENTS

The authors express their appreciation to Mary Sue Brown for her technical assistance in growing the cell cultures and to Cynthia Hosea for assisting in the purification of the glycoproteins.

REFERENCES

1 B. Sigurdsson, H.M. Grimsson and P.A. Palsson, *J. Infect. Dis.*, 90 (1951) 233.
2 B. Sigurdsson and P.A. Paulsson, *Br. J. Exp. Pathol.*, 39 (1958) 519.
3 R.C. Cutlip and G.A. Laird, *Am. J. Vet. Res.*, 37 (1976) 1377.
4 J.E. Dahlberg, J.M. Gaskin and K. Perk, *J. Virol.*, 39 (1981) 914.
5 W.P. Cheevers and T.C. McGuire, *Adv. Virus Res.*, 34 (1988) 189.
6 G. Querat, V. Barban, N. Sauze, P. Filippi, R. Vigne, P. Russo and C. Vitu, *J. Virol.*, 52 (1984) 672.
7 M.D. Lairmore, G.Y. Akita, H.I. Russell and J.C. DeMartini, *J. Virol.*, 61 (1987) 4038.
8 M.D. Lairmore, J.M. Poulson, T.A. Adducci and J.C. DeMartini, *Am. J. Pathol.*, 130 (1988) 80.
9 C.A. Lichtensteiger, D.P. Knowles, Jr., T.C. Mcguire and W.P. Cheevers, *Virol.*, 185 (1991) 2.
10 P. Sonigo, M. Alizon, K. Staskus, D. Klatzmann, S. Cole, O. Danos, E. Retzel, P. Tiollias, A. Haase and S. Wain-Hobson, *Cell*, 42 (1985) 369.
11 M.J. Braun, J.E. Clements and M.A. Gonda, *J. Virol.*, 61 (1987) 4046.
12 P. Knowles, W.P. Cheevers, T.C. McGuire, A.L. Brassfield, W.G. Harwood and T.A. Stem, *J. Virol.*, 65 (1991) 5744.
13 R.M. McCormick, *Anal. Chem.*, 60 (1988) 2322.
14 P.D. Grossmann, J.C. Colburn, H.H. Lauer, R.G. Nielsen, R.M. Riggin, G.S. Sittampalam and E.C. Rickard, *Anal. Chem.*, 61 (1989) 1186.
15 E.C. Rickard, M.M. Strohl and J.O. Nielson, *Anal. Biochem.*, 197 (1991) 197.
16 Z. Deyl and R. Struzinsky, *J. Chromatogr.*, 569 (1991) 63.
17 J.-E.S. Hansen, H. Clausen, C. Nielsen, L.S. Teglbjaerg, L.L. Hansen, C.M. Nielsen, E. Dabelsteen, L. Mathiesen, S. Hakomori, J.O. Nielsen and O. Jens, *J. Virol.*, 64 (1990) 2833.
18 J.-E.S. Hansen, C. Nielson, H. Clausen, L.R. Mathiesen and J.O. Nielsen, *Antiviral Res.*, 16 (1991) 233.
19 A. Benjouad, J.-C. Gluckman, H. Rochat, L. Montagnier and E. Bahraoui, *J. Virol.*, 66 (1992) 2473.
20 M.L. Poss, S.W. Dow and E.A. Hoover, *Virology*, 188 (1992) 25.
21 D.L. Huso, O. Narayan and G. Hart, *J. Virol.*, 62 (1987) 1974.
22 R.C. Montelaro, W.G. Robey, M.D. West, C.J. Issel and P.J. Fischinger, *J. Gen. Virol.*, 69 (1988) 1711.
23 O.H. Lowry, N.J. Rosebrough, A.L. Farr and R.J. Rendall, *J. Biol. Chem.*, 193 (1951) 265.
24 F. Bex, C. Bruck, D. Mammerickx, D. Portetelle, J. Ghysdael, Y. Cleuter, D. Lewckercq and A. Burny, *Cancer Res.*, 39 (1979) 1118.
25 M.S. Srikumaran, A.J. Guidry and R.A. Goldsby, *Am. J. Vet. Res.*, 43 (1982) 21.
26 F.-T.A. Chen, *Technical Information Bulletin DS818*, Beckman Instruments, Palo Alto, CA, 1991.
27 P.G. Pande, R.V. Nellore and H.R. Bhagat, *Anal. Biochem.*, 204 (1992) 103.
28 J.P. Landers, R.P. Oda, B.J. Madden and T.C. Spelsberg, *Anal. Biochem.*, 205 (1992) 115.
29 J.P. Landers, R.P. Oda, T.C. Spelsberg, J.A. Nolan and K.J. Ulfelder, *Biotechniques*, 14 (1993) 98.
30 M. Taverna, A. Baillet, D. Biou, M. Schluter, R. Werner and D. Ferrier, *Electrophoresis*, 13 (1992) 359.
31 A.N. Tran, S. Park and P.J. Lisi, *J. Chromatogr.*, 542 (1991) 459.

Journal of Chromatography A, 652 (1993) 207–213
Elsevier Science Publishers B.V., Amsterdam

CHROM. 25 179

Determination of milk proteins by capillary electrophoresis

N. de Jong, S. Visser and C. Olieman*

Departments of Analytical Chemistry and Biophysical Chemistry, Netherlands Institute for Dairy Research (NIZO), P.O. Box 20, 6710 BA Ede (Netherlands)

ABSTRACT

The determination of milk proteins by capillary zone electrophoresis (CZE) is hampered by the adsorption of the solute on the capillary wall. The effects of pH, ionic strength of the buffer and polymeric additives were studied in combination with a hydrophilically coated capillary. Optimum separations were obtained at low pH (2.5–3) in aqueous solutions containing 6 *M* urea and methylhydroxyethylcellulose, resulting in a complete separation of the serum proteins and caseins, including some genetic variants. The results were compared with those achieved with reversed-phase HPLC. With CZE, theoretical plate numbers in the range 300 000–700 000 were obtained. The relative standard deviations for migration times were below 0.08% and for peak areas were 2–4%. The separation of cow, goat and sheep milk proteins and of heat-damaged casein is reported.

INTRODUCTION

Bovine milk contains 3–3.5% of protein, of which 80% consists of caseins, insoluble at their isoelectric pH (pH 4.6). The serum proteins, soluble at pH 4.6, make up the remaining 20%. The casein fraction can be subdivided into α_{s1}-, α_{s2}-, β- and κ-casein components (α_{s1}CN, α_{s2}CN, βCN and κCN), which in milk occur as a micellar complex in the approximate proportions 4:1:4:1, respectively. The serum proteins are comprised mainly of β-lactoglobulin (βLg) and α-lactalbumin (αLa) in the ratio *ca.* 3:1.

The determination of milk proteins, including the separation of genetic variants, has been achieved by classical gel electrophoresis [1,2], isoelectric focusing [3–5] and high-performance liquid chromatography (HPLC) in the ion-exchange [6], hydrophobic interaction [7] and reversed-phase [8] modes. Each method has its own merits, but no single method gives an excellent separation between serum proteins and caseins in combination with possibilities for good quantification.

Capillary zone electrophoresis (CZE), a rapidly evolving technique, has the potential to give rapid separations with high resolutions and good quantification. The separation of proteins by CZE, however, might be hampered by adsorption on the negatively charged fused-silica surface of the capillary, leading to broad and/or tailing peaks and sometimes poor quantification [9]. These problems can be (partly) overcome by using a high pH buffer [10], a high ionic strength buffer [11,12], coated capillaries [13,14] or buffer additives [15,16].

In this paper, we describe the development of a CZE method by which the serum proteins and caseins are well separated from each other and some of their genetic variants.

EXPERIMENTAL

Reagents and chemicals

Phosphate buffer (10 m*M*) was prepared by dissolving in a 50-ml volumetric flask 69 mg of NaH_2PO_4 (Merck, Darmstadt, Germany) and 25

* Corresponding author.

0021-9673/93/$06.00

mg of methylhydroxyethylcellulose (MHEC, 30 000) (Serva, Heidelberg, Germany) in 37.5 ml of 8 *M* urea (Riedel-de Haën, Seelze, Germany); the pH was adjusted to 2.50 with 4 *M* phosphoric acid (AnalaR; BDH, Poole, UK) and the volume was made up with water. For some experiments MHEC was replaced with the same amount of methylhydroxypropylcellulose (MHPC, 15 000) (Serva) or poly(vinyl alcohol) (PVA, 15 000) (Fluka, Buchs, Switzerland).

Citrate buffer (10 m*M*) was prepared by dissolving in a 50-ml volumetric flask 147 mg of trisodium citrate dihydrate (Merck) and 25 mg of MHEC in 37.5 ml of 8 *M* urea. The pH was adjusted to 2.45 with 2.5 *M* citric acid solution and the volume was made up with water. Citrate buffer (20 m*M*) (pH 3.00) was prepared analogously.

Buffers were filtered through a 0.22-μm Millex GV filter (Millipore, Molsheim, France). Urea solution (8 *M*) was passed over a mixed-bed ion exchanger [AG 501-X8 (Bio-Rad Labs., Richmond, CA, USA)] in order to remove isocyanate and other ionic impurities.

Capillary zone electrophoresis

Electromigration was carried out with a Beckman P/ACE system 2050 controlled by a Laser 386/2 computer with Beckman P/ACE v. 2.0 software using a hydrophilically coated fused-silica capillary, either from SGE (Milton Keynes, UK) or CElect P1 from Supelco (Bellefonte, PA, USA), both with dimensions of 57 cm × 50 μm I.D. and fitted in a cartridge with a modified mandrel in order to improve cooling. A new SGE capillary required extensive flushing with methanol–water mixtures and with the buffer in order to obtain good electropherograms. In contrast, the Supelco capillary gave immediately repeatable electropherograms of high quality. Migrations were run at 45°C and the voltage across the capillary was maintained at 25 or 20 kV in the case of phosphate buffers, with ground at the detector side. Injections were carried out by pressure (duration 10–30 s). After each separation the capillary was flushed with the appropriate buffer for 4 min. Prior to storage the capillary was flushed for 10 min with water.

UV detection was performed at 214 nm (data collection rate 5 Hz). Peaks were identified by comparison with authentic samples and by analysing milks with a known genetic protein composition. Peak areas and peak heights were obtained from the same raw data after processing with Caesar NT software (v. 2.0, B*Wise, Geleen, Netherlands).

Liquid chromatography

Sample preparation and separations were carried out as described previously [17].

Sample treatment for CZE analysis

The reduction buffer was prepared by dissolving in a 50-ml volumetric flask 73 mg of trisodium citrate dihydrate (Merck) and 38 mg of DL-dithiothreitol (DTT) (Sigma, St. Louis, MO, USA) in 37.5 ml of 8 *M* urea. The pH was adjusted to 8 with dilute sodium hydroxide solution and the volume was made up with water. Skim milk (0.5 ml) was diluted with 2.5 ml of reduction buffer and incubated for 1 h at room temperature. The resulting clear solution was used for CZE analysis.

RESULTS AND DISCUSSION

The majority of caseins are present in milk in the form of micelles. The micelles can be disrupted by the combined action of a reducing agent (DTT) and 6 *M* urea. The reformation of micelles during electrophoresis can be prevented by using 6 *M* urea in the electrophoresis buffer. We investigated previously published electrophoretic separation methods [10,14,15] with and without the addition of 6 *M* urea to the buffers. The results obtained with serum proteins and caseins were in general disappointing, as broad and tailing peaks were observed or the selectivity was insufficient.

A Beckman application note showed an interesting separation of caseins at a low pH (10 m*M* phosphate, pH 2.5) in combination with a modified cellulose and an uncoated silica capillary. These conditions proved to be a good starting point for a systematic optimization of the analy-

sis. At pH 2.5 silica is almost without negative charge, and therefore the positively charged proteins are not attracted to the silica surface. Modified celluloses tend to adsorb on silica surfaces, shielding the polar nature and residual charges of the surface. Under these conditions adsorption of proteins is obviously prevented to a great extent.

We reasoned that the application of a hydrophilically coated capillary could suppress the adsorption of proteins even more, which indeed appeared to be the case. Elevation of the temperature to 45°C also improved the separation. In both instances the peaks became narrower and the migration times decreased. Electroosmotic flow is virtually zero under these conditions.

Fig. 1 shows the pH dependence of the electrophoretic pattern of bovine milk proteins using the phosphate buffer. It should be noted that the ionic strength was not the same at the different pH values, because the pH was adjusted starting with 10 m*M* sodium phosphate solution. At pH 2 and 2.5 serum proteins and caseins were well separated.

Fig. 2 shows the influence of various polymeric additives to the phosphate buffer of pH 2.5. MHEC gave the best performance, closely followed by MHPC. PVA gave rather broad peaks with long migration times. Recently Belder and Schomburg [18] described the beneficial properties of PVA and hydroxyethylcellulose on separations with bare silica capillaries. We investigated the effect of the average molecular mass of MHPC (viscosity of 2% solution in water of 5, 100 and 15 000 mPa s) on the separation. When the molecular mass of the polymer decreased the peak width increased. This cannot be overcome by using a higher mass percentage of the low molecular mass material.

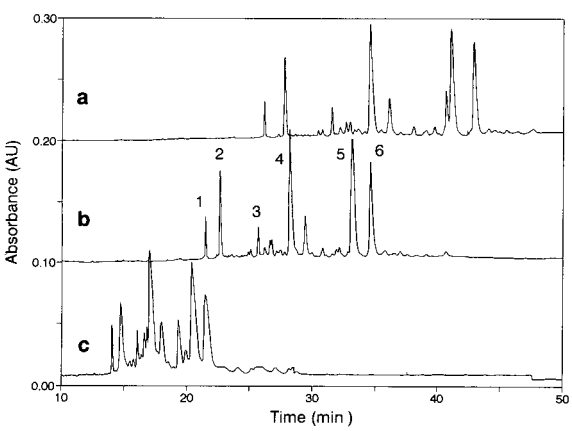

Fig. 1. Electropherograms of bovine milk proteins at (a) pH 2.0, (b) pH 2.5 and (c) pH 3.0. Buffer, 10 m*M* sodium phosphate containing 6 *M* urea and 0.05% MHEC; electromigration in a hydrophilically coated SGE capillary at 20 kV with ground at the detector side. Peaks: 1 = αLa; 2 = βLg; 3 = α_{s2}CN; 4 = α_{s1}CN; 5 = βCN-Al; 6 = βCN-A2.

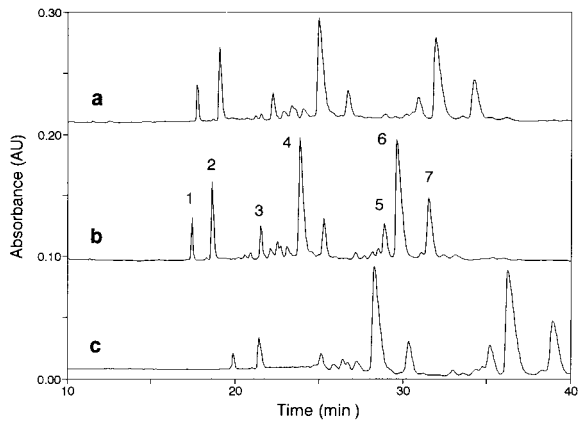

Fig. 2. Influence of polymeric additives (0.05%) on the electromigration of bovine milk proteins at pH 2.5. (a) MHPC; (b) MHEC; (c) PVA. Experimental conditions as in Fig. 1. Peaks: 1 = αLa; 2 = βLg; 3 = α_{s2}CN; 4 = α_{s1}CN; 5 = κCN; 6 = βCN-Al; 7 = βCN-A2.

The replacement of phosphate with citrate increased the theoretical plate number, calculated for the proteins in Fig. 3A, to the range 300 000–700 000. The conductivity of this buffer is lower than that of the phosphate buffer of the same concentration and pH, permitting an increase in the separation voltage to 25 kV, which generates a current of only *ca.* 60 μA. An excellent separation between serum proteins and caseins is observed. The A and B genetic variants of βLg and of κCN are not separated, and only a slight separation is observed for the B and C variants of α_{s1}CN. These genetic variants differ only in an acidic amino acid residue (Table I), which is almost not ionized at this pH, inducing no charge differences. The genetic variants of the β-caseins differ in the amount of

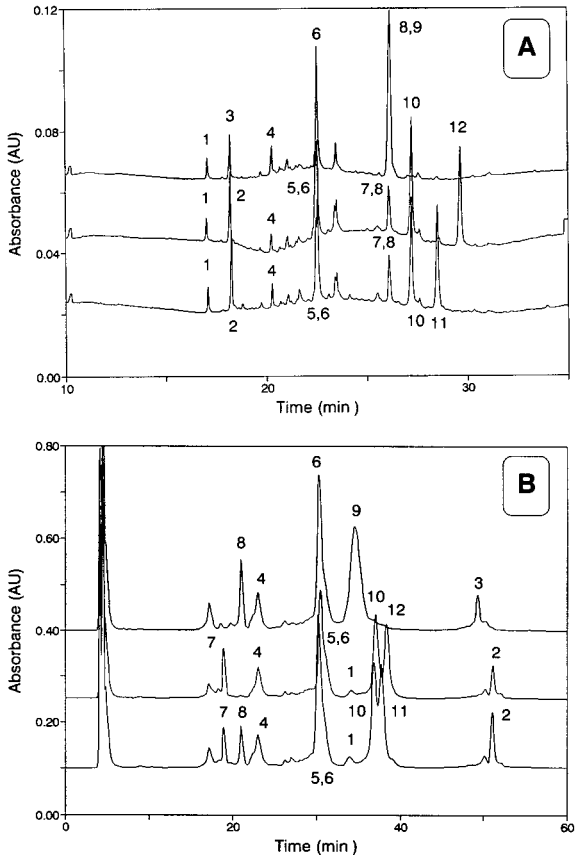

Fig. 3. Separation of genetic variants of proteins of three bovine milks by (A) capillary electrophoresis using a 10 m*M* sodium citrate buffer (pH 2.45) containing 6 *M* urea and 0.05% MHEC in combination with a hydrophilically coated SGE capillary run at 25 kV and (B) reversed-phase HPLC with an acetonitrile gradient on a Hi-Pore RP 318 column (Bio-Rad Labs.). Peaks: 1 = αLa; 2 = βLg-A; 3 = βLg-B; 4 = α_{s2}CN-A; 5 = α_{s1}CN-C; 6 = α_{s1}CN-B; 7 = κCN-A; 8 = κCN-B; 9 = βCN-B; 10 = βCN-Al; 11 = βCN-A2; 12 = βCN-A3.

basic amino acids residues. An excellent separation is observed (Fig. 3A). For comparison the reversed-phase HPLC results are shown in Fig. 3B. A completely different pattern is found, indicating that the two techniques are complementary to each other.

Increasing the pH of the electrophoresis buffer should allow the separation of genetic variants differing in acidic amino acid residues. However, a slight increase in the pH from 2.45 to 2.50 decreased the theoretical plate number by *ca.*

TABLE I

AMINO ACID DIFFERENCES IN GENETIC VARIANTS OF BOVINE MILK PROTEINS

Protein	Variant	Substitution
α_{s1}-Casein (α_{s1}CN)	B	Glu
	C	Gly
β-Casein (βCN)	A1	His His Ser
	A2	Pro His Ser
	A3	Pro Gln Ser
	B	His His Arg
κ-Casein (κCN)	A	Thr Asp
	B	Ile Ala
β-Lactoglobulin (βLg)	A	Asp Val
	B	Gly Ala

20%. At pH 3.00 we could obtain similar plate numbers (Fig. 4) if the concentration of trisodium citrate was increased from 10 to 20 m*M*, the conductivity of this buffer being the same as that of pH 2.45. This suggests that there is a minimum ionic strength needed to suppress adsorption of proteins on the capillary surface, similarly to the situation encountered in gel permeation chromatography. Fig. 4 shows a

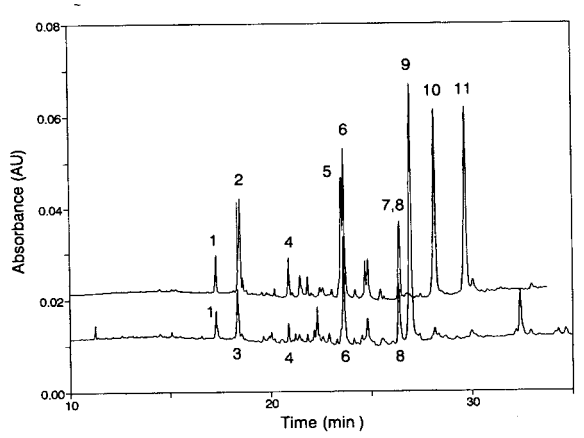

Fig. 4. Electromigration of genetic variants of proteins of two bovine milks at pH 3.00 (20 m*M* sodium citrate, 6 *M* urea and 0.05% MHEC) using a hydrophilically coated Supelco capillary at 25 kV. Peaks: 1 = αLa; 2 = βLg-A; 3 = βLg-B; 4 = α_{s2}CN-A; 5 = α_{s1}CN-C; 6 = α_{s1}CN-B; 7 = κCN-A; 8 = κCN-B; 9 = βCN-B; 10 = βCN-Al; 11 = βCN-A2. The dotted line near peak 2 in the upper trace indicates the position of βLg-B.

slight separation for the A and B forms of βLg and an improved separation for α_{s1}CN-B and -C. The A and B forms of κCN were not separated, but βCN-B was well separated from κCN.

A possible application is the determination of proteins from goat, sheep and, for comparison, cow milk (Fig. 5). For each species a distinctive pattern is found, which potentially could be used to detect the adulteration of each by addition of the other down to 1%.

During our investigations we observed that caseins, believed to be heat stable, were changed considerably on heating in milk. Caseins, isolated by isoelectric precipitation at pH 4.6 from evaporated milks (EVAP), show a dramatic change in their patterns (Fig. 6). All the caseins from EVAP show an additional peak after the main casein peaks. When the EVAP received an additional heat treatment, the peak of α_{s1}CN disappeared almost completely, leaving several partly separated peaks. The β-caseins show three additional peaks in addition to the original peak. This phenomenon could be used to detect heat treatments of milk more intensive than pasteurization, and to detect the addition of milk powder to fresh milk.

The repeatability of the electrophoresis separation system was assessed by analysing eight times a sample composed of standards (Table II). Excellent repeatabilities were found for the migration times (R.S.D. <0.085%). The absence of electroosmotic flow could be important for these results. For peak areas R.S.D.s of 2–4% were found. In real samples the identification of peaks is easy, owing to the insensitivity of migration times to matrix effects. In other electrophoretic systems these matrix components might influence the electroosmotic flow and thus the migration times. The response factors, calculated for peak areas, showed larger variations for the proteins studied, than expected for detection at 214 nm. Therefore, an equal response for every protein cannot be assumed.

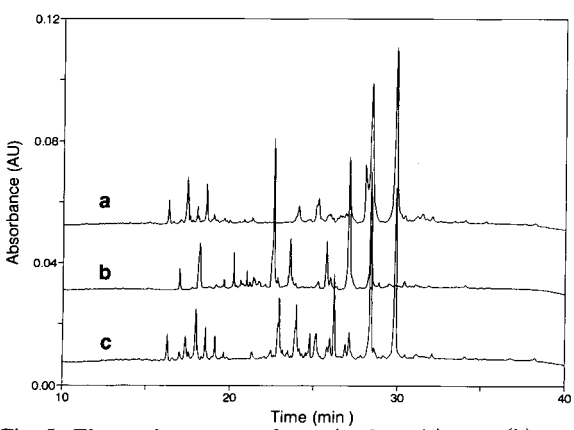

Fig. 5. Electropherograms of proteins from (a) goat, (b) cow and (c) sheep milk using a buffer of pH 2.45. Conditions as in Fig. 3.

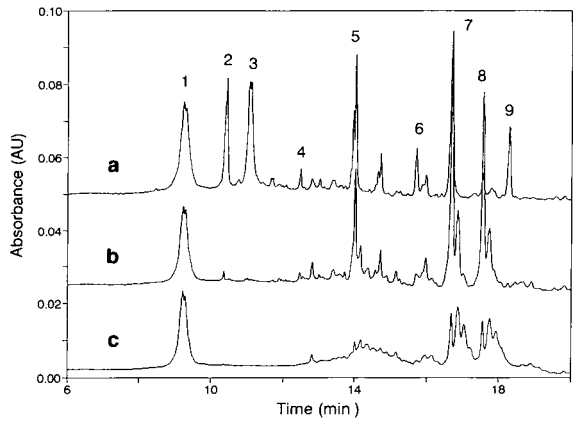

Fig. 6. Electropherograms of heat-damaged caseins. (a) Standard sample composed of serum proteins and caseins; (b) caseins isolated by isoelectric precipitation from EVAP; (c) caseins from EVAP that had received an additional heat treatment. A hydrophilically coated Supelco capillary (47 cm × 50 μm I.D.) was used; other conditions as in Fig. 4. Peaks: 1 = BSA (added as an internal standard); 2 = αLa; 3 = βLg-A and -B; 4 = α_{s2}CN; 5 = α_{s1}CN-B and -C; 6 = κCN; 7 = βCN-A1; 8 = βCN-A2; 9 = βCN-A3.

CONCLUSIONS

The CZE method described here is the first method for determining simultaneously serum proteins and caseins with high resolution and good possibilities for quantification in combination with a simple sample treatment.

Capillary electrophoresis proved to be a reliable method for the determination of milk proteins. The life of the coated capillary was at least 2 months, during which many hundreds of samples were analysed.

TABLE II

REPEATABILITY OF MIGRATION TIMES AND PEAK AREAS OF A STANDARD SAMPLE RUN WITH THE CITRATE BUFFER (pH 3.00) AT 25 kV

Injection No.	Migration time (min)									Peak area (area counts)						
	BSA-1	BSA-2	αLa	βLg-B	βLg-A	α_{s1}CN	κCN	βCN-A1	βCN-A2	BSA[a]	αLa	βLg[a]	α_{s1}CN	κCN	βCN-A1	βCN-A2
1	12.82	12.92	14.51	15.45	15.51	19.48	21.94	23.28	24.48	0.1315	0.0282	0.1204	0.0768	0.0216	0.1200	0.0483
2	12.82	12.93	14.51	15.47	15.53	19.48	21.94	23.28	24.48	0.1377	0.0290	0.1201	0.0782	0.0229	0.1224	0.0499
3	12.82	12.92	14.50	15.43	15.50	19.46	21.94	23.27	24.46	0.1303	0.0282	0.1203	0.0763	0.0210	0.1216	0.0504
4	12.83	12.93	14.51	15.45	15.51	19.48	21.94	23.28	24.48	0.1367	0.0284	0.1200	0.0753	0.0228	0.1203	0.0501
5	12.82	12.92	14.50	15.44	15.51	19.47	21.94	23.27	24.46	0.1294	0.0274	0.1146	0.0733	0.0206	0.1159	0.0473
6	12.83	12.93	14.51	15.45	15.51	19.48	21.94	23.28	24.48	0.1354	0.0277	0.1161	0.0756	0.0218	0.1188	0.0486
7	12.82	12.92	14.50	15.43	15.50	19.46	21.93	23.26	24.46	0.1289	0.0269	0.1155	0.0725	0.0218	0.1150	0.0477
8	12.82	12.92	14.50	15.44	15.50	19.46	21.93	23.26	24.46	0.1303	0.0270	0.1158	0.0736	0.0221	0.1160	0.0477
Mean	12.82	12.92	14.51	15.45	15.51	19.47	21.94	23.27	24.47	0.1325	0.0279	0.1178	0.0752	0.0218	0.1187	0.0488
S.D.	0.005	0.005	0.005	0.013	0.010	0.010	0.005	0.009	0.011	0.0035	0.0007	0.0026	0.0019	0.0008	0.0028	0.0012
R.S.D. (%)	0.036	0.040	0.037	0.085	0.064	0.051	0.021	0.038	0.044	2.6	2.6	2.2	2.6	3.7	2.3	2.5

[a] Sum of two partly separated peaks.

ACKNOWLEDGEMENTS

We are grateful to Dr. H.M. Farrell (Eastern Regional Research Center, Philadelphia, PA, USA) and Dr. H. Bovenhuis (Agricultural University, Wageningen, Netherlands) for providing samples of casein genetic variants and whole milk samples, respectively. We thank J.A.M. van Riel, K.J. Slangen, P. Tienstra and M. Casella for technical assistance.

REFERENCES

1 D.G. Schmidt and J. Koops, *Neth. Milk Dairy J.*, 19 (1965) 63.
2 M.P. Thompson, C.A. Kiddy, J.O. Johnston and R.M. Weinberg, *J. Dairy Sci.*, 47 (1964) 378.
3 F. Addeo, L. Chianese, A. Di Luccia, P. Petrilli, R. Mauriello and G. Anelli, *Milchwissenschaft*, 38 (1983) 586.
4 H. Bovenhuis and A.J.M. Verstege, *Neth. Milk Dairy J.*, 43 (1989) 447.
5 F. Braun, I. Krause and H. Klostermeyer, *Milchwissenschaft*, 45 (1990) 3.
6 A.T. Andrews, M.D. Taylor and A.J. Owen, *J. Chromatogr.*, 348 (1985) 177.
7 L.C. Chaplin, *J. Chromatogr.*, 363 (1986) 329.
8 S. Visser, Ch. J. Slangen and H.S. Rollema, *J. Chromatogr.*, 548 (1991) 361.
9 M.V. Novotny, K.A. Cobb and J. Liu, *Electrophoresis*, 11 (1990) 735.
10 H.H. Lauer and D. McManigill, *Anal. Chem.*, 58 (1986) 166.
11 F.A. Chen, L. Kelly, R. Palmieri, R. Biehler and H. Schwartz, *J. Liq. Chromatogr.*, 15 (1992) 1143.
12 F.A. Chen and J. Zang, *J. Assoc. Off. Anal. Chem.*, 75 (1992) 905.
13 K.A. Cobb, V. Dolnik and M. Novotny, *Anal. Chem.*, 62 (1990) 2478.
14 J.K. Towns and F.E. Regnier, *Anal. Chem.*, 63 (1991) 1126.
15 A. Emmer, M. Jansson and J. Roeraade, *J. Chromatogr.*, 547 (1991) 544.
16 W.G.H.M. Muijselaar, C.H.M.M. de Bruijn and F.M. Everaerts, *J. Chromatogr.*, 605 (1992) 115.
17 S. Visser and K.J. Slangen, *J. Chromatogr. Sci.*, 30 (1992) 466.
18 D. Belder and G. Schomburg, *J. High Resolut. Chromatogr.*, 15 (1992) 686.

Journal of Chromatography A, 652 (1993) 215–224
Elsevier Science Publishers B.V., Amsterdam

CHROM. 25 204

Analysis of a recombinant granulocyte macrophage colony stimulating factor dosage form by capillary electrophoresis, capillary isoelectric focusing and high-performance liquid chromatography

Guy G. Yowell*, Steven D. Fazio and Richard V. Vivilecchia

Sandoz Pharmaceuticals Corporation, 59 Route 10, East Hanover, NJ 07936 (USA)

ABSTRACT

The analysis of a recombinant granulocyte macrophage colony stimulating factor (GM-CSF) dosage form by free solution capillary electrophoresis (FSCE), capillary isoelectric focusing (cIEF), and high-performance liquid chromatography (HPLC) is described. The quantitative use of capillary electrophoresis, whether FSCE or cIEF, will always be prone to special problems, such as sensitivity to differences in salt concentrations between the standard and sample, and can not match the ruggedness of HPLC. The usable quantitative linear range for both HPLC and FSCE surpass that achieved for cIEF methods by a factor of 10 or greater. The FSCE system, utilizing an octyl bonded/Brij-35 coated capillary, did not work for all proteins examined. This is probably due to an interaction of the protein with the bonded phase or the adsorbed Brij-35. In contrast, the cIEF method worked well for all proteins tested thus far, yielding high efficiency and resolution comparable to slab gel isoelectric focusing. This paper addresses the potential for using free solution capillary electrophoresis and capillary isoelectric focusing as a quantitative analytical tool. Also, the effect of salt in the dosage form on quantitation, reproducibility, and efficiency of capillary electrophoresis methods is also discussed.

INTRODUCTION

The use of capillary electrophoresis (CE) for the analysis of pharmaceutical products has not yet reached a level where it is considered routine. There are many examples or application notes provided by instrument companies where CE can potentially be used, but these examples fail to discuss the quantitative aspect in the methods development process. The reasons for this are varied, but the detailed methods development and validation process is a time consuming event. The development and validation of quantitative methods is critical if CE is to be truly used, on a daily basis, for the analysis of pharmaceutical products. Analysis of a pharmaceutical dosage form has been reported by Guzman *et al.* [1] and other applications in the pharmaceutical industry have been reported by Hurni and Miller [2] and Compton [3]. This paper discusses the analytical use of free solution capillary electrophoresis (FSCE) and capillary isoelectric focusing (cIEF) in comparison with HPLC for the analysis of granulocyte macrophage colony stimulating factor (GM-CSF), a recombinant protein, in a dosage form.

The potential for using FSCE and/or cIEF as a quantitative analytical tool is now emerging as more applications are being developed. Protein separations in FSCE have been reported using both acidic and basic extremes of the pH range in uncoated capillaries [4,5]; however, undesirable problems sometimes occur. For certain proteins, the use of a pH 2.5 separation buffer causes protein aggregation, and therefore the

* Corresponding author.

0021-9673/93/$06.00

method is not an accurate representation of the protein composition in the dosage from. Generally, proteins should be separated and quantitated within one pH unit of physiological pH. However, to prevent protein adsorption on the capillary walls, the capillary surface must be chemically modified. Numerous buffer modifiers and wall chemistries have been described, such as ethylene glycol [6], a hydrophilic bonded surface [7], a polyethylene glycol (PEG) modified surface [8] as well as PEG as a protein modifier [9], carbohydrate [10] and polyethyleneimine [11] modified surfaces. Also, buffers containing high concentrations of zwitterionic salts [12] have been used. Success with GM-CSF was achieved using a coated/bonded capillary system developed by Towns and Regnier [13,14].

Capillary isoelectric focusing (cIEF) developed by Hjertén and co-workers [15–18] employed an acrylamide bonded capillary to reduce the electroosmotic flow. The application of cIEF to recombinant tissue plasminogen activator glycoforms [19] and other proteins [20,21] has been described. However, these cIEF methods consisted of a two-step process. The first was the focusing of the proteins in the capillary and the second required a change of either the cathode or anode buffers with a salt solution to mobilize the proteins past the detection window. Improvements and optimization of the cIEF separation parameters have included the use of tetramethylethylenediamine (TEMED) to adjust the pH range as described by Yao-Jun and Bishop [22], alternate mobilization agents, and the addition of non-ionic surfactants such as reduced Triton X-100 to minimize protein precipitation as described by Zhu *et al.* [23]. These improvements still required a salt mobilization of the focused bands for detection. This mobilization step and a lack of stable capillary wall chemistries have made cIEF unattractive for routine testing. Wu and Pawliszyn [24–26] discussed cIEF improvements for protein detection using a concentration gradient detector and imaging system, while Wang and Hartwick [27] used whole column absorbance detection.

Recently, cIEF bonded/coated chemistries developed by Mazzeo and Krull [28–35], without the need for salt mobilization of the focused protein bands past the detection window, have taken cIEF from a basic investigational tool to a readily automated method to study proteins. This procedure is successful for the analysis of GM-CSF, interleukin-3, and other recombinant proteins studied at Sandoz Research Institute. The cIEF method can be used to quantitative impurities and to study deamidation of proteins. In all cases, the stability of the capillary bonded/coated chemistries directly effect the reproducibility of the final analytical method.

If CE and cIEF methods are to succeed in the pharmaceutical industry, several issues must be addressed. These issues include reproducibility of migration time, peak area and peak height, within a capillary and from capillary to capillary. Also, parameters of ruggedness and capillary longevity must be fully evaluated. This paper addresses these issues in addition to others, such as ease of use and shorter analysis times with respect took both CE, other cIEF analytical methods and an existing HPLC method used for the analysis of GM-CSF.

EXPERIMENTAL

The octyl bonded capillaries were purchased from Supelco (Bellefonte, PA). The Pharmalyte 3-10 was purchased from Pharmacia LKB Biotechnology (Piscataway, NJ, USA). The Brij-35 was purchased from Aldrich (Milwaukee, WI, USA). The hydroxypropylmethylcellulose (HPMC), 4000 cP, as well as the sodium phosphate monobasic and sodium phosphate dibasic, were purchased from Sigma (St. Louis, MO, USA). The TEMED was purchased from Bio-Rad (Hercules, CA, USA); trifluoracetic acid (sequencing grade) was purchased from Pierce (Rockford, IL, USA). The capillary electrophoresis experiments described were carried out on the Beckman P/ACE 2050 (Fullerton, CA, USA). All data were collected and processed using Waters ExpertEase software (Milford, MA, USA).

The FSCE of GM-CSF was accomplished using a slightly modified version of the method described by Towns and Regnier [13]. A Beckman capillary cartridge was fitted with C_8

bonded capillary (the CElect H150 from Supelco) which had a total length of 37 cm (30 cm to the detector) and an internal diameter of 50 μm. The capillary was rinsed with a 0.5% (w/v) solution of Brij-35 for 2 h, then rinsed for 20 min the running buffer. The running buffer was 50 m*M* sodium phosphate (pH 6.8)–0.05% Brij-35. The effective field strength was 400 V/cm (14.8 kV overall). The polarity was negative. Detection was carried out at 200 nm. The capillary cartridge was maintained at a temperature of 23°C. The capillary was rinsed with running buffer for 2 min between each injection. The GM-CSF lyophilizate (0.4 mg/vial) was reconstructed with 1.0 ml sterile water-for-injection (WFI) and injected directly onto the capillary for 4 s under positive pressure. The total analysis time was 20 min.

The cIEF was accomplished using a method described by Mazzeo and Krull [28]. For the cIEF analysis, the Beckman cartridge was once again fitted with a CElect H150 capillary with a total length of 47 cm (40 cm to the detector) and an internal diameter of 50 μm. The volume of the capillary was 923 nl and the mass of GM-CSF loaded was 23 ng. The capillary was rinsed for 1 h with 0.5% (w/v) HPMC followed by water for 5 min. The GM-CSF lyophilizate was reconstituted as described above and diluted 1:1 with a 2× concentrate of the cIEF-ampholyte mixture which consisted of 970 μl of deionized water, 800 μl of 1% HPMC, 200 μl of Pharmalyte 3–10, and 30 μl of TEMED. The final running concentration of each of the components of the cIEF-ampholyte mixture was 0.2% HPMC, 2% Pharmalyte 3–10, and 0.75% TEMED. The capillary was rinsed for 4 min with 10 m*M* phosphoric acid and then filled with the sample preparation for 2 min using the high-pressure rinse capability of the Beckman P/ACE. The running field strength was 300 V/cm (14.1 kV overall) and the polarity again was negative. Detection was carried out at 280 nm; the capillary cartridge was maintained at a temperature of 23°C. The catholyte, 20 m*M* NaOH, was placed at the inlet and the anolyte, 10 m*M* phosphoric acid, was placed at the outlet. The total analysis time was 14 min.

The analysis of GM-CSF by reversed-phase HPLC was carried out on a Nucleosil C-4 column (Machery–Nagel) with a pore size of 300 Å and a particle size of 5 μm: The column dimensions were 10 cm × 4.6 mm I.D. Mobile phase A consisted of 0.1% (v/v) trifluoroacetic acid (TFA) in distilled-deionized water while mobile phase B consisted of 0.1% (v/v) TFA in acetonitrile–water (90:10, v/v). The protein was eluted from the column using a linear gradient from 38 to 58% B in 20 min; the flow-rate was 1.2 ml/min. The detector wavelength was 214 nm and the injection volume was 50 μl, corresponding to 20 μg of GM-CSF.

The UV spectrophotometric analysis was performed on a Perkin-Elmer Lambda 2 UV–Vis spectrophotometer. The GM-CSF was analyzed first at 280 nm at concentrations of 15.94, 7.97, 3.98 and 1.99 mg/ml using a 0.1 cm quartz cell. The absorptivity at 280 nm was found to be 1.15 ml/cm mg. The GM-CSF was then analyzed at 210 nm at concentrations of 1.594, 0.797, 0.398 and 0.199 mg/ml using the same quartz cell. The absorptivity at 210 nm was found to be 18.52 ml/cm mg.

RESULTS AND DISCUSSION

Free solution capillary electrophoresis

The free solution approach using the octyl bonded/Brij 35 coated phase shows good peak symmetry and an efficiency of 51 000 theoretical plates as shown in Fig. 1. The electropherogram shows adequate resolution between the GM-CSF and the human serum albumin (HSA). The HSA peak exhibits three major components with minor shoulders on the first and last components, also as shown in Fig. 1.

Both electrokinetic and pressure injection processes were examined. As shown in Table I, the assay results were found to be 16.3 and 9.3% of the labeled value for the 0.7 and the 0.4 mg/vial dosage forms, respectively, when employing the electrokinetic injection process. The assay results utilizing the pressure injection technique were 99.9 and 94.5% for the 0.7 and the 0.4 mg/vial, respectively. The reference standard, supplied in liquid form, was diluted in sterile WFI, while the GM-CSF lyophilizates were reconstituted with 1.0 ml of sterile WFI.

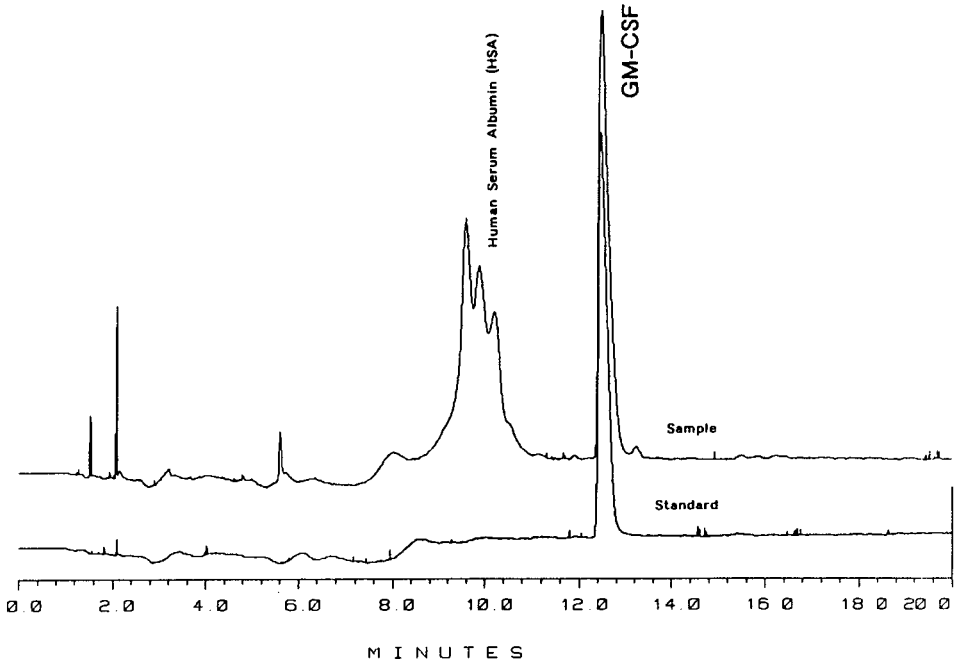

Fig. 1. Electropherogram of a GM-CSF standard and a GM-CSF sample with human serum albumin (HSA) by FSCE. Conditions: capillary, CElect H150, 37 cm × 50 μm I.D.; buffer, 50 m*M* NaH_2PO_4 (pH 7)/0.05% Brij 35; electric field strength, 400 V/cm (reverse polarity); detection, 200 nm; temperature, 23°C; injection 4 s pressure.

TABLE I

RESULTS FOR FSCE OF GM-CSF BY ELECTROKINETIC AND HYDROSTATIC INJECTION TECHNIQUES

Assay percent of two dosage forms using both electrokinetic and pressure injection.

Dosage form	% of Label	
	Electrokinetic injection	Hydrostatic injection
0.7 mg/vial	18.9	99.9
	15.1	99.4
	14.9	100.5
Mean	16.3	99.9
R.S.D. (%)	13.8	0.6
0.4 mg/vial	8.9	94.9
	9.4	94.0
	9.7	94.7
Mean	9.3	94.5
R.S.D. (%)	4.3	0.5

However, the GM-CSF lyophilizate contains a high salt concentration when reconstituted.

The effect of salt concentration of the sample on quantitation was examined for both the electrokinetic and pressure injection techniques, as shown in Fig. 2. These results indicate that the difference in salt concentration between the standard and the sample is critical for accurate

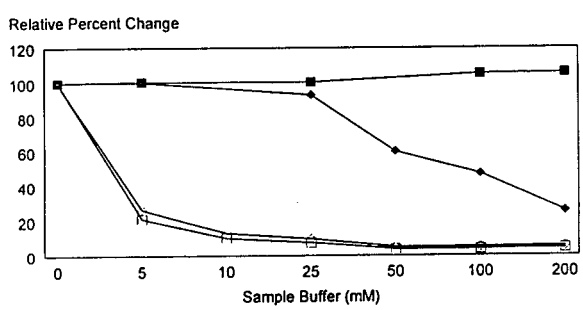

Fig. 2. The effect of salt concentration of peak area and peak height for both electrokinetic and pressure injections. □ = Electrokinetic injection, peak area; ■ = pressure injection, peak area; ◇ = electrokinetic injection, peak height; ◆ = pressure injection, peak height.

quantitation when employing the electrokinetic injection process. When the pressure injection technique was employed, these differences in salt concentration did not appear to effect peak area. The lack of change in peak area above 25 m*M* salt concentration was the result of severe peak broadening as shown in Fig. 3. In contrast, the peak heights decreased quickly as the salt concentration of the sample or standard approached that of the separation buffer. For these reasons, the ruggedness of the pressure injection technique is preferred. To maintain good efficiency, the salt concentration of both the sample and standard should be no greater than half that of the separation buffer.

Initially, the method was developed using a 75 μm I.D. capillary. The GM-CSF dosage form contains a high salt concentration when reconstituted. To achieve a stacking effect during the injection process, the sample must be of a lower ionic strength than that of the separation buffer. Therefore, the only way to achieve a stacking effect would be to increase the ionic strength of the running buffer. This approach was not possible due to the high current observed in a 75 μm I.D. capillary. Decreasing the capillary I.D. to 50 μm allowed the use of higher ionic strength separation buffers, 50 *versus* 10 m*M* phosphate buffer, in order to achieve stacking or injection plug compression. Linearity was observed from 1.0 mg/ml to 30 μg/ml with a correlation coefficient of 0.997, encompassing all dosage form strengths.

Capillary isoelectric focusing

The work of Mazzeo and Krull [28] demonstrated that a salt mobilization step was not necessary because a reduced electroosmotic flow exists allowing the focused protein bands to migrate past the detector window. Both the focusing and mobilization steps occur simultaneously, but the focusing step occurs more rapidly than mobilization. Mazzeo and Krull [28] first showed this work using a 60 cm unbonded capillary with 40 cm from the inlet to the detector and 20 cm from the detector to the outlet. The inlet reservoir contained the anolyte (10 m*M* phosphoric acid), the outlet contained the catholyte (20 m*M* sodium hydroxide), and forward polarity was employed. Adjusting the amount of TEMED in the sample allows all proteins to focus in the 40 cm capillary section before the detector and to drift towards the outlet with the electroosmotic flow past the detector window. This resulted in analysis times of 17 to 24 min.

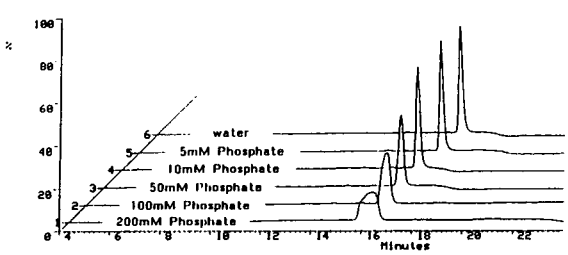

Fig. 3. The effect of salt on peak shape in FSCE.

Mazzeo and Krull [28] improved this method by employing reverse polarity, thus switching the anodic and cathodic reservoirs, using an octyl bonded capillary, and adjusting the amount of TEMED. Using this configuration, the TEMED now blocks the 40 cm from the inlet to just past the detector window. The proteins focus in the 20 cm past the detector window and the electroosmotic flow moves in the reverse direction towards the inlet. The proteins then drift past the detector window resulting in reduced analysis times of 4 to 6 min.

The improved cIEF configuration described above was used, with the addition of an octyl bonded/HPMC coated capillary, to quantitate the GM-CSF dosage forms as shown in the electropherogram in Fig. 4. Employing reverse polarity and adjusting the TEMED concentration, allowed over 40 cm (from the inlet to just past the detector) of a 47 cm capillary to be blocked, as schematically shown in Figs. 5 and 6. The pH gradient from 3 to 10 was located in the 7 cm from the detector to the outlet. The GM-CSF focused in a section of the 7 cm of capillary from the detector window to the outlet. The reduced electroosmotic flow in the octyl bonded capillary allowed the focused proteins, GM-CSF and HSA, to drift back towards the inlet reservoir past the detector window. The shortest capillary length obtainable from the detector to the outlet is a function of the manufacturer's instrument design. It appears that a short capil-

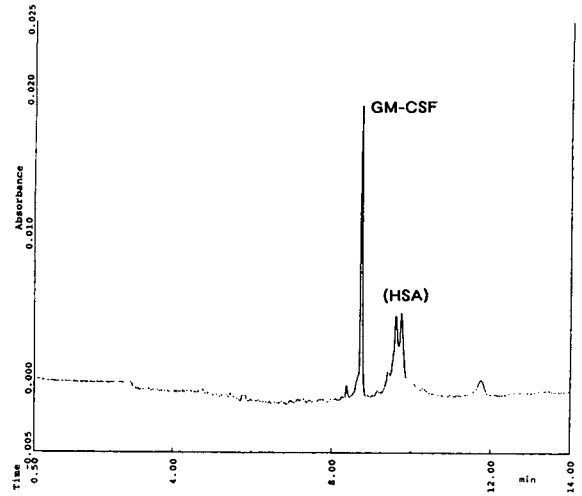

Fig. 4. A cIEF electropherogram of GM-CSF dosage form.

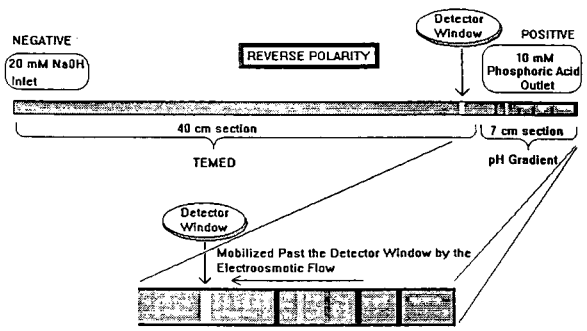

Fig. 5. A schematic of the capillary isoelectric focusing process showing position of focused bands on the outlet side of the detector.

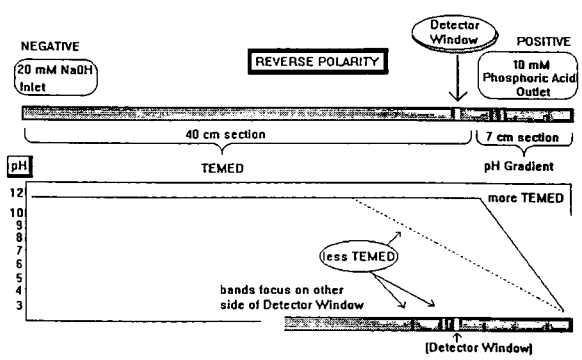

Fig. 6. A schematic of the capillary isoelectric focusing process showing the adjustment of TEMED on the location of the pH gradient and the problem of focused bands on the opposite side of the detector when too little TEMED is used.

lary section from the detector to the outlet (*i.e.* 7 *versus* 20 cm) is advantageous since this results in a shorter analysis time for a given electric field strength and should expose the protein to less capillary wall during the mobilization process resulting in a minimization of protein-wall interactions. The width of a focused band derived by Svensson [36] is given by the following equation:

$$x_i = \pm\left[\frac{D}{E(-\mathrm{d}\mu/\mathrm{d(pH)})(\mathrm{d(pH)}/\mathrm{d}x)}\right]^{1/2} \quad (1)$$

where x_i is the width of the focused band, D is the diffusion coefficient, E the electric field strength, $\mathrm{d}\mu/\mathrm{d(pH)}$ the rate of change of mobility with pH, and $\mathrm{d(pH)}/\mathrm{d}x$ is the pH gradient. The experimental parameters which determine the final width of a focused protein band are the range of ampholytes, the amount of TEMED, and the applied electric field gradient. Since the pH gradient is forced into a smaller section of the capillary (*i.e.* 7 *versus* 20 cm), the protein focuses in a narrower band which results in lower detection limits. However, since a higher concentration of the protein is achieved, precipitation may be observed earlier than if this section of capillary was longer.

The HSA contained in the dosage form exhibited 5 to 6 major components which were easily separated from the GM-CSF as shown in Fig. 4. The linear range for GM-CSF was observed from 10 to 40 μg/ml using a 47 cm capillary (overall length). GM-CSF concentrations from 60 to 250 μg/ml showed anomalous peaks which may represent precipitation [23] of the GM-CSF in the capillary. Concentrations above 250 μg/ml showed no peaks at all and again may represent protein precipitation. Another recombinant protein, interleukin-3, exhibited a linear range from 10 to 250 μg/ml without protein precipitation. The range of protein concentrations which may be used in cIEF vary from protein to protein and must therefore be optimized.

The capillary length represents an injection loop similar to HPLC. Since the overall length of the capillary represents the injection volume, shortening the capillary reduces the mass of protein loaded. Above a sample concentration of

40 μg/ml for GM-CSF, additional peaks were observed due to protein precipitation [23]. Precipitation occurs when a certain mass is exceeded for a given length of capillary as depicted by Fig. 7. The linear dynamic concentration range can be extended by shortening the length of the capillary. Shortening the capillary length to 27 cm (overall) allowed a higher concentration of sample, 50 to 100 μg/ml (less sample dilution) to be loaded while maintaining the same protein mass in the capillary, as shown in Fig. 8. Since the GM-CSF dosage form contains a large amount of salt, a higher concentration of the protein results in higher salt concentrations which effects migration time and efficiency. Therefore, a 47 cm capillary length is preferred for the GM-CSF method.

Detection in cIEF is performed at 280 nm due to the absorbance of the ampholytes below a wavelength of 235 nm. The absorptivity of GM-CSF at 280 nm is 16 times less than at 210 nm. To obtain a quantitative detection signal at 280 nm, the concentration of the focused protein bands must be much greater than the sample concentration which was loaded into the capillary. The focusing process results in a large increase in the sample band concentration. In FSCE analysis of GM-CSF, detection is performed at 200 nm. A comparison of the efficiency and band width was made. The efficiency for GM-CSF in cIEF is 270 000 theoretical plates while that achieved in FSCE is 51 000. The spatial width of the sample band, w_s, with units of length, in FSCE is calculated using the following equation as discussed by Huang *et al.* [37]:

$$w_s = \left(\frac{l_d}{t_m}\right) w_t - w_d \quad (2)$$

where l_d is the length of the capillary to the detector, in mm; w_t is the temporal peak width, in s, measured at the baseline; t_m is the migration time, in s; and w_d is the width of the detector window. The GM-CSF peak width in FSCE is 12 mm. The efficiency in cIEF for GM-CSF is approximately 5 times that observed in FSCE, the peak width in cIEF is assumed to be 1/5 that observed in FSCE. Therefore, the width of the band in cIEF is approximated to be 2 mm which corresponds to 4 nl. Since the capillary length represents an injection loop, filling the capillary with GM-CSF at a concentration of 25 μg/ml, yields 23 ng of protein which is loaded and focused. The protein concentration of the focused band is on the order of 5.8 mg/ml. Detection at 280 nm in FSCE is not possible for GM-CSF at 25 μg/ml due to the small injection volume typical in FSCE necessary to maintain good peak efficiency.

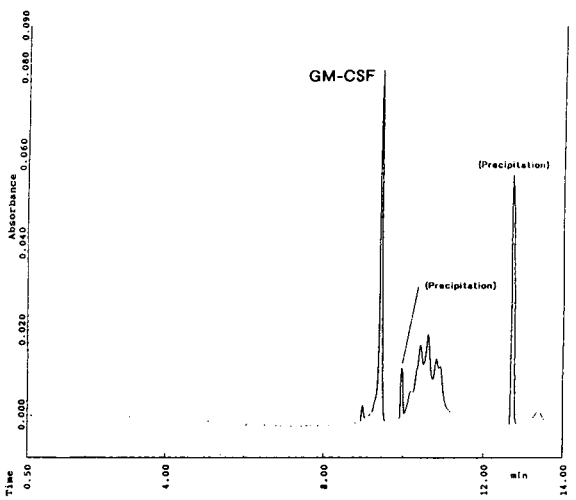

Fig. 7. A cIEF electropherogram of GM-CSF dosage form above the quantitative linear range showing precipitation peaks.

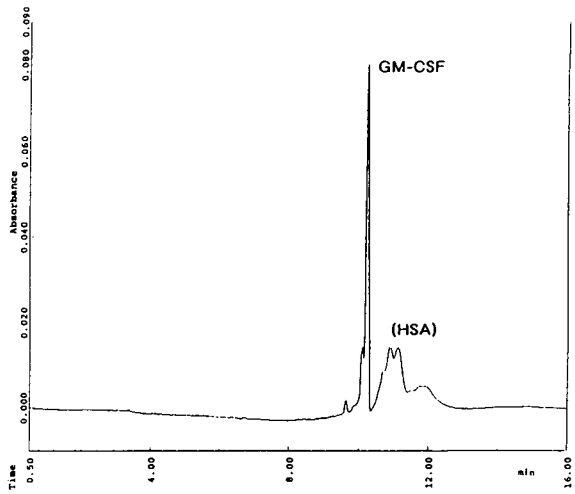

Fig. 8. A cIEF electropherogram of GM-CSF dosage form using a 27 cm capillary.

An additional peak, shown in Fig. 4, always eluting last in every cIEF electropherogram, may represent a small portion of the sample at the outlet of the capillary in contact with the anodic solution. This portion of the sample is not accessible during the focusing step and is eluted with the electroosmotic flow. This peak is used as a marker to indicate the end of the electropherogram and to calculate the electroosmotic flow. Using equation 1 yields a spatial width w_s of 1.5 mm, which corresponds to 3 nl. Using this approach the concentration of the focused band is 7.7 mg/ml. A third approach to estimate the concentration of the focused band is to measure the absorptivity. The absorptivity of GM-CSF was determined to be 1.15 ml/cm mg using a Perkin-Elmer Lambda-2 UV–Vis spectrophotometer. The GM-CSF peak in Fig. 4 shows an absorbance of 0.02 AU. Using Beer's law $\{A = abc$, where A is the absorbance, b is the optical pathlength (cm), a is the molar absorptivity [ml/(cm · mg)], and c is the sample concentration (mg/ml)}, and an optical pathlength of 50 μm, and solving for c yields a concentration for the focused band of 3.5 mg/ml.

Due to the relatively low absorptivity of proteins at 280 nm, detection can be achieved in cIEF at 280 nm because of the high concentration of the focused bands. When GM-CSF at 50 μg/ml is injected into a 47 cm capillary, the focused band has a concentration of 11.4 mg/ml. Above these concentrations, it is understandable that protein precipitation occurs, particularly due to the fact that the proteins are at their pI, the point of least solubility. The cIEF method concentrates the original sample of 25 μg/ml to 5.7 mg/ml, which is 228 times the original sample concentration.

The amount of TEMED used to extend the pH range, as described by Yao-Jun and Bishop [22], must also be considered, as well as the range of ampholytes and the concentration of HPMC in the development of the method. Migration time variability from capillary to capillary was observed and is caused by differences in electroosmotic flow. This may represent different degrees of capillary wall modification achieved by the manufacturer. Improvements of bonding procedures and/or the use of different mobile phase additives may reduce this variability. The purity of ampholytes influenced the resolution and resulted in the appearance of additional peaks.

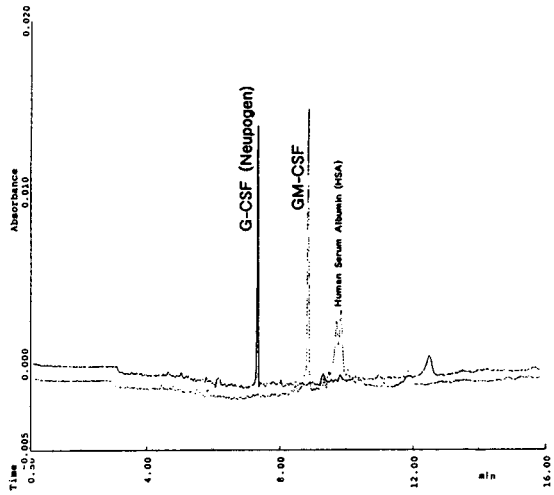

Fig. 9. A cIEF electropherogram of GM-CSF and G-CSF (Neupogen) showing different pI values as a method to distinguish product identification.

Although cIEF is being used to check GM-CSF concentration of dosage forms, it also offers the opportunity to distinguish different recombinant proteins of different pI values. Quick identifications can be accomplished as shown in Fig. 9 which distinguishes recombinant granulocyte colony stimulating factor (G-CSF), trade name Neupogen (Amgen) from GM-CSF. Assignment of pI to a protein for identification or estimation of pI values for degradation products can be achieved much more rapidly using cIEF than conventional slab gel isoelectric focusing as

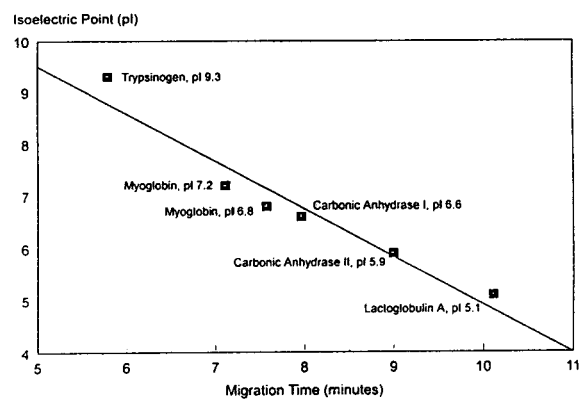

Fig. 10. Standard protein calibration curve showing migration time *versus* pI.

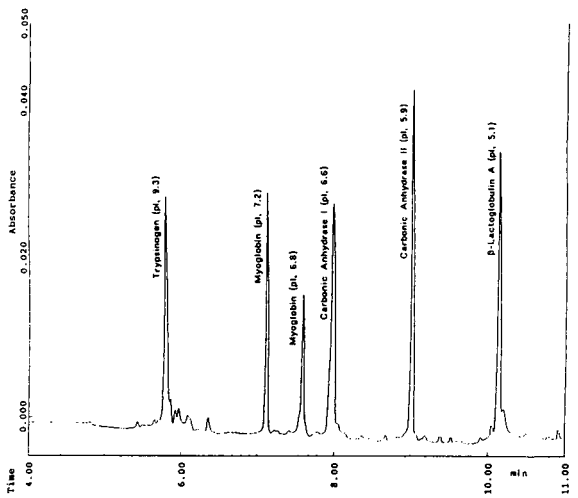

Fig. 11. Electropherogram of a protein standard mixture.

previously mentioned [28]. A reference standard curve is shown in Fig. 10 and the corresponding electropherogram in Fig. 11.

The cIEF methods have problems which again are protein dependent. It was observed that after analyzing GM-CSF, other protein standards did not separate in the same capillary as they had previously; the migration times were longer and the efficiency was substantially less. GM-CSF may be adsorbing to the capillary wall, changing the wall characteristics. Designating individual capillaries for a particular method or protein may prevent this problem.

Method comparison

A comparison of the quantitative results for HPLC, FSCE and cIEF is shown in Table II. The results are within acceptable ranges for all methods. The use of FSCE and cIEF methods for the testing of different dosage forms shows promise and offers to reduce analysis times and consumption of solvents. Method developments in FSCE and cIEF are prone to special problems such as sensitivity to salt differences between the standard and sample, or loss of separation due to high salt concentration in the sample. In general, HPLC is a more rugged technique and less prone to these difficulties. However, once these difficulties are overcome, the routine operation of a CE method appears to offer several advantages. These include the elimination of the problems associated with HPLC pump check values and plunger seal leaks, reduction in solvent consumption, reduced analysis times, and ease of use for daily operation.

TABLE II

COMPARISON OF ANALYTICAL RESULTS FOR FSCE, cIEF AND HPLC FOR GM-CSF DOSAGE FORMS

Sample	RP-HPLC	FSCE	cIEF
1-SFG-303	98.45	105.37	102.44
0-SFG-303	98.73	99.80	104.32
0-SFG-304	104.63	102.22	105.21

CONCLUSIONS

The usable quantitative linear range for both HPLC and FSCE surpass that achieved for cIEF methods by a factor of 10 or greater. The quantitative use of capillary electrophoresis, whether FSCE or cIEF, will always be prone to special problems, such as sensitivity to differences in salt concentrations between the standard and sample, and can not match the ruggedness of HPLC. Continued development of capillary wall chemical modifications in conjunction with solution additives continues to be a major avenue for uncovering new protein applications. However, the stability and reproducibility of these capillary wall and solution chemistries are the keys to solve the problem of reproducible electroosmotic flow observed from capillary to capillary.

The octyl bonded/Brij-35 coated capillary developed by Towns and Regnier [13] does not work for all proteins. The standard test mixture of proteins shown by Towns and Regnier [13], the GM-CSF, and some monoclonal antibodies used in our laboratory worked well with this system. However, other monoclonal antibodies, interleukin-3 and interleukin-6 showed poor efficiency. This is probably due to an interaction with the hydrophobic bonded phase or the adsorbed Brij-35, and may be dependent upon the hydrophobic or hydrophilic surface of the protein.

In contrast, cIEF worked well for all proteins tested thus far, yielding high efficiency and resolution comparable to slab gel isoelectric focusing. On a comparative basis to slab gel

isoelectric focusing (work which is presently being studied), cIEF offers reduced analysis times, direct transfer of data to a computer data base, and is 10 times more sensitive, on a concentration basis, than Coomassie stained gels. It is also remarkable that the original sample concentration is amplified by a factor of 228, resulting in a final detectable concentration of 5.7 mg/ml. Precipitation of the focused bands appears to be the major pathway leading to spurious peaks in cIEF. cIEF methods may be potentially interfaced with other spectroscopic techniques, such as light scattering, to determine the extent of aggregates present in focused bands. Also, since the protein concentration is so high, cIEF may be coupled to off-line techniques, such as sequencing, which is not practical for FSCE.

REFERENCES

1 N.A. Guzman, H.A.J. Moschero, K. Iqbal and A.W. Malick, *J. Chromatogr.*, 559 (1991) 307–315.
2 W.M. Hurni and W.J. Miller, *J. Chromatogr.*, 559 (1991) 337–343.
3 B.J. Compton, *J. Chromatogr.*, 559 (1991) 357–366.
4 H.H. Lauer and D. McManigill, *Anal. Chem.*, 58 (1986) 166–170.
5 R.M. McCormick, *Anal. Chem.*, 60 (1988) 2322–2328.
6 M.J. Gordon, K.-J. Lee, A.A. Arias and R.N. Zare, *Anal. Chem.*, 63 (1991) 69–72.
7 W. Nashabeh and Z. El Rassi, *J. Chromatogr.*, 559 (1991) 367–383.
8 G.J. Bruin, J.P. Chang, R.H. Kuhlman, K. Zegers, J.C. Kraak, H. Poppe, *J. Chromatogr.*, 471 (1989) 429–436.
9 R.L. Cunico, V. Gruhn, L. Kresin, D.E. Nitecki and J.E. Wiktorowicz, *J. Chromatogr.*, 559 (1991) 467–477.
10 G.J. Bruin, R. Huisden, J.C. Kraak and H. Poppe, *J. Chromatogr.*, 480 (1989) 339–349.
11 J.K. Towns and F.E. Regnier, *J. Chromatogr.*, 516 (1990) 69–78.
12 M.M. Bushey and J.W. Jorgenson, *J. Chromatogr.*, 480 (1989) 301–310.
13 J.K. Towns and F.E. Regnier, *Anal. Chem.*, 63 (1991) 1126–1132.
14 J.K. Towns and F.E. Regnier, *Anal. Chem.*, 64 (1992) 2473–2478.
15 S. Hjertén and J.L. Liao, *Protides Biol. Fluids*, 34 (1986) 727–730.
16 S. Hjertén and M.D. Zhu, *J. Chromatogr.*, 346 (1985) 265–270.
17 S. Hjertén, K. Elenbring, F. Kilar, J.L. Liao, A.J.C. Chen, C.J. Siebert and M.D. Zhu, *J. Chromatogr.*, 403 (1987) 47–61.
18 F. Kilar and S. Hjertén, *J. Chromatogr.*, 480 (1989) 351–357.
19 K.W. Yim, *J. Chromatogr.*, 559 (1991) 401–410.
20 T. Wehr, M. Zhu, R. Rodriguez, D. Burke and K. Duncan, *Am. Biotechnol. Lab.*, 8, No. 11 (1990) 22, 24–29.
21 M. Zhu, D.L. Hansen, S. Burd and F. Ganknon, *J. Chromatogr.*, 430 (1989) 311–319.
22 G. Yao-Jun and R. Bishop, *J. Chromatogr.*, 234 (1982) 459–462.
23 M. Zhu, R. Rodriguez and T. Wehr, *J. Chromatogr.*, 559 (1991) 479–488.
24 J. Wu and J. Pawliszyn, *Anal. Chem.*, 64 (1992) 219–224.
25 J. Wu and J. Pawliszyn, *Anal. Chem.*, 64 (1992) 224–227.
26 J. Wu and J. Pawliszyn, *Anal. Chem.*, 64 (1992) 2934–2941.
27 T. Wang and R.A. Hartwick, *Anal. Chem.*, 64 (1992) 1745–1747.
28 J.R. Mazzeo and I.S. Krull, *Anal. Chem.*, 63 (1991) 2852–2857.
29 J.R. Mazzeo and I.S. Krull, *J. Chromatogr.*, 606 (1992) 291–296.
30 J.R. Mazzeo and I.S. Krull, *BioTechniques*, 10 (1991) 638.
31 J.R. Mazzeo and I.S. Krull, *J. Microlumn Sep.*, 4 (1992) 29.
32 J.R. Mazzeo and I.S. Krull, *J. Chromatogr.*, 606 (1992) 291.
33 J.R. Mazzeo and I.S. Krull, in N. Guzman (Editor), *Capillary Electrophoresis-Technology*, Marcel Dekker, New York, in press.
34 J.R. Mazzeo, J.A. Martineau and I.S. Krull, *Anal. Biochem.*, 208 (1993) 323–329.
35 J.R. Mazzeo, J.A. Martineau and I.S. Krull, *Methods Enzymol.*, 4 (1992) 205–212.
36 H. Svensson, *Acta Chem. Scand.*, 15 (1961) 325–341.
37 X. Huang, W.F. Coleman and R.N. Zare, *J. Chromatogr.*, 480 (1989) 95–110.

Journal of Chromatography A, 652 (1993) 225–232
Elsevier Science Publishers B.V., Amsterdam

CHROM. 25 203

Separation of amino acid–oxazole derivatives of the redox coenzyme pyrroloquinoline quinone by capillary zone electrophoresis

Yukihiro Esaka, Yasuo Yamaguchi, Kenji Kano* and Masashi Goto

Gifu Pharmaceutical University, 5-6-1 Mitahora-higashi, Gifu 502 (Japan)

ABSTRACT

Condensation products (oxazole derivatives) from the reaction of the coenzyme pyrroloquinoline quinone (PQQ) with several α-amino acids were successfully separated by capillary zone electrophoresis. Addition of a certain organic solvent such as dimethyl sulphoxide to the electrolyte solution is essential for reproducible and complete separation. The organic modifier appears to prevent the oxazole derivatives from adsorbing on the capillary wall. Product analysis of the condensation reactions of PQQ with amino acids was performed by this method and the mechanism is discussed briefly. PQQ-spiked bovine serum was also analysed. Unsubstituted type 1 oxazole derivative was predominantly detected. This result suggests that most of the PQQ in mammalian fluids, if any, exists as PQQ derivatives, probably as a type 1 oxazole derivative.

INTRODUCTION

Pyrroloquinoline quinone (PQQ, see Fig. 1) was discovered in bacteria as a novel redox coenzyme of non-flavin or nicotinamide-dependent dehydrogenages in 1979 [1,2]. In early studies, several enzymes such as bovine serum amine oxidase [3,4] and methylamine dehydrogenase [5,6] were reputed to contain covalently bound PQQ and PQQ derivatives. Further, the occurrence of free PQQ in mammalian fluids and also, for example, in serum and milk was proposed [7,8]. Recently, however, topa quinone [9,10] and tryptophan tryptophyl quinone [11] have been proved to be the organic cofactors of copper-containing amine oxidases and methylamine dehydrogenase, respectively. In turn, the occurrence of PQQ in mammalian fluids has been questioned, while the biological importance [12–14] and pharmaceutical activity of PQQ in mammalian [11,15] continue to be emphasized.

Such confused circumstances appear to be partly due to a lack of reliable, sensitive and selective analytical methods for PQQ. We have reported a high-performance liquid chromatographic (HPLC) determination of free PQQ with an electrochemical detector coupled with amplification by a redox-cycling reaction of PQQ with glycine [7] and applied it to the determination of free PQQ in milk and swine serum [16]. However, no free PQQ was detected. In contrast, the immediate disappearance of free PQQ added to those biological fluids has been proved. This suggests that most of the PQQ in such biological media, if any, would be converted into some redox-inactive derivatives. Hence there seems to be an urgent need to develop an analytical method to speciate PQQ and its derivatives in biological fluids in order to provide some breakthrough in this confused field.

PQQ is known to be very reactive towards nucleophilic reagents [17–19]. Amino acids can be considered to be the most important and

* Corresponding author.

0021-9673/93/$06.00

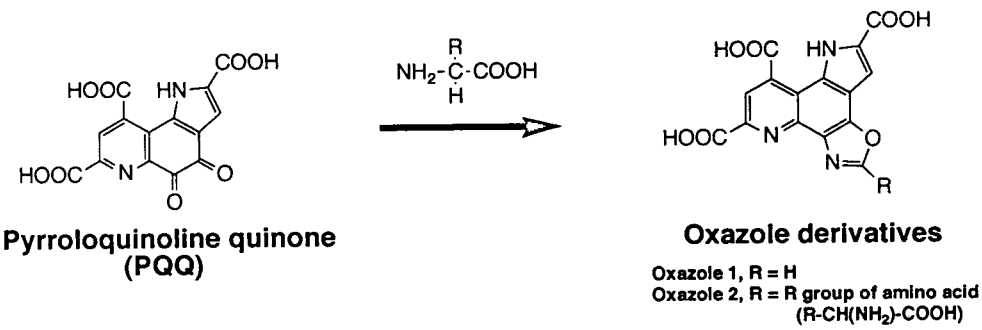

Fig. 1. Formation of amino acid–oxazole derivatives of PQQ.

widely distributed compounds among the many nucleophilic compound in biological fluids in view of the nucleophilic reaction towards PQQ. As shown in Fig. 1, free PQQ reacts readily with amino acids under aerobic conditions to yield corresponding oxazole derivatives as the final products [19–22]. The oxazole derivatives show variety in the structure of the R groups. Following Van Kleef *et al.* [21], the oxazoles with a hydrogen atom and amino acid residues as the R group will be called oxazoles 1 and 2, respectively, in this paper. All these oxazole derivatives have no redox–catalytic activity. Our hypothesis here is that the oxazole derivative(s) is (are) the major product(s) from PQQ in reactions in biological fluids.

Although reversed-phase (RP) HPLC with gradient elution [21] and ion-exchange chromatography [22] have been reported for the determination of the oxazoles, they might not necessarily be suitable for the separation of oxazole derivatives. The reasons are that the oxazole derivatives are strongly charged molecules owing to the three carboxyl groups and the acidic and basic amino acid residues and that their structures are only slightly different from each other (Fig. 1). RP-HPLC would not be suitable for the separation of such charged molecules and structurally related compounds with an identical charge might not be separated completely by ion-exchange chromatography.

Capillary zone electrophoresis (CZE) has a very high resolution for charged samples. Our aims in this work were to separate all oxazole derivatives by employing CZE with good resolution and to apply the method to the product analysis of the reaction between PQQ and each amino acid. Further, the speciation of PQQ in biological fluids will be discussed based on analyses of PQQ-spiked bovine serum samples.

EXPERIMENTAL

Materials

PQQ was obtained from Ube Industry (Tokyo, Japan) and used as received. Bovine serum was purchased from Nacalai Tesque (Kyoto, Japan). All other chemicals were of analytical-reagent grade.

Apparatus

Electrophoretic separation was performed in a fused-silica tube (GL Science, Tokyo, Japan) of 0.05 mm I.D. and a length of 550 mm, with an effective length for separation, *i.e.*, the length from the injection end to the detection cell, of 300 mm unless noted otherwise. A Matsusada Precision Devices (Kusatu, Japan) Model HCZE-30PNO high-voltage d.c. power supply, which can deliver high voltages up to 30 kV, was employed to supply the potential across the capillary. For UV–Vis spectrophotometric detection, a Jasco (Tokyo, Japan) 875-UV detector was employed. The detection wavelength was set at 250 or 420 nm. The flow cell was modified for capillary electrophoresis in our laboratory. A Shimadzu (Kyoto, Japan) Chromatopac C-R6A was used for data processing.

Sample preparation

Oxazole derivatives were generated by incubation of PQQ (0.01 *M*) and each amino acid

(0.004 g/ml) in 200 m*M* acetate buffer (pH 3.5) or 100 m*M* phosphate buffer (pH 7.9) at a volume ratio of 1:9. The incubation period was about 2 days at a room temperature. Oxazole 1 from glycine and oxazole 2 from valine were purified by thin-layer chromatography with silica gel plates (Kieselgel 60 F_{254}; Merck) in a mixed solvent of methanol–chloroform–water (70:30:7). These were used as the standard samples. In routine analysis, the reaction mixtures were subjected to CZE analysis without any purification.

A bovine serum sample was pretreated as follows. The sample was applied to an open column packed with DEAE-cellulose and washed with 200 ml of 0.1 *M* phosphate–Tris buffer (pH 6.0). The resin at the top of the column was removed and suspended in 30 ml of 0.5 *M* NaCl solution. After adjusting the pH of the solution to 0.5 with HCl to suppress the acid dissociation, adsorbed compounds were removed from the resin by shaking for 15 min and then extracted with isobutyl alcohol. The extracted solution was concentrated by evaporation. Control experiments for the standard oxazole 1 added to bovine serum showed a recovery of more than 95%.

Procedure

Just before each run, a separation capillary tube was purged with 0.1 *M* NaOH solution for 2 min and then with a desired buffer for 3 min by using an aspirator. The two ends of the tube were then dipped into two separate 1.5-ml reservoirs filled with the same buffer. The end at which samples were introduced was connected with a platinum electrode to positive high voltage, while the other end was connected with a platinum electrode to ground. Samples were introduced by siphoning at a height of 15 cm for a 5–10-s period.

RESULTS AND DISCUSSION

CZE separation of oxazole derivatives

In preliminary experiments in which electrophoresis of the standard samples (oxazole 1 from glycine and oxazole 2 from valine) was carried out with phosphate buffer containing no modifier, the oxazoles did not exhibit a peak or, even if a peak was detected, the electropherograms resulted in very poor reproducibility. We ascribe this phenomenon to the adsorption of the analytes on the capillary wall. To overcome such an adsorption effect, we examined several organic solvents as modifiers [23]. In this work, 10 m*M* phosphate buffer (pH 8.0) containing 5 or 10% (v/v) of a certain organic solvent was employed as an electrolyte solution, in which the three carboxyl groups in the oxazole derivatives are expected to be acid dissociated, as in the case of PQQ [24,25]. The addition of any one of dimethyl sulphoxide (DMSO), methanol (MeOH) and acetonitrile (ACN) was found to be efficient for obtaining reproducible peaks of the oxazoles. From the point of view of the complete separation of the oxazole derivatives (see below), however, DMSO was most preferred as a modifier for high resolution. The theoretical plate number (N) was calculated to be 2.75×10^5 for oxazole 1 based on the equation $N = l^2/2Dt$, where l, D and t are the separation distance, the diffusion coefficient and the migration time of a sample, respectively [26]. In the above calculation, the D value of PQQ ($3.9 \cdot 10^{-6}$ cm^2 s^{-1} [24]) was used. When MeOH was used as a modifier, a somewhat lower resolution was obtained with DMSO, and ACN gave an even lower resolution. This might be explained in terms of the relatively small value of D in the DMSO mixed solvent owing to its high viscosity and/or its large number of solvating molecules compared with the others. The electroosmotic flow-rate was virtually independent of the organic solvents used at such low concentrations, although at concentrations above 20% a marked effect on the flow-rate was observed, as has been reported elsewhere [27].

Reactions of PQQ with amino acids

Product analyses of the reactions of PQQ with several amino acids were performed by the present method together with absorption spectroscopy. Peak identification was performed by addition of standard samples and comparison of two electropherograms detected at 250 and 420 nm. Oxazoles are reported to exhibit a characteristic adsorption band around 420 nm [21], at

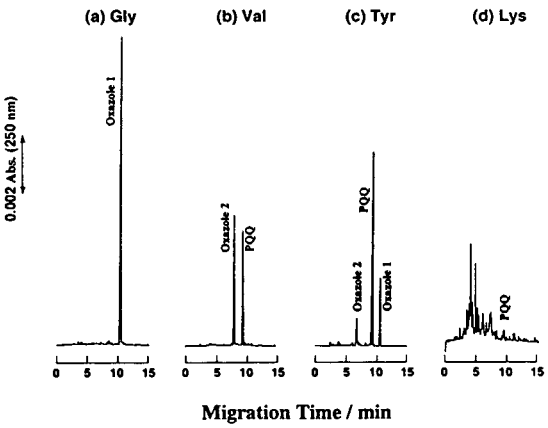

Fig. 2. Electropherograms of reaction solutions of PQQ with (a) glycine, (b) valine, (c) tyrosine and (d) lysine at pH 7.9 for 48 h at room temperature. Electrolyte solution, 10 m*M* phosphate buffer (pH 8.0) containing 5% (v/v) DMSO; capillary, 550 mm × 0.05 mm I.D. (300 mm effective length); separation voltage, 23 kV; current, 17 μA; injection (siphoning), 15 cm, 7 s; detection wavelength, 250 nm.

which the absorption of PQQ and other adducts is very weak compared with that at 250 nm.

Fig. 2 shows electropherograms of the reaction mixtures (pH 7.9) of four amino acids detected at 250 nm and Table I summarizes the yields of oxazoles 1 and 2 generated from several amino acids. Although the reaction products depend greatly on the amino acids and the reaction pH, we divided the amino acids into five classes (see Table I and below).

A typical amino acid in class 1 is glycine, with which the reaction led to the formation of oxazole 1 exclusively (Fig. 2a). The absorption spectrum of the reaction mixture gave a characteristic absorption maximum of oxazole 1 around 420 nm (Fig. 3, curve 1). Virtually identical results were obtained at pH 3.5 and 7.9. A similar behaviour was observed for the reaction with tryptophan (Table I). These results are in close agreement with those of other workers [20–22]. Threonine can be included in this class, although oxazole 2 was detected as a minor product.

In the reaction with valine, oxazole 2 was predominantly generated, while some PQQ remained unchanged (Fig. 2b). The absorption spectrum of the reaction mixture exhibited an

TABLE I

YIELDS OF OXAZOLES 1 AND 2 IN THE REACTIONS OF PQQ WITH SEVERAL AMINO ACIDS AT pH 3.5 AND 7.9

Incubation: 48 h at room temperature. Lys and Arg (class IV) yielded no detectable oxazoles but some adducts different from oxazoles. Pro, Hyp, Cys and Cys-Cys (class V) yielded no adducts.

Amino acid	Yield (%)				Class
	pH 3.5		pH 7.9		
	Oxazole 1	Oxazole 2	Oxazole 1	Oxazole 2	
Gly	100	–	100	–	I
Trp	97	–	92	–	I
Thr	75	22	84	12	I
Val	–	81	<1	67	II
Ala	3	87	13	72	II
Leu	–	93	6	72	II
Ile	–	84	3	61	II
Phe	3	97	2	83	II
Asn	–	95	6	70	II
Gln	–	97	3	90	II
Asp	–	85	–	38	II
Glu	4	92	6	50	II
Met	–	68	–	32	II
His	–	94	–	27	II
Tyr	–	73	23	12	III
Ser	2	94	91	8	III

absorption band around 420 nm (Fig. 3, curve 2). The product was virtually independent of the reaction pH. This class (class II) includes alanine, leucine, isoleucine, phenylalanine, asparagine, glutamine, aspartic acid and glutamic acid (Table I). For some of these amino acids, oxazole 1 was also formed as a minor product. Methionine and histidine yielded the corresponding oxazoles 2 as major products at pH 3.5 and 7.9 and can therefore be assigned to class II. However, there were several minor products different from the oxazoles.

With tyrosine, both oxazoles 1 and 2 were detected (Fig. 2c), but the ratio of oxazole 1 to oxazole 2 depended greatly on the reaction pH: at pH 3.5 oxazole 2 was generated preferentially, whereas at pH 7.9 oxazole 1 was the major product. A very similar behaviour was observed for serine. Such a pH-dependent reaction of

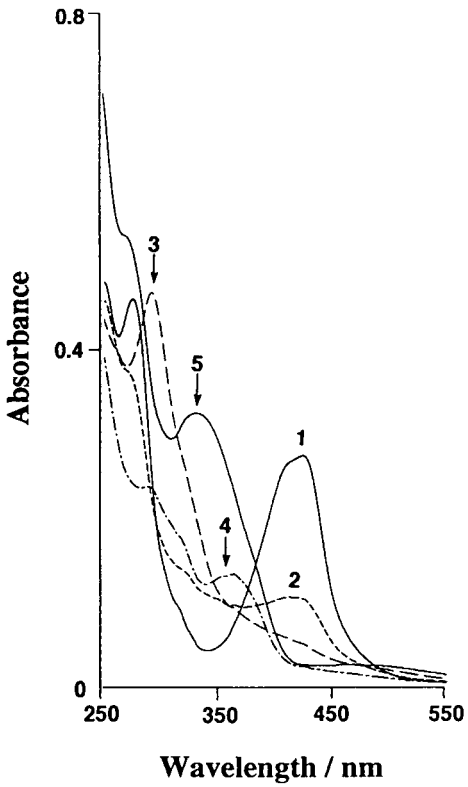

Fig. 3. Absorption spectra of reaction solutions of PQQ with (1) glycine, (2) valine, (3) lysine and (4) arginine and (5) free PQQ. Reaction conditions: PQQ (0.01 *M*)–amino acid (0.004 g/ml in 100 m*M* phosphate buffer, pH 7.9) (1:9) incubated for 48 h at room temperature. Before measurement, reaction solutions were diluted with a fivefold volume of 10 m*M* phosphate buffer (pH 7.9).

serine was reported first by Adachi [28] and then in detail by Itoh *et al.* [22].

Amino acids that did not yield any detectable oxazoles were assigned to class IV. Lysine exhibited a very complicated electropherogram (Fig. 2d), indicating the existence of several reaction pathways. The absorption spectrum of the reaction mixture was completely different from that of glycine. Although the formation of a small amount of oxazole derivatives is suggested by a shoulder around 420 nm (Fig. 3, curve 3), there appeared to be no significant peak in an electropherogram detected at 420 nm (not shown). The reaction with arginine resulted in the formation of one major adduct. This adduct, however, seems to be different from the oxazoles, because detection at 420 nm showed only a small peak and the absorption spectrum of the mixture was completely different from that of glycine (Fig. 3, curve 4).

Class V includes proline, hydroxyproline, cysteine and cystine. These amino acids did not give adducts, although cysteine is oxidized to cystine by PQQ [29].

The results suggest that there are two major competing reaction pathways to give oxazoles 1 and 2. We propose the mechanism shown in Fig. 4 for the formation of oxazoles. The reaction between PQQ and amino acids has been reported to proceed via an ionic mechanism involving carbinolamine-type intermediates which are dehydrated to give iminoquinones [9,28]. When C_α–C_β bond cleavage followed by decarboxylation proceeds from the iminoquinones, oxazole 1 is generated as a major product. The pathway is similar to that proposed by Van Kleef *et al.* [21]. In contrast, when decarboxylation is facilitated in the iminoquinone prior to the C_α–C_β bond fission, oxazole 2 will be predominantly produced. This reaction pathway has already been proposed by Ohshiro and co-workers [19,22].

The predominant path seems to depend on the amino acid residues and also the reaction conditions. For the amino acids in class I (except glycine), C_α–C_β bond cleavage would be facilitated, but decarboxylation is the path for the amino acids in class II. With serine and tyrosine (class III), base-catalysed C_α–C_β bond fission would occur rather than the decarboxylation at an elevated pH [22]. Lysine and arginine in class IV and histidine in class II are basic in nature and converted into some adducts different from oxazoles in major or minor processes. These amino acids have two nucleophilic groups in each molecule. In view of this, it is interesting to refer to the reactions of ethylenediamine [30] and aminoguanidine [31] with PQQ, in which pyrazine and triazine derivatives, respectively, are generated.

Fig. 5 illustrates an electropherogram of a mixture of the reaction solutions of PQQ with most of the amino acids in classes I, II and III (glycine, tryptophan, threonine, valine, alanine, leucine, phenylalanine, asparagine, glutamine,

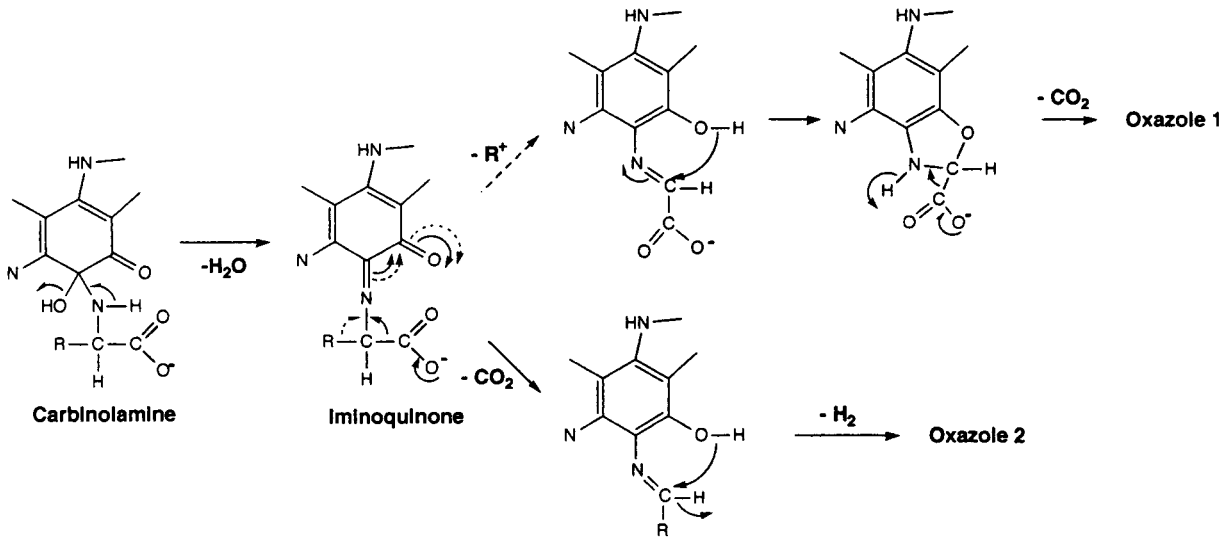

Fig. 4. Proposed mechanism of the formation of oxazoles 1 and 2.

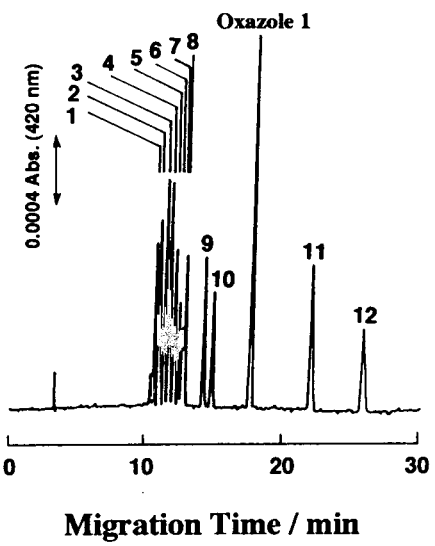

Fig. 5. Electropherogram of a mixture of reaction solutions of PQQ with several amino acids at pH 3.5. Electrolyte solution, 10 m*M* phosphate buffer (pH 8.0) containing 5% (v/v) DMSO; capillary, 700 mm × 0.05 mm I.D. (450 mm effective length); separation voltage, 25 kV; current, 14 μA; injection (siphoning), 15 cm, 7 s; detection wavelength, 420 nm. Peaks 1–12: oxazoles 2 generated from tyrosine, histidine, phenylalanine, leucine, glutamine, asparagine, threonine, valine, serine, alanine, glutamic acid and aspartic acid, in that order.

aspartic acid, glutamic acid, histidine, tyrosine and serine) except isoleucine and methionine. Each peak was identified by the addition of the corresponding oxazole derivative. The oxazole 2 from isoleucine gave a peak at a position identical with that of the oxazole 2 from leucine owing to their strong structural similarity. The peak of the oxazole 2 from methionine overlapped with that of glutamine. The amino acids in class IV would make the electropherograms complicated because they yield many kinds of minor products, as mentioned above.

Baseline resolution of most of the oxazole derivatives was obtained, except for two oxazoles 2 from threonine and valine, within *ca.* 25 min. The present separation appears to be much superior to those obtained with HPLC in terms of the resolution and the separation time. The detection limit for oxazole 1 was *ca.* 50 fmol ($S/N = 5$, 10 μM, *ca.* 5-nl injection).

The detailed mechanism of the reaction of PQQ with amino acids has not been completely elucidated. However, this work demonstrates that CZE is a powerful tool for such mechanistic and/or kinetic studies. Further research is in progress.

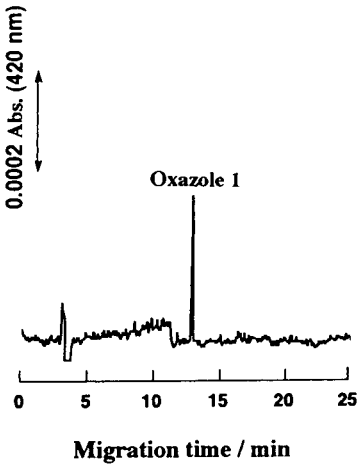

Fig. 6. Electropherogram of PQQ-spiked bovine serum sample. Electrolyte solution, 10 m*M* phosphate buffer (pH 8.0) containing 5% (v/v) DMSO; capillary, 550 mm × 0.05 mm I.D. (300 mm effective length); separation voltage, 17 kV; current, 13 μA, injection (siphoning), 15 cm, 7 s; detection wavelength, 250 nm. See text for pretreatment of the sample.

Analysis of PQQ-spiked bovine serum and native bovine serum

PQQ and its oxazole derivatives in PQQ-spiked bovine serum were determined using the present CZE method. The pretreatment was carried out about 48 h after the PQQ addition. An electropherogram of PQQ-spiked bovine serum sample is given in Fig. 6. For this sample, the PQQ concentration added to serum was $5 \cdot 10^{-6}$ *M* and a 30-fold concentration was carried out in the preparation. Oxazole 1 was observed as a major peak component. The peak of oxazole was identified by adding the standard oxazole 1 to the pretreated serum sample. The spectrum of the PQQ-spiked sample also supported the oxazole formation (not shown). When PQQ was added at a higher concentration of $2 \cdot 10^{-4}$ *M*, some oxazoles 2 together with the unreacted free PQQ were detected as minor peaks.

These results indicate that most of the PQQ existing in serum in the oxidized form is converted into oxazole 1 during the course of the reaction with free amino acids. The reason why oxazole 1 is a major product seems to be that the rate of the formation of oxazole 1 from glycine is much faster than that of oxazole 2 from other amino acids.

For a native (non-PQQ-spiked) bovine serum sample, however, no oxazole derivatives were found, even though a *ca.* 100-fold concentration was performed in the pretreatment. Hence the concentration of PQQ–oxazole derivatives in the bovine serum might be expected to be less than 10^{-7} *M*, if present at all. For further studies, some method of more effective and selective preconcentration seems to be required.

REFERENCES

1 J.A. Duine, J. Frank, Jr. and J.K. van Zeeland, *FEBS. Lett.*, 108 (1979) 443.
2 S.A. Salisbury, H.S. Forret, W.B.T. Cruse and O. Kennard, *Nature*, 280 (1979) 843.
3 C.L. Lobenstein-Verbeek, J.A. Jongejan, J. Frank and J.A. Duine, *FEBS Lett.*, 170 (1984) 305.
4 M. Ameyama, M. Hayashi, K. Matsushita, E. Shinagawa and O. Adachi, *Agric. Biol. Chem.*, 48 (1984) 561.
5 W.S. McIntire and J.T. Stults, *Biochem. Biophys. Res. Commun.*, 141 (1986) 562.
6 F.M.D. Vellieux and W.G. Hol, *FEBS Lett.*, 255 (1989) 460.
7 R. Flückiger, T. Woodtli and P.M. Gallop, *Biochem. Biophys. Res. Commun.*, 153 (1988) 353.
8 J.A. Jongejan and J.A. Duine (Editors), *PQQ and Quinoproteins*, Kluwer, Dordrecht, 1989, pp. 111–143.
9 S.M. Janes, D. Mu, D. Wemmer, A.J. Smith, S. Kaur, D. Maltby, A.J. Burlingame and J.P. Klinman, *Science*, 248 (1990) 981.
10 D.E. Brown, M.A. McGuirl, D.M. Dooley, S.M. Janes, D. Mu and J.P. Klinman, *J. Biol. Chem.*, 266 (1991) 4049.
11 W.S. McIntire, D.E. Wemmer, A. Chistoserdov and M.E. Lidstrom, *Science*, 252 (1991) 817.
12 P.M. Gallop, M.A. Paz, R. Flückiger and E. Henson, *2nd International Symposium on PQQ and Quinoproteins, November 1991, Yamaguchi, Japan*, Abstracts, p. 40.
13 J. Killgore, C. Smidt, L. Duich, N. Romero-Chapman, D. Tinker, K. Reiser, M. Merko, D. Hyde and R.B. Rucker, *Science*, 245 (1989) 850.
14 M. Ameyama, K. Matsushita, E. Shinagawa and O. Adachi, *Vitam. Horm.*, 46 (1991) 229.
15 H. Nishigori, *Nippon Nogeikagaku Kaishi*, 66 (1992) 1657 and references cited therein.
16 Y. Esaka, K. Kano, M. Sukeguchi and M. Goto, *Anal. Sci.*, 9 (1993) 207.
17 J.A. Duine, J. Frank, Jr. and J.A. Jongejan, *Adv. Enzymol.*, 59 (1987) 170–212; and references cited therein.
18 J.A. Jongejan and J.A. Duine (Editors), *PQQ and Quinoproteins*, Kluwer, 1989, pp. 195–241.

19 S. Itoh and Y. Ohshiro, *Bioorg. Chem.*, 19 (1991) 169, and references cited therein.
20 D.R. Sleath, J.B. Noar, G.A. Eberlein and T.C. Burice, *J. Am. Chem. Soc.*, 107 (1985) 3328.
21 M.A.G. van Kleef, J.A. Jongejan and J.A. Duine, *Eur. J. Biochem.*, 183 (1989) 41.
22 S. Ihoh, M. Mure, A. Suzuki, H. Murao and Y. Ohshiro, *J. Chem. Soc., Perkin Trans. 2* (1992) 1245.
23 N.J. Reinhoud, U.R. Tjaden, H. Irth and J. van der Greef, *J. Chromatogr.*, 574 (1992) 327.
24 K. Kano, K. Mori, B. Uno, T. Kubota, T. Ikeda and M. Senda, *Bioelectrochem. Bioenerg.*, 23 (1990) 227.
25 K. Kano, K. Mori, B. Uno, T. Kubota, T. Ikeda and M. Senda, *Bioelectrochem. Bioenerg.*, 24 (1990) 193.
26 J.W. Jorgenson and K.D. Lukacs, *Anal. Chem.*, 53 (1981) 1298.
27 C. Schwer and E. Kennder, *Anal. Chem.*, 63 (1991) 1801.
28 O. Adachi, *Nippon Nogeikagaku Kaishi*, 66 (1992) 1665, and references cited therein.
29 S. Itoh, N. Kato, M. Mure and Y. Ohshiro, *Bull. Chem. Soc. Jpn.*, 60 (1987) 420.
30 M. Mure, S. Itoh and Y. Ohshiro, *Chem. Lett.*, (1989) 1491.
31 M. Mure, K. Nii, S. Itoh and Y. Ohshiro, *Bull. Chem. Soc. Jpn.*, 63 (1990) 417.

Journal of Chromatography A, 652 (1993) 233–245
Elsevier Science Publishers B.V., Amsterdam

CHROM. 25 141

Capillary electrophoretic chiral separations using β-cyclodextrin as resolving agent

II. Bases: chiral selectivity as a function of pH and the concentration of β-cyclodextrin

Yasir Y. Rawjee, Robert L. Williams and Gyula Vigh*

Chemistry Department, Texas A&M University, College Station, TX 77843-3255 (USA)

ABSTRACT

An equilibrium model, first developed to describe the pH and cyclodextrin (CD) concentration dependence of the electrophoretic mobilities as well as the separation selectivities observed during the capillary electrophoretic (CE) separation of the enantiomers of weak acids, is extended to cover the separation of the enantiomers of weak bases as well. Model parameters are derived from three series of CE experiments: (i) one with cyclodextrin-free background electrolytes of varying pH values to obtain the ionic mobilities and base dissociation constant of the weak base enantiomers, (ii) one with constant, low pH background electrolytes with varying concentrations of β-cyclodextrin to obtain the mobilities and formation constants for the protonated base enantiomer–β-cyclodextrin complexes, and (iii) one with constant, high pH background electrolytes with varying concentrations of β-cyclodextrin to obtain the formation constants for the nonprotonated base enantiomer–β-cyclodextrin complexes. Homatropine was used as a model substance to test the validity of the model and an excellent agreement has been found between the calculated and the measured mobility and selectivity values. Baseline separation of the enantiomers of homatropine could be achieved in less than 15 min using a pH 6.25 phosphate buffer, which contained 15 m*M* β-cyclodextrin.

INTRODUCTION

In a recent paper [1] we reviewed the latest literature dealing with the use of cyclodextrins as chiral resolving agents in the capillary electrophoretic separations of enantiomers, and developed a theoretical model, based on simultaneous multiple equilibria, to describe the solute migration times, the solute mobilities, as well as the separation selectivities observed during the separation of the enantiomers of weak acids. The model contains, as parameters, the acid dissociation constants and ionic mobilities of the weak acid enantiomers, the formation constants and ionic mobilities of the dissociated enantiomer–β-cyclodextrin complexes, and the formation constants of the non-dissociated enantiomer–β-cyclodextrin complexes. Three different classes of separation problems were identified: in Type I separations only the non-dissociated acid enantiomers complex selectively with β-cyclodextrin, in Type II separations only the dissociated acid enantiomers complex selectively with β-cyclodextrin, while in Type III separations both the non-dissociated and dissociated acid enantiomers complex selectively with β-cyclodextrin. It was shown that for Type I acids, such as ibuprofen and fenoprofen, the separation selectivities were at their highest values in low pH background electrolytes (where the acids were only slightly dissociated), an entirely *non-intui-*

* Corresponding author.

0021-9673/93/$06.00

tive conclusion considering the coulombic nature of the CE separation process. Because we observed similar, often nonintuitive, migration and separation selectivity trends during the CE separation of the enantiomers of weak bases as well, the original theory developed for chiral weak acids is extended here to cover the separation of chiral weak bases as well. In Part I, the effects of the pH and the concentration of β-cyclodextrin in the background electrolyte will be studied experimentally using homatropine as a model substance, and the experimental results will be compared with the predictions of the theoretical model.

THEORY

The model

Let us assume that a background electrolyte contains a weak acid, HX, and its conjugate base, X^-, as the buffer components and β-cyclodextrin, CD, as the chiral resolving agent. The chiral weak base enantiomers to be separated from each other are R and S. Let the analytical concentration of the buffer be much higher than that of the CD and/or the analyte enantiomers, R and S. β-Cyclodextrin will complex with the buffer and the analyte, both in the non-dissociated and the dissociated form. If the buffer concentration is much higher than the CD concentration, and the CD concentration is much higher than the analyte concentration, then almost all the CD will be bonded in the CD–buffer complex, unless the formation constant for this complex is uncharacteristically small. Because the concentration of the chiral weak base analyte is very low with respect to the CD concentration, and because there is a sufficiently high excess of the uncomplexed buffer, to a first approximation, the analytical concentration of CD can be considered identical to the analytical concentration of the CD–buffer complexes. In addition, this analytical concentration remains constant and independent from the presence of the chiral weak base analyte. Therefore, to a first approximation, the equilibria which lead to the formation of the CD–buffer complexes may be omitted from the considerations, and, for the sake of simplicity, the terms CD and [CD] will be used instead of the proper but cumbersome CD–buffer and [CD–buffer] terms.

In an aqueous solution the weak base solute enantiomers, R and S, undergo base dissociation:

$$R + H_2O \rightleftarrows HR^+ + OH^- \quad (1)$$

$$S + H_2O \rightleftarrows HS^+ + OH^- \quad (2)$$

β-Cyclodextrin complexes with both the non-dissociated and dissociated analyte enantiomers:

$$R + CD \rightleftarrows RCD \quad (3)$$

$$S + CD \rightleftarrows SCD \quad (4)$$

$$HR^+ + CD \rightleftarrows HRCD^+ \quad (5)$$

$$HS^+ + CD \rightleftarrows HSCD^+ \quad (6)$$

The equilibrium expressions for these reactions are:

$$K_R = \frac{[HR^+][OH^-]}{[R]} \quad (7)$$

$$K_S = \frac{[HS^+][OH^-]}{[S]} \quad (8)$$

$$K_{RCD} = \frac{[RCD]}{[R][CD]} \quad (9)$$

$$K_{SCD} = \frac{[SCD]}{[S][CD]} \quad (10)$$

$$K_{HRCD^+} = \frac{[HRCD^+]}{[HR^+][CD]} \quad (11)$$

$$K_{HSCD^+} = \frac{[HSCD^+]}{[HS^+][CD]} \quad (12)$$

One can write mass balance equations for the R and the S related species using their analytical concentrations, c_R and c_S:

$$c_R = [R] + [HR^+] + [RCD] + [HRCD^+] \quad (13)$$

$$c_S = [S] + [HS^+] + [SCD] + [HSCD^+] \quad (14)$$

The mole fraction functions of the positively charged species HR^+, $HRCD^+$, HS^+, $HSCD^+$ become:

$$\alpha_{HR^+} = \frac{[HR^+]}{c_R} \quad (15)$$

$$\alpha_{HS^+} = \frac{[HS^+]}{c_S} \quad (16)$$

$$\alpha_{HRCD^+} = \frac{[HRCD^+]}{c_R} \quad (17)$$

$$\alpha_{HSCD^+} = \frac{[HSCD^+]}{c_S} \quad (18)$$

By combining eqns. 7–18 the mole fraction functions become:

$$\alpha_{HR^+} = \frac{\frac{K_R}{[OH^-]}}{1 + K_{RCD}[CD] + \frac{K_R}{[OH^-]} \cdot (1 + K_{HRCD^+}[CD])} \quad (19)$$

$$\alpha_{HS^+} = \frac{\frac{K_S}{[OH^-]}}{1 + K_{SCD}[CD] + \frac{K_S}{[OH^-]} \cdot (1 + K_{HSCD^+}[CD])} \quad (20)$$

$$\alpha_{HRCD^+} = \frac{K_{HRCD^+} \frac{K_R}{[OH^-]}[CD]}{1 + K_{RCD}[CD] + \frac{K_R}{[OH^-]} \cdot (1 + K_{HRCD^+}[CD])} \quad (21)$$

$$\alpha_{HSCD^+} = \frac{K_{HSCD^+} \frac{K_S}{[OH^-]}[CD]}{1 + K_{SCD}[CD] + \frac{K_S}{[OH^-]} \cdot (1 + K_{HSCD^+}[CD])} \quad (22)$$

The electroosmotic flow-corrected effective mobilities of the enantiomers are the linear combinations of the respective mole fractions and ionic mobilities [2]:

$$\mu_R^{eff} = \mu^0_{HR^+}\alpha_{HR^+} + \mu^0_{HRCD^+}\alpha_{HRCD^+} \quad (23)$$

$$\mu_S^{eff} = \mu^0_{HS^+}\alpha_{HS^+} + \mu^0_{HSCD^+}\alpha_{HSCD^+} \quad (24)$$

Combination of eqns. 19–24 results in:

$$\mu_R^{eff} = \mu^0_{HR^+} \cdot \frac{1 + \frac{\mu^0_{HRCD^+}}{\mu^0_{HR^+}} \cdot K_{HRCD^+}[CD]}{1 + K_{HRCD^+}[CD] + \frac{[OH^-]}{K_R} \cdot (1 + K_{RCD}[CD])} \quad (25)$$

$$\mu_S^{eff} = \mu^0_{HS^+} \cdot \frac{1 + \frac{\mu^0_{HSCD^+}}{\mu^0_{HS^+}} \cdot K_{HSCD^+}[CD]}{1 + K_{HSCD^+}[CD] + \frac{[OH^-]}{K_S} \cdot (1 + K_{SCD}[CD])} \quad (26)$$

Thus, the effective mobility of either enantiomer is a function of the ionic mobilities of both the free and the CD-complexed forms of that enantiomer, the base dissociation constants, the complex formation constants of both the ionic and the nondissociated forms of the enantiomers, as well as the hydroxide ion concentration and the CD concentration of the background electrolyte.

Separation selectivity, $A_{R/S}$, in CE can be expressed as the ratio of the effective mobilities [2]:

$$A_{R/S} = \frac{\mu_R^{eff}}{\mu_S^{eff}} \quad (27)$$

Substitution of eqns. 25 and 26 into eqn. 27 yields:

$$A_{R/S} = \frac{\mu^0_{HR^+}}{\mu^0_{HS^+}} \cdot \frac{1 + \frac{\mu^0_{HRCD^+}}{\mu^0_{HR^+}} \cdot K_{HRCD^+}[CD]}{1 + \frac{\mu^0_{HSCD^+}}{\mu^0_{HS^+}} \cdot K_{HSCD^+}[CD]} \cdot \frac{1 + K_{HSCD^+}[CD] + \frac{[OH^-]}{K_S} \cdot (1 + K_{SCD}[CD])}{1 + K_{HRCD^+}[CD] + \frac{[OH^-]}{K_R} \cdot (1 + K_{RCD}[CD])} \quad (28)$$

As long as the CD-free background electrolyte is an isotropic medium, the ionic mobilities of the two dissociated enantiomers are identical: $\mu^0_{HR+} = \mu^0_{HS+} = \mu^0_+$. The base dissociation constants of the two enantiomers are also identical: $K_R = K_S = K_b$. Thus, eqn. 28 is simplified to:

$$A_{R/S} = \frac{1 + \frac{\mu^0_{HRCD^+}}{\mu^0_+} \cdot K_{HRCD^+}[CD]}{1 + \frac{\mu^0_{HSCD^+}}{\mu^0_+} \cdot K_{HSCD^+}[CD]} \cdot \frac{1 + K_{HSCD^+}[CD] + \frac{[OH^-]}{K_b} \cdot (1 + K_{SCD}[CD])}{1 + K_{HRCD^+}[CD] + \frac{[OH^-]}{K_b} \cdot (1 + K_{RCD}[CD])} \quad (29)$$

Eqn. 29 indicates that the separation selectivity in a β-CD-based CE separation depends on both solute specific parameters and operator-dependent parameters. The solute specific parameters include the ionic mobilities of the free and the β-CD complexed enantiomers (μ^0_+, μ^0_{HRCD+} and μ^0_{HSCD+}), the base dissociation constant of the analyte (K_b), the complex formation constants of the ionic enantiomers (K_{HRCD+} and K_{HSCD+}), and the complex formation constants of the nondissociated enantiomers (K_{RCD} and K_{SCD}). The operator-dependent extensive parameters are the CD concentration and the hydroxide ion concentration (pH) of the background electrolyte.

Discussion of the model

Depending on whether (i) only the nonionic forms of the two enantiomers, (ii) only the ionic forms of the two enantiomers, or (iii) both forms of the two enantiomers interact differently with CD, there are three fundamentally different types of chiral CE separations.

Type I enantiomers. Type I enantiomers pose the simplest separation problem. Because only the non-ionic forms of the enantiomers interact differently with CD; K_{HRCD+} and K_{HSCD+} and μ^0_{HRCD+} and μ^0_{HSCD+} are identical:

$$K_{HRCD^+} = K_{HSCD^+} = K_{HBCD^+} \quad (30)$$

$$\mu^0_{HRCD^+} = \mu^0_{HSCD^+} = \mu^0_{HBCD^+} \quad (31)$$

Thus:

$$A_{R/S} = \frac{1 + \frac{\mu^0_{HBCD^+}}{\mu^0_+} \cdot K_{HBCD^+}[CD]}{1 + \frac{\mu^0_{HBCD^+}}{\mu^0_+} \cdot K_{HBCD^+}[CD]} \cdot \frac{1 + K_{HBCD^+}[CD] + \frac{[OH^-]}{K_b} \cdot (1 + K_{SCD}[CD])}{1 + K_{HBCD^+}[CD] + \frac{[OH^-]}{K_b} \cdot (1 + K_{RCD}[CD])} \quad (32)$$

The first term of eqn. 32 is reduced to unity, and the expression for separation selectivity becomes simply:

$$A_{R/S} = \frac{1 + K_{HBCD^+}[CD] + \frac{[OH^-]}{K_b} \cdot (1 + K_{SCD}[CD])}{1 + K_{HBCD^+}[CD] + \frac{[OH^-]}{K_b} \cdot (1 + K_{RCD}[CD])} \quad (33)$$

Therefore, the value of the separation selectivity factor will be different from unity, and its magnitude will depend on the values of K_{RCD}, K_{SCD}, K_{HBCD+}, K_b, [CD] and [OH^-]. If [CD] = 0, $A_{R/S}$ is unity, because there is no chiral separation without a resolving agent. $A_{R/S}$ increases with increasing hydroxide ion and β-cyclodextrin concentration. The theoretical maximum of separation selectivity (chiral selectivity, $A_{R/S} = K_{SCD}/K_{RCD}$) can be reached when the third term in both the numerator and the de-

nominator (the selective complexation term) becomes much larger than the second term in both the numerator and the denominator (the parasitic complexation term) as the concentrations of CD and OH^- are increased *ad infinitum*. This limiting value can be approximated when:

$$\frac{[OH^-]}{K_b} \cdot (1 + K_{SCD}[CD]) \geq 100(1 + K_{HBCD^+}[CD]) \quad (34)$$

i.e.:

$$K_{SCD} \geq \frac{100K_b - [OH^-]}{[OH^-][CD]} + \frac{100K_b}{[OH^-]} \cdot K_{HBCD^+} \quad (35)$$

If the hydroxide ion concentration is expressed as a multiple of the base dissociation constant,

$$[OH^-] = nK_b \quad (36)$$

(*i.e.* $pOH = pK_b - \log n$), then eqn. 35 becomes

$$K_{SCD} \geq \frac{100 - n}{n[CD]} + \frac{100}{n} \cdot K_{HBCD^+} \quad (37)$$

By taking $[CD] = 15$ m*M*, a value that can be safely maintained close to the ambient temperature solubility limit of β-CD, the highest pOH (lowest pH) values that lead to maximized chiral selectivities at the fastest migration rates can be calculated from eqn. 37. A few representative K_{SCD}, K_{HBCD+} and pOH combinations are listed in Table I. The minimum K_{SCD} requirement outlined in rows 1 and 2 of Table I is often fulfilled for Type I chiral bases resulting in a simple expression for separation selectivity:

$$A_{R/S} = \frac{1 + K_{SCD}[CD]}{1 + K_{RCD}[CD]} \quad (38)$$

These considerations explain the *non-intuitive* experimental observation that in the CE separation of some chiral weak bases, separation selectivity increases with increasing pH. Obviously, the parasitic complexation of the ionic enantiomers is reduced as, at higher pH values, the ionic species is gradually turned into the selectively complexing nonionic species. Optimization of such separations is very simple: the pH of the background electrolyte must be increased to increase selectivity until it becomes sufficiently large and produces the desired peak resolution with the available separation efficiency, resulting, automatically, in the shortest possible separation time.

Type II enantiomers. Type II enantiomer separations are more difficult to predict. Because only the dissociated forms of the enantiomers interact differently with CD, K_{RCD} and K_{SCD} are identical:

$$K_{RCD} = K_{SCD} = K_{BCD} \quad (39)$$

μ^0_{HRCD+} and μ^0_{HSCD+} may be equal or different, depending on the volume of the respective hydrated ionic enantiomer–CD complex. Thus, eqn. 29 is simplified only slightly:

$$A_{R/S} = \frac{1 + \frac{\mu^0_{HRCD^+}}{\mu^0_+} \cdot K_{HRCD^+}[CD]}{1 + \frac{\mu^0_{HSCD^+}}{\mu^0_+} \cdot K_{HSCD^+}[CD]} \cdot \frac{1 + K_{HSCD^+}[CD] + \frac{[OH^-]}{K_b} \cdot (1 + K_{BCD}[CD])}{1 + K_{HRCD^+}[CD] + \frac{[OH^-]}{K_b} \cdot (1 + K_{BCD}[CD])} \quad (40)$$

The R-enantiomer related values are in the numerator in the first term, and in the denominator in the second term of eqn. 40. Therefore, theoretically, $A_{R/S} < 1$, $A_{R/S} = 1$, and $A_{R/S} > 1$ are all possible, depending on the

TABLE I

REPRESENTATIVE COMPLEXATION CONSTANT AND MAXIMUM pOH VALUE PAIRS LEADING TO MAXIMUM SEPARATION SELECTIVITY FOR TYPE I AND TYPE II BASES

n	pOH	Type I base minimum K_{SCD} at [CD] = 15 m*M*	Type II base minimum K_{BCD} at [CD] = 15 m*M*
1000	$pK_b - 3$	$0.1K_{HBCD+} - 60$	$0.1K_{HSCD+} - 60$
100	$pK_b - 2$	K_{HBCD+}	K_{HSCD+}
10	$pK_b - 1$	$600 + 10K_{HBCD+}$	$600 + 10K_{HSCD+}$
1	pK_b	$6600 + 100K_{HBCD+}$	$6600 + 100K_{HSCD+}$

actual K and μ^0 values, and the hydroxide ion and the β-cyclodextrin concentrations, suggesting that the migration order of the enantiomers might be reversed by varying the concentration of the hydroxide ion.

For Type II enantiomers, because of the counteracting effects of the first and second terms in eqn. 40, separation selectivity can be maximized if one forces the second term to unity by increasing the value of the nonselective complexation term relative to the selective complexation term. This can be easily accomplished by increasing the concentration of the hydroxide ion, *i.e.* by going to higher pH values:

$$\frac{[OH^-]}{K_b} \cdot (1 + K_{BCD}[CD]) \geq 100(1 + K_{HSCD^+}[CD]) \quad (41)$$

or:

$$K_{BCD} \geq \frac{100K_b - [OH^-]}{[OH^-][CD]} + \frac{100K_b}{[OH^-]} \cdot K_{HSCD^+} \quad (42)$$

If, once again, the hydroxide ion concentration is expressed as a multiple of the base dissociation constant (*i.e.* $pOH = pK_b - \log n$), eqn. 42 becomes:

$$K_{BCD} \geq \frac{100 - n}{n[CD]} + \frac{100}{n} \cdot K_{HSCD^+} \quad (43)$$

Except for the subscripts, this relation is formally analogous to the one in eqn. 37. By taking [CD] = 15 mM as the limiting concentration, the highest pOH values that lead to maximized separation selectivities for Type II bases can be calculated from eqn. 43. A few representative K_{BCD}, K_{HSCD+} and pOH combinations are listed in Table I. Once again, the minimum K_{BCD} requirement shown in rows 1 and 2 of the last column of Table I is often easily fulfilled for Type II chiral bases resulting in a simple expression for separation selectivity:

$$A_{R/S} = \frac{1 + \frac{\mu^0_{HRCD^+}}{\mu^0_+} \cdot K_{HRCD^+}[CD]}{1 + \frac{\mu^0_{HSCD^+}}{\mu^0_+} \cdot K_{HSCD^+}[CD]} \quad (44)$$

These considerations explain the *non-intuitive* observation that in the CE separation of some chiral weak bases, selectivity increases with increasing pH. Optimization of the separation is still simple: the pH of the background electrolyte must be increased until the selectivity becomes sufficiently high, permitting the realization of the desired peak resolution, with the available separation efficiency, in the shortest period of time.

However, in the case of Type II bases, another alternative could also result in chiral resolution: one could suppress the last multiple in both the numerator and denominator of the second term in eqn. 40 by sufficiently lowering the pH of the background electrolyte. This would occur when

$$1 + K_{HSCD^+}[CD] \geq 100\frac{[OH^-]}{K_b} \cdot (1 + K_{BCD}[CD]) \quad (45)$$

that is, when

$$K_{HSCD^+} \geq \frac{100[OH^-] - K_b}{K_b[CD]} + \frac{100[OH^-]}{K_b} \cdot K_{BCD} \quad (46)$$

Using the $[OH^-] = nK_b$ approach, eqn. 46 becomes:

$$K_{HSCD^+} \geq \frac{100n - 1}{[CD]} + 100nK_{BCD} \quad (47)$$

By taking [CD] = 15 mM, the lowest pH values that lead to these alternative separation selectivity maxima can be calculated from eqn. 47. A few representative K_{BCD}, K_{HSCD+} and pH combinations are listed in Table I. Only the minimum K_{HSCD+} requirement shown in the last row of Table I is likely to occur in practice. In this case, the separation selectivity expression becomes:

$$A_{R/S} = \frac{1 + \frac{\mu^0_{HRCD^+}}{\mu^0_+} \cdot K_{HRCD^+}[CD]}{1 + \frac{\mu^0_{HSCD^+}}{\mu^0_+} \cdot K_{HSCD^+}[CD]} \cdot \frac{1 + K_{HSCD^+}[CD]}{1 + K_{HRCD^+}[CD]} \quad (48)$$

Although leading to higher mobilities, compared to the first approach, the use of low pH background electrolytes might be disadvantageous for

the separation selectivity of Type II weak bases. This is so, because the two terms in eqn. 48 counteract each other and result in separation selectivities that are lower than what could have been achieved in the high pH electrolytes (eqn. 44).

Type III enantiomers. It is very difficult to predict, a priori, what are the best conditions for maximization of the separation selectivity of Type III enantiomers. Since both the dissociated and the non-dissociated forms of the enantiomers interact differently with CD, eqn. 29 cannot be simplified and the "best" background electrolyte pH cannot be selected without the knowledge of the respective K and μ^0 values. A detailed pH study is indispensable if the optimum separation selectivity is to be determined. However, from a practical point of view, the use of a low pH electrolyte seems the most promising approach, because this would maximize the importance of the second term in eqn. 29 and result in as fast a separation as possible.

Determination of the model parameters

The model parameters (K_b, K_{RCD}, K_{SCD}, K_{HRCD+}, K_{HSCD+}, μ^0_{HR+}, μ^0_{HS+}, μ^0_{HRCD+}, μ^0_{HSCD+}), are generally not available from the literature for the particular chiral analyte studied. However, they can be determined by making a few simple assumptions and three sets of experiments, as follows.

In an isotropic, β-cyclodextrin-free background electrolyte both enantiomers have the same ionic mobilities and base dissociation constants. Therefore, both can be determined from electropherograms taken at different pH values, as widely discussed in the literature (*e.g.* ref. 3). When [CD] = 0, eqns. 25 and 26 simplify to eqn. 49:

$$\frac{\mu_+^{eff}}{\mu_+^0} = \frac{\mu_R^{eff}}{\mu_{R^+}^0} = \frac{\mu_S^{eff}}{\mu_{S^+}^0} = \frac{1}{1+\frac{[OH^-]}{K_R}} = \frac{1}{1+\frac{[OH^-]}{K_S}} = \frac{K_b}{K_b+[OH^-]} \quad (49)$$

$$\frac{1}{\mu_+^{eff}} = \frac{1}{\mu_+^0} + \frac{[OH^-]}{\mu_+^0 K_b} \quad (50)$$

from which the μ_+^0 and the K_b values can be determined by plotting $1/\mu_+^{eff}$ as a function of $[OH^-]$, where μ_+^{eff} is, naturally, corrected for the electroosmotic flow.

When $pOH = pK_b + 3$, $[R] \ll [HR^+]$ and $[S] \ll [HS^+]$, then eqns. 13 and 14 become:

$$c_R = [HR^+] + [HRCD^+] \quad (51)$$

$$c_S = [HS^+] + [HSCD^+] \quad (52)$$

and with these, eqns. 19–22 simplify to:

$$\alpha^*_{HR^+} = \frac{[HR^+]}{[HR^+]+[HRCD^+]} = \frac{1}{1+K_{HRCD^+}[CD]} \quad (53)$$

$$\alpha^*_{HS^+} = \frac{[HS^+]}{[HS^+]+[HSCD^+]} = \frac{1}{1+K_{HSCD^+}[CD]} \quad (54)$$

$$\alpha^*_{HRCD^+} = \frac{[HRCD^+]}{[HR^+]+[HRCD^+]} = \frac{K_{HRCD^+}[CD]}{1+K_{HRCD^+}[CD]} \quad (55)$$

$$\alpha^*_{HSCD^+} = \frac{[HSCD^+]}{[HS^+]+[HSCD^+]} = \frac{K_{HSCD^+}[CD]}{1+K_{HSCD^+}[CD]} \quad (56)$$

Substitution into eqns. 23 and 24 yields:

$$\mu_R^{eff} = \mu^0_{HR^+}\alpha^*_{HR^+} + \mu^0_{HRCD^+}\alpha^*_{HRCD^+} = \frac{\mu^0_{HR^+} + \mu^0_{HRCD^+}K_{HRCD^+}[CD]}{1+K_{HRCD^+}[CD]} \quad (57)$$

$$\mu_S^{eff} = \mu^0_{HS^+}\alpha^*_{HS^+} + \mu^0_{HSCD^+}\alpha^*_{HSCD^+} = \frac{\mu^0_{HS^+} + \mu^0_{HSCD^+}K_{HSCD^+}[CD]}{1+K_{HSCD^+}[CD]} \quad (58)$$

If $K_{HRCD+}[CD] \gg 1$ and $K_{HSCD+}[CD] \gg 1$, and the CD concentration is close to saturation (18 mM), that is, the enantiomer cations are sufficiently strongly complexed by CD ($K_{HRCD+} \geq$

500), then, considering that $\mu^0_{HR+} = \mu^0_{HS+} = \mu^0_+$, eqns. 57 and 58 can be rearranged to yield:

$$\mu_R^{eff} = \frac{\mu^0_+}{K_{HRCD^+}} \cdot \frac{1}{[CD]} + \mu^0_{HRCD^+} \quad (59)$$

$$\mu_S^{eff} = \frac{\mu^0_+}{K_{HSCD^+}} \cdot \frac{1}{[CD]} + \mu^0_{HSCD^+} \quad (60)$$

Both μ^0_{HRCD+} and K_{HRCD+} and μ^0_{HSCD+} and K_{HSCD+} can be determined by plotting μ_R^{eff} and μ_S^{eff} as a function of 1/[CD], because μ^0_+ is known from the previous calculations. With these values K_{RCD} and K_{SCD} can be obtained explicitly from eqns. 25 and 26 as:

$$K_{RCD} = \frac{K_b}{[OH^-][CD]\mu_R^{eff}} \left\{ (\mu^0_+ - \mu_R^{eff}) + K_{HRCD^+}[CD](\mu^0_{HRCD^+} - \mu_R^{eff}) - \frac{[OH^-]}{K_b} \cdot \mu_R^{eff} \right\} \quad (61)$$

$$K_{SCD} = \frac{K_b}{[OH^-][CD]\mu_S^{eff}} \left\{ (\mu^0_+ - \mu_S^{eff}) + K_{HSCD^+}[CD](\mu^0_{HSCD^+} - \mu_S^{eff}) - \frac{[OH^-]}{K_b} \cdot \mu_S^{eff} \right\} \quad (62)$$

If, on the other hand, $K_{HRCD+}[CD] \ll 1$ and $K_{HSCD+}[CD] \ll 1$, while the CD concentration is close to saturation (18 m*M*), that is, the enantiomer cations are very weakly complexed by CD ($K_{HRCD+} \leq 5$), then eqns. 57 and 58 can be rearranged to yield:

$$\mu_R^{eff} = \mu^0_+ + \mu^0_{HRCD^+} K_{HRCD^+}[CD] \quad (63)$$

$$\mu_S^{eff} = \mu^0_+ + \mu^0_{HSCD^+} K_{HSCD^+}[CD] \quad (64)$$

from which the multiples $\mu^0_{HRCD+}K_{HRCD+}$ and $\mu^0_{HSCD+}K_{HSCD+}$ can be determined. Assuming that $[OH^-] \geq 100K_b$, and that $K_{RCD}[CD] \gg 1$, substitution of these multiples into eqns. 25 and 26 results in eqns. 65 and 66,

$$\frac{\mu_R^{eff}[OH^-]}{K_b} = \frac{\mu^0_+}{K_{RCD}} \cdot \frac{1}{[CD]} + \frac{\mu^0_{HRCD^+} K_{HRCD^+}}{K_{RCD}} \quad (65)$$

$$\frac{\mu_S^{eff}[OH^-]}{K_b} = \frac{\mu^0_+}{K_{SCD}} \cdot \frac{1}{[CD]} + \frac{\mu^0_{HSCD^+} K_{HSCD^+}}{K_{SCD}} \quad (66)$$

which permit the determination of K_{RCD} and K_{SCD} from plots of the effective mobilities observed at low pOH as a function of 1/[CD].

If the complexation constants are intermediate values, $5 \leq K_{HRCD+} \leq 500$, then a least-square nonlinear parameter estimation method has to be used to extract the K_{HRCD+} and K_{HSCD+}, as well as the μ^0_{HRCD+} and μ^0_{HSCD+} values from the measured effective mobility values.

Once the ionic mobilities, the base dissociation constants, and the complex formation constants are known, the effective mobilities of the individual enantiomers and the separation selectivity of the given system can be calculated using eqns. 25, 26 and 29. The calculated values then can be compared with the measured values to test the validity of the model and predict the directions in which the background electrolyte parameters should be changed in order to achieve (or improve) the selectivity of a particular chiral CE separation.

EXPERIMENTAL

The electrophoretic experiments were completed with a P/ACE 2100 system, equipped with a variable-wavelength UV detector (Beckman, Fullerton, CA, USA). The UV detector was set at 210 nm. The electrode at the injection end of the capillary was kept at positive potential; the electrode at the detector end of the capillary was at ground potential.

Untreated, 25 μm I.D. × 150 μm O.D. fused-silica capillaries (Polymicro Technologies, Phoenix, AZ, USA) were used (39 cm from injector to detector, 45.8 cm total length). Before each and every series of measurements the capillaries were rinsed with deionized water and the background electrolyte (10 min and 15 min, respectively).

The samples were injected electrokinetically for 5 s at 10 kV potential. The sample concentrations were kept at 0.1 m*M*. In each run, a dilute solution of benzyl alcohol was coinjected

with the sample as a non-charged electroosmotic flow marker, providing us with the accurate corrected mobilities. All separations were completed at a thermostatting liquid bath temperature of 37°C.

The field strength used for the separations was varied between 150 and 660 V/cm, depending on the actual conductivity of the background electrolyte, in order to keep the power dissipation in the 80 to 100 mW range and insure linear potential *vs.* current plots (Ohm-plots).

β-Cyclodextrin was obtained from American Maize Products (Hammond, IN, USA). Reagent-grade phosphoric acid, lithium hydroxide, sodium hydroxide and racemic homatropine were obtained from Aldrich (Milwaukee, WI, USA), 250MHR PA hydroxyethyl cellulose (HEC) from Aqualon (Wilmington, DE, USA). All chemicals were used as received without further purification. All solutions were freshly prepared using deionized water from a Milli-Q unit (Millipore, Milford, MA, USA). The background electrolytes were prepared by adding 25 ml of a 140 m*M* H_3PO_4 stock solution, 25 ml of deionized water and 20 ml of a 1% (w/w) HEC stock solution to a 100 ml volumetric flask. Then the weighed amount of β-CD was added and the solution was stirred until the β-CD dissolved. Next, the flask was made up with deionized water almost to the mark, and the pH was adjusted to the desired value by adding up to a few hundred μl of saturated LiOH solution. Finally, the flask was made up to mark with deionized water. The background electrolyte was degassed prior to loading into the electrolyte reservoirs.

RESULTS AND DISCUSSIONS

First, the base dissociation constant, K_b, of homatropine was determined using background electrolytes which contained 0.2% (w/w) HEC and 35 m*M* phosphoric acid. The pH of the background electrolyte was varied in the 6 to 10.5 range by adding LiOH. The effective mobilities of homatropine, corrected for the electroosmotic flow, μ_+^{eff}, were determined in triplicate. The reciprocal effective mobilities were plotted as a function of the hydroxide ion concentration according to eqn. 50, for a power load of 85 mW and thermostatting liquid temperature of 37°C, and the K_b and μ_+^0 values were determined (Table II). In Fig. 1, the measured mobilities are shown by symbol ×, the least-square best-fit line is shown by the solid line. Because the background electrolytes used in these studies have a high ionic strength (in excess of 10 m*M*), accurate activity coefficient values cannot be calculated using the simple Debye–Hückel approach as suggested by Beckers *et al.* [3]. Yet, the experimentally found value, pK_b =

TABLE II

IONIC MOBILITY AND APPARENT EQUILIBRIUM CONSTANT DATA FOR HOMATROPINE

Conditions as in Figs. 1–4.

Parameter	Homatropine
μ_+^0 (10^{-5} cm^2/Vs)	23.40
K_b (*M*)	$3.47 \cdot 10^{-5}$
pK_b	4.46
pK_b (ref. 4)	4.1
$\mu^0_{HRCD+} = \mu^0_{HSCD+}$ (10^{-5} cm^2/Vs)	9.15
K^0_{HRCD+} (M^{-1})	87.8
K^0_{HSCD+} (M^{-1})	104.0
K_{RCD} (M^{-1})	1305
K_{SCD} (M^{-1})	1350

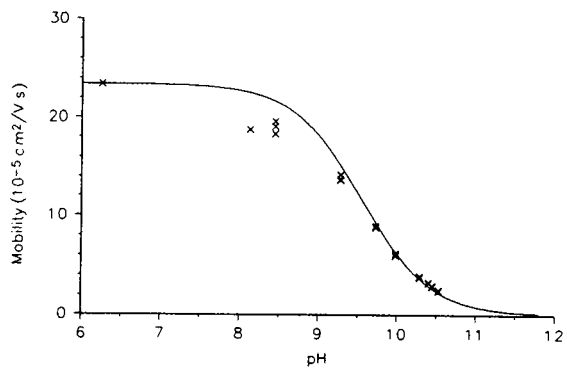

Fig. 1. The effective mobility *vs.* pH plot for homatropine in 35 m*M* H_3PO_4, 0.2% HEC background electrolyte (pH adjusted with saturated LiOH solution) at a thermostatting liquid temperature of 37°C and power load of 85 mW. Symbols: × = measured values; —— = least-square best-fit line.

4.46 is close to the infinite dilution $pK_b = 4.1$ value reported in the literature [4].

Second, the effects of the β-cyclodextrin concentration were tested in a high pOH (low pH) background electrolyte in which homatropine is almost completely dissociated (pH 6.25). When the effective mobilities were plotted against the reciprocal CD concentration according to eqns. 59 and 60, estimates could be obtained for μ^0_{HRCD+}, μ^0_{HSCD+}, K_{HRCD+} and K_{HSCD+} from the limiting slopes and the intercepts. These estimates were then used to find the parameters which assure the best fit between the measured values and the values calculated by eqns. 57 and 58. The μ^0_{HRCD+}, μ^0_{HSCD+}, K_{HRCD+} and K_{HSCD+} parameters obtained for homatropine are listed in Table II. The μ^0_{HRCD+} and the μ^0_{HSCD+} values are equal, and are about half as large as the μ^0_+ value, reflecting the size increase brought about by β-cyclodextrin. In Fig. 2, the measured values of the more mobile and the less mobile enantiomers of homatropine (symbols + and ×) are compared with the calculated effective mobilities (solid and dashed lines) obtained from eqns. 57 and 58 and the best-fit parameters listed in Table II. The agreement between the measured and calculated values is good.

Third, a series of mobility measurements were carried out in a pH 9.63 background electrolyte in which homatropine is only partially dissociated. The β-CD concentration was varied between 0 and 15 m*M*, all other conditions were kept the same as in Fig. 2, except for the pH. The complex formation constants of the nondissociated homatropine enantiomers (K_{RCD}, K_{SCD}) were calculated using the effective mobility values, eqns. 61 and 62, the respective parameters from Table II, and the actual [CD] and [OH^-] values. The result are listed in the last two lines of Table II. Interestingly, the complex formation constants of the nondissociated homatropine enantiomers (K_{RCD}, K_{SCD}) are about ten times larger than the respective complexation constants of the cations (K_{HRCD+}, K_{HSCD+}). In Fig. 3, the measured mobilities of homatropine

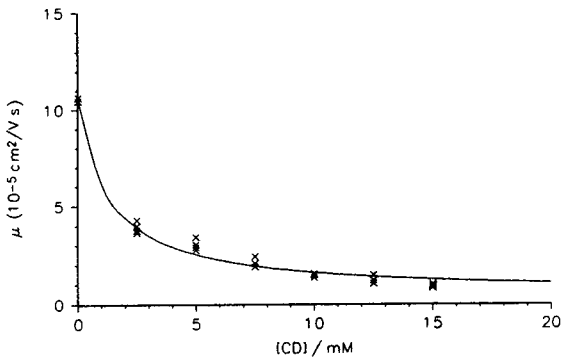

Fig. 3. Effective mobility of homatropine as a function of the β-cyclodextrin concentration in a pH 9.63 background electrolyte. Conditions as in Fig. 1. Symbols: × = measured values; —— = calculated values using the parameters in Table II.

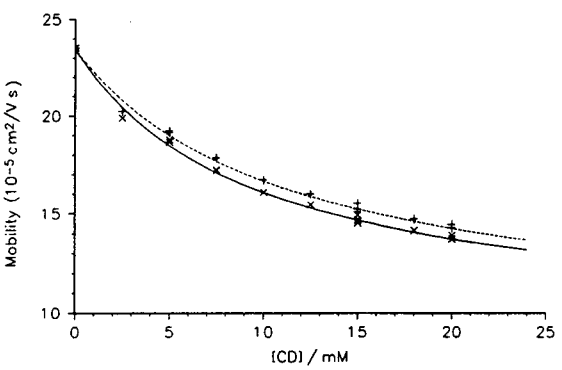

Fig. 2. Effective mobilities of the homatropine enantiomers as a function of the β-cyclodextrin concentration in a pH 6.25 background electrolyte. Conditions as in Fig. 1. Symbols: ×, + = measured values; lines = calculated values using the parameters in Table II.

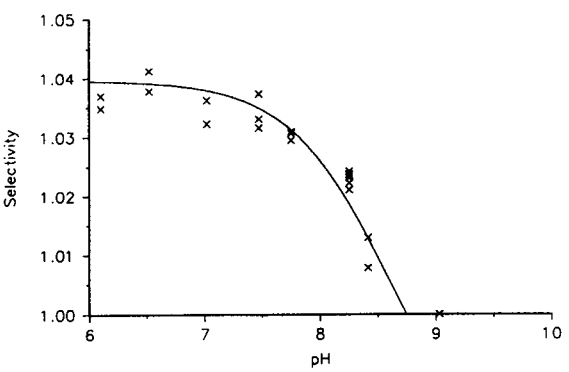

Fig. 4. Comparison of the measured and calculated separation selectivities for homatropine as a function of the pH. Conditions as in Fig. 1, except [CD] = 15 m*M*. Symbols: × = measured values; —— = calculated values using eqn. 29 and the parameters in Table II.

(symbol ×) are compared with the calculated effective mobilities (solid line) obtained from eqns. 25 and 26 using the best-fit parameters listed in Table II. The agreement between the measured and calculated values is good.

In order to further test the correctness of the estimated parameters, another series of measurements were made by keeping the β-CD concentration constant at 15 m*M* and varying the pH of the background electrolyte between 6 and 9. The measured separation selectivity values are shown by symbol × in Fig. 4, the values calculated by eqn. 29 using the parameters in Table II are shown as solid lines. The agreement is quite good. The quality of the fit between the calculated and the measured values can be tested in an orthogonal plane as well as shown in Fig. 5. The measured separation selectivity values obtained at pH 6.25 as a function of the β-cyclodextrin concentration (symbol ×) are compared here with the calculated values (solid line) obtained by eqn. 29 using the parameters in Table II. The agreement once again is good, indicating that the proposed model, indeed, correctly represents separation selectivity.

Using the parameter values in Table II and eqns. 25, 26 and 29, the electrophoretic mobility surface and the separation selectivity surface can be calculated as a function of both the pH and the β-cyclodextrin concentration as shown in Figs. 6–9. In Figs. 6 and 8 the mobility and the separation selectivity surfaces are shown up to 150 m*M* β-CD concentration. The same surfaces are shown in Figs. 7 and 9 up to the experimentally accessible 15 m*M* β-CD concentration. For the Type III solute, homatropine, mobility decreases rapidly as β-CD is added to the background electrolyte, and begins to level off above [CD] = 10 m*M* (Figs. 6 and 8). Along the pH axis, most of the mobility change occurs in the $8 < pH < 10$ range, in agreement with the $pK_b = 4.46$ value, where the mobility surface is shaped like a regular mole fraction function.

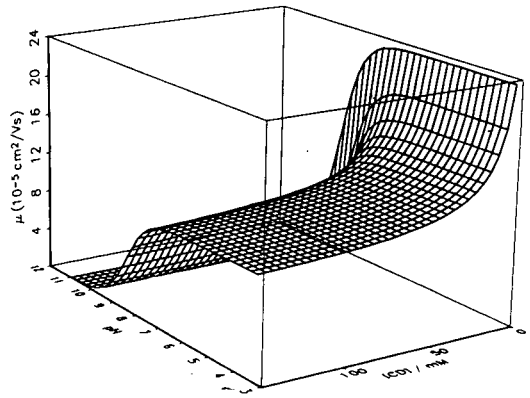

Fig. 6. Three-dimensional effective mobility surface for the more mobile enantiomer of homatropine as a function of the β-CD concentration and the pH, calculated using eqn. 25 and the parameters in Table II for the 0–150 m*M* β-CD range.

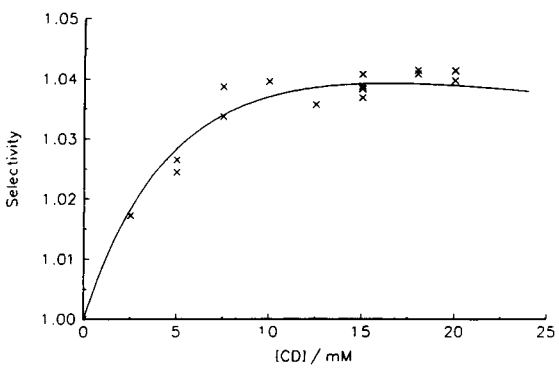

Fig. 5. Comparison of the measured and calculated separation selectivities for homatropine as a function of the β-CD concentration. Conditions as in Fig. 1, except pH 6.25. Symbols: × = measured values; —— = calculated values using eqn. 29 and the parameters in Table II.

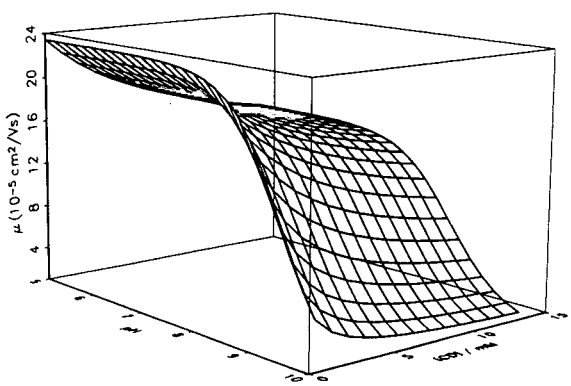

Fig. 7. Three-dimensional effective mobility surface for the more mobile enantiomer of homatropine as a function of the β-CD concentration and the pH, calculated using eqn. 25 and the parameters in Table II for the experimentally accessible 0–15 m*M* β-CD range.

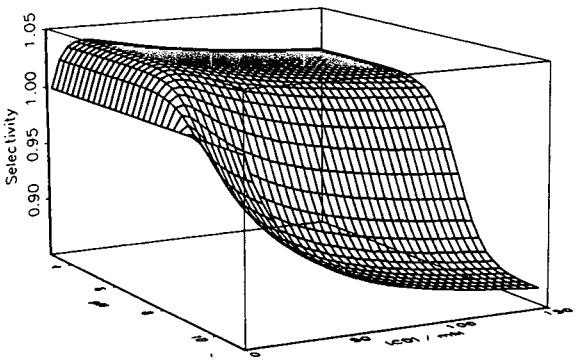

Fig. 8. Three-dimensional separation selectivity surface for homatropine as a function of the β-CD concentration and the pH, calculated using eqn. 25 and the parameters in Table II for the 0–150 m*M* β-CD range.

As shown in Fig. 8, the shape of the separation selectivity surface is much more complex. At any given pH in the acidic range, selectivity passes a maximum as the β-cyclodextrin concentration is increased. However, at low pH, this selectivity maximum is outside the experimentally accessible 0–15 m*M* range. As the pH is increased at a constant, sufficiently high β-CD concentration, the separation selectivity value falls below unity, indicating that the migration order of the two enantiomers is reversed. This is understandable when one considers that the second term in eqn. 29 approaches unity as the $[OH^-]/K_b$-multiplied terms in both the numerator and the denominator of eqn. 29 assume a large value with respect to both $(1 + K_{HSCD+}[CD])$ and $(1 + K_{HRCD+}[CD])$. This means that it is now the first term of eqn. 29, in which the R enantiomer-related parameters are in the numerator, that determines the value of the separation selectivity.

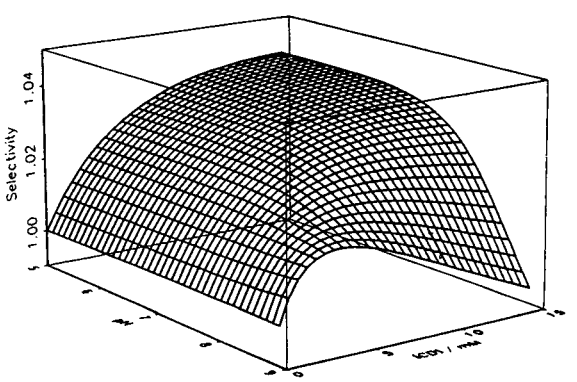

Fig. 9. Three-dimensional separation selectivity surface for homatropine as a function of the β-CD concentration and the pH, calculated using eqn. 25 and the parameters in Table II for the experimentally accessible 0–15 m*M* β-CD range.

As shown in Fig. 9, at low pH values, separation selectivity increases monotonously as the β-CD concentration is varied within the experimentally accessible 0–15 m*M* range. This indicates that as far as separation selectivity is concerned it is beneficial to use a saturated β-CD solution. However, as the pH is increased beyond 7, selectivity becomes lower than at low pH, and both the β-CD concentration-dependent maximum and the reversal in the migration order occur in the 0–15 m*M* β-CD concentration range. This indicates that, from a practical point of view, it is better and safer to operate in the low pH range when the solute is a Type II or Type III base, because there is a fairly broad selectivity plateau between pH 2 and 7. Experimentally, the reversal of the migration order could not be demonstrated, because the separation efficiency of the system was too low at high pH due to greater mobility dispersion, ion-exchange effects [5] and limited peak capacity caused by the electroosmotic flow.

By considering the shapes of both the mobility and the selectivity surfaces of homatropine, a Type III solute, one may conclude that the best selectivity optimization strategy would call for β-CD concentrations that are close to the solubility limit (15 m*M* is safe) and background electrolyte pH values that are at or below pH 7, providing the highest selectivity in the shortest separation time.

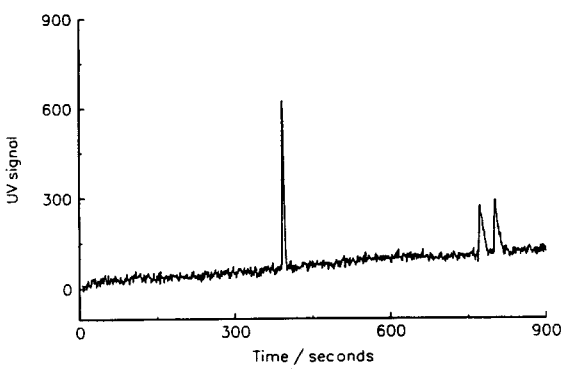

Fig. 10. CE separation of the benzyltrimethylammonium chloride (first peak) and enantiomers of homatropine. Conditions: 0.2% HEC, 35 m*M* H_3PO_4, 15 m*M* β-CD.

The electropherogram of a racemic mixture of homatropine is shown in Fig. 10. Baseline separation of the enantiomers can be achieved with 15 m*M* β-CD at pH 6.25 in about 15 min.

CONCLUSIONS

An equilibrium model has been developed to describe the electrophoretic mobilities of the enantiomers of chiral weak bases and the resulting separation selectivities, as a function of the pH and the β-cyclodextrin concentration of the background electrolyte. The parameters of the model can be readily derived from three sets of specifically designed separation experiments: the first at varying pH values without β-cyclodextrin in the background electrolyte, the second at low pH values with varying concentrations of β-cyclodextrin in the background electrolyte, and the third at high pH values with varying concentrations of β-cyclodextrin in the background electrolyte. The validity of the model has been demonstrated by comparing the measured and the calculated mobility and selectivity values for a test probe, homatropine. Homatropine behaves as Type III solute (defined under Theory) with β-cyclodextrin as the resolving agent, permitting rugged and fast separations in low pH background electrolytes which contain β-cyclodextrin at high concentrations. Further work is under way in our laboratory to extend the migration and separation selectivity model proposed here to other resolving agents as well [5].

ACKNOWLEDGEMENTS

Partial financial support of this project by the National Science Foundation (CHE-8919151), the Dow Chemical Company (Midland, MI, USA), Genentech (South San Francisco, CA, USA) and Beckman Instruments (Fullerton, CA, USA) is gratefully acknowledged. The authors are also indebted to Beckman Instruments for the loan of the P/ACE 2100 instrument. American Maize Products Corp. (Hammond, IN, USA) and Aqualon Corp. (Wilmington, DE, USA), respectively, are acknowledged for the donation of the β-cyclodextrin and the hydroxyethyl cellulose samples used in this project.

REFERENCES

1 Y.Y. Rawjee, D.U. Staerk and Gy. Vigh, *J. Chromatogr.*, 635 (1993) 291.
2 J.W. Jorgenson and K.D. Lukacs, *Anal. Chem.*, 53 (1981) 1298.
3 J.L. Beckers, F.M. Everaerts and M.T. Ackermans, *J. Chromatogr.*, 537 (1991) 407.
4 F.J. Muhtadi, M.M.A. Hassan and A.F.A. Afify, in K. Florey (Editor), *Analytical Profiles of Drug Substances*, Vol. 16, Academic Press, London, 1987, p. 245.
5 Y.Y. Rawjee and Gy. Vigh, *Anal. Chem.*, 65 (1993) in press.

Journal of Chromatography A, 652 (1993) 247–252
Elsevier Science Publishers B.V., Amsterdam

CHROM. 25 144

Chiral separations using an immobilized protein–dextran polymer network in affinity capillary electrophoresis

Peng Sun, Geoffrey E. Barker and Richard A. Hartwick*

Department of Chemistry, State University of New York at Binghamton, Binghamton, NY 13902 (USA)

Nelu Grinberg

Merck Research Laboratories, Rahway, NJ (USA)

Roman Kaliszan

Medical Academy, Gdansk (Poland)

ABSTRACT

An improvement in affinity capillary electrophoresis (ACE) was achieved by covalently linking bovine serum albumin (BSA) to a high-molecular-mass dextran (M_r 2 000 000) using cyanogen bromide. The efficiency of the binding reaction was greater than 99%, measured through quantitative separation of the protein and protein–dextran polymer network mixture on a bare capillary using capillary electrophoresis (CE). Baseline separation of leucovorin (LV) enantiomers was obtained under 9 min using a linear polyacrylamide-coated capillary (with an effective length of 20 cm) filled with the BSA–dextran polymer network. The present work offers several significant advantages over other approaches to ligand immobilization, and can be generally applied to a wide variety of ligand–substrate systems.

INTRODUCTION

With the improved understanding of the biological action of drugs with respect to their stereochemistry, investigations concerning the pharmacology and toxicology of individual drug enantiomers have become increasingly more important. Therefore chiral separation of pharmaceutical compounds is currently of great concern. Many liquid chromatographic techniques for the separation of enantiomers have been developed and chiral stationary phases are now widely available commercially. Among the various chiral stationary phases investigated, immobilized protein phases such as α-acid glycoprotein (AGP) [1,2], ovomucoid [3–5], and bovine serum albumin (BSA) [6–8] have been quite successful in a variety of separations, although separation efficiencies have often been poor [9]. Columns are also quite expensive, and have limited lifetimes.

CE is a technique which has developed considerably during the past several years [10–12]. CE distinguishes itself from other liquid-phase separation methods in that high efficiencies (usually greater than 100 000 plates) are obtained. Furthermore, CE can be viewed as a micro-scale to nano-scale analytical procedure and is advantageous when the availability of sample, mobile

* Corresponding author.

0021-9673/93/$06.00

phase, or separation phase is limited. Separation of racemic mixtures using CE has been reported so far using cyclodextrin (CD) [13,14], ligand-exchange principles [15,16], and mixed micelles in the run buffer [17,18]. Recently, a method for chiral separation of leucovorin (LV) using BSA as a run buffer additive was developed in our laboratory [19].

To date, capillary affinity gel electrophoresis (CAGE) has developed rapidly. It has opened up new horizons for the biospecific separation of DNA and RNA as well as investigating the interactions between biological molecules. Using capillaries filled with conjugated polyacrylamide-poly(9-vinyladenine) gel, Baba *et al.* [20] achieved the base-specific separation of oligodeoxynucleotides. A CAGE method for the separation of tryptophan enantiomers using capillaries filled with gel consisting of BSA cross-linked with glutaraldehyde was recently reported by Birnbaum and Nilsson [21]. Baseline separation of tryptophan enantiomers was obtained by this method. However, a limitation of this method is detection interference caused by the opaque off-white color of the BSA cross-linked gel. To overcome this problem, the capillary must be partially filled with the gel, with detection of sample occurring at a point on the capillary that is not occupied by the gel. This creates fabrication difficulties, and in addition, once the gel is formed in the capillary it is permanent and cannot be removed.

In this paper, a method is presented for synthesizing BSA–dextran conjugates. The covalent linking of a protein, DNA or other species to a high-molecular-mass, UV-transparent dextran polymer network [22] offers several significant advantages over existing methods. Since the network is replaceable, fresh stationary phase can be used after each injection if necessary, with good reproducibility. The phase ratio of the ligand site can be controlled by mixing ligand–polymer with plain polymer in any proportion. Polymer networks are also less subject to channeling and other defects arising when the capillaries are coiled or moved. The feasibility of using a replaceable BSA–dextran polymer network for chiral separations is presented in this paper.

EXPERIMENTAL

Chemicals

Acrylamide, N,N,N′,N′-tetramethylethylenediamine (TEMED), and ammonium persulfate (APS) were obtained from Bio-Rad Labs. (Richmond, CA, USA). Dextran (M_r 2 000 000), cyanogen bromide, and BSA were purchased from Sigma (St. Louis, MO, USA). 3-Methacryloxypropyltrimethoxysiline was obtained from HULS America (Bristol, PA, USA) and calcium leucovorin (LV) from Lederle Laboratories, American Cyanamid (Pearl River, NY, USA). All other chemicals were from Fisher Scientific (Fair Lawn, NJ, USA).

Apparatus

A CE apparatus which was designed and constructed in our laboratory was used. It contains a Spectra 100 UV detector (Spectra Physics, Reno, NV, USA), a CZE 1000 PN 30 high-power voltage supply (Spellman, Plainview, NY, USA), and a high-power supply local controller (Chamonix Industries, Binghamton, NY, USA). The controller box could be programmed for electrokinetic sample introduction as well as adjustment of the actual separation voltage. The electropherograms were processed on SP 4400 integrator (Spectra Physics).

Polymer network synthesis and preparation of capillaries

The immobilization of BSA on dextran was accomplished by the method reported by Takahura *et al.* [23] with some modification (scheme of synthesis reaction is shown in Fig. 1). Dextran (200 mg) was dissolved in 10 ml of 10 m*M* phosphate buffer at pH 7.12. This solution was degassed for 20 min, then it was activated by cyanogen bromide (20 mg) at pH 10.7 for 20 min [24]. Afterwards the pH was adjusted to 9.0 and BSA (20 mg) was added to this solution. The binding reaction was allowed to proceed for 12 h at room temperature. The efficiency of this binding reaction was determined by CE using a bare fused-silica capillary (75 μm I.D. × 360 μm O.D., Polymicro Technologies, Phoenix, AZ, USA).

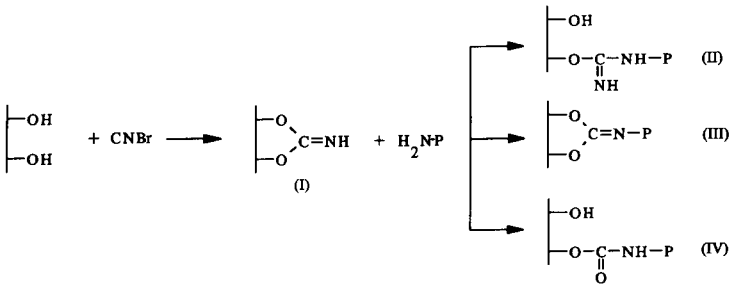

Fig. 1. Scheme of immobilization of BSA on dextran. I = Active imidocarbonate; II = N-substituted isoureas; III = N-substituted imido carbonate; IV = N-substituted carbamates.

Capillaries were coated with linear polyacrylamide by the method reported by Hjertén [25]. After being rinsed with water, the coated capillary was filled with the BSA–dextran network by flushing the capillary with the polymer network solution. The capillary was equilibrated by applying an electric field of 200 V/cm for 20 min using a run buffer consisting of 10 m*M* phosphate at pH 7.12. The samples, *e.g.* LV, were injected through electrokinetic injection. The BSA–dextran polymer network can be removed and replaced by means of a syringe.

The mobility of the BSA–dextran complex was estimated to be *ca.* $3 \cdot 10^{-6}$ cm^2 V^{-1} s^{-1}. It is interesting to note that this mobility results in a migration time of *ca.* 17 h for the BSA–dextran complex to travel one column length, in the absence of any electroosmotic flow. The capillaries used in this work are coated with linear polyacrylamide, and electroosmotic flow of the coated capillaries was found to be very slow (neutral molecules did not migrate to the detection window in several hours when 300 V/cm high voltage was applied). In many situations, a

RESULTS AND DISCUSSION

Immobilization of BSA on dextran

Complete reaction of the ligand to the polymer network is essential for good separation efficiency, otherwise the unbound ligand will travel at a velocity different from the bound fraction, creating the equivalent of active sites on a standard chromatographic separation. The efficiency of binding reaction of BSA on dextran was determined by CE to be greater than 99%. Fig. 2 shows an electropherogram of the BSA–dextran polymer network sample. Only a single peak is detectable at 5.65 min, which was identified as the BSA–dextran polymer network peak. No detectable peak was observed at the migration time for free BSA (7.7 min). The small shoulder on the front of the BSA–dextran peak is thought to be due to MW distributions within the dextran polymer, although it could also arise from different bonding densities of BSA with the dextran, with resultant small mobility differences.

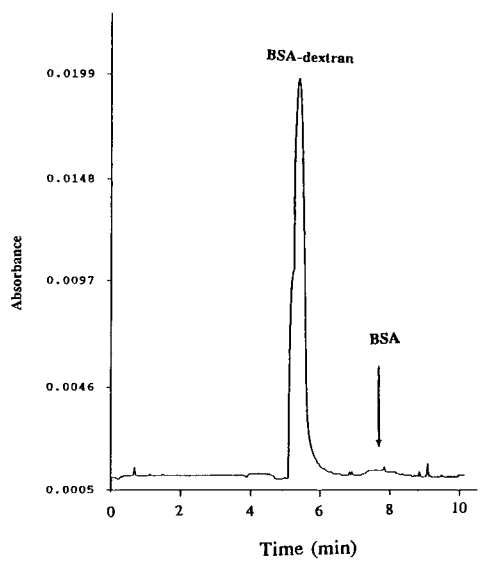

Fig. 2. Electropherogram of BSA–dextran polymer network sample. Capillary: fused silica (75 μm I.D. × 360 μm O.D.), 35.3 cm effective length. Voltage: 280 V/cm. Buffer: 20 m*M* phosphate at pH 7.4.

small electroosmotic flow will exist, usually opposite in direction to that of the protein complex. This results in a very stable system, in which the polymer will not flow out of the capillary to any significant extent during the course of several hours of running.

Chiral separation of leucovorin (LV) by BSA–dextran polymer network filled capillary

Baseline separation of the LV enantiomers could be obtained in just under 9 min on a BSA–dextran polymer network filled capillary with an effective length of 20 cm (Fig. 3). The short analysis time could not be achieved when using free BSA as the buffer additive [19] since in that method BSA moves in the same direction as the sample, creating a need for a relatively long effective capillary length to achieve adequate resolution. The stability of the BSA–dextran polymer network filled capillary was evaluated using the LV sample. No significant loss in efficiency was observed after 20 injections over the course of *ca.* 5 h. Replenishment of the capillary with fresh polymer when required is simple, and takes only minutes. The fresh BSA-polymer has the advantage of offering a virgin stationary phase for the solutes, such that if dirty samples are injected, capillaries can be recreated between injections if necessary.

The 6*R* isomer interacted more strongly with the immobilized BSA than did the 6*S* isomer, and also exhibited considerable peak distortion in comparison to the 6*S* species. Similar effects were observed in previous free solution separations of LV with BSA [19]. It is not known at this time whether the differences in peak width arise from differences in steric hindrance of the isomers for two distinct sites on (or within) the protein, or if the peak widths reflect differences in the adsorption energetics and kinetics of both isomers to the same site(s).

The advantage of covalent binding of a protein ligand to the polymer network is that the phase ratio of the ligand can be readily varied by dilution with non-derivatized dextran. This can be useful for solutes which absorb too strongly to the ligand for facile elution. The effect of phase dilution was studied for the BSA-LV system, and are presented in Fig. 4. Fig. 4A–D show the effect of diluting a 2 mg/mL BSA-dextran network with dextran. The resolution decreases systematically with decreasing phase ratio. The graph shown in Fig. 5 plots the trend. Both the resolution and the absolute migration times of both the 6*R* and 6*S* isomers decrease with decreasing phase ratio. This supports earlier conclusions that both isomers are retained to some extent by the BSA molecule [19], with the

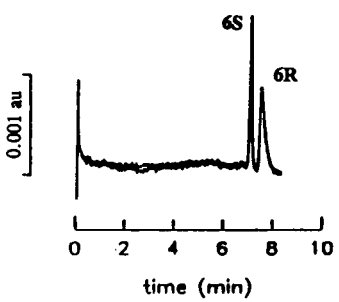

Fig. 3. Separation of leucovorin (LV) enantiomers on a capillary filled with BSA–dextran polymer network. Conditions: linear polyacrylamide-coated capillary with 20 cm effective length; electric field strength, 217 V/cm; pH 7.02, 20 m*M* phosphate buffer; injection, 5 kV × 5 s; sample, 0.1 mg/ml leukovorin (LV) in buffer; detection wavelength 230 nm.

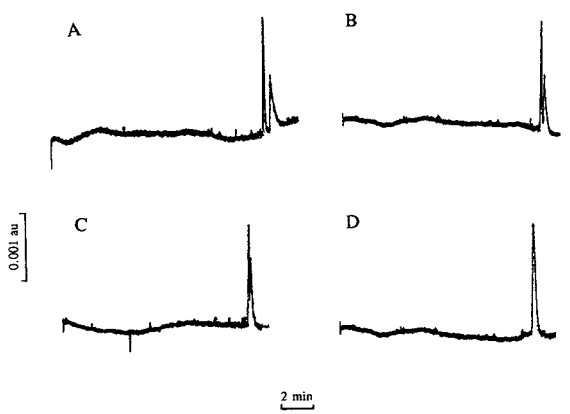

Fig. 4. Electropherograms showing the effect of diluting a 2 mg/ml BSA–dextran network with dextran solution. Conditions are the same as those of Fig. 3 except electric field strength is 250 V/cm and the effective length of the capillary is 40 cm. Sample: 0.5 mg/ml leukovorin (LV) in buffer. Injection: 5 kV × 4 s. BSA concentration: A = 2 mg/ml; B = 1 mg/ml; C = 0.5 mg/ml; D = 0.25 mg/ml. Time axes start at 0 min and chart speed is 0.5 cm/min.

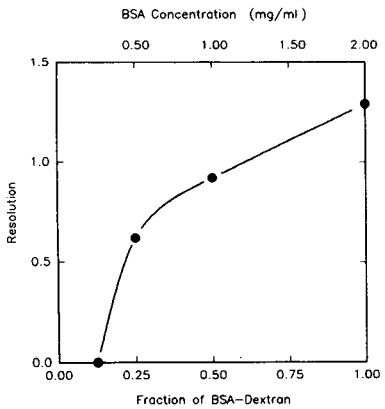

Fig. 5. Effect of BSA–dextran polymer network concentration on the resolution of leucovorin.

6*R* isomer being significantly more strongly retained than the 6*S*. It is possible that both isomers are retained by non-specific adsorption to BSA, with only the 6*R* isomer interacting with a particular site, or it is possible that both solutes are interacting with a chiral site, but to different degrees. Work is in progress in our laboratory to further elucidate the exact retention mechanisms operating in this LV–BSA system.

In conclusion, the authors have shown the feasibility of employing an immobilized protein–dextran polymer network for chiral separation via affinity capillary electrophoresis. Several significant technical advantages are created by using a covalently immobilized protein–polymer network over existing methodologies. Entrapment of BSA using gels cross-linked with glutaraldehyde (physical entrapment) [21] are not UV transparent, such that detection must be confined to a physically defined detection region. The polymer network used is UV transparent, eliminating this problem. In common with other polymer network methods, the lifetime of the capillary is extended by the ability to clear and refill the capillary at will with fresh polymer. For strongly retained solutes, resolution and retention times can be controlled by diluting the bound-polymer, thus controlling the phase ratio.

While data was presented only for a single test separation, that of leucovorin interacting with BSA, it is obvious that this is a completely general system. Not only can innumerable protein–solute interactions be used, often with rare and expensive proteins, but DNA–protein and DNA–DNA interactions can also be readily studied. A particularly exciting area of application is to the study of drug structure libraries. It should be possible to readily study drug–solute interactions, with the goal of screening structures for potential activity, at considerable savings in reduced animal studies. Another area of study is the competitive binding of different drugs to carrier proteins, such as the albumins or glycoproteins, which will yield useful in vitro information on potential cross-reactivity problems during dosing. Furthermore, in the area of chiral separations alone, other solutes, such as cyclodextrins, 3-point ligands and metal chelates can be used to advantage with polymer networks to create a convenient "stationary phase" for electrically driven separations.

ACKNOWLEDGEMENTS

The support of this work by Spectra-Physics Analytical Instruments and by the Center for Biotechnology at the State University of New York at Stonybrook, is gratefully acknowledged.

REFERENCES

1 J. Hermansson, *J. Chromatogr.*, 269 (1983) 71.
2 J. Hermansson and M. Eriksson, *J. Liq. Chromatogr.*, 9 (1986) 621.
3 T. Miwa, M. Ichikawa, M. Tsuno, T. Hattori, T. Miyakawa, M. Kayano and Y. Miyake, *Chem. Pharm. Bull.*, 35 (1987) 628.
4 T. Miwa, T. Miyakawa and M. Kayano, *J. Chromatogr.*, 480 (1987) 316.
5 K.M. Kirkland, K.L. Neilson and D.A. Mccombs, *J. Chromatogr.*, 545 (1991) 43.
6 S. Allenmark, B. Bomgren and H. Boren, *J. Chromatogr.*, 264 (1983) 63.
7 K. Choi and R.L. Schilsky, *Anal. Biochem.*, 168 (1988) 398.
8 P. Erlandsson and S. Nillsson, *J. Chromatogr.*, 482 (1989) 35.
9 R. Kuhn and S.H. Kuhn, *Chromatographia*, 34 (1992) 505.
10 J.W. Jorgenson and K. Lukaces, *Anal. Chem.*, 53 (1981) 1298.
11 S. Hjerten, *J. Chromatogr.*, 270 (1983) 1.
12 L. Karger, A.S. Cohen and A. Guttman, *J. Chromatogr.*, 492 (1989) 585.

13 S. Fanali, *J. Chromatogr.*, 477 (1989) 441.
14 A. Guttman, A. Paulus, A.S. Cohen, N. Grinberg and B.L. Karger, *J. Chromatogr.*, 448 (1988) 41.
15 E. Gassmann, J.E. Kuo and R.N. Zare, *Science (Washington, D.C.)*, 230 (1985) 813.
16 P. Gozel, E. Gassmann, H. Michelson and R.N. Zare, *Anal. Chem.*, 59 (1987) 44.
17 A.S. Cohen, A. Paulus and B.L. Karger, *Chromatographia*, 24 (1987) 15.
18 K. Otsuka and S. Terabe, *J. Chromatogr.*, 515 (1990) 221.
19 G.E. Barker, P. Russo and R.A. Hartwick, *Anal. Chem.*, 64 (1992) 3024.
20 Y. Baba, M. Tsuhako, T. Sawa, M. Akashi and E. Yashima, *Anal. Chem.*, 64 (1992) 1920.
21 S. Birnbaum and S. Nilsson, *Anal. Chem.*, 64 (1992) 2872.
22 K. Ganzler, K.S. Greve, A.S. Cohen, B.L. Karger, A. Guttman and N.C. Cooke, *Anal. Chem.*, 64 (1992) 2665.
23 Y. Takakura, Y. Kaneko, T. Fujita, M. Haside, H. Maeda and H. Sezak, *J. Pharm. Sci.*, 78 (1989) 117.
24 R. Axen and S. Ernback, *Eur. J. Biochem.*, 18 (1971) 351.
25 S. Hjertén, *J. Chromatogr.*, 347 (1985) 191.

Journal of Chromatography A, 652 (1993) 253–257
Elsevier Science Publishers B.V., Amsterdam

CHROM. 25 260

Optical resolution by high-performance capillary electrophoresis

Micellar electrokinetic chromatography with sodium N-dodecanoyl-L-glutamate and digitonin

Koji Otsuka*, Masanori Kashihara, Yasushi Kawaguchi, Ryo Koike and Toshio Hisamitsu

Department of Industrial Chemistry, Osaka Prefectural College of Technology, Saiwai-cho, Neyagawa, Osaka 572 (Japan)

Shigeru Terabe

Department of Material Science, Faculty of Science, Himeji Institute of Technology, Kamigori, Hyogo 678-12 (Japan)

ABSTRACT

Optical resolution by micellar electrokinetic chromatography with sodium N-dodecanoyl-L-glutamate (SDGlu) and with digitonin–sodium taurodeoxycholate (STDC) mixed micelles was investigated. Addition of sodium dodecyl sulphate, urea and methanol to SDGlu micellar solutions could give improved peak shapes and resolution. With SDGlu, phenylthiohydantoin (PTH) derivatives of five DL-amino acids (α-aminobutyric acid, methionine, norvaline, tryptophan and norleucine) were separated from each other and each pair of enantiomers was optically resolved. On the other hand, three PTH–DL-amino acids (norvaline, valine and α-aminobutyric acid) were also successfully resolved with a digitonin–STDC–urea solution (pH 2.5).

INTRODUCTION

High-performance capillary electrophoresis (HPCE) [1–3], which is a highly efficient separation technique, has become popular owing to the development of fully automated instruments. Among some modes of HPCE, capillary zone electrophoresis (CZE) is the most popular method because of the ease of operation, especially in terms of preparation of capillaries and separation solutions. Micellar electrokinetic chromatography (MEKC) [4–7], which is a branch of HPCE and uses an ionic micellar solution, has also become a well-known technique to separate small neutral molecules as well as charged solutes.

Optical resolution is one of the major objectives of HPCE, especially in the pharmaceutical field. Since Zare and co-workers [8,9] first reported enantiomeric separation by CZE using formation of copper (II) complexes, some papers on chiral separation have appeared. To achieve direct optical resolution by HPCE, the following three modes are usually employed: (1) CZE with chelating reagents or with cyclodextrins (CDs); (2) electrokinetic chromatography (EKC), which includes MEKC with chiral surfactants, cyclodextrin–modified MEKC (CD–MEKC), cyclodextrin EKC (CDEKC) and microemulsion

* Corresponding author.

0021-9673/93/$06.00

EKC (MEEKC); and (3) capillary gel electrophoresis with immobilized CDs. The direct enantiomeric separation by CZE using CD (CD–CZE) was first reported by Fanali [10]. This system can be applied to the optical resolution of charged enantiomers. We have also demonstrated the enantiomeric separation of *RS*-chlorpheniramine by CD–CZE [11]. In MEKC, sodium N-dodecanoyl-L-valinate (SDVal) [12–16], various bile salts [17–20], digitonin [14] and saponins [21] have been used as chiral surfactants. Optical resolution by CD–MEKC, in which achiral micelles such as sodium dodecyl sulphate (SDS) are normally used, has also been reported [11,22–24].

In the present investigation, we first used sodium N-dodecanoyl-L-glutamate (SDGlu) instead of SDVal. Some phenylthiohydantoin (PTH)–DL-amino acids were successfully resolved with a SDGlu–SDS–urea–methanol solution, although the selectivity difference between SDGlu and SDVal was not remarkable. Then, a digitonin–sodium taurodeoxycholate (STDC) comicellar system was employed. In the previous study [14], we found that a digitonin–SDS system was effective in enantiomeric resolution of PTH-DL-amino acids, but a long separation time was required. In this study, we changed some conditions so that a reduced separation time could be achieved.

EXPERIMENTAL

SDGlu was received from Ajinomoto (Tokyo, Japan), SDS and methanol from Nacalai Tesque (Kyoto, Japan), digitonin, urea, PTH–DL-amino acids and benzoin from Wako (Osaka, Japan) and STDC from Sigma (St. Louis, MO, USA). Separation solutions were prepared by dissolving surfactants and urea in a 50 m*M* phosphate buffer adjusted to an appropriate pH. Then, methanol was added to the micellar solutions when required. Sample solutions were made by dissolving solutes in a water–acetonitrile (1:1) solution. All the chemicals were of analytical reagent grade and used as received.

Capillary electrophoresis was performed with a laboratory-built system consisting of a Matsusada HepLL–30P0.08-LS or HCZE–30PN0.25-LDS regulated high-voltage power supply (Kusatsu, Shiga, Japan), a Shimadzu SPD-6A UV spectrophotometric detector (Kyoto, Japan) and a Shimadzu Chromatopac C-R6A data processor. An untreated fused-silica tube purchased from Polymicro Technologies (Phoenix, AZ, USA), 550 mm × 50 μm I.D. (effective length was 350 mm) was used as a separation capillary and on-column UV detection was employed.

Sample injection was carried out by the manual or hydrodynamic method. Separation was performed under the constant voltage and ambient temperature conditions.

RESULTS AND DISCUSSION

MEKC with SDGlu

As reported previously [16], by using a SDVal–SDS mixed micellar solution containing urea and methanol, six PTH–DL-amino acids were successfully separated from each other and each enantiomeric pair was resolved. Here, urea addition resulted in improved peak shapes compared with those obtained in the absence of urea, probably because of the adsorption of urea to the inside wall of the fused-silica capillary, which might prevent the irreversible adsorption of solutes.

In this study, SDGlu was employed to examine the possibility of optical resolution, instead of SDVal. As shown in Fig. 1, the structure of SDGlu is similar to that of SDVal: both have an N-dodecanoyl group and consist of an L-amino acid with five carbon atoms. SDGlu has an *n*-propyl and two carboxyl groups, whereas SDVal has isopropyl and carboxyl groups. Hence, resolution characteristics were expected to be similar in SDGlu and SDVal micellar

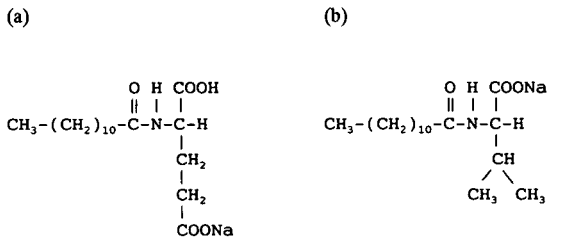

Fig. 1. Structures of (a) SDGlu and (b) SDVal.

systems. The critical micelle concentrations (CMCs) in an aqueous solution are reported to be 10.6 and 6.4 m*M* for SDGlu [25] and SDVal [26], respectively, at 40°C, and were measured by the conductivity method.

Similar to the case of SDVal, we used SDGlu–SDS mixed micellar solutions containing urea and methanol to obtain good peak shapes and enhanced selectivity. Three PTH–DL-amino acids, such as Nva, Val and Trp, were separated from each other and each pair was optically resolved, as shown in Fig. 2. Here, because the migration time window was not wide enough and also the capacity factor of the each pair was small, sufficient resolution could not be achieved.

The capacity factor (k') is represented with the concentration of the surfactant (C_{sf}) as [6]:

$$k' = K\bar{v}(C_{sf} - \mathrm{CMC}) \quad (1)$$

where K and $\bar{v}$ are the distribution coefficient and partial specific volume of the micelle, respectively. The term (C_{sf} – CMC) reveals the net concentration of the micelle. Therefore, an increase in C_{sf} causes an increase in k'. We then tried to use higher SDGlu or SDS concentrations than in Fig. 2, keeping the other conditions constant. However, higher SDGlu concentrations were not effective in improving resolution, but higher SDS concentrations led to improved results.

We could obtain improved resolution by using

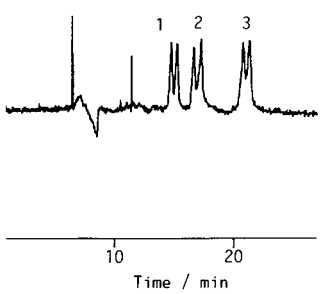

Fig. 2. Chiral separation of three PTH–DL-amino acids by MEKC with SDGlu. Corresponding amino acids: 1 = Nva; 2 = Val; 3 = Trp. Micellar solution, 75 m*M* SDGlu– 30 m*M* SDS–1 *M* urea (pH 9.0) containing 10% (v/v) methanol; separation capillary, 550 mm × 50 μm I.D.; effective length, 350 mm; total applied voltage, 12.5 kV (227 V cm^{-1}); current, 38 μA; detection wavelength, 260 nm; temperature, ambient.

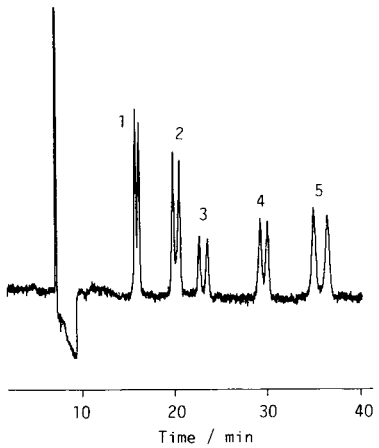

Fig. 3. Chiral separation of five PTH–DL-amino acids by MEKC with SDGlu. Corresponding amino acids: 1 = Aba; 2 = Met; 3 = Nva; 4 = Trp; 5 = Nle. Micellar solution, 75 m*M* SDGlu–50 m*M* SDS–1 *M* urea (pH 9.0) containing 10% (v/v) methanol; current, 32 μA. Other conditions are the same as in Fig. 2.

a 75 m*M* SDGlu–50 m*M* SDS–1 M urea (pH 9.0) solution containing 10% (v/v) methanol, as shown in Fig. 3. In this case, five PTH–DL-amino acids, α-aminobutyric acid (Aba), Met, Nva, Trp and Nle, were successfully separated and each enantiomeric pair was optically resolved. The separation characteristic was similar to that obtained with SDVal [16].

For each pair of the five PTH–DL-amino acids in Fig. 3, k' and the separation factor (α) are calculated according to the equations reported previously [6]. The results are listed in Table I. Here, the migration times of an unretained

TABLE I

CAPACITY FACTORS (k') AND SEPARATION FACTORS (α) OF FIVE PTH–DL-AMINO ACIDS IN THE SDGlu SOLUTION

Conditions as in Fig. 3

Solute	k'_1	k'_2	α
Aba	1.7	1.7	1.06
Met	2.7	2.9	1.07
Nva	3.8	3.9	1.01
Trp	6.2	6.6	1.08
Nle	9.7	11.0	1.14

solute (t_0) and the micelle (t_{mc}) were measured by acetonitrile and Sudan IV, respectively. Note that Sudan IV was assumed not to exist in the aqueous phase even containing 10% (v/v) methanol. For all the solutes, very similar k' values were observed compared with the case in SDVal, regardless of the difference in the micellar concentrations; in the SDVal solution, 50 m*M* SDVal–30 m*M* SDS–0.5 *M* urea (pH 9.0) containing 10% (v/v) methanol was employed. These results imply that SDGlu and SDVal have almost the same characteristics in terms of enantiomeric resolution of PTH–DL-amino acids. In the SDGlu solution, the value of t_0/t_{mc} was 0.12, and this value was smaller than that in the SDVal solution, 0.16, reported previously [16]. This reveals that a wider migration time window can be attained in the SDGlu system than in the SDVal system.

By using the same SDGlu–SDS–urea–methanol solution as in Fig. 3, optical resolution of benzoin was successfully resolved as shown in Fig. 4. This was the same result as in the SDVal system [16]. However, warfarin, which could be resolved with SDVal [16], was only partially resolved with the SDGlu solution.

Although the results are preliminary and SDGlu might have no advantage over SDVal, comparison of the resolution characteristics between the SDGlu and SDVal systems will provide useful information to investigate the chiral recognition mechanism of these N-acylamino acid micelles.

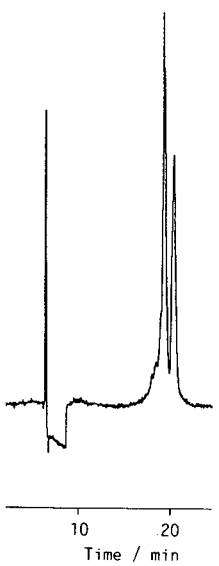

Fig. 4. Optical resolution of benzoin by MEKC with SDGlu. Current, 33 μA. Other conditions as in Fig. 3.

MEKC with digitonin

Digitonin is a natural surfactant with optical activity; it is a glycoside of digitogenin and is used for the determination of cholesterol. Since digitonin is electrically neutral, it is essential to add an ionic micelle to the digitonin solution to form charged mixed micelles that can be used as chiral carriers in MEKC. As reported previously [14], we used the digitonin–SDS co-micellar system for optical resolution of some PTH–DL-amino acids. Although good resolution could be achieved, a long separation time was required, *e.g.*, 90 min for Ala.

In the present investigation, we used a shorter column than the previous one and changed the co-surfactant from SDS to STDC. Although STDC alone has found to be capable of enantiomeric separation of dansylated DL-amino acids (Dns–DL-amino acids), it is not effective for optical resolution of PTH–DL-amino acids, which is similar to the case in other bile salts [27]. However, by using a 50 m*M* digitonin–50 m*M* STDC solution (pH 2.5) containing 1 *M* urea, three PTH–DL-amino acids such as Nva, Val and Aba were separated from each other and each

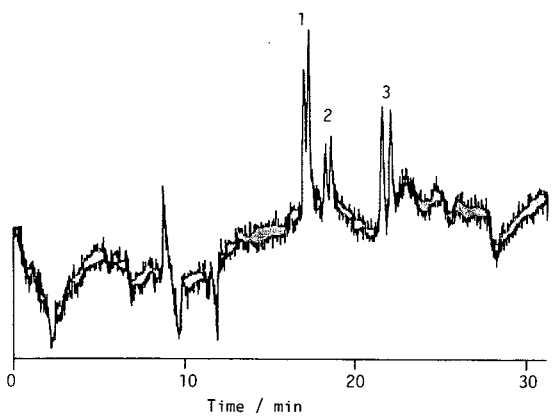

Fig. 5. Chiral separation of three PTH–DL-amino acids by MEKC with digitonin. 1 = Nva; 2 = Val; 3 = Aba. Micellar solution, 50 m*M* digitonin–50 m*M* STDC–1 *M* urea (pH 2.5); capillary, 540 mm × 50 μm I.D.; effective length, 340 mm; total applied voltage, 17.5 kV (324 V cm^{-1}); current, 46 μA. Other conditions as in Fig. 2.

pair was optically resolved, as shown in Fig. 5. In this instance, the electroosmotic velocity was sufficiently suppressed, and the migration direction of the mixed micelle was towards the positive electrode or opposite to the electroosmotic flow, as reported previously [14]: if the solutes are well incorporated into the micelle, they will migrate toward the positive electrode, while the solutes less incorporated into the micelle will migrate toward the negative electrode or the same direction as the electroosmosis [28]. Therefore, as long as the solute migrates toward the positive electrode, the larger the capacity factor, the shorter the migration time.

Although this was also a preliminary result and not optimized, a remarkably reduced separation time was achieved, *e.g.* for Aba *ca.* 22 min in Fig. 5, compared with *ca.* 43 min with the digitonin–SDS system in the previous study [14]. It should be noted that optical resolution of any Dns–DL-amino acids with the digitonin–STDC solution could not be achieved. This suggests that digitonin plays a major role in optical resolution in the digitonin–STDC system.

CONCLUSION

The use of SDGlu–SDS–urea–methanol solutions could give good results in the optical resolution of PTH–DL-amino acids, although the resolution characteristic was not very different from that in SDVal–SDS micellar solutions. The digitonin–STDC mixed micellar system was also effective for enantiomeric resolution of PTH–DL-amino acids, even using a shorter capillary than before. At present, chiral separation by MEKC and by CZE has not been fully investigated, especially compared with HPLC. Further applications on chiral separations of other compounds are being investigated with some other surfactants and additives.

ACKNOWLEDGMENTS

The authors are grateful to Dr. Akio Ishiwata of Ajinomoto for kindly providing SDGlu. This work was supported in part by a Grant-in-Aid for Scientific Research (No. 04750656) from the Ministry of Education, Science and Culture, Japan.

REFERENCES

1 F.E.P. Mikkers, F.M. Everaerts and Th.P.E.M. Verheggen, *J. Chromatogr.*, 169 (1979) 11–20.
2 J.W. Jorgenson and K.D. Lukacs, *Anal. Chem.*, 53 (1981) 1298–1302.
3 S. Hjertén, *J. Chromatogr.*, 270 (1983) 1–6.
4 S. Terabe, *Trends Anal. Chem.*, 8 (1989) 129–134.
5 S. Terabe, K. Otsuka, K. Ichikawa, A. Tsuchiya and T. Ando, *Anal. Chem.*, 56 (1984) 111–113.
6 S. Terabe, K. Otsuka and T. Ando, *Anal. Chem.*, 57 (1985) 834–841.
7 S. Terabe, K. Otsuka and T. Ando, *Anal. Chem.*, 61 (1989) 251–260.
8 E. Gassmann, J.E. Kuo and R.N. Zare, *Science*, 230 (1985) 813–814.
9 P. Gozel, E. Gassmann, H. Michelsen and R.N. Zare, *Anal. Chem.*, 59 (1987) 44–49.
10 S. Fanali, *J. Chromatogr.*, 474 (1989) 441–446.
11 K. Otsuka and S. Terabe, *J. Liq. Chromatogr.*, 16 (1993) 945–953.
12 A. Dobashi, T. Ono, S. Hara and J. Yamaguchi, *Anal. Chem.*, 61 (1989) 1984–1986.
13 A. Dobashi, T. Ono, S. Hara and J. Yamaguchi, *J. Chromatogr.*, 480 (1989) 413–420.
14 K. Otsuka and S. Terabe, *J. Chromatogr.*, 515 (1990) 221–226.
15 K. Otsuka and S. Terabe, *Electrophoresis*, 11 (1990) 982–984.
16 K. Otsuka, J. Kawahara, K. Tatekawa and S. Terabe, *J. Chromatogr.* 559 (1991) 209–214.
17 S. Terabe, M. Shibata and Y. Miyashita, *J. Chromatogr.*, 480 (1989) 403–411.
18 H. Nishi, T. Fukuyama, M. Matsuo and S. Terabe, *J. Microcol. Sep.*, 1 (1989) 234–241.
19 H. Nishi, T. Fukuyama, M. Matsuo and S. Terabe, *J. Chromatogr.*, 515 (1990) 233–243.
20 R.O. Cole, M.J. Sepaniak and W.L. Hinze, *J. High Resolut. Chromatogr.*, 13 (1990) 579–582.
21 Y. Ishihama and S. Terabe, *J. Liq. Chromatogr.*, 16 (1993) 933–944.
22 Y. Miyashita and S. Terabe, *Application Data*, High Performance Capillary Electrophoresis, DS–767, Beckman, Palo Alto, CA, 1990.
23 H. Nishi, T. Fukuyama and S. Terabe, *J. Chromatogr.*, 553 (1991) 503–516.
24 T. Ueda, F. Kitamura, R. Mitchel, T. Metcalf, T. Kuwana and A. Nakamoto, *Anal. Chem.*, 63 (1991) 2979–2981.
25 M. Takehara, K. Sakamoto and R. Yoshida, *Yukagaku*, 25 (1976) 789–792.
26 R. Yoshida, M. Takehara and K. Sakamoto, *Yukagaku*, 24 (1975) 538–541.
27 K. Otsuka, Y. Kawaguchi and M. Kashihara, unpublished results (1992).
28 K. Otsuka and S. Terabe, *J. Microcol. Sep.*, 1 (1989) 150–154.

Journal of Chromatography A, 652 (1993) 259–262
Elsevier Science Publishers B.V., Amsterdam

CHROM. 25 089

Separation of positional isomers and enantiomers using capillary zone electrophoresis with neutral and charged cyclodextrins

N.W. Smith

Chemical Analysis Department, Glaxo Group Research Limited, Greenford Road, Greenford, Middlesex UB6 0HE (UK)

ABSTRACT

Capillary zone electrophoresis is a highly efficient analytical technique that has been shown to be particularly useful for the analysis of isomers. The neutral chiral host compound β-cyclodextrin is capable of resolving analytes that possess charged functional groups. The enantiomers of two cyclic amines are resolved in a single run using a background electrolyte containing β-cyclodextrin at pH 2.7, conditions under which the compounds are positively charged. In order to resolve the enantiomers of neutral analytes, it is necessary to use a chiral selector capable of being ionised, and examples are given of the separation of neutral positional isomers and enantiomers using a carboxymethylethyl-β-cyclodextrin at high pH.

INTRODUCTION

Cyclodextrins are well established compounds capable of forming inclusion complexes in aqueous solutions. These cyclodextrins are cyclic oligosaccharides consisting of either 6, 7 or 8 glucose units and are termed α, β or γ, respectively. They consist of a truncated cone containing secondary hydroxyl groups at the entrance of the cavity, with a relatively hydrophobic interior. Therefore, molecules of certain size and stereochemistry can form inclusion complexes by hydrophobic interaction in the cyclodextrin cavity and from hydrogen bonding by the secondary hydroxyl groups at the entrance of the cavity. There have been numerous papers published on the use of cyclodextrins to separate positional and geometric isomers and also enantiomers [1–3]. In addition to the use of neutral cyclodextrins, Terabe *et al.* [1,4] advocated the use of cyclodextrins with ionic groups to separate enantiomers and geometrical isomers. Terabe *et al.* pointed out that carboxylated cyclodextrins behave in an analogous way to micelles in conventional micellar electrokinetic chromatography and will electrophorese towards the anode, but will be transported towards the cathode by the electroosmotic flow since this is much stronger than the electrophoretic mobility of the cyclodextrin. During this process, solutes will be separated by inclusion into the charged cyclodextrin as it travels towards the cathode, in a way that is analogous to micellar solubilisation.

EXPERIMENTAL

The data contained in this paper were produced using an Applied Biosystems (Foster City, CA, USA) Model 270HT instrument. β-Cyclodextrin was supplied by Sigma (Dorset, UK). The Resolvosil-7 column was supplied by Technicol (Cheshire, UK). All buffers and urea were supplied by BDH (Poole, UK). Capillaries were supplied by Polymicro Technologies (Phoenix, AZ, USA).

RESULTS AND DISCUSSION

o-Nitrobenzyl alcohol (Fig. 1) is used as a starting material for a new drug entity currently

0021-9673/93/$06.00

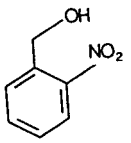

Fig. 1. *o*-Nitrobenzyl alcohol.

being progressed within Glaxo Group Research (GGR).

Attempts by HPLC to resolve *o*-nitrobenzyl alcohol from the *meta* and *para* analogues, as well as from *o*-nitrobenzoic acid have been unsuccessful. Although Terabe *et al.* [4] have shown that it was possible to resolve the *ortho*, *meta* and *para* isomers of nitrophenol using 0.1 *M* Na_2HPO_4 at pH 7.0 with and without α-cyclodextrin, we were unable to repeat these separations using the nitrobenzyl alcohol analogues. However, using carboxymethylethyl-β-cyclodextrin, we were able to achieve the desired separations (Fig. 2).

GR50360A and its N-benzyl analogue GR57732A (Fig. 3) are compounds passing through exploratory development within Glaxo Group Research.

The enantiomers of GR50360A have proved particularly difficult to resolve by HPLC, although some success was achieved using a Resolvosil column and 0.5 *M* K_2HPO_4–NaH_2PO_4 as mobile phase (Fig. 4).

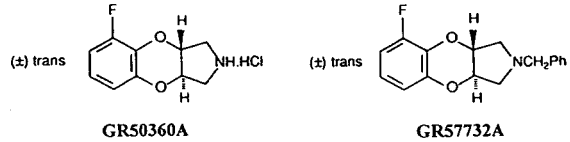

Fig. 3. GR50360A and its N-benzyl analogue GR57732A.

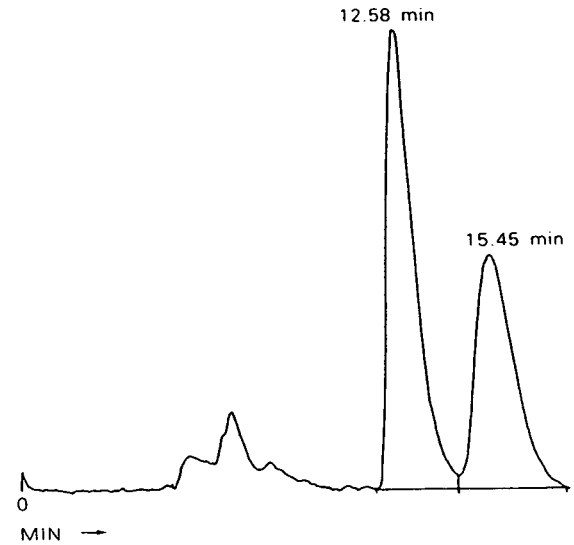

Fig. 4. Chiral HPLC separation of the enantiomers of GR50360A. Column: 150 mm × 4.6 mm I.D. Resolvosil-7; flow 0.3 ml/min; temperature 35°C; detection at 220 nm, 0.5 AUFS; injection volume 10 μl; mobile phase: 125 ml 0.5 *M* K_2HPO_4–250 ml 0.5 *M* NaH_2PO_4–250 ml water adjusted to pH 6.2.

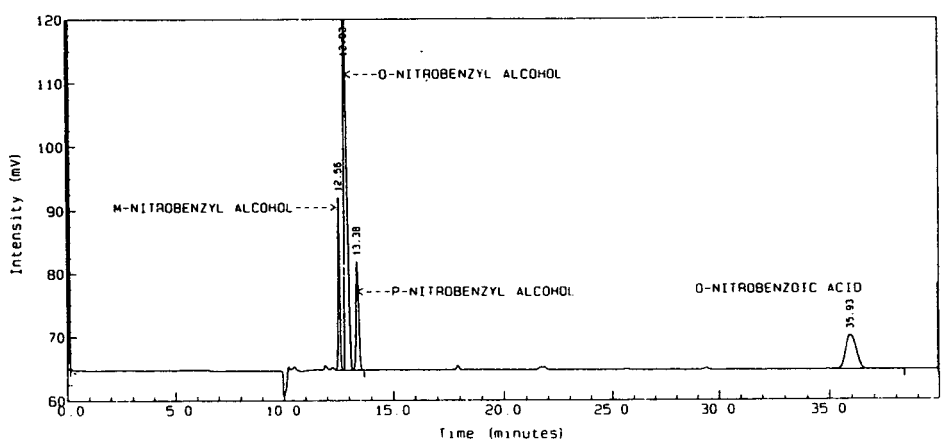

Fig. 2. Chiral separation of nitrobenzyl alcohols. Conditions: capillary 72 cm × 50 μm I.D.; applied voltage 15 kV; detection at 220 nm, range 0.03 AUFS; vacuum injection for 0.4 s; temperature 40°C; carrier: 0.025 *M* carboxymethylethyl-β-cyclodextrin in 0.05 *M* PO_4–0.03 *M* borate overall pH 8.4.

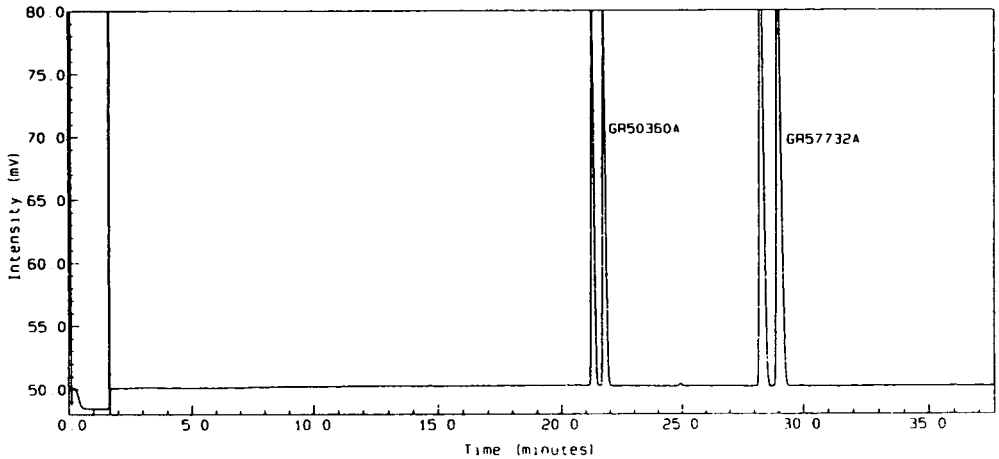

Fig. 5. Chiral separation of the enantiomers of GR50360A and the N-benzyl analogue GR57732A. Conditions: capillary 72 cm × 50 μm I.D.; applied voltage 30 kV; detection at 220 nm, range 0.03 AUFS; vacuum injection for 0.5 s; temperature 40°C; carrier: 0.1 *M* β-CD–5 *M* urea dissolved in 20% isopropanol in 0.01 *M* Tris–borate adjusted to pH 2.7 with dilute H_3PO_4.

Fig. 5 shows the baseline resolution of both pairs of enantiomers of GR50360A and the N-benzyl analogue in a single run, using β-CD as the chiral receptor.

GR50360A and its N-benzyl analogue are both

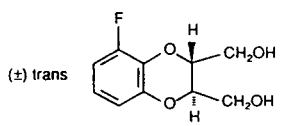

Fig. 6. GR57888X.

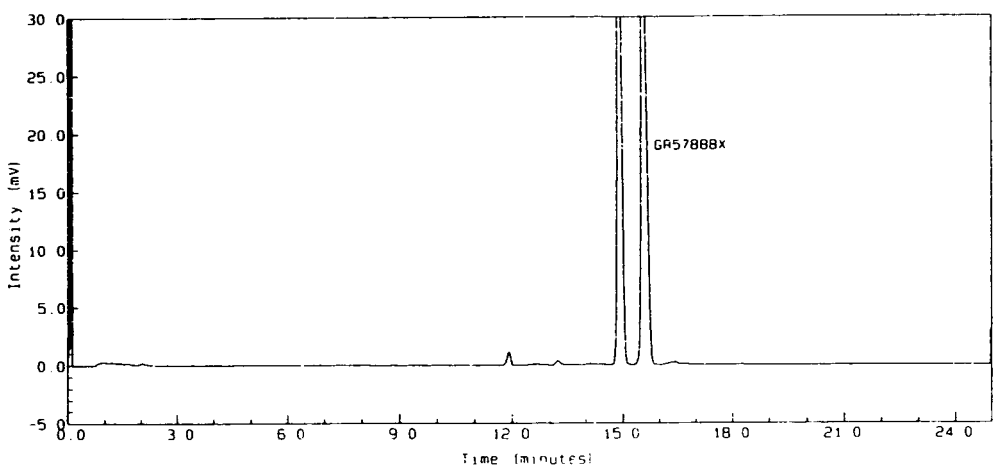

Fig. 7. Chiral separation of GR57888X. Conditions: capillary 72 cm × 50 μm I.D.; applied voltage 15 kV; detection at 220 nm, range 0.04 AUFS; vacuum injection for 1.5 s; temperature 30°C; carrier: 0.025 *M* carboxymethylethyl-β-cyclodextrin in 0.01 *M* Tris overall pH 12.4.

charged molecules at low pH and can therefore be separated using neutral cyclodextrins, however the related compound GR57888X, (Fig. 6) is neutral and can only be resolved by the use of a charged host compound.

Fig. 7 shows the baseline separation of enantiomers of GR57888X using a carboxylated methylethyl-β-cyclodextrin at pH 12.4.

DISCUSSION

There is an abundance of applications in the literature showing the use of cyclodextrins, particularly β-cyclodextrin, for the analysis of positional and geometrical isomers, as well as for enantiomers. However in order to achieve recognition for neutral species (without the use of a micelle) it is necessary to use charged cyclodextrins and we have been able to demonstrate in our laboratory several applications showing the resolution of enantiomers and positional isomers that would not be possible using neutral cyclodextrins, and that have also proved very difficult by HPLC.

REFERENCES

1 S. Terabe, *Trends Anal. Chem.*, 8 (1989) 129–134.
2 H. Nishi, T. Fukuyama and S. Terabe, *J. Chromatogr.*, 553 (1991) 503–516.
3 S. Fanali, *J. Chromatogr.*, 545 (1991) 437–444.
4 S. Terabe, H. Ozaki, K. Otsuka and T. Ando, *J. Chromatogr.*, 332 (1985) 211–217.

Journal of Chromatography A, 652 (1993) 263–275
Elsevier Science Publishers B.V., Amsterdam

CHROM. 25 410

Timescales of transient processes in capillary electrophoresis

Eric V. Dose[☆] and Georges Guiochon[*]

Department of Chemistry, University of Tennessee, Knoxville, TN 37996-1501 (USA) and Analytical Chemistry Division, Oak Ridge National Laboratory, Oak Ridge, TN 37831-6120 (USA)

ABSTRACT

We apply numerical simulation based on fundamental physical properties to the study of the development of electroosmotic flow and thermal gradient formation that occur immediately after a potential is applied to a capillary filled with electrolyte. Electroosmotic flow requires a few hundred microseconds to develop. We confirm others' findings that radial thermal gradients are generally too small to dominate zone dispersion for capillaries with lumen diameters smaller than about 100 μm. The radial thermal gradient within the capillary lumen requires a few milliseconds to develop, but the general, whole-capillary temperature rise requires ten to a thousand times longer. We combine on one scale the major time-dependent processes that occur when an axial potential gradient is applied, and we demonstrate the theoretical feasibility of using modulated driving potentials to suppress thermal zone broadening.

INTRODUCTION

Much current interest in theory and practice of capillary electrophoresis (CE) is driven quite properly by the technique's very high efficiency. Experiments generally develop over 100 theoretical plates per second, as expected from steady-state theory. However, transient processes in CE resulting from altering the applied potential are not nearly as well understood. When this potential is first applied at the beginning of a CE separation, several changes occur in the capillary including propagation of the electric field down the length of the column, capacitative charging of the double layer at the silica-electrolyte interface, resistive heating of the electrolyte and subsequent development of thermal gradients in the electrolyte and silica, and the start of electroosmotic flow, if any. Also, in real instruments the power supply and electrolyte together constitute a low-pass electric filter so that the potential gradient in the capillary lumen requires some time to rise to the steady-state gradient magnitude.

Each of these processes has a characteristic timescale, and these timescales cover a range of roughly ten orders of magnitude. However, when two or more of these processes have similar timescales, the processes probably interact. The effect of a given process on separation efficiency is probably most complex when its timescale is on the same order as the characteristic time for an analyte molecule to diffuse through the zone either radially (through the distance from the capillary center to the lumen wall or *vice versa*) or axially (from one end of an analyte zone to the other).

We examine below the progress of two major transient processes that occur immediately after a potential is applied to a capillary filled with electrolyte. First, we show that electroosmotic

* Corresponding author. Address for correspondence: Department of Chemistry, University of Tennessee, Knoxville, TN 37996-1501, USA.
☆ Present address: Ross Laboratories, Analytical R&D, 625 Cleveland Avenue, Columbus, OH 43215, USA.

0021-9673/93/$06.00

flow does not develop immediately after potential is applied but that it requires a few hundred microseconds to develop. Second, we use numerical simulation based directly on very fundamental physical assumptions to confirm others' findings [1–3] that radial thermal gradients are generally too small to dominate zone dispersion for capillaries with lumen diameters smaller than about 100 μm. Finally, we combine on one scale the relative rates of several transient processes in CE and comment on the feasibility of using modulated driving potentials to suppress thermal zone broadening. In the interests of clarity we present our methods and results for each process before proceeding to the next.

NUMERICAL SIMULATION OF ELECTROOSMOTIC FLOW CHANGES

Methods

This simulation is based on the integration of simple differential equations in one spatial (radial) dimension. The boundary conditions in the radial dimension simply consist of the initial electrolyte velocity (V) at all radii (r) in the lumen, or $V(t=0; r)$. Boundary conditions in the time dimension consist of time history of the axial flow velocity just inside the aqueous-silica surface at the wall of the lumen, or $V(t; r=r_{aq})$, which is the same as the equilibrium flow rate across the lumen. In fact, we divide the lumen space into N_{aq} concentric annuli each of thickness Δr, so that the boundary conditions are specified as $V(t=0; i)$ and $V(t; N_{aq}+1)$.

We based the electroosmotic simulations on some simplifying assumptions. We include no temperature dependence of the electrolyte viscosity because, as we show below, the timescale of relaxation of the electrolyte velocity is much shorter than heating timescales at the lumen wall so that the viscosity is nearly constant over the time required to reestablish velocity steady state. Thus, while electrolyte heating certainly does alter electroosmotic flow rates [4–7], that process is slower than the one investigated here. Further, we assume that the slipping zone at the wall, that is the very thin boundary layer of electrolyte solution where the electrolyte velocity increases from zero at the silica wall itself to the asymptotic electroosmotic velocity, is very small compared to the lumen diameter. This assumption is supported by the very small depth, on the order of 10 nm, that one calculates for the double layer in concentrated electrolytes [8–10]. Though there exist reports that the double layers may effectively be as thick as 1 or 2 μm [11], even this would directly affect only the very outermost annuli in our model, and the timescale indicated by the model would probably not be affected significantly.

Integration resolution Δr in the radial dimension was chosen to be 0.25–1.0% of the lumen (inside) diameter for electroosmotic simulations. The propagation of axial velocities was assumed to arise by simple diffusion through the action of viscous forces $\vec{F}_i$ per unit length transmitted through interannulus interfaces i (which lie between annuli i and $i+1$) as

$$\vec{F}_i = 2\pi i\eta(V_{i+1} - V_i) \tag{1}$$

which depends on axial velocities V_i and V_{i+1} in adjacent annuli i and $i+1$. These forces cause accelerations $\dot{V}_i$ in annulus i

$$\dot{V}_i = \frac{\vec{F}_i}{M_i} \qquad \text{for } i = 1\,,$$

$$= \frac{(\vec{F}_i - \vec{F}_{i-1})}{M_i} \qquad \text{for } 1 < i \leq N_{aq} \tag{2}$$

where M_i is the mass of electrolyte in annulus i. Integrating $\dot{V}_i$ in each annulus from its initial velocity $V(t=0; i)$ gives the history of its velocity V_i.

The integration time increment Δt_{max} depends on Δr and was computed as one-half the maximum time during which, given each annulus's calculated accelerations integrated forward linearly in time, no annulus's velocity may extrapolate past the mean velocity of its two adjacent rings. To calculate this, consider a radial velocity discontinuity between two annuli, calculate the viscous force in the interface between them, calculate the initial acceleration of the electrolyte in one of the two annuli, double the acceleration to account for the possibility of an equally large velocity discontinuity on the other side of the annulus, compute the time for

the electrolyte in this annulus to accelerate by half the initial velocity difference in the discontinuity and halve the time for safety. By this method, the maximum time increment is

$$\Delta t_{max} = \frac{(\Delta r)^2 d}{8\eta} \quad (3)$$

where d is the electrolyte density and η is the electrolyte viscosity. Note that Δt_{max} is time-independent and need be computed only once before integration begins. Were the integration time increment to exceed Δt_{max}, oscillation and simulation instability would rapidly result. Restricting the time increment to less than Δt_{max} always prevented this oscillatory instability in our work.

Results and discussion

When the electrolyte velocity at the capillary wall suddenly changes because of the application of electrical potential down the capillary axis, viscous forces accelerate the bulk of the electrolyte until the electrolyte all moves in plug flow at the same velocity as the electrolyte at the wall, as expected. This radial propagation occurs at a rate proportional to the electrolyte solution's kinematic viscosity, or its intrinsic viscosity divided by its density. By taking advantage of the analogy between wall-driven electroosmotic flow propagation and well-thermostatted heat transfer, we calculate a characteristic relaxation time for this process as

$$t_{char} = \frac{R_{aq}^2}{\alpha_1^2(\eta/d)} \quad (4)$$

where α_1 is the first root of the Bessel equation $J_0(\alpha) = 0$, about 2.4048 [12]. For a capillary of inside diameter 50 micrometers filled with an electrolyte similar to water at room temperature is about 110 μs. From our simulation results given in Fig. 1 it is clear that the electroosmotic flow has in fact regained its radial uniformity by 200 to 300 ms after potential is initially applied. Eqn. 4 also predicts that the electroosmotic relaxation time is proportional to the square of the capillary inside diameter, and simulation results like those in Fig. 2 are consistent with this expectation.

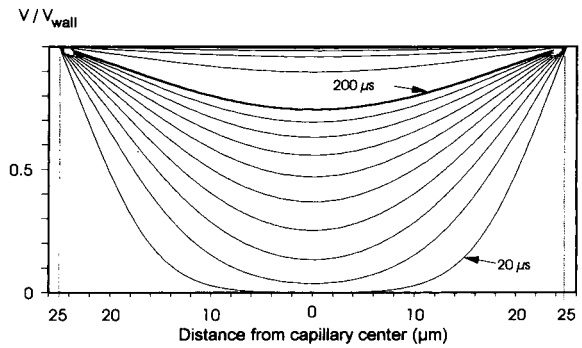

Fig. 1. Axial electrolyte velocity profiles at 20, 40, 60, . . . , 180, 200 (bold curve), 300, 400, and 500 μs after potential applied.

Except for instruments designed specifically to induce high-frequency, high-voltage potential changes in the capillary, most CE instruments will have rise times considerably longer than 1 ms [13]. The present analysis concludes that for these usual instruments, electroosmotic flow effectively propagates instantaneously across the capillary lumen, and electroosmotic flow delays generally need not be taken into consideration. This process appears to be faster than all thermal and all other transient mechanical processes in CE. This is especially true for capillaries with very small inside diameters [14,15].

Even for an instrument with zero potential gradient rise time, the zone broadening effects of electroosmotic relaxation are small. Because analyte molecular diffusion is much slower than effective velocity–propagation diffusion (whose effective diffusion coefficient is equal to the

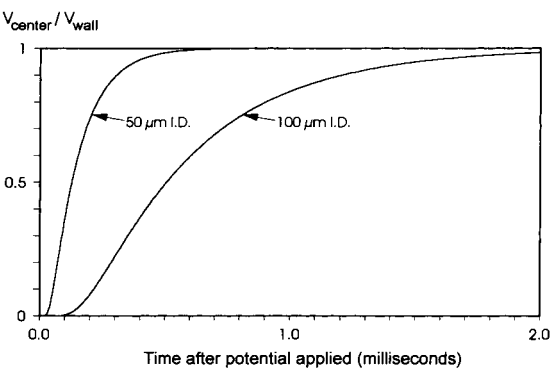

Fig. 2. Axial electrolyte velocity profiles at the lumen center.

kinematic viscosity, about 10^{-2} cm^2/s for water), electroosmotic relaxation will have its full effect on the analyte's radial concentration profile before diffusion can significantly blur it.

The zone broadening effect of electroosmotic relaxation during a cycle where the potential is applied and withdrawn could therefore be measured in principle by moving an analyte zone past the detector and measuring the zone's breadth (variance), applying one or more axial potential changes each separated from the next by enough time to allow radial diffusional mixing, and then moving the zone back across the detector to measure the peak variance increase. Performing this experiment by numerical simulation on a column of inside diameter 50 μm, one measures the axial zone variance introduced for one voltage-switching cycle as about 0.4 V_{EO} micrometers^2, where V_{EO} is the electrolyte velocity at the wall in cm/s. We also find that this axial variance induced by electroosmotic relaxation is proportional to the fourth power of the capillary inside diameter. Voltage-switching variance contributions calculated in this way are five orders of magnitude smaller than upper limits previously deduced by experiment [16], suggesting either that some addition source of voltage-switching dispersion exists or that determination of dispersion by subtraction of calculated variance contributions from measured zone variances is inherently difficult. It is also possible that heterogeneity of the silica surface and therefore of its zeta potential is more important than is the observed (average) rate of electroosmotic flow itself. Though it is clear that neither ideal electroosmotic flow nor its modulation causes much zone broadening, electroosmotic flow heterogeneity may be inevitable whenever electroosmotic flow exists at all, and this may be the reason electroosmotic flow is often observed to lower the plate count to a fraction of that expected.

NUMERICAL SIMULATION AND THERMAL CHANGES

Methods

For cases where the temperature coefficient of electrolyte conductivity is nonzero, the radial temperature profile in a capillary heated by power dissipation in the lumen is solvable to any desired degree of accuracy only by numerical simulation [17]. As in the electroosmotic problem in the previous section, we divide the space within the capillary's outer wall into concentric annuli each of thickness Δr, the radial integration resolution, chosen to be 0.25–1.0% of the capillary outside diameter. The model could be adapted to rectangular capillaries [18–20] or etched channels [21–22] with some loss of simplicity. For thermal simulations the boundary conditions in the space dimension consist of initial temperature (T) at all annuli i in the capillary, or $T(t = 0; i)$, and the boundary conditions in the time dimension consist of the history of the temperature of the air at the polyimide-air interface, or $T(t; r = N_{pi} + 1)$, where N_{pi} is the total number of annuli representing the space within the capillary lumen, silica, and polyimide coating.

We made some simplifying assumptions in the thermal simulations. First, we set to zero the temperature coefficients of thermal conductivities Λ_{th}, specific heats C_p, and densities D for electrolyte, silica, and polyimide coating and we assumed that there is little double layer reorganization after application of the axial potential, though there may be experimental evidence in favor of some very slow such processes [23]. We assumed that the thermal transfer coefficient to air was temperature-independent, though the temperature of the outer capillary wall is very difficult to measure, as noted in other work [6]. We assumed that the temperature of the capillary's surroundings are radially symmetric [24] and held constant at a known temperature; real instruments will satisfy this assumption to varying extents [25]. We ignore radiative heat losses [26] and surface conductivity at the double layer [10], each of which is expected to be very small. Finally, electrolyte conductivity temperature dependence in a given simulation was assumed to be either linear

$$\Lambda_{th}(T) = \Lambda_{th}(T_0)(1 + j(T - T_0)) \quad (5)$$

or exponential

$$\Lambda_{th}(T) = \Lambda_{th}(T_0)e^{j(T-T_0)} \quad (6)$$

in form, where T_0 is the temperature of the capillary's surroundings, and j is the temperature coefficient of electrical conductivity at T_0

$$j = \frac{1}{\Lambda_{th}(T_0)} \cdot \frac{d\Lambda_{th}}{dT}(T_0) \quad (7)$$

The value of j is usually about 0.02 [27]. We used exponential temperature dependence except in simulations intended to model previously published work which employed linear or zero temperature dependence. When comparing our results to those of other work we adopted all capillary dimensions and physical properties used in that work.

The enthalpy rate of change $\dot{H}_{IR,i}$ generated by electrical resistance per unit length within each annulus i is

$$\dot{H}_{IR,i} = \begin{cases} (2i+1)\pi(\Delta r)^2 E^2 \Lambda_{IR} & \text{for } i \leq N_{aq}, \text{ and} \\ 0 & \text{for } i > N_{aq} \end{cases} \quad (8)$$

where E is the axial potential gradient (electrical field), Λ_{IR} is the electrolyte's electrical conductivity, and N_{aq} is the number of annuli representing the lumen space. The outward heat flux F_i per unit length across each boundary i (which lies on the outside surface of annulus i) is

$$F_i = \begin{cases} 2\pi i[T_i - T_{i+1}]\bar{\Lambda}_{th} & \text{for } i < N_{pi}, \text{ and} \\ 2\pi R_{pi} h & \text{for } i = N_{pi} \end{cases} \quad (9)$$

where T_i and T_{i+1} are the temperatures in annuli i and $i+1$, $\bar{\Lambda}_{th}$ is the mean thermal conductivity of the materials in annuli i and $i+1$, h is the extrinsic heat transfer coefficient from the outside to the capillary's polyimide coating to the surrounding medium, and R_{pi} is the capillary outside radius. Thus the total enthalpy rate of change $\dot{H}_i$ per unit length for annulus i is

$$\dot{H}_i = \begin{cases} -\Delta F_{H,i} + \dot{H}_{IR,i} & \text{for } i = 1, \\ \Delta F_{H,i-1} - \Delta F_{H,i} + \dot{H}_{IR,i} & \text{for } 2 \leq i \leq N_{pi} \end{cases} \quad (10)$$

and the rate of temperature change $\dot{T}_i$ in annulus i is

$$\dot{T}_i = \frac{\dot{H}_i}{\pi(2i-1)(\Delta r)^2 D_i C_{p,i}} \quad (11)$$

Given an integration cycle time increment Δt (see below), the temperature change ΔT_i resulting from one integration cycle for each annulus i is

$$\Delta T_i = \dot{T}_i \Delta t \quad (12)$$

For thermal simulations, the integration time increment Δt_{max} must be no greater than the lesser of two upper limits. The first prevents integration oscillation in the same manner as does eqn. 3 described above and is given by

$$\Delta t_{max}(1) = (\Delta r)^2 \min\left(\frac{d_i C_{p,i}}{4\Lambda_{th,i}}\right) \quad \text{over } 1 \leq i \leq N_{pi} \quad (13)$$

where $C_{p,i}$ is the heat capacity and $\Lambda_{th,i}$ is the thermal conductivity within a given annulus i. Under the simplifying assumptions above, $\Delta t_{max}(1)$ is time-independent and need be computed only once before integration begins. The second limit prevents resistive heating from causing the lumen temperature to increase in one integration cycle by more than an arbitrarily chosen limit ΔT_{max}, so that

$$\Delta t_{max}(2) = \min\left|\frac{\Delta T_{max}}{\dot{T}_i}\right| \quad \text{over } 1 \leq i \leq N_{pi} \quad (14)$$

We chose ΔT_{max} to be less than about 0.1% of the total temperature rise at the capillary lumen center. Unfortunately, $\Delta t_{max}(2)$ depends on the temperature profile and so must be computed in every integration cycle. Except at extremely high applied power or extremely low arbitrary limit ΔT_{max}, $\Delta t_{max}(1)$ was always smaller than $\Delta t_{max}(2)$ and thus defined the time increment we actually used, but to ensure computational stability we always computed both.

Results and discussion

We first ran our numerical simulations to long times to compare our steady state to results given in various other literature reports. Temperature profiles within the capillary lumen are very nearly parabolic, as noted by other workers

TABLE I

COMPARISON OF PRESENT NUMERICAL SIMULATION (A) WITH ANALYTICAL APPROXIMATION OF REF. 25 (B)

Zone	Percent of total temperature range falling within given zone (%)	
	A	B
Electrolyte	2.7	2.7
Silica wall	2.8	2.8
Polyimide coating	1.3	1.4
Air–polyimide interface	93.2	93.1

TABLE II

COMPARISON OF PRESENT NUMERICAL SIMULATION (A) WITH ANALYTICAL APPROXIMATION OF REF. 27 (B)

Lumen radius (μm)	Lumen temperature range (K)		Lumen wall temperature (K)	
	A	B	A	B
25	0.33	0.53 (0.35?)	299.1	299.0
50	1.37	1.39	301.5	301.2
75	3.10	3.14	304.8	304.2
100	5.52	5.58	308.8	307.7
125	8.64	8.72	313.2	311.6

[28], though exceptions may exist [29]. Using the physical parameters of Table II of ref. 26, we obtain steady state profiles (Table I) that agree closely with those obtained from the analytical approximation given in ref. 26. In Table II we show that our numerical results agree with other analytical approximations over a wide range of capillary lumen radii (we suspect that the lumen temperature range of 0.53 K given by ref. 28 for lumen radius 25 μm is a typographical error because it is inconsistent with other results in the same table). The steady-state temperature profile we obtain from numerical simulation also agrees closely with the results in ref. 30 using the analytical approximations of ref. 30 as given in the last column of our Table III.

Numerical simulation under conditions given in ref. 25 predicts a lumen temperature increase of 5.0°C given thermal transfer coefficients typical of liquid cooling and 1.7°C given perfect thermal dissipation at the outer surface, compared with the *experimental* temperature measurement [25] of 1.9°C, suggesting that if the measurements were accurate, thermal dissipation in those experiments was extremely efficient.

However, it is in the study of non-steady-state thermal behavior that numerical simulation has the greatest advantages. One major advantage is that it provides direct access to simulated thermal profiles at any time during the equilibration process, as illustrated by Fig. 3. Another feature of the numerical approach is its ability to employ any boundary conditions or physical conditions

TABLE III

COMPARISON OF PRESENT NUMERICAL SIMULATION (A) WITH ANALYTICAL APPROXIMATION OF REF. 29 (B)

Position (μm from center)	Temperature increase (K)							
	0.034 s		0.34 s		1.36 s		"Steady state"	
	A	B	A	B	A	B	A	B
Center (0 μm)	4.31	4.23	19.1	18.9	28.7	28.4	29.2	28.9
Aqueous–Si (75 μm)	2.52	2.49	16.3	16.0	25.2	24.8	25.2	25.3
Si–polyimide (166 μm)	1.66	1.70	14.7	14.3	22.9	22.6	23.4	22.9
Polyimide–air (180 μm)	1.40	1.49	13.2	13.0	20.6	20.5	20.9	20.9

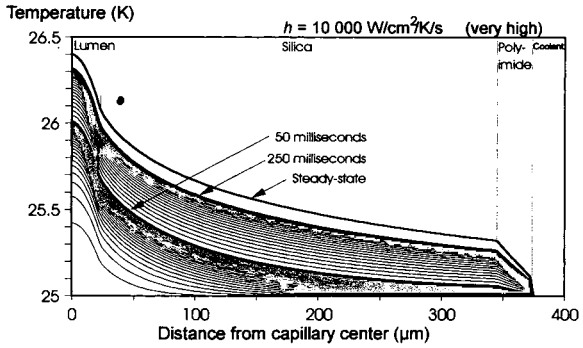

Fig. 3. Electrolyte velocity temperature profiles at 2, 4, 6, . . . , 48, 50, 60, 70, 80, . . . , 240 and 250 ms after potential first applied. Simulated conditions as given in ref. 28: capillary radii: lumen 25 μm, silica 345 μm, polyimide 375 μm; potential gradient 300 V/cm; resulting current 88.4 μA.

whatsoever. Especially, one may set any initial temperature conditions one likes, and in fact may integrate backwards in time, though this technique is prone to oscillation because the profile-broadening effects of thermal conduction are reversed. One may include the effects of varying the surroundings' temperature, for example when the thermostatting system has a lag time or is influenced by air conditioning. One may even include sudden, gradual, or cyclical changes in the applied potential, thermal or electrical conductivities, or other physical parameters, though many combinations may not be physical consistent.

The conditions of the separation considered in ref. 28 include extremely efficient thermal transfer from the capillary's outer surface to its surroundings, and as expected most of the steady-state temperature drop is predicted to occur within the silica and the lumen with very little drop at the capillary outer surface (Fig. 3). Temperatures at the interfaces agree with those predicted by analytical means [28]. However, even in this nearly ideal case, the whole-capillary temperature rise takes about 100 times as long to develop as does the parabolic profile in the lumen, even with efficient thermal transfer at the outer surface. The lumen profile is fully developed within a very few milliseconds. Such results confirm the need to distinguish between rates of thermal gradient development within the capillary's inside and outside diameters [26].

Assuming a smaller, more realistic thermal transfer rate h at the outer wall, we find that temperature profiles given by the present numerical simulation method agree at several radial positions and at several time points after first application of axial potential (Table III) with results of analytical approximations previously published [30,31]. Again we find that the parabolic temperature profile shape and gradient magnitude in the lumen develop in the first few milliseconds (Fig. 4). However, in most other ways the development of thermal profiles depends greatly on thermal transfer efficiency at the capillary outer wall —at lower thermal transfer efficiency the temperature rise across the column is much larger in proportion to the power dissipation, a much greater fraction of the temperature gradient across the capillary occurs at the outer surface, and the temperature rise throughout the capillary, including inside the lumen, take longer to complete.

Once thermal steady state is achieved, setting the applied potential to zero reverses the processes (Fig. 5). First, the parabolic temperature profile across the lumen flattens in a very few milliseconds, and the whole capillary cools more slowly and in a nearly exponential fashion.

In the case of very inefficient thermal transfer from the outer surface of a capillary in contact only with still air, almost all of the radial tem-

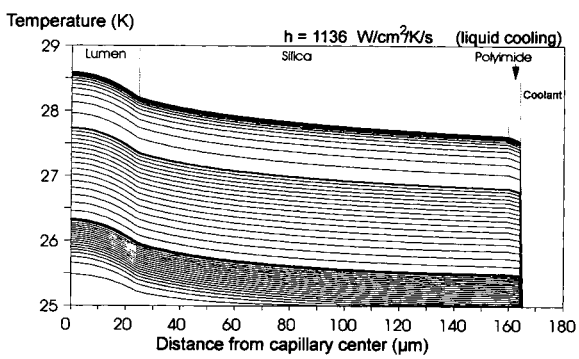

Fig. 4. Electrolyte temperature profiles (beginning with lowermost curve) at 2, 4, 6, . . . , 38, 40 (bold curve), 50, 60, . . . , 180, 200 (bold curve), 250, 300, . . . , and 1000 ms after potential applied beginning at power-off steady state. Simulated conditions after ref. 30: capillary radii: 25 μm, silica 160 μm, and polyimide 165 μm; potential gradient 300 V/cm; resulting current 100 μA.

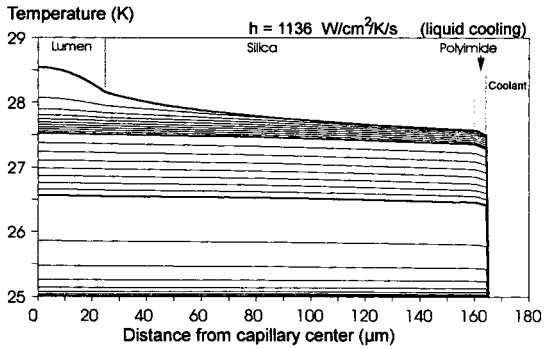

Fig. 5. Electrolyte temperature profiles (beginning with uppermost curve) at 0, 2, 4, 6, . . . , 18, 20 (bold curve), 30, 40, . . . , 90, 100 (bold curve), 200, 300, . . . , and 700 μs after potential set to zero after thermal steady state established. Conditions as in Fig. 4 except that potential gradient and current refer to preexisting steady state.

perature drop occurs at the outer surface (Fig. 6), that is, the temperature profile across the entire capillary is relatively very flat [9,26,27]. The inefficient heat dissipation requires that the applied potential be kept very small so that the temperatures in the lumen are kept low enough to prevent "thermal runaway" caused by positive feedback between temperature rise and electrolyte conductivity increases [24,26] large thermally induced pH changes [32], chemical changes like protein denaturation [27,33] or reduction [33], and other problems. The low power dissipation causes very little parabolic,

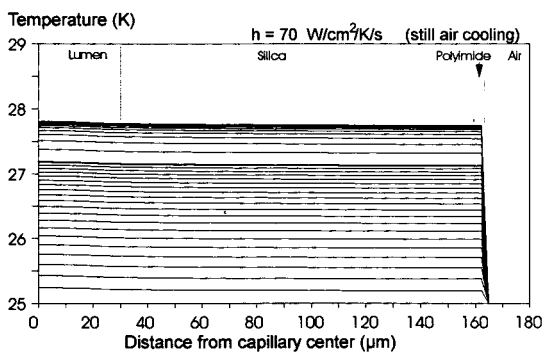

Fig. 6. Electrolyte temperature profiles (beginning with lowermost curve) at 200, 400, 600, . . . , 3800, 4000 (bold curve), 5000, 6000, . . . , and 20 000 ms after potential applied. Simulated conditions after ref. 30: capillary radii: 25 μm, silica 160 μm, and polyimide 165 μm; potential gradient 75 V/cm; resulting current 25 μA.

zone-broadening radial thermal gradient in the lumen, but it also means that ion velocities will be so slow that the electrophoretic analysis will be slow. The capillary's approach to thermal steady state requires several seconds in this case. The use of capillaries with extremely small inside diameters [14,15] helps in two ways: by suppressing thermal broadening by decreasing the parabolic [34], zone-broadening thermal gradients inside the lumen, and simply by decreasing the amount of power that the outer capillary surface is required to dissipate. However, note that at constant electrolyte composition, smaller inside diameters can cause the electric field rise time *in the capillary* to lengthen dramatically [13].) Further, there is experimental evidence [35] that the extent of convection and therefore the effective thermal transfer rate in still air depend on the outer surface temperature in unpredictable ways [36]. Fortunately, in electrokinetic sample injection the injection end of the capillary is immersed in the sample solution, so that the degree of temperature changes and the unpredictability of thermal transfer rates at the injection end of the capillary will not be as important as they might at first appear, though electroosmotic flow changes caused by slow capillary heating during injection may impair quantitative precision.

Thus we confirm by independent means that efficient thermal transfer at the capillary outer walls are required for analyses that require both high separation efficiency and short analysis times. Air-cooled silica capillaries are known to limit the power dissipation to about 1 W/m [37,38] for efficient separations. Our results are consistent with others' findings that efficient capillary cooling over the length of the capillary including near the detector [24] suppresses thermal zone broadening [9] and that under very efficient capillary cooling the thermal zone broadening is smaller than other sources of broadening [2,9,28,30,39] and especially that it contributes less broadening than does the length of the injection zone itself [1–3] in the efficient cooling case. Such efficient thermal transfer also speeds thermal equilibration of the whole capillary (though not of radial thermal gradients in the lumen) so that it is probably especially

important for efficient, quantitative CE separations in short capillaries with large inside diameters and relatively high electrolyte conductivities.

TIMESCALES OF TRANSIENT EVENTS IN CAPILLARY ELECTROPHORESIS

We can now compare the timescales of several transient processes in CE (see Fig. 7). The fastest process is certainly the propagation of axial potential gradients down the length of the capillary lumen. For a capillary of length l filled with electrolyte of refractive index n, this characteristic propagation time is $t_{char} = ln/c$, where c is the speed of light in a vacuum. For a 1 m column filled with aqueous electrolyte t_{char} is on the order of a few nanoseconds, depending on the refractive index of the electrolyte at the effective frequency at which the axial potential is applied. Thus even with the fastest power supplies one need not be concerned with electric field phase changes in a CE capillary. Though ion migration under an abrupt potential gradient change may indeed occur on a picosecond timescale [40], one can do very little to decrease the potential propagation time, so the former timescale must defer to the latter.

Electroosmotic flow radial propagation occurs on the order of hundreds of microseconds as demonstrated above. This relaxation time can be accelerated greatly by increasing the electrolyte solution viscosity, but the most apparent effect will be the suppression of electroosmotic flow altogether.

Thermal changes following application of potential to a CE capillary fall into two categories: the first, which occurs inside the capillary lumen and causes some zone dispersion, and the second one a more general temperature rise over most of the capillary. The relaxation time of the thermal gradient in the capillary lumen is much faster than that of the general temperature rise largely because the distance over which heat must be conducted is much shorter in the first case than in the second; the resistance to heat flow presented by the capillary outer surface also serves to slow the general temperature rise, but not the parabolic profile formation in the lumen.

The relaxation time of the thermal gradient in the lumen depends mostly on the capillary's inside diameter and not on applied potential [2], while the relaxation time of the general temperature rise depends greatly on the efficiency of heat transfer at the outer surface of the capillary, and to a lesser extent on the capillary outside diameter. Inefficient heat removal from the capillary's outer surface may cause serious quantitation problems in electrokinetic injection by making non-linear the relation of analyte amount injected with the product of injection voltage and duration of injection. Convective cooling in unstirred air worsens this problem still more because the surface thermal transfer coefficient h probably depends in complex ways on the capillary surface temperature [36].

The electric field rise time in the capillary lumen is probably the most readily controlled of the transient processes considered in this work [3,40]. Though it is probably in the hundreds of milliseconds in most instruments, with care this rise time can be shortened to the millisecond range [13]. This electric field rise time in the capillary makes irrelevant all clearly shorter rise times.

Analyte diffusion across the lumen is the only process whose timescale depends directly on analyte properties, specifically on the analyte diffusion coefficient D_x. This process's timescale is the most variable of those considered in this work. The diffusion coefficient is directly calculable from the measured signed mobility m_x and charge Z_x of analyte x as

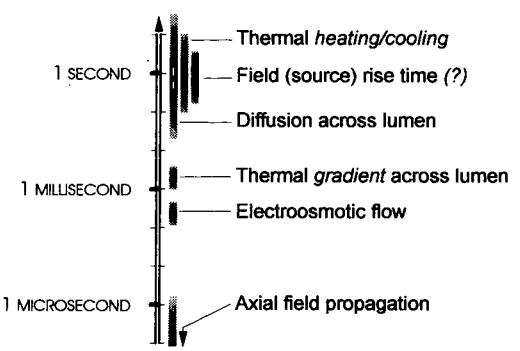

Fig. 7. Summary of timescales of CE transient processes, given here for capillary of 50 μm inside diameter, 360 μm outside diameter.

$$D_x = RTm_x/FZ_x \quad (15)$$

where R is the ideal gas constant, T is the local temperature, F is the Faraday constant, and Z_x is the signed charge on analyte x. Note that eqn. 15 neatly accounts for the temperature dependence of the ratio D_x/m_x previously noted in experimental results [2].

We note here that the diffusion coefficient and mobility are directly linked by fundamental statistical mechanics and not through viscosity. Attributions to the contrary notwithstanding [2], we have never doubted the validity of eqn. 15. Viscosity cannot be derived from either analyte diffusion coefficients or mobilities, or *vice versa* [1], except under assumptions which are tenuous in homogeneous solution and patently invalid in the presence of gels and viscosity-enhancing polymers. One should not rely too much on any connection between ion mobility and electrolyte viscosity as is often done [2,41] but should use the Stokes–Einstein equation (15 above) instead when at all possible.

MINIMIZING THERMAL DISPERSION THROUGH POTENTIAL MODULATION

Methods

Thermal simulations demonstrate that the parabolic thermal profile in the capillary lumen rises and falls rapidly when the driving potential is applied or withdrawn, respectively, and the initial temperature changes occur rapidly and slow considerably after only a few milliseconds (Figs. 3–6). This behaviour suggests that when driving potential is applied, the ions immediately reach a nearly constant velocity, but that the dispersion-generating temperature difference between the center and the wall of the lumen requires a few milliseconds to reach its maximum. In this section we explore whether it is possible to maximize the ion migration while minimizing zone dispersion by taking advantage of the two process's different timescales. Because the disparities in the processes' time-dependent behaviour exist for only a few milliseconds, a much shorter time than any feasible CE separation requires, we are constrained to exploit it in some repetitive fashion. The applied potential is the only whole-column experimental condition we can think of manipulating in just a few seconds. These two constraints suggest that in order to suppress the effects of thermal broadening, we investigate the use of driving potential modulation.

All repetitive modulation patterns contained only three parts, applied in this order: a period a of duration l_a during which a positive potential gradient of magnitude E_a is applied, followed by a period b of duration l_b of negative potential gradient of magnitude E_b, followed in turn by a period c of duration of l_c of zero applied potential (see Fig. 8). Rather than using the potential gradients, we found it convenient to work instead from capillary-center ballistic heating rates B_a and B_b

$$B_a = \frac{E_a^2 \Lambda_{aq} D_{aq}}{C_{p,aq}}$$
$$B_b = \frac{E_b^2 \Lambda_{aq} D_{aq}}{C_{p,aq}} \quad (16)$$

that one would obtain from instantaneously switching from zero potential gradient to E_a and E_b, respectively, where Λ_{aq} is the specific electrical conductivity within the electrolyte solution, D_{aq} is the electrolyte density, and $C_{p,aq}$ is the electrolyte specific heat. Our assumption that the rate k of radial thermal gradient relaxation within the electrolyte is slow compared to diffusional and column-wide heating relaxation rates is supported by results of previous sections of

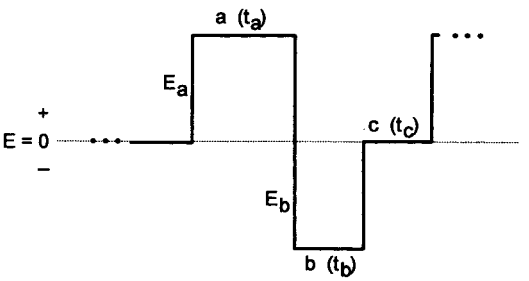

Fig. 8. Definition of potential modulation sequence used in this work. E_a and E_b are potential gradients during periods a and b, and E_a, E_b and E_c are the durations of periods a, b and c.

this work. Assuming that a single radial thermal gradient relaxation time exists implies that temperature *vs.* time curves represent exponential decays. We expect that the results of this feasibility study do not depend strongly on minor deviations from exponential relaxation curve shapes. Our assumption that the decay curves during periods *a* and *b* are exponential implies in turn that conductivity changes caused by the electrolyte temperature excursions are linear, that is, that eqn. 16 holds. This assumption is very probably valid over the few degree's temperature fluctuations expected within the lumen of real capillaries. Finally, we assume that rectangular-wave modulation patterns can in fact be delivered to the capillary, that is, that the power source can deliver high-frequency components. For a capillary of inside diameter 50 μm, k is about 500 s^{-1} (see Fig. 5). The power source must deliver alternating current components of at least a few kilohertz to synthesize a reasonable approximation of a 500-Hz square wave. Sine-wave modulation at 390 Hz [23] and reasonably square-wave modulation at 500 Hz [13] of the CE driving potential have been reported previously.

The steady state (identical thermal profiles in sequential cycles) is achieved only after very many identical modulation cycles. The present model considers only the analytes' behavior at steady state. Under the assumptions of the previous paragraph, steady-state capillary center temperatures $T_{a,t}$, $T_{b,t}$ and $T_{c,t}$ during periods *a*, *b* and *c* are given by

$$T_{a,t} = T_{a,\infty} - T_{a,\infty}\, e^{-k(t-t_{a,0})}$$

$$T_{b,t} = T_{b,\infty} + (T_{a,\infty} - T_{b,\infty})\, e^{-k(t-t_{b,0})} \quad (17)$$

$$T_{c,t} = T_{b,\infty}\, e^{-k(t-t_{c,0})}$$

where $T_{a,\infty}$ and $T_{b,\infty}$ are the asymptotic capillary-center temperatures, relative to ambient temperature, at times long compared to the intralumen thermal relaxation time k^{-1} but short compared to the column-wide thermal relaxation time, and where $t_{a,0}$, $t_{b,0}$ and $t_{c,0}$ are times at the beginning of periods *a*, *b* and *c*, respectively, within a given cycle. One can solve by substitution for the capillary-center temperatures $T_{a,0}$, $T_{b,0}$ and $T_{c,0}$ at potential-switching times $t_{a,0}$, $t_{b,0}$ and $t_{c,0}$ to obtain

$$T_{a,0} = T_{a,\infty} + (T_{c,\infty} - T_{a,\infty})\, e^{-kt_a}$$

$$T_{b,0} = \frac{T_{b,\infty}(1 - e^{-kt_b}) + T_{a,\infty}\, e^{-kt_b}(1 - e^{-kt_a})}{1 - e^{-kt_a}\, e^{-kt_b}\, e^{-kt_c}} \quad (18)$$

$$T_{c,0} = T_{b,\infty}\, e^{-kt_c}$$

To judge the success of any given modulation sequence defined by B_a, B_b, kt_a, kt_b and kt_c requires that one integrate over one steady-state modulation cycle the capillary-center displacement of analyte x with velocity temperature coefficient j_x relative to its displacement at the capillary wall, assuming that electroosmotic flow is either absent, laminar, or relaxing radially much faster than radial thermal relaxation. This dispersion-generating net displacement difference Δd_x is

$$\begin{aligned}\Delta d_x &= j_x\left\{B_a \int_0^{t_a} (T - T_{a,0})\, dt + B_b \int_0^{t_b} (T - T_{b,0})\, dt\right\} \\ &= j_x\{B_a[T_{a,\infty}t_a - (T_{c,0} - T_{a,\infty})(e^{-kt_a} - 1)/k] \\ &\quad - B_b[T_{b,\infty}t_b - (T_{a,0} - T_{b,\infty})(e^{-kt_b} - 1)/k]\}\end{aligned} \quad (19)$$

Our strategy is thus to explore modulation sequences giving zero net axial displacement difference Δd_x, selecting for further consideration those which yield significant net forward displacement. Because modulation sequences vary in duration, we found it most useful to compare the usefulness of modulation sequences with zero Δd_x by comparing values of R_d, the ratio of d_{max}, the forward displacement one would achieve by applying a constant potential equal to the modulation sequence's maximum potential, to d_{mod}, the forward displacement under modulation.

$$\begin{aligned}R_d = \frac{d_{max}}{d_{mod}} &= \frac{(t_a + t_b + t_c)\cdot \max(|E_a|, |E_b|)}{|t_a|E_a| - t_b|E_b||} \\ &= \frac{(t_a + t_b + t_c)\cdot \max(B_a, B_b)}{|t_aB_a - t_bB_b|}\end{aligned} \quad (20)$$

This measure of comparison is conservative in that it disfavors modulation sequences relative to constant potentials because capillary-center temperatures under modulation will generally not rise as high as they would under a given sequence's maximum potential held constant.

Results and discussion

The minimum set of properly scaled and dimensionless parameters defining a modulation sequence is: B_b/B_a, kt_a and kt_b. The absolute magnitudes of B_a and B_b are unimportant if the maximum applied potentials are small enough that ion velocity temperature coefficients are constant. The dimensionless duration of the zero-potential (cooling) period, defined by kt_c, is adjusted to set Δd_i to zero, so kt_c is only a dependent parameter of the modulation cycle's definition. For many combinations of B_b/B_a, kt_a and kt_b values there exists no positive kt_c yielding zero Δd_i.

We find that under this model there do exist modulation sequences that completely suppress thermally generated CE zone dispersion (Table IV). The optimal sequence appears to have the parameters $B_b/B_a = 1.0$, $kt_a = 1.5$ and $kt_b = 1.0$. This is probably a global optimum, as the range of parameters allowing for zero calculated thermal dispersion is very limited.

These sequences work because most of the forward displacement during period *a* occurs when the radial thermal gradients are small, and most of the reverse displacement during period *b* occurs when the radial thermal gradients are fully developed. Thus, if the applied potential in the two periods are of equal magnitude, t_a may be longer than t_b, so that while the axial dispersion in the two periods exactly cancel, there is net forward ion migration.

TABLE IV

SOME MODULATION SEQUENCES GIVING ZERO CALCULATED THERMAL DISPERSION

Adjustable parameters			Results	
B_b/B_a	kt_a	kt_b	kt_c	R_d
1.00	1.1	1.0	0.22	23.2
↓	1.2	↓	0.46	13.3
	1.3		0.72	10.1
	1.4		1.04	8.6
	1.5		1.48	8.0[a]
	1.6		2.18	8.0[a]
	1.7		5.9	12.3
	1.8		[b]	[b]

[a] Very near apparent global optimum.
[b] No kt_c value gives zero calculated thermal dispersion.

Whether one can achieve such zone sharpening in practice we cannot say due to the number of assumptions we were required to make. To remove the assumption that relaxation is exponential in time and to explore more realistic, non-rectangular waveforms with fewer high-frequency components would require micrometer-resolution, two-dimensional (axial and radial), time-dependent integration in ion velocity and temperature, and perhaps in electroosmotic flow. Further, there has been reported experimental evidence of *radial* ion migration under modulated applied potentials [23,42] whose inclusion would complicate matters still further. Such complete integrations would be computationally demanding in the extreme.

However, because the present model's simplifying assumptions are probably close to reality, we speculate that there may exist real modulation sequences which are accessible experimentally and which suppress the dispersive effects of radial thermal gradients. We note an interesting previous report of similar suppression results obtained by introducing a steady-state retrograde hydrodynamic flow [43].

Sequences such as the ones presented herein would be most valuable when applied to highly conductive electrolyte solutions or perhaps to capillaries with large inside diameters, provided the model's timescale assumptions still apply. Preparative CE of large molecules (with small diffusion coefficients) might best make use of the proposed method. We have had to make a considerable number of assumptions in the interest of mathematical tractability. It is not clear whether the thermal states generated by optimal sequences will be near enough to steady state that exponential decay will be a useful approximation [12]. Thus, nothing can take the place of careful experimental demonstration, including

error analysis, of this proposed antibroadening effect.

REFERENCES

1 R.-L. Chien and D.S. Burgi, *Anal. Chem.*, 64 (1992) 489A–496A.
2 S.L. Delinger and J.M. Davis, *Anal. Chem.*, 64 (1992) 1947–1959.
3 X. Huang, W.F. Coleman and R.N. Zare, *J. Chromatogr.*, 480 (1989) 95–110.
4 K.D. Altria and C.F. Simpson, *Anal. Proc.*, 23 (1986) 453–454.
5 C.L. Rice and R. Whitehead, *J. Phys. Chem.*, 69 (1965) 4017–4024.
6 J.M. Davis, *J. Chromatogr.*, 517 (1990) 521–547.
7 H.T. Rasmussen and H.M. McNair, *J. Chromatogr.*, 516 (1990) 223–231.
8 J.H. Knox and I.H. Grant, *Chromatographia*, 24 (1987) 135–143.
9 J.H. Knox, *Chromatographia*, 26 (1988) 329–337.
10 J.C. Reijenga, G.V.A. Aben, T.P.E.M. Verheggen and F.M. Everaerts, *J. Chromatogr.*, 260 (1983) 241–254.
11 M. Martin and G. Guiochon, *Anal. Chem.*, 56 (1984) 614–620.
12 H.S. Carslaw and J.C. Jaeger, *Conduction of Heat in Solids*, Clarendon Press, Oxford, 2nd ed., 1959, Ch. 7 and appendix 4.
13 D.N. Heiger, S.M. Carson, A.S. Cohen and B.L. Karger, *Anal. Chem.*, 64 (1992) 192–199.
14 T.M. Olefirowicz and A.G. Ewing, *Anal. Chem.*, 62 (1990) 1872–1876.
15 R.A. Wallingford and A.G. Ewing, *Anal. Chem.*, 60 (1988) 1972–1975.
16 H.K. Jones, N.T. Nguyen and R.D. Smith, *J. Chromatogr.*, 504 (1990) 1–19.
17 J.F. Brown and J.O.N. Hinckley, *J. Chromatogr.*, 109 (1975) 218–224.
18 M. Jansson, Å. Emmer and J. Roeraade, *J. High Resolut. Chromatogr.*, 12 (1989) 797–801.
19 T. Tsuda, J.V. Sweedler and R.N. Zare, *Anal. Chem.*, 62 (1990) 2149–2152.
20 J.F. Brown and J.O.N. Hinckley, *J. Chromatogr.*, 109 (1975) 225–231.
21 D.J. Harrison, A. Manz, Z. Fan, H. Lüdi and H.M. Widmer, *Anal. Chem.*, 64 (1992) 1926–1932.
22 A. Manz, D.J. Harrison, E.M.J. Verpoorte, J.C. Fettinger, A. Paulus, H. Lüdi and H.M. Widmer, *J. Chromatogr.*, 593 (1992) 253–258.
23 C.-Y. Chen, T. Demana, S.-D. Huang and M.D. Morris, *Anal. Chem.*, 61 (1989) 1590–1593.
24 J.O.N. Hinckley, *J. Chromatogr.*, 109 (1975) 209–217.
25 H. Wätzig, *Chromatographia*, 33 (1992) 445–448.
26 A. Vinther and H. Søeberg, *J. Chromatogr.*, 559 (1991) 27–42.
27 R.J. Nelson, A. Paulus, A.S. Cohen, A. Guttman and B.L. Karger, *J. Chromatogr.*, 480 (1989) 111–127.
28 E. Grushka, R.M. McCormick and J.J. Kirkland, *Anal. Chem.*, 61 (1989) 241–246.
29 M. Coxon and M.J. Binder, *J. Chromatogr.*, 101 (1974) 1–16.
30 M.S. Bello and P.G. Righetti, *J. Chromatogr.*, 606 (1992) 103–111.
31 M.S. Bello and P.G. Righetti, *J. Chromatogr.*, 606 (1992) 95–102.
32 C.-W. Whang and E.S. Yeung, *Anal. Chem.*, 64 (1992) 502–506.
33 R.S. Rush, A.S. Cohen and B.L. Karger, *Anal. Chem.*, 63 (1991) 1346–1350.
34 A.E. Jones and E. Grushka, *J. Chromatogr.*, 466 (1989) 219–225.
35 Y. Kurosu, K. Hibi, T. Sasaki and M. Saito, *J. High Resolut. Chromatogr.*, 14 (1991) 200–203.
36 G.O. Roberts, P.H. Rhodes and R.S. Snyder, *J. Chromatogr.*, 480 (1989) 35–67.
37 M.J. Sepaniak and R.O. Cole, *Anal. Chem.*, 59 (1987) 472–476.
38 S. Terabe, K. Otsuka and T. Ando, *Anal. Chem.*, 57 (1985) 834–841.
39 S. Terabe, K. Otsuka and T. Ando, *Anal. Chem.*, 61 (1989) 251–260.
40 T.T. Lee and E.S. Yeung, *Anal. Chem.*, 64 (1992) 1226–1231.
41 H.J. Issaq, I.Z. Atamna, G.M. Muschik and G.M. Janini, *Chromatographia*, 32 (1991) 155–161.
42 T. Demana, U. Guhathakurta and M.D. Morris, *Anal. Chem.*, 64 (1992) 390–394.
43 W.A. Gobie and C.F. Ivory, *J. Chromatogr.*, 516 (1990) 191–210.

Journal of Chromatography A, 652 (1993) 277–281
Elsevier Science Publishers B.V., Amsterdam

CHROM. 25 135

Leakage current consideration of capillary electrophoresis under electroosmotic control

Chin-Tiao Wu, Tung-Liang Huang and Cheng S. Lee*

Department of Chemical and Biochemical Engineering, University of Maryland Baltimore County Campus, Baltimore, MD 21228 (USA)

ABSTRACT

The leakage current phenomenon at the capillary–solution interface was investigated with the application of *high* radial electric potential gradients across the capillary wall for the direct control of electroosmosis. The leakage current traveling through the capillary wall gave rise to a different surface potential between the controlled and uncontrolled regions, and resulted in a linear electroosmotic velocity profile from the controlled region to the ends of the capillary. The mismatch between the electroosmotic velocities was then balanced by the additional laminar flow over the entire length of the capillary. The additional dispersion induced by the laminar flow under the leakage current situation was demonstrated and compared with theoretical prediction.

INTRODUCTION

The concept of electroosmotic control in capillary electrophoresis under the influence of applied radial electric potential gradient has been intensively investigated in several laboratories [1–8]. In all the experimental devices, a radial electric potential gradient is applied over the major portion, but not the entire length of the capillary. This is to ensure the separation and isolation of applied radial electric potential gradient from the axial electric field in the capillary for electrophoresis. The potential mismatch between electroosmotic velocities in the controlled (under the influence of a radial electric potential gradient) and uncontrolled regions, and the resultant dispersion and band broadening are the subjects in our recent study [6].

It is found that there is no measurable additional dispersion and band broadening induced by the direct control of electroosmosis [6]. A d.c. short circuit phenomenon at the capillary–solution interface is proposed for averaging the surface potential over the entire length of the capillary. Thus, there is no difference in the ζ potential and the resultant electroosmosis between the controlled and uncontrolled regions. One major assumption for the "short circuiting effect", however, is that the leakage current through the capillary wall in the controlled region must be negligible. The extra current traveling through the capillary wall would give rise to a different surface potential between the controlled and uncontrolled regions. It is anticipated that the measured dispersion will increase due to this leakage current with the application of a high enough radial electric potential gradient across the capillary wall [6].

In this report, the leakage current in capillary electrophoresis with the application of a high enough radial electric potential gradient is investigated. The magnitude of applied radial electric potential gradient required for causing the leakage current and the irreversible dielectric breakdown of capillary tubing are measured. The flow profiles of bulk fluid in the capillary and the additional dispersion of solute induced

* Corresponding author.

0021-9673/93/$06.00

by the leakage current phenomenon at the capillary–solution interface are presented and discussed both experimentally and theoretically.

EXPERIMENTAL

The experimental setup for measuring the leakage current across the capillary wall under the influence of applied radial electric potential gradient is shown in Fig. 1. A 25 cm long capillary (Polymicro Technologies, Phoenix, AZ, USA) with 50 μm I.D. and 150 μm O.D. was placed between two buffer reservoirs. About 85% of the external surface of capillary tubing was coated with the nickel print (GC Electronics, Rockford, IL, USA) and then connected to the ground. Platinum-wire electrodes were affixed to both reservoirs. One high-voltage power supply (Spellman High-Voltage Electronics, Plainview, NY, USA) was connected to the two reservoirs so that *a constant electric potential* was applied across the buffer solution in the capillary. Thus, a constant radial electric potential gradient across the capillary wall with respect to the external grounding (connected through the nickel print) was generated. A 10-MΩ resistor was inserted between the nickel print conductive layer and the external grounding. This means that a 1-nA leakage current is monitored as a 10-mV potential drop across the resistor.

The experimental setup of capillary electrophoresis in a coaxial configuration for the direct control of electroosmosis has been described in details in the previous study [3]. A smaller (inner) capillary was placed inside a larger (outer) capillary. A radial electric potential gradient was employed along the annular space between the two capillaries for controlling the ζ potential and then the electroosmosis in the inner capillary.

Frontal analyses of a 0.1% dimethyl sulfoxide in phosphate buffer solution were studied with various percentages of the inner capillary under the direct control of electroosmosis. The values of total spatial variance and the changes in the bulk velocity were measured with the application of various radial electric potential gradients. The measured solute dispersion in terms of equivalent plate height was then compared with the theoretical analyses for investigating any additional dispersion induced by the leakage current phenomenon. Sodium phosphate buffer, hydrochloric acid, and dimethyl sulfoxide were purchased from Sigma (St. Louis, MO, USA). The pH of the buffer solution was adjusted with 0.1 *M* hydrochloric acid.

RESULTS AND DISCUSSION

The leakage current across the capillary wall was only measurable when the applied radial electric potential gradient was at or greater than −10 kV. In the experimental setup, an electric potential equal to or greater than +10 kV was employed at both buffer reservoirs containing 10

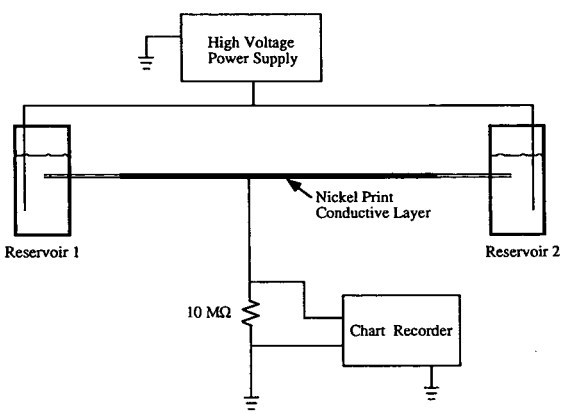

Fig. 1. Test setup for measuring the leakage current across the capillary wall.

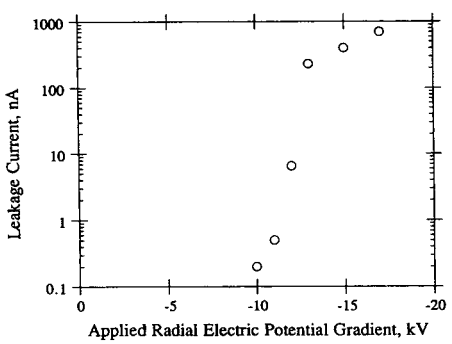

Fig. 2. Plot of leakage current *vs.* applied radial electric potential gradient across a fused-silica capillary with 50 μm I.D. and 150 μm O.D.

m*M* phosphate at pH 3. As shown in Fig. 2, a significant increase in the leakage current was observed with the application of a −13-kV or higher potential gradient. There was no hysteresis effect in the leakage current measurement. The experimental error for measuring the leakage current was about 10–15% for over 5 repeated runs. The capillary tubing was broken by applying any potential gradients which were greater than −17 kV. The irreversible dielectric breakdown of fused-silica capillary with 50 μm I.D. and 150 μm O.D. was thus occurred at a field strength around 17 kV/50 μm = $3.4 \cdot 10^8$ V/m in our study. This measured dielectric strength was about one order of magnitude greater than those reported by Polymicro Technologies (Phoenix, AZ, USA) in the range of $2.5 \cdot 10^7$–$4 \cdot 10^7$ V/m.

In our previous study [6], the d.c. short circuit phenomenon at the inner capillary–solution interface is proposed for averaging the surface potential over the entire length of the capillary. Thus, there is no difference in the ζ potential and the resultant electroosmosis between the controlled and uncontrolled regions. Furthermore, there is no additional laminar flow and dispersion induced by the use of a radial electric potential gradient for the electronic adjustment of electroosmosis. The averaged electroosmotic flow which is constant over the entire length of the capillary is equal to

$$V_{eo,avg} = xV_{eo,100\%} + (1-x)V_{eo,0\%} \quad (1)$$

where x is a fraction of the total length of the capillary under the influence of a radial electric potential gradient and $V_{eo,0\%}$ is the measured electroosmotic velocity in the absence of a radial electric potential gradient. Based on eqn. 1, $V_{eo,100\%}$ is estimated by

$$V_{eo,100\%} = (V_{eo,85\%} - 0.15V_{eo,0\%})/0.85 \quad (2)$$

where $V_{eo,85\%}$ is the measured electroosmotic velocity with 85% of the inner capillary under the influence of a radial electric potential gradient.

To satisfy the proposed "short circuit effect" at the capillary–solution interface, the leakage current across the capillary wall must be negligible [6]. In combination with the surface conductivity, the extra current traveling through the capillary wall would give rise to a difference in the surface potentials between the controlled and uncontrolled regions. By assuming a linear change in the ζ potential from the controlled region to the ends of the capillary, the electroosmotic velocity is thus varied linearly from $V_{eo,100\%}$ in the controlled region to $V_{eo,0\%}$ at the ends of the capillary. Under the leakage current situation, the mismatch between the electroosmotic velocities will have to be balanced by the additional laminar flow. The averaged bulk velocity of fluid over the entire length of the capillary is thus equal to

$$V_{avg} = xV_{eo,100\%} + (1-x)\bar{V} \quad (3)$$

where $\bar{V}$ is the average of $V_{eo,100\%}$ and $V_{eo,0\%}$. Based on the theory of field-amplified capillary electrophoresis, the laminar flow caused by the mismatch between the electroosmotic velocities will then result in extra dispersion and band broadening for solutes inside the capillary [9].

Thus, the flow profiles and solute dispersion in the capillary are dependent on the "short circuit effect" or the "leakage current phenomenon" at the capillary–solution interface. To demonstrate such difference in the flow profiles and solute dispersion between these two surface phenomena, the percentage of the inner capillary under the direct control of electroosmosis was varied from 85, 60, 40, to 20%. The inner capillary was filled with 10 m*M* phosphate buffer at pH 3. A constant inner electric field strength equal to 5.5 kV/25 cm = 220 V/cm was applied during the experiment.

As shown in Fig. 3, the measured velocities of bulk fluid in the capillary with various percentages of tubing under the influence of a −5-kV potential gradient were in good agreement with those predicted by eqn. 1 as the "short circuit effect" at the capillary–solution interface. In contrast, the measured bulk velocities as shown in Fig. 4 with various percentages of tubing under the influence of a −10-kV potential gradient were more close to the prediction based on eqn. 3 as the "leakage current phenomenon" at the capillary–solution interface. The difference

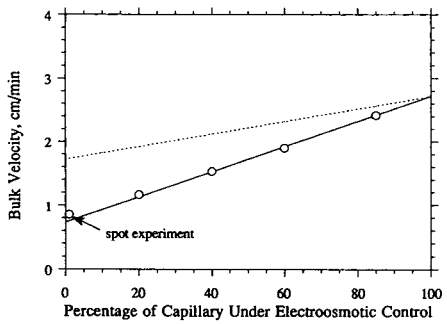

Fig. 3. Plot of bulk velocity *vs.* various percentages of capillary under the influence of a − 5-kV potential gradient. The experimental data are shown as open circles. The prediction obtained from eqn. 1 and eqn. 3 are represented as the solid and dashed lines, respectively.

in the prediction obtained from eqn. 1 (the solid line) and eqn. 3 (the dashed line) was more pronounced with the lower percentage of capillary under the direct control of electroosmosis. It was interesting to notice that the predicted bulk velocity at 0% of the capillary under the influence of a radial electric potential gradient was $V_{eo,0\%}$ from eqn. 1, but became $\bar{V}$ (as the average of $V_{eo,100\%}$ and $V_{eo,0\%}$) from eqn. 3.

To further reduce the percentage of the capillary under the direct control of electroosmosis, we simply applied a spot of nickel print on the external surface of capillary tubing. An electrical connection was then made between the spot of nickel print and a (external) high-voltage power supply. By assuming a linear potential drop across the buffer solution in the capillary, various radial electric potential gradients were applied at the spot of nickel print through the (external) high-voltage power supply. As shown in Fig. 3, there was almost no change for the measured velocity in the absence or presence of a −5-kV potential gradient through the spot of nickel print. In contrast, the measured velocity shown in Fig. 4 was increased to a value close to $\bar{V}$ (as the average of $V_{eo,100\%}$ and $V_{eo,0\%}$) in the presence of a −10-kV potential gradient. The experimental error in the measurement of bulk velocity was about 0–4% for over 5 repeated runs.

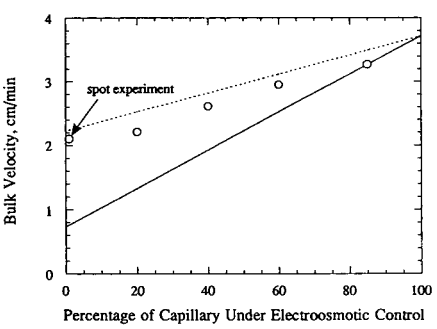

Fig. 4. Plot of bulk velocity *vs.* various percentages of capillary under the influence of a − 10-kV potential gradient. The experimental data are shown as open circles. The prediction obtained from eqn. 1 and eqn. 3 are represented as the solid and dashed lines, respectively.

For dispersion studies, the inner capillary was filled with 1 m*M* phosphate buffer at pH 3. A constant electric field strength equal to 7.5 kV/25 cm = 300 V/cm was applied in the inner capillary. 85% of the inner capillary was under the influence of various radial electric potential gradients from 0 to −8 kV. As shown in Fig. 5, the experimental results (the open circles) were in good agreement with the theoretical plate height based on only molecular diffusion (the solid line). A diffusion coefficient equal to $1 \cdot 10^{-5}$ cm^2/s was used for dimethyl sulfoxide in the calculation of molecular diffusion. With the application of low pH and ionic strength buffer, the electroosmotic flow was enhanced easily with

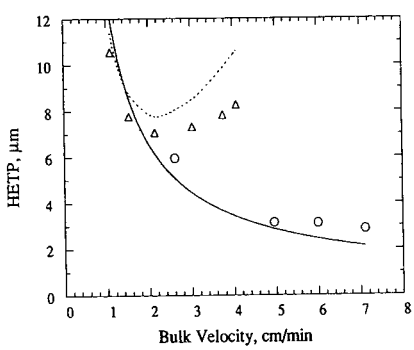

Fig. 5. The comparison of the prediction and the measured values of plate height at various operation conditions. The experimental data are shown as open circles for 85% and open triangles for 40% of the inner capillary under the direct control of electroosmosis. The solid line is the prediction based on only molecular diffusion. The solute dispersion contributed by molecular diffusion and laminar flow is represented by a dashed line. HETP = Height equivalent to a theoretical plate.

85% of the inner capillary under the direct control of electroosmosis.

The ionic strength of buffer solution in the inner capillary was increased to 10 m*M* phosphate at the same pH. The percentage of the inner capillary under the influence of a radial electric potential gradient was reduced from 85% to 40%. Various radial electric potential gradients ranged from 0 to −14 kV were thus required to obtain the bulk velocities similar to those discussed previously. The measured solute dispersion (the open triangles) shown in Fig. 5 started to deviate from the theoretical plate height based on only molecular diffusion (the solid line) when the bulk velocity was around 2.1 cm/min with the application of a −8-kV potential gradient. In fact, the measured solute dispersion was increased with the enhancement of bulk velocity from 2.1 cm/min to 4.1 cm/min under the influence of a radial electric potential gradient from −8 to −14 kV.

Under the leakage current situation at high radial electric potential gradients, the mismatch between the electroosmotic velocities over the entire length of the capillary would induce the additional laminar flow and result in extra dispersion and band broadening for sample inside the capillary. As discussed in our previous study [6], a model based on Chien and Helmer's [9] theory in field-amplified capillary electrophoresis was developed for calculating the additional dispersion and band broadening induced by the laminar flow. As shown in Fig. 5, the measured solute dispersion under the influence of high radial electric potential gradients (from −8 to −14 kV) was quite close to the theoretical plate height contributed by molecular diffusion and laminar flow. The experimental error in the measurement of solute dispersion was about 10–15% for over 5 repeated runs.

Depending on the "short circuit effect" or the "leakage current phenomenon" at the capillary–solution interface, the flow profiles and band broadening of solute in the capillary under the direct control of electroosmosis could be significantly different. The difference in the flow profiles and solute dispersion between the "short circuit effect" and the "leakage current phenomenon" was increased with the decrease in the percentage of the capillary under the direct control of electroosmosis. The required potential gradient across the capillary wall for inducing the leakage current was determined as 10 kV/50 μm = $2 \cdot 10^8$ V/m for a 25-cm long capillary with 50 μm I.D. and 150 μm O.D. used in this study.

ACKNOWLEDGEMENT

We thank Cary J. Miller for his helpful discussion. Support for this work by NSF Instrumentation and Instrument Development Program (DIR-9105016), and NSF Research Initiation Award (CTS-9108875) is gratefully acknowledged. C.S.L. is a National Science Foundation Young Investigator (BCS-9258652).

REFERENCES

1 C.S. Lee, W.C. Blanchard and C.T. Wu, *Anal. Chem.*, 62 (1990) 1550.
2 C.S. Lee, D. McManigill, C.T. Wu and B. Patel, *Anal. Chem.*, 63 (1991) 1519.
3 C.S. Lee, C.T. Wu, T. Lopes and B. Patel, *J. Chromatogr.*, 559 (1991) 133.
4. C.T. Wu, T. Lopes, B. Patel and C.S. Lee, *Anal. Chem.*, 64 (1992) 886.
5 C.T. Wu, T.J. Miller and C.S. Lee, *Anal. Chem.*, 64 (1992) 2310.
6 C.T. Wu, T.J. Miller, T.L. Huang and C.S. Lee, *Anal. Chem.*, 65 (1993) 568.
7 M.A. Hayes and A.G. Ewing, *Anal. Chem.*, 64 (1992) 512.
8 R.R. Holloway, C.A. Keely, J.A. Lux, D. McManigill and J.E. Young, presented at the *4th International Symposium on High Performance Capillary Electrophoresis, Amsterdam, February 9–13, 1992*, poster PT-27.
9 R.L. Chien and J.C. Helmer, *Anal. Chem.*, 63 (1991) 1354.

Journal of Chromatography A, 652 (1993) 283–289
Elsevier Science Publishers B.V., Amsterdam

CHROM. 25 306

Dispersion in capillary electrophoresis with external flow control methods

Catherine A. Keely, Robert R. Holloway, Tom A.A.M. van de Goor and Douglass McManigill*

Hewlett Packard Laboratories, 3500 Deer Creek Road, P.O. Box 10350, Palo Alto, CA 94303-0867 (USA)

ABSTRACT

Recently, methods for controlling the bulk flow of the buffer which are independent of the electrophoretic migration have been demonstrated in capillary electrophoresis (CE) systems. These methods include controlling the electroosmosis by radially directed electric fields, and controlling the bulk flow by siphoning. This paper investigates basic dispersion mechanisms at work by examining the dispersion of dimethyl sulfoxide under various external control methods. It is found that the electroosmotic flow control methods exhibit the same dispersive behavior as the conventional CE system. In particular, the results for pH 7 buffers obey the theoretical expression for the plate height in all configurations. However, in all configurations, pH 2.7 buffers do not follow the theory, and counter to intuition, additional pressure can improve the plate height at pH 2.7. Taking all these methods together, one can develop a technique to appropriately adjust the electrophoretic and bulk flow to optimize resolution.

INTRODUCTION

Capillary electrophoresis (CE) makes use of electroosmotic flow (EOF) and electrophoretic migration induced by a strong electrical field along the axis of the capillary [1,2]. Traditionally these two transport mechanisms were linked because one could not be adjusted by external means without affecting the other. However, in the past few years it has been observed that an external *radial* field can significantly affect the electroosmotic flow while electrophoretic migration remains dependent only on the axial field [3–5]. Adjustment of the radial field allows electroosmotic flow to be increased, decreased, or even reversed. Since electrophoretic migration depends only on the axial field, it is not influenced by the radial adjustment. The EOF control serves to set the bulk flow so that the sample is held in the column to increase resolution, or is flushed through to increase speed. Thus, the electroosmotic and electrophoretic velocities can be adjusted independently.

In CE, electroosmosis generates bulk flow. A pressure differential can also be used to generate bulk flow. Models for the flow profile resulting from EOF and pressure driven flow have been derived [6–8], and from the flow profile an expression for the plate height (height equivalent to a theoretical plate, or HETP) has been formed [7,8] as a measure of system efficiency.

This paper compares the plate height theory with the experimental results of CE systems using three methods of bulk flow control, which include radial field methods and pressure driven flow. It is found that the pH of the buffer–electrolyte solution has a significant impact on the plate height in all systems, yet is not accounted for in the flow profile models or the resulting plate height expression. It is further shown that because of this pH effect, using pressure-driven flow with electroosmosis can actually improve the plate height in many cases.

* Corresponding author.

0021-9673/93/$06.00

Electroosmotic flow control

In 1989, Lee *et al.* [3] and Ghowsi and Gale [5] independently introduced the concept of constraining the electrical field in the radial direction as a means of controlling the EOF without affecting the electrophoretic migration rate. One advantage of such a system would be the ability to perform different kinds of separations on the same capillary where otherwise capillaries of different lengths might be required in order to be time efficient. Another advantage would be the ability to program the fields to optimize the separation at each subsection of an electropherogram. The approach was demonstrated to effectively adjust the bulk velocity over a wide range when using low-pH buffers, but the effectiveness diminishes as pH values increase [9].

The above advantages of external flow control could also be realized by simply pressure driving the bulk flow [10], which is also independent of the electrophoretic migration. However, this option is not always useful because of the extra dispersion caused by the resulting Hagen–Poiseuille velocity profile. The velocity profile resulting from controlling the EOF by radial fields is not currently known, but it is usually assumed to be mostly plug flow as is normally generated by EOF at small dimensions [6]. Chien and Helmer [11] and Towns and Regnier [12] have described profiles when the flow is perturbed by other means, and their findings may be related to the EOF controlled profiles.

This paper studies two separate configurations for controlling EOF via radial fields, in addition

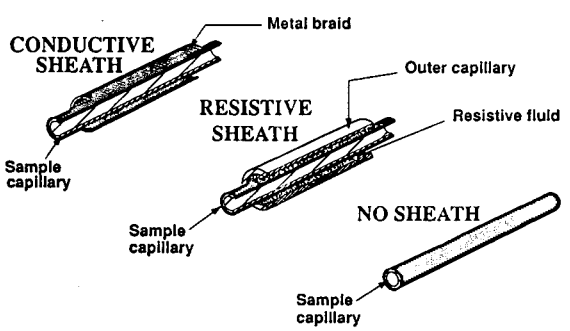

Fig. 1. General capillary configurations used: conductive sheath made by threading capillary through metal webbing; resistive sheath made by surrounding capillary by resistive fluid; and no sheath.

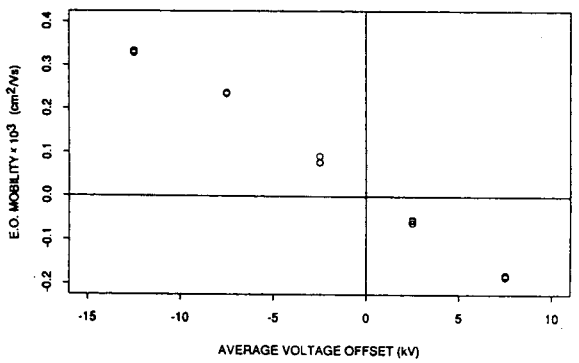

Fig. 2. Electroosmotic (E.O.) mobility plotted as a function of average voltage offset of conductive sheath [$V_{sheath} - (V_{inlet} + V_{outlet})/2$]. Conditions: capillary length 65.5 cm to detector, conductive sheath covering 70%, phosphate buffer pH 2.7, 170 V/cm axial field.

to a conventional configuration. Fig. 1 shows these three configurations schematically. The first method constrains the radial electric field by placing a conductive coating or jacket around the outside of the capillary and holding it at a uniform voltage or ground [9], thus producing a radial field that varies along the length of the capillary. A demonstration of the velocity control possible by radial field adjustment with phosphate buffer pH 2.7 is shown by Fig. 2 where the electroosmotic mobility of dimethyl sulfoxide (DMSO) is plotted as a function of the average voltage difference between the conductive jacket and the buffer fluid. The second method constrains the radial field by placing a resistive coating or fluid around the capillary and holding the ends at specific voltages to create a uniform radial field across the capillary wall everywhere along the capillary [3,9,13]. Conventional systems do not explicitly constrain the radial field, although objects near the capillary, *e.g.* detectors, may affect it.

THEORETICAL MODEL

Datta and Kotamarthi [7] developed a model for dispersion when both electroosmotic flow and Poiseuille flow exist, using the electroosmotic velocity profile developed by Rice and Whitehead [6]. From this model, an expression for plate height H (or HETP) can be written as:

$$H = \frac{2D}{v_{tot}} + \frac{a^2}{24Dv_{tot}} \cdot (v_p^2 + \delta_2 v_p v_e + \delta_3 v_e^2) \quad (1)$$

where

$$\delta_2 = \frac{1}{48} \cdot \frac{\eta}{(1-\eta)} \cdot \left[\frac{1}{12} - \frac{2}{(\kappa a)^2} + \frac{16}{(\kappa a)^4}\left(\frac{1-\eta}{\eta}\right)\right]$$

$$\delta_3 = \frac{1}{48} \cdot \frac{\eta^2}{(1-\eta)^2} \cdot \left[\frac{3}{8} + \frac{2}{(\kappa a)^2} - \frac{1}{\eta(\kappa a)^2} - \frac{1}{\eta^2(\kappa a)^2}\right]$$

$$\eta = \frac{2}{\kappa a} \cdot \frac{I_1(\kappa a)}{I_0(\kappa a)}$$

and where D is the diffusion coefficient, v_{tot} is the total average velocity, a is the capillary inside radius, v_p is the Poiseuille flow velocity component, v_e is the electroosmotic flow velocity component, κ^{-1} is the double layer thickness, and $I_n(x)$ is the modified Bessel function of the first kind, order n. Note how the δ terms depend on the parameter κa, which is the ratio of the capillary radius to the double layer thickness, and the terms are negligible for values of $\kappa a > 200$. For ionic strengths ranging from 1 to 100 mM, the double layer thickness κ^{-1} ranges from 10 nm to 1 nm [14,15]. Thus, under normal CE conditions, capillary diameters greater than about 4 μm reduce the plate height expression to

$$H = \frac{2D}{v_{tot}} + \frac{a^2}{24Dv_{tot}} v_p^2 \quad (2)$$

This formula has also been derived by Grushka [8].

One extreme of this expression occurs when there is no Poiseuille velocity component, or $v_p = 0$, and the equation reduces to the familiar diffusion limited dispersion. The other extreme occurs when the total velocity results from pure Poiseuille flow, or $v_{tot} = v_p$, and then the last term becomes linearly related to the velocity.

EXPERIMENTAL

Apparatus

Fig. 3 schematically shows the apparatus used in the plate height experiments. As described above and shown in Fig. 1, three capillary configurations were used: a conductive sheath, a resistive sheath, and a configuration with no sheath used as a reference. For the conductive sheath, the capillary was threaded through a metal braid which covered 56% of the capillary length. The 50 μm I.D. × 180 μm O.D. fused-silica capillary used in the experiments (Polymicro Technologies, Phoenix, AZ, USA) was typically 40 cm long, with a detector window 16.5 cm from the inlet. The inlet side was connected to a high-voltage supply (Spellman High Voltage, Plainview, NY, USA), and the outlet end and the sheath were both typically connected to ground, but for certain experiments one or the other were connected to a second high-voltage supply. The conventional "no-sheath" configuration was identical except that the metal braid was removed.

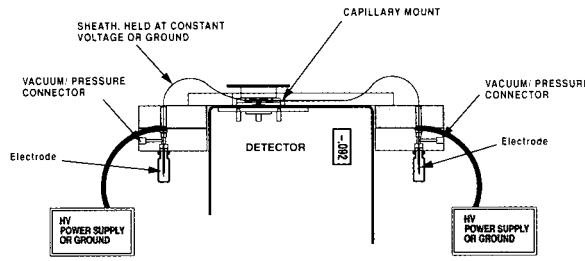

Fig. 3. Capillary electrophoresis apparatus used in experiments. Shown with conductive sheath. HV = High voltage.

For the resistive sheath, the method of Lee *et al.* [3] was used in which the sample capillary rests inside a second capillary filled with a resistive buffer, allowing a constant field to be held across the wall of the inner capillary. The inner capillary dimensions were as stated above, and the outer capillary dimensions were 540 μm I.D. × 680 μm O.D., and 22.5 cm long centered lengthwise along the inner capillary.

A UV absorbance detector (Linear Instruments, Reno, NV, USA) set to 210 nm was used to detect the sample front. A window was burned in the polyimide coating of the capillaries for UV transmission.

In the pressure-driven flow experiments, pressure was connected to ports indicated in Fig. 3 and controlled by an in-house designed pressure regulator. The pressure was adjusted to be 10, 20

or 30 cmH_2O (1, 2 or 3 kPa, respectively) and it was connected to one side or the other of the CE system to push with or against the EOF.

Chemicals

DMSO (Alltech, Deerfield, IL, USA) was normally used as the neutral molecule under study. For a few experiments, mesityl oxide (Aldrich, Milwaukee, WI, USA) and benzene (Aldrich) were substituted for DMSO. The background buffer was 10 m*M* phosphate buffer with 0.5% DMSO, and the run was made using a front of the same 10 m*M* phosphate buffer with 1% DMSO. Certain experiments used 10 m*M* glycine buffer instead of phosphate. The outer capillary in the resistive sheath system contained 1 m*M* phosphate buffer pH 2.8.

Phosphate buffers at pH 2.7 were prepared by titrating 10 m*M* phosphoric acid (J.T. Baker, Jackson, TN, USA) to pH 2.7 with 50% sodium hydroxide (J.T. Baker), resulting in a nominal ionic strength of 7.8 m*M*. The alternative glycine buffer was prepared by titrating 10 m*M* glycine (Bio-Rad, Richmond, CA, USA) to pH 2.7 with concentrated hydrochloric acid (Fluka, Ronkonkoma, NY, USA), the final ionic strength being 5.1 m*M*. Phosphate buffers at pH 7 were made by titrating 10 m*M* monobasic potassium phosphate (J.T. Baker) with 4 *M* potassium hydroxide (Fluka) to pH 7, resulting in an ionic strength of 17.7 m*M*. The pH 8.6 glycine buffer was made from the pH 2.7 glycine buffer by titration with 50% sodium hydroxide, producing an ionic strength of 6.0 m*M*.

Procedure

The background buffer contained DMSO to eliminate any skew in the front caused by adsorption-desorption to the wall of the capillary. Frontal analysis was used to eliminate the additional variance of the injection, and the detector variance was assumed to be negligible. An in-house program using standard formulas and S-Plus (Statistical Sciences, Seattle, WA, USA) operations was used to calculate statistical moments of the UV absorbance signal. The program would take the derivative of the raw signal, trim the data to an approximately 6σ wide region centered on the peak, smooth the data, and perform a moments analysis to obtain the length-based variance σ^2. This variance was related to the experimental plate height,

$$H = \frac{\sigma^2}{l}$$

where l is the capillary length from the inlet to the detector.

RESULTS AND DISCUSSION

Configuration study

Results of the experiments are in the form of plate height (10^{-6} m) *versus* velocity (10^{-3} m/s) plots (H–u curves). The first set of experiments compared the behavior of the three configurations with a pH 2.7 buffer and with a pH 7 buffer. Fig. 4 shows these results, along with the

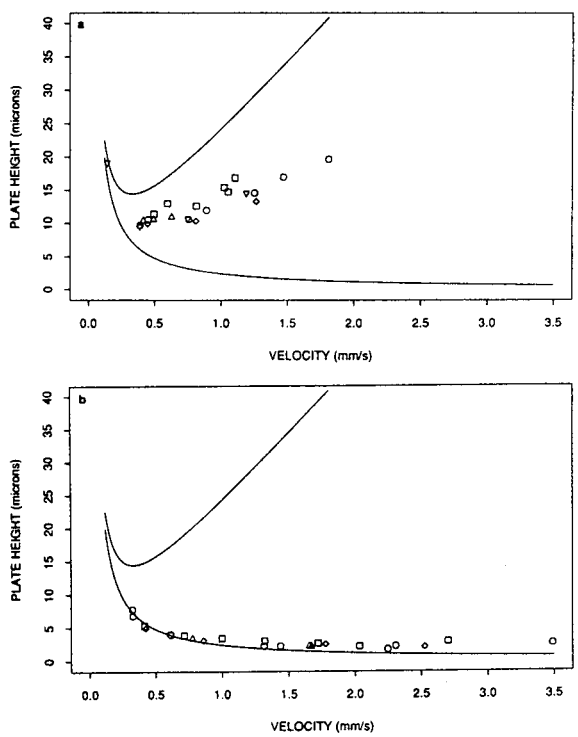

Fig. 4. Plate height *vs.* velocity for three configurations. Theoretical curves are for diffusion-limited dispersion (lower curve) and pressure-limited dispersion (higher curve). ○ = Conductive sheath and phosphate buffer; △ = resistive sheath and phosphate buffer; □ = no sheath and phosphate buffer; ◇ = no sheath and glycine buffer; ▽ = conductive sheath and glycine buffer. (a) Buffer pH 2.7; (b) buffer pH 7.

theoretical curve for diffusion limited dispersion, and the curve for pure pressure-driven flow, the extremes of eqn. 2. Note that in all configurations the pH 7 buffer data points fall on the diffusion limit line, while the pH 2.7 data points ascend at about 70% of the pressure limit level. This is contrary to theoretical expectations. Glycine buffer substituted for phosphate buffer produced the same results. Although not shown here, samples which used mesityl oxide and benzene as the neutral molecule also gave similar results.

Experiments were also run with two smaller diameter capillaries. As Fig. 5 shows, the theoretical pressure limit curve is different for each capillary, yet as in the original case, it can still be seen that the observed plate heights rise as the velocity increases.

Relating the results to the EOF control, it is seen that the EOF control methods do not cause any significant additional dispersion compared to the conventional no-sheath configuration. The pH was the only parameter which caused a change in the dispersion behavior, but at this time we have no plate height expression that describes this pH dependence. Temperature gradients were examined as a possible cause, but were found to be insignificant. It should be recalled that the radial field EOF control methods also have a pH dependence, in that the velocity adjustment range is large with low-pH buffers but minimal with high-pH buffers. Thus, the phenomena that allows control may also perturb the velocity profile, but actively controlling EOF does not seem to affect the resulting plate height–velocity relationship.

Pressure study

Fig. 6 shows data taken at pH 7 with a 20 cmH_2O head (20 mbar or 2 kPa) attached at the capillary inlet or outlet. The range of experimental velocities was obtained by varying the axial field and by changing the direction, but not magnitude, of the pressure head. Overlaid on the data is the diffusion limit curve, and the theoretical plate height curve determined by eqn. 2 with v_p obtained by the Hagen–Poiseuille law [16]. Because the v_p term is squared, its contribution to the plate height is not dependent on direction, and thus experiments could be made with the pressure head pushing in either direction. As can be seen, the data points follow the plate height theory very well.

The implications of the plate height theory are demonstrated more graphically by Fig. 7. This plot shows a series of runs all taken under identical electrical conditions, but with varying amounts of applied pressure. It can be seen that with a given axial field, pressure may be used to increase or decrease the bulk flow velocity with a minor increase in plate height. Since the data obey eqn. 2, it follows that added pressure will not cause as great an increase in plate height

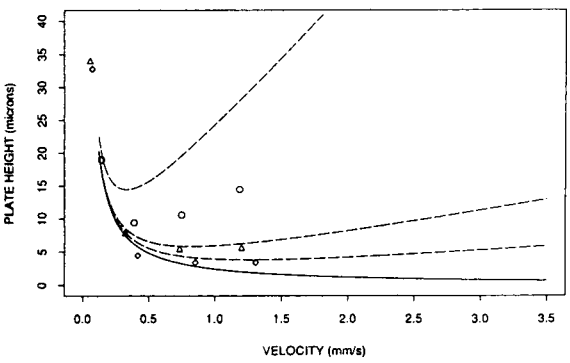

Fig. 5. Performance of three capillary diameters with glycine buffer pH 2.7. Three upper dashed theoretical curves are for pressure-limited dispersion corresponding to the three diameters. Lowest curve is for diffusion-limited dispersion. ○ = 50 μm I.D.; △ = 20 μm I.D.; ◇ = 13 μm I.D. Conditions: axial field varied, conductive sheath.

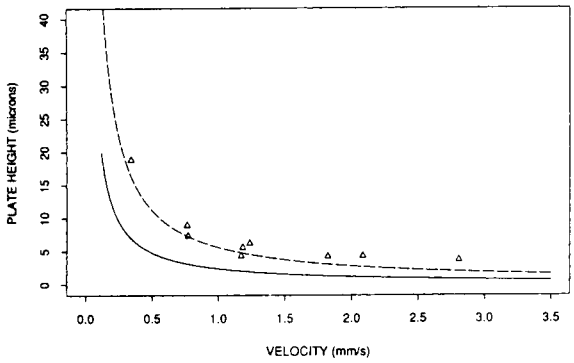

Fig. 6. Phosphate buffer pH 7 with 20 cmH_2O head attached to inlet or outlet end of capillary during run. Dashed curve is eqn. 2 with v_p corresponding to a 20 cmH_2O head. Lower curve is diffusion-limited dispersion. Conditions: axial field varied, conductive sheath.

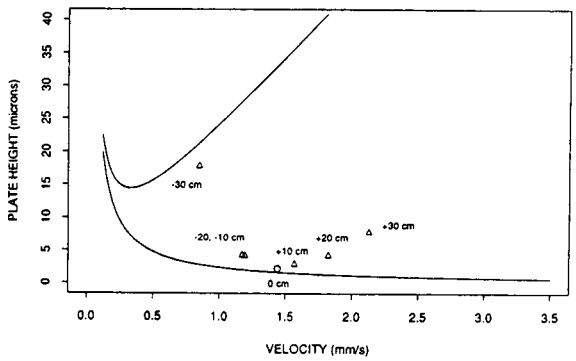

Fig. 7. Phosphate buffer pH 7 with 250 V/cm axial field. ○ = No pressure head; △ = additional pressure head varied from −30 cmH_2O to +30 cmH_2O (−3 kPa to +3 kPa). Conditions: constant axial field, conductive sheath.

when smaller diameter capillaries are used. On the other hand, when larger molecules are used (lower D), the added pressure will cause a more significant plate height increase [8].

Fig. 8 illustrates the data from a similar experiment using the pH 2.7 buffer. The ascending data points (open circles) are from Fig. 4 and show the trend when there is no pressure applied. The main data points (△) show the effect of changing pressure using a constant axial field. As is clear, additional pressure in the direction of the bulk flow improves the plate height over that obtained for the same velocity without the use of pressure. In fact, the minimum of the curve of data points obtained with the same

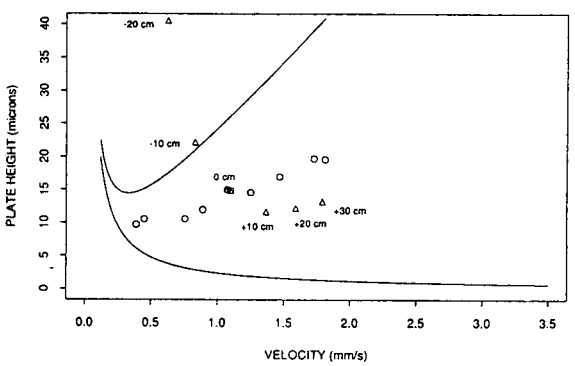

Fig. 8. Phosphate buffer pH 2.7 with applied pressure. ○ show the trend of data with no applied pressure, radial and axial field varied. △ are points where pressure is varied from −20 cmH_2O to +30 cmH_2O (−2 kPa to +3 kPa) while the axial field remains constant at 500 V/cm. Conditions: conductive sheath.

voltage settings occurs when pressure is added.

These results seem to indicate that at pH 2.7 there is some type of disturbance of the velocity profile that is not quite normal Poiseuille flow and acts against the bulk flow. Transient effects of the sudden voltage initiation have been ruled out as a cause.

CONCLUSIONS

Plate height *versus* velocity curves have been used to examine the performance of different external flow control methods. It has been found that radial field EOF control methods do not change the plate heights relative to the conventional no-sheath configuration. In all cases, pH 7 buffers follow the diffusion limit theory. When pressure is added, pH 7 buffers continue to follow the theory containing the additional pressure driven flow term. The theory and data also predict that pressure may be useful to adjust the bulk flow velocity with a small increase in plate height.

A pH 2.7 the EOF methods do not change the plate height, but all configurations produce data fitting between the diffusion limit and the pure pressure driven limit. We do not have an expression to predict this pH dependency. However, the plate height can be improved by adding pressure in the direction of bulk flow, thus the implication that at pH 2.7 there is a back flow.

ACKNOWLEDGMENT

The authors wish to acknowledge and thank Jim Young for his contribution to this work.

REFERENCES

1 J.W. Jorgenson and K.D. Lukacs, *Anal. Chem.*, 53 (1981) 1298.
2 F.E.P. Mikkers, F.M. Everaerts and Th.P.E.M. Verheggen, *J. Chromatogr.*, 169 (1979) 11.
3 C.S. Lee, W.C. Blanchard and C.-T. Wu, *Anal. Chem.*, 62 (1990) 1550.
4 C.S. Lee, D. McManigill, C.-T. Wu and B. Patel, *Anal. Chem.*, 63 (1991) 1519.
5 K. Ghowsi and R.J. Gale, in R.P. Buck (Editor), *Proceedings of the International Symposium on Biosensor Technology 1989*, Marcel Dekker, New York, 1990, pp. 55–62.

6 C.L. Rice and R. Whitehead, *J. Phys. Chem.*, 69 (1965) 4017.
7 R. Datta and V.R. Kotamarthi, *AIChE J.*, 36 (1990) 916.
8 E. Grushka, *J. Chromatogr.*, 559 (1991) 81.
9 R.R. Holloway, C.A. Keely, J.A. Lux, D. McManigill and J.E. Young, presented at the *4th International Symposium on High Performance Capillary Electrophoresis, Amsterdam, February 9–13, 1992*, poster PT-27.
10 F.M. Everaerts, T.P.E.M. Verheggen and J.L.M. van de Venne, *J. Chromatogr.*, 123 (1976) 139.
11 R.-L. Chien and J.C. Helmer, *Anal. Chem.*, 63 (1991) 1354.
12 J.K. Towns and F.E. Regnier, *Anal. Chem.*, 64 (1992) 2473.
13 M.A. Hayes and A.G. Ewing, *Anal. Chem.*, 64 (1992) 512.
14 P.C. Hiemenz, *Principles of Colloid and Surface Chemistry*, Marcel Dekker, New York, 2nd ed., 1986.
15 R.J. Hunter, *Zeta Potential in Colloid Science*, Academic Press, London, 1981.
16 J.C. Giddings, *Unified Separation Science*, Wiley, New York, 1991.

Journal of Chromatography A, 652 (1993) 291–294
Elsevier Science Publishers B.V., Amsterdam

CHROM. 25 134

On-line measurement of electroosmosis in capillary electrophoresis using a conductivity cell

Bart J. Wanders*, Tom A.A.M. van de Goor☆ and Frans M. Everaerts

Eindhoven University of Technology, Laboratory of Instrumental Analysis, P.O. Box 513, 5600 MB Eindhoven (Netherlands)

ABSTRACT

A common phenomenon in capillary electrophoresis is electroendosmotic flow (EOF). Although often useful, EOF fluctuations introduce extra variances in the overall reproducibility of the analysis. In order to correct for these fluctuations, an on-line EOF monitoring method is required. The method presented utilizes a conductivity cell as the ground electrolyte reservoir, filled with dilute running buffer. During the separation the EOF will cause a continuous flow of non-diluted buffer into this reservoir. From the resulting continuously rising conductivity signal, the EOF can be calculated and used for, *e.g.*, migration time and peak area corrections.

INTRODUCTION

Capillary electrophoresis (CE) is a separation method in which species are separated in a fused-silica capillary tube based on the different velocities obtained in an electric field [1]. A phenomenon often occurring in these capillaries is electroosmotic flow (EOF). This is a buffer flow which originates when an electric field is applied over a capillary having a charged inner surface. Under most separation conditions in CE this is the case, although the extent can vary considerably. Often the silica surface is negatively charged, compensated for by a diffuse positive charge in the electrolyte. This charge separation is called the electric double layer. When an electric field is applied the negative surface charge is immobile, while the positive ions in solution are able to move in the field. These ions drag solvent along, resulting in a flow of the liquid directed towards the cathode [2].

Owing to the EOF it is possible to determine both anions and cations in a single experiment using electrophoresis. The conditions, however, should be such that the mobility of the EOF is higher than that of any of the anions. Tuning of the flow can be important in optimizing the separation conditions because optimum resolution is achieved when the mobility of electrophoresis and electroosmosis are equal but of opposite sign [1].

The EOF can be influenced by many parameters. Adsorption of compounds on the capillary wall or pH changes can cause shifts from run to run. To compensate, a marker molecule (often a neutral compound) is co-migrated in the analysis so that the magnitude of the flow can be established [3–5].

Several methods have been developed to measure the EOF under various electrolyte conditions. Reijenga *et al.* [6] measured the EOF in PTFE tubing using the streaming potential method. This method was later automated and ap-

* Corresponding author. Present address: Beckman Instruments, 2500 Harbor Boulevard, Fullerton, CA 92634, USA.
☆ Present address: Hewlett Packard Laboratories, 3500 Deer Creek Road, Palo Alto, CA 94304, USA.

0021-9673/93/$06.00

plied to fused silica by Van de Goor *et al.* [7]. Altria and Simpson [8] used a balance to measure the EOF by mass. Huang *et al.* [9] used the current monitoring method to obtain information on the EOF by replacing the buffer in the capillary tube. Wanders *et al.* [10] proposed the addition of a UV-absorbing compound to obtain EOF information. Both the weighing and the UV addition methods could be used in an on-line set-up [7,10].

The aim of measuring the EOF is always to determine whether the desired flow has been achieved. Several ways to change the flow can be used, such as capillary coating, the use of a surfactant [11], viscosity changes in the buffer [12] or the addition of a radial external field [13–15] to influence the zeta potential on the inner surface and hence the EOF.

The direct coupling of an EOF flow detector to an EOF flow modification method would be the ultimate goal [16]. Here, we investigated the use of a conductivity cell to measure accurately the electroosmotic flow without extensive modification to the separation set-up, based on osmotic flow.

EXPERIMENTAL

The conductivity cell used was laboratory made in the following way. A hole of 1 cm was drilled in a cylindrical Perspex rod. In the centre of this hole a stainless steel rod of 5 mm diameter was positioned. Two platinum wires were wrapped tightly around this rod and the ends were passed through a hole in the side, shown in Fig. 1. The empty space was filled with Insulcast 510 (Permagil Industries, Plainview, NY, USA) and subsequently polymerized. After hardening, the stainless steel rod was removed, leaving a cylindrical space with platinum wires mounted in the wall. This conductivity cell was mounted on a stirring mechanism, consisting of either a small magnetic stirrer or an air-driven rotor.

The electrodes were connected to a digital conductivity meter (CDM 83; Radiometer, Copenhagen, Denmark) isolated electrically by a d.c. shield (Philips DC250V, No. 2222-344-41225

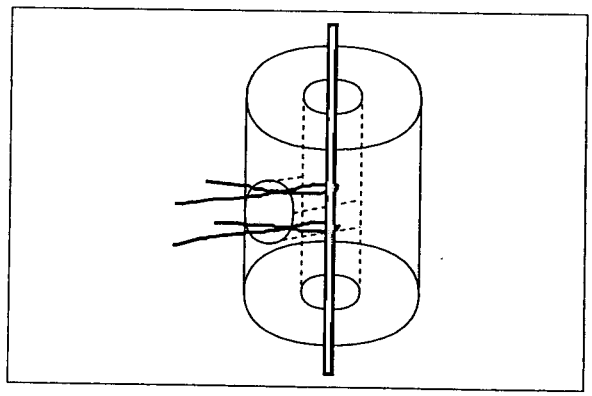

Fig. 1. Schematic diagram of the construction of the flow cell.

MKT metallized film capacitor). The set-up is shown in Fig. 2; a magnetic stirrer is used. The conductivity cell was also used as the ground electrolyte reservoir in the electrophoresis scheme. At the beginning of the experiment the capillary (Siemens, 50 cm total length × 75 μm I.D.) and the inlet/high-voltage reservoir were filled with running buffer (*e.g.*, 100 m*M* boric acid at pH 8.3). In the ground reservoir/conductivity cell a dilute buffer/deionized water is used. Then the high voltage is applied and EOF starts to occur, transporting buffer to the ground reservoir. Owing to this

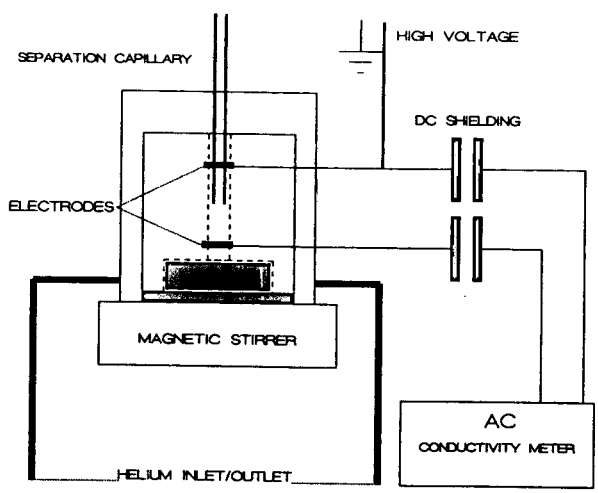

Fig. 2. Set-up of the conductivity cell and the measurement system.

flow the conductivity in the cell increases and the signal is measured.

RESULTS AND DISCUSSION

Fig. 3 shows the result from the conductivity measurements as a function of time. Line I shows the increase in conductivity when a gravity flow of buffer is used. To induce this flow the injection end of the capillary was lifted with respect to the ground end. Using the microbalance method [7], this flow was measured to correspond to 6 nl/s. This value was further used to calibrate the conductivity measurements.

Line II indicates the increase in conductivity due to the electroosmotic flow using different potential differences over the capillary. At 0 kV a constant value was measured as no buffer was transported. Then about every 60 s, the power supply setting was increased by 5 kV and the conductivity in the cell monitored. At 10 kV an increase in signal was observed having a slope comparable to the gravity flow. At higher voltages an even steeper curve was found. Using the calibration value, the EOF for these different situations can be calculated. The values are given in Table I.

A clear increase in EOF is observed when the applied voltage is increased, according to the theory. It shows that about every 20 s sufficient data are collected to calculate accurately the EOF. The linearity is fairly poor, however, especially for the higher voltages. This may be due to the fact that a non-thermostatted system is used, so a temperature increase can lead to an increased EOF.

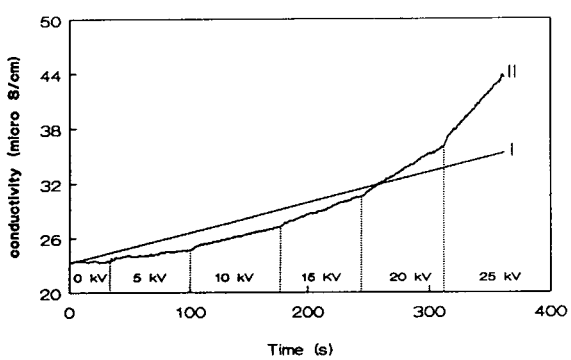

Fig. 3. Measured increase in conductivity in the cell as a function of time. Line I is for gravity flow (6 nl/s = 1 mm/s) and line II is for electroosmotic flow generated using different voltages across the capillary tube as indicated.

TABLE I

MEASURED CHANGE IN CONDUCTIVITY PER SECOND AND CALCULATED ELECTROOSMOTIC FLOW PER SECOND AS A FUNCTION OF APPLIED VOLTAGE

Voltage (kV)	Conductivity (μS/s)	EOF (nl/s)
0	0	0
5	0.019	3.4
10	0.034	6.1
15	0.049	8.8
20	0.082	14.7
25	0.161	23.2

Another problem which can occur is the influence of the electrode reactions on the increase in the conductivity in the cell. As electrode reactions must occur to allow current to flow, this can contribute to the conductivity in the cell. Even a change in pH is observed in the buffer reservoirs during longer runs. In a long run, at a high electric current this was found to disturb the accuracy of the method.

An advantage of the system, however, is that continuous information about the EOF is obtained and that the original situation can easily be restored by rinsing the ground reservoir. The set-up can easily be implemented in existing CE instrumentation without major modifications. The accuracy of the method is comparable to that of previously described methods.

ACKNOWLEDGEMENT

Part of this research was supported by a grant from the Dutch Foundation for Scientific Research.

REFERENCES

1 J.W. Jorgenson and K.D. Lukacs, *Anal. Chem.*, 53 (1981) 1298.
2 R.J. Hunter, *Zeta Potential in Colloid Science*, Academic Press, London, 1981.
3 T.S. Stevens and H.J. Cortes, *Anal. Chem.*, 55 (1983) 1365.
4 K.D. Lukacs and J.W. Jorgenson, *J. High Resolut. Chromatogr. Chromatogr. Commun.*, 8 (1985) 407.
5 H.H. Lauer and D. McManigill, *Anal. Chem.*, 58 (1986) 166.
6 J.C. Reijenga, G.V.A. Aben, Th.P.E.M. Verheggen and F.M. Everaerts, *J. Chromatogr.*, 260 (1983) 241.
7 A.A.A.M. van de Goor, B.J. Wanders and F.M. Everaerts, *J. Chromatogr.*, 470 (1989) 95.
8 K.D. Altria and C.F. Simpson, *Anal. Proc.*, 23 (1986) 453.
9 X. Huang, M.J. Gordon and R.N. Zare, *Anal. Chem.*, 60 (1988) 1837.
10 B.J. Wanders, A.A.A.M. van de Goor and F.M. Everaerts, *J. Chromatogr.*, 470 (1989) 89.
11 T. Tsuda, *J. Liq. Chromatogr.*, 12 (1989) 2501.
12 C. Schwer and E. Kenndler, *Anal. Chem.*, 63 (1991) 1801.
13 C.S. Lee, W.C. Blanchard and C.T. Wu, *Anal. Chem.*, 62 (1990) 1550.
14 C.S. Lee, D. McManigill, C.T. Wu and B. Patel, *Anal. Chem.*, 63 (1991) 1519.
15 M.A. Hayes and A.G. Ewing, *Anal. Chem.*, 64 (1992) 512.
16 B.J. Wanders, A.A.A.M. van de Goor, F.M. Everaerts and C.A.M. Cramers, *Neth. Pat. Appl.*, nr. NL88-2273 (1990).

Journal of Chromatography A, 652 (1993) 295–299
Elsevier Science Publishers B.V., Amsterdam

CHROM. 25 099

In vitro observation of interactions of iron and transferrin by capillary isoelectric focusing with a concentration gradient imaging detection system

Jiaqi Wu and Janusz Pawliszyn*

Department of Chemistry, University of Waterloo, Waterloo, Ontario N2L 3G1 (Canada)

ABSTRACT

A capillary isoelectric focusing–concentration gradient imaging detector system was used for *in vitro* observation of dynamics of interaction between iron and bovine transferrin. Transferrin was first focused inside the capillary by isoelectric focusing. A plug of ferric ion was then introduced into the capillary. The iron-free and the iron-complexed transferrins have different isoelectric points, hence they were focused at different positions inside the capillary. Concentration changes of different isoforms of iron-free and iron-complexed transferrins were monitored in an on-line fashion during the interaction by the imaging detector. One advantage of using this detector for studying the protein interaction is that the 633 nm wavelength probe beam used in the detector does not pump energy into the reaction system, which will interfere with the reaction. The results show that iron-binding and dissociation rates of different isoforms are different. This is the first report that the reaction speed of different isoforms of a protein can be observed in an on-line fashion.

INTRODUCTION

Capillary electrophoresis (CE) has become an important separation method in analytical chemistry and biochemistry. Separation and detection of different components in small amounts of sample (pl–nl in volume) can be achieved in a few minutes [1]. Because of its high separation efficiency and speed, CE is also a promising tool for the study of interactions between biologically active molecules, such as in the characterization of enzyme–antibody conjugates [2], the separation of antibody–antigen complexes [3], and the study of protein–drug binding [4]. In these works, studies of the interactions of those molecules under different concentration ratios were achieved by capillary zone electrophoresis (CZE) which separated the conjugates and the complexes from unreacted molecules based on their differences in electrophoretic mobility [2–4]. In this way, binding parameters between molecules could be determined. However, until now there is no method in which one can observe the dynamics of the interactions between the different isoforms of different molecules in an on-line fashion.

In order to observe the interaction dynamics, two conditions are required. First, a special "container" is needed, in which the interaction takes place. In the "container", different isoforms of a protein, and the reacted and unreacted species can be distinguished. An on-line detector is also necessary to monitor the concentration changes of all species. Capillary isoelectric focusing (cIEF) [5] is a suitable "container" for this purpose. In cIEF, all proteins inside the capillary are focused at the positions where their isoelectric points (pI) are equivalent to the pH. It is a static situation. It has a resolution of 0.02 pH units [5]. It is a powerful method for resolving different isoforms of protein samples. Also,

* Corresponding author.

0021-9673/93/$06.00

if the reacted species and unreacted species have different p*I* values, they will be focused at different positions inside the capillary. However, in order to observe changes of concentrations of all these species inside the capillary during the interaction process, protein zones need to be detected by an on-line imaging detector. All present commercial CE detectors are not suitable for the purpose.

In our laboratory, a concentration gradient imaging detector based on Schlieren optics [6] and a UV–Vis absorption imaging detector [7] were developed for cIEF detection. For observation of dynamics of protein reaction, concentration gradient imaging detection had advantages over other optical and spectroscopic detectors. A low-power, long-wavelength He–Ne laser (633 nm) was employed in the detector. This eliminated the possibility of pumping energy into the reaction system, which might disturb the reaction. Thus, the cIEF–concentration gradient imaging detector system [6] is an ideal instrument for the observation of the dynamics of interaction between biological molecules. In this report, the feasibility of using the cIEF–concentration gradient imaging detector system for observing the dynamics of interaction between biological molecules will be shown by observing the interactions between bovine transferrin and iron.

EXPERIMENTAL

Instrumental

The cIEF–concentration gradient imaging detector system used has been described in detail in our previous paper [6]. It consists of a capillary cartridge holding a 100 μm I.D., 4 cm long square glass capillary (Dynamics, Rockaway, NJ, USA), a low-power He–Ne laser (Model 1103P, Uniphase, Manteca, CA, USA), and a 1024 pixel CCD sensor (S3903-1024Q, Hamamatsu, Hamamatsu City, Japan). The capillary inner wall was coated with non-cross-linked acrylamide to eliminate electroosmosis by the reported method [5].

Reagents

All solutions used in the experiment were prepared using deionized water. All chemicals were reagents grade. Solutions of 10 m*M* H_3PO_4 and 20 m*M* NaOH were used as anolyte and catholyte, respectively. Proteins were purchased from Sigma, St. Louis, MO, USA. Iron-free and iron-saturated bovine transferrin were used in the experiment. Protein samples were mixed with the carrier ampholytes (Pharmalyte pH 5–8, Sigma) solution to a final concentration of 2% ampholytes. Protein concentrations were 0.5 mg/ml. Iron(III) solution of $5 \cdot 10^{-4}$ *M* was prepared in 10 m*M* H_3PO_4.

Procedures

The protein solution was introduced into the capillary by pressure. Two buffer reservoirs at the two ends of the capillary were filled with anolyte and catholyte, respectively. Then a 3.5 kV dc voltage was applied to the two ends of the capillary. The current which passed through the capillary was monitored to follow the focusing process and interaction dynamics between iron and transferrin. The current dropped from about 30 to 3 μA in two min before stabilizing. After 2 min of focusing, the anolyte in the reservoir at the anodic end of the capillary was replaced by the iron solution for 20 s, and the reservoir was filled again with the anolyte. In this way, a plug of iron solution was introduced into the capillary. Protein zones inside the capillary were monitored on-line by the concentration gradient imaging detector. All experiments were done in duplicate or triplicate to ensure reproducibility.

RESULTS AND DISCUSSION

In the experiment, carrier ampholytes having pH values ranging from 5 to 8 were used, giving good resolution for isoforms of transferrin. After application of the dc voltage, a pH gradient from pH 5 to pH 8 was established along the capillary, and proteins having p*I* values in this range were focused inside the capillary. Proteins are focused where the pH equals their p*I* values. All these protein zones inside the capillary can be detected by the concentration gradient imaging detector. The signal profile of the detected image is proportional to the second derivative of the protein sample concentration [6].

First, iron-free and iron-saturated transferrin

were separated by the cIEF instrument. As shown in Fig. 1a and c, at least four isoforms can be distinguished for the iron-free transferrin by this method. The isoforms are located in the pH range of 5.30–5.60. Each isoform may bind iron at several binding sites [8], so there can be many iron-complexed isoforms. The focused pattern

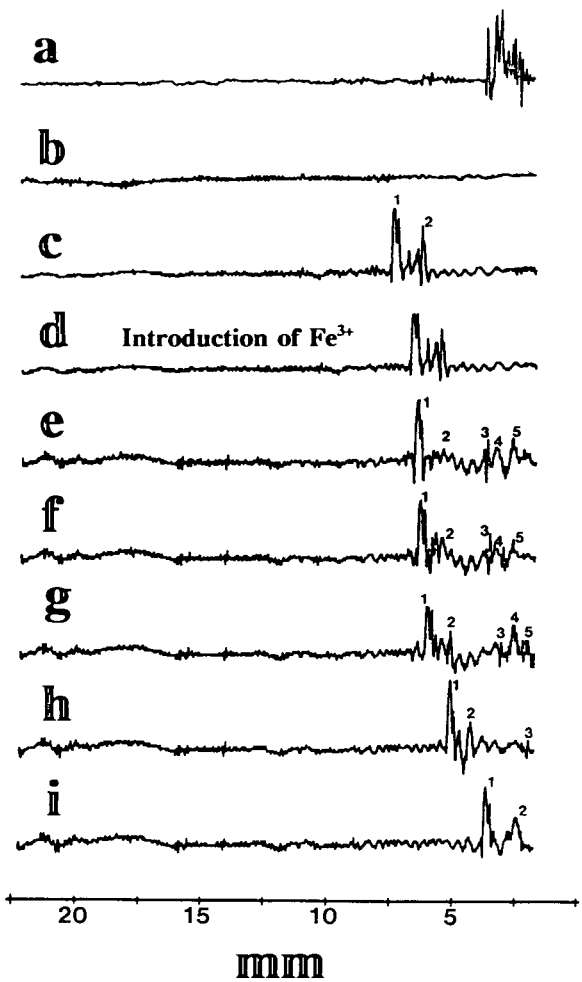

Fig. 1. (a) Focused pattern of iron-saturated bovine transferrin after 2 min focusing. Bovine transferrin of 0.5 mg/ml concentration are focused by the cIEF instrument, and the focused patterns were detected by the imaging detector (b, c). After 2 min focusing, a plug of ferric ion was introduced into the capillary, and the changes in the focused pattern were monitored (d–i). (b) Image of iron-free bovine transferrin after 3 s of focusing, and (c) after 2 min of focusing. (d) Focused pattern of iron-free transferrin 20 s after the introduction of the ferric ion plug, (e) 0.5 min, (f) 2 min, (g) 4 min, (h) 8 min, and (i) 12 min. Peaks 1 and 2 are iron-free forms of transferrin, peaks 3–5 correspond to iron–transferrin complexes.

for iron-saturated transferrin is rather complicated as shown in Fig. 1a. The iron-transferrin complexes have different p*I* values from those of iron-free transferrin [8]. As shown in Fig. 1a, they distribute in the pH range of 5.15–5.30.

The focused pattern of the proteins became stable after 2 min. If ferric ions are introduced into the capillary at this point, they should be bounded by the transferrin, and the position of each isoform of the protein inside the capillary should change upon binding [8]. This position change could be observed on-line by the imaging detector. Thus, the dynamics of the interaction between iron and transferrin could be monitored. The iron–transferrin complexes were formed with the participation of anions [9]. Furthermore, the existence of the carrier ampholytes facilities their formation [8]. In our experiment, the H_3PO_4 solution of ferric ion effectively prevented the ion from precipitating at high pH conditions due to $Fe(HPO_4)^+$ formation.

There is a problem with the introduction of the ferric solutions into the capillary. Introducing ions other than H^+ to the anodic end of the capillary will destroy the pH gradient along the capillary, and cause the focused proteins to mobilize toward this end of the capillary [5]. If the concentration of the ferric ion is too high, all focused proteins will be mobilized out of the capillary in a short time, which makes it difficult to observe the interaction between ferric ion and the protein. If the concentration is too low, the concentrations of iron–transferrin complexes will be too small to be detected by the detection system. These difficulties can be solved by introducing a ion plug into the capillary. We found in experiments that when a K^+ plug ($2 \cdot 10^{-3} M$) was introduced into the anodic end of the capillary after all proteins were focused, mobilization caused by the plug was slow. All focused zones could stay in the 4-cm long capillary for more than 10 min. Mobilization of the pH gradient caused by a low concentration Fe^{3+} plug is also slow. The mobilization speed can be monitored by measuring the current passing through the capillary. As illustrated in Fig. 2, after application of the dc voltage, the current stabilized in about 2 min. This shows that a stable pH gradient is established in the capillary. When a

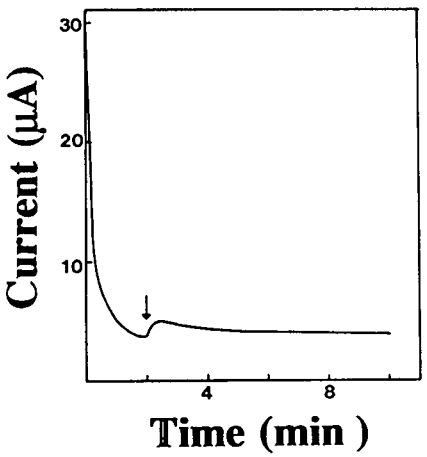

Fig. 2. The current passing through the capillary during the focusing process of the protein and the interaction between iron and transferrin. The time the ferric ion plug is added was marked by the arrow.

plug of $5 \cdot 10^{-4}$ *M* ferric ion was introduced, there was an increase in current passing through the capillary. However, because of the short length of the plug, the plug moves through the capillary. The current almost becomes stable in 1 min, and just increases very slowly, which means that after 1 min the mobilization of the pH gradient inside the capillary is slow.

Peaks in Fig. 1c represent different isoforms of iron-free transferrin, and each isoform may exist in iron-free and iron-complexed molecular forms. In addition, because each isoform has several iron binding sites, every iron-free isoform can create several different iron-complexed isoforms. The major advantage of using the cIEF-imaging detector system to observe the interaction between iron and transferrin is that the association and dissociation rates of different isoforms can be monitored in an on-line fashion. The association constants for different iron-complexed isoforms can be estimated since the peak height in the detected image is approximately proportional to the concentration of the protein.

Fig. 1c shows two main peaks (peaks 1 and 2) for iron-free transferrin. Immediately after the introduction of the ferric ion plug, as shown in Fig. 1d, all focused zones are mobilized quickly toward the anodic end of the capillary by the ferric ion. This corresponds to the current increase in Fig. 2 marked by the arrow. However, the focused pattern of the iron-free transferrin does not change. The quick mobilization only lasts for about 1 min. After 1 min, the mobilization is very slow in 10 min as shown in Fig. 1e–i, which allows observation of the interaction between ferric ion and transferrin.

The focused pattern begins to change 1 min after the introduction of ferric ion due to the interaction between the ion and the protein (Fig. 1e). After the addition of ferric ion, peak 2 quickly disappears. However, several new peaks (peaks 3–5) appear in the positions of iron–transferrin complexes as shown in Fig. 1a. Peak 1, which corresponds to an isoform of iron-free transferrin, also becomes lower slowly as shown by Fig. 1e–g. These results show that peaks 3, 4, and 5, which are iron–transferrin complexes are mainly formed from peak 2. Under these conditions, after the ferric ion zone passes through the capillary, peaks 3–5 become lower as shown in Fig. 1f–h. This is because under these conditions any ferric ions dissociated from the complexes are immediately rejected from the capillary by the applied high dc voltage applied at the two ends of the capillary, the dissociated transferrin returns to its original position. This is observed in Fig. 1f–i, where peaks 1 and 2 slowly become higher again. Another interesting phenomenon is the formation and dissociation speed of peaks 3–5. The formation speed of peak 3 is the fastest; however, it also disappears in the fastest rate (Fig. 1e–h). The formation and dissociation speeds of peaks 4 and 5 are both slower than that of peak 3. After 12 minutes, most of iron–transferrin complexes are dissociated, and the peak shapes of the iron-free transferrin are almost restored to their original forms (Fig. 1c and i). By this instrument, much information can be obtained for the interaction between iron and transferrin during the short time interaction. This achievement is impossible for a conventional cIEF instrument with a single point on-column detector using mobilization processes [5].

The above results show that the cIEF–concentration gradient imaging detector system is a powerful tool for the study of the interactions between biochemical molecules. Future work will concentrate on the study of interactions between monoclonal antibodies and antigens,

and the evaluation of the association constants of their conjugates.

REFERENCES

1 J.W. Jorgenson, *Anal. Chem.*, 58 (1986) 743A.
2 S.J. Harrington, R. Varro and T.M. Li, *J. Chromatogr.*, 559 (1991) 385.
3 R.G. Nielsen, E.C. Rickard, P.F. Santa, D.A. Sharknas and G.S. Sittampalam, *J. Chromatogr.*, 539 (1991) 177.
4 J.C. Kraak, S. Busch and H. Poppe, *J. Chromatogr.*, 608 (1992) 257.
5 T. Wehr, M. Zhu, R. Rodriguez, D. Burke and K. Duncan, *Am. Biotechnol. Lab.*, 8 (1990) 22.
6 J. Wu and J. Pawliszyn, *Anal. Chem.*, 64 (1992) 2934.
7 J. Wu and J. Pawliszyn, *J. Liq. Chromatogr.*, 16 (1993) in press.
8 F. Kilar and S. Hjerten, *Electrophoresis*, 10 (1989) 23.
9 J.W. Young and D.J. Perkins, *European J. Biochem.*, 4 (1968) 285.

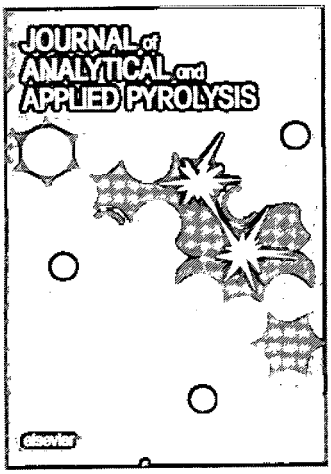

JOURNAL OF ANALYTICAL AND APPLIED PYROLYSIS

Audience

Analytical Chemists; Researchers involved in Chromatography, Mass Spectrometry, and Polymer Science; Geochemists, Technologists in Plastic and Rubber Industries; Bacteriologists; Food and Medical Chemists.

AIMS AND SCOPE

The international *Journal of Analytical and Applied Pyrolysis* is devoted to the publication of qualitative and quantitative results relating to: Controlled thermal degradation and pyrolysis of technical and biological macromolecules; environmental, geochemical, biological and medical applications of analytical pyrolysis; basic studies in high temperature chemistry, reaction kinetics and pyrolysis mechanisms; pyrolysis investigations of energy related problems, fingerprinting of fossil and synthetic fuels, coal extraction and liquefaction products.

ABSTRACTED/INDEXED IN: Analytical Abstracts, Biological Abstracts, Chemical & Earth Sciences, Chemical Abstracts, Current Contents/Physical, Mass Spectrometry Bulletin, Science Citation Index.

SUBSCRIPTION INFORMATION

1993: Volumes 24-26 in 9 issues

Dfl. 1098.00 / US $ 627.50 (including postage)

ISSN 0165-2370

CHROM

I would like ☐ a free sample copy of Journal of Analytical and Applied Pyrolysis.

☐ Instructions to Authors.

☐ to enter a subscription for 1993. Please send me a Proforma Invoice.

Name _____

Address _____

_____

_____

The Dutch Guilder price (Dfl.) is definitive. US$ prices are for your convenience only and are subject to exchange fluctuations. Customers in the European Community should add the appropriate VAT rate applicable in their country to the price(s).

Elsevier Science Publishers
Attn. Carla G.C. Stokman
P.O. Box 330, 1000 AH Amsterdam
The Netherlands
Fax: (+31-20) 5862 845

In the USA & Canada
Attn. Judy Weislogel
P.O. Box 945, Madison Square Station
New York, NY 10160-0757, USA
Fax: (212) 633 3880

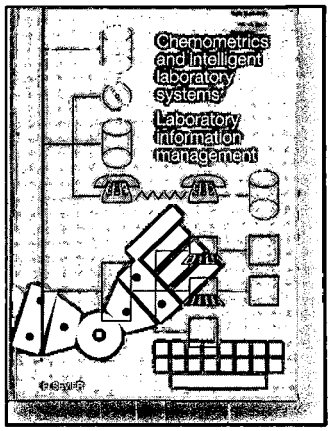

Audience

Chemists, pharmacists, computer scientists and managers working in academic, clinical, industrial and government laboratories.

Elsevier Science Publishers
Attn. Carla G.C. Stokman
P.O. Box 330, 1000 AH Amsterdam
The Netherlands
Fax: (+31-20) 5862 845
In the USA & Canada
Attn. Judy Weislogel
P.O. Box 945, Madison Square Station
New York, NY 10160-0757, USA
Fax: (212) 633 3880

LABORATORY INFORMATION MANAGEMENT

Section of CHEMOMETRICS AND INTELLIGENT LABORATORY SYSTEMS

AIMS AND SCOPE

The journal covers all aspects of information management in a laboratory environment, such as information technology, storage, processing and flow of data. The following topics are covered:

- **Laboratory Information Management Systems (LIMS):** Systems architecture, database design, novel aspects of interfacing, methods of data acquisition and integration with other computer applications and instruments.
- **Means of integrating and merging laboratory information:** Document preparation using chemical structures, spectra, results and text; corporate communication.
- **Networks:** Novel technology for the dissemination, storage and retrieval of information.
- **Regulatory Aspects:** Development and implementation of governmental guidelines and regulations and industry standards, and their effect on information management.
- **Electronic Laboratory Notebooks.**
- **Human aspects of laboratory automation:** The application of chemometrics and expert systems to handle laboratory information is within the scope of the journal. The application of robotics or dedicated automation systems is of interest where these systems form part of an integrated solution for information management. The journal aims to cover micro-, mini-, and mainframe applications and systems, both those designed in-house or available commercially.

The journal publishes five types of papers: **Original research papers, Tutorial articles, Case studies, State-of-the-art review articles, and Short communications. A Monitor Section** provides news on meetings, book and software reviews, a calendar of forthcoming events, etc.

ABSTRACTED/INDEXED IN: ASCA, Analytical Abstracts, BioSciences Information Service, Cambridge Scientific Abstracts, Chromatography Abstracts, Current Contents, Current Index to Statistics, Excerpta Medica, INSPEC, SCISEARCH.

1993: SUBSCRIPTION INFORMATION
Volume 21 in 3 issues
Dfl. 448.00 / US $ 256.00 (including postage) ISSN 0925-5281 CHROM

I would like ☐ a free sample copy of Laboratory Information Management.
☐ Instructions to Authors.
☐ to enter a subscription for 1993. Please send me a Proforma Invoice.

Name _____

Address _____

_____

_____

The Dutch Guilder price (Dfl.) is definitive. US$ prices are for your convenience only and are subject to exchange fluctuations. Customers in the European Community should add the appropriate VAT rate applicable in their country to the price(s).

PUBLICATION SCHEDULE FOR THE 1994 SUBSCRIPTION

Journal of Chromatography A and *Journal of Chromatography B: Biomedical Applications*

MONTH	O 1993	N 1993	D 1993	
Journal of Chromatography A	652/1 652/2 653/1	653/2 654/1 654/2 655/1	655/2 656/1 + 2 657/1 657/2	The publication schedule for further issues will be published later
Bibliography Section				
Journal of Chromatography B: Biomedical Applications				

INFORMATION FOR AUTHORS

(Detailed *Instructions to Authors* were published in Vol. 609, pp. 437–443. A free reprint can be obtained by application to the publisher, Elsevier Science Publishers B.V., P.O. Box 330, 1000 AH Amsterdam, Netherlands.)

Types of Contributions. The following types of papers are published: Regular research papers (Full-length papers), Review articles, Short Communications and Discussions. Short Communications are usually descriptions of short investigations, or they can report minor technical improvements of previously published procedures; they reflect the same quality of research as Full-length papers, but should preferably not exceed five printed pages. Discussions (one or two pages) should explain, amplify, correct or otherwise comment substantively upon an article recently published in the journal. For Review articles, see inside front cover under Submission of Papers.

Submission. Every paper must be accompanied by a letter from the senior author, stating that he/she is submitting the paper for publication in the *Journal of Chromatography A* or *B*.

Manuscripts. Manuscripts should be typed in **double spacing** on consecutively numbered pages of uniform size. The manuscript should be preceded by a sheet of manuscript paper carrying the title of the paper and the name and full postal address of the person to whom the proofs are to be sent. As a rule, papers should be divided into sections, headed by a caption (*e.g.*, Abstract, Introduction, Experimental, Results, Discussion, etc.) All illustrations, photographs, tables, etc., should be on separate sheets.

Abstract. All articles should have an abstract of 50–100 words which clearly and briefly indicates what is new, different and significant. No references should be given.

Introduction. Every paper must have a concise introduction mentioning what has been done before on the topic described, and stating clearly what is new in the paper now submitted.

Experimental conditions should preferably be given on a *separate* sheet, headed "Conditions". These conditions will, if appropriate, be printed in a block, directly following the heading "Experimental".

Illustrations. The figures should be submitted in a form suitable for reproduction, drawn in Indian ink on drawing or tracing paper. Each illustration should have a legend, all the *legends* being typed (with double spacing) together on a *separate sheet.* If structures are given in the text, the original drawings should be supplied. Coloured illustrations are reproduced at the author's expense, the cost being determined by the number of pages and by the number of colours needed. The written permission of the author and publisher must be obtained for the use of any figure already published. Its source must be indicated in the legend.

References. References should be numbered in the order in which they are cited in the text, and listed in numerical sequence on a separate sheet at the end of the article. Please check a recent issue for the layout of the reference list. Abbreviations for the titles of journals should follow the system used by *Chemical Abstracts*. Articles not yet published should be given as "in press" (journal should be specified), "submitted for publication" (journal should be specified), "in preparation" or "personal communication".

Vols. 1–651 of the *Journal of Chromatography*; *Journal of Chromatography, Biomedical Applications* and *Journal of Chromatography, Symposium Volumes* should be cited as *J. Chromatogr.* From Vol. 652 on, *Journal of Chromatography A* (incl. Symposium Volumes) should be cited as *J. Chromatogr. A* and *Journal of Chromatography B: Biomedical Applications* as *J. Chromatogr. B.*

Dispatch. Before sending the manuscript to the Editor please check that the envelope contains four copies of the paper complete with references, legends and figures. One of the sets of figures must be the originals suitable for direct reproduction. Please also ensure that permission to publish has been obtained from your institute.

Proofs. One set of proofs will be sent to the author to be carefully checked for printer's errors. Corrections must be restricted to instances in which the proof is at variance with the manuscript. "Extra corrections" will be inserted at the author's expense.

Reprints. Fifty reprints will be supplied free of charge. Additional reprints can be ordered by the authors. An order form containing price quotations will be sent to the authors together with the proofs of their article.

Ovomucoid Bonded Column for Direct Chiral Separation

ULTRON ES-OVM

Narrow-Bore Column (2.0 I.D. x 150 mm) for Trace Analyses
Analytical Column (4.6 I.D., 6.0 I.D. x 150 mm) for Regular Analyses
Semi-Preparative Column (20.0 I.D. x 250 mm) for Preparative Separation

Analysis of Trace FLURBIPROFEN in Metabolite with NARROW-BORE COLUMN

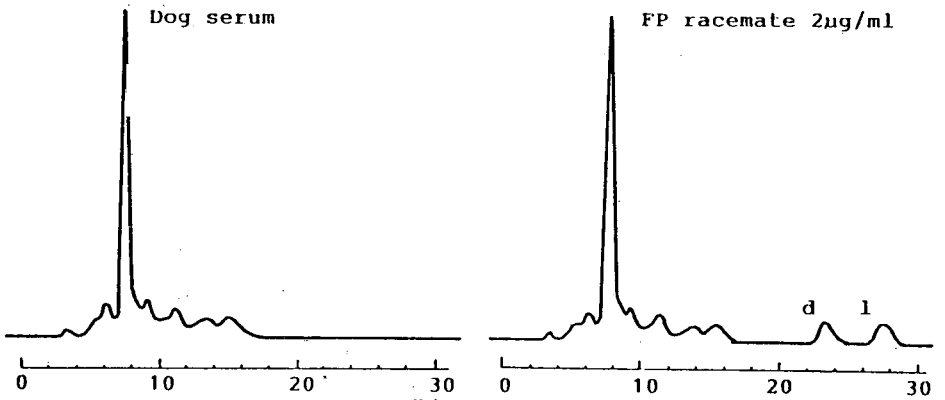

Conditions

Column: ULTRON ES-OVM(2.0I.D. x 150mm)
Mobile Phase: 20mMPhosphate Buffer(pH=3.0)/CH3CN =100/15
Flow Rate: 0.1ml/min
Temperature: 25°C
Injection: 5µl
Detection: UV- 247nm(0.05AUFS)

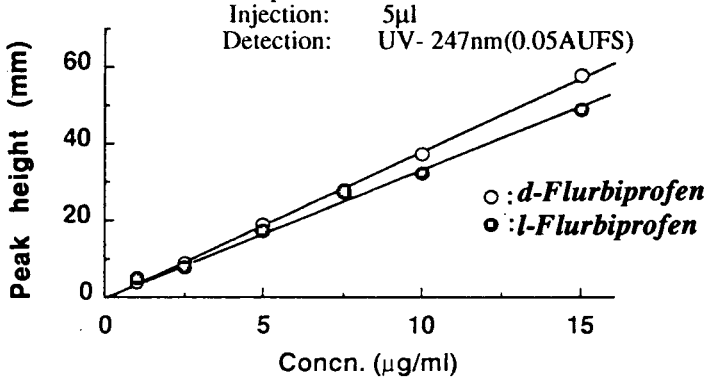

Calibration Curve for Each Enantiomer of Flurbiprofen

SHINWA CHEMICAL INDUSTRIES, LTD.

50 Kagekatsu-cho, Fushimi-ku, Kyoto 612, JAPAN
Phone:+81-75-621-2360 Fax:+81-75-602-2660

In the United States and Europe, please contact:

Rockland Technologies, Inc.

538 First State Boulevard, Newport, DE 19804, U.S.A.
Phone: 302-633-5880 Fax: 302-633-5893

This product is licenced by Eisai Co., Ltd.